

Supramolecular Chemistry and Halogenation

Reactions of Pentaphosphaferrocenes



Dissertation zur Erlangung des
Doktorgrades der Naturwissenschaften

DR. RER. NAT.

am Institut für Anorganische Chemie
der Fakultät für Chemie und Pharmazie
der Universität Regensburg

vorgelegt von

HELENA HOIDN

(geb. Brake)

aus Schramberg

im Jahr 2020

Diese Arbeit wurde angeleitet von Prof. Dr. Manfred Scheer.

Das Promotionsgesuch wurde eingereicht am: Mo, 14.12.2020

Tag der mündlichen Prüfung: Fr, 05.02.2021

Vorsitzender: Apl. Prof. Dr. Rainer Müller

Prüfungsausschuss: Prof. Dr. Manfred Scheer

Prof. Dr. Henri Brunner

Prof. Dr. Frank-Michael Matysik



Universität Regensburg

Eidesstattliche Erklärung

Ich erkläre hiermit an Eides statt, dass ich die vorliegende Arbeit ohne unzulässige Hilfe Dritter und ohne Benutzung anderer als der angegebenen Hilfsmittel angefertigt habe; die aus anderen Quellen direkt oder indirekt übernommenen Daten und Konzepte sind unter Angabe des Literaturzitats gekennzeichnet.

Helena Hoidn

This thesis was elaborated within the period from January 2016 until December 2020 in the Institute of Inorganic Chemistry at the University of Regensburg under supervision of Prof. Dr. Manfred Scheer.

Parts of this work have already been published.

List of Publications:

E. Peresykina, C. Heindl, A. Virovets, H. Brake, E. Mädl, M. Scheer, *Chem. Eur. J.* **2018**, *24*, 2503-2508.

H. Brake, E. Peresykina, C. Heindl, A. V. Virovets, W. Kremer, M. Scheer, *Chem. Sci.* **2019**, *10*, 2940-2944.

H. Brake, E. Peresykina, A. V. Virovets, M. Piesch, W. Kremer, L. Zimmermann, C. Klimas, M. Scheer, *Angew. Chem. Int. Ed.* **2020**, *59*, 16241-16246.

To my family

Preface

This thesis deals with the supramolecular chemistry and halogenation reactions of pentaphosphaferrocenes. At the beginning, an introduction into supramolecular chemistry in general and that of polyphosphorus ligands in particular is given, followed by an outline of the research objectives.

The results are discussed in self-contained chapters 3 – 7. At the beginning of each of these chapters, a list of authors, who contributed to the respective work, is given. The extent of their contribution is listed in detail in the 'Author Contributions' at the end of the respective chapter. Additionally, if some of the presented results have already partly been discussed in other theses, it is stated there.

The chapters are subdivided into 'Introduction', 'Results and Discussion', 'Conclusion', 'Experimental Part', 'Crystallographic Details', 'Author Contributions' and 'References'. All chapters have the same text settings, and the numeration of compounds, figures, schemes and tables begins anew for each chapter.

Chapter 8 contains the thesis treasury with separate results not yet suitable for publication. A comprehensive conclusion of this work is presented at the end of the thesis.

Table of Contents

1	Introduction	1
1.1	Supramolecular Chemistry.....	1
1.2	Self-Assembly of Extended Structures.....	3
1.3	Self-Assembly of Discrete Structures.....	5
1.4	Covalently linked Discrete Hosts.....	9
1.5	Organometallic Building Blocks.....	10
1.5.1	P _n ligand complexes – Synthesis	11
1.5.2	P _n ligand complexes – Coordination Polymers.....	12
1.5.3	P _n ligand complexes – Discrete Supramolecules	14
1.6	References.....	19
2	Research Objectives	31
3	Fine-Tuning the supramolecular chemistry of Pentaphosphaferrocenes – Achieving versatility, selectivity and solubility	33
3.1	Introduction.....	34
3.2	Results and Discussion	35
3.3	Conclusion	45
3.4	Experimental Part	46
3.5	Crystallographic Details	62
3.6	Author Contributions	70
3.7	References.....	71
4	From Nano-Balls to Nano-Bowls	75
4.1	Introduction.....	76
4.2	Results and Discussion	77
4.3	Conclusion	82
4.4	Experimental Part	82

4.5	Crystallographic Details	85
4.6	Author Contributions.....	88
4.7	References	89
5	Nano-Bowls as Hosts for Triple Decker Complexes	93
5.1	Introduction	94
5.2	Results and Discussion.....	95
5.3	Conclusion.....	114
5.4	Experimental Part.....	116
5.5	Crystallographic Details	131
5.6	Author Contributions.....	138
5.7	References	139
6	The first Au-containing Coordination Polymers based on Polyphosphorus Ligand Complexes	145
6.1	Introduction	146
6.2	Results and Discussion.....	148
6.3	Conclusion.....	166
6.4	Experimental Part.....	167
6.5	Crystallographic Details	179
6.6	Author Contributions.....	188
6.7	References	189
7	Iodination of <i>cyclo</i>-E₅-Complexes (E = P, As)	195
7.1	Introduction	196
7.2	Results and Discussion.....	197
7.3	Conclusion.....	204
7.4	Experimental Part.....	205
7.5	Crystallographic Details	216
7.6	Computational Details	222
7.7	Author Contributions.....	235

7.8	References.....	236
8	Thesis Treasury.....	241
8.1	Self-Assembly of $[\text{Cp}^{\text{R}}\text{Fe}(\eta^5\text{-P}_5)]$ ($\text{Cp}^{\text{R}} = \text{Cp}^*, \text{Cp}^{\times}$) with CuGaCl_4	241
8.2	Self-Assembly of $[\text{Cp}^*\text{Fe}(\eta^5\text{-As}_5)]$ and $[\text{CpMo}(\text{CO})_2(\eta^3\text{-P}_3)]$ with Au Salts	246
8.3	Supramolecular Chemistry of Polyphospholyl Salts	249
8.4	Early Transition Metal Complexes of Polyphospholyl Ligands	252
8.5	Halogenations of $[\text{Cp}^*\text{Fe}(\eta^5\text{-P}_5)]$	255
8.6	Experimental Part	258
8.7	Crystallographic Details	264
8.8	Author Contributions	271
8.9	References.....	272
9	Conclusion.....	275
10	Appendices.....	289
10.1	Alphabetic List of Abbreviations	289
10.2	Curriculum Vitae	292
10.3	Acknowledgments.....	294

1. Introduction

1.1 Supramolecular Chemistry

Though essential to life itself, it was not until the late 1960s that *Supramolecular Chemistry* has evolved as a distinct area of chemical research, when Pedersen first studied the complexing of alkali metal cations to cyclic polyethers ('crowns').^[1] Shortly afterwards, Lehn reported on the complexation of metal cations by macrobicyclic compounds ('cryptands'),^[2] and Cram developed optically pure crowns for chiral recognition, as well as 'spherands' in which the synthetic ligand system is pre-organized for the first time.^[3] In 1987, they conjointly received the Nobel Prize in Chemistry '*for their development and use of molecules with structure-specific interactions of high selectivity*'.^[4] In his Nobel lecture, Lehn described supramolecular chemistry as '*chemistry beyond the molecule*', in which two or more species (covalent molecules or ions) display building blocks held together by intermolecular, non-covalent forces.^[5]

Supramolecular chemistry can roughly be split into two categories. Whilst '*host-guest chemistry*' rather relates to a large molecule (host) capable of enwrapping a smaller species (guest), the term '*self-assembly*' is referred to in case no significant difference concerning the size of the building blocks exists.^[6] An enzyme with its substrate would thus be described as a host-guest complex, whereas the biosynthesis of DNA for example is allocated to the field of self-assembly. With the DNA's famous double helix structure, nature demonstrates in an impressive manner the extraordinary potential of self-assembly processes in the bottom-up synthesis of intricate structures. Instead of an elaborate step-by-step construction, this approach merely requires the design and synthesis of few, relatively simple building blocks and their subsequent spontaneous aggregation.^[6,7] The reversibility of this process ensures the formation of thermodynamic, stable supramolecules, since the system is allowed to self-correct errors in possible initially formed, kinetic products.^[8]

Supramolecular aggregates can further be categorized based on the interactions directing their assembly, like i) H-bonding interactions; ii) other non-covalent interactions such as ion-ion, ion-dipole, π - π stacking, cation- π , van der Waals and hydrophobic interactions; and iii) coordinative bonds between metals and ligands.^[9] In the latter approach, called '*metallo-supramolecular chemistry*', the crucial feature is the highly directional and predictable nature of the metal-ligand interaction. This is due to the defined acceptor properties of the metal ion (size, coordination number and geometry) on the one hand in combination with the defined donor properties of the ligand (number and spatial arrangement of the donor atoms) on the other hand.^[10] Moreover, coordinative bond energies are relatively high (15-50 kcal/mol), lying in between those of organic covalent bonds (60-120 kcal/mol) and weak interactions

(0.5-10 kcal/mol) as can be found in natural self-assembly products. Nevertheless, they are still labile enough to assure kinetic reversibility and thus the formation of thermodynamically stable products.^[9]

The building blocks in coordination-driven self-assembly, i.e. the Lewis-acidic metal centers (metal ions, clusters, organometallic fragments or others) and Lewis-basic ligands (organic, inorganic or metal-containing), are each at least ditopic.^[11] The coordination sites of most ligands typically are functional groups with nitrogen (e.g. pyridyl, nitrile groups) or oxygen (e.g. carboxylate groups) as donating elements,^[12] while phosphorus^[13] or sulfur^[14] donor atoms are less frequently found. By installing rigid spacers such as ethynyl or phenyl groups in the ligand, expanded structures may be formed while retaining their original topology.^[11] A selection of multitopic ligands is given in Figure 1.

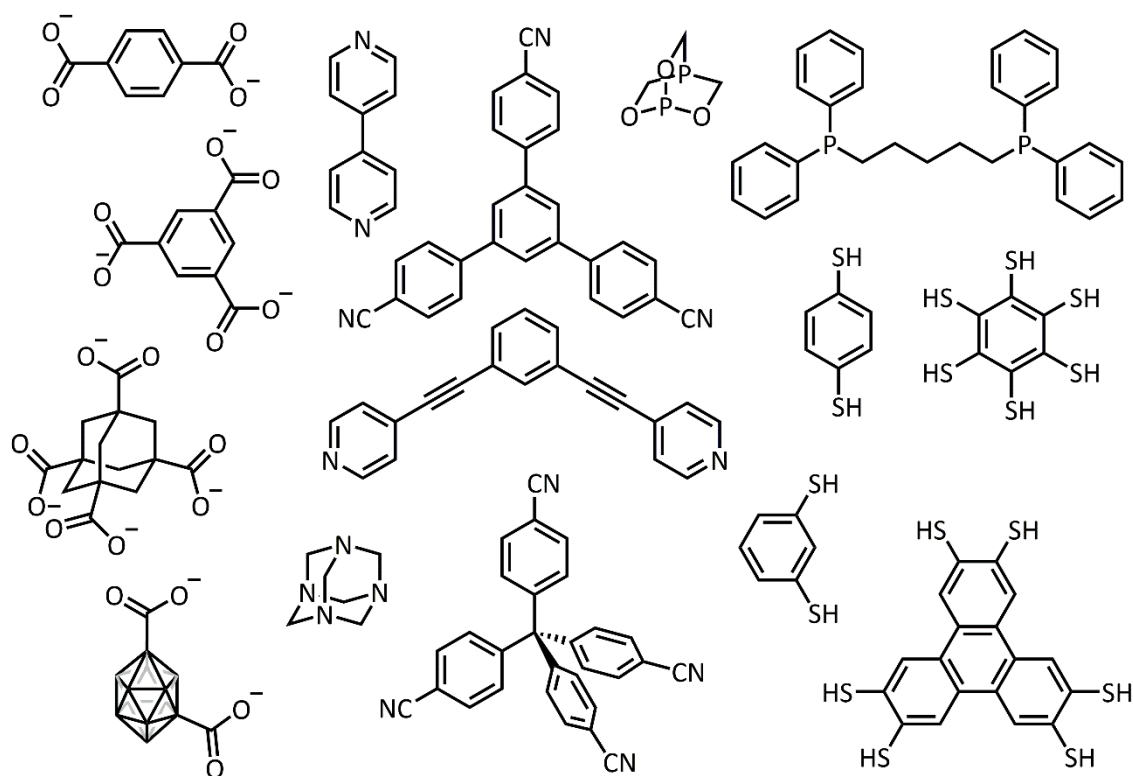


Figure 1. A selection of multitopic ligands used for coordination-driven self-assembly.

Moreover, both building blocks may each be classified as convergent or divergent.^[11] For the self-assembly of discrete aggregates at least one component must be convergent – in case both components are divergent, only extended polymeric structures may be formed.^[15] Since naked metal ions are inherently divergent (Figure 2a), for the synthesis of discrete structures either convergent ligands are applied, or capping ligands are introduced onto the metal ions leaving only convergent coordination sites available (Figure 2b,c).^[11] While conceptually, naked metal ions are suitable for the synthesis of extended structures when combined with divergent ligands, in practice, clusters have proven beneficial (Figure 2d).^[15] These ‘secondary building units’ (SBUs)

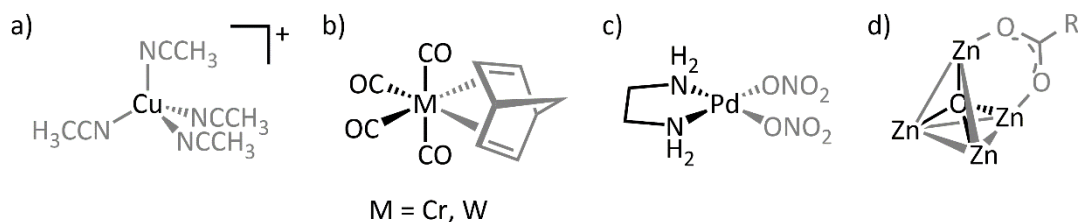


Figure 2. A selection of metal building blocks used for coordination-driven self-assembly. Grey ligands in a)-c) are labile and exchanged during self-assembly. Grey lines in d) indicate the coordination sites for six bridging multitopic ligands, one of which is exemplarily depicted.

are often formed *in situ* and avoid the geometric ambiguity of naked metal ions. This ‘decoration’ of an extended structure can also be taken one step further, by employing discrete, supramolecular aggregates themselves as supramolecular building blocks (‘SBBs’) instead of metal ions or clusters in a hierarchical self-assembly process.^[16] Similarly, discrete supramolecules may be ‘decorated’, e.g. by replacing a single *n*-connected node by a group of *n* nodes, a process referred to as ‘augmentation’ and leading to truncated structures.^[15]

1.2 Self-Assembly of Extended Structures

In nature, extended structures formed by self-assembly are ubiquitous. The DNA double helix, secondary, tertiary and quaternary protein structures and the phospholipid layers building up the cell membrane are examples, in which supramolecular interactions (here mainly hydrogen bonding and hydrophobic interactions) play a crucial role for their functionality.^[9,17]

In the field of *metallo-supramolecular chemistry*, coordination-driven self-assembly of metals and ligands may also be used to build up extended, polymeric structures. Such a ‘*coordination polymer*’ is defined as “a coordination compound with repeating coordination entities in 1, 2, or 3 dimensions”, where there is no restriction in the nature of the ligand (i.e. organic, inorganic or organometallic).^[18] Accordingly, fully inorganic *Prussian Blue* was in fact not only the first man-made coordination compound, but at the same time the first synthetic coordination polymer,^[19] as structural characterization in 1977 revealed (Figure 3a).^[20] Nevertheless, coordination polymers merely attracted researchers’ attention before the late 1980s.^[19] Then, advances in X-ray diffraction equipment and the Cambridge Structural Database, amongst other developments, provided excellent conditions for the emerging research field.^[21] A plethora of coordination polymers have been reported since.^[19] Originating from the field of crystal engineering, a technique for the analysis and design of solids by reducing their crystal structures to networks of nodes and spacers was described by A. F. Wells.^[22] This ‘net approach’ was later applied to the design of new coordination polymers by Robson and co-workers.^[23] In their seminal papers, they describe the deliberate synthesis of a diamond-like framework from

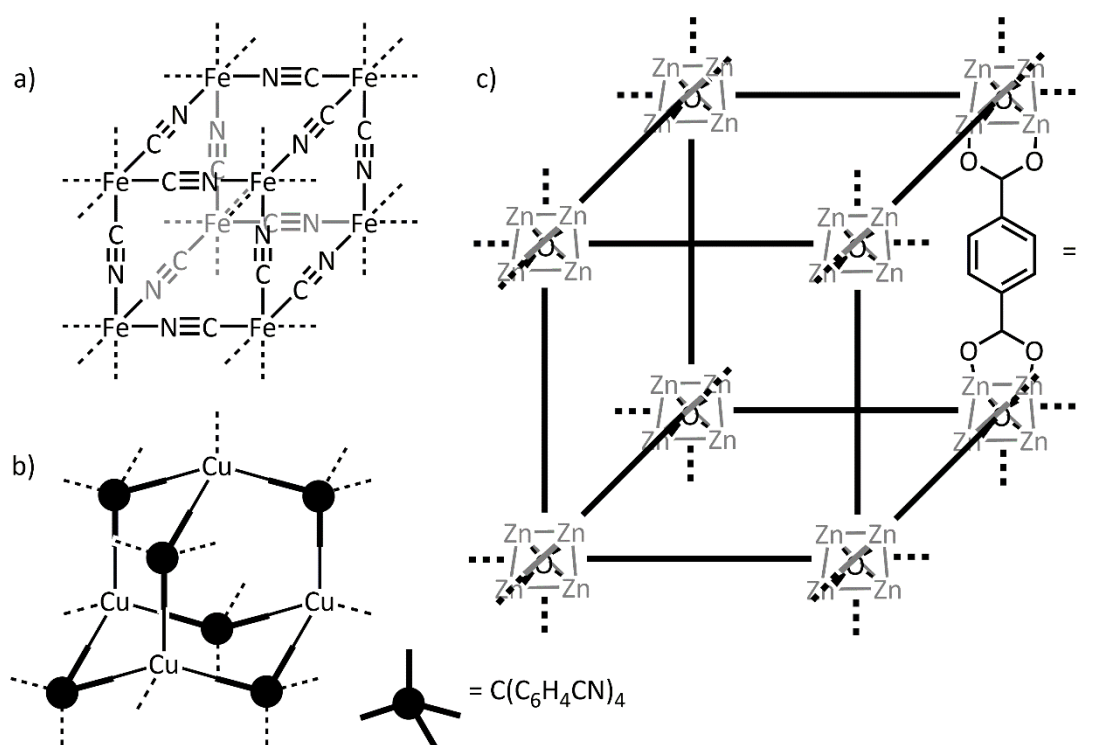


Figure 3. Sections of the 3D coordination networks a) Prussian blue $Fe_4[Fe(CN)_6]_3$, b) $[Cu\{C(C_6H_4CN)_4\}]_n^{n+}$ and c) $[Zn_4O\{O_2C(C_6H_4)CO_2\}_3]_n$ (MOF-5) with Zn_4O tetrahedra highlighted in grey.

$[Cu(CH_3CN)_4]BF_4$ and 4,4',4'',4'''-tetracyanotetraphenylmethane containing large cavities that make up two-thirds of the crystal volume (Figure 3b). Inspired by zeolites, they envisioned the use of such porous frameworks as molecular sieves and heterogeneous catalysts. Constituting a subset of coordination polymers, these materials soon came to be known as metal-organic frameworks (MOFs) and are defined as 'a coordination network with organic ligands containing potential voids'.^[18] In the following years, the groups of Zaworotko and Yaghi each published frameworks of Cu(I) centers connected by 4,4'-bipyridine, which yet adopted different topologies due to the geometric ambiguity of the Cu nodes.^[24] To overcome this problem, clusters have been employed as rigid, well-defined SBUs.^[11] Quite often, these are only formed in situ during MOF synthesis and not isolable individually, hence leaving the organic linkers as important set screw. Since many applications of MOFs base on the accessibility of voids, strong metal-ligand bonds are favorable to guarantee permanent porosity. This can be achieved by application of chelating carboxylate linkers, which additionally may participate in cluster (SBU) formation through versatile binding modes and provide charge balance, thus keeping counterions from occupying the voids. A prominent example is the notorious MOF-5 by Yaghi and co-workers, which consists of $\{Zn_4O\}$ clusters connected by 1,4-benzenedicarboxylate as linkers (Figure 3c).^[25] Notably, MOF-5 exhibits a permanently porous nature even upon guest removal by heating up to 300°C while retaining crystallinity. These design principles (combining

rigid molecular building blocks by strong bonding) facilitate the deliberate synthesis of predetermined ordered networks and are dubbed ‘reticular synthesis’ by Yaghi.^[26] However, since strong metal-ligand bonds may hinder kinetic reversibility, harsh conditions as found in the solvothermal synthesis of MOFs are often applied to overcome kinetic intermediates.^[11] In contrast, Kitagawa and co-workers published a permanently porous MOF based on pyridyl-linkers already in 1997.^[27]

As suggested by Robson and co-workers (*vide supra*),^[23] the applications of porous MOFs by now indeed span gas storage,^[28] separations (gas, vapor, liquid),^[29] catalysis,^[30] photophysical applications such as sensing^[31] and more.^[29,32] Furthermore, as introduced by Fujita and co-workers,^[33] MOFs may be employed as crystalline sponges enabling X-ray crystallographic structural determination of e.g. liquid or even volatile compounds upon encapsulation.^[34]

Other applications are not (solely) based on the porosity and host-guest chemistry of the framework. Instead, the applied building blocks may impart chirality, redox activity, photophysical characteristics,^[11] as well as magnetic^[32] and conductive^[35] behavior. In fact,

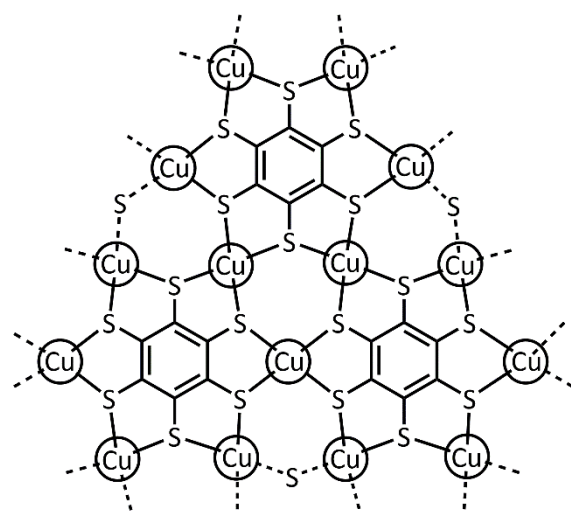


Figure 4. Section of the coordination network $[Cu_3(BHT)]_n$ (BHT = benzenhexathiolate).

increased framework density appears to correlate with higher conductivities. Accordingly, the conductivities of 2D polymeric $Cu_3(BHT)$ (BHT = benzenhexathiolate) currently hold the record for coordination polymers and even the transition into a superconducting state was reported for the first time (Figure 4).^[36] Moreover, the metal-ligand bond strengths can be varied over a large range by chelation and donor/metal pairing according to the concept of ‘hard and soft acids and bases’

(HSAB), enabling the synthesis of coordination polymers with fine-tuned properties.^[37] Some coordination polymers may readily depolymerize in solution, while others may retain their polymeric structure, sometimes depending on external stimuli such as sonication, hence introducing mechano-chemical features.

1.3 Self-Assembly of Discrete Structures

Conceptually, the transformation of extended to discrete supramolecular aggregates can be achieved by employing convergent rather than divergent building blocks.^[15] Thus, the first coordination macrocycles synthesized by Verkade in 1983 were obtained by mixing metal carbonyl precursors with cis-arranged labile ligands and ditopic phosphorus (metallo)ligands

(Figure 5a-e).^[38] Moreover, entropy favors the formation of discrete structures rather than polymeric assemblies.^[9] However, if the competing polymeric assembly is insoluble, once formed, the reversibility of the self-assembly is no longer given and polymeric byproducts may become a concern.^[11] In contrast, if all intermediate species remain soluble throughout self-assembly, thermodynamic products may be isolated in high yields. Discrete coordination-driven assemblies evince immense structural diversity, ranging from 2D helicates,^[39] grids^[40] and polygons^[41] to 3D polyhedra^[42] and others.^[43] Among these, metal-organic polyhedra (MOPs) have been of special interest due to their confined cavities and often take the shape of Platonic or Archimedean solids.^[42b,12a] Contrarily to MOFs, MOPs are frequently constructed with neutral, organic N-donor ligands,^[11,42b] since the dynamic interactions and kinetic reversibility are crucial for the deliberate synthesis of targeted structures.^[44] Nevertheless, many reported MOPs were discovered by coincidence,^[12a] and minor changes in components can lead to major differences in the resulting assemblies.^[45] Considerable effort has been made to develop methodologies for the rational design and preparation. In general, the assembly of MOPs may be edge-directed, meaning that the building blocks occupy the edges and vertices of the polyhedral structure, or face-directed, with either of the building blocks occupying the faces.^[11] Stang introduced the concept of ‘directional bonding’,^[46] based on the supramolecular squares of Verkade^[38] (*vide supra*, Figure 5a-e) and later examples of Fujita^[47] and his own group,^[48] employing cis-capped Pd^{II} and Pt^{II} centers and 4,4'-bipyridine (Figure 5f,g).

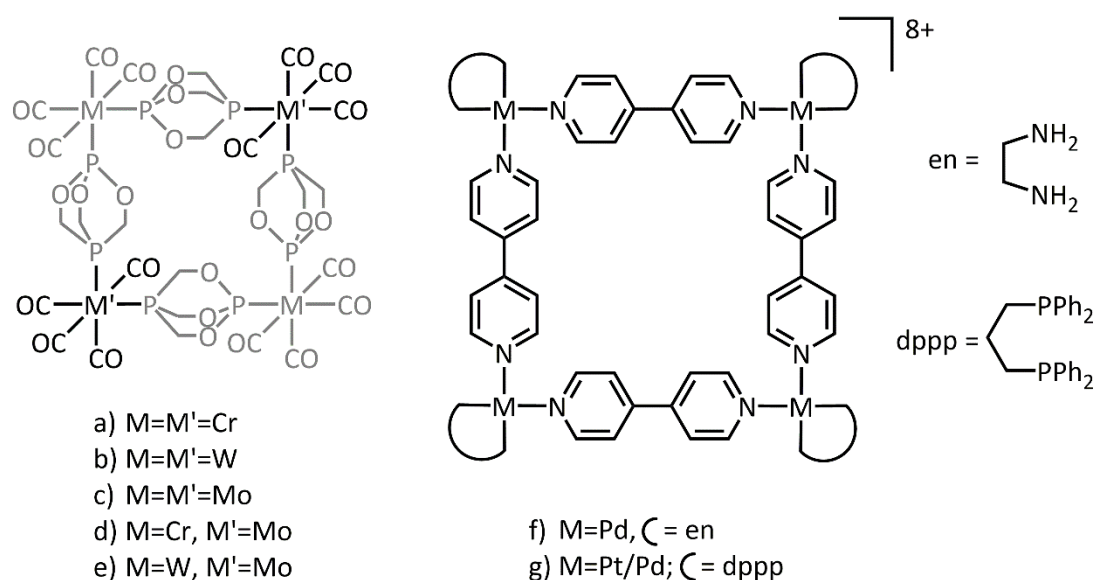


Figure 5. Supramolecular squares of (a-e) metalloligands (grey) and M(CO)₄ fragments by Verkade^[38], f) (en)Pd fragments and 4,4'-bipyridine by Fujita^[47] and g) (dppp)M fragments and 4,4'-bipyridine by Stang.^[48]

It relies on the combination of structurally rigid building blocks with predefined bite angles in a given stoichiometric ratio and thus is sometimes also termed ‘molecular library model’.^[46,43b]

The self-assembly of ditopic building blocks gives 2D metallacycles, while 3D MOPs are formed in case at least one of the building blocks is more than ditopic. As a subset of the directional bonding approach, ‘molecular paneling’ may be mentioned, describing the face-directed self-assembly of MOPs by panel-like ligands designed to occupy some or all of the faces of the polyhedral structure.^[9,11] Fujita and co-workers pioneered this design strategy by publishing the synthesis of a supramolecular octahedron with six, cis-capped Pd^{II} vertices and four of the eight faces paneled by rigid, tritopic pyridyl ligands (Figure 6, left).^[49] In contrast, the very first MOP was serendipitously found by Saalfrank and co-workers, constituting a tetrahedron built up from four naked Mg²⁺ centers and six bis-chelating ligands (Figure 6, right).^[50] This strategy, later called ‘symmetry interaction model’,^[43b] was conceptualized by Raymond and co-workers and makes use of rigid polychelating linkers, thus rendering cis-capping of divergent, naked metal ions unnecessary.^[51]

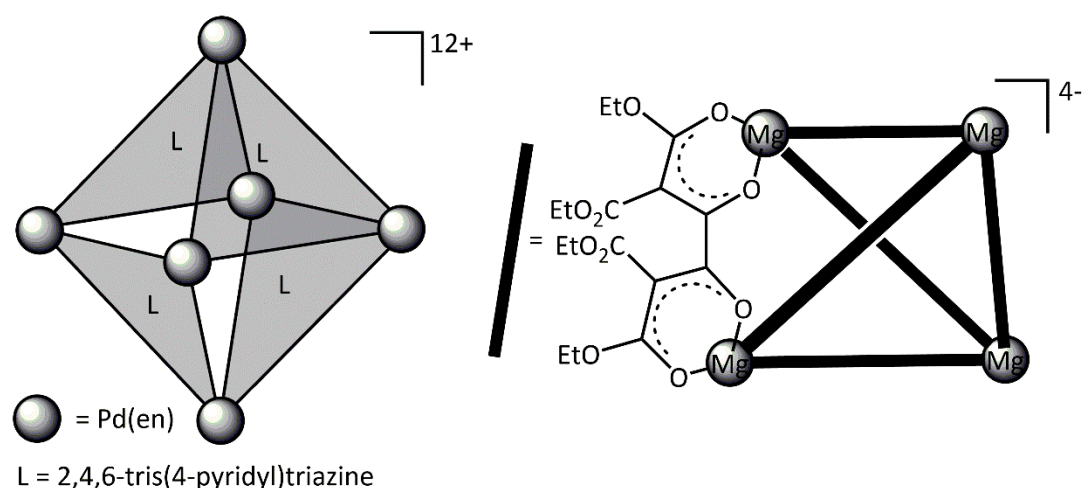


Figure 6. (Left) Face-directed octahedral assembly of four tritopic ligands (grey triangles) and six ditopic metal centers. (Right) Edge-directed tetrahedral assembly of six dicarboxylate ligands (black bars) and four hexatopic metal centers.

As outlined for MOFs, the stability of MOPs can as well be enhanced by applying SBUs instead of single metal ions as acceptor building blocks. For instance, Cotton and co-workers pioneered the use of paddlewheel complexes as dimetallic SBUs for the construction of MOPs.^[52] By this approach, MOPs with extraordinary stability comparable to that of MOFs are accessible.^[53]

The enormous structural diversity resulting from the modular synthesis with a large variety of available building blocks has translated into multifaceted functions.^[45] As for MOFs, applications of 2D coordination cycles and 3D coordination cages are often based on their ability to act as hosts. By now, they have found use in sensing, chemical purifications and extractions, the stabilization of reactive species, biomedical applications such as imaging and drug delivery, as molecular flasks for stoichiometric reactions and in catalysis.^[9,44,45,54] Purely organic, covalent

hosts such as crown ethers, calixarenes, cyclodextrins and cucurbiturils, as well as organic, self-assembled hosts held together by hydrogen-bonding are applied similarly.^[55] However, their supramolecular coordination-based counterparts often exhibit higher selectivities in sensing and their facile modular synthesis enables rapid screening for the appropriate hosts.^[54a]

A pioneering example of stabilization of reactive species was given by Nitschke and co-workers.^[56] By encapsulation of P_4 into a self-assembled coordination cage the host-guest aggregate was air-stable for four months since oxidation products of P_4 would not fit into the cavity of the host. Moreover, the host-guest assembly was water-soluble and P_4 could be released by adding benzene as a competing guest.

Fujita's group used an octahedral MOP for the encapsulation of four molecules methylcymantrene.^[57] Upon photoirradiation of a single crystal of the host-guest complex, one CO ligand was dissociated from one of the guest molecules leaving a coordinatively unsaturated 16VE species, while retaining the crystallinity of the sample. Hence, X-ray crystallographic structure determination of this labile complex was feasible for the first time and revealed its pyramidal geometry.

Bergman and Raymond reported on a self-assembled coordination tetrahedron capable of catalyzing the Nazarov cyclization of 1,4-pentadien-3-ol derivatives to give Cp^*H with a rate acceleration exceeding a million-fold, which is comparable to enzymes.^[58] The addition of a Cp^*H trapping agent proved to be of crucial importance in order to avoid product inhibition. Next to such a cavity promoted catalytic behavior, catalytic function may also be imparted by embedding active sites in the cage structure or by encapsulating catalysts themselves within the cage.^[54b] Contrarily to solid MOFs, the oftentimes well-soluble MOPs may be employed as homogeneous catalysts, with the accompanying advantages and disadvantages.

Sometimes, a template is needed to direct the formation of MOPs.^[11] Such templates often are weakly coordinating anions (WCAs), at the same time acting as counterions for the MOP, but may as well be cations, solvent molecules or an additional component, which then act as guest molecules.^[59] The synthetic potential of the template effect was demonstrated not only in the synthesis of crown ethers,^[60] but also by Sauvage in the synthesis of pseudorotaxanes, which then may act as precursors to rotaxanes and catenanes, so called mechanically interlocked materials (MIMs).^[61] Interestingly, pseudorotaxanes themselves are supramolecular host-guest complexes.^[62] These pseudorotaxanes may in turn serve as building blocks in coordination driven self-assembly, resulting in discrete molecular necklaces (Figure 7, left) or extended polypseudorotaxanes (Figure 7, right).^[63] Poly-pseudorotaxanes may also be constructed solely upon the host-guest interactions, which constitute a special case of non-covalent interactions.^[64] Similarly to the abovementioned organic MIMs, there are also examples of catenated metal-

organic cycles^[65] and 3D interpenetrated metal-organic cages.^[12a,66] Just as intercalation (e.g. the encapsulation of guest or solvent molecules), this interpenetration is a way in which a crystal can maximize its packing efficiency.^[67] Interpenetration mostly constitutes a problem in MOFs by reducing available pore sizes, but for both MOFs and MOPs it also may give rise to some interesting properties and applications.^[66b]

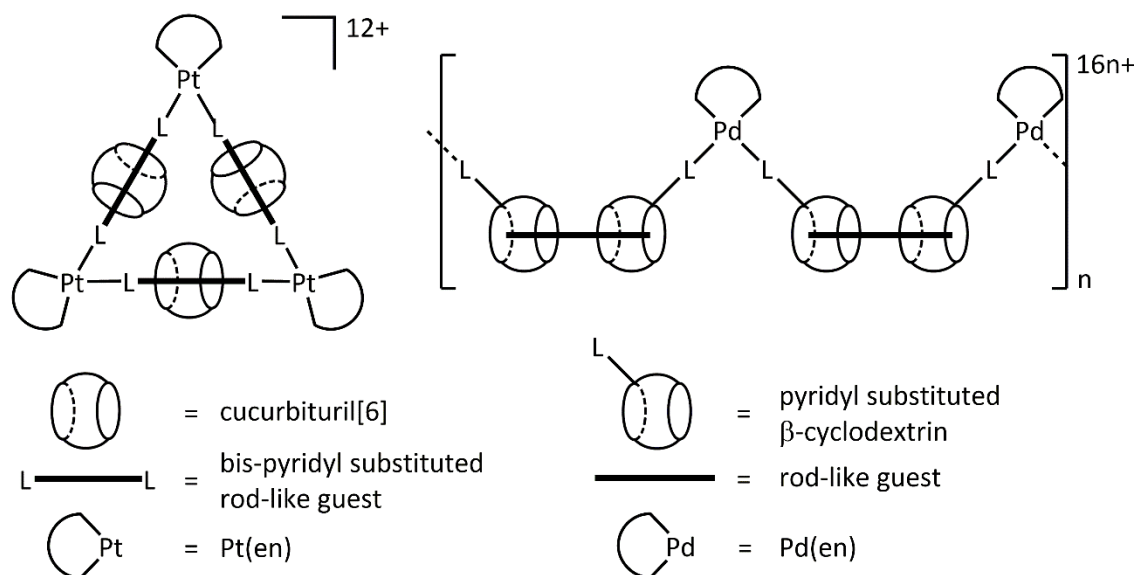


Figure 7. (Left) Molecular necklace constructed by self-assembly of a pseudorotaxane and Pt(en) vertices. (Right) Polypseudorotaxane constructed by self-assembly of pseudorotaxane and Pd(en) vertices.

1.4 Covalently linked Discrete Hosts

Host molecules capable of encapsulating smaller guest species do not necessarily have to be coordinative assemblies, but may also be covalently linked species, such as the aforementioned organic hosts (crown ethers, cryptands, etc.) or even hosts of purely inorganic nature. Concerning the latter class, especially fullerenes must be mentioned, the third allotropic modification of carbon, whose discovery in 1985 by Kroto, Curl, Smalley and co-workers^[68] was honored with the Nobel Prize in 1996.^[69] The proposed soccer-ball-like spherical structure of C₆₀^[68] was later confirmed by single-crystal X-ray diffraction of an exohedrally osmylated derivative.^[70] Owing to the hollow structures of fullerenes, encapsulation of single atoms or small molecules was soon accomplished. This class of endohedral fullerenes by now spans carbon cages hosting one or more metal atoms,^[71] a variety of clusters,^[72] single main group atoms (N or P),^[73] one or two noble gas atoms^[74] and small molecules like H₂,^[75] CO,^[76] N₂^[77] or H₂O.^[78] Analogously, carbon nanotubes have been used as hosts, e.g. in turn for fullerenes,^[79] and as nanovessels for stoichiometric and catalytic reactions.^[80] The synthesis of fullerenes and carbon nanotubes has sometimes been called “covalent self-assembly”, since the harsh reaction conditions allows a certain structural fluidity.^[81]

Another class of inorganic, covalent and hollow substances are polyoxometalates (POMs), nanoscale oxides of group 5 and 6 metals in high oxidation states constructed of fused $\{MO_x\}$ polyhedral units.^[82] Their immense molecular and electronic structural diversity^[83] together with the remarkable stability^[82b] endow them with applications in catalysis,^[84] medicine,^[85] materials science^[86] and others.^[87] With cage-, basket-, barrel-, wheel- or sphere-like shapes, POMs may also function as hosts e.g. for a single H₂O molecule, H₂O 'nanodrops' or smaller POMs, or serve as building blocks for polypseudorotaxanes (wheel-type hosts), MOFs and MOPs.^[87b,88]

Apart from fullerenes and POMs, other classes of inorganic substances that can act as host molecules are to be mentioned. As inorganic crown or cryptand analogues, cyclosiloxanes or -silazanes, bicyclic phosphanyl siloxanes, cyclophosphazanes or -phosphazenes have been studied in that respect.^[89]

1.5 Organometallic Building Blocks

The previous examples of coordination-driven assemblies are primarily based on the combination of metal ions or clusters as acceptor building blocks with organic ligands as donor building blocks. However, either component may also be a coordination compound itself.

Abovementioned supramolecular squares by Verkade,^[38] Fujita^[47] and Stang^[48] are examples, where a metal complex fragment is employed rather than a metal ion or cluster. While the first example is formed from a complex with *cis*-arranged labile ligands, the latter two additionally encompass *cis*-capping chelate ligands (ethylenediamine (en) and bis(diphenylphosphino)propane (dppp), respectively) blocking the other two coordination sites. The blocking of three coordination sites can be achieved by introducing an arene or Cp ligand. The resulting or $\{CpM\}$ (M = Rh, Ir)^[90] organometallic acceptor building blocks hence have merely three convergently arranged coordination sites left available (Figure 8a). Similarly, $\{(arene)Ru\}$ ^[91] units have been employed especially by Therrien and co-workers, which are often bridged by oxalate or dihydroxybenzoquinone to give bimetallic, ditopic acceptor units (Figure 8b). Further di- and tritopic acceptor building blocks are so called 'molecular clips', where metal centers (often Pd or Pt) are connected via alkynyl^[92] or aryl^[93] groups (Figure 8c,d). Thereby, a specific angle can be installed between the available coordination sites, which is hence not restricted to the coordination geometry of a single metal ion anymore.

On the other hand, the ligand may be formally substituted by an organometallic compound. This is possible in case a metal complex possesses peripheral donor atoms, allowing the complex to function as ligand. These so-called 'metalloligands' or 'ligand complexes' often comprise pyridyl substituents.^[94] Organometallic examples are given by Stang,^[95] Lee & Lee,^[96] Clemmer,^[97] Cotton & Murrillo^[98] and Williams,^[99] comprising M₂C₂ tetrahedra, alkynyl or metallocene complex derivatives (Figure 8e-g).

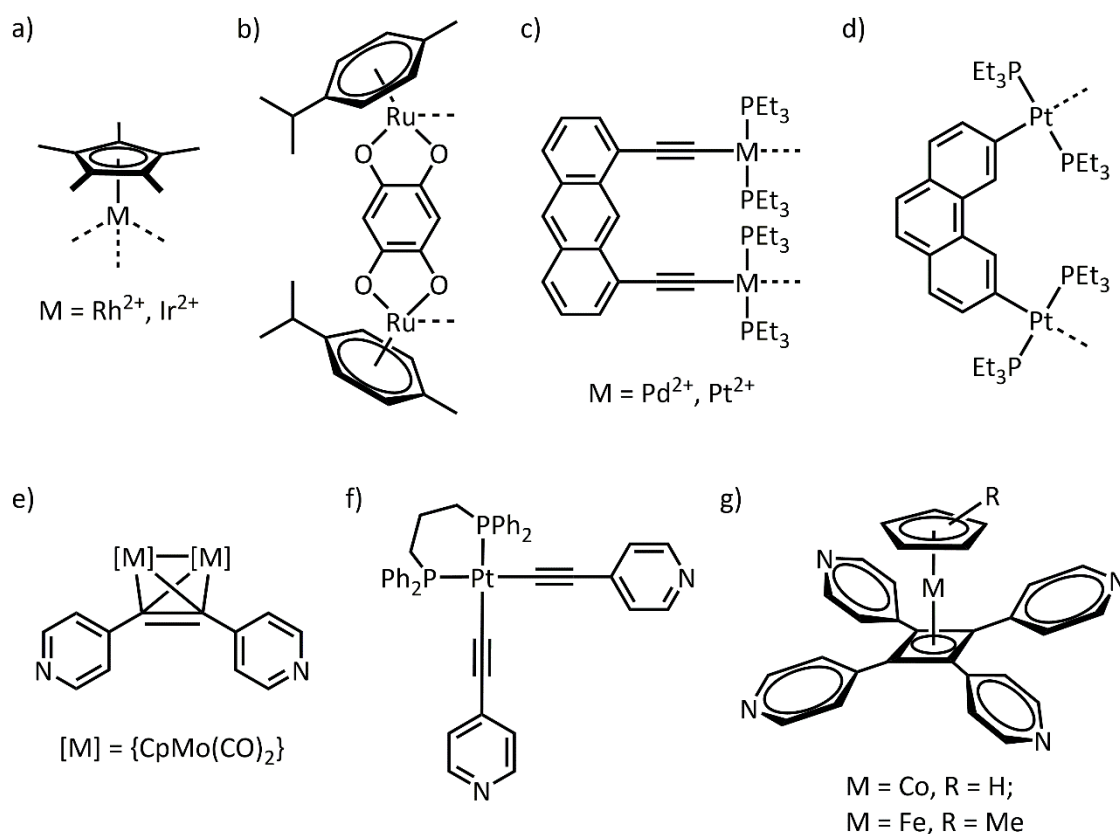


Figure 8. Selected examples of organometallic building blocks employed in self-assembly processes as acceptors (a-d) or donors (e-g).

Apart from these organometallic ligand complexes, numerous other metalloligands have been employed in coordination driven self-assembly, thereby spanning salen,^[100] porphyrine^[101] and clathrochelate^[102] based ligand complexes, in which the ligand is itself can already function as a multitopic linker, as well as metalloligands, in which the metal center is crucial for the arrangement of the donor sites. This is the case in Verkade's supramolecular square^[13] (*vide supra*) and others.^[94,103] Subsequent coordination of these metalloligands (organometallic or not) to a second set of metal ions results in the desired supramolecular assemblies. Hence, this approach is useful for the synthesis of heterometallic aggregates, providing additional functionality and enhanced complexity.

1.5.1 P_n ligand complexes – Synthesis

In contrast to the widespread use of N or O donor ligands, our group focuses on the construction of supramolecular aggregates based on polyphosphorus (P_n) ligand complexes as organometallic ligands. P_n ligand complexes are characterized by substituent-free P atoms, which are solely bound to other P or metal atoms. Some neutral complexes with cyclic P_n ligands are depicted in Figure 9, although a wide variety of P_n ligand complexes is known to date, also including further dinuclear complexes^[104] and complexes with other metals^[105] or Cp ligands^[106] as well as E_n ligand complexes of heavier group 15 elements ($E = \text{As}, \text{Sb}, \text{Bi}$).^[107]

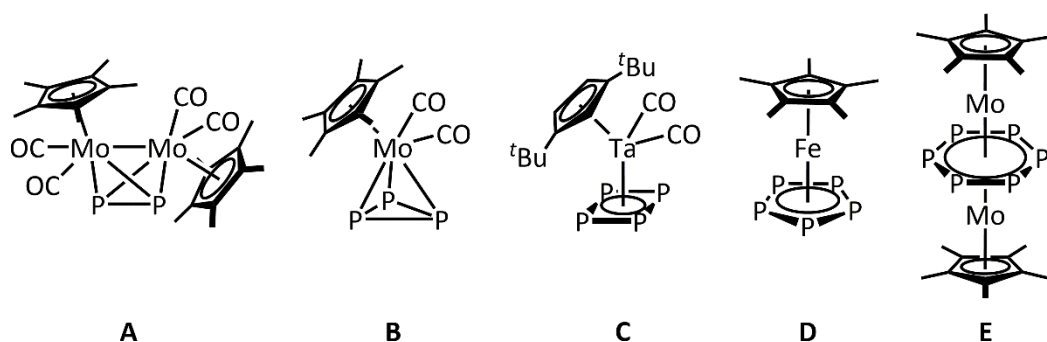


Figure 9. Selected P_n ligand complexes ($n = 2 - 6$) as building blocks for supramolecular chemistry.

The complexes in Figure 9 are accessible from thermolysis or photolysis of white phosphorus (P_4) with the respective carbonyl complex $[Cp^*Mo(CO)_3]_2$ (**A**, **B**, **E**),^[108] $[Cp^tTa(CO)_4]$ (**C**)^[109] and $[Cp^*Fe(CO)_2]_2$ (**D**).^[110] This transition metal-mediated P_4 activation is a flourishing research field of its own, since it not only brings forth exciting P_n ligand complexes, but subsequent functionalization may also yield industrially relevant phosphorus compounds via milder reaction conditions.^[111] In contrast, the currently applied route encompasses hazardous reagents and generates stoichiometric amounts of waste under partially harsh conditions.

1.5.2 P_n ligand complexes – Coordination Polymers

Since all P_n ligand complexes comprise a lone pair per P atom accessible for further coordination, in case $n > 1$, this substance class may well act as polytopic organometallic ligands for the construction of supramolecular assemblies. Building on early results of coinage metal bridged *cyclo*- P_3 complexes,^[112] our group published first coordination polymers constructed by self-assembly of $[CpMo(CO)_2]_2[\mu, \eta^{2:2}-P_2]$ (type **A**) with $AgNO_3$ and $CuBr$ (Figure 10a), respectively.^[113] From then on, numerous dimeric or 1D polymeric assemblies based on $[CpM(CO)_2]_2[\mu, \eta^{2:2}-P_2]$ (type **A**, $M = Cr, Mo$) ligand complexes have been reported with coinage metal salts of halides or weakly coordinating anions (WCAs).^[114] Interestingly, the addition of an N donor linker as a third component to reactions of type **A** complexes $[CpM(CO)_2]_2[\mu, \eta^{2:2}-P_2]$ ($M = Cr, Mo$) with coinage metal salts mostly leads to further polymerization to 1D, 2D and even 3D organometallic-organic hybrid polymers.^[114f,115] The supramolecular chemistry of type **B** and **E** complexes is less explored. While reactions of $[CpM(CO)_2(\eta^3-P_3)]$ (type **B**, $M = Cr, Mo$) with $CuTEF$ ($TEF = Al(OC(CF_3)_3)_4$) lead to monomeric or dimeric coordination products,^[114c] self-assembly of $[Cp^R Mo(CO)_2(\eta^3-P_3)]$ (type **B**, $Cp^R = Cp, Cp^*$) with $AgOTf$ or $AgTEF$ salts yields 1D coordination polymers (Figure 10b).^[116] Concerning the P_6 ligand complexes, the reactions of $[Cp^*Mo]_2[\mu, \eta^{6:6}-P_6]$ (type **E**) with $CuTEF$ or $AgTEF$ lead to monomeric coordination products,^[117] whereas sterically less hindered $[CpMo]_2[\mu, \eta^{6:6}-P_6]$ (type **E**) forms 2D coordination polymers with $CuBr$ or CuI (Figure 10f).^[118]

The supramolecular chemistry of type **A**, **B** and **E** complexes towards main group metals has been explored as well. Type **A** complexes $[\{\text{Cp}^R\text{M}(\text{CO})_2\}_2\{\mu, \eta^{2:2}\text{-P}_2\}]$ ($\text{Cp}^R = \text{Cp}, \text{Cp}^*$) arrange to oligomeric coordination products upon reaction with InTEF or TITEF.^[119] On the contrary, type **B** complexes $[\text{CpM}(\text{CO})_2(\eta^3\text{-P}_3)]$ ($\text{M} = \text{Cr}, \text{Mo}$) arrange to 1D polymeric assemblies with InTEF or TITEF.^[119b,c] Triple-decker complex $[\{\text{Cp}^*\text{Mo}\}_2\{\mu, \eta^{6:6}\text{-P}_6\}]$ (type **E**) was shown to form layers with TITEF, which may be interpreted as a 2D coordination polymer (although the connectivity is not unambiguously clarified due to disorder in the TI positions).^[117]

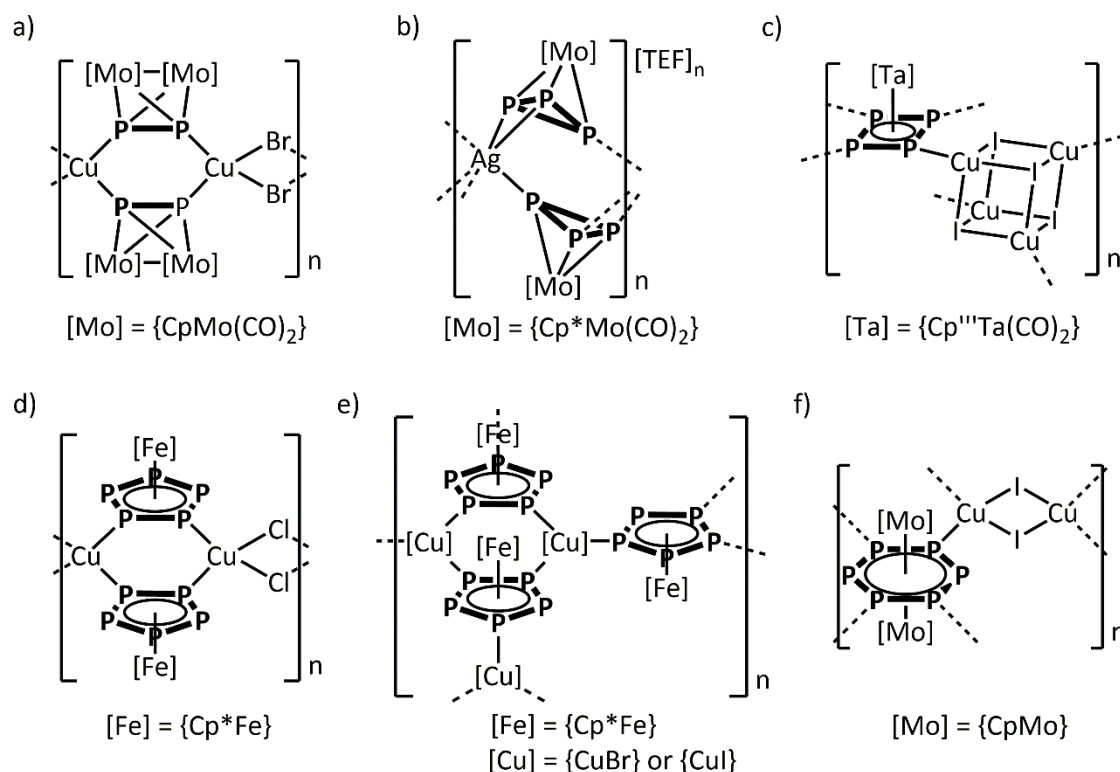


Figure 10. Selected coordination polymers obtained from P_n ligand complexes of type **A** – **E**.

The supramolecular chemistry of *cyclo*- P_4 and *cyclo*- P_5 complexes of type **C** and **D** step out of line, since not only oligomeric or polymeric assemblies may be achieved, but spherical aggregates are reported as well. The first polymers were obtained by self-assembly of $[\text{Cp}^*\text{Fe}(\eta^5\text{-P}_5)]$ (**D**) and $\text{Cu}(\text{I})$ halides and exhibit a 1,2- (Figure 10d) or a 1,2,4-coordination mode (Figure 10e) of the pentaphosphaferrocene.^[120] A closer look into the reaction of $[\text{Cp}^*\text{Fe}(\eta^5\text{-P}_5)]$ (**D**) with CuCl revealed the additional formation of a soluble, 90-vertex spherical aggregate $[\{\text{Cp}^*\text{Fe}(\eta^5\text{-P}_5)\}_{12}\{\text{CuCl}\}_{25}\{\text{CH}_3\text{CN}\}_{10}]$ (Figure 11a, *vide infra*), cocrystallizing with an ionic derivative in the ratio of 3:1.^[121] By now, a myriad of 1D and 2D coordination polymers of the type $[\{\text{Cp}^*\text{Fe}(\eta^5\text{-P}_5)\}_a\{\text{CuX}\}_b]_n$ ($\text{X} = \text{Cl}, \text{Br}, \text{I}$) is known,^[122] as opposed to only one 2D polymer based on $[\text{Cp}^{\text{Bn}}\text{Fe}(\eta^5\text{-P}_5)]$ (type **D**, $\text{Cp}^{\text{Bn}} = \text{C}_5(\text{CH}_2\text{C}_6\text{H}_5)_5$) and CuI .^[123] Interestingly, the recently developed synthesis of the parent pentaphosphaferrocene $[\text{CpFe}(\eta^5\text{-P}_5)]$ (type **D**) enabled investigations of its reactivity towards $\text{Cu}(\text{I})$ halides as well, and next to 2D polymers for the first time also a 3D

polymeric assembly was obtained.^[124] Apart from coinage metal salts, again main group metal salts MTEF (M = Ga, In, Tl) have been employed in reactions with $[\text{Cp}^*\text{Fe}(\eta^5\text{-P}_5)]$ (**D**) to give a series of isostructural 1D polymers.^[119a,125] Additionally, 1D coordination polymers were synthesized using pre-assembled linear $[\text{Cu}_3]$ building blocks as SBUs in self-assembly reactions with $[\text{Cp}^*\text{Fe}(\eta^5\text{-P}_5)]$ (**D**).^[126]

Moreover, the self-assembly of $[\text{Cp}^R\text{Fe}(\eta^5\text{-P}_5)]$ (type **D**, $\text{Cp}^R = \text{Cp}^*, \text{Cp}''$) with CuWCA salts (WCA = OTf, GaCl_4 , TEF, FAI; FAI = $\text{FAI}\{\text{OC}_6\text{F}_{10}(\text{C}_6\text{F}_5)_3\}$) has been investigated, bringing forth 2D polymers with coordinating OTf and GaCl_4 anions,^[127] or a 1D polymer or dimeric species encompassing non-coordinated TEF or FAI anions.^[114d,g,128] The application of WCAs is especially of importance, when the self-assembly with Ag salts should be achieved, since Ag(I) halides suffer from poor solubility. Type **D** complexes $[\text{Cp}^R\text{Fe}(\eta^5\text{-P}_5)]$ ($\text{Cp}^R = \text{Cp}^*, \text{Cp}^{\text{Bn}}$) as well as their huge Cp^{BIG} analogue ($\text{Cp}^{\text{BIG}} = \text{C}_5(4\text{-}^i\text{BuC}_6\text{H}_4)_5$) were hence reacted with AgOTf, AgSbF_6 , AgTEF or AgFAI, proving dimers and coordination polymers are accessible also with Ag.^[127a,129] Similarly, $[\text{Cp}^R\text{Ta}(\text{CO})_2(\eta^4\text{-P}_4)]$ (type **C**, $\text{Cp}^R = \text{Cp}''$, Cp''') forms 1D, 2D, or even 3D coordination polymers when reacted with CuI (Figure 10c) or AgSbF_6 .^[130]

As found for P_2 complexes of type **A**, the addition of a third component capable of acting as further linking moiety may lead to hybrid polymers with higher dimensionality. However, the three-component self-assembly of $[\text{Cp}^*\text{Fe}(\eta^5\text{-P}_5)]$ (**D**) with CuCl and P_4 or As_4 , respectively, yielded coordination polymers structurally resembling the previously mentioned 1D polymer $[\{\text{Cp}^*\text{Fe}(\eta^5\text{-P}_5)\}\{\text{CuCl}\}]_n$ (Figure 10d).^[120] The P_4 or As_4 molecules function as guests occupying tetrahedral voids in between the chains, thus interconnecting them into the second dimension by weak $\text{P}\cdots\text{P}$ or $\text{As}\cdots\text{P}$ host-guest-interactions.^[131] However, P_4 may also act as a terminal ligand, as found in the 1D coordination polymer obtained from P_4 , $[\text{Cp}^*\text{Fe}(\eta^5\text{-P}_5)]$ (**D**) and AgSbF_6 , thus not adding dimensionality to the products.^[129b] On the contrary, the addition of rigid or flexible ditopic N donor ligands to $[\text{Cp}^R\text{Fe}(\eta^5\text{-P}_5)]$ (type **D**, $\text{Cp}^R = \text{Cp}^*, \text{Cp}^{\text{Bn}}$) and CuA (A = Cl, BF_4 , PF_6) or AgA (A = SbF_6 , TEF) has been thoroughly investigated and gives rise to 1D, 2D or 3D metalorganic-organic hybrid coordination polymers.^[129b,132]

1.5.3 P_n ligand complexes – Discrete Supramolecules

The very first spherical aggregate obtained by self-assembly of P_n ligand complexes as multitopic donor component is the aforementioned 90-vertex sphere $[\{\text{Cp}^*\text{Fe}(\eta^5\text{-P}_5)\}_{12}\{\text{CuCl}\}_{25}\{\text{CH}_3\text{CN}\}_{10}]$ (Figure 11a).^[121] Soon, further neutral or ionic analogues with Cp^* or Cp^\times ($\text{Cp}^\times = \text{C}_5\text{Me}_4\text{Et}$), with CuCl or CuBr have been reported, all encapsulating up to one molecule of $[\text{Cp}^R\text{Fe}(\eta^5\text{-P}_5)]$ (type **D**, $\text{Cp}^R = \text{Cp}^*, \text{Cp}^\times$).^[133] Additionally, with $[\text{Cp}^*\text{Fe}(\eta^5\text{-P}_5)]$ (**D**) and CuCl a capsule constructed of two half-shells held together by dispersion interactions is

accessible under certain conditions, where each half-shell encapsulates one molecule $[\text{Cp}^*\text{Fe}(\eta^5\text{-P}_5)]$ (**D**).^[122a] Based on these findings, the host-guest chemistry has been investigated by adding potential guest molecules as a third component into reactions of $[\text{Cp}^*\text{Fe}(\eta^5\text{-P}_5)]$ (**D**) and Cu(I) halides. By now, numerous small and medium sized molecules have been encapsulated into such spherical aggregates, spanning P_4 , As_4 (ellipsoid-shaped host, Figure 11b),^[131] C_{60} (barrel-like host, Figure 11c),^[134] $o\text{-C}_2\text{B}_{10}\text{H}_{12}$, $[\text{FeCp}_2]$, $[\text{CpCr}(\eta^5\text{-As}_5)]$, $[\text{CpFe}(\eta^5\text{-P}_5)]$, $[\text{NiCp}_2]$, P_4S_3 , P_4Se_3 , adamantane, $[\text{CpV}(\eta^7\text{-C}_7\text{H}_7)]$, $[\text{CpMn}(\text{CO})_3]$, $[\text{Cr}(\text{C}_6\text{H}_6)_2]^+$ (80-vertex spherical hosts, Figure 11d),^[124,135] $[\text{CoCp}_2]^+$ (prism- or cube-shaped host),^[136] $[(\text{CpCr})_2(\mu, \eta^{5:5}\text{-As}_5)]$ (90-vertex spherical host, Figure 11a).^[135b]

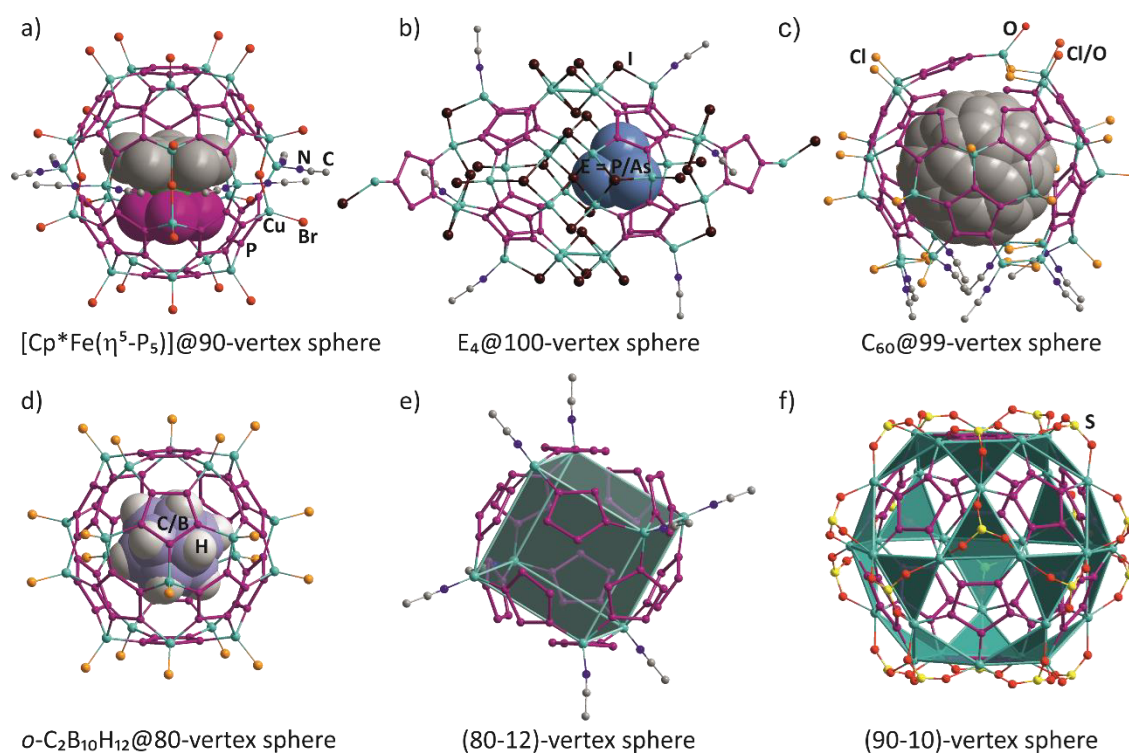


Figure 11. Selected molecular structures of spherical supramolecules consisting of type **D** complexes and Cu(I) salts. $\{\text{Cp}^*\text{Fe}\}$ and $\{\text{CF}_3\}$ moieties, TEF counterions, H atoms, uncoordinated solvent molecules and minor parts of disorder are omitted for clarity. Host scaffolds are depicted in the ball-and-sticks model, guest molecules are highlighted in the space-filling model.

These spheres (Figure 11b-d) only form in presence of the respective guest molecule as a template. An especially remarkable host is the 80-vertex spherical aggregate $\{[\text{Cp}^*\text{Fe}(\eta^5\text{-P}_5)]_{12}\{\text{CuX}\}_{20-n}\}$ ($\text{X} = \text{Cl}, \text{Br}, \text{I}$, Figure 11d), whose idealized scaffold ($n = 0$) is solely constructed of 12 five-membered (P_5) rings separated by 30 six-membered (Cu_2P_4) rings and exhibits icosahedral symmetry. Its core therefore displays an inorganic analogue of the $I_h\text{-C}_{80}$ fullerene. With the most templates so far being encapsulated into this 80-vertex spherical host, it is particularly unfortunate that they suffer from low solubility. A general way to more solubility is the application of large WCAs. Hence, $[\text{Cp}^*\text{Fe}(\eta^5\text{-P}_5)]$ (type **D**) was reacted with $[\text{Cu}(\text{CH}_3\text{CN})_4]\text{TEF}$ resulting in the formation of the polycationic spherical aggregate

$[\{\text{Cp}^{\text{R}}\text{Fe}(\eta^5\text{-P}_5)\}_{12}\{\text{Cu}(\text{CH}_3\text{CN})\}_8]^{8+}$ (Figure 11e).^[128] Interestingly, its scaffold can be regarded as an 80-vertex sphere $[\{\text{Cp}^{\text{R}}\text{Fe}(\eta^5\text{-P}_5)\}_{12}\{\text{CuL}\}_{20-n}]$ with the maximum number of vacancies $n = 12$, with the eight remaining Cu atoms now spanning a cube (highlighted in cyan in Figure 11e). Unfortunately, the compound is nearly insoluble except under partial fragmentation.

In order to address the solubility issue by other means, also more organic groups were introduced to the Cp ligand, and $[\text{Cp}^{\text{Bn}}\text{Fe}(\eta^5\text{-P}_5)]$ (type **D**) has been applied as a supramolecular building block instead.^[137] Indeed, the self-assembly with CuCl or CuBr, respectively, leads to 80-vertex spheres (host of Figure 11d) with enhanced solubility. Moreover, the spheres are already formed in the absence of a template. Then, merely solvent molecules are occupying the void. The solubility was sufficient for NMR spectroscopic investigations, providing evidence for interconversions between 80-vertex spheres of different porosities ($n = 0 - 4.8$), a tetrahedrally shaped aggregate $[\{\text{Cp}^{\text{Bn}}\text{Fe}(\eta^5\text{-P}_5)\}_{12}\{\text{CuBr}\}_{51}\{\text{CH}_3\text{CN}\}_8]$ and even reversible $[\text{FeCp}_2]$ encapsulation into the 80-vertex spheres. However, structural characterization of $[\text{Cp}^{\text{Bn}}\text{Fe}(\eta^5\text{-P}_5)]$ -based host-guest assemblies is limited to $[\text{FeCp}_2]$ and $[\text{CpV}(\eta^7\text{-C}_7\text{H}_7)]$ as guests, so far.^[124] The self-assembly of $[\text{Cp}^{\text{Bn}}\text{Fe}(\eta^5\text{-P}_5)]$ (type **D**) with CuI is dependent on the stoichiometry applied.^[123] While three equivalents of CuI lead to a polymeric assembly, the use of six equivalents yields $[\{\text{Cp}^{\text{Bn}}\text{Fe}(\eta^5\text{-P}_5)\}_{12}\{\text{CuI}\}_{54}\{\text{CH}_3\text{CN}\}_{1.46}]$ as a further soluble spherical aggregate. A noteworthy result was obtained from the self-assembly of $[\text{Cp}^{\text{Bn}}\text{Fe}(\eta^5\text{-P}_5)]$ (type **D**) with CuBr_2 .^[138] Here, the formation of a giant rugby ball with outer dimensions of 3.7×4.6 nm was observed (Figure 12a). Large spherical aggregates were also obtained by two further methods. On the one hand, $[\text{Cp}^{\text{Bn}}\text{Fe}(\eta^5\text{-P}_5)]$ (type **D**) was allowed to react with CuOTf, resulting in an icosidodecahedral assembly with OTf anions capping the 20 triangular faces and Cu cations occupying only 20 of the 30 vertices (Figure 11f).^[127b] This example illustrates the concept of ‘augmentation’ (cf. chapter 1.1), since the 20 Cu atoms of abovementioned smaller 80-vertex spheres (Figure 11d) describe a dodecahedron, and truncation thereof by conceptually replacing every Cu atom by a group of three Cu positions leads to said icosidodecahedron (highlighted in cyan in Figure 11f). On the other hand, the use of the huge pentaphosphaferrocene derivative $[\text{Cp}^{\text{BIG}}\text{Fe}(\eta^5\text{-P}_5)]$ (type **D**) in combination with CuBr gives a 3.5 nm large spherical assembly with a three-shell core structure described as icosahedron@dodecahedron@ $[\{\text{Cp}^{\text{BIG}}\text{Fe}(\eta^5\text{-P}_5)\}_{12}\text{Cu}_{70}\text{Br}_{83}]$, the latter shell exhibiting $I\text{-C}_{140}$ topology (Figure 12b).^[139] Here, the steric influence of the Cp^{BIG} ligand (about three times the size of Cp^*) forces the formation of larger Cu_xBr_y aggregates connecting two pentaphosphaferrocene units. If no such aggregates are formed and pentaphosphaferrocene units are connected only via one metal atom, the only way to avoid steric repulsion of the Cp ligands is to arrange the $\{\text{FeCp}\}$ units alternately, leading to a polymer (cf. chapter 1.5.1).^[127a]

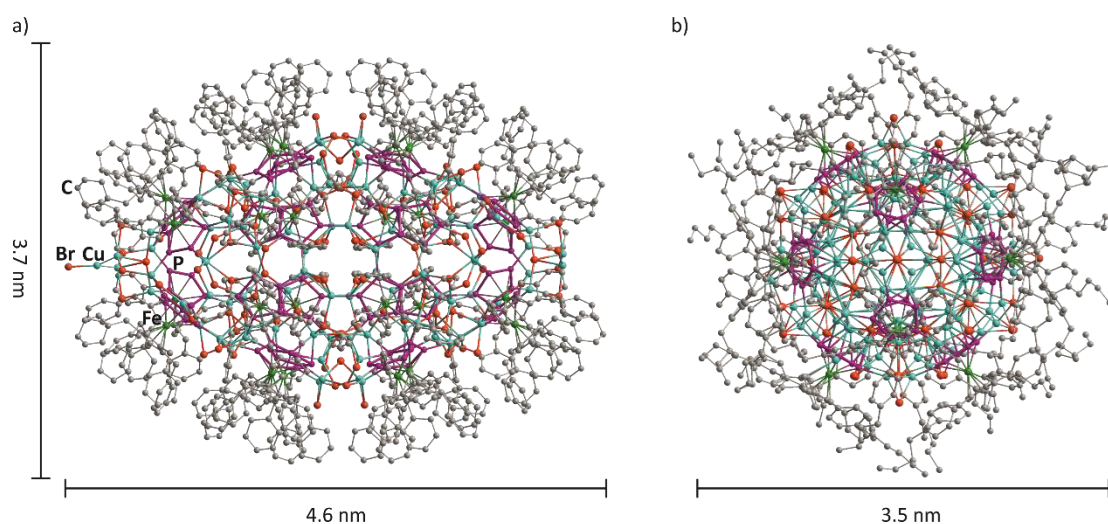


Figure 12. Molecular structures of the large spherical supramolecules consisting of type **D** complexes and Cu_xBr_y aggregates. Solvent molecules, H atoms and minor positions of disorder are omitted for clarity.

Similarly to complexes of type **D**, also *cyclo*- P_4 complexes of type **C** are capable of forming spherical assemblies. The first example was reported in already in 2006 and is obtained by the reaction of $[\text{Cp}^{\text{II}}\text{Ta}(\text{CO})_2(\eta^4\text{-P}_4)]$ (**C**) with CuCl (Figure 13a).^[140] The resulting sphere $[\{\text{Cp}^{\text{II}}\text{Ta}(\text{CO})_2(\eta^4\text{-P}_4)\}_6\{\text{CuCl}\}_8]$ possesses 32 inorganic core atoms and is constructed of 6 four-membered (P_4) and 12 six-membered (Cu_2P_4) rings. It may be described as a cubic structure with Cu atoms occupying the vertices and P_4 ligand complexes occupying the faces. Later, CuBr and Cp^{III} analogues have been reported.^[130a] As often observed with *cyclo*- P_5 (type **D**) complexes, the supramolecular products obtained with CuI differ from the Cl or Br counterparts. Nevertheless, CuI also assembles with $[\text{Cp}^{\text{III}}\text{Ta}(\text{CO})_2(\eta^4\text{-P}_4)]$ (type **C**) to give two other spherical aggregates, while reaction with $[\text{Cp}^{\text{II}}\text{Ta}(\text{CO})_2(\eta^4\text{-P}_4)]$ (**C**) only leads to a polymer (cf. chapter 1.5.1).^[130a]

Spherical supramolecules have as well been obtained with Ag salts. Again, WCA salts were used for solubility reasons. Thus, $[\text{Cp}^{\text{R}}\text{Fe}(\eta^5\text{-P}_5)]$ (type **D**, $\text{Cp}^{\text{R}} = \text{Cp}^*$, Cp^{Bn}) complexes were brought to reaction with AgWCA ($\text{WCA} = \text{OTf}$, OTs , SbF_6) salts, resulting in the formation of spherical aggregates exhibiting topologies similar to Cu containing 80-vertex spheres, (90-10)-vertex icosidodecahedral spheres or others.^[129b] In the case of $[\text{Cp}^*\text{Fe}(\eta^5\text{-P}_5)]$ (**D**) containing spheres, the presence of a larger number of Ag vacancies (≈ 10) in the core scaffold of the 80-vertex-like sphere enables the encapsulation of $[\text{Cp}^*\text{Fe}(\eta^5\text{-P}_5)]$ in such a small sphere for the first time. Furthermore, the conceptual expansion of the spherical assembly by augmentation to a (90-10)-vertex sphere (previously described for $[\text{Cp}^{\text{Bn}}\text{Fe}(\eta^5\text{-P}_5)]$ and CuOTf) even allows for the encapsulation of stacked $[\text{Cp}^*\text{Fe}(\eta^5\text{-P}_5)]$ and toluene as guest molecules. In contrast, the abovementioned Cu analogue was only obtained from $[\text{Cp}^{\text{Bn}}\text{Fe}(\eta^5\text{-P}_5)]$, which is too large to act as guest.^[127b] In the absence of CH_3CN , $[\text{Cp}^{\text{Bn}}\text{Fe}(\eta^5\text{-P}_5)]$ (type **D**) and AgSbF_6 form a dimer with Ag atoms coordinatively saturated by the benzyl groups.^[129b] This promoted the idea to use nitriles

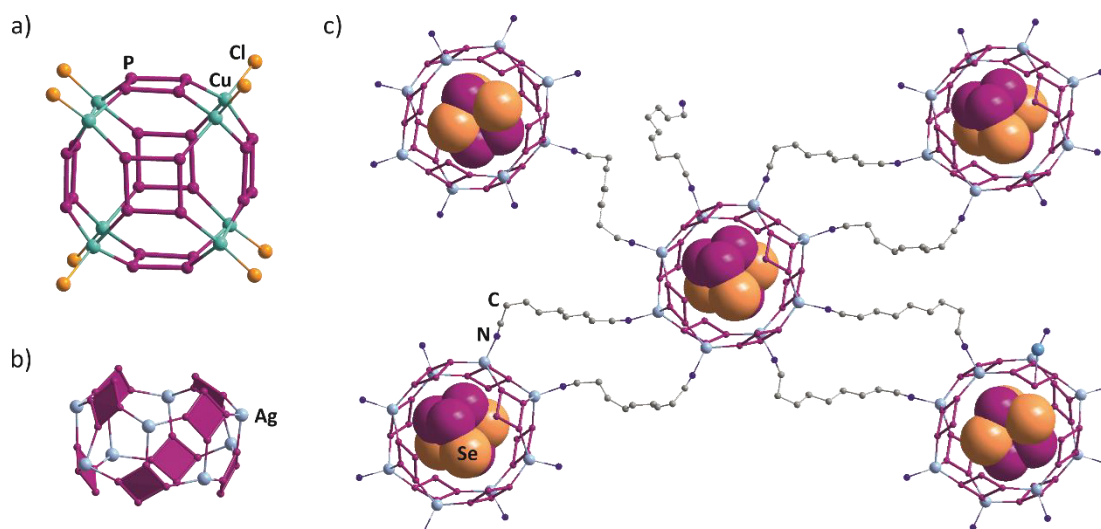


Figure 13. a) Example of a spherical supramolecule as obtained from type **D** complexes and CuCl or CuBr; b) supramolecular building block (SBB) constructed of $[\text{Cp}^{\text{II}}\text{Ta}(\text{CO})_2(\eta^4\text{-P}_4)]$ (**D**) and Ag cations, as found in c) a 2D polymer of spherical supramolecules obtained from $[\text{Cp}^{\text{II}}\text{Ta}(\text{CO})_2(\eta^4\text{-P}_4)]$ (**D**), AgSbF_6 , P_4Se_3 and dinitrile linkers. $\{\text{Cp}^{\text{II}}\text{Ta}(\text{CO})_2\}$ moieties, SbF_6 counterions, H atoms, solvent molecules and minor positions of disorder are omitted for clarity. P_4Se_3 host molecules are highlighted in the space-filling model.

for coordinative saturation of Ag atoms instead. The analogue reactions in presence of CH_3CN or $\text{Cl}(\text{C}_6\text{H}_4)\text{CN}$ yield either anti-prismatic supramolecular hosts with encapsulated SbF_6 anions or a half-shell shaped aggregate, all encompassing terminal nitrile ligands. When flexible, ditopic dinitrile linkers were employed, hence metalorganic-organic hybrid polymers were obtained from self-assembly of $[\text{Cp}^{\text{Bn}}\text{Fe}(\eta^5\text{-P}_5)]$ (type **D**) and $[\text{Cu}(\text{CH}_3\text{CN})_4]\text{BF}_4$, AgSbF_6 or AgTEF . Similarly, such hybrid polymers are obtained from $[\text{Cp}^*\text{Fe}(\eta^5\text{-P}_5)]$ (**D**), AgSbF_6 and $\text{NC}(\text{CH}_2)_x\text{CN}$ ($x = 5 - 7, 10$). The most remarkable products however are obtained with $[\text{Cp}^*\text{Fe}(\eta^5\text{-P}_5)]$ (**D**), AgSbF_6 and dinitrile linkers $\text{NC}(\text{CH}_2)_x\text{CN}$ of the length $x = 7 - 10$. Then, supramolecular spheres of the type $[\{\text{Cp}^*\text{Fe}(\eta^5\text{-P}_5)\}_9\{\text{Ag}\}_{11}]$ or $[\{\text{Cp}^*\text{Fe}(\eta^5\text{-P}_5)\}_{12}\{\text{Ag}\}_{12}]$ are formed, which act as supramolecular building blocks (SBBs, cf. chapter 1.1) further connected by the respective dinitriles to give 3D polymers. At the same time, these SBBs act as hosts for SbF_6 anions or $[\text{Cp}^*\text{Fe}(\eta^5\text{-P}_5)]$. When P_4 is added to the reaction with $\text{NC}(\text{CH}_2)_{10}\text{CN}$, SBBs built up from $[\text{Cp}^*\text{Fe}(\eta^5\text{-P}_5)]$ and Ag atoms encapsulate P_4 and polymerize to 1D – 3D polymers of spheres. Analogously, the four-component reaction of $[\text{Cp}^{\text{II}}\text{Ta}(\text{CO})_2(\eta^4\text{-P}_4)]$ (**C**), AgSbF_6 , $\text{NC}(\text{CH}_2)_7\text{CN}$ and P_4Se_3 results in barrel-shaped $[\{\text{Cp}^{\text{II}}\text{Ta}(\text{CO})_2(\eta^4\text{-P}_4)\}_8\{\text{Ag}\}_8]$ SBBs (Figure 13b) encapsulating P_4Se_3 and further interconnected to a 2D network of SBBs (Figure 13c).^[130b]

1.6 References

- [1] C. J. Pedersen, *J. Am. Chem. Soc.* **1967**, *89*, 7017-7036.
- [2] B. Dietrich, J. M. Lehn, J. P. Sauvage, *Tetrahedron Lett.* **1969**, 2885-2888.
- [3] a) E. B. Kyba, K. Koga, L. R. Sousa, M. G. Siegel, D. J. Cram, *J. Am. Chem. Soc.* **1973**, *95*, 2692-2693; b) K. N. Trueblood, C. B. Knobler, E. Maverick, R. C. Helgeson, S. B. Brown, D. J. Cram, *J. Am. Chem. Soc.* **1981**, *103*, 5594-5596.
- [4] "The Nobel Prize in Chemistry 1987". *NobelPrize.org*. Nobel Media AB 2020. Tue. 30 Jun 2020. <https://www.nobelprize.org/prizes/chemistry/1987/summary/>
- [5] J.-M. Lehn, *Angew. Chem. Int. Ed. Engl.* **1988**, *27*, 89-112.
- [6] J. W. Steed, D. R. Turner, K. Wallace, in *Core Concepts in Supramolecular Chemistry and Nanochemistry*, John Wiley & Sons, Ltd, Chichester, **2007**.
- [7] F. Mancin, E. Rampazzo, P. Tecilla, U. Tonellato, *Chem. Eur. J.* **2006**, *12*, 1844-1854.
- [8] D. L. Caulder, K. N. Raymond, *Acc. Chem. Res.* **1999**, *32*, 975-982.
- [9] R. Chakrabarty, P. S. Mukherjee, P. J. Stang, *Chem. Rev.* **2011**, *111*, 6810-6918.
- [10] a) J.-M. Lehn, *Supramol. Chem.* **1995**, 139-197; b) E. C. Constable, *Pure Appl. Chem.* **1996**, *68*, 253-260.
- [11] T. R. Cook, Y.-R. Zheng, P. J. Stang, *Chem. Rev.* **2013**, *113*, 734-777.
- [12] a) M. Han, D. M. Engelhard, G. H. Clever, *Chem. Soc. Rev.* **2014**, *43*, 1848-1860; b) C. J. Brown, F. D. Toste, R. G. Bergman, K. N. Raymond, *Chem. Rev.* **2015**, *115*, 3012-3035; c) A. Gorczyński, J. M. Harrowfield, V. Patroniak, A. R. Stefankiewicz, *Chem. Rev.* **2016**, *116*, 14620-14674; d) S. Chakraborty, G. R. Newkome, *Chem. Soc. Rev.* **2018**, *47*, 3991-4016; e) C. E. Housecroft, E. C. Constable, *J. Inorg. Organomet. Polym.* **2018**, *28*, 414-427; f) A. E. Thorarinsdottir, T. D. Harris, *Chem. Rev.* **2020**, *120*, 8716-8789; g) S. Peng, Q. He, G. I. Vargas-Zúñiga, L. Qin, I. Hwang, S. K. Kim, N. J. Heo, C.-H. Lee, R. Dutta, J. L. Sessler, *Chem. Soc. Rev.* **2020**, *49*, 865-907.
- [13] a) P. Stricklen, J. Verkade, *J. Am. Chem. Soc.* **1983**, *105*, 2494-2495; b) Y. Jiang, B. Li, Y. Wang, D. Liu, X. Song, X. Chang, *J. Organomet. Chem.* **2014**, *759*, 37-45.
- [14] a) X. Huang, P. Sheng, Z. Tu, F. Zhang, J. Wang, H. Geng, Y. Zou, C.-a. Di, Y. Yi, Y. Sun, W. Xu, D. Zhu, *Nat. Commun.* **2015**, *6*, 7408; b) A. J. Clough, J. W. Yoo, M. H. Mecklenburg, S. C. Marinescu, *J. Am. Chem. Soc.* **2015**, *137*, 118-121; c) Z. Ji, C. Trickett, X. Pei, O. M. Yaghi, *J. Am. Chem. Soc.* **2018**, *140*, 13618-13622.
- [15] J. L. Atwood, J. W. Steed, in *Supramolecular Chemistry, 2nd Edition*, John Wiley & Sons, Ltd, Chichester **2009**, p. 620.

- [16] S. Datta, M. L. Saha, P. J. Stang, *Acc. Chem. Res.* **2018**, *51*, 2047-2063.
- [17] a) J.-M. Lehn, *Supramol. Chem.* **1995**, 139-197; b) J. L. Atwood, J. W. Steed, in *Supramolecular Chemistry, 2nd Edition*, John Wiley & Sons, Ltd, Chichester **2009**, p. 598-602.
- [18] S. R. Batten, N. R. Champness, X.-M. Chen, J. Garcia-Martinez, S. Kitagawa, L. Ohrstrom, M. O'Keeffe, M. P. Suh, J. Reedijk, *Pure Appl. Chem.* **2013**, *85*, 1715-1724.
- [19] S. R. Batten, S. M. Neville, D. R. Turner, in *Coordination Polymers: Design, Analysis and Application*, The Royal Society of Chemistry, Cambridge **2009**, pp. 1-3.
- [20] H. J. Buser, D. Schwarzenbach, W. Petter, A. Ludi, *Inorg. Chem.* **1977**, *16*, 2704-2710.
- [21] S. R. Batten, S. M. Neville, D. R. Turner, in *Coordination Polymers: Design, Analysis and Application*, The Royal Society of Chemistry, Cambridge **2009**, p. V (preface).
- [22] S. R. Batten, S. M. Neville, D. R. Turner, in *Coordination Polymers: Design, Analysis and Application*, The Royal Society of Chemistry, Cambridge **2009**, p. 19-20.
- [23] a) B. F. Hoskins, R. Robson, *J. Am. Chem. Soc.* **1989**, *111*, 5962-5964; b) B. F. Hoskins, R. Robson, *J. Am. Chem. Soc.* **1990**, *112*, 1546-1554.
- [24] a) L. R. MacGillivray, S. Subramanian, M. J. Zaworotko, *J. Chem. Soc., Chem. Commun.* **1994**, 1325-1326; b) O. M. Yaghi, H. Li, *J. Am. Chem. Soc.* **1995**, *117*, 10401-10402.
- [25] H. Li, M. Eddaoudi, M. O'Keeffe, O. M. Yaghi, *Nature* **1999**, *402*, 276-279.
- [26] O. M. Yaghi, M. O'Keeffe, N. W. Ockwig, H. K. Chae, M. Eddaoudi, J. Kim, *Nature* **2003**, *423*, 705-714.
- [27] M. Kondo, T. Yoshitomi, H. Matsuzaka, S. Kitagawa, K. Seki, *Angew. Chem. Int. Ed. Engl.* **1997**, *36*, 1725-1727.
- [28] Y.-X. Tan, F. Wang, J. Zhang, *Chem. Soc. Rev.* **2018**, *47*, 2130-2144.
- [29] W. Lu, Z. Wei, Z.-Y. Gu, T.-F. Liu, J. Park, J. Park, J. Tian, M. Zhang, Q. Zhang, T. Gentle III, M. Bosch, H.-C. Zhou, *Chem. Soc. Rev.* **2014**, *43*, 5561-5593.
- [30] a) A. Bavykina, N. Kolobov, I. S. Khan, J. A. Bau, A. Ramirez, J. Gascon, *Chem. Rev.* **2020**, *120*, 8468-8353; b) Y.-S. Wei, M. Zhang, R. Zou, Q. Xu, *Chem. Rev.* **2020**, *120*, 12089-12174.
- [31] L. E. Kreno, K. Leong, O. K. Farha, M. Allendorf, R. P. Van Duyne, J. T. Hupp, *Chem. Rev.* **2012**, *112*, 1105-1125.
- [32] A. E. Thorarinsdottir, T. D. Harris, *Chem. Rev.* **2020**, *120*, 8716-8789.
- [33] a) Y. Inokuma, S. Yoshioka, J. Ariyoshi, T. Arai, Y. Hitora, K. Takada, S. Matsunaga, K. Rissanen, M. Fujita, *Nature* **2013**, *495*, 461-466; b) Y. Inokuma, S. Yoshioka, J. Ariyoshi, T. Arai, Y. Hitora, K. Takada, S. Matsunaga, K. Rissanen, M. Fujita, *Nature* **2013**, *501*, 262-262.

- [34] K. Rissanen, *Chem. Soc. Rev.* **2017**, *46*, 2638-2648.
- [35] L. S. Xie, G. Skorupskii, M. Dincă, *Chem. Rev.* **2020**, *120*, 8536-8580.
- [36] a) X. Huang, P. Sheng, Z. Tu, F. Zhang, J. Wang, H. Geng, Y. Zou, C.-a. Di, Y. Yi, Y. Sun, W. Xu, D. Zhu, *Nat. Commun.* **2015**, *6*, 7408; b) X. Huang, S. Zhang, L. Liu, L. Yu, G. Chen, W. Xu, D. Zhu, *Angew. Chem. Int. Ed.* **2018**, *57*, 146-150.
- [37] A. Winter, U. S. Schubert, *Chem. Soc. Rev.* **2016**, *45*, 5311-5357.
- [38] P. Stricklen, J. Verkade, *J. Am. Chem. Soc.* **1983**, *105*, 2494-2495.
- [39] a) J. M. Lehn, A. Rigault, J. Siegel, J. Harrowfield, B. Chevrier, D. Moras, *Proc. Natl. Acad. Sci. USA* **1987**, *84*, 2565-2569; b) J.-M. Lehn, A. Rigault, *Angew. Chem. Int. Ed. Engl.* **1988**, *27*, 1095-1097; c) H. S. Sahoo, D. K. Chand, *Dalton Trans.* **2010**, *39*, 7223-7225.
- [40] a) P. N. W. Baxter, J.-M. Lehn, J. Fischer, M.-T. Youinou, *Angew. Chem. Int. Ed. Engl.* **1994**, *33*, 2284-2287; b) J. Rojo, J.-M. Lehn, G. Baum, D. Fenske, O. Waldmann, P. Müller, *Eur. J. Inorg. Chem.* **1999**, 517-522; c) P. N. W. Baxter, J.-M. Lehn, G. Baum, D. Fenske, *Chem. Eur. J.* **2000**, *6*, 4510-4517; d) M. Ruben, J. Rojo, F. J. Romero-Salguero, L. H. Uppadine, J.-M. Lehn, *Angew. Chem. Int. Ed.* **2004**, *43*, 3644-3662.
- [41] a) L. Xu, Y.-X. Wang, L.-J. Chen, H.-B. Yang, *Chem. Soc. Rev.* **2015**, *44*, 2148-2167; b) M.-M. Gan, J.-Q. Liu, L. Zhang, Y.-Y. Wang, F. E. Hahn, Y.-F. Han, *Chem. Rev.* **2018**, *118*, 9587-9641; c) S. Chakraborty, G. R. Newkome, *Chem. Soc. Rev.* **2018**, *47*, 3991-4016.
- [42] a) T. R. Cook, P. J. Stang, *Chem. Rev.* **2015**, *115*, 7001-7045; b) E.-S. M. El-Sayed, D. Yuan, *Chem. Lett.* **2019**, *49*, 28-53.
- [43] a) P. N. W. Baxter, G. S. Hanan, J.-M. Lehn, *Chem. Commun.* **1996**, 2019-2020; b) S. Leininger, B. Olenyuk, P. J. Stang, *Chem. Rev.* **2000**, *100*, 853-908; c) G. F. Swiegers, T. J. Malefetse, *Chem. Rev.* **2000**, *100*, 3483-3538; d) R. S. Forgan, J.-P. Sauvage, J. F. Stoddart, *Chem. Rev.* **2011**, *111*, 5434-5464; e) J. E. Beves, B. A. Blight, C. J. Campbell, D. A. Leigh, R. T. McBurney, *Angew. Chem. Int. Ed.* **2011**, *50*, 9260-9327.
- [44] Y. Sun, C. Chen, J. Liu, P. J. Stang, *Chem. Soc. Rev.* **2020**, *49*, 3889-3919.
- [45] F. J. Rizzuto, L. K. S. von Krbek, J. R. Nitschke, *Nat. Rev. Chem.* **2019**, *3*, 204-222.
- [46] a) P. J. Stang, B. Olenyuk, *Acc. Chem. Res.* **1997**, *30*, 502-518; b) B. Olenyuk, A. Fechtenkötter, P. J. Stang, *J. Chem. Soc., Dalton Trans.* **1998**, 1707-1728.
- [47] M. Fujita, J. Yazaki, K. Ogura, *J. Am. Chem. Soc.* **1990**, *112*, 5645-5647.
- [48] P. J. Stang, D. H. Cao, *J. Am. Chem. Soc.* **1994**, *116*, 4981-4982.
- [49] M. Fujita, D. Oguro, M. Miyazawa, H. Oka, K. Yamaguchi, K. Ogura, *Nature* **1995**, *378*, 469-471.
- [50] R. W. Saalfrank, A. Stark, K. Peters, H. G. von Schnering, *Angew. Chem. Int. Ed. Engl.* **1988**, *27*, 851-853.

- [51] D. L. Caulder, K. N. Raymond, *Acc. Chem. Res.* **1999**, *32*, 975-982.
- [52] F. A. Cotton, C. Lin, C. A. Murillo, *Acc. Chem. Res.* **2001**, *34*, 759-771.
- [53] M. Eddaoudi, J. Kim, J. B. Wachter, H. K. Chae, M. O'Keeffe, O. M. Yaghi, *J. Am. Chem. Soc.* **2001**, *123*, 4368-4369.
- [54] a) T. L. Mako, J. M. Racicot, M. Levine, *Chem. Rev.* **2019**, *119*, 322-477; b) Y. Fang, J. A. Powell, E. Li, Q. Wang, Z. Perry, A. Kirchon, X. Yang, Z. Xiao, C. Zhu, L. Zhang, F. Huang, H.-C. Zhou, *Chem. Soc. Rev.* **2019**, *48*, 4707-4730; c) D. Zhang, T. K. Ronson, J. R. Nitschke, *Acc. Chem. Res.* **2018**, *51*, 2423-2436.
- [55] a) R. Hein, P. D. Beer, J. J. Davis, *Chem. Rev.* **2020**, *120*, 1888-1935; b) I. V. Kolesnichenko, E. V. Anslyn, *Chem. Soc. Rev.* **2017**, *46*, 2385-2390; c) G. Crini, *Chem. Rev.* **2014**, *114*, 10940-10975; d) D. J. Cram, M. E. Tanner, R. Thomas, *Angew. Chem. Int. Ed. Engl.* **1991**, *30*, 1024-1027; e) J. Kang, J. Rebek, *Nature* **1997**, *385*, 50-52; f) J. Kang, J. Santamaría, G. Hilmersson, J. Rebek, *J. Am. Chem. Soc.* **1998**, *120*, 7389-7390.
- [56] P. Mal, B. Breiner, K. Rissanen, J. R. Nitschke, *Science* **2009**, *324*, 1697-1699.
- [57] M. Kawano, Y. Kobayashi, T. Ozeki, M. Fujita, *J. Am. Chem. Soc.* **2006**, *128*, 6558-6559.
- [58] C. J. Hastings, M. D. Pluth, R. G. Bergman, K. N. Raymond, *J. Am. Chem. Soc.* **2010**, *132*, 6938-6940.
- [59] a) H. Amouri, C. Desmarets, J. Moussa, *Chem. Rev.* **2012**, *112*, 2015-2041; b) W. Wang, Y.-X. Wang, H.-B. Yang, *Chem. Soc. Rev.* **2016**, *45*, 2656-2693.
- [60] D. Ajami, L. Liu, J. Rebek Jr, *Chem. Soc. Rev.* **2015**, *44*, 490-499.
- [61] G. A. Breault, C. A. Hunter, P. C. Mayers, *Tetrahedron* **1999**, *55*, 5265-5293; a) C. O. Dietrich-Buchecker, J. P. Sauvage, J. P. Kintzinger, *Tetrahedron Lett.* **1983**, *24*, 5095-5098; b) C. O. Dietrich-Buchecker, J. P. Sauvage, J. M. Kern, *J. Am. Chem. Soc.* **1984**, *106*, 3043-3045.
- [62] J. L. Atwood, J. W. Steed, in *Supramolecular Chemistry, 2nd Edition*, John Wiley & Sons, Ltd, Chichester **2009**, p. 653.
- [63] a) K.-M. Park, S.-Y. Kim, J. Heo, D. Whang, S. Sakamoto, K. Yamaguchi, K. Kim, *J. Am. Chem. Soc.* **2002**, *124*, 2140-2147; b) Z. Han, Q. Zhou, Y. Li, *J. Incl. Phenom. Macrocycl. Chem.* **2018**, *92*, 81-101; c) L. Zhu, M. Lu, Q. Zhang, D. Qu, H. Tian, *Macromolecules* **2011**, *44*, 4092-4097; d) P. Wei, X. Yan, F. Huang, *Chem. Soc. Rev.* **2015**, *44*, 815-832.
- [64] a) A. Harada, A. Hashidzume, H. Yamaguchi, Y. Takashima, *Chem. Rev.* **2009**, *109*, 5974-6023; b) F. M. Raymo, J. F. Stoddart, *Chem. Rev.* **1999**, *99*, 1643-1664.
- [65] a) M. Fujita, F. Ibukuro, H. Hagihara, K. Ogura, *Nature* **1994**, *367*, 720-723; b) W.-X. Gao, H.-J. Feng, B.-B. Guo, Y. Lu, G.-X. Jin, *Chem. Rev.* **2020**, *120*, 6288-6325.

- [66] a) M. Fujita, N. Fujita, K. Ogura, K. Yamaguchi, *Nature* **1999**, *400*, 52-55; b) M. Frank, M. D. Johnstone, G. H. Clever, *Chem. Eur. J.* **2016**, *22*, 14104-14125.
- [67] S. R. Batten, S. M. Neville, D. R. Turner, in *Coordination Polymers: Design, Analysis and Application*, The Royal Society of Chemistry, Cambridge **2009**, pp. 59-95.
- [68] H. W. Kroto, J. R. Heath, S. C. O'Brien, R. F. Curl, R. E. Smalley, *Nature* **1985**, *318*, 162-163.
- [69] "The Nobel Prize in Chemistry 1996". *NobelPrize.org*. Nobel Media AB 2020. Tue. 1 Sep 2020. <https://www.nobelprize.org/prizes/chemistry/1996/summary/>
- [70] J. M. Hawkins, A. Meyer, T. A. Lewis, S. Loren, F. J. Hollander, *Science* **1991**, *252*, 312.
- [71] a) J. R. Heath, S. C. O'Brien, Q. Zhang, Y. Liu, R. F. Curl, F. K. Tittel, R. E. Smalley, *J. Am. Chem. Soc.* **1985**, *107*, 7779-7780; b) Y. Chai, T. Guo, C. Jin, R. E. Haufler, L. P. F. Chibante, J. Fure, L. Wang, J. M. Alford, R. E. Smalley, *J. Phys. Chem.* **1991**, *95*, 7564-7568; c) H. Shinohara, H. Yamaguchi, N. Hayashi, H. Sato, M. Ohkohchi, Y. Ando, Y. Saito, *J. Phys. Chem.* **1993**, *97*, 4259-4261; d) C.-R. Wang, T. Kai, T. Tomiyama, T. Yoshida, Y. Kobayashi, E. Nishibori, M. Takata, M. Sakata, H. Shinohara, *Nature* **2000**, *408*, 426-427; e) M. M. Alvarez, E. G. Gillan, K. Holczer, R. B. Kaner, K. S. Min, R. L. Whetten, *J. Phys. Chem.* **1991**, *95*, 10561-10563.
- [72] a) S. Stevenson, G. Rice, T. Glass, K. Harich, F. Cromer, M. R. Jordan, J. Craft, E. Hadju, R. Bible, M. M. Olmstead, K. Maitra, A. J. Fisher, A. L. Balch, H. C. Dorn, *Nature* **1999**, *401*, 55-57; b) S. Yang, T. Wei, F. Jin, *Chem. Soc. Rev.* **2017**, *46*, 5005-5058.
- [73] a) T. Almeida Murphy, T. Pawlik, A. Weidinger, M. Höhne, R. Alcalá, J. M. Spaeth, *Phys. Rev. Lett.* **1996**, *77*, 1075-1078; b) C. Knapp, N. Weiden, H. Kass, K. P. Dinse, B. Pietzak, M. Waiblinger, A. Weidinger, *Mol. Phys.* **1998**, *95*, 999-1004.
- [74] a) M. Saunders, H. A. Jiménez-Vázquez, R. J. Cross, R. J. Poreda, *Science* **1993**, *259*, 1428; b) M. Saunders, H. A. Jiménez-Vázquez, R. J. Cross, S. Mroczkowski, M. L. Gross, D. E. Gibling, R. J. Poreda, *J. Am. Chem. Soc.* **1994**, *116*, 2193-2194; c) M. Saunders, R. J. Cross, H. A. Jiménez-Vázquez, R. Shimshi, A. Khong, *Science* **1996**, *271*, 1693; d) A. Khong, H. A. Jiménez-Vázquez, M. Saunders, R. J. Cross, J. Laskin, T. Peres, C. Lifshitz, R. Strongin, A. B. Smith, *J. Am. Chem. Soc.* **1998**, *120*, 6380-6383; e) J. Laskin, T. Peres, C. Lifshitz, M. Saunders, R. J. Cross, A. Khong, *Chem. Phys. Lett.* **1998**, *285*, 7-9.
- [75] K. Komatsu, M. Murata, Y. Murata, *Science* **2005**, *307*, 238.
- [76] T. Peres, B. Cao, W. Cui, A. Khong, R. J. Cross, M. Saunders, C. Lifshitz, *Int. J. Mass spectrom.* **2001**, *210-211*, 241-247.
- [77] T. Suetsuna, N. Dragoie, W. Harneit, A. Weidinger, H. Shimotani, S. Ito, H. Takagi, K. Kitazawa, *Chem. Eur. J.* **2002**, *8*, 5079-5083.

- [78] K. Kurotobi, Y. Murata, *Science* **2011**, 333, 613.
- [79] a) B. W. Smith, D. E. Luzzi, *Chem. Phys. Lett.* **2000**, 321, 169-174; b) H. Itoi, H. Muramatsu, M. Inagaki, *RSC Advances* **2019**, 9, 22823-22840.
- [80] S. A. Miners, G. A. Rance, A. N. Khlobystov, *Chem. Soc. Rev.* **2016**, 45, 4727-4746.
- [81] J.-M. Lehn, *Supramol. Chem.* **1995**, 139-197.
- [82] a) A. Müller, F. Peters, M. T. Pope, D. Gatteschi, *Chem. Rev.* **1998**, 98, 239-272; b) A. V. Anyushin, A. Kondinski, T. N. Parac-Vogt, *Chem. Soc. Rev.* **2020**, 49, 382-432.
- [83] P. Gouzerh, A. Proust, *Chem. Rev.* **1998**, 98, 77-112.
- [84] a) S.-S. Wang, G.-Y. Yang, *Chem. Rev.* **2015**, 115, 4893-4962; b) C. L. Hill (Ed.), "Polyoxometalates in Catalysis", special issue in *J. Mol. Catal. A: Chem.* **2007**, 262(1-2), 1-242; c) I. V. Kozhevnikov, *Chem. Rev.* **1998**, 98, 171-198.
- [85] a) G. Absillis, E. Cartuyvels, R. Van Deun, T. N. Parac-Vogt, *J. Am. Chem. Soc.* **2008**, 130, 17400-17408; b) J. T. Rhule, C. L. Hill, D. A. Judd, R. F. Schinazi, *Chem. Rev.* **1998**, 98, 327-358.
- [86] a) Y. Martinetto, B. Pégot, C. Roch-Marchal, B. Cottyn-Boitte, S. Floquet, *Eur. J. Inorg. Chem.* **2020**, 2020, 228-247; b) L. Chen, W.-L. Chen, X.-L. Wang, Y.-G. Li, Z.-M. Su, E.-B. Wang, *Chem. Soc. Rev.* **2019**, 48, 260-284.
- [87] a) A. Bijelic, A. Rompel, *Coord. Chem. Rev.* **2015**, 299, 22-38; b) A. Müller, P. Gouzerh, *Chem. Soc. Rev.* **2012**, 41, 7431-7463.
- [88] a) K. Y. Monakhov, W. Bensch, P. Kögerler, *Chem. Soc. Rev.* **2015**, 44, 8443-8483; b) H. N. Miras, L. Vilà-Nadal, L. Cronin, *Chem. Soc. Rev.* **2014**, 43, 5679-5699; c) D. Yang, Y. Liang, P. Ma, S. Li, J. Wang, J. Niu, *Inorg. Chem.* **2014**, 53, 3048-3053; d) D. Yang, S. Li, P. Ma, J. Wang, J. Niu, *Inorg. Chem.* **2013**, 52, 8987-8992; e) Z. Zhang, L. Wojtas, M. J. Zaworotko, *Chem. Sci.* **2014**, 5, 927-931.
- [89] a) D. S. Wright, in *Comprehensive Inorganic Chemistry II, 2nd Edition, Vol. 1* (Eds.: J. Reedijk, K. Poeppelmeier), Elsevier, Amsterdam **2013**, pp. 953-967; b) F. Dankert, L. Erlemeier, C. Ritter, C. von Hänisch, *Inorg. Chem. Front.* **2020**, 7, 2138-2153.
- [90] a) W.-Y. Zhang, Y.-J. Lin, Y.-F. Han, G.-X. Jin, *J. Am. Chem. Soc.* **2016**, 138, 10700-10707; b) Y.-Y. Zhang, L. Zhang, Y.-J. Lin, G.-X. Jin, *Chem. Eur. J.* **2015**, 21, 14893-14900; c) L. Zhang, Y.-J. Lin, Z.-H. Li, G.-X. Jin, *J. Am. Chem. Soc.* **2015**, 137, 13670-13678; d) W.-G. Jia, Y.-F. Han, Y.-J. Lin, L.-H. Weng, G.-X. Jin, *Organometallics* **2009**, 28, 3459-3464.
- [91] a) J. Y. Ryu, Y. J. Park, H.-R. Park, M. L. Saha, P. J. Stang, J. Lee, *J. Am. Chem. Soc.* **2015**, 137, 13018-13023; b) A. Pitto-Barry, N. P. E. Barry, O. Zava, R. Deschenaux, P. J. Dyson, B. Therrien, *Chem. Eur. J.* **2011**, 17, 1966-1971; c) A. Granzhan, C. Schouwey, T. Riis-

- Johannessen, R. Scopelliti, K. Severin, *J. Am. Chem. Soc.* **2011**, *133*, 7106-7115; d) B. Therrien, *Eur. J. Inorg. Chem.* **2009**, *2009*, 2445-2453.
- [92] a) S. Shanmugaraju, A. K. Bar, K.-W. Chi, P. S. Mukherjee, *Organometallics* **2010**, *29*, 2971-2980; b) L. Zhao, K. Ghosh, Y.-R. Zheng, P. J. Stang, *J. Org. Chem.* **2009**, *74*, 8516-8521; c) H.-B. Yang, B. H. Northrop, Y.-R. Zheng, K. Ghosh, M. M. Lyndon, D. C. Muddiman, P. J. Stang, *J. Org. Chem.* **2009**, *74*, 3524-3527; d) S. Ghosh, R. Chakrabarty, P. S. Mukherjee, *Inorg. Chem.* **2009**, *48*, 549-556; e) A. K. Bar, B. Gole, S. Ghosh, P. S. Mukherjee, *Dalton Trans.* **2009**, 6701-6704.
- [93] a) J. B. Pollock, G. L. Schneider, T. R. Cook, A. S. Davies, P. J. Stang, *J. Am. Chem. Soc.* **2013**, *135*, 13676-13679; b) A. Kaloudi-Chantzea, N. Karakostas, F. Pitterl, C. P. Raptopoulou, N. Glezos, G. Pistoris, *Chem. Commun.* **2012**, *48*, 12213-12215; c) Y.-R. Zheng, P. J. Stang, *J. Am. Chem. Soc.* **2009**, *131*, 3487-3489; d) H.-B. Yang, B. H. Northrop, Y.-R. Zheng, K. Ghosh, P. J. Stang, *J. Org. Chem.* **2009**, *74*, 7067-7074.
- [94] a) Y.-Y. Zhang, W.-X. Gao, L. Lin, G.-X. Jin, *Coord. Chem. Rev.* **2017**, *344*, 323-344; b) G. Kumar, R. Gupta, *Chem. Soc. Rev.* **2013**, *42*, 9403-9453.
- [95] a) L. Zhao, K. Ghosh, Y. Zheng, M. M. Lyndon, T. I. Williams, P. J. Stang, *Inorg. Chem.* **2009**, *48*, 5590-5592; b) D. C. Caskey, T. Yamamoto, C. Addicott, R. K. Shoemaker, J. Vacek, A. M. Hawkrige, D. C. Muddiman, G. S. Kottas, J. Michl, P. J. Stang, *J. Am. Chem. Soc.* **2008**, *130*, 7620-7628; c) J. Manna, C. J. Kuehl, J. A. Whiteford, P. J. Stang, D. C. Muddiman, S. A. Hofstadler, R. D. Smith, *J. Am. Chem. Soc.* **1997**, *119*, 11611-11619.
- [96] J. Y. Ryu, J. M. Lee, Y. J. Park, N. V. Nghia, M. H. Lee, J. Lee, *Organometallics* **2013**, *32*, 7272-7274.
- [97] S. C. Johannessen, R. G. Brisbois, J. P. Fischer, P. A. Grieco, A. E. Counterman, D. E. Clemmer, *J. Am. Chem. Soc.* **2001**, *123*, 3818-3819.
- [98] a) F. A. Cotton, C. Lin, C. A. Murillo, *Inorg. Chem.* **2001**, *40*, 478-484; b) F. A. Cotton, L. M. Daniels, C. Lin, C. A. Murillo, *J. Am. Chem. Soc.* **1999**, *121*, 4538-4539.
- [99] a) L. H. Tong, L. Guénée, A. F. Williams, *Inorg. Chem.* **2011**, *50*, 2450-2457; b) O. Oms, T. Jarrosson, L. H. Tong, A. Vaccaro, G. Bernardinelli, A. F. Williams, *Chem. Eur. J.* **2009**, *15*, 5012-5022.
- [100] a) N. C. Gianneschi, P. A. Bertin, S. T. Nguyen, C. A. Mirkin, L. N. Zakharov, A. L. Rheingold, *J. Am. Chem. Soc.* **2003**, *125*, 10508-10509; b) S.-S. Sun, C. L. Stern, S. T. Nguyen, J. T. Hupp, *J. Am. Chem. Soc.* **2004**, *126*, 6314-6326.
- [101] a) N. Fujita, K. Biradha, M. Fujita, S. Sakamoto, K. Yamaguchi, *Angew. Chem. Int. Ed.* **2001**, *40*, 1718-1721; b) S. K. Samanta, M. Schmittel, *J. Am. Chem. Soc.* **2013**, *135*, 18794-18797.

- [102] a) M. D. Wise, J. J. Holstein, P. Pattison, C. Besnard, E. Solari, R. Scopelliti, G. Bricogne, K. Severin, *Chem. Sci.* **2015**, *6*, 1004-1010; b) M. D. Wise, A. Ruggi, M. Pascu, R. Scopelliti, K. Severin, *Chem. Sci.* **2013**, *4*, 1658-1662.
- [103] a) A. J. Metherell, M. D. Ward, *Chem. Commun.* **2014**, *50*, 6330-6332; b) K. Li, L.-Y. Zhang, C. Yan, S.-C. Wei, M. Pan, L. Zhang, C.-Y. Su, *J. Am. Chem. Soc.* **2014**, *136*, 4456-4459; c) V. Vajpayee, H. Kim, A. Mishra, P. S. Mukherjee, P. J. Stang, M. H. Lee, H. K. Kim, K.-W. Chi, *Dalton Trans.* **2011**, *40*, 3112-3115.
- [104] O. J. Scherer, J. Schwalb, G. Wolmershäuser, W. Kaim, R. Gross, *Angew. Chem. Int. Ed. Engl.* **1986**, *25*, 363-364.
- [105] O. J. Scherer, T. Brück, G. Wolmershäuser, *Chem. Ber.* **1988**, *121*, 935-938.
- [106] O. J. Scherer, H. Sitzmann, G. Wolmershäuser, *J. Organomet. Chem.* **1984**, *268*, C9-C12.
- [107] a) O. J. Scherer, C. Blath, G. Wolmershäuser, *J. Organomet. Chem.* **1990**, *387*, C21-C24; b) J. R. Harper, A. L. Rheingold, *J. Organomet. Chem.* **1990**, *390*, C36-C38; c) W. Clegg, N. A. Compton, R. J. Errington, N. C. Norman, *Polyhedron* **1988**, *7*, 2239-2241.
- [108] O. J. Scherer, H. Sitzmann, G. Wolmershäuser, *Angew. Chem. Int. Ed. Engl.* **1985**, *24*, 351-353.
- [109] O. J. Scherer, R. Winter, G. Wolmershäuser, *Z. Anorg. Allg. Chem.* **1993**, *619*, 827-835.
- [110] O. J. Scherer, T. Brück, *Angew. Chem. Int. Ed. Engl.* **1987**, *26*, 59.
- [111] C. M. Hoidn, D. J. Scott, R. Wolf, *Chem. Eur. J.* **2020**; DOI: 10.1002/chem.202001854.
- [112] a) M. Di Vaira, P. Stoppioni, M. Peruzzini, *J. Chem. Soc., Dalton Trans.* **1990**, 109-113; b) M. Di Vaira, M. P. Ehses, M. Peruzzini, P. Stoppioni, *Polyhedron* **1999**, *18*, 2331-2336.
- [113] J. Bai, E. Leiner, M. Scheer, *Angew. Chem. Int. Ed.* **2002**, *41*, 783-786.
- [114] a) M. Scheer, L. Gregoriades, J. Bai, M. Sierka, G. Brunklaus, H. Eckert, *Chem. Eur. J.* **2005**, *11*, 2163-2169; b) M. Scheer, L. J. Gregoriades, M. Zabel, M. Sierka, L. Zhang, H. Eckert, *Eur. J. Inorg. Chem.* **2007**, 2775-2782; c) M. Scheer, L. J. Gregoriades, M. Zabel, J. Bai, I. Krossing, G. Brunklaus, H. Eckert, *Chem. Eur. J.* **2008**, *14*, 282-295; d) M. Fleischmann, S. Welsch, E. V. Peresykina, A. V. Virovets, M. Scheer, *Chem. Eur. J.* **2015**, *21*, 14332-14336; e) M. Elsayed Moussa, M. Fleischmann, E. V. Peresykina, L. Dütsch, M. Seidl, G. Balázs, M. Scheer, *Eur. J. Inorg. Chem.* **2017**, *2017*, 3222-3226; f) M. Elsayed Moussa, S. Welsch, L. J. Gregoriades, G. Balázs, M. Seidl, M. Scheer, *Eur. J. Inorg. Chem.* **2018**, *2018*, 1683-1687; g) M. Elsayed Moussa, M. Piesch, M. Fleischmann, A. Schreiner, M. Seidl, M. Scheer, *Dalton Trans.* **2018**, *47*, 16031-16035.
- [115] a) B. Attenberger, S. Welsch, M. Zabel, E. Peresykina, M. Scheer, *Angew. Chem. Int. Ed.* **2011**, *50*, 11516-11519; b) B. Attenberger, E. V. Peresykina, M. Scheer, *Inorg. Chem.* **2015**, *54*, 7021-7029; c) M. Elsayed Moussa, B. Attenberger, E. V. Peresykina, M.

- Fleischmann, G. Balázs, M. Scheer, *Chem. Commun.* **2016**, 52, 10004-10007; d) M. Elsayed Moussa, B. Attenberger, M. Seidl, A. Schreiner, M. Scheer, *Eur. J. Inorg. Chem.* **2017**, 2017, 5616-5620; e) M. E. Moussa, M. Seidl, G. Balázs, M. Zabel, A. V. Virovets, B. Attenberger, A. Schreiner, M. Scheer, *Chem. Eur. J.* **2017**, 23, 16199-16203; f) M. Elsayed Moussa, E. Peresyphkina, A. V. Virovets, D. Venus, G. Balázs, M. Scheer, *CrystEngComm* **2018**, 20, 7417-7422.
- [116] L. J. Gregoriades, B. K. Wegley, M. Sierka, E. Brunner, C. Gröger, E. V. Peresyphkina, A. V. Virovets, M. Zabel, M. Scheer, *Chem. Asian J.* **2009**, 4, 1578-1587.
- [117] M. Fleischmann, F. Dielmann, L. J. Gregoriades, E. V. Peresyphkina, A. V. Virovets, S. Huber, A. Y. Timoshkin, G. Balázs, M. Scheer, *Angew. Chem. Int. Ed.* **2015**, 54, 13110-13115.
- [118] C. Heindl, E. V. Peresyphkina, D. Lüdeker, G. Brunklaus, A. V. Virovets, M. Scheer, *Chem. Eur. J.* **2016**, 22, 2599-2604.
- [119] a) S. Welsch, L. J. Gregoriades, M. Sierka, M. Zabel, A. V. Virovets, M. Scheer, *Angew. Chem. Int. Ed.* **2007**, 46, 9323-9326; b) S. Welsch, M. Bodensteiner, M. Dusek, M. Sierka, M. Scheer, *Chem. Eur. J.* **2010**, 16, 13041-13045; c) M. Fleischmann, S. Welsch, L. J. Gregoriades, C. Gröger, M. Scheer, *Z. Naturforsch. B.* **2014**, 69, 1348-1356.
- [120] J. Bai, A. V. Virovets, M. Scheer, *Angew. Chem. Int. Ed.* **2002**, 41, 1737-1740.
- [121] J. Bai, A. V. Virovets, M. Scheer, *Science* **2003**, 300, 781-783.
- [122] a) S. Welsch, C. Gröger, M. Sierka, M. Scheer, *Angew. Chem. Int. Ed.* **2011**, 50, 1435-1438; b) F. Dielmann, A. Schindler, S. Scheuermayer, J. Bai, R. Merkle, M. Zabel, A. V. Virovets, E. V. Peresyphkina, G. Brunklaus, H. Eckert, M. Scheer, *Chem. Eur. J.* **2012**, 18, 1168-1179.
- [123] F. Dielmann, C. Heindl, F. Hastreiter, E. V. Peresyphkina, A. V. Virovets, R. M. Gschwind, M. Scheer, *Angew. Chem. Int. Ed.* **2014**, 53, 13605-13608.
- [124] C. Heindl, *Dissertation (University of Regensburg)* **2015**.
- [125] M. Fleischmann, S. Welsch, H. Krauss, M. Schmidt, M. Bodensteiner, E. V. Peresyphkina, M. Sierka, C. Gröger, M. Scheer, *Chem. Eur. J.* **2014**, 20, 3759-3768.
- [126] a) M. Fleischmann, L. Dütsch, M. E. Moussa, A. Schindler, G. Balázs, C. Lescop, M. Scheer, *Chem. Commun.* **2015**, 51, 2893-2895; b) M. Fleischmann, L. Dütsch, M. Elsayed Moussa, G. Balázs, W. Kremer, C. Lescop, M. Scheer, *Inorg. Chem.* **2016**, 55, 2840-2854.
- [127] a) C. Heindl, S. Heindl, D. Lüdeker, G. Brunklaus, W. Kremer, M. Scheer, *Inorg. Chim. Acta* **2014**, 422, 218-223; b) C. Heindl, E. Peresyphkina, A. V. Virovets, I. S. Bushmarinov, M. G. Medvedev, B. Krämer, B. Dittrich, M. Scheer, *Angew. Chem. Int. Ed.* **2017**, 56, 13237-13243.

- [128] J. Schiller, E. Peresyphkina, A. V. Virovets, M. Scheer, *Angew. Chem. Int. Ed.* **2020**, *59*, 13647-13650.
- [129] a) M. Scheer, L. J. Gregoriades, A. V. Virovets, W. Kunz, R. Neueder, I. Krossing, *Angew. Chem. Int. Ed.* **2006**, *45*, 5689-5693; b) Barbara Hiltl, *Dissertation (University of Regensburg)* **2018**.
- [130] a) F. Dielmann, E. V. Peresyphkina, B. Krämer, B. P. Johnson, M. Zabel, C. Heindl, M. Scheer, E. V. Peresyphkina, F. Hastreiter, *Angew. Chem. Int. Ed.* **2016**, *55*, 14833-14837; b) E. Peresyphkina, M. Bielmeier, A. Virovets, M. Scheer, *Chem. Sci.* **2020**, *11*, 9067-9071.
- [131] C. Schwarzmaier, A. Schindler, C. Heindl, S. Scheuermayer, E. V. Peresyphkina, A. V. Virovets, M. Neumeier, R. Gschwind, M. Scheer, *Angew. Chem. Int. Ed.* **2013**, *52*, 10896-10899.
- [132] a) M. Elsayed Moussa, B. Attenberger, E. V. Peresyphkina, M. Scheer, *Dalton Trans.* **2018**, *47*, 1014-1017; b) M. E. Moussa, S. Welsch, M. Lochner, E. V. Peresyphkina, A. V. Virovets, M. Scheer, *Eur. J. Inorg. Chem.* **2018**, *2018*, 2689-2694.
- [133] a) M. Scheer, J. Bai, B. P. Johnson, R. Merkle, A. V. Virovets, C. E. Anson, *Eur. J. Inorg. Chem.* **2005**, 4023-4026; b) M. Scheer, A. Schindler, J. Bai, B. P. Johnson, R. Merkle, R. Winter, A. V. Virovets, E. V. Peresyphkina, V. A. Blatov, M. Sierka, H. Eckert, *Chem. Eur. J.* **2010**, *16*, 2092-2107.
- [134] M. Scheer, A. Schindler, R. Merkle, B. P. Johnson, M. Linseis, R. Winter, C. E. Anson, A. V. Virovets, *J. Am. Chem. Soc.* **2007**, *129*, 13386-13387.
- [135] a) M. Scheer, A. Schindler, C. Gröger, A. V. Virovets, E. V. Peresyphkina, *Angew. Chem. Int. Ed.* **2009**, *48*, 5046-5049; b) A. Schindler, C. Heindl, G. Balázs, C. Gröger, A. V. Virovets, E. V. Peresyphkina, M. Scheer, *Chem. Eur. J.* **2012**, *18*, 829-835; c) E. V. Peresyphkina, C. Heindl, A. Schindler, M. Bodensteiner, A. V. Virovets, M. Scheer, *Z. Kristallogr. - Cryst. Mater.* **2014**, *229*, 735-740.
- [136] E. Peresyphkina, C. Heindl, A. Virovets, H. Brake, E. Mädl, M. Scheer, *Chem. Eur. J.* **2018**, *24*, 2503-2508.
- [137] F. Dielmann, M. Fleischmann, C. Heindl, E. V. Peresyphkina, A. V. Virovets, R. M. Gschwind, M. Scheer, *Chem. Eur. J.* **2015**, *21*, 6208-6214.
- [138] C. Heindl, E. V. Peresyphkina, A. V. Virovets, W. Kremer, M. Scheer, *J. Am. Chem. Soc.* **2015**, *137*, 10938-10941.
- [139] S. Heinl, E. Peresyphkina, J. Sutter, M. Scheer, *Angew. Chem. Int. Ed.* **2015**, *54*, 13431-13435.

- [140] B. P. Johnson, F. Dielmann, G. Balázs, M. Sierka, M. Scheer, *Angew. Chem. Int. Ed.* **2006**, *45*, 2473-2475.

2 Research Objectives

As demonstrated in the introduction, polyphosphorus complexes display versatile building blocks for supramolecular chemistry when combined with Lewis acidic metal salts. Thus, a myriad of polymeric assemblies (chapter 1.5.2) or, with $[\text{Cp}^{\text{R}}\text{Fe}(\eta^5\text{-P}_5)]$, discrete nano-sized spherical aggregates (chapter 1.5.3) are accessible. The investigations on such spherical assemblies faced some challenges in the past, including insolubility of the spheres, selectivity of the self-assembly reaction, template encapsulation and crystal quality, with all these factors being highly dependent on, *inter alia*, the nature of the R group and the applied template. Hence, the objectives of this thesis are:

- Variation of the $[\text{Cp}^{\text{R}}\text{Fe}(\eta^5\text{-P}_5)]$ building block and investigation of the self-assembly processes with Cu(I) halides
- Investigations on the templating properties of triple decker complexes with respect to the formation of host aggregates of different size and shape as well as potential fragmentation of the triple decker complexes

The self-assembly of $[\text{Cp}^{\text{R}}\text{Fe}(\eta^5\text{-P}_5)]$ so far has been merely investigated in combination with Cu or Ag salts. Concerning other polyphosphorus complexes, only two examples of Au coordination have been reported with $[\{\text{CpMo}(\text{CO})_2\}_2(\mu, \eta^2\text{-P}_2)]$. Hence, a further research objective for this work is:

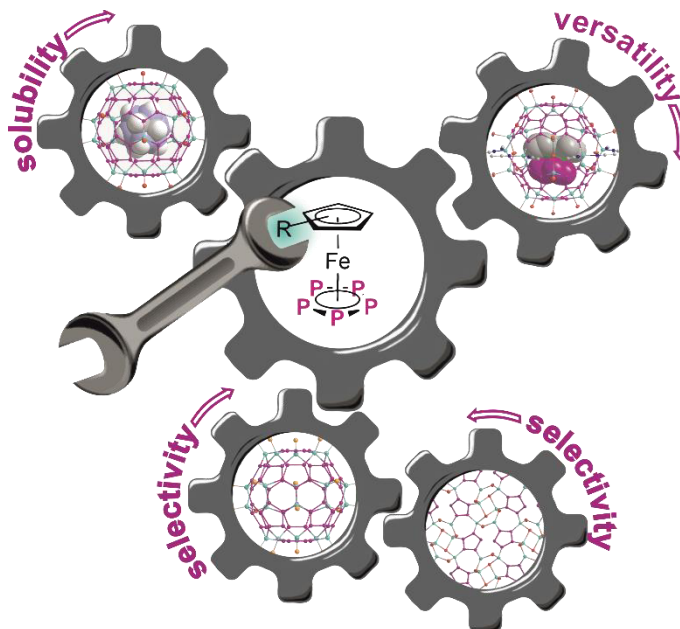
- Transferring the supramolecular chemistry of $[\text{Cp}^{\text{R}}\text{Fe}(\eta^5\text{-P}_5)]$ to Au salts

Moreover, iodinations of P_4 or its complexes have led to unprecedented polyphosphorus compounds by not only P-P bond cleavage but also recombination. Investigations on these iodination reactions are confined to P_4 complexes and have been left untouched for other polyphosphorus complexes. Thus, a further objective is:

- Investigations on the halogenation reactions of $[\text{Cp}^*\text{Fe}(\eta^5\text{-P}_5)]$ and its heavier homologues $[\text{Cp}^*\text{Fe}(\eta^5\text{-As}_5)]$, $[\text{Cp}^*\text{Ru}(\eta^5\text{-P}_5)]$ and $[\text{Cp}^*\text{Ru}(\eta^5\text{-As}_5)]$

3 Fine-Tuning the supramolecular chemistry of Pentaphosphaferrocenes – Achieving versatility, selectivity and solubility

H. Brake, E. Peresytkina, A. V. Virovets, S. Rank, R. Szlosek, W. Kremer, C. Klimas, M. Scheer



Abstract:

The self-assembly of $[\text{Cp}^x\text{Fe}(\eta^5\text{-P}_5)]$ ($\mathbf{1}^x$) and Cu(I) halides is highly selective and controllable by the applied reaction conditions. In two-component reactions in presence of CH_3CN , 90-vertex spheres $[\text{Cp}^x\text{Fe}(\eta^5\text{-P}_5)]@[\{\text{Cp}^x\text{Fe}(\eta^5\text{-P}_5)\}_{12}\{\text{CuX}\}_{25}\{\text{CH}_3\text{CN}\}_{10}]$ ($\mathbf{2}$, $X = \text{Cl}, \text{Br}$) and a 2D polymer $[\{\text{Cp}^x\text{Fe}(\eta^5\text{-P}_5)\}\{\text{CuI}\}_3]$ ($\mathbf{5-I}$) are obtained. By avoiding CH_3CN , instead (80- n)-vertex metal-deficient spheres $(\text{CH}_2\text{Cl}_2)_m@[\{\text{Cp}^x\text{Fe}(\eta^5\text{-P}_5)\}_{12}\{\text{CuX}\}_{20-n}]$ ($\mathbf{3}$, $X = \text{Cl}$: $m \geq 0.84$, $n = 1.20$; $X = \text{Br}$) are formed. These rearrange in solution to give 2D polymers $[\{\text{Cp}^x\text{Fe}(\eta^5\text{-P}_5)\}\{\text{CuX}\}_3]$ ($X = \text{Cl}$: $\mathbf{4-Cl}$; $X = \text{Br}$: $\mathbf{5-Br}$). In the presence of P_4S_3 or $o\text{-C}_{20}\text{H}_{12}$, the formation of host-guest aggregates $(\text{P}_4\text{S}_3)_m@[\{\text{Cp}^x\text{Fe}(\eta^5\text{-P}_5)\}_{12}\{\text{CuX}\}_{20-n}]$ ($\mathbf{6}$, $X = \text{Cl}, \text{Br}$; $0.68 \leq m \leq 1$; $2.8 \geq n \geq 1.4$) and $(o\text{-C}_{20}\text{H}_{12})_m@[\{\text{Cp}^x\text{Fe}(\eta^5\text{-P}_5)\}_{12}\{\text{CuX}\}_{20-n}]$ ($\mathbf{7}$, $X = \text{Cl}, \text{Br}$; $0.5 \leq m \leq 1$; $2.27 \geq n \geq 1.75$) is realized. Astonishingly, $\mathbf{1}^x$ combines all advantages of the previously applied building blocks $[\text{Cp}^x\text{Fe}(\eta^5\text{-P}_5)]$ and $[\text{Cp}^{\text{Bn}}\text{Fe}(\eta^5\text{-P}_5)]$, respectively, since its spherical assemblies are well soluble, selectively synthesizable, encapsulate templates and crystallize well. Stoichiometry- or template-driven interconversions of (80- n)-vertex spheres $\mathbf{3}$ to 90-vertex spheres $\mathbf{2}$ or to host-guest aggregates $\mathbf{7}$ could be observed for the first time.

3.1 Introduction

Originally dominated by organic receptors, such as calixarenes, cyclodextrins, crown ethers and cryptands, host-guest chemistry has evolved into a fascinating topic in current research, by now also spanning inorganic or metal-organic systems.^[1] Metallosupramolecular architectures offer the advantage of well-balanced strength of the coordinative bond often assuring dynamic behavior in solution, while at the same time multidentate ligand design in combination with the preferred coordination number and geometry of metal ions allows for a rational design of host aggregates with well-defined size and shape of cavities.^[2]

Our group makes use of substituted pentaphosphaferrocenes [$\text{Cp}^R\text{Fe}(\eta^5\text{-P}_5)$] as five-fold symmetric building blocks in supramolecular chemistry (Figure 1a-c). In combination with Lewis acidic metal cations, a large variety of polymers^[3] and discrete spherical compounds have been discovered.^[4] Spherical aggregates of [$\text{Cp}^*\text{Fe}(\eta^5\text{-P}_5)$] ($\mathbf{1}^*$) and $\text{Cu}(\text{I})\text{X}$ ($\text{X} = \text{Cl}, \text{Br}, \text{I}$) are only stable when formed in the presence of an adequate template. This may be $\mathbf{1}^*$ itself, thus under certain conditions yielding the 90-vertex spheres [$\mathbf{1}^*$]@{ $\mathbf{1}^*$ }₁₂{ CuX }₂₅{ CH_3CN }₁₀} ($\text{X} = \text{Cl}, \text{Br}$; scaffold **A**, Figure 1d).^[4a,5] On the other hand, a third component may act as a template, such as $o\text{-C}_2\text{B}_{10}\text{H}_{12}$, [FeCp_2], C_{60} , P_4 , As_4 and [$(\text{CpCr})_2(\mu, \eta^{5:5}\text{-As}_5)$], resulting in host molecules of various shapes and topologies.^[6] In particular, the (80-n)-vertex spherical hosts [{ $\mathbf{1}^*$ }]₁₂{ CuX }_{20-n}} ($\text{X} = \text{Cl}, \text{Br}$; scaffold **B**, Figure 1e) should be highlighted, since their framework represents an entirely carbon-free analogue of the $I_h\text{-C}_{80}$ fullerene.

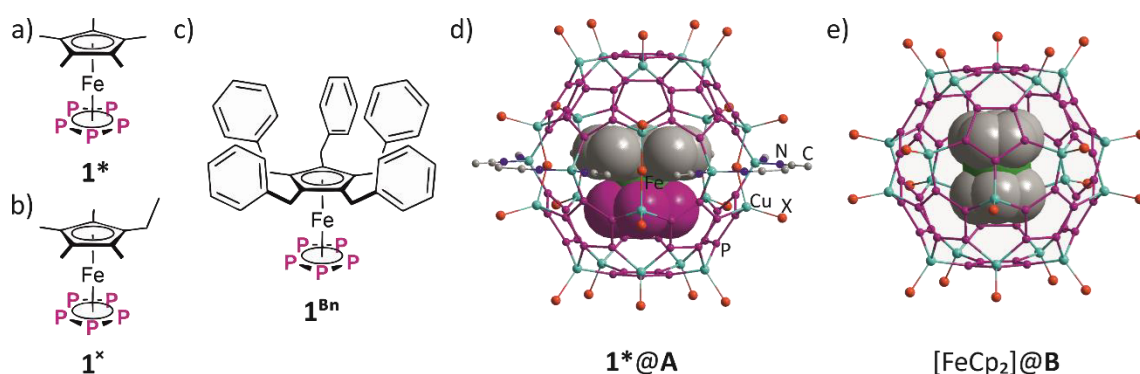


Figure 1. Molecular structures of a) [$\text{Cp}^*\text{Fe}(\eta^5\text{-P}_5)$] ($\mathbf{1}^*$); b) [$\text{Cp}^X\text{Fe}(\eta^5\text{-P}_5)$] ($\mathbf{1}^X$); c) [$\text{Cp}^{\text{Bn}}\text{Fe}(\eta^5\text{-P}_5)$] ($\mathbf{1}^{\text{Bn}}$). Inclusion of d) $\mathbf{1}^*$ into the 90-vertex sphere **A**; e) [FeCp_2] into the 80-vertex sphere **B**. H atoms and { FeCp^R } units of the host scaffold are omitted for clarity. Incorporated molecules are displayed in the space-filling model.

Unfortunately, host-guest aggregates based on $\mathbf{1}^*$ are often sparingly soluble or even completely insoluble, impeding further characterization in solution and investigations on the formation pathway.^[6a,b,e,7] In contrast, reactions of [$\text{Cp}^{\text{Bn}}\text{Fe}(\eta^5\text{-P}_5)$] ($\mathbf{1}^{\text{Bn}}$, $\text{Cp}^{\text{Bn}} = \text{C}_5(\text{CH}_2\text{Ph})_5$) with

Cu(I)X (X = Cl, Br, I) result in highly soluble spherical assemblies, also spanning an 80-vertex sphere (scaffold **B**, Figure 1e) with I_h -C₈₀ topology.^[8] Its formation is observed already in the absence of a template and instead, solvent molecules occupy the void. Due to dynamic behavior of the 80-vertex sphere (scaffold **B**) in solution, [FeCp₂] can be reversibly incorporated into the spherical host.^[8b] However, the host-guest chemistry of **1^{Bn}** is quite limited. On the one hand, a 90-vertex sphere (scaffold **A**) is not formed from **1^{Bn}**. On the other hand, encapsulation into **B** was proven crystallographically merely for [FeCp₂] and [CpV(η⁷-C₇H₇)], but not for any other template despite numerous attempts.^[8b,9] While in the synthesis of **1*** based spherical assemblies, polymeric by-products can barely be avoided,^[9] these are not observed in reactions of **1^{Bn}** with Cu(I)X (X = Cl, Br), but only when X = I is used.^[8b]

Since both [Cp^{*}Fe(η⁵-P₅)] (**1***) and [Cp^{Bn}Fe(η⁵-P₅)] (**1^{Bn}**) show some disadvantages when used as supramolecular building blocks, the question arises as to whether selectivity, solubility and template encapsulation can be fine-tuned by further variation of the Cp ligand. Also, post-synthetic encapsulation and rearrangement to a 90-vertex ball has never been observed due to the limited solubility of the spheres and/or limited versatility. Hence, the use of [Cp^xFe(η⁵-P₅)] (**1^x**, Cp^x = C₅Me₄Et)^[10] comes to mind, for which so far, only one 90-vertex sphere [1^x]@[1^x]₁₂{CuBr}₂₅{CH₃CN}₁₀ (**2-Br**, scaffold **A** in Figure 1d) was reported.^[5] We wondered, whether **1^x** as a building block might for the first time combine the solubility and selectivity observed for **1^{Bn}** with the versatility and crystallization ease observed for **1***.

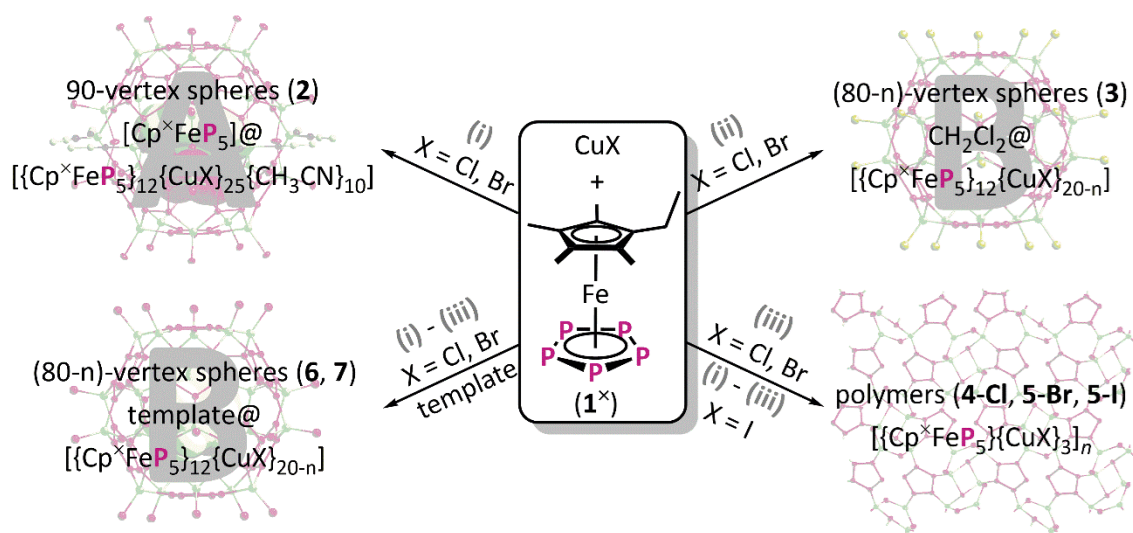
Herein, we present the results of the self-assembly of **1^x** with CuX (X = Cl, Br, I). Thereby, the outcome can be controlled easily by variation of the applied reaction conditions and the resulting products are formed selectively. The high solubility of the spherical products additionally enables studies in solution addressing their rearrangement capabilities.

3.2 Results and Discussion

Similarly to the synthesis of **2-Br**, [Cp^xFe(η⁵-P₅)] (**1^x**) was allowed to react with CuCl (2.2 eq.) in a CH₂Cl₂ / CH₃CN mixture (either by stirring or layering both components; Scheme 1, top left). Unfortunately, no crystals of sufficient quality for X-ray crystallography were obtained despite numerous attempts, but NMR spectroscopy confirmed the formation of [1^x]@[1^x]₁₂{CuCl}₂₅{CH₃CN}₁₀ (**2-Cl**, scaffold **A**), the Cl analogue of the previously reported 90-vertex sphere **2-Br**.^[5] After one month, also the formation of crystals of a novel 2D polymer [1^x]₂{CuCl}₆{CH₃CN}]_n·nCH₃CN (**4-Cl-CH₃CN**) was observed. **4-Cl-CH₃CN** could be reproduced selectively by layering **1^x** in toluene with a solution of CuCl in CH₃CN. Performing layering

experiments with CuI (2 or 3 eq.) results in the exclusive crystallization of the 2D polymer $[\{1^x\}\{CuI\}_3]_n$ (**5-I**) in 82% yield (Scheme 1, bottom right).

Since the 90-vertex spheres **2** (scaffold **A**) comprise coordinated CH_3CN molecules, the question arose, which products would be formed in the absence of CH_3CN . Hence, a solution of 1^x in CH_2Cl_2 was stirred over solid CuX ($X = Cl, Br$). After 45 minutes, an orange solution was obtained, from which by layering with toluene (80- n)-vertex spheres $(CH_2Cl_2)_m@[\{1^x\}_{12}\{CuX\}_{20-n}]$ (**3-Cl** and **3-Br**, scaffold **B**) crystallized initially (< 2 weeks; Scheme 1, top right). The void is occupied by solvent molecules (**3-Cl**: $m \geq 0.84$)^[11] and the inorganic scaffold may contain CuX-vacancies (**3-Cl**: $n = 1.20$), which is reminiscent of a 1^{Bn} -based (80- n)-vertex sphere.^[8b,12]



Scheme 1. Selective self-assembly of $[Cp^xFe(\eta^5-P_5)]$ (1^x) and Cu(I) halides depending on the applied reaction conditions: (i) layering of CH_2Cl_2 solutions with CH_3CN solutions, (ii) stirring briefly in CH_2Cl_2 , (iii) stirring longer in CH_2Cl_2 . Template = P_4S_3 (**6**) or $o-C_2B_{10}H_{12}$ (**7**). Grey capital letters indicate the scaffold of the formed supramolecule (**A**: 90-vertex sphere; **B**: (80- n)-vertex sphere).

Occasionally, after some time (> 2 weeks) also crystals of the 2D polymeric compounds $[\{1^x\}\{CuX\}_3]_n$ (**4-Cl** and **5-Br**) were obtained. These could be synthesized more conveniently when the reaction solutions of 1^x and CuX are allowed to stir longer (several hours to days; Scheme 1, bottom right). Then, a yellow solid of the respective 2D polymer (**4-Cl** or **5-Br**) precipitates, indicating a certain instability of the initially formed (80- n)-vertex spheres **3-Cl** and **3-Br** in solution. The solids could be identified as **4-Cl** (mixed with **4-Cl- CH_3CN**)^[13] and **5-Br** by elemental analysis, X-ray powder diffraction (Figure 2) and solid-state NMR spectroscopy (*vide infra*). In contrast, when 1^x is stirred with CuI (2 eq.) in CH_2Cl_2 , **5-I** precipitates immediately while uncoordinated 1^x resides in the green supernatant and no spherical assemblies could be observed.

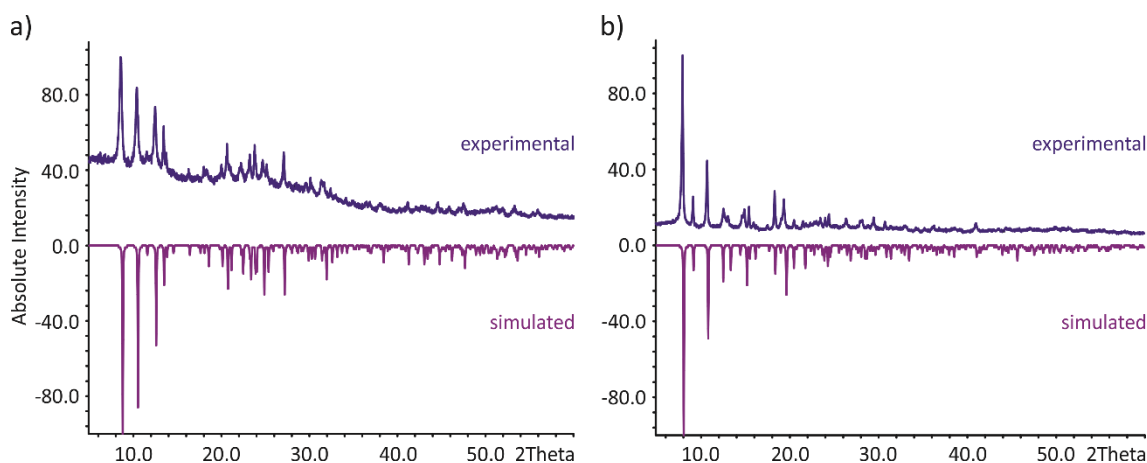


Figure 2. Experimental (top) X-ray powder diffraction patterns of precipitated a) **4-Cl** (+ **4-Cl-CH₃CN**)^[14] and b) **5-Br** in comparison to the diffraction pattern simulated from the single crystal X-ray data of a) **4-Cl** and b) **5-Br** (bottom), respectively.

In order to stabilize the desired scaffolds **B** and avoid polymer formation, the self-assembly of **1^x** and CuX was additionally carried out in the presence of a template. For this purpose, P₄S₃ and *o*-C₂B₁₀H₁₂ were selected as third components in self-assembly processes, since their presence can easily be detected by NMR spectroscopy, and both have been successfully encapsulated into 80-vertex spheres of **1^{*}**, but proper crystallization of **1^{Bn}** analogues was unsuccessful despite numerous attempts.^[6a,9,15] By stirring a CH₂Cl₂ solution of **1^x** and P₄S₃ or *o*-C₂B₁₀H₁₂ over solid CuX (X = Cl, Br), the desired host-guest aggregates (P₄S₃)_m@[{**1^x**]₁₂{CuX}_{20-n}] (**6-Cl** and **6-Br**; 0.68 ≤ m ≤ 1; 2.8 ≥ n ≥ 1.4) or (*o*-C₂B₁₀H₁₂)_m@[{**1^x**]₁₂{CuX}_{20-n}] (**7-Cl** and **7-Br**; 0.5 ≤ m ≤ 1; 2.52 ≥ n ≥ 1.52) were obtained (Scheme 1, bottom left).^[11,12] The yields amount up to 63% and are higher for shorter reaction times (stirring for 1-3 hours), while they decrease with longer reaction times (stirring for 2-3 days) due to the formation of insoluble yellow precipitates (presumably polymers **4-Cl** and **5-Br**). Furthermore, compounds **6** and **7** can be synthesized by layering CH₃CN solutions of Cu(I)X (X = Cl, Br) onto CH₂Cl₂ solutions of **1^x** and P₄S₃ or *o*-C₂B₁₀H₁₂ in up to 89% yield, surprisingly without the accompanying formation of 90-vertex spheres (scaffold **A**) or polymers.

Characterization of the polymeric products

Polymer **4-Cl** crystallizes in the orthorhombic space group *Pbcm*. Its molecular structure consists of 1D polymeric {CuCl}_∞ strands interconnected by **1^x** units (Figure 3a). Thereby, every two of three Cu atoms link two neighboring **1^x** units, resulting in a distorted tetrahedral coordination geometry. Every third Cu atom is only coordinated by one **1^x**, resulting in a distorted trigonal planar coordination mode and a change in helicity of the {CuCl}_∞ strands

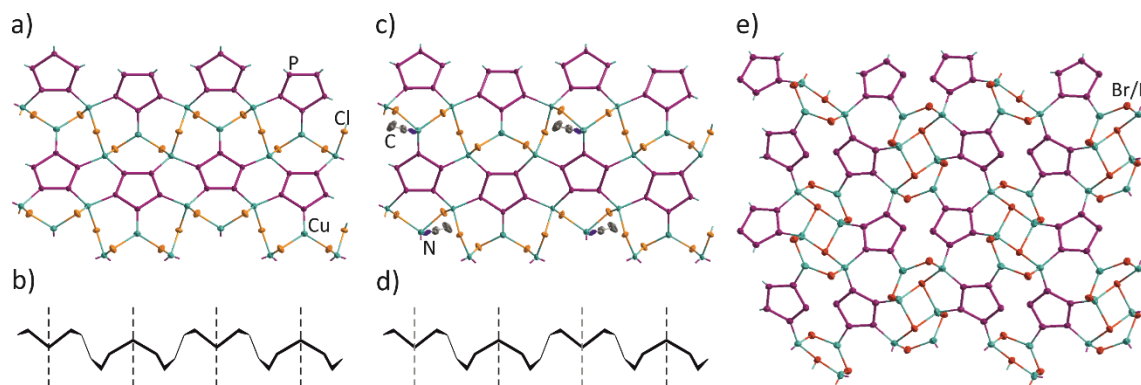


Figure 3. Molecular structures of a) **4-Cl**, c) **4-Cl-CH₃CN**, e) **5-Br** and **5-I**. H atoms, non-coordinating solvent molecules, {Cp^xFe} moieties and positions of minor occupancies are omitted for clarity. A.d.p. ellipsoids at 50% probability level. Schematic representations of the {CuCl}_∞ helices in b) **4-Cl** and d) **4-Cl-CH₃CN** with changes in helicity indicated by dashed lines at every trigonally coordinated Cu atom (black) or every additionally by CH₃CN coordinated Cu atom (grey).

(Figure 3b). Polymer **4-Cl-CH₃CN** is built up similarly (Figure 3c,d), but every sixth Cu atom (corresponding to every second of the trigonally coordinated Cu atoms in **4-Cl**) is additionally coordinated by CH₃CN. It crystallizes in the monoclinic space group $P2_1/n$. Moreover, **4-Cl** and **4-Cl-CH₃CN** represent the first examples of polymers with [Cp^RFe(η⁵-P₅)] building blocks coordinated to 5 Cu atoms in a σ-fashion, which so far has only been observed in spherical aggregates of pentaphosphaferrocenes.^[3-9,16] In contrast to the spherical compounds, however, the {FeCp^R} units in **4-Cl** and **4-Cl-CH₃CN** are oriented alternating above and below the layer. This seems to render angulation along the Cu...Cu axes of the {P₄Cu₂} six-membered rings unnecessary, which is in turn mainly responsible for the curvature of the shell in the spherical compounds reported before^[4-9] and herein (*vide infra*). Compounds **5-Br** and **5-I** are isostructural. They crystallize in the monoclinic space group $P2_1/c$ (Figure 3e) and are similar to the reported [Cp^{*}Fe(η⁵-P₅)] (**1***) based polymer [(Cp^{*}Fe(η⁵-P₅)){CuI₃}]_n·*no*-C₆H₄Cl₂.^[16] While in the latter the 2D layers are separated by *o*-C₆H₄Cl₂ molecules, in compounds **5-Br** and **5-I** the concave parts of the puckered 2D-layer instead are occupied by the additional CH₃ group of the Cp^x ligands. The **1*** units in both polymers exhibit a 1,2,3,4-coordination mode.

Polymers **4-Cl**, **4-Cl-CH₃CN**, **5-Br** and **5-I** are insoluble in all common solvents, but soluble in pyridine under depolymerization. The ¹H and ³¹P{¹H} NMR spectra in pyridine-d₅ thus only exhibit signals for the uncoordinated pentaphosphaferrocene **1***. In contrast, the respective solid state ³¹P{¹H} NMR magic angle spinning (MAS) spectra of the polymeric products show broad signals ranging from 0 to 120 ppm. While compound **4-Cl** comprises three crystallographically unique P atoms, the ³¹P{¹H} MAS NMR spectrum shows more than three signals (Figure 4a), due to the unavoidable contamination of precipitated **4-Cl** with **4-Cl-CH₃CN**

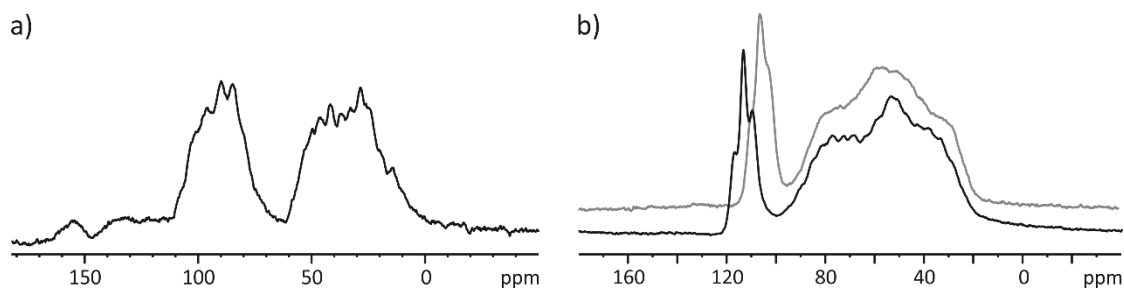


Figure 4. $^{31}\text{P}\{^1\text{H}\}$ MAS NMR spectra of a) a mixture of **4-Cl** and **4-Cl-CH₃CN** and b) **5-Br** (grey) and **5-I** (black) acquired at a spinning frequency of 25000 Hz.

during washing with CH_3CN .^[13] The $^{31}\text{P}\{^1\text{H}\}$ MAS NMR spectra of **5-Br** and **5-I** are expected to show five signals for the five crystallographically unique P atoms found in the solid state structures. Each spectrum shows one distinct broad *pseudo*-triplet at 107 or 113 ppm, which can be assigned to the P atom not coordinating to Cu (Figure 4b). The remaining four signals overlap in the region of 20 to 100 ppm, and the resulting broad set of signals can be assigned to the four P atoms coordinating to Cu. Accordingly, the integral ratios of the *pseudo*-triplet to the broad signal set amount to 1:4. Unfortunately, line shape fitting was hampered due to the overlapping of the signals, why $^1J_{\text{PP}}$ and $^1J_{\text{PCu}}$ couplings are partially unresolved. However, two $^1J_{\text{PP}}$ couplings can be derived from the *pseudo*-triplet and $^1J_{\text{PCu}}$ couplings are visible at some parts of the broad signal set, especially in the better resolved spectrum of **5-I**. Although the spectra were acquired from crystals of **5-I** and powder of **5-Br**, they merely differ in the chemical shift of the *pseudo*-triplet, thus also confirming the composition and purity of the precipitated **5-Br**.

Solid state structures of the supramolecules

When synthesized by stirring in CH_2Cl_2 and layering with toluene for crystallization, the spherical products **3**, **6** and **7** (scaffold **B**) all crystallize in the face-centered cubic structure type with an a lattice constant varying between 41.4 – 41.9 Å. However, the obtained crystals are often not of sufficient quality for full structure determination, but the presence of (80- n)-vertex spheres is nevertheless confirmed. For the Cl spheres luckily the crystal quality was satisfactory. All three compounds (**3-Cl**, **6b-Cl** and **7b-Cl**, Figure 5) are isostructural. They crystallize in the cubic space group $Fm\bar{3}c$ and respective supramolecules occupy $m\bar{3}$ special positions, represented by a half a unit of 1^* and two {CuCl} moieties in the asymmetric unit.

Interestingly, host-guest compounds **6** and **7** are also formed by the layering approach in $\text{CH}_2\text{Cl}_2/\text{CH}_3\text{CN}$ and then crystallize isostructurally in the space group $P4_2/n$ (**6a-Cl**, **6a-Br**, **7a-Cl**, **7a-Br**). As minor phases, **6a'-Br**, crystallizing in the space group $C2/m$, and **7a'-Br**, crystallizing in the trigonal space group $R\bar{3}$, are found. **7a'-Br** is isotypic to the 1^* based (80- n)-vertex spheres crystallized from $\text{CH}_2\text{Cl}_2/\text{CH}_3\text{CN}$.^[9]

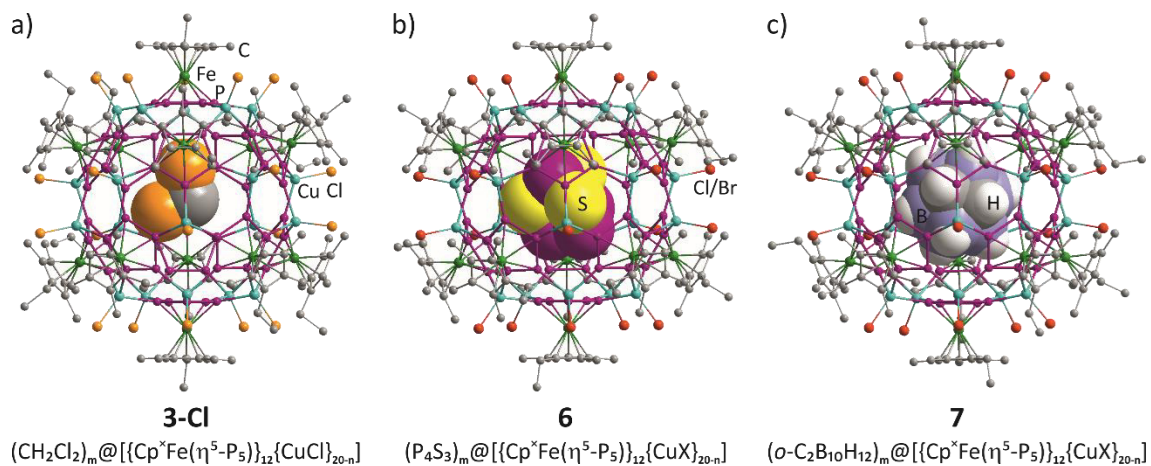


Figure 5. Molecular structures of a) **3-Cl**, b) **6** and c) **7**. H atoms, solvent molecules and minor positions of disorder are omitted for clarity. Host molecules are depicted in the ball-and-sticks model and guest molecules in the space-filling model.

The core of the host molecule found in all phases of **3-Cl**, **6** and **7** is composed of 12 *cyclo*-P₅ rings | connected by (20-n) {CuX} units (Figure 5), similar to the (80-n)-vertex spheres of **1*** and **1^{Bn}** (scaffold **B** in Figure 1e). Likewise, {CuX} contents, listed in Table 1, differ from the idealized scaffold containing 20 {CuX} units.^[12] Since the {CuX} amount found is not an integer, compounds **3-Cl**, **6** and **7** must display solid solutions of spheres with different metal-deficiency. For crystals obtained by the stirring approach (**3-Cl**, **6b-Cl**, **7b-Cl**) the average {CuCl} amount found (18.25 – 18.80) cannot be unambiguously interpreted, but could be e.g. a mixture of (80-1) vertex spheres and (80-2) vertex spheres in the ratios of 80:20 for **3-Cl**, 60:40 for **6b-Cl** and 25:75 for **7b-Cl**. For the (80-2) vertex spheres, different isomers are conceivable, as already reported for **1^{Bn}** based spheres.^[17] However, while for **1^{Bn}** based spheres the vacancies are found in the 12-fold CuX position,^[8b] for the **1^x** spheres **3-Cl**, **6b-Cl** and **7b-Cl** partial occupation is only found in the 8-fold positions, so in these compounds the presence of C_{2v} isomers can be ruled out. For the crystals obtained by the layering approach (**6a-Cl**, **6a-Br**, **6a'-Br**, **7a-Cl**, **7a-Br**, **7a'-Br**), the average {CuX} contents found (17.20 – 17.75) also suggest the presence of more metal-deficient, for instance, (80-3)-vertex spherical supramolecules. At least 8 of the 20 {CuX} positions are fully occupied, while the other 12 {CuX} positions are partly vacant. In fact, the hypothetically derived minimal scaffold of a (80-12)-vertex sphere was proven to exist recently for a cationic sphere of [Cp^{''}Fe(η⁵-P₅)].^[18] Hence, the {CuX} content in the bulk phase may differ from the one found in the respective crystal and may vary from 8 to 20 {CuX} moieties per supramolecule. Moreover, in the crystals obtained by layering (CH₂Cl₂/CH₃CN), Cl atoms of CH₂Cl₂ or N atoms of CH₃CN may point towards the vacant X positions. This is not observed for crystals obtained by stirring (CH₂Cl₂/toluene), although in principle it is possible also for toluene to occupy vacant X positions, as once observed.^[9] The trend that crystallization from toluene mixtures results in less dense

packing of the spheres (as found for spheres of **1***)^[9] continues for the spheres of **1*** presented herein ($V/Z \approx 6600 - 6900 \text{ \AA}^3$ vs. 9000 \AA^3).

Table 1. Number of {CuX} vacancies n , resulting total {CuX} contents ($20-n$), guest occupancies m , inner diameter (range) and max. outer diameters for crystallographically unique molecules in **3-Cl**, **6** and **7**.

Compound	n ^[11]	$20-n$ ^[11]	m ^[12]	inner diameter [Å] ^[19]	max. outer diameter [Å] ^[19]
3-Cl	1.2	18.8	0.84	7.72	25.3
6a-Cl	2.6	17.4	1	7.57 – 7.77	25.4
6a-Br	2.6	17.4	0.83	7.60 – 7.81	25.4
6a'-Br ^[a]	2.8,	17.2,	0.68,	7.64 – 7.86,	25.5,
	2.8	17.2	0.68	7.60 – 7.82	25.6
6b-Cl	1.4	18.6	0.8	7.69	25.3
7a-Cl	2.25	17.75	1	7.58 – 7.78	25.5
7a-Br	2.25	17.75	1	7.60 – 7.83	25.5
7a'-Br ^[a]	2.52,	17.48,	0.77,	7.69 – 7.79,	25.5,
	1.52	18.48	1	7.64 – 7.77	25.2
7b-Cl	1.75	18.25	0.5	7.70	25.3

[a] The data separated by a comma correspond to crystallographically unique spheres occupying two different special positions with site symmetry $2/m$ for **6a'-Br** and $\bar{1}$ or $\bar{3}$ for **7a'-Br**, respectively.

The outer diameter of the host molecules amounts up to 25.6 Å, while the inner diameter is about 7.7 Å (Table 1).^[19,20] In contrast to the spheres of **1***, the formation of the (80- n)-vertex spheres reported herein is not template-controlled, but instead the void of **3-Cl** is occupied by molecules of CH_2Cl_2 . In the host-guest aggregates **6** and **7**, the void is occupied by up to one molecule of P_4S_3 or $o\text{-C}_2\text{B}_{10}\text{H}_{12}$, respectively.^[11] With maximum sizes of 6.99 Å (P_4S_3)^[21] and 7.77 Å ($o\text{-C}_2\text{B}_{10}\text{H}_{12}$),^[22] both templates fit perfectly inside the cavity of the host molecules when considering that the van-der-Waals radii have been taken into account for the size calculations. Neither attractive interactions nor resulting preferred orientations towards the host molecule were found. However, due to its size, $o\text{-C}_2\text{B}_{10}\text{H}_{12}$ does not take in an orientation where its C-H or B-H bonds point towards the P_5 cycles of the host being the narrowest points of the void.

Characterization of the supramolecules in solution

The 90-vertex spherical compounds **2-Cl** and **2-Br** (scaffold **A**) are soluble in mixtures of CH_2Cl_2 and CH_3CN (2:1). The $^{31}\text{P}\{^1\text{H}\}$ NMR spectra both exhibit a broad signal at 68 ppm assigned to the P atoms of the host. The signal assigned to the encapsulated molecule of **1*** (**2-Cl**: 157.8 ppm; **2-Br**: 160.8 ppm) is shifted downfield in comparison to free **1*** (152.8 ppm).^[10,23] This downfield shift was similarly observed in the $^{31}\text{P}\{^1\text{H}\}$ MAS NMR spectrum of the Cp^* analogue with scaffold **A**.^[4a] In the ^1H NMR spectrum, the encapsulation of **1*** does not affect the chemical

shift, and signals of free^[24] and encapsulated 1^x are superimposed. Additionally, the signal expected for the CH_2 group is superimposed by the CD_3CN signal, as was shown by $^1\text{H}, ^1\text{H}$ -COSY NMR spectroscopy. In contrast, the signals observed for 1^x units building the host sphere are shifted to lower field and broadened. Interestingly, they split up into two groups with an integral ratio of 2:10, suggesting the first set of signals is assigned to the top and bottom 1^x unit while the second set of signals is assigned to the ten 1^x units coordinating to the middle belt. In addition, few small singlets are always observed at -2.52 to -1.81 ppm (**2-Cl**) or -3.26 to -1.35 ppm (**2-Br**) and 1.83 ppm. These presumably might be assigned to coordinated CH_3CN .

Compound **3**, **6** and **7** (scaffold **B**) are insoluble in pentane, toluene, THF and CH_3CN , though astonishingly well soluble in CH_2Cl_2 . The high solubility of the spherical supramolecules in CH_2Cl_2 allows for their comprehensive characterization in solution, which was so far only possible for 1^{Bn} -based spherical aggregates, but often not for 1^* -based ones.

In the ^1H NMR spectra of **3**, **6** and **7** in CD_2Cl_2 , the signals for the Cp^x ligands comprise chemical shifts of 1.07 to 1.08 ($-\text{CH}_2\text{CH}_3$), 2.09 to 2.33 (CH_3) and 2.75 to 3.10 ppm ($-\text{CH}_2\text{CH}_3$) and thus are shifted downfield compared to free 1^x .^[24] Moreover, the signals are broadened, and while for the $-\text{CH}_2\text{CH}_3$ protons only one broadened triplet is observed, all other groups of signals split up to give up to three broad signals. This is most probably due to the presence of spherical aggregates with different CuX -deficiency, as already observed for 1^* and 1^{Bn} -based spheres of scaffold **B**.^[8b,9] According to $^1\text{H}, ^1\text{H}$ -COSY NMR spectroscopy, the three broad signals assigned to the $-\text{CH}_2\text{CH}_3$ protons all couple to the one broad triplet assigned to the $-\text{CH}_2\text{CH}_3$ protons. Hence, the chemical shift of the latter protons does not seem to be affected by the presence of $\{\text{CuX}\}$ vacancies, since these protons are turned away from the inorganic core of the sphere.

In the $^{31}\text{P}\{^1\text{H}\}$ NMR spectra of **3**, **6** and **7** in CD_2Cl_2 up to three broad signals at ca. 67, 75 and 110 ppm are found, sometimes accompanied by a sharp singlet at about 65 ppm. In analogy to studies based on spheres of 1^{Bn} ,^[8b] the broad signals may be assigned to incomplete spheres with $\{\text{CuX}\}$ vacancies while the sharp singlet at 65 ppm may be attributed to complete spheres $[\{1^x\}_{12}\{\text{CuX}\}_{20}]$. Moreover, in all spectra a small singlet for free 1^x (152 ppm) is present indicating some disaggregation of 1^x in solution, which is in accordance to the behavior of 1^* and 1^{Bn} based spheres of scaffold **B**.^[8b,9] For compounds **6**, also signals for encapsulated P_4S_3 are detected at -128 ppm (basal P atoms) but the signal for the apical P atom is superimposed by the broad signal of the host. Interestingly, for compounds **7**, not only the presence of $o\text{-C}_2\text{B}_{10}\text{H}_{12}$ but this time also its encapsulation can be corroborated by $^{11}\text{B}\{^1\text{H}\}$ NMR spectroscopy. In CD_2Cl_2 solution, four signals are found at about -7, -14, -19 and -20 ppm, which fit nicely to the signals observed in the $^{11}\text{B}\{^1\text{H}\}$ MAS NMR spectrum of insoluble $o\text{-C}_2\text{B}_{10}\text{H}_{12}@[\{\text{Cp}^*\text{Fe}(\eta^5\text{-P}_5)\}_{12}\{\text{CuX}\}_{20}]$

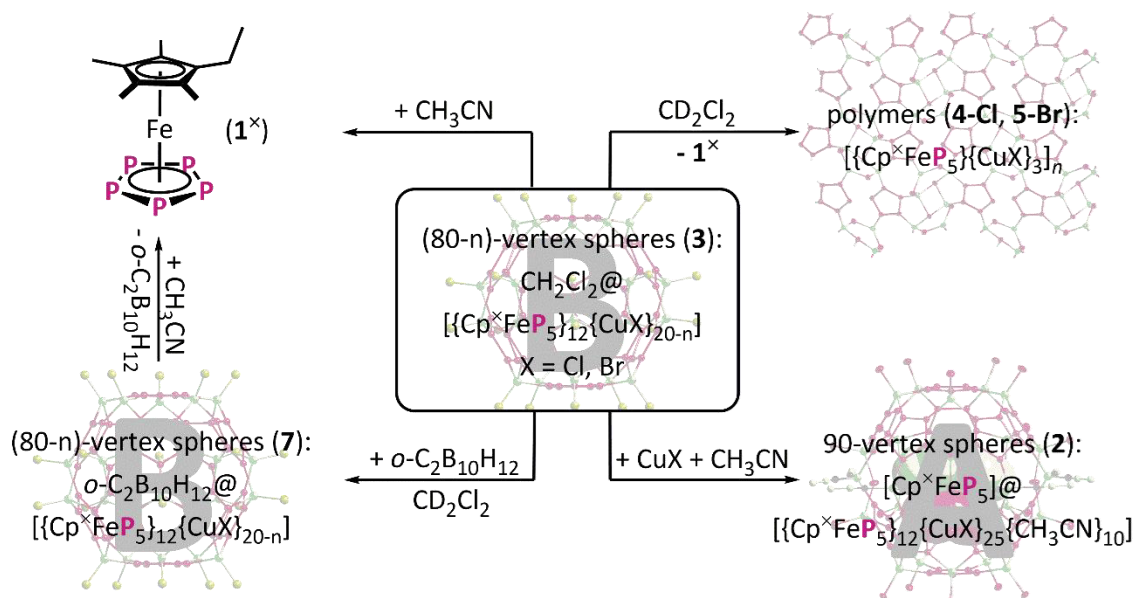
(-7.4, -14.3, -18.8 and -19.7 ppm).^[6a] Again, compared to free *o*-C₂B₁₀H₁₂, these signals are shifted upfield by about 5 ppm. This shows that *o*-C₂B₁₀H₁₂ stays encapsulated in solution.

Compounds **3**, **6** and **7** are also soluble in pyridine, however under complete disaggregation. Hence, in the respective ¹H and ³¹P{¹H} NMR spectra merely uncoordinated **1^x** is detected. For pyridine-d₅ solutions of **6**, also signals for released P₄S₃ are detected in the ³¹P{¹H} NMR spectra (-113 and 87 ppm). Analogously, *o*-C₂B₁₀H₁₂ is released by dissolving **7-Cl** in pyridine-d₅. Thus, in the ¹¹B{¹H} NMR spectrum four broad signals at -2.6, -9.2, -13.2 and -14.1 ppm for the free *o*-C₂B₁₀H₁₂ are found.

For compounds **6** and **7**, the presence of the corresponding template molecules is also confirmed by EI mass spectrometry. While for compounds **3**, only {**1^x**}⁺, {**1^x**-P₂}⁺ and solvents are detected, in the spectra of compounds **6** also P₄S₃⁺ is found. In the spectra of compounds **7**, a peak is detected at a mass/charge ratio of 142.2, corresponding to C₂B₁₀H₁₀⁺. Only once, also the expected peak at a mass/charge ratio of 144.2 for C₂B₁₀H₁₂⁺ was detected. Therefore, EI mass spectrometry was also performed on pure *o*-C₂B₁₀H₁₂ and the resulting spectrum indeed featured a main peak at 142.2, superimposed by a smaller peak at 144.2. This indicates the cleavage of two H atoms from *o*-C₂B₁₀H₁₂ to give C₂B₁₀H₁₀ under mass spectrometric conditions and thus indirectly confirms the presence of *o*-C₂B₁₀H₁₂ in all samples of compounds **7**. Remarkably, the templates are detected by EI mass spectrometry and ³¹P{¹H} or ¹¹B{¹H} NMR spectroscopy regardless of the synthesis method applied (layering vs. brief stirring vs. long stirring). For comparison, applying more than 17 vol% CD₃CN to solutions of [FeCp₂]@[Cp^{Bn}Fe(η⁵-P₅)₁₂{CuBr}_{20-n}] (Figure 1e) leads to release of [FeCp₂], being the reason why template encapsulation experiments with **1^{Bn}** were always carried out by stirring in the absence of CH₃CN.^[8b] On the contrary, the synthesis of host-guest aggregates from **1^x** is restricted to the layering approach, since the products are too insoluble for the stirring approach and rapid precipitation is observed.

Reactivity of the supramolecules

Compounds **3** (scaffold **B**) seem to be unstable in solution over time, as the polymers **4-Cl** and **5-Br** precipitate when stirring the reaction mixture longer and crystallize from the mother liquor while crystals of **3** vanish. Hence, the stability of **3** in solution and solid state was further investigated. For this purpose, compounds **3** were dissolved in CH₂Cl₂ and CH₃CN was added. Thereby, the reaction mixture turned greenish, indicating the release of uncoordinated **1^x** (Scheme 2, top left). NMR spectroscopy after one day proved the disaggregation of **1^x**, which



Scheme 2. Conversions of (80-n)-vertex spheres **3** to uncoordinated building block 1^x (top left), polymers **4-Cl** and **5-Br** (top right), 90-vertex spheres **2** (bottom right) and host guest aggregates **7** (bottom left). Grey capital letters indicate the scaffold of the formed supramolecule (**A**: 90-vertex sphere; **B**: (80-n)-vertex sphere).

was complete for **3-Cl**. Moreover, crystals of compounds **3** were also re-dissolved in pure CD_2Cl_2 and stirred for one day. While NMR spectroscopy again confirmed the disaggregation to 1^x , also a yellow solid precipitates. Presumably, this is due to the formation of polymers **4-Cl** or **5-Br**, in which the ratio of 1^x to CuX is 1:3. While the ratio in **3** is 12:(20-n) ($\geq 1:1.7$), it becomes clear that 1^x has to be released while the polymers are formed from decomposing compounds **3** (Scheme 2, top right). In contrast, the (80-n)-vertex spheres (scaffold **B**) of 1^{Bn} are stable even without template encapsulation, and polymers of 1^{Bn} with CuCl or CuBr are not known.^[8b]

In an attempt to stabilize compounds **3** in the solid state, crystals were stored under pure toluene. This way, crystals of **3** were preserved for one month without significant loss of crystallinity. On the other hand, crystals of **3** were also found to be stable in the mother liquor, as long as no precipitate is present. When, during the crystallization of **3**, also precipitate is formed and the crystals are left in this suspension, then crystals of **3** vanish with more precipitate being formed. In contrast, if some mother liquor is decanted into a different Schlenk flask without the precipitate and crystals of **3** are transferred into this mother liquor, these crystals are still present after one month. Hence, the presence of a crystallization seeds seems to be crucial for the formation of polymers **4-Cl** and **5-Br** from decomposing spheres **3**, since this transformation is only observed either in the presence of precipitate or in the presence of a stirring bar.

As compounds **3** are formed only in the absence of CH₃CN, the question arose whether 80-vertex spheres **3** (scaffold **B**) can be transformed into 90-vertex spheres **2** (scaffold **A**) by adding CuX and CH₃CN. Indeed, when a solution of the respective CuX salt in CH₃CN is added to a solution of the 80-vertex spheres **3** in CH₂Cl₂ according to the NMR spectra the corresponding 90-vertex spheres **2** are formed (scaffold **A**, Scheme 2, bottom right). Interestingly, first NMR experiments also suggest the formation of a mixed 90-vertex sphere [1^x]₁₂@[{1^x]₁₂{CuCl}_(25-y){CuI}_y{CH₃CN}₁₀] by this method (cf. Supporting Information).

Moreover, since compounds **3** show partial disaggregation releasing 1^x in CH₂Cl₂ solution, it becomes conceivable to subsequently add a template. For these experiments, *o*-C₂B₁₀H₁₂ was applied as its encapsulation is traceable by ¹¹B{¹H} NMR spectroscopy. According to the ¹¹B{¹H} NMR spectra, stirring **3** (scaffold **B**) with *o*-C₂B₁₀H₁₂ in CD₂Cl₂ results in the encapsulation of *o*-C₂B₁₀H₁₂ to give compounds **7** (scaffold **B**, Scheme 2, bottom left). On the other hand, when compounds **7** are dissolved in CH₂Cl₂ and CH₃CN is added, partial degradation of the 80-vertex spherical host (scaffold **B**) occurs and *o*-C₂B₁₀H₁₂ is being released (Scheme 2, left).

3.3 Conclusion

In conclusion, it was shown that the self-assembly of 1^x with Cu(I) halides occurs in a highly selective manner. On the one hand, new polymers **4-Cl**, **4-Cl-CH₃CN**, **5-Br** and **5-I** can be obtained. Remarkably, **4-Cl** and **4-Cl-CH₃CN** are the first pentaphosphaferrocene-based polymers comprising σ -coordination to Cu from all five P atoms, a mode otherwise only found in spherical aggregates so far. All polymers were characterized by solid state ³¹P{¹H} NMR magic angle spinning (MAS) spectroscopy, thus complementing previous MAS NMR investigations on 1^{*} based compounds with polymers comprising 1,2,3,4- and 1,2,3,4,5-coordination modes.

On the other hand, spherical aggregates are obtained including 90-vertex spheres **2** (scaffold **A**), (80-*n*)-vertex spheres **3** and template-stabilized (80-*n*)-vertex spheres **6** and **7** (scaffold **B**). The synthesis of these spherical aggregates occurs in a highly selective manner and the products are significantly more soluble than the Cp* analogues, allowing for their comprehensive characterization in solution as well as investigations on interconversions. Thus, post-synthetic encapsulation of *o*-C₂B₁₀H₁₂ into (80-*n*)-vertex spheres **3** to give template-stabilized (80-*n*)-vertex spheres **7** was observed for the first time. Remarkably, an unprecedented interconversion of the (80-*n*)-vertex scaffold of **3** to the 90-vertex scaffold of **2** was achieved upon addition of CuX salts in CH₃CN. Higher solubility had also been obtained by application of 1^{Bn} as a building block, however encapsulation into 1^{Bn}-based spherical aggregates

could be proven crystallographically only for a very limited number of templates, and 90-vertex spheres were never found. In comparison, spheres of 1^x and CuX tend to form crystals of better quality than those of 1^{Bn} , thus proving advantageous for X-ray crystallographic characterization. In summary, 1^x combines all advantages of 1^* and 1^{Bn} as a supramolecular building block concerning solubility, selectivity, versatility, template encapsulation and crystallization ease, while ruling out their respective disadvantages. Future investigations hence could profit from using 1^x as a building block. Due to the fact, that host-guest aggregates starting from 1^x are synthesizable by the stirring as well as the layering approach, more synthetic methods towards host-guest aggregates become available. Thus, the chances to obtain crystals of novel host-guest assemblies with X-ray quality are increased, being the limiting factor to this chemistry so far. Prospective research will address the synthesis of mixed-halide and mixed-metal 90-vertex spheres (scaffold **A**) and competitive displacements of templates encapsulated in (80-n)-vertex spheres (scaffold **B**) by NMR studies.

3.4 Experimental Part

General Remarks

All reactions were performed under an inert atmosphere of dry nitrogen or argon with standard vacuum, Schlenk and glove-box techniques. Solvents were purified, dried and degassed prior to use by standard procedures. $[Cp^xFe(\eta^5-P_5)]$ (1^x)^[25] and P_4S_3 were synthesized following reported procedures, although the synthesis of 1^x was performed in *meta*-diisopropylbenzene with an improved yield of 80%. $CuCl$, $CuBr$, CuI and $o-C_2B_{10}H_{12}$ are commercially available and were used without further purification. Solution NMR spectra were recorded on a BRUKER Avance 400 spectrometer. MAS NMR spectra were acquired on a Bruker Avance 300 spectrometer. Chemical shifts δ are given in [ppm] referring to external standards of tetramethylsilane (1H NMR spectra), 85% phosphoric acid ($^{31}P\{^1H\}$ NMR spectra), NaH_2PO_4 ($^{31}P\{^1H\}$ MAS NMR spectra) or $BH_3 \cdot Et_2O$ ($^{11}B\{^1H\}$ NMR spectra). ESI-MS spectra were recorded on a ThermoQuest Finnigan MAT TSQ 7000 and EI-MS spectra were recorded on a Finnigan MAT 95 mass spectrometer. Elemental analyses were performed on a Vario EL III apparatus.

Synthesis of $\{Cp^xFe(\eta^5-P_5)\}@[\{Cp^xFe(\eta^5-P_5)\}_{12}\{CuCl\}_{25}\{CH_3CN\}_{10}]\$ (**2-Cl**)

To a mixture of $[Cp^xFe(\eta^5-P_5)]$ (1^x , 49 mg, 0.14 mmol) and $CuCl$ (29 mg, 0.29 mmol) 5 mL CH_3CN and 5 mL CH_2Cl_2 were added. After stirring for ten minutes, the deeply orange-brown solution was filtered and layered with 20 mL hexane. Already after one day, large black rods of

2-Cl (within mother liquor) and yellow plates of **4-Cl-CH₃CN** (above mother liquor) crystallized. However, all attempts to obtain crystals of **2-Cl** suitable for X-ray crystallographic characterization failed. Crystals of **2-Cl** were taken from the Schlenk wall and quickly dipped into a Schlenk tube with pentane, washed with pentane (3 x 3 mL) and dried.

Analytical data of **2-Cl**:

Yield: 6 mg (0.8 μmol, 8%)

¹H NMR (CD₂Cl₂/CD₃CN): δ [ppm] = -2.52 (br), -2.43 (s), -2.36 (s), -1.81 (br), 0.72 (t, ³J_{HH} = 7.0 Hz, {Cp^xFeP₅}_{enc.+free}), 0.84 (t, ³J_{HH} = 7.0 Hz, C₆H₁₄), 0.98 (t, ³J_{HH} = 7.5 Hz, 36 H, {Cp^xFeP₅}_{sphere}), 1.26 (m, C₆H₁₄), 1.42 (br, {Cp^xFeP₅}_{enc.+free}), 1.83 (s), 1.94 (CD₃CN and {Cp^xFeP₅}_{enc.+free}), 2.18 – 2.25 (br, 144 H, {Cp^xFeP₅}_{sphere}), 2.89 – 3.04 (br, 24 H, 36 H, {Cp^xFeP₅}_{sphere}), 5.32 (CD₂Cl₂).

³¹P{¹H} NMR (CD₂Cl₂/CD₃CN): δ [ppm] = 68 (br, 60 P, {Cp^xFeP₅}_{sphere}), 149.9 (s, {Cp^xFeP₅}_{free}), 157.8 (s, 5 P, {Cp^xFeP₅}_{enc.}).

Elemental Analysis: Calculated (%) for (C₁₁H₁₇FeP₅)₁₃(CuCl)₂₅(CH₃CN)(C₆H₁₄)₂ (7368 g/mol): C 25.59, H 3.45, N 0.19; found (%): C 25.44, H 3.40, N traces.

Synthesis of {Cp^xFe(η⁵-P₅)}@[{Cp^xFe(η⁵-P₅)}]₁₂{CuBr}₂₅{CH₃CN}₁₀ (**2-Br**)^[5]

To a mixture of [Cp^xFe(η⁵-P₅)] (**1^x**, 48 mg, 0.13 mmol) and CuBr (43 mg, 0.30 mmol) 3 mL CH₃CN and 7 mL CH₂Cl₂ were added. After stirring for ten minutes, the deeply orange-brown solution was filtered and layered with 15 mL hexane. Already after one day, large black rods of **2-Br** crystallized. The crystals were taken from the Schlenk wall with a spatula and quickly dipped into a Schlenk flask with pentane, washed with pentane (3 x 3 mL) and dried.

Analytical data of **2-Br**:

Yield: 42 mg (4.9 μmol, 48%)

¹H NMR (CD₂Cl₂/CD₃CN): δ [ppm] = -3.26 (br), -2.01 (br), -1.35 (br), 0.72 (t, ³J_{HH} = 7.3 Hz, {Cp^xFeP₅}_{enc.+free}), 0.85 (t, ³J_{HH} = 6.9 Hz, C₆H₁₄), 0.98 (t, ³J_{HH} = 7.5 Hz, 36 H, {Cp^xFeP₅}_{sphere}), 1.25 (m, C₆H₁₄), 1.41 (br, {Cp^xFeP₅}_{enc.+free}), 1.83 (s), 1.92 (CD₃CN and {Cp^xFeP₅}_{enc.+free}), 2.22 – 2.26 (br, 144 H, {Cp^xFeP₅}_{sphere}), 2.96 – 3.09 (br, 24 H, 36 H, {Cp^xFeP₅}_{sphere}), 5.32 (CD₂Cl₂).

³¹P{¹H} NMR (CD₂Cl₂/CD₃CN): δ [ppm] = 68 (br, 60 P, {Cp^xFeP₅}_{sphere}), 150.4 (s, {Cp^xFeP₅}_{free}), 160.8 (s, 5 P, {Cp^xFeP₅}_{enc.}).

Elemental Analysis: Calculated (%) for (C₁₁H₁₇FeP₅)₁₃(CuBr)₂₅(CH₃CN)₂(C₆H₁₄)₂ (8520 g/mol): C 22.41, H 3.02, N 0.33; found (%): C 22.38, H 2.86, N 0.29.

Synthesis of $(\text{CH}_2\text{Cl}_2)_m@[\{\text{Cp}^*\text{Fe}(\eta^5\text{-P}_5)\}_{12}\{\text{CuCl}\}_{20-n}]$ (**3-Cl**)

$[\text{Cp}^*\text{Fe}(\eta^5\text{-P}_5)]$ (**1**^{*}, 54 mg, 0.15 mmol) and CuCl (30 mg, 0.30 mmol) were dissolved in 7 mL CH_2Cl_2 and stirred for 45 minutes. After filtration, the orange solution was layered with 15 mL toluene. After complete diffusion the mother liquor was decanted and the black cubic crystals of **3-Cl** were washed with toluene (3 x 5 mL) and pentane (3 x 5 mL) and dried.

Analytical data of **3-Cl**:

Yield: 50 mg (7.8 μmol , 62%).

^1H NMR (CD_2Cl_2): δ [ppm] = 1.08 (br, 36 H, $-\text{C}_5\text{Me}_4\text{CH}_2\text{CH}_3$), 2.09 – 2.26 (144 H, $-\text{C}_5\text{Me}_4\text{Et}$), 2.34 (s, C_7H_8), 2.85 – 2.96 (m, 24 H, $-\text{C}_5\text{Me}_4\text{CH}_2\text{CH}_3$), 5.33 (CH_2Cl_2), 7.14 – 7.26 (m; C_7H_8).

$^{31}\text{P}\{^1\text{H}\}$ NMR (CD_2Cl_2): δ [ppm] = 67.8, 75 (br), 109 (br), 151.5 (s, $[\text{Cp}^*\text{Fe}(\eta^5\text{-P}_5)]$).

^1H NMR (pyridine- d_5): δ [ppm] = 0.65 (t, $^3J_{\text{HH}} = 7.6$ Hz, 3 H, Cp^*FeP_5), 1.37 (s, 6 H, Cp^*FeP_5), 1.40 (s, 6 H, Cp^*FeP_5), 1.92 (q, $^3J_{\text{HH}} = 7.6$ Hz, 2 H, Cp^*FeP_5), 2.22 (s, C_7H_8), 5.69 (s, CH_2Cl_2), 7.16 – 7.30 (m; C_7H_8).

$^{31}\text{P}\{^1\text{H}\}$ NMR (pyridine- d_5): δ [ppm] = 146.2 (s, $[\text{Cp}^*\text{Fe}(\eta^5\text{-P}_5)]$).

Positive ion ESI-MS (CH_2Cl_2 , CH_3CN): m/z = 980.6062 $[(\text{Cp}^*\text{FeP}_5)_2\text{Cu}_3\text{Cl}_2]^+$, 882.7082 $[(\text{Cp}^*\text{FeP}_5)_2\text{Cu}_2\text{Cl}]^+$, 782.8104 $[(\text{Cp}^*\text{FeP}_5)_2\text{Cu}]^+$, 504.9241 $[(\text{Cp}^*\text{FeP}_5)\text{Cu}(\text{CH}_3\text{CN})_2]^+$, 463.8972 $[(\text{Cp}^*\text{FeP}_5)\text{Cu}(\text{CH}_3\text{CN})]^+$, 422.8693 $[(\text{Cp}^*\text{FeP}_5)\text{Cu}]^+$.

Negative ion ESI-MS (CH_2Cl_2 , CH_3CN): m/z = 332.6571 $[\text{Cu}_3\text{Cl}_4]^-$, 232.7623 $[\text{Cu}_2\text{Cl}_3]^-$, 134.8647 $[\text{CuCl}_2]^-$.

EI-MS (70 eV): m/z = 359.9340 $[\text{Cp}^*\text{FeP}_5]^+$, 297.9864 $[(\text{Cp}^*\text{FeP}_5)\text{-P}_2]^+$, 92.0586 (C_7H_8)⁺.

Elemental Analysis: Calculated (%) for $(\text{C}_{11}\text{H}_{17}\text{FeP}_5)_{12}(\text{CuCl})_{17}(\text{C}_7\text{H}_8)_2(\text{CH}_2\text{Cl}_2)_3$ (6441 g/mol): C 27.78, H 3.54; found (%): C 27.61, H 3.61.

Synthesis of $(\text{CH}_2\text{Cl}_2)_m@[\{\text{Cp}^*\text{Fe}(\eta^5\text{-P}_5)\}_{12}\{\text{CuBr}\}_{20-n}]$ (**3-Br**)

$[\text{Cp}^*\text{Fe}(\eta^5\text{-P}_5)]$ (**1**^{*}, 47 mg, 0.13 mmol) and CuBr (40 mg, 0.28 mmol) were dissolved in 7 mL CH_2Cl_2 and stirred for 40 minutes. After filtration, the orange solution was layered with 9 mL toluene. After complete diffusion the mother liquor was decanted and the black cubic crystals of **3-Br** were washed with toluene (3 x 5 mL) and pentane (3 x 5 mL) and dried.

Analytical data of **3-Br**:

Yield: 56 mg (7.7 μmol , 71%)

^1H NMR (CD_2Cl_2): δ [ppm] = 1.08 (br, 36 H, $-\text{C}_5\text{Me}_4\text{CH}_2\text{CH}_3$), 2.13 – 2.33 (144 H, $-\text{C}_5\text{Me}_4\text{Et}$), 2.34 (s, C_7H_8), 2.92 – 3.07 (m, 24 H, $-\text{C}_5\text{Me}_4\text{CH}_2\text{CH}_3$), 5.33 (CH_2Cl_2), 7.12 – 7.26 (m, C_7H_8).

$^{31}\text{P}\{^1\text{H}\}$ NMR (CD_2Cl_2): δ [ppm] = 64.9, 65 (br), 74 (br), 107 (br), 151.6 (s, $[\text{Cp}^*\text{Fe}(\eta^5\text{-P}_5)]$).

¹H NMR (pyridine-d₅): δ [ppm] = 0.65 (t, ³J_{HH} = 7.6 Hz, 3 H, Cp^xFeP₅), 1.37 (s, 6 H, Cp^xFeP₅), 1.39 (s, 6 H, Cp^xFeP₅), 1.91 (q, ³J_{HH} = 7.6 Hz, 2 H, Cp^xFeP₅), 2.22 (s, C₇H₈), 5.68 (s, CH₂Cl₂), 7.16 – 7.30 (m; C₇H₈).

³¹P{¹H} NMR (pyridine-d₅): δ [ppm] = 146.7 (s, [Cp^xFe(η⁵-P₅)]).

Positive ion ESI-MS (CH₂Cl₂, CH₃CN): *m/z* = 1070.4954 [(Cp^xFeP₅)₂Cu₃Br₂]⁺, 926.6508 [(Cp^xFeP₅)₂Cu₂Br]⁺, 782.8043 [(Cp^xFeP₅)₂Cu]⁺, 607.7387 [(Cp^xFeP₅)Cu₂Br(CH₃CN)]⁺, 566.7123 [(Cp^xFeP₅)Cu₂Br]⁺, 504.9201 [(Cp^xFeP₅)Cu(CH₃CN)₂]⁺, 463.8934 [(Cp^xFeP₅)Cu(CH₃CN)]⁺.

Negative ion ESI-MS (CH₂Cl₂, CH₃CN): *m/z* = 939.9872 [Cu₆Br₇]⁻, 796.1431 [Cu₅Br₆]⁻, 654.2966 [Cu₄Br₅]⁻, 510.4520 [Cu₃Br₄]⁻, 366.6081 [Cu₂Br₃]⁻, 322.6583 [Cu₂ClBr₂]⁻, 222.7634 [CuBr₂]⁻, 178.8139 [CuClBr]⁻.

EI-MS (70 eV): *m/z* = 359.9346 [Cp^xFeP₅]⁺, 297.9867 [(Cp^xFeP₅)-P₂]⁺, 92.0595 (C₇H₈)⁺, 83.9510 (CH₂Cl₂)⁺.

Elemental Analysis: Calculated (%) for (C₁₁H₁₇FeP₅)₁₂(CuBr)₁₇(C₇H₈)₃(CH₂Cl₂)₃ (7290 g/mol): C 25.70, H 3.24; found (%): C 25.76, H 3.19.

Synthesis of [(Cp^xFe(η⁵-P₅))₃(CuCl)₃] (4-Cl) and [(Cp^xFe(η⁵-P₅))₂(CuCl)₆(CH₃CN)]·CH₃CN (4-Cl-CH₃CN)

[Cp^xFe(η⁵-P₅)] (**1^x**, 101 mg, 0.281 mmol) and CuCl (83 mg, 0.83 mmol) were dissolved in 15 mL CH₂Cl₂ and stirred for 4 d. The suspension was filtered over a G4 frit, the precipitate washed with CH₂Cl₂ (3 x 10 mL) and CH₃CN (3 x 10 mL) and dried. Elemental analysis suggests a mixture of **4-Cl** and **4-Cl-CH₃CN** (3:1) has formed. Presumably, **4-Cl** reacts with CH₃CN while washing to give **4-Cl-CH₃CN**. However, washing with CH₃CN is crucial to remove residual unreacted CuCl.

Crystals of **4-Cl** were obtained by stirring [Cp^xFe(η⁵-P₅)] (**1^x**, 20 mg, 0.056 mmol) and CuCl (11 mg, 0.11 mmol) in 8 mL CH₂Cl₂ only for 1.5 hrs, filtering and layering with 10 mL toluene. While after 2 d crystals of **3-Cl** were obtained, after one month instead crystals of **4-Cl** were present.

Analytical data of **4-Cl** and **4-Cl-CH₃CN**:

Yield (precipitated): 134 mg (0.201 mmol, 72% for (C₁₁H₁₇FeP₅)(CuCl)₃(CH₃CN)_{0.25})

³¹P{¹H} MAS NMR: δ [ppm] = 0 – 60 (br, at least 3 signals superimposed), 70 – 110 (br, at least two signals superimposed).

¹H NMR (pyridine-d₅): δ [ppm] = 0.66 (t, ³J_{HH} = 7.6 Hz, 3 H, Cp^xFeP₅), 1.47 (s, 6 H, Cp^xFeP₅), 1.49 (s, 6 H, Cp^xFeP₅), 1.86 (s, CH₃CN), 2.03 (q, ³J_{HH} = 7.6 Hz, 2 H, Cp^xFeP₅), 5.69 (s, CH₂Cl₂).

³¹P{¹H} NMR (pyridine-d₅): δ [ppm] = 131.0 (s, [Cp^xFe(η⁵-P₅)]).

Positive ion ESI-MS (CH₂Cl₂, CH₃CN):^[26] $m/z = 980.5983$ [(Cp^xFeP₅)₂Cu₃Cl₂]⁺, 882.7007 [(Cp^xFeP₅)₂Cu₂Cl]⁺, 782.8047 [(Cp^xFeP₅)₂Cu]⁺, 620.6613 [(Cp^xFeP₅)Cu₃Cl₂]⁺, 601.8056 [(Cp^xFeP₅)Cu₂Cl(NC₅H₅)]⁺, 563.7899 [(Cp^xFeP₅)Cu₂Cl(CH₃CN)]⁺, 522.7629 [(Cp^xFeP₅)Cu₂Cl]⁺, 501.9087 [(Cp^xFeP₅)Cu(NC₅H₅)]⁺, 463.8933 [(Cp^xFeP₅)Cu(CH₃CN)]⁺, 422.8661 [(Cp^xFeP₅)Cu]⁺.

Negative ion ESI-MS (CH₂Cl₂, CH₃CN):^[26] $m/z = 332.6592$ [Cu₃Cl₄]⁻, 232.7632 [Cu₂Cl₃]⁻, 134.8651 [CuCl₂]⁻.

Elemental Analysis: Calculated (%) for (C₁₁H₁₇FeP₅)(CuCl)₃(CH₃CN)_{0.25} (667.2 g/mol): C 20.70, H 2.68, N 0.52 ; found (%): C 20.87, H 2.65, N 0.3.

Synthesis of [(Cp^xFe(η⁵-P₅))₂{CuCl}₆{CH₃CN}]-CH₃CN (4-Cl-CH₃CN)

Crystals of **4-Cl-CH₃CN** were obtained by layering a solution of [Cp^xFe(η⁵-P₅)] (**1^x**, 30 mg, 0.083 mmol) in 5 mL toluene with a solution of CuCl (25 mg, 0.25 mmol) in 5 mL CH₃CN. After four months crystals of **4-Cl-CH₃CN** were formed. The crystals were taken from the Schlenk wall with a spatula and quickly dipped into a Schlenk tube with CH₂Cl₂, washed with CH₂Cl₂ (3 x 3 mL) and dried.

Analytical data of **4-Cl-CH₃CN**:

Yield: 34 mg (0.024 mmol, 58%)

Elemental Analysis: Calculated (%) for (C₁₁H₁₇FeP₅)₂(CuCl)₆(CH₃CN)₂ (1396 g/mol): C 22.37, H 2.89, N 2.01; found (%): C 22.46, H 2.84, N 1.88.

Crystals of **4-Cl-CH₃CN** were also obtained by layering a solution of [Cp^xFe(η⁵-P₅)] (**1^x**, 46 mg, 0.13 mmol) in 5 mL CH₂Cl₂ with a solution of CuCl (30 mg, 0.30 mmol) in 4 mL CH₃CN. While after one week crystals of **2-Cl** were obtained, after one month instead crystals of **4-Cl-CH₃CN** were present.

Synthesis of [(Cp^xFe(η⁵-P₅))₂{CuBr}₃] (5-Br)

[Cp^xFe(η⁵-P₅)] (**1^x**, 102 mg, 0.283 mmol) and CuBr (120 mg, 0.837 mmol) were dissolved in 15 mL CH₂Cl₂ and stirred for 4 d. The suspension was filtered over a G4 frit, the precipitate washed with CH₂Cl₂ (3 x 10 mL) and CH₃CN (3 x 10 mL) and dried.

Few crystals of **5-Br** could be obtained by layering the combined washing liquors with toluene. Alternatively, crystals of **5-Br** were obtained by stirring [Cp^xFe(η⁵-P₅)] (**1^x**, 20 mg, 0.053 mmol) and CuBr (19 mg, 0.11 mmol) in 10 mL CH₂Cl₂ only for 1.5 hrs, filtering and layering with 10 mL toluene. After two weeks, only crystals **5-Br** were present.

Analytical data of **5-Br**:

Yield (precipitated): 169 mg (0.214 mmol, 77%)

$^{31}\text{P}\{^1\text{H}\}$ MAS NMR: δ [ppm] = 20 – 90 (br, 4 P), 107 (t, 1 P).

^1H NMR (pyridine- d_5): δ [ppm] = 0.66 (t, $^3J_{\text{HH}} = 7.6$ Hz, 3 H, Cp^*FeP_5), 1.39 (s, 6 H, Cp^*FeP_5), 1.42 (s, 6 H, Cp^*FeP_5), 1.95 (q, $^3J_{\text{HH}} = 7.6$ Hz, 2 H, Cp^*FeP_5), 5.70 (s, CH_2Cl_2).

$^{31}\text{P}\{^1\text{H}\}$ NMR (pyridine- d_5): δ [ppm] = 144.0 (s, [$\text{Cp}^*\text{Fe}(\eta^5\text{-P}_5)$]).

Positive ion ESI-MS (CH_2Cl_2 , CH_3CN):^[26] $m/z = 1070.4942$ [$(\text{Cp}^*\text{FeP}_5)_2\text{Cu}_3\text{Br}_2$]⁺, 782.8024 [$(\text{Cp}^*\text{FeP}_5)_2\text{Cu}$]⁺, 722.7796 [$(\text{Cp}^*\text{FeP}_5)\text{Cu}_2\text{Br}(\text{NC}_5\text{H}_5)$]⁺, 710.5572 [$(\text{Cp}^*\text{FeP}_5)\text{Cu}_3\text{Br}_2$]⁺, 645.7539 [$(\text{Cp}^*\text{FeP}_5)\text{Cu}_2\text{Br}(\text{NC}_5\text{H}_5)$]⁺, 607.7379 [$(\text{Cp}^*\text{FeP}_5)\text{Cu}_2\text{Br}(\text{CH}_3\text{CN})$]⁺, 566.7115 [$(\text{Cp}^*\text{FeP}_5)\text{Cu}_2\text{Br}$]⁺, 501.9079 [$(\text{Cp}^*\text{FeP}_5)\text{Cu}(\text{NC}_5\text{H}_5)$]⁺, 463.8924 [$(\text{Cp}^*\text{FeP}_5)\text{Cu}(\text{CH}_3\text{CN})$]⁺, 227.0354 [$\text{Cu}(\text{CH}_3\text{CN})_4$]⁺.

Negative ion ESI-MS (CH_2Cl_2 , CH_3CN):^[26] $m/z = 510.4565$ [Cu_3Br_4]⁻, 366.6107 [Cu_2Br_3]⁻, 222.7655 [CuBr_2]⁻, 178.8153 [CuClBr]⁻.

Elemental Analysis: Calculated (%) for $(\text{C}_{11}\text{H}_{17}\text{FeP}_5)(\text{CuBr})_3$ (790.3 g/mol): C 16.72, H 2.17, N 0; found (%): C 16.70, H 2.05, N 0.

Synthesis of [$\text{Cp}^*\text{Fe}(\eta^5\text{-P}_5)\{\text{CuI}\}_3$] (**5-I**)

A solution of [$\text{Cp}^*\text{Fe}(\eta^5\text{-P}_5)$] (**1^x**, 50 mg, 0.14 mmol) in 10 mL CH_2Cl_2 was layered with a solution of CuI (83 mg, 0.44 mmol) in 15 mL CH_3CN . After complete diffusion, the mother liquor was decanted. The crystals were washed with toluene (3 x 5 mL) and pentane (3 x 5 mL) and dried.

Analytical data of **5-I**:

Yield: 106 mg (0.114 mmol, 82%)

$^{31}\text{P}\{^1\text{H}\}$ MAS NMR: δ [ppm] = 20 – 90 (br, 4 P), 113 (t, 1 P).

^1H NMR (pyridine- d_5): δ [ppm] = 0.64 (t, $^3J_{\text{HH}} = 7.6$ Hz, 3 H, Cp^*FeP_5), 1.35 (s, 6 H, Cp^*FeP_5), 1.38 (s, 6 H, Cp^*FeP_5), 1.89 (q, $^3J_{\text{HH}} = 7.6$ Hz, 2 H, Cp^*FeP_5), 5.69 (s, CH_2Cl_2).

$^{31}\text{P}\{^1\text{H}\}$ NMR (pyridine- d_5): δ [ppm] = 149.0 (s, [$\text{Cp}^*\text{Fe}(\eta^5\text{-P}_5)$]).

Positive ion ESI-MS (CH_3CN):^[27] $m/z = 1164.4675$ [$(\text{Cp}^*\text{FeP}_5)_2\text{Cu}_3\text{I}_2$]⁺, 972.6360 [$(\text{Cp}^*\text{FeP}_5)_2\text{Cu}_2\text{I}$]⁺, 804.5320 [$(\text{Cp}^*\text{FeP}_5)\text{Cu}_3\text{I}_2$]⁺, 782.8027 [$(\text{Cp}^*\text{FeP}_5)_2\text{Cu}$]⁺, 653.7263 [$(\text{Cp}^*\text{FeP}_5)\text{Cu}_2\text{I}(\text{CH}_3\text{CN})$]⁺, 612.7000 [$(\text{Cp}^*\text{FeP}_5)\text{Cu}_2\text{I}$]⁺, 504.9109 [$(\text{Cp}^*\text{FeP}_5)\text{Cu}(\text{CH}_3\text{CN})_2$]⁺, 463.8930 [$(\text{Cp}^*\text{FeP}_5)\text{Cu}(\text{CH}_3\text{CN})$]⁺.

Negative ion ESI-MS (CH_3CN):^[27] $m/z = 698.4079$ [Cu_3I_4]⁻, 506.5751 [Cu_2I_3]⁻, 316.7408 [CuI_2]⁻, 224.8046 [CuClI]⁻, 134.8662 [CuCl_2]⁻, 126.9060 (I⁻).

Elemental Analysis: Calculated (%) for $(\text{C}_{11}\text{H}_{17}\text{FeP}_5)(\text{CuI})_3$ (931.3 g/mol): C 14.19, H 1.84, N 0; found (%): C 14.33, H 1.78, N 0.

Synthesis of $(P_4S_3)_m@[\{Cp^*Fe(\eta^5-P_5)\}_{12}\{CuCl\}_{20-n}]$ (**6-Cl**)

Method A (layering = **6a-Cl**):

A solution of $[Cp^*Fe(\eta^5-P_5)]$ (**1^x**, 26 mg, 0.072 mmol) and P_4S_3 (13 mg, 0.059 mmol) in 10 mL CH_2Cl_2 was layered with a solution of $CuCl$ (20 mg, 0.20 mmol) in 10 mL CH_3CN . After complete diffusion, the mother liquor was decanted together with the orange precipitate. The crystals **6a-Cl** were washed with toluene (3 x 5 mL) and pentane (3 x 5 mL) and dried.

Analytical data of **6a-Cl**:

Yield: 23 mg (3.9 μ mol, 64%).

1H NMR (CD_2Cl_2): δ [ppm] = 1.08 (t, 36 H, $-C_5Me_4CH_2CH_3$), 2.10 – 2.27 (144 H, C_5Me_4Et), 2.34 (s, C_7H_8), 2.85 – 2.97 (m, 24 H, $C_5Me_4CH_2CH_3$), 5.32 (CH_2Cl_2), 7.14 – 7.26 (m, C_7H_8).

$^{31}P\{^1H\}$ NMR (CD_2Cl_2): δ [ppm] = -128.0 (P_4S_3 , basal), 66.6 (br), 68.0 (P_4S_3 , apical), 68.4 (br), 75 (br), 111 (br), 151.7 (s, $[Cp^*FeP_5]_{free}$).

1H NMR (pyridine- d_5): δ [ppm] = 0.65 (t, $^3J_{HH} = 7.6$ Hz, 3 H, Cp^*FeP_5), 1.37 (s, 6 H, Cp^*FeP_5), 1.40 (s, 6 H, Cp^*FeP_5), 1.92 (q, $^3J_{HH} = 7.6$ Hz, 2 H, Cp^*FeP_5), 2.22 (s, C_7H_8), 5.68 (s, CH_2Cl_2), 7.16 – 7.30 (m; C_7H_8).

$^{31}P\{^1H\}$ NMR (pyridine- d_5): δ [ppm] = -113.4 (d, $^2J_{PP} = 59$ Hz, P_4S_3 , basal), 146.1 (s, $[Cp^*Fe(\eta^5-P_5)]$).

Positive ion ESI-MS (CH_2Cl_2 , CH_3CN): $m/z = 980.5976$ $[(Cp^*FeP_5)_2Cu_3Cl_2]^+$, 882.7006 $[(Cp^*FeP_5)_2Cu_2Cl]^+$, 782.8042 $[(Cp^*FeP_5)_2Cu]^+$, 563.7893 $[(Cp^*FeP_5)Cu_2Cl(CH_3CN)]^+$, 522.7625 $[(Cp^*FeP_5)Cu_2Cl]^+$, 504.9193 $[(Cp^*FeP_5)Cu(CH_3CN)_2]^+$, 463.8933 $[(Cp^*FeP_5)Cu(CH_3CN)]^+$, 422.8660 $[(Cp^*FeP_5)Cu]^+$.

Negative ion ESI-MS (CH_2Cl_2 , CH_3CN): $m/z = 232.7648$ $[Cu_2Cl_3]^-$, 134.8663 $[CuCl_2]^-$.

EI-MS (70 eV): $m/z = 359.9348$ $[Cp^*FeP_5]^+$, 297.9866 $[(Cp^*FeP_5)-P_2]^+$, 219.8083 $[P_4S_3]^+$, 92.0589 (C_7H_8) $^+$.

Elemental Analysis: Calculated (%) for $(P_4S_3)(C_{11}H_{17}FeP_5)_{12}(CuCl)_{14}$ (5926 g/mol): C 26.76, H 3.47, N 0, S 1.62; found (%): C 26.80, H 3.45, N 0, S 1.48.

Method B (stirring briefly = **6b-Cl**):

$[Cp^*Fe(\eta^5-P_5)]$ (**1^x**, 30 mg, 0.083 mmol), P_4S_3 (10 mg, 0.045 mmol) and $CuCl$ (20 mg, 0.20 mmol) were stirred in 10 mL CH_2Cl_2 for 2.5 hours. The red solution was filtered from the yellow precipitate and layered with 17 mL toluene. After complete diffusion, the mother liquor was decanted. The crystals of **6b-Cl** were washed with toluene (5 x 5 mL) and hexane (3 x 5 mL) and dried.

Analytical data of **6b-Cl**:

Yield: 19 mg (3.1 μ mol, 45%)

¹H NMR (CD₂Cl₂): δ [ppm] = 1.08 (t, 36 H, -C₅Me₄CH₂CH₃), 2.10 – 2.27 (144 H, C₅Me₄Et), 2.34 (s, C₇H₈), 2.75 – 2.98 (24 H, C₅Me₄CH₂CH₃), 5.33 (CH₂Cl₂), 7.14 – 7.26 (m, C₇H₈).

³¹P{¹H} NMR (CD₂Cl₂): δ [ppm] = -128.3 (P₄S_{3, basal}), 66.2 (P₄S_{3, apical}), 69 (br, [Cp^xFeP₅]_{host}), 77 (br, [Cp^xFeP₅]_{host}), 111 (br, [Cp^xFeP₅]_{host}), 151.9 (s, [Cp^xFeP₅]_{free}).

¹H NMR (pyridine-d₅): δ [ppm] = 0.65 (t, ³J_{HH} = 7.6 Hz, 3 H, Cp^xFeP₅), 1.36 (s, 6 H, Cp^xFeP₅), 1.39 (s, 6 H, Cp^xFeP₅), 1.91 (q, ³J_{HH} = 7.6 Hz, 2 H, Cp^xFeP₅), 2.22 (s, C₇H₈), 5.68 (s, CH₂Cl₂), 7.16 – 7.30 (m; C₇H₈).

³¹P{¹H} NMR (pyridine-d₅): δ [ppm] = -113.4 (d, ²J_{PP} = 59 Hz, P₄S_{3, basal}), 147.1 (s, [Cp^xFe(η⁵-P₅)]).

EI-MS (70 eV): *m/z* = 359.9240 [Cp^xFeP₅]⁺, 297.9779 [(Cp^xFeP₅)-P₂]⁺, 219.8016 [P₄S₃]⁺, 92.0563 (C₇H₈)⁺.

Elemental Analysis: Calculated (%) for (P₄S₃)(C₁₁H₁₇FeP₅)₁₂(CuCl)_{15.5} (6074 g/mol): C 26.10, H 3.39, N 0, S 1.58; found (%): C 26.05, H 3.40, N 0, S 1.48.

Synthesis of (P₄S₃)_m@[{Cp^xFe(η⁵-P₅)}]₁₂{CuBr}_{20-n} (6-Br)

Method A (layering = 6a-Br and 6a'-Br):

A solution of [Cp^xFe(η⁵-P₅)] (**1**^x, 30 mg, 0.083 mmol) and P₄S₃ (12 mg, 0.055 mmol) in 8 mL CH₂Cl₂ was layered with a solution of CuBr (24 mg, 0.17 mmol) in 7 mL CH₃CN. After complete diffusion, the mother liquor was decanted together with the yellow precipitate. The crystals of **6a-Br** and **6a'-Br** were washed with a mixture of CH₂Cl₂ / CH₃CN (2:1, 3 x 10 mL) and pentane (3 x 5 mL) and dried.

Analytical data of **6a-Br** and **6a'-Br**:

Yield: 25 mg (3.7 μmol, 53%)

¹H NMR (CD₂Cl₂): δ [ppm] = 1.07 (br, 36 H, -C₅Me₄CH₂CH₃), 2.13 – 2.32 (144 H, -C₅Me₄Et), 2.81 – 3.08 (m, 24 H, -C₅Me₄CH₂CH₃), 5.33 (CH₂Cl₂).

³¹P{¹H} NMR (CD₂Cl₂): δ [ppm] = -128.3 (d, P₄S_{3, basal}), 66.1 (br), 73 (br), 109 (br), 151.8 (s, [Cp^xFe(η⁵-P₅)]_{free}).

¹H NMR (pyridine-d₅): δ [ppm] = 0.64 (t, ³J_{HH} = 7.6 Hz, 3 H, Cp^xFeP₅), 1.35 (s, 6 H, Cp^xFeP₅), 1.38 (s, 6 H, Cp^xFeP₅), 1.89 (q, ³J_{HH} = 7.6 Hz, 2 H, Cp^xFeP₅), 2.22 (s, C₇H₈), 5.68 (s, CH₂Cl₂), 7.18 – 7.28 (m; C₇H₈).

³¹P{¹H} NMR (pyridine-d₅): δ [ppm] = -113.2 (d, ²J_{PP} = 59 Hz, P₄S_{3, basal}), 86.7 (P₄S_{3, apical})^{*}, 149.0 (s, [Cp^xFe(η⁵-P₅)]). ^{*}Signal almost below noise floor

Positive ion ESI-MS (CH₂Cl₂, CH₃CN): *m/z* = 1070.4946 [(Cp^xFeP₅)₂Cu₃Br₂]⁺, 926.6500 [(Cp^xFeP₅)₂Cu₂Br]⁺, 782.8044 [(Cp^xFeP₅)₂Cu]⁺, 607.7384 [(Cp^xFeP₅)Cu₂Br(CH₃CN)]⁺, 566.7120 [(Cp^xFeP₅)Cu₂Br]⁺, 504.9197 [(Cp^xFeP₅)Cu(CH₃CN)₂]⁺, 463.8931 [(Cp^xFeP₅)Cu(CH₃CN)]⁺.

Negative ion ESI-MS (CH₂Cl₂, CH₃CN): m/z = 796.1503 [Cu₅Br₆]⁻, 654.3024 [Cu₄Br₅]⁻, 510.4565 [Cu₃Br₄]⁻, 366.6108 [Cu₂Br₃]⁻, 322.6612 [Cu₂ClBr₂]⁻, 222.7649 [CuBr₂]⁻, 178.8155 [CuClBr]⁻, 134.8654 [CuCl₂]⁻.

EI-MS (70 eV): m/z = 359.9424 [Cp[×]FeP₅]⁺, 297.9935 [(Cp[×]FeP₅)-P₂]⁺, 219.8142 [P₄S₃]⁺.

Elemental Analysis: Calculated (%) for (P₄S₃)(C₁₁H₁₇FeP₅)₁₂(CuBr)_{15.5} (6763 g/mol): C 23.44, H 3.04, N 0, S 1.42; found (%): C 23.48, H 3.10, N 0, S 1.53.

Method B (stirring briefly = **6b-Br**)

[Cp[×]Fe(η⁵-P₅)] (**1**[×], 30 mg, 0.083 mmol), P₄S₃ (9 mg, 0.041 mmol) and CuBr (27 mg, 0.19 mmol) were stirred in 10 mL CH₂Cl₂ for 2.5 hours. The red solution was filtered from the yellow precipitate and layered with 17 mL toluene. After complete diffusion, the mother liquor was decanted. The crystals of **6b-Br** were washed with toluene (3 x 5 mL) and hexane (3 x 5 mL) and dried.

Analytical data of **6b-Br**:

Yield: 30 mg (4.4 μmol, 63%)

¹H NMR (CD₂Cl₂): δ [ppm] = 1.08 (br, 36 H, -C₅Me₄CH₂CH₃), 2.13 – 2.33 (144 H, -C₅Me₄Et), 2.34 (s, C₇H₈), 2.91 – 3.10 (m, 24 H, -C₅Me₄CH₂CH₃), 5.33 (CH₂Cl₂), 7.12 – 7.26 (m, C₇H₈).

³¹P{¹H} NMR (CD₂Cl₂): δ [ppm] = -128.3 (P₄S_{3, basal}), 65.6 (P₄S_{3, apical}), 66.0 ([Cp[×]Fe(η⁵-P₅)]_{host}), 74 (br, [Cp[×]Fe(η⁵-P₅)]_{host}), 109 (br, [Cp[×]Fe(η⁵-P₅)]_{host}), 151.8 (s, [Cp[×]Fe(η⁵-P₅)]_{free}).

¹H NMR (pyridine-d₅): δ [ppm] = 0.64 (t, ³J_{HH} = 7.6 Hz, 3 H, Cp[×]FeP₅), 1.36 (s, 6 H, Cp[×]FeP₅), 1.39 (s, 6 H, Cp[×]FeP₅), 1.90 (q, ³J_{HH} = 7.6 Hz, 2 H, Cp[×]FeP₅), 2.22 (s, C₇H₈), 5.68 (s, CH₂Cl₂), 7.16 – 7.30 (m; C₇H₈).

³¹P{¹H} NMR (pyridine-d₅): δ [ppm] = -113.1 (d, ²J_{PP} = 59 Hz, P₄S_{3, basal}), 87.4 (P₄S_{3, apical})*, 147.7 (s, [Cp[×]Fe(η⁵-P₅)]). *Signal almost below noise floor

EI-MS (70 eV): m/z = 359.9366 [Cp[×]FeP₅]⁺, 297.9884 [(Cp[×]FeP₅)-P₂]⁺, 219.8094 [P₄S₃]⁺.

Elemental Analysis: Calculated (%) for (P₄S₃)(C₁₁H₁₇FeP₅)₁₂(CuBr)₁₆ (6835 g/mol): C 23.20, H 3.01, N 0, S 1.41; found (%): C 23.29, H 2.95, N 0, S 1.38.

Method C (stirring longer = **6b-Br**)

[Cp[×]Fe(η⁵-P₅)] (**1**[×], 30 mg, 0.083 mmol), P₄S₃ (9 mg, 0.041 mmol) and CuBr (24 mg, 0.17 mmol) were stirred in 10 mL CH₂Cl₂ for three days. The red solution was filtered from the yellow precipitate and layered with 10 mL toluene. After complete diffusion, the mother liquor was decanted. The crystals of **6b-Br** were washed with toluene (3 x 10 mL) and pentane (3 x 5 mL) and dried.

Analytical data of **6b-Br**:

Yield: 6 mg (0.81 μmol , 12%)

EI-MS (70 eV): m/z = 359.9372 $[\text{Cp}^*\text{FeP}_5]^+$, 297.9891 $[(\text{Cp}^*\text{FeP}_5)\text{-P}_2]^+$, 219.8106 $(\text{P}_4\text{S}_3)^+$.

Synthesis of $(o\text{-C}_2\text{B}_{10}\text{H}_{12})_m@[\{\text{Cp}^*\text{Fe}(\eta^5\text{-P}_5)\}_{12}\{\text{CuCl}\}_{20-n}]$ (**7-Cl**)

Method A (layering = **7a-Cl**):

A solution of $[\text{Cp}^*\text{Fe}(\eta^5\text{-P}_5)]$ (**1^x**, 33 mg, 0.092 mmol) and $o\text{-C}_2\text{B}_{10}\text{H}_{12}$ (10 mg, 0.069 mmol) in 7 mL CH_2Cl_2 was layered with a solution of CuCl (24 mg, 0.24 mmol) in 7 mL CH_3CN . After complete diffusion, the mother liquor was decanted. The crystals of **7a-Cl** were washed with toluene (3 x 5 mL) and pentane (3 x 5 mL) and dried.

Analytical data of **7a-Cl**:

Yield: 30 mg (4.9 μmol , 64%)

¹H NMR (CD_2Cl_2): δ [ppm] = 1.08 (br, 36 H, $-\text{C}_5\text{Me}_4\text{CH}_2\text{CH}_3$), 2.10 – 2.26 (144 H, $-\text{C}_5\text{Me}_4\text{Et}$), 2.34 (s, C_7H_8), 2.75 – 2.96 (m, 24 H, $-\text{C}_5\text{Me}_4\text{CH}_2\text{CH}_3$), 5.33 (CH_2Cl_2), 7.12 – 7.26 (m, C_7H_8).

³¹P{¹H} NMR (CD_2Cl_2): δ [ppm] = 68.0 ($[\text{Cp}^*\text{Fe}(\eta^5\text{-P}_5)]_{\text{host}}$), 75 (br, $[\text{Cp}^*\text{Fe}(\eta^5\text{-P}_5)]_{\text{host}}$), 78 (br, $[\text{Cp}^*\text{Fe}(\eta^5\text{-P}_5)]_{\text{host}}$), 110 (br, $[\text{Cp}^*\text{Fe}(\eta^5\text{-P}_5)]_{\text{host}}$), 151.8 (s, $[\text{Cp}^*\text{Fe}(\eta^5\text{-P}_5)]_{\text{free}}$).

¹¹B{¹H} NMR (CD_2Cl_2): δ [ppm] = -7.4, -14.3, -19.0, -20.1.

¹H NMR (pyridine-*d*₅): δ [ppm] = 0.65 (t, $^3J_{\text{HH}}$ = 7.6 Hz, 3 H, Cp^*FeP_5), 1.39 (s, 6 H, Cp^*FeP_5), 1.42 (s, 6 H, Cp^*FeP_5), 1.94 (q, $^3J_{\text{HH}}$ = 7.6 Hz, 2 H, Cp^*FeP_5), 2.22 (s, C_7H_8), 5.69 (s, CH_2Cl_2), 7.16 – 7.30 (m; C_7H_8).

³¹P{¹H} NMR (pyridine-*d*₅): δ [ppm] = 143.3 (s, $[\text{Cp}^*\text{Fe}(\eta^5\text{-P}_5)]$).

¹¹B{¹H} NMR (pyridine-*d*₅): δ [ppm] = -2.6, -9.2, -13.2, -14.1.

Positive ion ESI-MS (CH_2Cl_2 , CH_3CN): m/z = 980.5985 $[(\text{Cp}^*\text{FeP}_5)_2\text{Cu}_3\text{Cl}_2]^+$, 882.7014 $[(\text{Cp}^*\text{FeP}_5)_2\text{Cu}_2\text{Cl}]^+$, 782.8043 $[(\text{Cp}^*\text{FeP}_5)_2\text{Cu}]^+$, 563.7894 $[(\text{Cp}^*\text{FeP}_5)\text{Cu}_2\text{Cl}(\text{CH}_3\text{CN})]^+$, 522.7625 $[(\text{Cp}^*\text{FeP}_5)\text{Cu}_2\text{Cl}]^+$, 504.9196 $[(\text{Cp}^*\text{FeP}_5)\text{Cu}(\text{CH}_3\text{CN})_2]^+$, 463.8935 $[(\text{Cp}^*\text{FeP}_5)\text{Cu}(\text{CH}_3\text{CN})]^+$.

Negative ion ESI-MS (CH_2Cl_2 , CH_3CN): m/z = 332.6613 $[\text{Cu}_3\text{Cl}_4]^-$, 232.7652 $[\text{Cu}_2\text{Cl}_3]^-$, 134.8665 $[\text{CuCl}_2]^-$.

EI-MS (70 eV): m/z = 359.9350 $[\text{Cp}^*\text{FeP}_5]^+$, 297.9868 $[(\text{Cp}^*\text{FeP}_5)\text{-P}_2]^+$, 142.1762 $(\text{C}_2\text{B}_{10}\text{H}_{10})^+$.

Elemental Analysis: Calculated (%) for $(\text{C}_2\text{B}_{10}\text{H}_{12})(\text{C}_{11}\text{H}_{17}\text{FeP}_5)_{12}(\text{CuCl})_{15}(\text{C}_7\text{H}_8)_2$ (6133 g/mol): C 28.98, H 3.81, N 0; found (%): C 28.94, H 3.80, N 0.

Method B (stirring briefly = **7b-Cl**):

$[\text{Cp}^*\text{Fe}(\eta^5\text{-P}_5)]$ (**1^x**, 34 mg, 0.094 mmol), $o\text{-C}_2\text{B}_{10}\text{H}_{12}$ (10 mg, 0.069 mmol) and CuCl (18 mg, 0.18 mmol) were stirred in 7 mL CH_2Cl_2 for 45 minutes. The red solution was filtered and layered

with 12 mL toluene. After complete diffusion, the mother liquor was decanted. The crystals of **7b-Cl** were washed with toluene (3 x 5 mL) and pentane (3 x 5 mL) and dried.

Analytical data of **7b-Cl**:

Yield: 29 mg (4.5 μ mol, 57%)

EI-MS (70 eV): m/z = 359.9362 [Cp^xFeP_5] $^+$, 297.9880 [(Cp^xFeP_5)- P_2] $^+$, 142.1773 ($\text{C}_2\text{B}_{10}\text{H}_{10}$) $^+$.

Method C (stirring longer = **7b-Cl**)

[$\text{Cp}^x\text{Fe}(\eta^5\text{-P}_5)$] (**1 x** , 30 mg, 0.083 mmol), $o\text{-C}_2\text{B}_{10}\text{H}_{12}$ (12 mg, 0.083 mmol) and CuCl (17 mg, 0.17 mmol) were stirred in 10 mL CH_2Cl_2 for three days. The orange-brown solution was filtered from the yellow-greenish precipitate and layered with 15 mL toluene. After two weeks the solution was again layered with 10 mL hexane. After complete diffusion, the mother liquor was decanted. The crystals of **7b-Cl** were washed with toluene (4 x 5-10 mL) and pentane (3 x 3 mL) and dried.

Analytical data of **7b-Cl**:

Yield: 6 mg (0.9 μ mol, 13%)

EI-MS (70 eV): m/z = 359.9438 [Cp^xFeP_5] $^+$, 297.9948 [(Cp^xFeP_5)- P_2] $^+$, 142.1814 ($\text{C}_2\text{B}_{10}\text{H}_{10}$) $^+$.

Synthesis of ($o\text{-C}_2\text{B}_{10}\text{H}_{12}$) $_m$ @{[$\text{Cp}^x\text{Fe}(\eta^5\text{-P}_5)$] $_{12}$ {CuBr} $_{20-n}$ } (7-Br**)**

Method A (layering = **7a-Br** and **7a'-Br**):

A solution of [$\text{Cp}^x\text{Fe}(\eta^5\text{-P}_5)$] (**1 x** , 32 mg, 0.089 mmol) and $o\text{-C}_2\text{B}_{10}\text{H}_{12}$ (8 mg, 0.06 mmol) in 6 mL CH_2Cl_2 was layered with a solution of CuBr (29 mg, 0.20 mmol) in 6 mL CH_3CN . After complete diffusion, the mother liquor was decanted. The crystals of **7a-Br** and **7a'-Br** were washed with toluene (3 x 5 mL) and pentane (3 x 5 mL) and dried.

Analytical data of **7a-Br** and **7a'-Br**:

Yield: 46 mg (6.6 μ mol, 89%)

EI-MS (70 eV): m/z = 359.9365 [Cp^xFeP_5] $^+$, 297.9881 [(Cp^xFeP_5)- P_2] $^+$, 142.1768 ($\text{C}_2\text{B}_{10}\text{H}_{10}$) $^+$, 92.0593 (C_7H_8) $^+$.

Elemental Analysis: Calculated (%) for ($\text{C}_2\text{B}_{10}\text{H}_{12}$)($\text{C}_{11}\text{H}_{17}\text{FeP}_5$) $_{12}$ (CuBr) $_{16}$ (C_7H_8) $_2$ (6943 g/mol): C 25.60, H 3.37, N 0; found (%): C 25.60, H 3.10, N 0.

Method B (stirring briefly = **7b-Br**)

[$\text{Cp}^x\text{Fe}(\eta^5\text{-P}_5)$] (**1 x** , 29 mg, 0.081 mmol), $o\text{-C}_2\text{B}_{10}\text{H}_{12}$ (10 mg, 0.069 mmol) and CuBr (24 mg, 0.17 mmol) were stirred in 10 mL CH_2Cl_2 for one hour. The red solution was filtered and layered

with 10 mL toluene. After complete diffusion, the mother liquor was decanted. The crystals of **7b-Br** were washed with toluene (3 x 5 mL) and pentane (3 x 5 mL) and dried.

Analytical data of **7b-Br**:

Yield: 21 mg (3.1 μmol , 46%)

^1H NMR (CD_2Cl_2): δ [ppm] = 1.07 (br, 36 H, $-\text{C}_5\text{Me}_4\text{CH}_2\text{CH}_3$), 2.13 – 2.33 (144 H, $-\text{C}_5\text{Me}_4\text{Et}$), 2.34 (s, C_7H_8), 2.92 – 3.08 (m, 24 H, $-\text{C}_5\text{Me}_4\text{CH}_2\text{CH}_3$), 5.33 (CH_2Cl_2), 7.14 – 7.26 (m, C_7H_8).

$^{31}\text{P}\{^1\text{H}\}$ NMR (CD_2Cl_2): δ [ppm] = 64.9 (s, $[\text{Cp}^\times\text{Fe}(\eta^5\text{-P}_5)]_{\text{host}}$), 72 (br, $[\text{Cp}^\times\text{Fe}(\eta^5\text{-P}_5)]_{\text{host}}$), 108 (br, $[\text{Cp}^\times\text{Fe}(\eta^5\text{-P}_5)]_{\text{host}}$), 151.7 (s, $[\text{Cp}^\times\text{Fe}(\eta^5\text{-P}_5)]_{\text{free}}$).

$^{11}\text{B}\{^1\text{H}\}$ NMR (CD_2Cl_2): δ [ppm] = -7.2, -14.3, -18.8, -20.0.

^1H NMR (pyridine- d_5): δ [ppm] = 0.64 (t, $^3J_{\text{HH}} = 7.6$ Hz, 3 H, $\text{Cp}^\times\text{FeP}_5$), 1.33 (s, 6 H, $\text{Cp}^\times\text{FeP}_5$), 1.35 (s, 6 H, $\text{Cp}^\times\text{FeP}_5$), 1.87 (q, $^3J_{\text{HH}} = 7.6$ Hz, 2 H, $\text{Cp}^\times\text{FeP}_5$), 2.22 (s, C_7H_8), 5.68 (s, CH_2Cl_2).

$^{31}\text{P}\{^1\text{H}\}$ NMR (pyridine- d_5): δ [ppm] = 151.6 (s, $[\text{Cp}^\times\text{Fe}(\eta^5\text{-P}_5)]$).

$^{11}\text{B}\{^1\text{H}\}$ NMR (pyridine- d_5): δ [ppm] = no signals detected.

Positive ion ESI-MS (CH_2Cl_2 , CH_3CN): m/z = 2433.3542 $[(\text{Cp}^\times\text{FeP}_5)_3\text{Cu}_{10}\text{Br}_9]^+$, 2291.5082 $[(\text{Cp}^\times\text{FeP}_5)_3\text{Cu}_9\text{Br}_8]^+$, 2147.6613 $[(\text{Cp}^\times\text{FeP}_5)_3\text{Cu}_8\text{Br}_7]^+$, 2003.8126 $[(\text{Cp}^\times\text{FeP}_5)_3\text{Cu}_7\text{Br}_6]^+$, 1859.9692 $[(\text{Cp}^\times\text{FeP}_5)_3\text{Cu}_6\text{Br}_5]^+$, 1070.4957 $[(\text{Cp}^\times\text{FeP}_5)_2\text{Cu}_3\text{Br}_2]^+$, 926.6504 $[(\text{Cp}^\times\text{FeP}_5)_2\text{Cu}_2\text{Br}]^+$, 782.8045 $[(\text{Cp}^\times\text{FeP}_5)_2\text{Cu}]^+$, 566.7122 $[(\text{Cp}^\times\text{FeP}_5)\text{Cu}_2\text{Br}]^+$, 504.9195 $[(\text{Cp}^\times\text{FeP}_5)\text{Cu}(\text{CH}_3\text{CN})_2]^+$, 463.8930 $[(\text{Cp}^\times\text{FeP}_5)\text{Cu}(\text{CH}_3\text{CN})]^+$.

Negative ion ESI-MS (CH_2Cl_2 , CH_3CN): m/z = 939.9912 $[\text{Cu}_6\text{Br}_7]^-$, 796.1462 $[\text{Cu}_5\text{Br}_6]^-$, 654.2990 $[\text{Cu}_4\text{Br}_5]^-$, 510.4540 $[\text{Cu}_3\text{Br}_4]^-$, 366.6091 $[\text{Cu}_2\text{Br}_3]^-$, 222.7641 $[\text{CuBr}_2]^-$.

EI-MS (70 eV): m/z = 359.9358 $[\text{Cp}^\times\text{FeP}_5]^+$, 297.9881 $[(\text{Cp}^\times\text{FeP}_5)\text{-P}_2]^+$, 144.1822 $(\text{C}_2\text{B}_{10}\text{H}_{12})^+$, 142.1785 $(\text{C}_2\text{B}_{10}\text{H}_{10})^+$.

Elemental Analysis: Calculated (%) for $(\text{C}_2\text{B}_{10}\text{H}_{12})(\text{C}_{11}\text{H}_{17}\text{FeP}_5)_{12}(\text{CuBr})_{16}$ (6759 g/mol): C 23.81, H 3.22, N 0; found (%): C 23.79, H 3.20, N 0.

Method C (stirring longer = **7b-Br**)

$[\text{Cp}^\times\text{Fe}(\eta^5\text{-P}_5)]$ (**1 $^\times$** , 30 mg, 0.083 mmol), *o*- $\text{C}_2\text{B}_{10}\text{H}_{12}$ (12 mg, 0.083 mmol) and CuBr (24 mg, 0.17 mmol) were stirred in 8 mL CH_2Cl_2 for three days. The red solution was filtered from the yellow precipitate and layered with 16 mL toluene. After complete diffusion, the mother liquor was decanted. The crystals of **7b-Br** were washed with toluene (2 x 5 mL) and Et_2O (3 x 5 mL) and dried.

Analytical data of **7b-Br**:

Yield: 19 mg (2.6 μmol , 37%)

^1H NMR (CD_2Cl_2): δ [ppm] = 1.08 (br, 36 H, $-\text{C}_5\text{Me}_4\text{CH}_2\text{CH}_3$), 2.14 – 2.33 (144 H, $-\text{C}_5\text{Me}_4\text{Et}$), 2.34 (s, C_7H_8), 2.93 – 3.10 (m, 24 H, $-\text{C}_5\text{Me}_4\text{CH}_2\text{CH}_3$), 5.33 (CH_2Cl_2), 7.12 – 7.26 (m, C_7H_8).

$^{31}\text{P}\{^1\text{H}\}$ NMR (CD_2Cl_2): δ [ppm] = 65.0 (s, $[\text{Cp}^\times\text{Fe}(\eta^5\text{-P}_5)]_{\text{host}}$), 66 (br, $[\text{Cp}^\times\text{Fe}(\eta^5\text{-P}_5)]_{\text{host}}$), 73 (br, $[\text{Cp}^\times\text{Fe}(\eta^5\text{-P}_5)]_{\text{host}}$), 109 (br, $[\text{Cp}^\times\text{Fe}(\eta^5\text{-P}_5)]_{\text{host}}$), 151.8 (s, $[\text{Cp}^\times\text{Fe}(\eta^5\text{-P}_5)]_{\text{free}}$).

$^{11}\text{B}\{^1\text{H}\}$ NMR (CD_2Cl_2): δ [ppm] = -7.1, -14.1, -18.8, -20.0.

EI-MS (70 eV): m/z = 359.9333 $[\text{Cp}^\times\text{FeP}_5]^+$, 297.9854 $[(\text{Cp}^\times\text{FeP}_5)\text{-P}_2]^+$, 142.1756 ($\text{C}_2\text{B}_{10}\text{H}_{10}$) $^+$, 92.0586 (C_7H_8) $^+$.

Stability of 3-Cl in CH_3CN solution

A few crystals of **3-Cl** were dissolved in 3 mL CH_2Cl_2 to give an orange solution. Upon adding 1 mL CH_3CN , the solution turned green immediately. After stirring for one day, the solvent was evaporated, and the residue dissolved in CD_2Cl_2 to give an orange solution again.

^1H NMR (CD_2Cl_2): δ [ppm] = 0.75 (t, $^3J_{\text{HH}} = 7.6$ Hz, 3 H, $\text{Cp}^\times\text{FeP}_5$), 1.43 (s, 6 H, $\text{Cp}^\times\text{FeP}_5$), 1.45 (s, 6 H, $\text{Cp}^\times\text{FeP}_5$), 1.94 (q, $^3J_{\text{HH}} = 7.6$ Hz, 2 H, $\text{Cp}^\times\text{FeP}_5$), 1.97 (s, CH_3CN), 5.32 (s, CH_2Cl_2).

$^{31}\text{P}\{^1\text{H}\}$ NMR (CD_2Cl_2): δ [ppm] = 151.8 (s, $[\text{Cp}^\times\text{Fe}(\eta^5\text{-P}_5)]$).

Stability of 3-Br in CH_3CN solution

A few crystals of **3-Br** were dissolved in 3 mL CH_2Cl_2 to give an orange solution. Upon adding 1 mL CH_3CN , the solution was stirred for one day. The solvent was evaporated from the brown suspension, and the residue dissolved in CD_2Cl_2 .

^1H NMR (CD_2Cl_2): δ [ppm] = 0.75 (t, $^3J_{\text{HH}} = 7.6$ Hz, 3 H, $\text{Cp}^\times\text{FeP}_5$), 1.06 (br, $[\text{Cp}^\times\text{FeP}_5]_{\text{sphere}}$), 1.44 (s, 6 H, $\text{Cp}^\times\text{FeP}_5$), 1.45 (s, 6 H, $\text{Cp}^\times\text{FeP}_5$), 1.94 (q, $^3J_{\text{HH}} = 7.6$ Hz, 2 H, $\text{Cp}^\times\text{FeP}_5$), 1.95 (s, CH_3CN), 2.13 – 2.32 (br, $[\text{Cp}^\times\text{FeP}_5]_{\text{sphere}}$), 2.81 – 3.10 (br, $[\text{Cp}^\times\text{FeP}_5]_{\text{sphere}}$), 5.32 (s, CH_2Cl_2).

$^{31}\text{P}\{^1\text{H}\}$ NMR (CD_2Cl_2): δ [ppm] = 66 (br, $[\text{Cp}^\times\text{Fe}(\eta^5\text{-P}_5)]_{\text{sphere}}$), 72 (br, $[\text{Cp}^\times\text{Fe}(\eta^5\text{-P}_5)]_{\text{sphere}}$), 107 (br, $[\text{Cp}^\times\text{Fe}(\eta^5\text{-P}_5)]_{\text{sphere}}$), 151.8 (s, $[\text{Cp}^\times\text{Fe}(\eta^5\text{-P}_5)]_{\text{free}}$).

Stability of 3-Cl in CH_2Cl_2 solution

A few crystals of **3-Cl** were dissolved in 2 mL CD_2Cl_2 to give an orange solution. After stirring for 30 minutes, the resulting yellow suspension was analyzed by NMR spectroscopy.

^1H NMR (CD_2Cl_2): δ [ppm] = 0.75 (t, $^3J_{\text{HH}} = 7.6$ Hz, 3 H, $\text{Cp}^\times\text{FeP}_5$), 1.44 (s, 6 H, $\text{Cp}^\times\text{FeP}_5$), 1.45 (s, 6 H, $\text{Cp}^\times\text{FeP}_5$), 1.95 (q, $^3J_{\text{HH}} = 7.6$ Hz, 2 H, $\text{Cp}^\times\text{FeP}_5$), 2.34 (s, C_7H_8), 5.33 (s, CH_2Cl_2), 7.15 – 7.24 (m, C_7H_8).

$^{31}\text{P}\{^1\text{H}\}$ NMR (CD_2Cl_2): δ [ppm] = 151.8 (s, $[\text{Cp}^\times\text{Fe}(\eta^5\text{-P}_5)]_{\text{free}}$).

Stability of **3-Br** in CH₂Cl₂ solution

A few crystals of **3-Br** were dissolved in 2 mL CD₂Cl₂ to give an orange solution. After stirring for one day, the resulting yellow suspension was analyzed by NMR spectroscopy.

¹H NMR (CD₂Cl₂): δ [ppm] = 0.75 (t, ³J_{HH} = 7.6 Hz, 3 H, Cp[×]FeP₅), 1.06 (br, [Cp[×]FeP₅]_{sphere}), 1.44 (s, 6 H, Cp[×]FeP₅), 1.45 (s, 6 H, Cp[×]FeP₅), 1.94 (q, ³J_{HH} = 7.6 Hz, 2 H, Cp[×]FeP₅), 2.13 – 2.32 (br, [Cp[×]FeP₅]_{sphere}), 2.34 (s, C₇H₈), 2.82 – 3.09 (br, [Cp[×]FeP₅]_{sphere}), 5.32 (s, CH₂Cl₂), 7.12 – 7.26 (m, C₇H₈).

³¹P{¹H} NMR (CD₂Cl₂): δ [ppm] = 151.8 (s, [Cp[×]Fe(η⁵-P₅)]_{free}).

Stability of **3-Cl** in toluene or mother liquor

[Cp[×]Fe(η⁵-P₅)] (**1^x**, 52 mg, 0.14 mmol) and CuCl (32 mg, 0.32 mmol) were dissolved in 6 mL CH₂Cl₂ and stirred for 45 minutes. After filtration, the orange solution was layered with 8 mL toluene. Already after four days, the formation of black cubic crystals of **3-Cl** and powder was observed. After complete diffusion, some of the black crystals of **3-Cl** were a) taken from the Schlenk wall with a spatula and dipped into a Schlenk tube with toluene or b) taken from Schlenk wall with a spatula and dipped into a Schlenk tube with some of the mother liquor or c) left in the Schlenk tube with some of the mother liquor and the precipitated powder. After one month, crystals of **3-Cl** were still found in a) and b), while in c) they have vanished.

Stability of **3-Br** in toluene or mother liquor

[Cp[×]Fe(η⁵-P₅)] (**1^x**, 55 mg, 0.15 mmol) and CuBr (46 mg, 0.32 mmol) were dissolved in 8 mL CH₂Cl₂ and stirred for 45 minutes. After filtration, the orange solution was layered with 12 mL toluene. Already after four days, the formation of black cubic crystals of **3-Br** was observed. After complete diffusion, some of the black crystals of **3-Br** were a) taken from the Schlenk wall with a spatula and dipped into a Schlenk tube with toluene or b) left in the Schlenk tube with the mother liquor. After one month, crystals of **3-Br** were still found in a) and b).

Reaction of **3-Cl** with CuCl

A few crystals of **3-Cl** (5 mg, 0.8 μmol) were dissolved in 2 mL CH₂Cl₂ and added to a solution of CuCl (~1 mg, 10 μmol) in 2 mL CH₃CN. After stirring for three hours, the resulting dark orange solution was analyzed by NMR spectroscopy.

¹H NMR (CD₂Cl₂/CD₃CN): δ [ppm] = -2.56 (br), -2.41 (s), -2.35 (s), -2.07 (br), 0.75 (t, ³J_{HH} = 7.4 Hz, 3 H, Cp[×]FeP₅), 0.99 (t, ³J_{HH} = 7.2 Hz, **2-Cl**), 1.45 (s, 6 H, Cp[×]FeP₅), 1.46 (s, 6 H, Cp[×]FeP₅), 1.94 (CD₃CN

and Cp^xFeP_5), 2.06 (s), 2.19 (br, **2-Cl**), 2.20 (br, **2-Cl**), 2.26 (br, **2-Cl**), 2.28 (br, **2-Cl**), 2.93 (br, **2-Cl**), 3.08 (br, **2-Cl**), 5.40 (s, CH_2Cl_2).

$^{31}\text{P}\{^1\text{H}\}$ NMR ($\text{CD}_2\text{Cl}_2/\text{CD}_3\text{CN}$): δ [ppm] = 72 (br, 60 P, **2-Cl**_{host}), 150.1 (s, 5 P, $[\text{Cp}^x\text{Fe}(\eta^5\text{-P}_5)]_{\text{free}}$), 161.5 (s, 5 P, **2-Cl**_{guest}).

Reaction of **3-Cl** with CuI

A few crystals of **3-Cl** (5 mg, 0.8 μmol) were dissolved in 2 mL CH_2Cl_2 and added to a solution of CuI (~1 mg, 5 μmol) in 2 mL CH_3CN . After stirring for three hours, the resulting dark orange solution was analyzed by NMR spectroscopy.

^1H NMR ($\text{CD}_2\text{Cl}_2/\text{CD}_3\text{CN}$): δ [ppm] = -2 (br), 0.78 (br, 3 H, $[\text{Cp}^x\text{FeP}_5]_{\text{enc.+free}}$), 0.99 (br, $[\text{Cp}^x\text{FeP}_5]_{\text{host}}$), 1.49 (s, 12 H, $[\text{Cp}^x\text{FeP}_5]_{\text{enc.+free}}$), 1.94 (CD_3CN and $[\text{Cp}^x\text{FeP}_5]_{\text{enc.+free}}$), 2.03 (s), 2.20 – 2.36 (br, $[\text{Cp}^x\text{FeP}_5]_{\text{host}}$), 2.94 (br, $[\text{Cp}^x\text{FeP}_5]_{\text{host}}$), 5.39 (s, CH_2Cl_2).

$^{31}\text{P}\{^1\text{H}\}$ NMR ($\text{CD}_2\text{Cl}_2/\text{CD}_3\text{CN}$): δ [ppm] = 74 (br, 60 P, $[\text{Cp}^x\text{FeP}_5]_{\text{host}}$), 151.4 (s, 5 P, $[\text{Cp}^x\text{Fe}(\eta^5\text{-P}_5)]_{\text{free}}$), 164 (br, 5 P, $[\text{Cp}^x\text{FeP}_5]_{\text{enc.}}$)*. * Signal almost below noise floor.

Reaction of **3-Br** with CuBr

A few crystals of **3-Br** (13 mg, 1.8 μmol) and CuBr (2 mg, 14 μmol) were dissolved in a mixture of CH_2Cl_2 and CH_3CN (3 mL, 2:1) and stirred for one hour. The resulting dark orange suspension was analyzed by NMR spectroscopy.

^1H NMR ($\text{CD}_2\text{Cl}_2/\text{CD}_3\text{CN}$): δ [ppm] = -3.26 (br)*, -2.01 (s), -1.35 (s), 0.71 (t, $^3J_{\text{HH}} = 7.6$ Hz, $[\text{Cp}^x\text{FeP}_5]_{\text{enc.+free}}$), 0.98 (t, $^3J_{\text{HH}} = 7.5$ Hz, 36 H, $\{\text{Cp}^x\text{FeP}_5\}_{\text{sphere}}$), 1.40 (s, 6 H, $[\text{Cp}^x\text{FeP}_5]_{\text{enc.+free}}$), 1.41 (s, 6 H, $[\text{Cp}^x\text{FeP}_5]_{\text{enc.+free}}$), 1.84 (s), 1.92 (CD_3CN and $\{\text{Cp}^x\text{FeP}_5\}_{\text{enc.+free}}$ superimposed), 2.22 – 2.26 (br, 144 H, $\{\text{Cp}^x\text{FeP}_5\}_{\text{sphere}}$), 2.96 – 3.11 (br, 24 H, 36 H, $\{\text{Cp}^x\text{FeP}_5\}_{\text{sphere}}$), 5.32 (CD_2Cl_2).

$^{31}\text{P}\{^1\text{H}\}$ NMR ($\text{CD}_2\text{Cl}_2/\text{CD}_3\text{CN}$): δ [ppm] = 67 (br, 60 P, $\{\text{Cp}^x\text{FeP}_5\}_{\text{sphere}}$)*, 150.5 (s, $\{\text{Cp}^x\text{FeP}_5\}_{\text{free}}$).

*Signals almost below noise floor.

Reaction of **3-Cl** with *o*- $\text{C}_2\text{B}_{10}\text{H}_{12}$

3-Cl (5 mg, 0.8 μmol) and *o*- $\text{C}_2\text{B}_{10}\text{H}_{12}$ (1 mg, 7 μmol) were dissolved in 3 mL CD_2Cl_2 to give an orange solution. After stirring for 30 minutes, a yellow solid had precipitated, and the dark orange supernatant was analyzed by NMR spectroscopy.

^1H NMR (CD_2Cl_2): δ [ppm] = 0.75 (t, $^3J_{\text{HH}} = 7.6$ Hz, 3 H, Cp^xFeP_5), 1.07 (br, $[\text{Cp}^x\text{FeP}_5]_{\text{sphere}}$), 1.43 (s, 6 H, Cp^xFeP_5), 1.45 (s, 6 H, Cp^xFeP_5), 1.94 (q, $^3J_{\text{HH}} = 7.6$ Hz, 2 H, Cp^xFeP_5), 1.49 – 2.00 (br, *o*- $\text{C}_2\text{B}_{10}\text{H}_{12}$), 2.10 – 2.27 (br, $[\text{Cp}^x\text{FeP}_5]_{\text{sphere}}$), 2.34 (s, C_7H_8), 2.53 (br, *o*- $\text{C}_2\text{B}_{10}\text{H}_{12}$), 2.72 (br,

$o\text{-C}_2\text{B}_{10}\text{H}_{12}$), 2.86 – 2.98 (br, $[\text{Cp}^*\text{FeP}_5]_{\text{sphere}}$), 3.66 (br, $o\text{-C}_2\text{B}_{10}\text{H}_{12}$), 5.32 (s, CH_2Cl_2), 7.13 – 7.26 (m, C_7H_8).

$^{31}\text{P}\{^1\text{H}\}$ NMR (CD_2Cl_2): δ [ppm] = 69 (br, $[\text{Cp}^*\text{Fe}(\eta^5\text{-P}_5)]_{\text{sphere}}$), 76 (br, $[\text{Cp}^*\text{Fe}(\eta^5\text{-P}_5)]_{\text{sphere}}$), 78 (br, $[\text{Cp}^*\text{Fe}(\eta^5\text{-P}_5)]_{\text{sphere}}$), 110 (br, $[\text{Cp}^*\text{Fe}(\eta^5\text{-P}_5)]_{\text{sphere}}$), 120 (br, $[\text{Cp}^*\text{Fe}(\eta^5\text{-P}_5)]_{\text{sphere}}$), 151.8 (s, $[\text{Cp}^*\text{Fe}(\eta^5\text{-P}_5)]_{\text{free}}$).

$^{11}\text{B}\{^1\text{H}\}$ NMR (CD_2Cl_2): δ [ppm] = -2.9 ($\{o\text{-C}_2\text{B}_{10}\text{H}_{12}\}_{\text{free}}$), -7.6 ($\{o\text{-C}_2\text{B}_{10}\text{H}_{12}\}_{\text{guest}}$), -9.6 ($\{o\text{-C}_2\text{B}_{10}\text{H}_{12}\}_{\text{free}}$), -13.9 ($\{o\text{-C}_2\text{B}_{10}\text{H}_{12}\}_{\text{free}}$), -14.9 ($\{o\text{-C}_2\text{B}_{10}\text{H}_{12}\}_{\text{free}}$), -19.1 ($\{o\text{-C}_2\text{B}_{10}\text{H}_{12}\}_{\text{guest}}$), -20.4 ($\{o\text{-C}_2\text{B}_{10}\text{H}_{12}\}_{\text{guest}}$).

Reaction of 3-Br with $o\text{-C}_2\text{B}_{10}\text{H}_{12}$

3-Br (5 mg, 0.7 μmol) and $o\text{-C}_2\text{B}_{10}\text{H}_{12}$ (2 mg, 14 μmol) were dissolved in 2 mL CD_2Cl_2 to give an orange solution. After stirring for one day, a yellow solid had precipitated, and the dark orange supernatant was analyzed by NMR spectroscopy.

^1H NMR (CD_2Cl_2): δ [ppm] = 0.75 (t, $^3J_{\text{HH}} = 7.6$ Hz, 3 H, Cp^*FeP_5), 1.06 (br, $[\text{Cp}^*\text{FeP}_5]_{\text{sphere}}$), 1.44 (s, 6 H, Cp^*FeP_5), 1.45 (s, 6 H, Cp^*FeP_5), 1.94 (q, $^3J_{\text{HH}} = 7.6$ Hz, 2 H, Cp^*FeP_5), 1.50 – 2.08 (br, $o\text{-C}_2\text{B}_{10}\text{H}_{12}$), 2.13 – 2.33 (br, $[\text{Cp}^*\text{FeP}_5]_{\text{sphere}}$), 2.34 (s, C_7H_8), 2.53 (br, $o\text{-C}_2\text{B}_{10}\text{H}_{12}$), 2.72 (br, $o\text{-C}_2\text{B}_{10}\text{H}_{12}$), 2.80 – 3.09 (br, $[\text{Cp}^*\text{FeP}_5]_{\text{sphere}}$), 3.66 (br, $o\text{-C}_2\text{B}_{10}\text{H}_{12}$), 5.32 (s, CH_2Cl_2), 7.12 – 7.26 (m, C_7H_8).

$^{31}\text{P}\{^1\text{H}\}$ NMR (CD_2Cl_2): δ [ppm] = 66 (br, $[\text{Cp}^*\text{Fe}(\eta^5\text{-P}_5)]_{\text{sphere}}$), 73 (br, $[\text{Cp}^*\text{Fe}(\eta^5\text{-P}_5)]_{\text{sphere}}$), 109 (br, $[\text{Cp}^*\text{Fe}(\eta^5\text{-P}_5)]_{\text{sphere}}$), 151.9 (s, $[\text{Cp}^*\text{Fe}(\eta^5\text{-P}_5)]_{\text{free}}$).

$^{11}\text{B}\{^1\text{H}\}$ NMR (CD_2Cl_2): δ [ppm] = -2.9 ($\{o\text{-C}_2\text{B}_{10}\text{H}_{12}\}_{\text{free}}$), -7.7 ($\{o\text{-C}_2\text{B}_{10}\text{H}_{12}\}_{\text{guest}}$), -9.6 ($\{o\text{-C}_2\text{B}_{10}\text{H}_{12}\}_{\text{free}}$), -13.9 ($\{o\text{-C}_2\text{B}_{10}\text{H}_{12}\}_{\text{free}}$), -14.9 ($\{o\text{-C}_2\text{B}_{10}\text{H}_{12}\}_{\text{free}}$), -19.0 ($\{o\text{-C}_2\text{B}_{10}\text{H}_{12}\}_{\text{guest}}$), -20.2 ($\{o\text{-C}_2\text{B}_{10}\text{H}_{12}\}_{\text{guest}}$).

Reaction of 7-Cl with CH_3CN

A few crystals of **7-Cl** were dissolved in 3 mL CH_2Cl_2 to give an orange-brown solution. After adding 1 mL CH_3CN , the solution was stirred for one day. The solvent was evaporated from the orange-brown suspension and the residue dissolved in 1 mL CD_2Cl_2 .

^1H NMR (CD_2Cl_2): δ [ppm] = 0.75 (t, $^3J_{\text{HH}} = 7.8$ Hz, 3 H, Cp^*FeP_5), 1.08 (br, $[\text{Cp}^*\text{FeP}_5]_{\text{sphere}}$), 1.45 (br, 12 H, Cp^*FeP_5), 1.54 (br, $o\text{-C}_2\text{B}_{10}\text{H}_{12}$), 1.92 (2 H, Cp^*FeP_5)*, 1.97 (s, CH_3CN), 2.11 – 2.26 (br, $[\text{Cp}^*\text{FeP}_5]_{\text{sphere}}$), 2.73 – 2.97 (br, $[\text{Cp}^*\text{FeP}_5]_{\text{sphere}}$), 3.66 (br, $o\text{-C}_2\text{B}_{10}\text{H}_{12}$), 5.32 (s, CH_2Cl_2). *Signal almost below noise floor.

$^{31}\text{P}\{^1\text{H}\}$ NMR (CD_2Cl_2): δ [ppm] = 68 (br, $[\text{Cp}^*\text{Fe}(\eta^5\text{-P}_5)]_{\text{sphere}}$), 78 (br, $[\text{Cp}^*\text{Fe}(\eta^5\text{-P}_5)]_{\text{sphere}}$), 110 (br, $[\text{Cp}^*\text{Fe}(\eta^5\text{-P}_5)]_{\text{sphere}}$), 151.7 (s, $[\text{Cp}^*\text{Fe}(\eta^5\text{-P}_5)]_{\text{free}}$).

$^{11}\text{B}\{^1\text{H}\}$ NMR (CD_2Cl_2): δ [ppm] = -2.8 ($\{o\text{-C}_2\text{B}_{10}\text{H}_{12}\}_{\text{free}}$), -7.5 ($\{o\text{-C}_2\text{B}_{10}\text{H}_{12}\}_{\text{guest}}$), -9.6 ($\{o\text{-C}_2\text{B}_{10}\text{H}_{12}\}_{\text{free}}$), -13.9 ($\{o\text{-C}_2\text{B}_{10}\text{H}_{12}\}_{\text{free}}$), -14.4 ($\{o\text{-C}_2\text{B}_{10}\text{H}_{12}\}_{\text{guest}}$), -14.9 ($\{o\text{-C}_2\text{B}_{10}\text{H}_{12}\}_{\text{free}}$), -19.0 ($\{o\text{-C}_2\text{B}_{10}\text{H}_{12}\}_{\text{guest}}$), -20.3 ($\{o\text{-C}_2\text{B}_{10}\text{H}_{12}\}_{\text{guest}}$).

Reaction of 7-Br with CH_3CN

A few crystals of **7-Br** were dissolved in 3 mL CH_2Cl_2 to give an orange solution. After adding 1 mL CH_3CN , the solution was stirred for one day. The solvent was evaporated from the orange-brown suspension and the residue dissolved in 1 mL CD_2Cl_2 .

^1H NMR (CD_2Cl_2): δ [ppm] = 0.75 (t, $^3J_{\text{HH}} = 7.6$ Hz, 3 H, $\text{Cp}^\times\text{FeP}_5$), 1.07 (br, $[\text{Cp}^\times\text{FeP}_5]_{\text{sphere}}$), 1.44 (s, 6 H, $\text{Cp}^\times\text{FeP}_5$), 1.45 (s, 6 H, $\text{Cp}^\times\text{FeP}_5$), 1.94 (q, $^3J_{\text{HH}} = 7.4$ Hz, 2 H, $\text{Cp}^\times\text{FeP}_5$)*, 1.97 (s, CH_3CN), 2.13 – 2.32 (br, $[\text{Cp}^\times\text{FeP}_5]_{\text{sphere}}$), 2.81 – 3.09 (br, $[\text{Cp}^\times\text{FeP}_5]_{\text{sphere}}$), 3.66 (br, $o\text{-C}_2\text{B}_{10}\text{H}_{12}$), 5.32 (s, CH_2Cl_2).
*Signal almost below noise floor.

$^{31}\text{P}\{^1\text{H}\}$ NMR (CD_2Cl_2): δ [ppm] = 64.9 (s, $[\text{Cp}^\times\text{Fe}(\eta^5\text{-P}_5)]_{\text{sphere}}$), 66 (br, $[\text{Cp}^\times\text{Fe}(\eta^5\text{-P}_5)]_{\text{sphere}}$), 74 (br, $[\text{Cp}^\times\text{Fe}(\eta^5\text{-P}_5)]_{\text{sphere}}$), 79 (br, $[\text{Cp}^\times\text{Fe}(\eta^5\text{-P}_5)]_{\text{sphere}}$), 108 (br, $[\text{Cp}^\times\text{Fe}(\eta^5\text{-P}_5)]_{\text{sphere}}$), 151.7 (s, $[\text{Cp}^\times\text{Fe}(\eta^5\text{-P}_5)]_{\text{free}}$).

$^{11}\text{B}\{^1\text{H}\}$ NMR (CD_2Cl_2): δ [ppm] = -2.9 ($\{o\text{-C}_2\text{B}_{10}\text{H}_{12}\}_{\text{free}}$), -7.2 ($\{o\text{-C}_2\text{B}_{10}\text{H}_{12}\}_{\text{guest}}$), -9.4 ($\{o\text{-C}_2\text{B}_{10}\text{H}_{12}\}_{\text{free}}$), -13.9 ($\{o\text{-C}_2\text{B}_{10}\text{H}_{12}\}_{\text{free}}$), -14.3 ($\{o\text{-C}_2\text{B}_{10}\text{H}_{12}\}_{\text{guest}}$), -18.9 ($\{o\text{-C}_2\text{B}_{10}\text{H}_{12}\}_{\text{guest}}$), -20.1 ($\{o\text{-C}_2\text{B}_{10}\text{H}_{12}\}_{\text{guest}}$).

The observed signals indicate a degradation of the host scaffold while the guest molecule $o\text{-C}_2\text{B}_{10}\text{H}_{12}$ is released. Seen in this light, it is especially interesting that host-guest aggregates **6** and **7** are nevertheless formed from the layering approach in the presence of 50 vol% CH_3CN (cf. syntheses of **6a-Cl**, **6a-Br+6a'-Br**, **7a-Cl**, **7a-Br**, **7a'-Br**). This might be caused by the insolubility of **6** and **7** in premixed mixtures of CH_2Cl_2 and CH_3CN , so that the host-guest aggregates immediately crystallize upon their formation at the solvent interface in the layering reaction. In contrast, the for the degradation reactions of **7-Cl** and **7-Br** with CH_3CN , both compounds have to be dissolved in CH_2Cl_2 first, and CH_3CN is added subsequently.

3.5 Crystallographic Details

Crystals of **3-Cl** – **7b-Cl** were taken from a Schlenk flask under a stream of argon and immediately covered with mineral oil to prevent decomposition and a loss of solvent. The quickly chosen single crystals covered by a drop of the oil were directly placed into a stream of cold nitrogen with the pre-centered goniometer head with CryoMount[®] and attached to the

goniometer of a diffractometer. The data for **3-Cl**, **4-Cl**, **4-Cl-CH₃CN**, **5-Br**, **5-I**, **6b-Cl**, **7a-Br**, **7a'-Br** and **7b-Cl** were collected on an Agilent Technologies diffractometer equipped with a Titan^{S2} CCD detector and a SuperNova CuK α microfocus source using 0.5° ω scans at 90 K or 123 K (only for **5-I**). Absorption correction for these was applied based on crystal faces. The crystals for **6a'-Br** showed systematic twinning featuring very close reflections, and an attempt to measure high quality data at the laboratory device failed due to relatively low resolution of the detector preventing separation of the diffraction maxima during integration.

Therefore, to collect diffraction data for **6a-Br** and **6a'-Br**, at the DESY PETRA III synchrotron, the crystals were carefully selected, mounted on a magnetic holder, checked for quality and placed into a Dewar vessel with liquid nitrogen using standard cryocrystallography tools. Using standard procedures, it was placed into a special Dewar vessel filled with liquid nitrogen among other crystals in the P11 hutch. A robotic mounting/demounting was used for further manipulations.^[28] The measurements were performed at 80 K on a 1-axis goniostat using 360°-rotation around ϕ with an exposure of 60 ms per 0.1° frame at 18 keV for **6a-Br**, and 40 ms per 0.05° frame at 20 keV for of **6a'-Br**. DECTRIS PILATUS 6M photo-counting detector was used to register diffraction pattern in a shutterless mode. Due to partial radiation damage, only those frames were taken into integration, which were not affected by decomposition of the crystal. Empirical absorption correction using equivalent reflections was applied. The dataset collected for **6a'-Br** was integrated with de-twin procedure implemented in *CrysAlisPro* software^[29] and confirmed supposed earlier $x/-x$ twinning law. The experimental strategy chosen to separate twinned reflections with narrow scans allowed for the dataset with $R_{\text{int}} = 0.0496$ compared to $R_{\text{int}} = 0.0713$, which was obtained at a laboratory device.

To collect diffraction data at helium temperature in order to check if it was possible to suppress severe disorder of the guest molecules, the crystals of **6a-Cl** and **7a-Cl** were taken to the DESY PETRA III synchrotron. X-ray diffraction experiments for **6a-Cl** and **7a-Cl** were measured at P24 EH2 beamline^[30] using four-circle HUBER diffractometer with Eulerian DECTRIS PILATUS3 CdTe 1M pixel array detector at 15(1) K (**6a-Cl**) or 20(1) K (**7a-Cl**) using open-flow helium cryosystem. The data for were acquired by 360° ϕ -rotation with 0.1° scan width and exposure 0.2 s per frame at wavelength $\lambda = 0.50000 \text{ \AA}$ (24.8 keV). Data reduction for all data sets was performed with *CrysAlisPro* software. Empirical absorption correction using equivalent reflections was applied.

The structures **3-Cl** – **7-Br** were solved by direct methods with *SHELXT*^[31] and refined by full-matrix least-squares method against F^2 in anisotropic approximation using multi-processor variable memory versions of *SHELXL* (2014-2018). For the refinement of the structures of the

cubic structure type **6b-Cl** and **7b-Cl**, the model obtained from **3-Cl** was used, and for structures of tetragonal structure type **6a-Cl**, **6a-Br** and **7a-Br**, the model obtained from **7a-Cl**. The models were individually adapted in structural detail concerning refinement of the occupation factors for partly vacant CuX positions, refinement of the guest and solvent molecules, which can vary from sample to sample. The occupation factors for disordered positions of heavy atoms in all structures of **3**, **6** and **7** were refined with fixed isotropic U_{iso} similar to the average U_{iso} (0.025-0.035 \AA^{-2} depending on temperature) for the fully occupied heavy atoms in the corresponding structure. To model severe disorder of the guest molecules the rigid body refinement was used, as applicable for rigid cage molecules *o*-carborane and P_4S_3 . The model for the refinement of *o*-carborane was extracted using CSD^[32] from the crystal structure determination from neutron diffraction^[33] (QEQFUN), in which all B-H distances were additionally averaged to give 1.04 \AA . The carbon atoms were placed arbitrarily to maintain correct chemical composition without overdue complication of the model, and give no information on the real orientation of the *o*-carborane molecule. The model for the refinement of P_4S_3 cage molecule was extracted using CSD^[34] from the crystal structure determination^[35] (ZEGSUZ04). The carbon atoms were placed arbitrarily to maintain correct chemical composition without overdue complication of the model, and give no information on the real orientation of the *o*-carborane molecule.

The solvent molecules CH_3CN and CH_2Cl_2 or toluene are severely disordered, and in supramolecular compounds **3**, **6** and **7** their real content can be seriously underestimated.

Table 2. Experimental details for compounds **3-Cl**, **4-Cl** and **4-Cl-CH₃CN**.

Crystal data	3-Cl	4-Cl	4-Cl-CH₃CN
Chemical formula	C ₁₃₂ H ₂₀₄ Cl _{18.80} Cu _{18.80} Fe ₁₂ P ₆₀ ·6(C ₇ H ₈)·3(CH ₂ Cl ₂)	C ₁₁ H ₁₇ Cl ₃ Cu ₃ FeP ₅	C ₂₅ H ₃₇ Cl ₆ Cu ₆ Fe ₂ NP ₁₀ ·CH ₃ CN
<i>M_r</i>	6987.93	656.91	1395.94
Crystal system, space group	Cubic, <i>Fm3c</i>	Orthorhombic, <i>Pbcm</i>	Monoclinic, <i>P2₁/n</i>
Temperature (K)	90	90	90
<i>a</i> , <i>b</i> , <i>c</i> (Å)	41.5600 (3)	10.05280(16), 15.2613(3), 12.7940(2)	12.6711(2), 15.6252(3), 23.1053(5)
<i>β</i> (°)	90	90	99.3555(18)
<i>V</i> (Å ³)	71783.9 (16)	1962.85(6)	4513.72(16)
<i>Z</i>	8	4	4
<i>F</i> (000)	27990	1288	2752
<i>D_x</i> (Mg m ⁻³)	1.293	2.223	2.054
Radiation type	Cu <i>Kα</i>	Cu <i>Kα</i>	Cu <i>Kα</i>
<i>μ</i> (mm ⁻¹)	9.39	16.99	14.78
Crystal shape	Prism	Prism	Needle
Colour	Dark brown	Yellow	Yellow
Crystal size (mm)	0.17 × 0.16 × 0.13	0.09 × 0.08 × 0.06	0.35 × 0.02 × 0.01
Data collection			
Diffractometer	SuperNova, Titan ^{S2}	SuperNova, Titan ^{S2}	SuperNova, Titan ^{S2}
Absorption correction	Gaussian	Gaussian	Gaussian
<i>T_{min}</i> , <i>T_{max}</i>	0.312, 0.545	0.379, 0.503	0.207, 1.000
No. of measured, independent and observed [<i>I</i> > 2σ(<i>I</i>)] reflections	12944, 3162, 2543	4654, 2065, 1748	15064, 8805, 5227
<i>R_{int}</i>	0.022	0.030	0.060
(sin θ/λ) _{max} (Å ⁻¹)	0.627	0.627	0.627
Range of <i>h</i> , <i>k</i> , <i>l</i>	<i>h</i> = -47→37, <i>k</i> = -6→51, <i>l</i> = -29→23	<i>h</i> = -11→12, <i>k</i> = -14→18, <i>l</i> = -15→7	<i>h</i> = -8→15, <i>k</i> = -14→18, <i>l</i> = -28→27
Refinement			
<i>R</i> [<i>F</i> ² > 2σ(<i>F</i> ²)], <i>wR</i> (<i>F</i> ²), <i>S</i>	0.067, 0.204, 1.06	0.023, 0.052, 0.95	0.058, 0.133, 0.91
No. of reflections	3162	2065	8805
No. of parameters	172	116	491
No. of restraints	6	0	13
H-atom treatment	constrained	constrained	constrained
Δ _{max} , Δ _{min} (e Å ⁻³)	0.85, -0.78	0.59, -0.45	1.66, -1.04

Computer programs: CrysAlis PRO 1.171.39.37b (Rigaku OD, 2017), SHELXT2018/5 (Sheldrick, 2018), SHELXL2018/3 (Sheldrick, 2018). SHELXT2014/7 (Sheldrick, 2014), SHELXL2014/7 (Sheldrick, 2014).

Table 3. Experimental details for compounds **5-Br**, **5-I** and **6b-Cl**.

Crystal data	5-Br	5-I	6b-Cl
Chemical formula	C ₁₁ H ₁₇ Br ₃ Cu ₃ FeP ₅	C ₁₁ H ₁₇ Cu ₃ FeI ₃ P ₅	(P ₄ S ₃) _{0.8} @C ₁₃₂ H ₂₀₄ Cl _{18.60} Cu _{18.60} Fe ₁₂ P ₆₀ (C ₇ H ₈) ₆ (CH ₂ Cl ₂) _{0.96}
<i>M_r</i>	790.29	931.26	6970.96
Crystal system, space group	Monoclinic, <i>P2₁/c</i>	Monoclinic, <i>P2₁/c</i>	Cubic, <i>Fm3c</i>
Temperature (K)	90	123	90
<i>a</i> , <i>b</i> , <i>c</i> (Å)	11.0228(5), 12.2772(4), 15.6863(5)	11.18729(11), 12.62201(13), 16.08805(15)	41.55007(13)
<i>β</i> (°)	94.749(3)	96.3307(9)	90
<i>V</i> (Å ³)	2115.53(13)	2257.88(4)	71732.4(7)
<i>Z</i>	4	4	8
<i>F</i> (000)	1504	1720	27923
<i>D_x</i> (Mg m ⁻³)	2.481	2.740	1.291
Radiation type	Cu <i>Kα</i>	Cu <i>Kα</i>	Cu <i>Kα</i>
<i>μ</i> (mm ⁻¹)	18.93	43.74	9.42
Crystal shape	Plate	prism	Prism
Colour	Yellow	black	Dark brown
Crystal size (mm)	0.09 × 0.04 × 0.02	0.13 × 0.09 × 0.07	0.07 × 0.06 × 0.05
Data collection			
Diffractometer	SuperNova, Titan ^{S2}	SuperNova, Titan ^{S2}	SuperNova, Titan ^{S2}
Absorption correction	Gaussian	Gaussian	Gaussian
<i>T_{min}</i> , <i>T_{max}</i>	0.357, 0.756	0.031, 0.207	0.549, 0.664
No. of measured, independent and observed [<i>I</i> > 2σ(<i>I</i>)] reflections	8248, 4206, 3031	22323, 4430	4508, 17592, 3148, 2401
<i>R_{int}</i>	0.050	0.037	0.033
(sin θ/λ) _{max} (Å ⁻¹)	0.627	0.625	0.624
Range of <i>h</i> , <i>k</i> , <i>l</i>	<i>h</i> = -9→13, <i>k</i> = -15→12, <i>l</i> = -17→19	<i>h</i> = -13→13, <i>k</i> = -15→15, <i>l</i> = -19→20	<i>h</i> = -15→50, <i>k</i> = -34→41, <i>l</i> = -42→22
Refinement			
<i>R</i> [<i>F</i> ² > 2σ(<i>F</i> ²)], <i>wR</i> (<i>F</i> ²), <i>S</i>	0.043, 0.110, 1.02	0.020, 1.11	0.050, 0.059, 0.193, 1.04
No. of reflections	4206	4508	3148
No. of parameters	213	214	156
No. of restraints	0	0	5
H-atom treatment	H-atom parameters constrained	H-atom parameters constrained	H-atom parameters constrained
Δ _{max} , Δ _{min} (e Å ⁻³)	0.87, -0.87	1.09, -0.83	0.91, -0.59

Computer programs: CrysAlis PRO, Agilent Technologies, different versions 2014-2017, SHELXS (Sheldrick, 2008), SHELXL2014/7 (Sheldrick, 2014), SHELXT2018/5 (Sheldrick, 2018), SHELXL2018/3 (Sheldrick, 2018).

Table 4. Experimental details for compounds **6a-Cl** and **6a-Br**.

Crystal data	6a-Cl	6a-Br
Chemical formula	(P ₄ S ₃)@C ₁₃₂ H ₂₀₄ Fe ₁₂ P ₆₀ Cl _{17.40} Cu _{17.40} ·(CH ₃ CN) _{6.25} ·(CH ₂ Cl ₂) _{2.2}	(P ₄ S ₃) _{0.833} @C ₁₃₂ H ₂₀₄ Fe ₁₂ P ₆₀ Cl _{17.40} Cu _{17.40} ·(CH ₃ CN) _{2.8} ·(CH ₂ Cl ₂) _{1.42}
<i>M_r</i>	6705.25	7234.27
Crystal system, space group	Tetragonal, <i>P4₂/n</i>	Tetragonal, <i>P4₂/n</i>
Temperature (K)	15	80
<i>a</i> , <i>c</i> (Å)	36.43436(6), 20.49028(15)	36.66093(4), 20.67071(5)
<i>V</i> (Å ³)	27200.1(2)	27781.93(9)
<i>Z</i>	4	4
<i>F</i> (000)	13385	14131
<i>D_x</i> (Mg m ⁻³)	1.637	1.730
Radiation type	Synchrotron, λ = 0.500 Å	Synchrotron, λ = 0.6888 Å
μ (mm ⁻¹)	0.97	4.45
Crystal shape	Prism	Prism
Colour	Dark brown	Dark brown
Crystal size (mm)	0.40 × 0.30 × 0.30	0.4 × 0.2 × 0.2
Data collection		
Diffractometer	P24 beamline, PETRA III, DESY, Huber diffractometer, Pilatus3 CdTe 1M	P11 beamline, PETRA III, DESY, Decries PILATUS 6M
Absorption correction	Multi-scan	Multi-scan
<i>T_{min}</i> , <i>T_{max}</i>	0.769, 1.000	0.417, 1.000
No. of measured, independent and observed [<i>I</i> > 2σ(<i>I</i>)] reflections	550742, 49692, 44165	333067, 43780, 40134
<i>R_{int}</i>	0.028	0.033
(sin θ/λ) _{max} (Å ⁻¹)	0.823	0.760
Range of <i>h</i> , <i>k</i> , <i>l</i>	<i>h</i> = -58→59, <i>k</i> = -58→58, <i>l</i> = -30→30	<i>h</i> = -48→48, <i>k</i> = -44→48, <i>l</i> = -30→29
Refinement		
<i>R</i> [<i>F</i> ² > 2σ(<i>F</i> ²)], <i>wR</i> (<i>F</i> ²), <i>S</i>	0.040, 0.129, 1.05	0.037, 0.123, 1.03
No. of reflections	49692	43780
No. of parameters	1511	1363
No. of restraints	9	29
H-atom treatment	H-atom parameters constrained	H-atom parameters constrained
Δ _{max} , Δ _{min} (e Å ⁻³)	2.20, -1.42	2.70, -1.45
Computer programs: CrysAlis PRO 1.171.41.21a (Rigaku OD, 2019), SHELXT2018/5 (Sheldrick, 2018), SHELXL2018/3 (Sheldrick, 2018).		

Table 5. Experimental details for compounds **6a'-Br** and **7b-Cl**.

Crystal data	6a'-Br	7b-Cl
Chemical formula	(P ₄ S ₃) _{0.68} @C ₁₂₃ H ₂₀₄ Fe ₁₂ P ₆₀ Cu _{17.20} Cl _{17.20} · (CH ₂ Cl ₂) _{1.4} · (CH ₃ CN) _{2.25}	(C ₂ B ₁₀ H ₁₂) _{0.5} · C ₁₃₂ H ₂₀₄ Fe ₁₂ P ₆₀ Cu _{18.25} Cl _{18.25} · (C ₇ H ₈) _{5.4} · (CH ₂ Cl ₂) _{1.2}
<i>M_r</i>	7147.59	6797.45
Crystal system, space group	Monoclinic, <i>C2/m</i>	Cubic, <i>Fm3c</i>
Temperature (K)	80	90
<i>a</i> , <i>b</i> , <i>c</i> (Å)	33.6038 (4), 23.74502 (14), 34.6012 (2)	41.26543 (16)
β (°)	103.3649 (7)	90
<i>V</i> (Å ³)	26861.3 (4)	70268.3 (8)
<i>Z</i>	4	8
<i>F</i> (000)	13962	27239
<i>D_x</i> (Mg m ⁻³)	1.767	1.285
Radiation type	Synchrotron, λ = 0.61991 Å	Cu <i>K</i> α
μ (mm ⁻¹)	3.44	9.27
Crystal shape	Prism	Prism
Colour	Dark brown	Dark brown
Crystal size (mm)	0.10 × 0.10 × 0.08	0.23 × 0.16 × 0.09
Data collection		
Diffractometer	P11 beamline, PETRA III, DESY, SuperNova, Titan ^{S2} Dectris PILATUS 6M	
Absorption correction	Multi-scan	Gaussian
<i>T_{min}</i> , <i>T_{max}</i>	0.572, 1.000	0.325, 0.595
No. of measured, independent and observed [<i>I</i> > 2σ(<i>I</i>)] reflections	83620, 83620, 67511	14536, 3060, 2326
<i>R_{int}</i>	0.050	0.023
(sin θ / λ) _{max} (Å ⁻¹)	0.845	0.623
Range of <i>h</i> , <i>k</i> , <i>l</i>	<i>h</i> = -48→48, <i>k</i> = -36→36, <i>l</i> = -54→55	<i>h</i> = -19→44, <i>k</i> = -45→50, <i>l</i> = -36→34
Refinement		
<i>R</i> [<i>F</i> ² > 2σ(<i>F</i> ²)], <i>wR</i> (<i>F</i> ²), <i>S</i>	0.059, 0.194, 1.05	0.080, 0.270, 1.12
No. of reflections	83620	3060
No. of parameters	1352	151
No. of restraints	19	5
H-atom treatment	H-atom parameters constrained	H-atom parameters constrained
Δ _{max} , Δ _{min} (e Å ⁻³)	2.61, -2.80	1.23, -0.63

Computer programs: CrysAlis PRO 1.171.41.21a (Rigaku OD, 2019), CrysAlis PRO 1.171.38.46 (Rigaku OD, 2015), SHELXT2018/5 (Sheldrick, 2018), SHELXL2018/3 (Sheldrick, 2018).

Table 6. Experimental details for compounds **7a-Cl**, **7a-Br** and **7a'-Br**.

Crystal data	7a-Cl	7a-Br	7a'-Br
Chemical formula	(C ₂ B ₁₀ H ₁₂)@C ₁₃₂ H ₂₀₄ Fe ₁₂ P ₆₀ Cl _{17.75} Cu _{17.75} ·(CH ₃ CN) _{5.95} ·(CH ₂ Cl ₂) _{2.25}	(C ₂ B ₁₀ H ₁₂)@C ₁₃₂ H ₂₀₄ P ₆₀ Fe ₁₂ Cu _{17.75} Br _{17.75} ·(CH ₃ CN) _{3.7} ·(CH ₂ Cl ₂) _{1.3}	(C ₂ B ₁₀ H ₁₂) _{0.83} @C ₁₃₂ H ₂₀₄ P ₆₀ Fe ₁₂ Cu _{17.73} Br _{17.73} ·(CH ₃ CN) ₂ ·(CH ₂ Cl ₂) _{2.28}
<i>M_r</i>	6655.98	7272.10	7258.15
Crystal system, space group	Tetragonal, <i>P</i> 4 ₂ / <i>n</i>	Tetragonal, <i>P</i> 4 ₂ / <i>n</i>	Trigonal, <i>R</i> $\bar{3}$
Temperature (K)	20	90	90
<i>a</i> , <i>b</i> , <i>c</i> (Å)	36.41565 (11), 20.48100 (11)	36.59223 (13), 20.65336 (19)	42.18984 (13), 51.3601 (2)
<i>V</i> (Å ³)	27159.8 (2)	27654.7 (3)	79172.0 (6)
<i>Z</i>	4	4	12
<i>F</i> (000)	13296	14216	42527
<i>D_x</i> (Mg m ⁻³)	1.628	1.747	1.827
Radiation type	Synchrotron, λ = 0.500 Å	Cu <i>K</i> α	Cu <i>K</i> α
μ (mm ⁻¹)	0.96	13.11	13.90
Crystal shape	Prism	Elongated prism	Rhombohedron
Colour	Dark brown	Dark brown	Dark brown
Crystal size (mm)	0.40 × 0.35 × 0.30	0.15 × 0.06 × 0.03	0.20 × 0.15 × 0.09
Data collection			
Diffractometer	P24 beamline, PETRA III, DESY, Huber diffractometer, Pilatus3 CdTe 1M	SuperNova, Titan ^{S2}	SuperNova, Titan ^{S2}
Absorption correction	Multi-scan	Gaussian	Gaussian
<i>T_{min}</i> , <i>T_{max}</i>	0.181, 1.000	0.308, 0.749	0.265, 0.605
No. of measured, independent and observed [<i>I</i> > 2σ(<i>I</i>)] reflections	552525, 55644, 48375	93029, 27808, 21479	121223, 35282, 28168
<i>R_{int}</i>	0.042	0.048	0.043
(sin θ/λ) _{max} (Å ⁻¹)	0.824	0.624	0.625
Range of <i>h</i> , <i>k</i> , <i>l</i>	<i>h</i> = -59→59, <i>k</i> = -58→57, <i>l</i> = -33→33	<i>h</i> = -45→43, <i>k</i> = -41→32, <i>l</i> = -23→25	<i>h</i> = -52→49, <i>k</i> = -52→39, <i>l</i> = -62→57
Refinement			
<i>R</i> [<i>F</i> ² > 2σ(<i>F</i> ²)], <i>wR</i> (<i>F</i> ²), <i>S</i>	0.038, 0.122, 1.04	0.042, 0.108, 0.95	0.046, 0.131, 0.97
No. of reflections	55644	27808	35282
No. of parameters	1523	1397	1760
No. of restraints	26	30	24
H-atom treatment	H-atom parameters constrained	H-atom parameters constrained	H-atom parameters constrained
Δ _{max} , Δ _{min} (e Å ⁻³)	1.55, -1.28	1.65, -1.63	2.22, -0.82

Computer programs: CrysAlis PRO 1.171.41.21a (Rigaku OD, 2019), CrysAlis PRO 1.171.40.18c (Rigaku OD, 2018), SHELXT2018/5 (Sheldrick, 2018), SHELXL2018/3 (Sheldrick, 2018).

3.6 Author Contributions

- The synthesis and characterization of compounds **2-Cl**, **5-I**, **6a-Br** and **6a'-Br** and the characterization of compound **2-Br** was performed by Helena Brake
- The synthesis of compounds **3-Cl**, **3-Br** and **4-Cl-CH₃CN** was performed by Helena Brake and Robert Szlosek and are also part of his Bachelor thesis; their characterization was performed by Helena Brake
- The synthesis of compounds **4-Cl** and **5-Br** was performed by Helena Brake and Robert Szlosek and are also part of his Bachelor thesis and their characterization was performed by Helena Brake and Susan Rank
- The synthesis of compounds **6a-Cl**, **6b-Cl**, **7a-Cl**, **7b-Cl**, **7a-Br**, and **7a'-Br** was performed by Helena Brake and their characterization was performed by Helena Brake and Susan Rank.
- The investigations on the reaction behavior of compounds **3** and **7** were performed by Helena Brake
- X-ray structure analyses of compounds **3-Cl**, **4-Cl**, **4-Cl-CH₃CN**, **5-Br**, **5-I**, **6a-Cl**, **6b-Cl**, **6a-Br**, **6a'-Br**, **7a-Cl**, **7b-Cl**, **7a-Br**, and **7a'-Br** were performed by Dr. Eugenia Peresyphkina, Dr. Sc. Alexander Virovets and Helena Brake. Parts of this research (projects I-20170135, I-20180049 and I-20180967) were carried out at PETRA III at DESY, a member of the Helmholtz Association (HGF), by Dr. Eugenia Peresyphkina and Dr. Sc. Alexander V. Virovets. EP and AV are grateful to Dr. A. Burkhardt and Dr. Martin Tolkiehn for the assistance regarding the use of the beamlines P11 and P24, respectively.
- X-ray powder diffraction of compounds **4-Cl**, **5-Br** and **5-I** was performed by Dr. Christian Klimas (group of Prof. Dr. Arno Pfitzner)
- Solid-state MAS NMR spectroscopy of compounds **4-Cl**, **5-Br** and **5-I** was performed by Prof. Dr. W. Kremer
- The manuscript (introduction, results and discussion, experimental part, conclusion; including figures and graphical abstract) was written by Helena Brake
- The section 'crystallographic details' was written by Dr. Eugenia Peresyphkina

3.7 References

- [1] a) D. J. Cram, *Angew. Chem. Int. Ed. Engl.* **1988**, *27*, 1009-1020; b) J.-M. Lehn, *Angew. Chem. Int. Ed. Engl.* **1988**, *27*, 89-112; c) C. J. Pedersen, *Angew. Chem. Int. Ed. Engl.* **1988**, *27*, 1021-1027; d) D. S. Wright in *Comprehensive Inorganic Chemistry II (Second Edition)*, Vol. 1 (Eds.: J. Reedijk, K. Poeppelmeier), Elsevier, Amsterdam, **2013**, pp. 953-967; e) D. Zhang, T. K. Ronson, J. R. Nitschke, *Acc. Chem. Res.* **2018**, *51*, 2423-2436; f) T. L. Mako, J. M. Racicot, M. Levine, *Chem. Rev.* **2019**, *119*, 322-477; g) F. Dankert, L. Erlemeier, C. Ritter, C. von Hänisch, *Inorg. Chem. Front.* **2020**, *7*, 2138-2153.
- [2] a) E. C. Constable, *Pure Appl. Chem.* **1996**, *68*, 253-260; b) R. Chakrabarty, P. S. Mukherjee, P. J. Stang, *Chem. Rev.* **2011**, *111*, 6810-6918; c) Y.-Y. Zhang, W.-X. Gao, L. Lin, G.-X. Jin, *Coord. Chem. Rev.* **2017**, *344*, 323-344; d) S. Chakraborty, G. R. Newkome, *Chem. Soc. Rev.* **2018**, *47*, 3991-4016.
- [3] a) J. Bai, A. V. Virovets, M. Scheer, *Angew. Chem. Int. Ed.* **2002**, *41*, 1737-1740; b) M. Scheer, L. J. Gregoriades, A. V. Virovets, W. Kunz, R. Neueder, I. Krossing, *Angew. Chem. Int. Ed.* **2006**, *45*, 5689-5693; c) S. Welsch, L. J. Gregoriades, M. Sierka, M. Zabel, A. V. Virovets, M. Scheer, *Angew. Chem. Int. Ed.* **2007**, *46*, 9323-9326; d) M. Fleischmann, S. Welsch, H. Krauss, M. Schmidt, M. Bodensteiner, E. V. Peresykina, M. Sierka, C. Gröger, M. Scheer, *Chem. Eur. J.* **2014**, *20*, 3759-3768; e) F. Dielmann, C. Heindl, F. Hastreiter, E. V. Peresykina, A. V. Virovets, R. M. Gschwind, M. Scheer, *Angew. Chem. Int. Ed.* **2014**, *53*, 13605-13608; f) C. Heindl, S. Heindl, D. Lüdeker, G. Brunklaus, W. Kremer, M. Scheer, *Inorg. Chim. Acta* **2014**, *422*, 218-223.
- [4] a) J. Bai, A. V. Virovets, M. Scheer, *Science* **2003**, *300*, 781-783; b) F. Dielmann, C. Heindl, F. Hastreiter, E. V. Peresykina, A. V. Virovets, R. M. Gschwind, M. Scheer, *Angew. Chem. Int. Ed.* **2014**, *53*, 13605-13608; c) S. Heindl, E. Peresykina, J. Sutter, M. Scheer, *Angew. Chem. Int. Ed.* **2015**, *54*, 13431-13435.
- [5] M. Scheer, J. Bai, B. P. Johnson, R. Merkle, A. V. Virovets, C. E. Anson, *Eur. J. Inorg. Chem.* **2005**, 4023-4026.
- [6] a) M. Scheer, A. Schindler, C. Gröger, A. V. Virovets, E. V. Peresykina, *Angew. Chem. Int. Ed.* **2009**, *48*, 5046-5049; b) A. Schindler, C. Heindl, G. Balázs, C. Gröger, A. V. Virovets, E. V. Peresykina, M. Scheer, *Chem. Eur. J.* **2012**, *18*, 829-835; c) M. Scheer, A. Schindler, R. Merkle, B. P. Johnson, M. Linseis, R. Winter, C. E. Anson, A. V. Virovets, *J. Am. Chem. Soc.* **2007**, *129*, 13386-13387; d) C. Schwarzmaier, A. Schindler, C. Heindl, S. Scheuermayer, E. V. Peresykina, A. V. Virovets, M. Neumeier, R. Gschwind, M. Scheer, *Angew. Chem. Int.*

- Ed.* **2013**, *52*, 10896-10899; e) H. Brake, E. Peresykina, C. Heindl, A. V. Virovets, W. Kremer, M. Scheer, *Chem. Sci.* **2019**, *10*, 2940-2944.
- [7] S. Welsch, C. Gröger, M. Sierka, M. Scheer, *Angew. Chem. Int. Ed.* **2011**, *50*, 1435-1438.
- [8] a) F. Dielmann, C. Heindl, F. Hastreiter, E. V. Peresykina, A. V. Virovets, R. M. Gschwind, M. Scheer, *Angew. Chem. Int. Ed.* **2014**, *53*, 13605-13608; b) F. Dielmann, M. Fleischmann, C. Heindl, E. V. Peresykina, A. V. Virovets, R. M. Gschwind, M. Scheer, *Chem. Eur. J.* **2015**, *21*, 6208-6214.
- [9] C. Heindl, *Dissertation (University of Regensburg)*, **2015**.
- [10] O. J. Scherer, T. Brück, G. Wolmershäuser, *Chem. Ber.* **1988**, *121*, 935-938.
- [11] The amount of CH₂Cl₂ occupying the void of **3-Cl** is most probably underestimated due to severe disorder. The P₄S₃ and *o*-C₂B₁₀H₁₂ occupancy factors (<1) in the structures of **6b-Cl**, **6a-Br**, **6a'-Br**, **7b-Cl** and the $\bar{1}$ position of **7a'-Br** are most probably underestimated for the same reason.
- For P₄S₃ and *o*-C₂B₁₀H₁₂, the refined occupancies *m* reach the maximum occupancy of 1, which is found in the structures of **6a-Cl**, **7a-Cl**, **7a-Br** and the $\bar{3}$ position of **7a'-Br** and thus, in these crystal structures, the modeling of the disorder of the guest molecules can be considered complete and the chemical composition reliable in this respect.
- [12] For **3-Br**, no crystals of sufficient quality for complete structural characterization were found, but the determined unit cell parameters are characteristic for (80-*n*)-vertex spherical scaffolds of **1^x**. Since no template was added and **1^x** itself is too large to be encapsulated into an (80-*n*)-vertex sphere, the compound obtained was identified as (80-*n*)-vertex sphere with CH₂Cl₂ occupying the void. This is confirmed by further analytics and by the similar behavior in solution as found for **3-Cl**. The number of vacancies *n* is only an average value found in the single measured crystal of **3-Cl**. Implying possible CuCl-deficiency, the average CuCl amount in the bulk hence may differ from this value.
- [13] By washing with CH₃CN, an excess of uncoordinated CuCl was washed out of the product. However, CH₃CN also seems to be coordinated to the initially formed polymer **4-Cl** by washing, resulting in a 3:1 mixture of **4-Cl** and **4-Cl-CH₃CN**, as indicated by the presence of 25% CH₃CN in the elemental analysis despite thorough drying under vacuum and additional signals in the ³¹P{¹H} MAS NMR spectrum.
- [14] Although additionally 25% **4-Cl-CH₃CN** seem to be present (cf. elemental analysis and ³¹P{¹H} MAS NMR spectrum), this is not clearly reflected in the X-ray powder diffraction pattern. However, it is possible that the reflections of **4-Cl-CH₃CN** are too weak in intensity

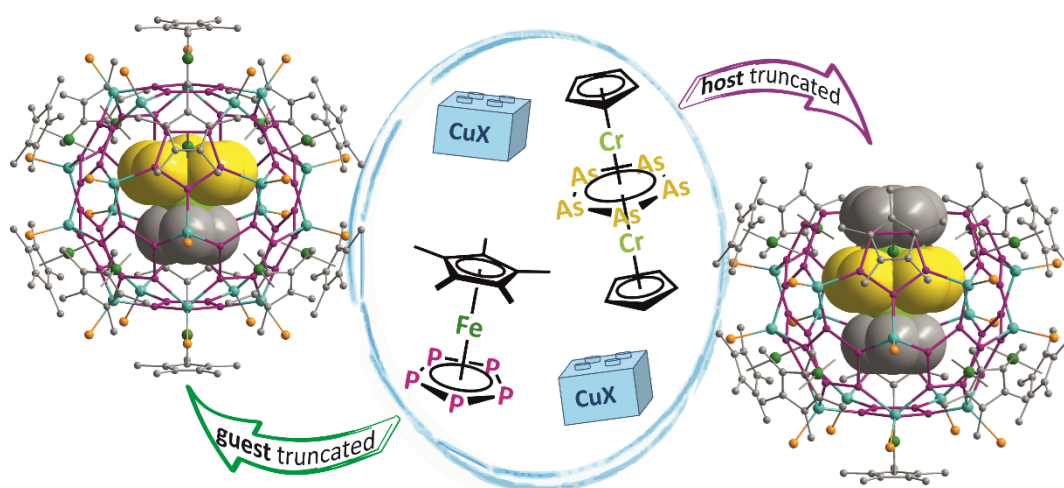
and partly lie underneath the reflections of **4-Cl**, resulting in the comparatively large (amorphous) background.

- [15] E. V. Peresykina, C. Heindl, A. Schindler, M. Bodensteiner, A. V. Virovets, M. Scheer, *Z. Kristallogr.* **2014**, *229*, 735-740.
- [16] F. Dielmann, A. Schindler, S. Scheuermayer, J. Bai, R. Merkle, M. Zabel, A. V. Virovets, E. V. Peresykina, G. Brunklaus, H. Eckert, M. Scheer, *Chem. Eur. J.* **2012**, *18*, 1168-1179.
- [17] E. Peresykina, C. Heindl, A. Virovets, M. Scheer, *Struct. Bonding (Berlin, Ger.)* **2017**, *174*, 1-53.
- [18] J. Schiller, E. Peresykina, A. V. Virovets, M. Scheer, *Angew. Chem. Int. Ed.* **2020**, *59*, 13647-13650.
- [19] The outer diameters were calculated from the largest C...C distance between two furthestmost ethyl groups plus twice the van-der-Waals radius of C (1.70 Å). The range of the inner diameters were calculated from the shortest and longest centroid-centroid distances between two opposing P₅ planes minus twice the van-der-Waals radius of P (1.80 Å). Van-der-Waals radii were taken from reference [20].
- [20] M. Mantina, A. C. Chamberlin, R. Valero, C. J. Cramer, D. G. Truhlar, *J. Phys. Chem. A* **2009**, *113*, 5806-5812, and references therein.
- [21] L. Y. Goh, W. Chen, R. C. S. Wong, K. Karaghiosoff, *Organometallics* **1995**, *14*, 3886-3896. The size was calculated from the largest P...S distance (3.39 Å) plus the van-der-Waals radii of P (1.80 Å) and S (1.80 Å). Van-der-Waals radii were taken from reference [20].
- [22] M. G. Davidson, T. G. Hibbert, J. A. K. Howard, A. Mackinnon, K. Wade, *Chem. Commun.* **1996**, 2285-2286. The size was calculated as the largest distance of two furthestmost H atoms (5.57 Å) plus twice the van-der-Waals radius of H (1.10 Å). The van-der-Waals radius was taken from reference [20].
- [23] Free **1*** is additionally detected in the ³¹P{¹H} NMR spectra. Its presence might indicate some disaggregation of 90-vertex spherical compounds **2** in solution, a feature already observed e.g. for (80-n)-vertex spheres of **1*** and **1^{Bn}**, cf. references [8b,9].
- [24] NMR data of pure **1***:
¹H NMR (CD₂Cl₂): δ [ppm] = 0.75 (t, ³J_{HH} = 7.6 Hz, 3 H, -CH₂CH₃), 1.43 (s, 6 H, -CH₃), 1.45 (s, 6 H, -CH₃), 1.94 (q, ³J_{HH} = 7.6 Hz, 2 H, -CH₂CH₃).
³¹P{¹H} NMR (CD₂Cl₂): δ [ppm] = 151.9 (s).
- [25] M. Detzel, G. Friedrich, O. J. Scherer, G. Wolmershäuser, *Angew. Chem. Int. Ed. Engl.* **1995**, *34*, 1321.

- [26] At first, the sample was dissolved in pyridine under decomposition. After removal of the solvent the residue was re-dissolved in CH₂Cl₂ and CH₃CN.
- [27] At first, the sample was dissolved in pyridine under decomposition. After removal of the solvent the residue was re-dissolved in CH₃CN.
- [28] A. Burkhardt, T. Pakendorf, B. Reime et al, *Eur. Phys. J. Plus* **2016**, *131*, 56-64.
- [29] *CrysAlisPRO*, different versions **2006-2020**, Rigaku Oxford Diffraction.
- [30] https://photon-science.desy.de/facilities/petra_iii/beamlines/p24_chemical_crystallography/eh2/index_eng.html
- [31] G. M. Sheldrick. *Acta Cryst. Sect. C* **2015**, *C71*, 3-8.
- [32] C. R. Groom, I. J. Bruno, M. P. Lightfoot and S. C. Ward, *Acta Cryst. Sect. B* **2016**, *B72*, 171-179.
- [33] M. Schultz, C. J. Burns, D. J. Schwartz, R. A. Andersen, *Organometallics* **2000**, *19*, 781.
- [34] C. R. Groom, I. J. Bruno, M. P. Lightfoot and S. C. Ward, *Acta Cryst. Sect. B* **2016**, *B72*, 171-179.
- [35] T. K. Chattopadhyay, W. May, H. G. von Schnering, G. S. Pawley, *Z. Kristallogr. Cryst. Mater.* **1983**, *165*, 47.

4 From Nano-Balls to Nano-Bowls

H. Brake, E. Peresykina, C. Heindl, A. V. Virovets, W. Kremer, M. Scheer, *Chem. Sci.* **2019**, *10*, 2940-2944. – Adapted with permission of The Royal Society of Chemistry ([view online](#)).



Abstract:

Pentaphosphaferrocene [$\text{Cp}^*\text{Fe}(\eta^5\text{-P}_5)$] in combination with Cu(I) halides is capable of a template-directed synthesis of fullerene-like spheres. Herein, we present the use of a triple decker complex as template that leads to the formation of unprecedented 'nano-bowls'. These spherical domes resemble the truncated fullerenes $I_h\text{-C}_{80}$ and represent a novel spherical arrangement in the chemistry of spherical molecules.

4.1 Introduction

Supramolecular chemistry is one of the most fascinating topics in current research, as it is inspired by highly complex biochemical systems where the efficiency and selectivity of chemical processes are triggered by weak interactions between small subunits. During the last decades, it was successfully extended to non-biological systems. Here, the coordinative bond turned out to be an excellent tool, since it combines the advantages of both covalent bonds and weak interactions: it is relatively strong, but often weak enough to enable dynamic behavior in solution. Hence, the self-assembly of metal salts and organic linkers has produced a wide variety of metal-organic frameworks (MOFs) on the one hand^[1] and discrete nano-sized supramolecules on the other hand.^[2] The latter often provide defined inner cavities and can be used e.g. as molecular containers.

Recently, we have introduced pentaphosphaferrocene [$\text{Cp}^{\text{R}}\text{Fe}(\eta^5\text{-P}_5)$] ($\text{Cp}^{\text{R}} = \text{Cp}^* = \eta^5\text{-C}_5\text{Me}_5$; $\text{Cp}^{\text{Bn}} = \eta^5\text{-C}_5(\text{CH}_2\text{Ph})_5$; $\text{Cp}^{\text{BIG}} = \eta^5\text{-C}_5(4\text{-}^i\text{BuC}_6\text{H}_4)_5$) as an outstanding five-fold symmetric organometallic building block and an auspicious alternative to the often used di- or tridentate organic linkers (Figure 1a).^[3] Astonishingly, under certain conditions the *cyclo*- P_5 ligand in combination with Cu(I) halides leads to the formation of spheres with fullerene-like topologies or beyond them.^[4,5] The synthesis of such nanospheres is often template-directed, thus, various molecules such as e.g. C_{60} ^[4f] and ferrocene^[4d] are encapsulated within these nano-balls. Among all templates, the triple decker complex $[(\text{CpCr})_2(\mu, \eta^{5:5}\text{-As}_5)]$ (**1**)^[6] is an exceptional case (Figure 1b).

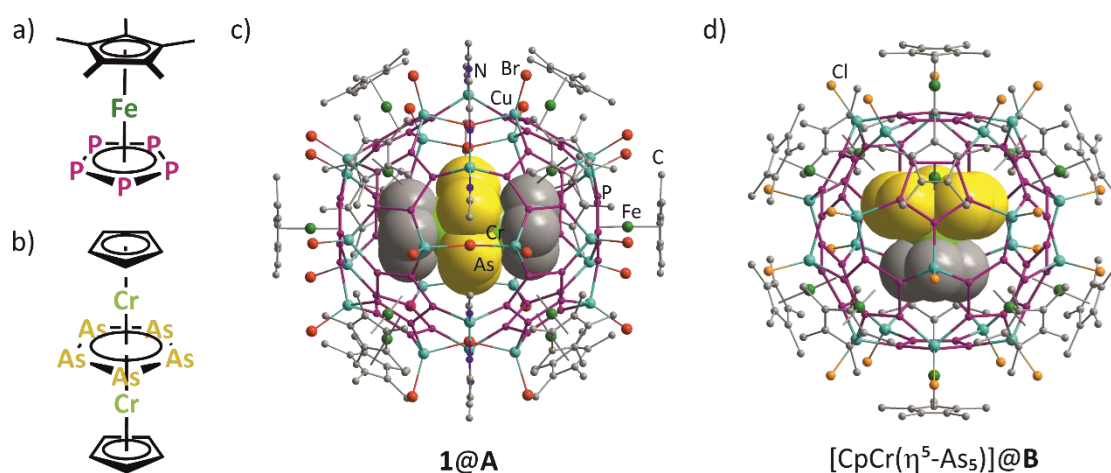


Figure 1. a) Building block [$\text{Cp}^*\text{Fe}(\eta^5\text{-P}_5)$]; b) template $[(\text{CpCr})_2(\mu, \eta^{5:5}\text{-As}_5)]$ (**1**); c) inclusion of **1** into the 90-vertex sphere **A**; d) inclusion of the 16 VE fragment [$\text{CpCr}(\eta^5\text{-As}_5)$] generated from **1** into the 80-vertex sphere **B**.

Together with CuBr, it is incorporated into the 90-vertex host $[(\text{Cp}^*\text{Fe}(\eta^5\text{-P}_5))_{12}(\text{CuBr})_{25}(\text{CH}_3\text{CN})_{10}]$ (host **A**), while, in the case of CuCl, a reproducible cleavage of the template takes place, and in the free-state, the unstable molecule [$\text{CpCr}(\eta^5\text{-As}_5)$] is encapsulated into the slightly smaller

80-vertex sphere $[\{\text{Cp}^*\text{Fe}(\eta^5\text{-P}_5)\}_{12}(\text{CuCl})_{20}]$ (host **B**) (Figure 1c,d).^[4d] Both reactions were carried out under similar conditions in a mixture of toluene/ CH_3CN only differing by the nature of the Cu(I) halide applied. Since not only the used Cu(I) halide affects the reaction pathway, but self-assembly processes also strongly depend on the reaction conditions used,^[7] the question arose in what way the applied solvent mixtures influence the reaction outcome. Addressing this issue is of general importance since it may open the way for going different pathways within one and the same reaction in supramolecular chemistry.

Herein, the solvent-dependent self-assembly of the systems containing **1**, $[\text{Cp}^*\text{Fe}(\eta^5\text{-P}_5)]$ and CuX ($X = \text{Cl}, \text{Br}$) is demonstrated, which mainly depends on the solvent used and only to some extent on the used Cu(I) salt (formation of a 80- or 90-vertex ball). Remarkably, the change of the reaction media from toluene/ CH_3CN to $\text{CH}_2\text{Cl}_2/\text{CH}_3\text{CN}$ tunes the self-assembly to the unprecedented nano-bowls **2** with an open fullerene topology. These truncated spheres are able to incorporate the intact triple decker complexes **1**.

4.2 Results and Discussion

To apply the triple decker complex **1**^[6,8] as a template in the systems $[\text{Cp}^*\text{Fe}(\eta^5\text{-P}_5)]$ and CuX ($X = \text{Cl}, \text{Br}$), a solution of $[\text{Cp}^*\text{Fe}(\eta^5\text{-P}_5)]$ and **1** in CH_2Cl_2 is layered with a solution of CuX in CH_3CN . By using CuCl and CuBr , the products **1@2a** and **1@2b** crystallize as dark brown rods in the monoclinic non-centrosymmetric space group *Cc*. The X-ray structure analysis reveals that these crystals represent the novel host-guest complexes $[\mathbf{1}]@[\{\text{Cp}^*\text{Fe}(\eta^5\text{-P}_5)\}_{11}\{\text{CuCl}\}_{13.45}]$ (**1@2a**) and $[\mathbf{1}]@[\{\text{Cp}^*\text{Fe}(\eta^5\text{-P}_5)\}_{11}\{\text{CuBr}\}_{14.55}]$ (**1@2b**) with an open structure resembling the truncated spheres **B** (Figure 2). The 80-vertex scaffold of the spheres **B** contains 12 five-membered P_5 ligands in a 1,2,3,4,5-coordination mode and 30 six-membered $\{\text{Cu}_2\text{P}_4\}$ rings, whereas the halide atoms are all terminal, resembling the $I_h\text{-C}_{80}$ fullerene structure. In most cases,^[5c] some positions of the CuBr fragments are partly vacant leading to the CuX -reduced scaffolds $[\{\text{Cp}^*\text{Fe}(\eta^5\text{-P}_5)\}_{12}\{\text{CuBr}\}_{20-n}]$ as was found by measuring different crystals from different batches of reaction mixtures.^[4b,5c,d,9]

Surprisingly, in **2a** and **2b**, for the first time, a pentaphosphaferrocene vacancy is observed along with n minor vacancies in CuX positions. As a consequence, a $\{\text{Cp}^*\text{Fe}(\eta^5\text{-P}_5)(\text{CuX})_5\}$ moiety is formally cut-off when compared to the spheres **B**, leaving the bowl-like truncated spheres $[\mathbf{1}]@[\{\text{Cp}^*\text{Fe}(\eta^5\text{-P}_5)\}_{11}\{\text{CuX}\}_{15-n}]$ (**1@2a**: $X = \text{Cl}$, $n = 0.45$; **1@2b**: $X = \text{Br}$, $n = 1.55$) (Figure 2). In these unprecedented nano-bowls **2**, the coordination mode of the P_5 rings on the upper ‘bottleneck’ part is reduced to a 1,2,3-fashion and the idealized scaffold of the supramolecule consists of 70 vertices (55 P + 15 Cu) arranged into 11 five-membered P_5 ligands and 25 six-membered $\{\text{Cu}_2\text{P}_4\}$ rings (Figure 2a). The diameter of the cavity in the truncated sphere therefore amounts to a

width of 0.79 nm in the middle of the bowl and 0.61 nm at the bottleneck.^[10,11] The template, with a width of 0.78 nm at the As₅ deck and 0.62 nm at the Cp deck, respectively, fits perfectly in the host cavity.^[11,12] The cavity is open at the top so that the template with its length of 0.99 nm is allowed to protrude from the 0.79 nm deep host but can be incorporated despite this protrusion (Figure 2b, c).

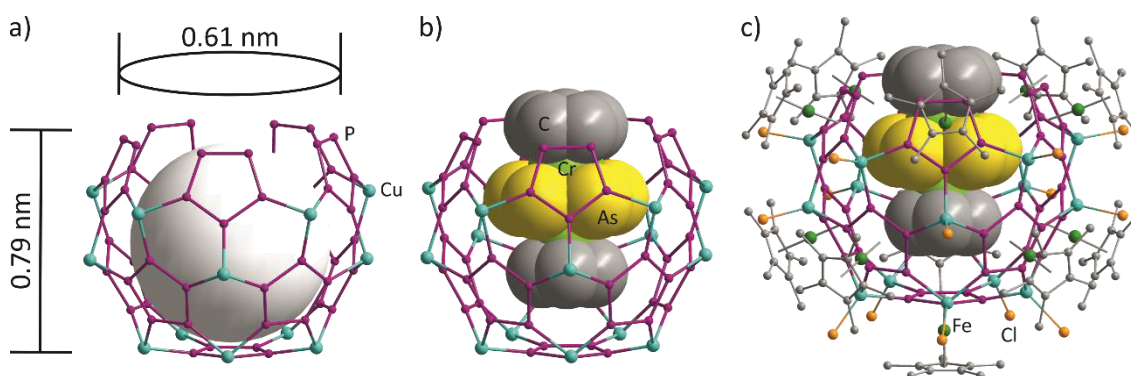


Figure 2. a) Inorganic scaffold of **2**; b) with the encapsulated template **1** with the scaffold; c) molecular structure of **1@2a**. Hydrogen atoms and minor parts of disorder are omitted for clarity; the template is depicted in the space-filling model.

The only comparable open-shelled assembly based on pentaphosphaferrocene observed so far is the nano-capsule [Cp*Fe(η^5 -P₅)]₂@{[Cp*Fe(η^5 -P₅)]₉(CuCl)₁₀]₂, consisting of two open host shells each incorporating a [Cp*Fe(η^5 -P₅)] molecule.^[13] However, these shells are weakly bound together to give an isolated closed capsule *via* π -stacking interactions between Cp* ligands of the guest molecules, as well as by a number of weak non-valent P...P interactions between the P₅ ligands of the open shells. Therefore, this structure is not related to the ones of **1@2a,b**.

In the previously reported complex **1@A**, the triple decker complex **1** forms a similar eclipsed stacking of its Cp rings with the P₅ ring of the 90-vertex host **A** (3.56 Å).^[4d] However, the *cyclo*-As₅ middle deck of **1** is disordered over three positions due to weak interactions with alternating {Cu(CH₃CN)₂} and Br bridges of the middle part of host **A** (Fig. 1c). The As...Br distances of 4.03 – 4.58 Å exceed the sum of the van-der-Waals radii (3.68 Å) by far.^[11a,b] In contrast, the guest molecule **1** is ordered when encapsulated in the novel nano-bowls **2**. As in **1@A**, the Cp ligands show an eclipsed orientation towards the *cyclo*-P₅ rings of the host molecule, indicating π - π host-guest interactions with interplanar Cp...P₅ distances of 3.50 Å in **1@2a** and 3.46 Å in **1@2b** (Fig. 3a). In the As₅ middle deck, each As-As edge is arranged parallel to the corresponding *cyclo*-P₅ ligand of the host (line-to-plane angles deviate by 0.2° – 2.4° for **1@2a** and by 0.2° – 1.5° for **1@2b**). The shortest intermolecular As...P contacts amounting to 3.69 – 3.94 Å (**1@2a**) and 3.78 – 3.89 Å (**1@2b**) are in the range of normal van-der-Waals contacts (3.65 Å).^[11a,b] Therefore, the guest molecule prefers an orientation supported by van-der-Waals interactions, which is the most distant from the inner surface of the host molecule.

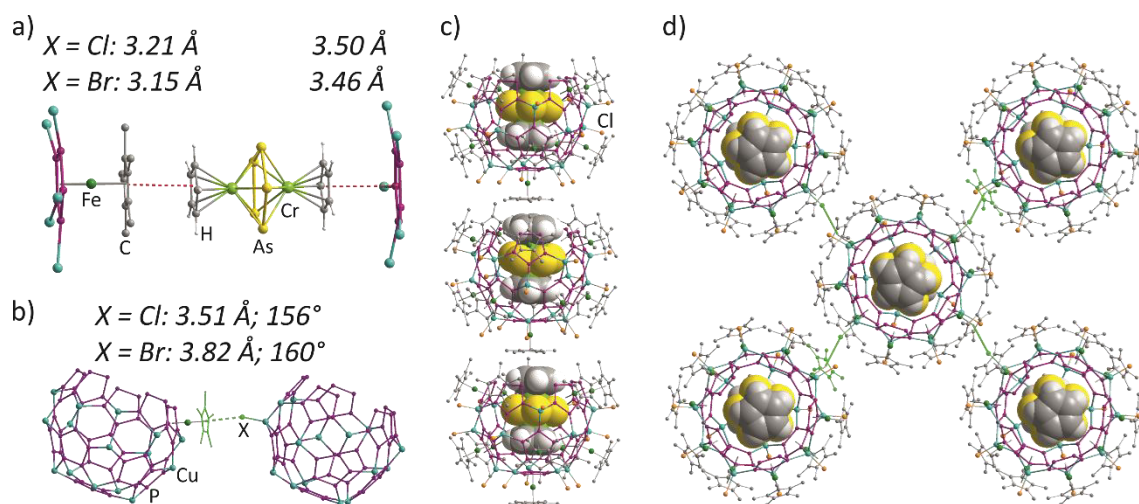


Figure 3. Intermolecular interactions in **1@2a** and **1@2b**; a) host-guest π -interactions between the guest molecule **1** and hosts **2** schematically shown as (*cyclo*-P₅)Cu₅ shells; b) inorganic cores **2** forming a σ - π supramolecular synthon based on X...Cp* interactions (shown in green). Other {Cp*Fe} fragments are not shown; c) a column based on π - π host-guest interactions; d) a packing of host-guest columns in **1@2a** connected *via* σ - π synthons (b). Hydrogen atoms are omitted for clarity; the template is shown in the space-filling model.

Interestingly, the host-guest interactions are not restricted to the encapsulation of **1** into the cavity of **2**. Each guest molecule protruding from the open bowl further interacts with the Cp* ligand on the opposite side of the next host-guest assembly **1@2**, resulting in unprecedented head-to-tail infinite columns (Fig. 3c). The short intra-column π - π contacts amount to 3.21 and 3.15 Å in **1@2a** and **1@2b**, respectively. In contrast, the aforementioned assembly **C** forms a nano-capsule and thus isolates the two guest molecules from extended intermolecular interactions. Interestingly, another type of intermolecular interactions controls the packing of these columns in the solid state, namely the X...Cp*-specific interactions of σ - π type, also observed in some packings of other pentaphosphaferrocene-based supramolecules.^[14] Every bowl-like supramolecule participates in four supramolecular σ - π synthons with the four neighboring supramolecules of other columns (Fig. 3b, d). The geometry of the σ - π synthons is in agreement with the previously reported examples and amounts to 3.48 – 3.55 Å (**1@2a**) and 3.54 – 4.13 Å (**1@2b**) for X...Cp* contacts and to 155.7 – 157.0° (**1@2a**) and 158.8 – 160.5° (**1@2b**) for Cu-X...Cp* angles. The earlier-noticed tendency of heavier halogens to form more obtuse angles is also valid here.

This bowl-like scaffold is observed for the first time and demonstrates that the formation of pentaphosphaferrocene-based host molecules is indeed template-directed.

Compared to [CpCr(η^5 -As₅)]@**B**, the nano-bowls **1@2** are less soluble in CH₂Cl₂. The Br compound **1@2b** is slightly more soluble in CHCl₃ than in CH₂Cl₂, still the detection of the guest complex **1** by solution NMR spectroscopy was hampered. Therefore, both compounds **1@2** were investigated in the solid state by magic angle spinning (MAS) NMR spectroscopy. In the

^1H MAS NMR spectra, a signal at 21.3 ppm is assigned to the triple decker complex **1** encapsulated in the bowl-like hosts **2**. Compared to free **1** (23.8 ppm),^[6] the signal is shifted to higher field upon encapsulation. This effect has previously been observed for the chemical shifts of various other templates in pentaphosphaferrocene-based host systems,^[4b,d-g] especially for the encapsulation of **1** into the 90-vertex sphere **A**, resulting in a similar chemical shift of 20.5 ppm.^[4d] Moreover, two signals at 1.4 ppm and 6.7 ppm (6.8 ppm for **1@2b**) can be assigned to the Cp* protons of the host, partially low-field shifted due to their proximity to the paramagnetic guest complex. Additionally, signals of low intensities can be observed in the ^1H MAS NMR spectra, with chemical shifts of about 16 ppm and -13 ppm for both compounds **1@2**. For **1@2b**, the $^{31}\text{P}\{^1\text{H}\}$ MAS NMR spectrum shows two broad signals at 126 ppm and 70 ppm, which are due to different coordination spheres of the $[\text{Cp}^*\text{Fe}(\eta^5\text{-P}_5)]$ complex within the host **2b**. For **1@2a**, the $^{31}\text{P}\{^1\text{H}\}$ chemical shifts are similar and amount to 125 ppm and 74 ppm. The products **1@2** are well soluble in pyridine, resulting in a fragmentation of the hosts. Hence, in the ^1H NMR spectra in pyridine- d_5 , a singlet at 23.9 ppm (24.0 ppm for **1@2b**) is detected corresponding to the free complex **1**, next to a singlet at 1.33 ppm assigned to free $[\text{Cp}^*\text{Fe}(\eta^5\text{-P}_5)]$. The presence of the latter is confirmed by the detection of a singlet at 150.5 ppm in the $^{31}\text{P}\{^1\text{H}\}$ NMR spectra.

Thus, the previously reported cleavage of the triple decker complex **1** in the $[\text{Cp}^*\text{Fe}(\eta^5\text{-P}_5)]/\text{CuCl}$ system is not observed when performing the reaction in $\text{CH}_2\text{Cl}_2/\text{CH}_3\text{CN}$ *in lieu* of toluene/ CH_3CN , but instead the novel nano-bowls **1@2** were obtained.

These results motivated us to revisit the reaction of $[\text{Cp}^*\text{Fe}(\eta^5\text{-P}_5)]$ with CuCl and **1** in toluene/ CH_3CN . Crystals of $[\text{CpCr}(\eta^5\text{-As}_5)]@[\{\text{Cp}^*\text{Fe}(\eta^5\text{-P}_5)\}_{12}(\text{CuCl})_{20}]$ ($[\text{CpCr}(\eta^5\text{-As}_5)]@**B**$) were obtained by a slightly altered synthetic method: before being layered with a CuCl solution in CH_3CN , the toluene solution of $[\text{Cp}^*\text{Fe}(\eta^5\text{-P}_5)]$ and **1** was sonicated and filtered. Both steps proved to be crucial due to the low solubility of crystalline **1** in toluene. The crystals of the product were isolated by washing with toluene/ CH_3CN (1:1), since they can be redissolved in $\text{CH}_2\text{Cl}_2/\text{CH}_3\text{CN}$ (2:1, previously reported method)^[4d] and were investigated by EPR spectroscopy. The spectrum clearly showed a half-field line indicating the presence of a triplet molecule that agrees well with the calculated triplet ground state for the encapsulated 16 VE $[\text{CpCr}(\eta^5\text{-As}_5)]$ molecule (Figure 4).^[4d] In contrast, these signals were observed neither in the EPR spectrum of the intact 27 VE triple decker complex **1** nor in the EPR spectrum of the crystals of **1@2a** obtained from the $\text{CH}_2\text{Cl}_2/\text{CH}_3\text{CN}$ reaction, which reconfirms the cleavage of the triple decker complex **1** when toluene/ CH_3CN is used as reaction medium. Additionally, according to the ^1H NMR spectrum, the triple decker complex **1** itself stays intact when its toluene solution is

sonicated and filtered, suggesting that the cleavage of **1** only occurs during the reaction with $[\text{Cp}^*\text{Fe}(\eta^5\text{-P}_5)]$ and CuCl and is not induced by the sonication.

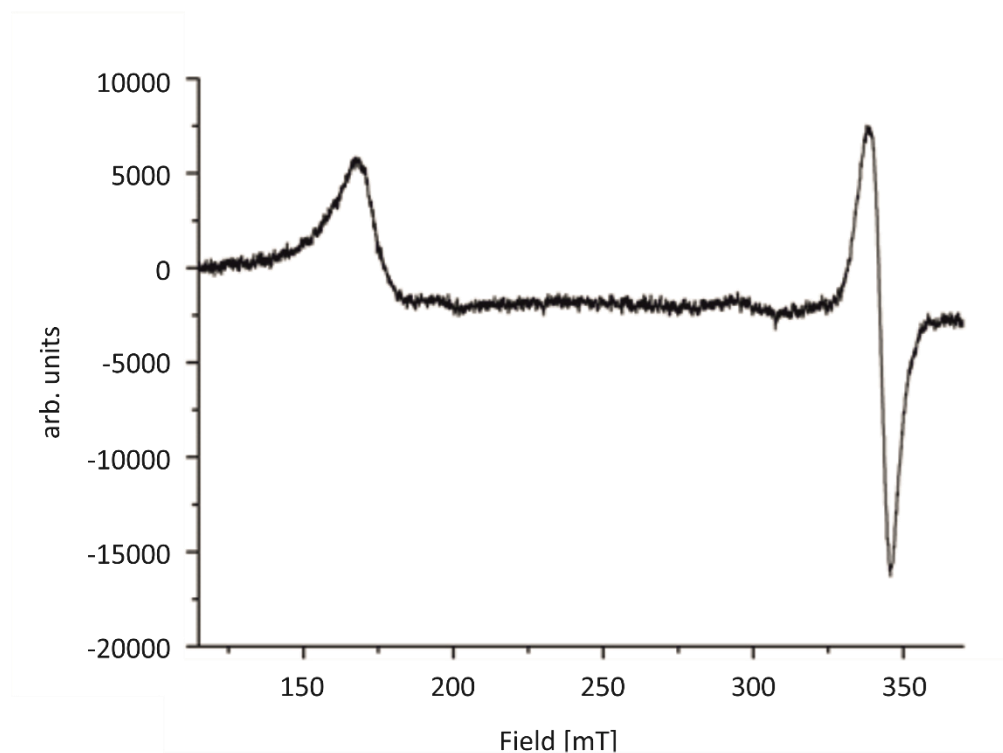


Figure 4. EPR spectrum of crystals of $[\text{CpCr}(\eta^5\text{-As}_5)]@B$ in a quartz tube at r.t.

Moreover, NMR spectroscopy of the crystalline product $[\text{CpCr}(\eta^5\text{-As}_5)]@B$ was carried out in solution since it can sparingly be dissolved in CD_2Cl_2 . Here, two broad signals at 120 ppm and 69 ppm in the $^{31}\text{P}\{^1\text{H}\}$ NMR spectrum as well as a signal at 19.8 ppm in the ^1H NMR spectrum were detected, which can be assigned to $[\text{CpCr}(\eta^5\text{-As}_5)]@B$.^[4d] This demonstrates that $[\text{CpCr}(\eta^5\text{-As}_5)]@B$ is quite stable in a CH_2Cl_2 solution. On the other hand, a sharp singlet at 151.5 ppm in the $^{31}\text{P}\{^1\text{H}\}$ NMR spectrum can tentatively be assigned to free $[\text{Cp}^*\text{Fe}(\eta^5\text{-P}_5)]$. In the ^1H -NMR spectrum, also a signal at 21.3 ppm is observed, which may be assigned to the intact triple decker complex **1** encapsulated in the CuCl analogue of the host **A** (for the CuBr analogue **1@A**: 20.5 ppm, free **1**: 23.8 ppm)^[4d] or in a nano-bowl **2a** (**1@2a**: 21.3 ppm, *vide supra*). Since the latter compound has a similar size and shape as $[\text{CpCr}(\eta^5\text{-As}_5)]@B$, a cocrystallization of both compounds cannot be completely excluded. In both cases, in the $^{31}\text{P}\{^1\text{H}\}$ NMR spectrum, the expected signals for the hosts (CuCl analogue of host **A**: 68 ppm,^[4g] host **2a**: 125 ppm and 74 ppm, *vide supra*) would overlap with the signals of host **B**, so no further conclusion can be drawn. In pyridine, crystals of $[\text{CpCr}(\eta^5\text{-As}_5)]@B$ are well soluble again resulting in a fragmentation of the hosts and subsequent release of the guest molecules. Hence, in the $^{31}\text{P}\{^1\text{H}\}$ NMR spectrum, solely a singlet at 147.2 ppm is detected, assigned to free $[\text{Cp}^*\text{Fe}(\eta^5\text{-P}_5)]$. In the ^1H NMR spectrum in pyridine- d_5 , a signal at 23.9 ppm is assigned to the free triple decker

complex **1**, whereas a very broad signal at approximately 6 ppm is also detected and might be assigned to subsequent products formed by the conversion of the released unstable complex $[\text{CpCr}(\eta^5\text{-As}_5)]$. These results are also in line with a cocrystallization of $[\text{CpCr}(\eta^5\text{-As}_5)]@**B**$ and **1@2a** in the toluene/ CH_3CN reaction.

4.3 Conclusion

In summary, different pathways of self-assembly in the system $[(\text{CpCr})_2(\mu, \eta^{5:5}\text{-As}_5)]/[\text{Cp}^*\text{Fe}(\eta^5\text{-P}_5)]/\text{CuX}$ ($X = \text{Cl}, \text{Br}$) were addressed and the crucial role of the used solvents was demonstrated. The previously reported **1**/ $[\text{Cp}^*\text{Fe}(\eta^5\text{-P}_5)]/\text{CuCl}$ system in toluene/ CH_3CN was revisited and the cleavage of the triple decker **1** and the encapsulation of the resulting unstable 16 VE complex $[\text{CpCr}(\eta^5\text{-As}_5)]$ into a 80-vertex sphere (**B**) were proven by EPR and solution NMR spectroscopy. By changing the solvent mixture toluene/ CH_3CN to $\text{CH}_2\text{Cl}_2/\text{CH}_3\text{CN}$, unprecedented open shell bowl-like host molecules incorporating the triple decker complex **1** were obtained irrespective of the nature of the halogen: $[\mathbf{1}]@[\{\text{Cp}^*\text{Fe}(\eta^5\text{-P}_5)\}_{11}\{\text{CuX}\}_{15-n}]$ (**1@2a**: $n = 0.45$; **1@2b**: $n = 1.55$). They resemble truncated fullerene-like 80-vertex spheres **B**. Due to the opening in the hosts, the guest molecules can be trapped despite their protruding from the opening and still participate for the first time in π interactions not only with their own hosts, but also with the neighboring host molecules. Thus, the supramolecular π - π columns formed in the solid state are further connected into a 3D supramolecular assembly by a system of σ - π synthons. These results do not only nicely demonstrate that supramolecular self-assembly strongly depends on the conditions applied, but also prove that the formation of spherical assemblies in the $[\text{Cp}^*\text{Fe}(\eta^5\text{-P}_5)]/\text{CuX}$ system is template-directed. Investigations regarding the transferability of these results to other triple decker complexes and guest molecules as templates are currently under way.

4.4 Experimental Part

General Remarks

All reactions were performed under an inert atmosphere of dry nitrogen or argon with standard vacuum, Schlenk and glove-box techniques. Solvents were purified, dried, and degassed prior to use by standard procedures. $[(\text{CpCr})_2(\mu, \eta^{5:5}\text{-As}_5)]^{[6]}$ and $[\text{Cp}^*\text{Fe}(\eta^5\text{-P}_5)]^{[15]}$ were synthesized following reported procedures. CuCl and CuBr are commercially available and were used without further purification. Solution NMR spectra were recorded on a BRUKER Avance 400. MAS NMR spectra were acquired on a Bruker Avance 300 spectrometer. Chemical shifts δ are given in [ppm] referring to external standards of tetramethylsilane (^1H NMR spectra), 85%

phosphoric acid ($^{31}\text{P}\{^1\text{H}\}$ NMR spectra) or NaH_2PO_4 ($^{31}\text{P}\{^1\text{H}\}$ MAS NMR spectra). ESI-MS and EI-MS spectra were recorded on a ThermoQuest Finnigan MAT TSQ 7000 and on a Finnigan MAT 95 mass spectrometer, respectively. Elemental analyses were determined by Mikroanalytisches Labor, Lehrbereich Anorganische Chemie, TU Munich for all elements. EPR spectroscopy was carried out on a MiniScope MS400 device with a frequency of 9.44 GHz.

Synthesis of $[(\text{CpCr})_2(\mu, \eta^{5:5}\text{-As}_5)]@[\{\text{Cp}^*\text{Fe}(\eta^5\text{-P}_5)\}_{11}(\text{CuCl})_{13.5}] \cdot 8 \text{CH}_2\text{Cl}_2 \cdot 0.5 \text{CH}_3\text{CN}$ (1@2a** · 8 CH_2Cl_2 · 0.5 CH_3CN)**

$[\text{Cp}^*\text{Fe}(\eta^5\text{-P}_5)]$ (102 mg, 0.30 mmol) and **1** (19 mg, 0.031 mmol) are dissolved in CH_2Cl_2 (22 mL). After treatment in a warm ultrasonic bath (1 h, 60°C, 35 kHz), the dark green solution is filtered into a thick Schlenk tube and carefully layered with a colorless solution of CuCl (64 mg, 0.65 mmol) in CH_3CN (22 mL). After 1-2 weeks, the mother liquor is decanted, and the crystals are washed three times each with $\text{CH}_2\text{Cl}_2/\text{CH}_3\text{CN}$ (2:1) and pentane and dried.

Analytical data of **1@2a**:

Yield: 72 mg (11 μmol , 42%)

^1H MAS NMR: δ [ppm] = -13.6 (br), 1.4 (s, br), 6.7 (s, br), 16.4 (br), 21.3 (s, br).

$^{31}\text{P}\{^1\text{H}\}$ MAS NMR: δ [ppm] = 74 (br), 125 (br); a small shoulder at 150 ppm is detected, which can most probably be assigned to free $[\text{Cp}^*\text{Fe}(\eta^5\text{-P}_5)]$.

^1H NMR (CD_2Cl_2): δ [ppm] = 1.42 (s, br), 1.43 (s, br), 1.97 (s, CH_3CN), 2.08 (s, br), 2.18 (s, br), 2.20 (s, br), 3.26 (s, br), 3.33 (s, br).

$^{31}\text{P}\{^1\text{H}\}$ NMR (CD_2Cl_2): δ [ppm] = 60 (br), 120 (br), 152.2 (s, $[\text{Cp}^*\text{Fe}(\eta^5\text{-P}_5)]$); signals almost below noise floor.

^1H NMR (pyridine- d_5): δ [ppm] = 1.33 (s, $[\text{Cp}^*\text{Fe}(\eta^5\text{-P}_5)]$), 1.87 (s, CH_3CN), 23.9 (s, br, $[(\text{CpCr})_2(\mu, \eta^{5:5}\text{-As}_5)]$).

$^{31}\text{P}\{^1\text{H}\}$ NMR (pyridine- d_5): δ [ppm] = 150.5 (s, $[\text{Cp}^*\text{Fe}(\eta^5\text{-P}_5)]$).

EI-MS (70 eV): 608.5668 $[(\text{CpCr})_2(\mu, \eta^{5:5}\text{-As}_5)]$, 345.9187 $[\text{Cp}^*\text{Fe}(\eta^5\text{-P}_5)]$, 299.6829 $[\text{As}_4]$, 283.9715 $[\{\text{Cp}^*\text{Fe}(\eta^5\text{-P}_5)\}\text{-P}_2]$.

Positive ion ESI-MS ($\text{CH}_2\text{Cl}_2/\text{CH}_3\text{CN}$): m/z = 2635.4 $[\{\text{Cp}^*\text{Fe}(\eta^5\text{-P}_5)\}_4\text{Cu}_{13}\text{Cl}_{12}]^+$, 2535.5 $[\{\text{Cp}^*\text{Fe}(\eta^5\text{-P}_5)\}_4\text{Cu}_{12}\text{Cl}_{11}]^+$, 2337.7 $[\{\text{Cp}^*\text{Fe}(\eta^5\text{-P}_5)\}_4\text{Cu}_{10}\text{Cl}_9]^+$, 1794.0 $[\{\text{Cp}^*\text{Fe}(\eta^5\text{-P}_5)\}_3\text{Cu}_8\text{Cl}_7]^+$, 1744.0 $[\{\text{Cp}^*\text{Fe}(\eta^5\text{-P}_5)\}_4\text{Cu}_4\text{Cl}_3]^+$, 1694.1 $[\{\text{Cp}^*\text{Fe}(\eta^5\text{-P}_5)\}_3\text{Cu}_7\text{Cl}_6]^+$, 1596.2 $[\{\text{Cp}^*\text{Fe}(\eta^5\text{-P}_5)\}_3\text{Cu}_6\text{Cl}_5]^+$, 952.6 $[\{\text{Cp}^*\text{Fe}(\eta^5\text{-P}_5)\}_2\text{Cu}_3\text{Cl}_2]^+$, 854.7 $[\{\text{Cp}^*\text{Fe}(\eta^5\text{-P}_5)\}_2\text{Cu}_2\text{Cl}]^+$, 754.8 $[(\text{Cp}^*\text{Fe}(\eta^5\text{-P}_5))_2\text{Cu}]^+$, 490.9 $[\{\text{Cp}^*\text{Fe}(\eta^5\text{-P}_5)\}\text{Cu}(\text{CH}_3\text{CN})_2]^+$, 449.9 $[\{\text{Cp}^*\text{Fe}(\eta^5\text{-P}_5)\}\text{Cu}(\text{CH}_3\text{CN})]^+$, 408.9 $[\{\text{Cp}^*\text{Fe}(\eta^5\text{-P}_5)\}\text{Cu}]^+$.

Negative ion ESI-MS (CH₂Cl₂/CH₃CN): $m/z = 232.8$ [Cu₂Cl₃]⁻.

Elemental analysis: Calculated (%) for [(CpCr)₂(μ,η^{5:5}-As₅)@{(Cp*Fe(η⁵-P₅))₁₁(CuCl)_{13.5}} · 8 CH₂Cl₂ · 0.5 CH₃CN (6451 g/mol): C 24.02, H 3.01, N 0.11, Cu 13.30, P 26.41; found (%): C 23.88, H 3.35, N 0.07, Cu 13.4, P 26.81.

Synthesis of [(CpCr)₂(μ,η^{5:5}-As₅)@{(Cp*Fe(η⁵-P₅))₁₁(CuBr)_{12.5}} · 2 CH₂Cl₂ (1@2b · 2 CH₂Cl₂)

[Cp*Fe(η⁵-P₅)] (106 mg, 0.31 mmol) and **1** (21 mg, 0.034 mmol) are dissolved in CH₂Cl₂ (21 mL). After treatment in a warm ultrasonic bath (1 h, 60°C, 35 kHz), the dark green solution is filtered into a thick Schlenk tube and carefully layered with a colorless solution of CuBr (87 mg, 0.61 mmol) in CH₃CN (21 mL). After 1-2 weeks, the mother liquor is decanted, and the crystals are washed three times each with CH₂Cl₂/CH₃CN (2:1) and pentane and dried.

Analytical data of **1@2b**:

Yield: 122 mg (19 μmol, 67%)

¹H MAS NMR: δ [ppm] = -13.4 (br), 1.4 (s, br), 6.8 (s, br), 16.2 (br), 21.3 (s, br).

³¹P{¹H} MAS NMR: δ [ppm] = 70 (br), 126 (br).

¹H NMR (CDCl₃): δ [ppm] = 1.44 (s, br), 1.48 (s, br), 1.49 (s, br), 2.13 (s, br), 2.14 (s, CH₃CN), 2.25 (s, br), 3.32 (s, br), 3.40 (s, br).

³¹P{¹H} NMR (CDCl₃): δ [ppm] = 152.8 (s, [Cp*Fe(η⁵-P₅)]).

¹H NMR (pyridine-d₅): δ [ppm] = 1.33 (s, [Cp*Fe(η⁵-P₅)]), 1.87 (s, CH₃CN), 5.69 (s, CH₂Cl₂), 24.0 (s, br, [(CpCr)₂(μ,η^{5:5}-As₅)]).

³¹P{¹H} NMR (pyridine-d₅): δ [ppm] = 150.5 (s, [Cp*Fe(η⁵-P₅)]).

EI-MS (70 eV): 608.5667 [(CpCr)₂(μ,η^{5:5}-As₅)], 345.9197 [Cp*Fe(η⁵-P₅)], 299.6853 [As₄], 283.9724 [(Cp*Fe(η⁵-P₅))-P₂].

Positive ion ESI-MS (CH₂Cl₂/CHCl₃/CH₃CN): $m/z = 1042.4600$ [(Cp*Fe(η⁵-P₅))₂Cu₃Br₂]⁺, 898.6152 [(Cp*Fe(η⁵-P₅))₂Cu₂Br]⁺, 754.7710 [(Cp*Fe(η⁵-P₅))₂Cu]⁺, 449.8758 [(Cp*Fe(η⁵-P₅))Cu(CH₃CN)]⁺.

Negative ion ESI-MS (CH₂Cl₂/CHCl₃/CH₃CN): $m/z = 222.7643$ [CuBr₂]⁻, 178.8144 [CuClBr]⁻, 134.8649 [CuCl₂]⁻.

Elemental analysis: Calculated (%) for [(CpCr)₂(μ,η^{5:5}-As₅)@{(Cp*Fe(η⁵-P₅))₁₁(CuBr)_{12.5}} · 2 CH₂Cl₂ (6377 g/mol): C 22.98, H 2.83, Cu 12.46, P 26.71; found (%): C 23.01, H 2.90, Cu 12.44, P 26.77.

Synthesis of [CpCr(η^5 -As₅)]@[{Cp*Fe(η^5 -P₅)}₁₂(CuCl)₂₀] ([CpCr(η^5 -As₅)]@B)

[Cp*Fe(η^5 -P₅)] (105 mg, 0.30 mmol) and **1** (23 mg, 0.038 mmol) are dissolved in toluene (26 mL). After treatment in a warm ultrasonic bath (1 h, 50°C, 35 kHz), the dark green solution is filtered into a thick Schlenk tube and carefully layered with a colorless solution of CuCl (58 mg, 0.59 mmol) in CH₃CN (20 mL). After 2-3 weeks, the mother liquor is decanted, and the crystals are washed twice with toluene/CH₃CN (1:1) and dried.

Analytical data of [CpCr(η^5 -As₅)]@B:

Yield: 44 mg (6.6 μ mol, 26%)

¹H NMR (CD₂Cl₂): δ [ppm] = 1.42 (s, br), 1.43 (s, br), 2.08 (s, br), 2.17 (s, br), 2.34 (s, C₇H₈), 3.26 (s, br), 3.33 (s, br), 7.14-7.26 (m, C₇H₈), 19.8 (s, br), 21.3 (s, br).

³¹P{¹H} NMR (CD₂Cl₂): δ [ppm] = 69 (br), 120 (br), 151.5 (s, [Cp*Fe(η^5 -P₅)]); signals almost below noise floor.

¹H NMR (pyridine-d₅): δ [ppm] = 1.35 (s, [Cp*Fe(η^5 -P₅)]), 1.84 (s, CH₃CN), 2.23 (s, C₇H₈), 6.0 (br), 23.9 (s, br, [(CpCr)₂(μ , $\eta^{5:5}$ -As₅))].

³¹P{¹H} NMR (pyridine-d₅): δ [ppm] = 147.2 (s, [Cp*Fe(η^5 -P₅)]).

4.5 Crystallographic Details

Crystals of **1** and **1@2a** and **1@2b** were taken from a Schlenk flask under a stream of argon and immediately covered with mineral oil (**1**) or perfluorinated Fomblin[®] mineral oil (**1@2a**, **1@2b**) to prevent both decomposition and a loss of solvent. The quickly chosen single crystals covered by a thin layer of the oil were taken to the pre-centered goniometer head with suitable CryoMount[®] and directly attached to the goniometer into a stream of cold nitrogen. The X-ray diffraction study of **2a** and **2b** faced many challenges since the crystals were systematically twinned by merohedry and quickly decomposed due to the loss of solvent. Due to the low diffraction power of **1@2a** and **1@2b** at high theta angles the collection of data required high exposure times.

The data for **1** and **1@2a** were collected using 1° (**1**) or 0.5° (**1@2a**) ω scans on a Rigaku Oxford Diffraction diffractometer equipped with a Titan^{S2} CCD detector and a SuperNova CuK α microfocus source. The data for **1@2b** were collected at P11 beamline of PETRA III (DESY, Hamburg) using 20 keV synchrotron radiation (λ = 0.6199 Å) and scan width 0.3 deg. The measurements of **1** and **2a** were performed at 123 K, the experiment for **1@2b** was performed at 80 K.

The data processing and reduction was performed with CrysAlis*PRO* Software.^[16] The structures were solved by direct methods with *SHELX97* and refined by full-matrix least-squares method on $|F|^2$ using multiprocessor and variable memory version *SHELXL2014*.^[17] All ordered non-hydrogen atoms were refined in an anisotropic approximation, while the disordered atoms with occupancy factors less than 0.5 were refined isotropically. The hydrogen atoms were refined as riding on pivot atoms. Crystallographic data and details of the diffraction experiments are given in Table 1.

CIF files with comprehensive information on the details of the diffraction experiments and full tables of bond lengths and angles for **1**, **1@2a** and **1@2b** are deposited in Cambridge Crystallographic Data Centre under the deposition codes CCDC-1875092, CCDC-1875093 and CCDC-1875094, respectively.

Table 1. Experimental details for compounds **1**, **1@2a** and **1@2b**.

Crystal Data	1	1@2a	1@2b
CCDC-Code	CCDC 1875092	CCDC 1875093	CCDC 1875094
Chemical formula	C ₁₀ H ₁₀ As ₅ Cr ₂	C ₁₁₀ H ₁₆₅ Cl _{13.35} Cu _{13.35} Fe ₁₁ P ₅₅ ·C ₁₀ H ₁₀ As ₅ Cr ₂ ·2.96(CH ₂ Cl ₂)·3.825(CH ₃ CN)	C ₁₁₀ H ₁₆₅ Br _{14.55} Cu _{14.55} Fe ₁₁ P ₅₅ ·C ₁₀ H ₁₀ As ₅ Cr ₂ ·3.4(CH ₂ Cl ₂)·0.9(CH ₃ CN)
<i>M_r</i>	608.78	6143.82	6826.78
Crystal system, space group	Monoclinic, <i>P</i> 2 ₁ / <i>n</i>	Monoclinic, <i>Cc</i>	Monoclinic, <i>Cc</i>
Temperature (K)	123	123(2)	80
<i>a</i> , <i>b</i> , <i>c</i> (Å)	8.1149(2), 14.8158(3), 12.0097(3)	30.4118(4), 29.4289(2), 28.8188(3)	27.08802(13), 33.62013(12), 25.36593(11)
β (°)	104.644(3)	112.8746(13)	103.3511(5)
<i>V</i> (Å ³)	1397.00(6)	23764.1(4)	22476.47(17)
<i>Z</i>	4	4	4
<i>F</i> (000)	1132	12166	13251
<i>D_x</i> (Mg m ⁻³)	2.895	1.717	2.017
Radiation type	Cu Kα	Cu Kα	Synchrotron, λ = 0.6199 Å
μ (mm ⁻¹)	25.87	13.74	4.11
Crystal color and shape	Black rod	brown rod	brown rod
Crystal size (mm)	0.32×0.12×0.10	0.19 × 0.06 × 0.04	0.15 × 0.07 × 0.05
Data collection			
Diffractometer	SuperNova, Titan ^{S2}	SuperNova, Titan ^{S2}	P11 beamline, PETRA III, DESY, Dectris PILATUS 6M
Absorption correction	Gaussian	Gaussian	Multi-scan
<i>T_{min}</i> , <i>T_{max}</i>	0.047, 0.306	0.239, 0.651	0.868, 1.000
No. of measured, independent and observed [<i>I</i> > 2σ(<i>I</i>)] reflections	4560, 2404	2677, 83809, 31629, 26711	256480, 81091, 64928
<i>R_{int}</i>	0.071	0.109	0.045
(sin θ/λ) _{max} (Å ⁻¹)	0.624	0.624	0.845
Range of <i>h</i> , <i>k</i> , <i>l</i>	<i>h</i> = -8→10, <i>k</i> = -17→17, <i>l</i> = -9→14	<i>h</i> = -23→37, <i>k</i> = -35→35, <i>l</i> = -35→34	<i>h</i> = -44→45, <i>k</i> = -49→49, <i>l</i> = -41→42
Refinement			
<i>R</i> [<i>F</i> ² > 2σ(<i>F</i> ²)]	0.071,	0.205, 0.056, 0.144, 1.01	0.039, 0.107, 0.96
<i>wR</i> (<i>F</i> ²), <i>S</i>	1.08		
No. of reflections	2677	31627	81064
No. of parameters	154	2341	2260
No. of restraints	0	117	12
H-atom treatment	H-atom parameters constrained	H atom parameters constrained	H-atom parameters constrained
Δ _{max} , Δ _{min} (e Å ⁻³)	2.33, -1.97	1.51, -1.32	2.02, -1.26
Absolute structure	-	Refined as an inversion twin	Refined as an inversion twin

Computer programs: CrysAlis PRO 1.171.38.46 and 1.171.38.37b (Rigaku OD, 2015), SHELXL97 (Sheldrick, 1998), SHELXL2014/7 (Sheldrick, 2014).

4.6 Author Contributions

- The reinvestigation of compound $[\text{CpCr}(\eta^5\text{-As}_5)]@B$ was performed by Helena Brake
- The synthesis of compounds **1@2a** and **1@2b** was performed by Dr. Claudia Heindl
- The characterization of compounds **1@2a** and **1@2b** was performed by Helena Brake
- X-ray structure analyses of compounds **1**, **1@2a** and **1@2b** were performed by Dr. Eugenia Peresykina, Dr. Sc. Alexander Virovets and Dr. Claudia Heindl. Parts of this research (project I-20170135) were carried out at PETRA III at DESY, a member of the Helmholtz Association (HGF), by Dr. Eugenia Peresykina and Dr. Sc. Alexander V. Virovets. EP and AV are grateful to Dr. O. Lorbeer for his assistance regarding the use of the beamline P11.
- Solid-state MAS NMR spectroscopy of compounds **1@2a** and **1@2b** was performed by Prof. Dr. W. Kremer
- The manuscript (results and discussion, experimental part, conclusion; including figures and graphical abstract) was written by Helena Brake and Dr. Eugenia Peresykina
- The introduction was written by Helena Brake, Dr. Eugenia Peresykina and Dr. Claudia Heindl and is also part of her dissertation (University of Regensburg, **2015**)
- The section ‘crystallographic details’ was written by Dr. Eugenia Peresykina

4.7 References

- [1] a) M. Bosch, S. Yuan, W. Rutledge, H.-C. Zhou, *Acc. Chem. Res.* **2017**, *50*, 857-865; b) B. Manna, A. V. Desai, S. K. Ghosh, *Dalton Trans.* **2016**, *45*, 4060-4072; c) L. E. Kreno, K. Leong, O. K. Farha, M. Allendorf, R. P. Van Duyne, J. T. Hupp, *Chem. Rev.* **2012**, *112*, 1105-1125; d) O. K. Farha, J. T. Hupp, *Acc. Chem. Res.* **2010**, *43*, 1166-1175; e) C. Janiak, J. K. Vieth, *New J. Chem.* **2010**, *34*, 2366-2388; f) J. L. C. Rowsell, O. M. Yaghi, *Microporous Mesoporous Mat.* **2004**, *73*, 3-14.
- [2] a) J. Jiao, C. Tan, Z. Li, Y. Liu, X. Han, Y. Cui, *J. Am. Chem. Soc.* **2018**, *140*, 2251-2259; b) S. Bestgen, O. Fuhr, B. Breitung, V. S. K. Chakravadhanula, G. Guthausen, F. Hennrich, Wen Yu, M. M. Kappes, P. W. Roesky, D. Fenske, *Chem. Sci.* **2017**, *8*, 2235-2240; c) J. Uchida, M. Yoshio, S. Sato, H. Yokoyama, M. Fujita, T. Kato, *Angew. Chem. Int. Ed.* **2017**, *56*, 14085-14089; d) D. A. Roberts, B. S. Pilgrim, J. R. Nitschke, *Chem. Soc. Rev.* **2018**, *47*, 626-644; e) N. A. Sakthivel, S. Theivendran, V. Ganeshraj, A. G. Oliver, A. Dass, *J. Am. Chem. Soc.* **2017**, *139*, 15450-15459; f) T. Mitra, K. E. Jelfs, M. Schmidtman, A. Ahmed, S. Y. Chong, D. J. Adams, A. I. Cooper, *Nat. Chem.* **2013**, *5*, 276-281; g) R. W. Saalfrank, A. Scheurer, *Top. Curr. Chem.* **2012**, *319*, 125-170; h) F. J. Rizzuto, J. R. Nitschke, *Nat. Chem.* **2017**, *9*, 903-908; i) K. Tiefenbacher, D. Ajami, J. Rebek, *Angew. Chem. Int. Ed.* **2011**, *50*, 12003-12007; j) L. Qin, G.-J. Zhou, Y.-Z. Yu, H. Nojiri, C. Schröder, R. E. P. Winpenny, Y.-Z. Zheng, *J. Am. Chem. Soc.* **2017**, *139*, 16405-16411.
- [3] (a) O. J. Scherer, T. Brück, *Angew. Chem. Int. Ed. Engl.* **1987**, *26*, 59-61; (b) F. Dielmann, R. Merkle, S. Heintl, M. Scheer, *Z. Naturforsch., B: J. Chem. Sci.* **2009**, *64*, 3-10; (c) S. Heintl, G. Balázs, M. Scheer, *Phosphorus, Sulfur, Silicon Relat. Elem.* **2014**, *189*, 924-932.
- [4] a) S. Heintl, E. V. Peresyphkina, A. V. Virovets, M. Scheer, *Angew. Chem. Int. Ed.* **2015**, *54*, 13431-13435; b) F. Dielmann, M. Fleischmann, C. Heindl, E. V. Peresyphkina, A. V. Virovets, R. M. Gschwind, M. Scheer, *Chem. Eur. J.* **2015**, *21*, 6208-6214; c) F. Dielmann, C. Heindl, F. Hastreiter, E. V. Peresyphkina, A. V. Virovets, R. M. Gschwind, M. Scheer, *Angew. Chem. Int. Ed.* **2014**, *53*, 13605-13608; d) A. Schindler, C. Heindl, G. Balázs, C. Gröger, A. V. Virovets, E. V. Peresyphkina, M. Scheer, *Chem. Eur. J.* **2012**, *18*, 829-835; e) M. Scheer, A. Schindler, C. Gröger, A. V. Virovets, E. V. Peresyphkina, *Angew. Chem. Int. Ed.* **2009**, *48*, 5046-5049; f) M. Scheer, A. Schindler, R. Merkle, B. P. Johnson, M. Linseis, R. Winter, C. E. Anson, A. V. Virovets, *J. Am. Chem. Soc.* **2007**, *129*, 13386-13387; g) J. Bai, A. V. Virovets, M. Scheer, *Science* **2003**, *300*, 781-783.
- [5] a) E. V. Peresyphkina, C. Heindl, A. Virovets, H. Brake, E. Mädl, M. Scheer, *Chem. Eur. J.* **2018**, *24*, 2503-2508; b) C. Heindl, E. Peresyphkina, A. V. Virovets, I. S. Bushmarinov, M. G.

- Medvedev, B. Krämer, B. Dittrich, M. Scheer, *Angew. Chem Int. Ed.* **2017**, *56*, 13237-13243; c) E. Peresykina, C. Heindl, A. Virovets, M. Scheer, Inorganic Superspheres, in *Clusters – Contemporary Insight in Structure and Bonding*, Ed. S. Dehnen **2016**, *174*, 321-373; d) F. Dielmann, E. V. Peresykina, B. Krämer, F. Hastreiter, B. P. Johnson, M. Zabel, C. Heindl, M. Scheer, *Angew. Chem. Int. Ed.* **2016**, *55*, 14833-14837; e) C. Heindl, E. V. Peresykina, A. V. Virovets, W. Kremer, M. Scheer, *J. Am. Chem. Soc.* **2015**, *137*, 10938-10941.
- [6] O. J. Scherer, W. Wiedemann, G. Wolmershäuser, *J. Organomet. Chem.* **1989**, *361*, C11-C14.
- [7] a) A. J. Savyasachi, O. Kotova, S. Shanmugaraju, S. J. Bradberry, G. M. Ó'Máille, T. Gunnlaugsson, *Chem.* **2017**, *3*, 764-811; b) K. Suzuki, M. Kawano and M. Fujita, *Angew. Chem. Int. Ed.* **2007**, *46*, 2819-2822; c) M. Scheer, J. Bai, B. P. Johnson, R. Merkle, A. V. Virovets, C. E. Anson, *Eur. J. Inorg. Chem.* **2005**, *20*, 4023-4026.
- [8] In the course of this work, we have also determined the crystal structure of **1**. For the details see crystallographic section.
- [9] E. V. Peresykina, C. Heindl, A. Schindler, M. Bodensteiner, A. V. Virovets, M. Scheer, *Z. Kristallogr.* **2014**, *229*, 735-740.
- [10] The width of the host is measured as the average distance between opposite P₅ plane centroids minus twice the van-der-Waals radius of phosphorus ($r_{\text{vdW}}(\text{P}) = 1.80 \text{ \AA}$ [ref. 11a]); the bottleneck is measured as twice the distance between the geometric centre and the closest P atom of the open top minus $2 \times r_{\text{vdW}}(\text{P})$. The height of the cavity is measured as the distance between the centroid of all 10 P atoms of the bottleneck and the centroid of the P₅ ligand at the bottom minus the $r_{\text{vdW}}(\text{P})$.
- [11] a) M. Mantina, A. C. Chamberlin, R. Valero, C. J. Cramer, D. G. Truhlar, *J. Phys. Chem. A* **2009**, *113*, 5806-5812; b) A. Bondi, *J. Phys. Chem.* **1964**, *68*, 441-445; c) S. Alvarez, *Dalton Trans.* **2013**, *42*, 8617-8636.
- [12] The dimensions of the template are measured as the distances between two opposite As atoms of the middle deck and the distance between the centroids of the Cp rings, respectively, plus twice the van-der-Waals radius of As (1.85 Å) and C (1.70 Å) [ref. 11a], respectively.
- [13] S. Welsch, C. Gröger, M. Sierka, M. Scheer, *Angew. Chem. Int. Ed.* **2011**, *50*, 1435-1438.
- [14] a) E. V. Peresykina, A. V. Virovets, M. Scheer, *Cryst. Growth Des.* **2016**, *16*, 2335-2341; (b) M. Scheer, A. Schindler, J. Bai, B. P. Johnson, R. Merkle, R. Winter, A. V. Virovets, E. V. Peresykina, V. A. Blatov, M. Sierka, H. Eckert, *Chem. Eur. J.* **2010**, *16*, 2092-2107.

- [15] M. Detzel, G. Friedrich, O. J. Scherer, G. Wolmershäuser, *Angew. Chem. Int. Ed. Engl.* **1995**, *34*, 1321-1323.
- [16] *CrysAlis PRO* 1.171.38.46 (Rigaku OD, **2015**)
- [17] G. M. Sheldrick, *Acta Cryst. sect. C.* **2015**, *C71*, 3.

5 Nano-Bowls as Hosts for Triple Decker Complexes

H. Brake, E. Peresyphkina, A. V. Virovets, C. Heindl, A. Kunz, W. Kremer, M. Scheer

Abstract:

Herein, the capability of triple decker complexes to act as a template in the self-assembly of pentaphosphaferrocenes with copper halides is investigated by variation of concentration, solvents and the applied pentaphosphaferrocene. The system $[\text{Cp}^*\text{Fe}(\eta^5\text{-P}_5)]$ (**1***) / $[(\text{CpCr})_2(\mu, \eta^{5:5}\text{-As}_5)]$ (**2**) / CuX ($X = \text{Cl, Br}$) was further investigated. Thereby, the formation of “80-vertex spheres” vs. 90-vertex spheres was found to be dependent on the concentration. Switching solvents leads to the formation of nano-bowls $[(\text{CpCr})_2(\mu, \eta^{5:5}\text{-As}_5)]@[\{\text{Cp}^*\text{Fe}(\eta^5\text{-P}_5)\}_{11}\{\text{CuX}\}_{15-n}]$ (**2@3***, $X = \text{Cl, Br}$). In order to synthesize more soluble nano-bowls, $[\text{Cp}^x\text{Fe}(\eta^5\text{-P}_5)]$ (**1^x**) was applied as a building block as well. With the soluble nano-bowls $[(\text{CpCr})_2(\mu, \eta^{5:5}\text{-As}_5)]@[\{\text{Cp}^x\text{Fe}(\eta^5\text{-P}_5)\}_{11}\{\text{CuX}\}_{15-n}]$ (**2@3^x**, $X = \text{Cl, Br}$) in hand, novel conclusions on the obtained NMR spectroscopic data could be drawn. Therefore, the structure of the proposed 80-vertex spheres “ $[(\text{CpCr}(\eta^5\text{-As}_5)]@[\{\text{Cp}^*\text{Fe}(\eta^5\text{-P}_5)\}_{12}\{\text{CuX}\}_{20-n}]$ ” ($X = \text{Cl, Br}$), for which also the novel Br analogue is presented, was carefully reconsidered. It could not be unambiguously clarified whether the triple decker template **2** undergoes cleavage to $[\text{CpCr}(\eta^5\text{-As}_5)]$ or oxidation to $[(\text{CpCr})_2(\mu, \eta^{5:5}\text{-As}_5)]^+$. Moreover, the hitherto unknown triple decker complex $[(\text{CpMo})_2(\mu, \eta^{3:3}\text{-P}_3)(\mu, \eta^{2:2}\text{-PS})]$ (**7**) was synthesized in order to be applied as a template in reactions of **1*** or **1^x** with CuX . Thereby, the nano-bowls $[(\text{CpMo})_2(\mu, \eta^{3:3}\text{-P}_3)(\mu, \eta^{2:2}\text{-PS})]@[\{\text{Cp}^R\text{Fe}(\eta^5\text{-P}_5)\}_{11}\{\text{CuX}\}_{15-n}]$ ($\text{Cp}^R = \text{Cp}^*$: **7@3***, $\text{Cp}^R = \text{Cp}^x$: **7@3^x**, $X = \text{Cl, Br}$) or an unprecedented 2D polymer, $[\{(\text{CpMo})_2(\mu_4, \eta^{3:3:1:1}\text{-P}_3)(\mu_3, \eta^{2:2:1}\text{-PS})\}\text{CuCl}]_n$ (**8**), are obtained depending on the applied conditions. Due to the diamagnetic behavior of the guest molecule **7**, more insight on the NMR chemical shifts of the host molecules is gained. In the course of these studies, also the remarkable polymer $[\{\text{Cp}^*\text{Fe}(\eta^{5:1:1:1}\text{-P}_5)\}_2\{\text{Cp}^*\text{Fe}(\eta^{5:1:1}\text{-P}_5)\}\text{Cu}_4(\mu\text{-I})_4]_n$ (**9**) was obtained, constituting the first 3D coordination polymer based on $[\text{Cp}^*\text{Fe}(\eta^5\text{-P}_5)]$ (**1***) building blocks.

5.1 Introduction

In 1985, a Noble Prize-winning discovery was made, when Kroto, Curl, Smalley and co-workers published a proposed structure for the C_{60} molecule, also known as “Buckminster-Fullerene”.^[1] The structure of this third allotrope of carbon constitutes a soccer-ball-like sphere, as confirmed later for a derivative.^[2] As a result of its hollow structure, soon encapsulation of single atoms or small molecules was investigated.^[3] Apart from aesthetic appeal and academic curiosity, encapsulation of guest molecules into a confined space is of great interest as it paves the way to a myriad of applications, e.g. in sensing,^[4] purification,^[5] drug delivery^[6] and molecular flasks.^[7]

However, the host molecules may not only be covalently bound spheres like fullerenes but can also be supramolecules obtained by self-assembly. Here, the field of metallocupramolecular chemistry, making use of the coordinative bond, is particularly well investigated.^[8] This is due to the highly directional donor and acceptor properties of ligand and metal and the intermediate strength of their bond.^[4,9] While most supramolecular coordination cages (SCCs) are based on N or O donor ligands,^[8c,10] our group employs polyphosphorus complexes as ligands. As probably the most prominent polyphosphorus ligand complex, pentaphosphaferrocene [$Cp^*Fe(\eta^5-P_5)$] (**1***, Figure 1a) should be mentioned. First synthesized by Scherer in 1987,^[11] it is isolobal to ferrocene [$FeCp_2$] but in contrast to the {CH} fragments of the Cp ligand, the P atoms of the *cyclo*- P_5 ligand each bear a lone pair available to further coordination.

Thus, by self-assembly with Lewis acidic Cu(I), a multitude of coordination polymers^[12] and even spherical assemblies^[12b,13] have been obtained. Under certain conditions, the two-component self-assembly of **1*** with CuX ($X = Cl, Br$) leads to 90-vertex spherical assemblies of the general formula [$Cp^*Fe(\eta^5-P_5)$]@{ $[Cp^*Fe(\eta^5-P_5)]_{12}[CuX]_{25}[CH_3CN]_{10}$ } (**1*@A**, Figure 1b) comprising fullerene topology.

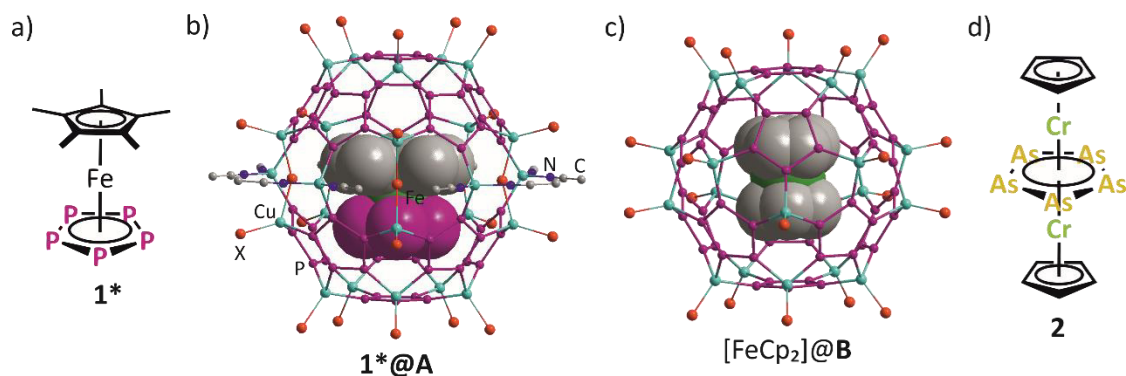


Figure 1. a) Building block [$Cp^*Fe(\eta^5-P_5)$] (**1***); b) core of the 90-vertex sphere **A** with encapsulated guest **1***; c) core of the 80-vertex sphere **B** with encapsulated guest [$FeCp_2$]; d) triple decker complex [$(CpCr)_2(\mu, \eta^5:5-As_5)$] (**2**). Guest molecules are depicted in the space filling model.

Moreover, it was soon recognized that addition of a small molecule as a third component gives access to further spherical host structures encapsulating the small molecule rather than **1*** as guest.^[14] These molecules span P_4 , As_4 (ellipsoid-shaped host), C_{60} (barrel-like host), $o-C_{2}B_{10}H_{12}$, $[FeCp_2]$, $[CpFe(\eta^5-P_5)]$, $[NiCp_2]$, P_4S_3 , P_4Se_3 , adamantane (80-vertex spherical host type **B**, Figure 1c) and $[CoCp_2]^+$ (prism- or cube-shaped host). The two largest templates of this series are $[NiCp_2]$ ^[15] with a diameter of about 7.88 Å^[16,17] and C_{60} with a diameter of about 10.49 Å.^[18,19] Hence, the question arises, whether a larger, but non-spherical template can be as well encapsulated, and if so, which kind of host molecule will form. For this purpose, the triple decker complex $[(CpCr)_2(\mu, \eta^{5:5}-As_5)]$ ^[20] (**2**, Figure 1d) came to mind, with a maximum diameter of 10.05 Å^[21,22] and a rather rod-like shape.

5.2 Results and Discussion

$[(CpCr)_2(\mu, \eta^{5:5}-As_5)]$ as guest

Self-assembly of $[Cp^*Fe(\eta^5-P_5)]$ (**1***) with CuX ($X = Cl, Br$) in the presence of $[(CpCr)_2(\mu, \eta^{5:5}-As_5)]$ (**2**) in CH_2Cl_2 / CH_3CN leads to the crystallization of dark brown rods of $[(CpCr)_2(\mu, \eta^{5:5}-As_5)]@[\{Cp^*Fe(\eta^5-P_5)\}_{11}\{CuCl\}_{13,45}]$ (**2@3*-Cl**, host type **C**) and $[(CpCr)_2(\mu, \eta^{5:5}-As_5)]@[\{Cp^*Fe(\eta^5-P_5)\}_{11}\{CuBr\}_{14,55}]$ (**2@3*-Br**, host type **C**, Figure 2a and Scheme 1, top), respectively.^[21] The structures were elucidated by X-ray structural analysis, revealing intact triple decker guest molecules encapsulated into an opened host structure resembling a truncated sphere **B** (Figure 1c).

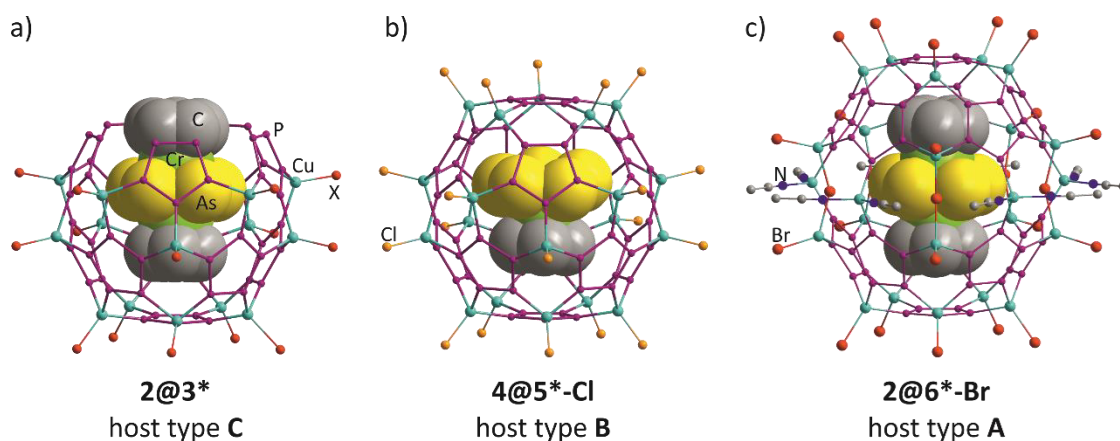
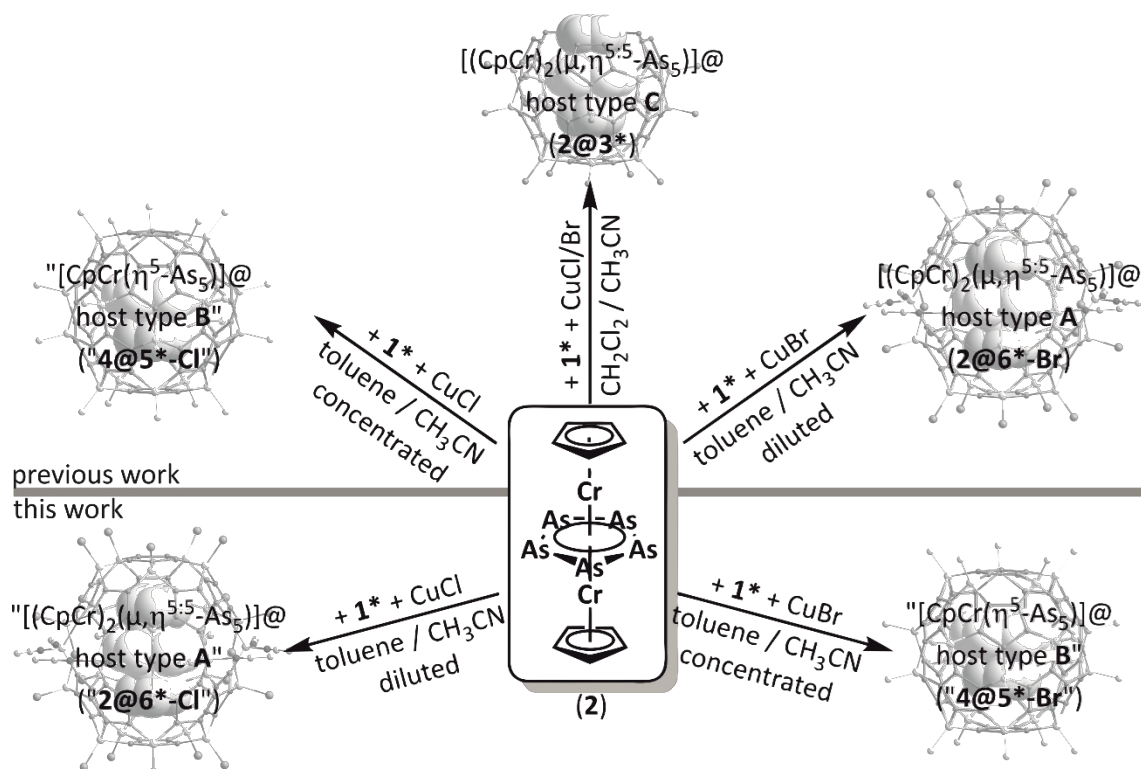


Figure 2. a) Core of the nano-bowl shaped host **3*** (type **C**) with encapsulated guest **2**; b) Core of the 80-vertex spherical host **5*-Cl** (type **B**) with encapsulated guest $[CpCr(\eta^5-As_5)]$ (**4**); c) Core of the 90-vertex spherical host **6*-Br** (type **A**) with encapsulated guest **2**.

In contrast, from the reaction of **1***, **2** and $CuCl$ in toluene / CH_3CN a different phase crystallized, interpreted as $[CpCr(\eta^5-As_5)]@[\{Cp^*Fe(\eta^5-P_5)\}_{12}\{CuCl\}_{20}]$ (**4@5*-Cl**, type **B** host, Figure 2b and Scheme 1, top left).^[14c,21] In this case, the triple decker molecule is thought to be cleaved and

encapsulated by the well-known 80-vertex spherical host of type **B**. A third type of product is obtained by reacting **1***, **2** and CuBr in toluene / CH₃CN.^[14c] Thereby, dark brown blocks of $[(\text{CpCr})_2(\mu, \eta^{5:5}\text{-As}_5)]@[(\text{Cp}^*\text{Fe}(\eta^5\text{-P}_5))_{12}\{\text{CuBr}\}_{25}\{\text{CH}_3\text{CN}\}_{10}]$ (**2@6*-Br**, type **A** host, Figure 2c and Scheme 1, top right) crystallized, in which an intact triple decker guest molecule is encapsulated into the larger 90-vertex spherical host of type **A**.

However, the 90-vertex spherical hosts **A** are known to form in more diluted reactions than the smaller 80-vertex spherical hosts **B**.^[14g] Hence, the questions arise, whether a type **B** host is also accessible from CuBr by performing more concentrated reactions, and whether a type **A** host is accessible from CuCl by performing more diluted reactions. On the one hand, **2@6*-Br** (host **A**) was obtained from a diffusion reaction in toluene / CH₃CN with $c(\mathbf{1}^*) \approx 7.2 \text{ mmol}\cdot\text{L}^{-1}$ (Scheme 1, top right).^[14c] Hence, the reaction with CuBr was repeated under more concentrated conditions with $c(\mathbf{1}^*) \approx 9.2 \text{ mmol}\cdot\text{L}^{-1}$, leading to crystallization of "**4@5*-Br** (host **B**)" with a similar structure as **4@5*-Cl** (Scheme 1, bottom right). On the other hand, "**4@5*-Cl**" was obtained from a diffusion reaction in toluene / CH₃CN with $c(\mathbf{1}^*) \approx 13 \text{ mmol}\cdot\text{L}^{-1}$ (Scheme 1, top left).^[21] Performing the reaction with CuCl under more diluted conditions with $c(\mathbf{1}^*) \approx 10 \text{ mmol}\cdot\text{L}^{-1}$ results in the formation of a 90-vertex spherical host **A** (proposed structure "**2@6*-Cl**", Scheme 1, bottom left).



Scheme 1. Self-assembly of $[\text{Cp}^*\text{Fe}(\eta^5\text{-P}_5)]$ (**1***) with $[(\text{CpCr})_2(\mu, \eta^{5:5}\text{-As}_5)]$ (**2**) and CuCl or CuBr under various conditions.

Thus, the formation of "**4@5***" (cleavage of guest and smaller 80-vertex spherical host **B**) vs. "**2@6***" (triple decker or **1*** as guest and larger 90-vertex spherical host **A**) is indeed dependent

on the concentration, not on the halide (Cl or Br) as previously assumed. Moreover, Cl spheres are known to possess better solubility as the Br analogues,^[14g] which is why the CuBr reactions generally are carried out under slightly more diluted conditions than the CuCl reactions.

Unfortunately, complete X-ray structure determination of the proposed compound “**2@6*-Cl**” proved that the guest molecule within the 90-vertex spheres obtained from CuCl is [Cp*Fe(η^5 -P₅)] (**1***) instead of [(CpCr)₂(μ , $\eta^{5:5}$ -As₅)] (**2**) for the sole measured crystal, so **1*@6*-Cl** (host **A**) is formed.^[23] Since the encapsulated template does not influence the unit cell parameters of the supramolecular compound, it cannot be excluded that other crystals of this batch contained the proposed target product “**2@6*-Cl**” and the experiment obviously only reflects the situation within a single measured crystal. Thus, also NMR spectroscopy of the isolated bulk of crystals was performed. The ¹H NMR spectrum in pyridine-d₅ showed a signal for free **2** at 24.1 ppm but according to the integral ratio of free **1*** to free **2** (1285 : 10), **2** could have only been present as a guest in up to 15% of the spheres.^[24]

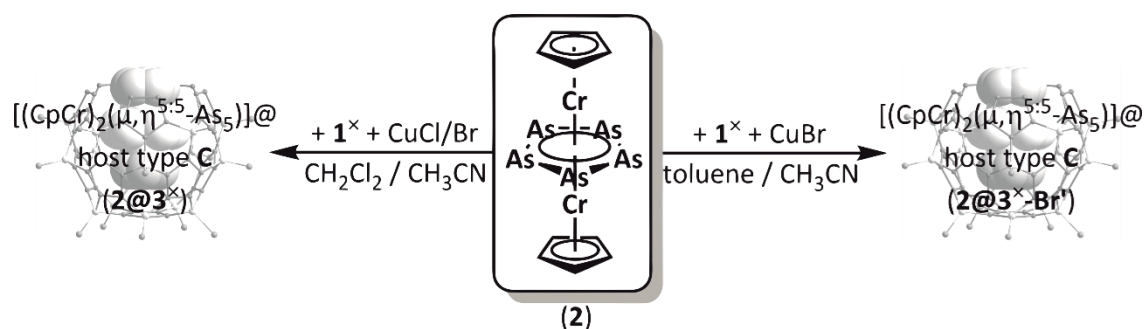
While “**4@5*-Cl**” crystallizes in the cubic space group $Fm\bar{3}c$,^[14c] crystals of “**4@5*-Br**” were of insufficient quality for single crystal X-ray characterization despite numerous crystallization attempts, but their unit cell constants analogously suggest the presence of 80-vertex spheres.^[25] Unfortunately, the X-ray structural data for both compounds “**4@5***” is ambiguous due to high (cubic holohedral) symmetry and entailed disorder and may be interpreted in at least three different ways (borderline cases):

- a) as the previously proposed structure [CpCr(η^5 -As₅)]@{[Cp*Fe(η^5 -P₅)]₁₂{CuX}_{20-n}} (**4@5***, X = Cl, Br), with a cleft guest molecule and a host type **B**, or
- b) as a disordered nano-bowl [(CpCr)₂(μ , $\eta^{5:5}$ -As₅)]@{[Cp*Fe(η^5 -P₅)]₁₁{CuX}_{15-n}} (**2@3***, X = Cl, Br) with all [Cp*Fe(η^5 -P₅)] (**1***) units occupied by 11/12 and an addition {CpCr} fragment being disordered over 12 positions just like the [CpCr(η^5 -As₅)] fragment, thus constituting an intact triple decker guest molecule and an open host type **C**, or
- c) as a disordered nano-bowl [(CpCr)₂(μ , $\eta^{5:5}$ -As₅)]⁺@{[Cp*Fe(η^5 -P₅)]₁₁Cu_{14-n}X_{15-n}} (**2⁺@3***, X = Cl, Br), with the intact triple decker molecule being oxidized by one electron and an open host type **C** with overall site occupancy factors of Cu being reduced by 1 compared to those of X.

Due to similar size and shape these tentative host-guest complexes may also co-crystallize, all these borderline cases can be presumably mixed. To clarify this ambiguity further characterization techniques were used (*vide infra*).

While 90-vertex spherical compounds **2@6*** and proposed 80-vertex spherical compounds “**4@5***” are soluble in CH₂Cl₂ / CH₃CN mixtures or CH₂Cl₂, respectively, the nano-bowls **2@3*** are completely insoluble.^[21] Hence, for a better comparability of the NMR spectra and thereby

bringing more light into the ambiguous structure of “**4@5***”, it was aimed to synthesize more soluble nano-bowls similar to **2@3***. Previously, our group investigated the supramolecular chemistry of $[\text{Cp}^x\text{Fe}(\eta^5\text{-P}_5)]$ (**1^x**, $\text{Cp}^x = \text{C}_5\text{Me}_4\text{Et}$).^[26] The obtained 80-vertex spherical compounds $\{[\text{Cp}^x\text{Fe}(\eta^5\text{-P}_5)]_{12}\{\text{CuX}\}_{20-n}\}$ ($\text{X} = \text{Cl}, \text{Br}$) exhibit a decisively better solubility in CH_2Cl_2 than the analogue compounds based on **1***. Hence, following the syntheses of **2@3***,^[21] $[\text{Cp}^x\text{Fe}(\eta^5\text{-P}_5)]$ (**1^x**) was reacted with $[(\text{CpCr})_2(\mu, \eta^{5:5}\text{-As}_5)]$ (**2**) and CuCl or CuBr in $\text{CH}_2\text{Cl}_2 / \text{CH}_3\text{CN}$ to give $\{[(\text{CpCr})_2(\mu, \eta^{5:5}\text{-As}_5)]@[\text{Cp}^x\text{Fe}(\eta^5\text{-P}_5)]_{11}\{\text{CuCl}\}_{15-n}\}$ (**2@3^x-Cl**, host type **C**) and $\{[(\text{CpCr})_2(\mu, \eta^{5:5}\text{-As}_5)]@[\text{Cp}^x\text{Fe}(\eta^5\text{-P}_5)]_{11}\{\text{CuBr}\}_{15-n}\}$ (**2@3^x-Br**, host type **C**, Scheme 2, left), respectively.



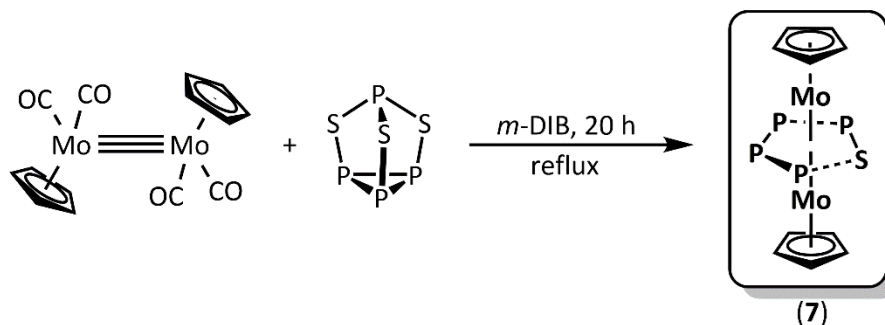
Scheme 2. Self-assembly of $[\text{Cp}^x\text{Fe}(\eta^5\text{-P}_5)]$ (**1^x**) with $[(\text{CpCr})_2(\mu, \eta^{5:5}\text{-As}_5)]$ (**2**) and CuCl or CuBr.

Both compounds possess enhanced solubility in CH_2Cl_2 and CHCl_3 compared to the Cp^* analogues, enabling solution NMR spectroscopic investigations. Moreover, the reactions of **1^x**, **2** and CuCl or CuBr were also performed in toluene / CH_3CN (conditions for **4@5***). For CuCl, under diluted reaction conditions no solids were observed and NMR spectroscopy of the mother liquor rather suggested the formation of nano-bowls (type **C**) or 80-vertex spheres (type **B**), with no hint of the encapsulated species. Under more concentrated conditions only an unidentified precipitate was obtained. For CuBr, under diluted conditions no solid was observed but NMR spectroscopy of the mother liquor proved the formation of **2@3^x-Br**. Under more concentrated conditions indeed the crystallization of another phase of the nano-bowl $\{[(\text{CpCr})_2(\mu, \eta^{5:5}\text{-As}_5)]@[\text{Cp}^x\text{Fe}(\eta^5\text{-P}_5)]_{11}\{\text{CuBr}\}_{15-n}\}$ (**2@3^x-Br'**, Scheme 2, right) is observed.

$[(\text{CpMo})_2(\mu, \eta^{3:3}\text{-P}_3)(\mu, \eta^{2:2}\text{-PS})]$ – a novel template

In order to examine the generality of these observations, we were interested in the application of further triple decker complexes in this host-guest system. For this purpose, we developed a synthesis for the hitherto unknown parent compound $[(\text{CpMo})_2(\mu, \eta^{3:3}\text{-P}_3)(\mu, \eta^{2:2}\text{-PS})]$ (**7**).^[14g] While the Cp^* ^[27] and Cp° ($\text{Cp}^\circ = 1\text{-}^t\text{Bu-3,4-Me}_2\text{C}_5\text{H}_2$)^[28] derivatives of this triple decker complex are already known, they display less appropriate templates for the **1***/CuX self-assembly. In contrast, the Cp containing parent compound should

be preferred for encapsulation due to the least steric bulk on the one hand and favored Cp...P₅ π-π-interactions on the other. Unfortunately, **7** could not be obtained by reaction of [CpMo(CO)₂]₂ with P₄S₃ in refluxing toluene, the method published for the known derivatives. Instead, the use of a higher-boiling solvent proved beneficial. Hence, when [CpMo(CO)₂]₂ is reacted with P₄S₃ in refluxing 1,3-diisopropylbenzene (*m*-DIB, b.p. = 205°C), [(CpMo)₂(μ,η^{3:3}-P₃)(μ,η^{2:2}-PS)] (**7**) was isolable after chromatographic work-up in 18% crystalline yield (for comparison: 13% for the Cp^o derivative, Scheme 3).^[28]



Scheme 3. Synthesis of [(CpMo)₂(μ,η^{3:3}-P₃)(μ,η^{2:2}-PS)] (**7**).

Compound **7** is soluble in toluene and CH₂Cl₂, yet only sparingly soluble in hexane and insoluble in CH₃CN. The ¹H and ¹³C{¹H} NMR spectra of **7** in C₆D₆ each show one singlet at δ = 4.73 ppm and δ = 91.2 ppm for the Cp ligand, respectively. ¹H NMR spectra were additionally recorded in CD₂Cl₂, CDCl₃ and pyridine-*d*₅ for the sake of better comparability of the chemical shifts of free **7** and encapsulated **7**. In CD₂Cl₂ and CDCl₃, the Cp ligand resonates at δ = 5.21 ppm, in pyridine-*d*₅ a singlet at δ = 5.23 ppm is observed. In the ³¹P{¹H} NMR spectrum, four multiplets, spread over a wider range of almost 750 ppm, represent an ABMX spin system: δ = 336.6 (ddd, P_A), 318.9 (ddd, P_B), -168.6 (ddd, P_M), -403.8 (ddd, P_X) ppm with respective coupling constants of *J*_{PP}(AB) = 19 Hz, *J*_{PP}(AM) = 59 Hz, *J*_{PP}(AX) = 376 Hz, *J*_{PP}(BM) = 6 Hz, *J*_{PP}(BX) = 376 Hz and *J*_{PP}(MX) = 20 Hz. These observations are in accordance with weakly interacting η³-P₃ and η²-PS ligands within the middle deck. Compared to the Cp* and Cp^o derivatives, all signals are shifted to higher field by up to 18 ppm.^[27,28]

By layering a solution **7** in CH₂Cl₂ with CH₃CN, red plate-like crystals suitable for X-ray structure analysis could be obtained for the first time for a [(Cp^RMo)₂(μ,η^{3:3}-P₃)(μ,η^{2:2}-PS)] triple decker complex. For Cp^R = Cp* or Cp^o, only coordination compounds containing the complexes and not the starting material themselves were characterized by X-ray crystallography.^[27,28,29] Compound **7** crystallizes in the monoclinic space group *C*2/*c*. Its molecular structure reveals a triple decker complex bearing a *pseudo* five-membered middle deck (Figure 3a). In accordance with the ³¹P{¹H} NMR spectrum, it can be best described as an η³-P₃ and an η²-PS ligand. The latter is disordered in the crystal structure by rotation about the 2-fold axis, passing through the

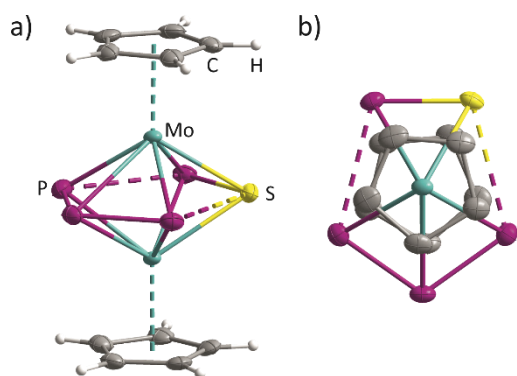


Figure 3. Molecular structure of **7**. a) side view; b) top view with H atoms omitted for clarity.

center of the PS bond and the middle P atom of the $\eta^3\text{-P}_3$ ligand. The P-S distance of 2.0791(12) Å as well as the P-P bond lengths of 2.1590(8) Å are in the region between a single and a double bond.^[30] The P_3 and the PS ligand are separated by 2.8899(9) Å in the middle deck, whereas the Mo-P distances range from 2.4170(6) to 2.5995(7) Å. The Cp ligands deviate from an eclipsed conformation by 9.78(19)° (Figure 3b). In the crystal structure,

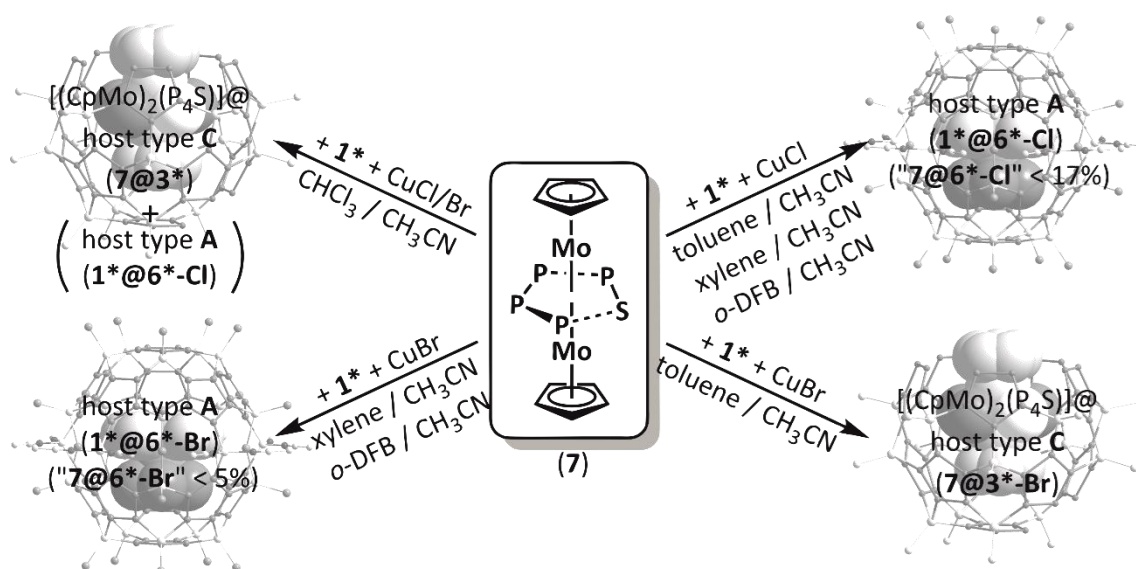
the molecules form lengthwise chains with short Cp...Cp distances of 3.222(6) Å evident for quite strong π - π -interactions.

[(CpMo)₂($\mu,\eta^{3:3}\text{-P}_3$)($\mu,\eta^{2:2}\text{-PS}$)] as guest

With [(CpMo)₂($\mu,\eta^{3:3}\text{-P}_3$)($\mu,\eta^{2:2}\text{-PS}$)] (**7**) in hand, we were interested in its function as a template in the [Cp*Fe($\eta^5\text{-P}_5$)] (**1***) / CuX (X = Cl, Br) system. In analogy to the reactions with [(CpCr)₂($\mu,\eta^{5:5}\text{-As}_5$)] (**2**), a solution of **7** and **1*** in CH₂Cl₂ was layered with a solution of CuBr in CH₃CN.^[14g] Then, next to brown plates of the 2D polymer [Cp*Fe($\eta^5\text{-P}_5$)CuBr]_n^[12a] and sometimes brown rods of **1*@A** (90-vertex supramolecule),^[13b,c] also black rhombohedra are obtained.^[14g] The latter crystallize in the trigonal space group $R\bar{3}$ with unit cell parameters of $a = b = 41.7763(5)$ Å, $c = 104.785(1)$ Å, $V = 158377(4)$ Å³, reminiscent of the parameters obtained for 80-vertex spheres **B** when crystallized from CH₂Cl₂ / CH₃CN,^[14g] except for a doubled c unit cell constant. Hence, these crystalline phases are crystallographically related as structure and superstructure. However, due to disorder, the X-ray data obtained are ambiguous and can again be interpreted in different ways.

In the attempt to prevent this disorder, two different methods were applied. On the one hand, the reaction was carried out by layering a CHCl₃ solution instead of a CH₂Cl₂ solution in order to slow down crystallization. On the other hand, [Cp*Fe($\eta^5\text{-P}_5$)] (**1***) was applied as a building block instead of **1*** for the same reason.

When a solution of **1*** and **7** in CHCl₃ is layered with a solution of CuCl or CuBr in CH₃CN, dark brown rods of [(CpMo)₂($\mu,\eta^{3:3}\text{-P}_3$)($\mu,\eta^{2:2}\text{-PS}$)][Cp*Fe($\eta^5\text{-P}_5$)]₁₁{CuCl}_{13.3} (**7@3*-Cl**) or [(CpMo)₂($\mu,\eta^{3:3}\text{-P}_3$)($\mu,\eta^{2:2}\text{-PS}$)][Cp*Fe($\eta^5\text{-P}_5$)]₁₁{CuBr}_{13.235} (**7@3*-Br**), respectively, crystallize in the monoclinic non-centrosymmetric space group Cc , isostructurally to **2@3*-Cl** (Scheme 4, top left).^[21] Here, no positional disorder is observed and the structure is unambiguously identified as an intact triple decker guest molecule encapsulated in a nano-bowl host (type **C**).



Scheme 4. Self-assembly of $[\text{Cp}^*\text{Fe}(\eta^5\text{-P}_5)]$ ($\mathbf{1}^*$) with $[(\text{CpMo})_2(\mu, \eta^{3:3}\text{-P}_3)(\mu, \eta^{2:2}\text{-PS})]$ ($\mathbf{7}$) and CuCl or CuBr under various conditions.

Remarkably, this time also the Cl compound $\mathbf{7@3^*-Cl}$ is obtained. $\mathbf{7@3^*-Cl}$ and $\mathbf{7@3^*-Br}$ can be isolated in 40% and 39% crystalline yield, respectively. For the reaction of $\mathbf{1}^*$ with $\mathbf{7}$ and CuCl, longer crystallization times (>3 weeks) lead to additional crystallization of 90-vertex spheres $\mathbf{6^*-Cl}$ (host type A) in a new crystalline phase.^[31] The X-ray diffraction experiment showed the encapsulation of $\mathbf{1}^*$ instead of $\mathbf{7}$. Additionally, the isolated crystals were dissolved in pyridine- d_5 for complete disaggregation, and in the ^1H and $^{31}\text{P}\{^1\text{H}\}$ NMR spectra of this solution no signals for $\mathbf{7}$ are detected. Hence, only $\mathbf{1^*@6^*-Cl}$ is formed instead of $\mathbf{7@6^*-Cl}$.

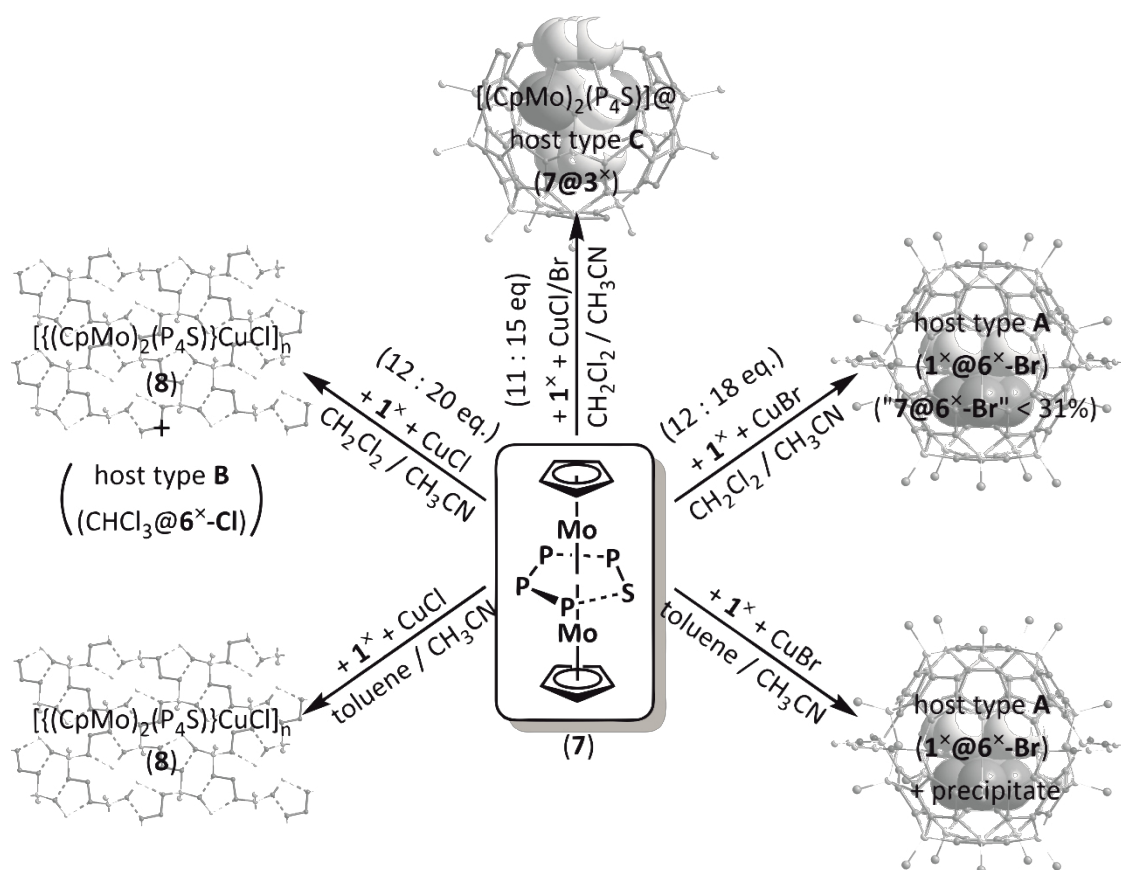
Furthermore, 90-vertex spheres $\mathbf{6^*-Cl}$ (host type A) were also obtained by layering a solution of CuCl in CH_3CN onto solutions of $\mathbf{1}^*$ and $\mathbf{7}$ in toluene, xylene or *o*-difluorobenzene (*o*-DFB), partially crystallizing as new phases (Scheme 4, top right).^[32] Again, all X-ray diffraction data point to encapsulation of $\mathbf{1}^*$ instead of $\mathbf{7}$, and integral ratios in the ^1H NMR spectra of the isolated crystals dissolved in pyridine- d_5 show that a maximum of 17% of the $\mathbf{6^*-Cl}$ hosts spheres could have encapsulated $\mathbf{7}$.^[24] Therefore, the chances to find the desired crystals of $\mathbf{7@6^*-Cl}$ are very low since the obtained batches predominantly consist of $\mathbf{1^*@6^*-Cl}$.

Analogously, 90-vertex spheres $\mathbf{6^*-Br}$ (host type A) were obtained by layering a solution of CuBr in CH_3CN onto solutions of $\mathbf{1}^*$ and $\mathbf{7}$ in xylene or *o*-DFB, crystallizing as new phases (Scheme 4, bottom left).^[33] Preliminary X-ray data point to encapsulation of $\mathbf{1}^*$ and ^1H NMR spectra of the isolated crystals in pyridine- d_5 reveal that only up to 5% of the host spheres could have encapsulated triple decker complex $\mathbf{7}$.^[24]

On the contrary, the reaction of $\mathbf{1}^*$, $\mathbf{7}$ and CuBr in toluene / CH_3CN indeed furnishes crystals with unit cell parameters reminiscent of those obtained for 80-vertex spheres (Scheme 4, bottom right).^[34] Hence, the three borderline interpretations discussed above also account for

these crystals. However, the absence of an EPR signal as expected for a paramagnetic 17VE $[(\text{CpMo}(\eta^3\text{-P}_3)(\eta^2\text{-PS}))]$ fragment or a 27VE $[(\text{CpMo})_2(\mu, \eta^{3:3}\text{-P}_3)(\mu, \eta^{2:2}\text{-PS})]^+$ (7^+) oxidized triple decker (presumably doublet states) gives no hint for cleavage or oxidation of the triple decker **7**. Moreover, the ^1H NMR spectrum in pyridine- d_5 exhibits a singlet at $\delta = 5.23$ ppm attributed to free **7**. Therefore, it is more likely that a nano-bowl $7@3^*\text{-Br}$ is formed and crystallized with orientational disorder probably co-crystallized with 80-vertex spheres hosting solvent molecules.

In contrast to compounds $7@3^*$, their Cp^x analogues $7@3^x$ can already be crystallized in an ordered fashion from $\text{CH}_2\text{Cl}_2 / \text{CH}_3\text{CN}$ layering reactions (Scheme 5, top). $7@3^x\text{-Cl}$ is isolable in 48% crystalline yield, $7@3^x\text{-Br}$ in 22% crystalline yield. Both reactions are highly dependent on the stoichiometry and the nano-bowls $7@3^x$ are only obtained from stoichiometric molar ratios of 11 : 15 ($1^x : \text{Cu}$).



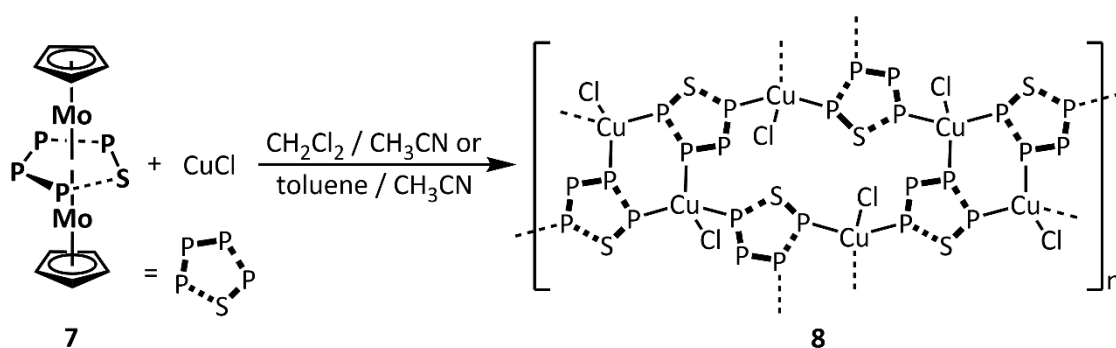
Scheme 5. Self-assembly of $[\text{Cp}^x\text{Fe}(\eta^5\text{-P}_5)]$ (1^x) with $[(\text{CpMo})_2(\mu, \eta^{3:3}\text{-P}_3)(\mu, \eta^{2:2}\text{-PS})]$ (**7**) and CuCl or CuBr under various conditions.

For CuBr reactions, when a ratio of 12 : >18 ($1^x : \text{CuBr}$) is applied, instead of host types **C**, the 90-vertex spherical product $6^x\text{-Br}^{[13b]}$ is obtained in a novel crystalline phase (Scheme 5, top right).^[35] ^1H NMR spectroscopy of the isolated crystals in pyridine- d_5 suggests encapsulation of triple decker **7** in 31% of the supramolecular hosts at most (integral ratio of **7** : (Me groups of 1^x) = 10 : 494).^[36]

For CuCl reactions, when a ratio of 12 : 20 (1^* : CuCl) is applied, crystals of the novel 2D polymer $[(\text{CpMo})_2(\mu_4, \eta^{3:3:1:1}\text{-P}_3)(\mu_3, \eta^{2:2:1}\text{-PS})\text{CuCl}]_n$ (**8**) are obtained (Scheme 5, top left). When the mother liquor is decanted, dried and re-dissolved in CDCl_3 , the 80-vertex sphere $(\text{CHCl}_3)_m @ \{[\text{Cp}^*\text{Fe}(\eta^5\text{-P}_5)]_{12}[\text{CuCl}]_{20-n}\}$ (host type **B**) is detected by NMR spectroscopy. Crystals obtained from the concentrated NMR solution were as well identified as 80-vertex sphere $(\text{CHCl}_3)_m @ \{[\text{Cp}^*\text{Fe}(\eta^5\text{-P}_5)]_{12}[\text{CuCl}]_{20-n}\}$ with solvent molecules occupying its void since no electron density that could be attributed to heavy Mo atoms of the guest was found.^[37] Unlike 1^* , 1^x is known to form 80-vertex spheres also in the absence of a template (cf. chapter 3).^[26] Polymer **8** constitutes the first 2D polymer obtained from $[(\text{Cp}^R\text{Mo})_2(\mu, \eta^{3:3}\text{-P}_3)(\mu, \eta^{2:2}\text{-PS})]$ ($\text{Cp} = \text{Cp}, \text{Cp}^*, \text{Cp}^\circ$). So far, only the coordination behavior of the Cp^* and Cp° derivatives towards CuI, Ag[TEF] and Ti[TEF] ($\text{TEF}^- = \text{Al}(\text{OC}(\text{CF}_3)_3)_4^-$) has been examined, whereby mostly 1D and only once a 3D polymer was obtained.^[28,29]

Compound **8** is also the only crystalline product obtained from the reaction of 1^x , **7** and CuCl in toluene / CH_3CN . In the analogous reaction with CuBr, only the 90-vertex spherical product $1^x @ 6^x\text{-Br}$ (host type **A**) is detected in the $^{31}\text{P}\{^1\text{H}\}$ NMR spectrum of the mother liquor, while a black precipitate is obtained (Scheme 5, bottom right). This precipitate is insoluble in toluene, CH_2Cl_2 and a 1:1 CH_2Cl_2 / CH_3CN mixture but is soluble in pyridine. The ^1H and $^{31}\text{P}\{^1\text{H}\}$ NMR spectra of the precipitate in pyridine- d_5 merely exhibit signals of free **7** next to trace amounts of 1^x . Therefore, it is likely that the precipitate is composed of a CuBr-coordination polymer of **7**.

Polymer **8** can as well be synthesized directly by layering a solution of **7** in CH_2Cl_2 or toluene with a solution of CuCl in CH_3CN in 38% crystalline yield (Scheme 6). However, it can be isolated in up to 83% yield referring to **7** when obtained as by-product in the abovementioned reactions.



Scheme 6. Self-assembly of $[(\text{CpMo})_2(\mu, \eta^{3:3}\text{-P}_3)(\mu, \eta^{2:2}\text{-PS})]$ (**7**) and CuCl.

Within the unsuccessful attempts to synthesize a CuI derivative of nano-bowl shaped host molecules, the novel polymer $\{[\text{Cp}^*\text{Fe}(\eta^{5:1:1:1}\text{-P}_5)]_2[\text{Cp}^*\text{Fe}(\eta^{5:1:1}\text{-P}_5)]\text{Cu}_4(\mu\text{-I})_4\}_n$ (**9**) is obtained by reaction of $[\text{Cp}^*\text{Fe}(\eta^5\text{-P}_5)]$ (1^*), $[(\text{CpMo})_2(\mu, \eta^{6:6}\text{-P}_6)]$ ^[38] and CuI (Scheme 7).^[14g]

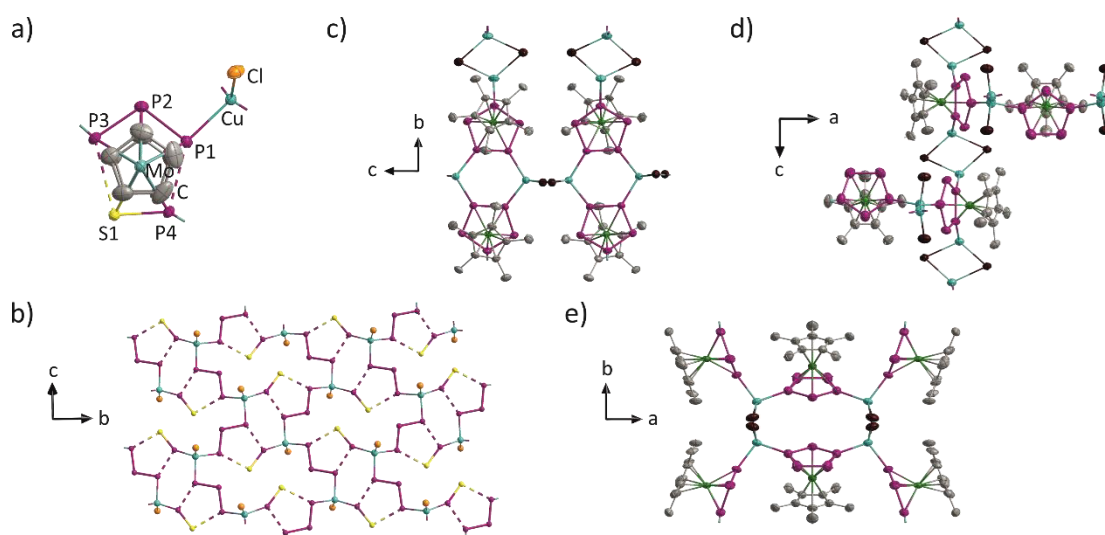


Figure 4. a) Repeating unit and b) section of the polymeric structure of **8** with {CpMo} moieties omitted. c) – e) Sections of the polymeric structure of **9**. H atoms and solvate molecules are omitted.

of the van-der-Waals-radii: 2.85 Å).^[17] Additionally, exceedingly short Cp...Cp distances (3.093(6) – 3.293(6) Å) are found in between the 2D layers indicating quite strong π - π -interactions (normal range: 3.3 – 3.8 Å).^[39]

3D polymer **9** crystallizes as brownish-red needles in the orthorhombic space group *Pmna*. The *cyclo*-P₅ ligands in **9** show two different coordination modes: Two thirds of the P₅ rings are connected to copper *via* three atoms in a 1,2,4-fashion, whereas the remaining ones show a 1,3-bridging coordination mode of two P atoms (Figure 4c-e). In turn, each Cu atom links two P₅ rings and is additionally coordinated by two iodine atoms to reach tetrahedral environment. By this, 12-membered {Cu₄P₆I₂} rings, six-membered {Cu₂P₄} rings and four-membered {Cu₂I₂} rings are formed. The individual structural motifs and connectivity pattern are well-known in this chemistry.^[12] Despite this, the first combination of these coordination modes leads to a hitherto unknown topological type of 3-connected 3-periodic nets. Thereby, the Cu atoms and the 1,2,4-coordinating [Cp*Fe(η^5 -P₅)] moieties form the nodes of the polymeric framework whereas iodine and the 1,3-coordinating [Cp*Fe(η^5 -P₅)] molecules act as spacers (see crystallographic part, Figure 8).

Compounds **8** and **9** are insoluble in all common solvents (pentane or hexane, toluene, CH₂Cl₂, CH₃CN, THF). Only in the strong donor solvent pyridine the networks are soluble under disassembly into the building blocks as evidenced by ³¹P{¹H} NMR spectroscopy. The positive ion ESI mass spectrum of **8** displays peaks for triple decker containing fragments up to $m/z = 1597.0937$ attributed to [((CpMo)₂P₄S)₃Cu₂Cl]⁺.

Supramolecules: Crystal Structures

The structures of compounds **2@3***^[21] and **2@6*-Br**^[14c] have already been described elsewhere and will therefore not be discussed herein. The ambiguous structure of “**4@5*-Cl**”^[14c,21] is reinvestigated together with the novel Br analogue “**4@5*-Br**” by further characterization techniques and an additional interpretation of the X-ray data (borderline case c, **2*@3***) is introduced above. Unfortunately, the crystallization of “**4@5*-Cl**” in the face-centered cubic structure type ($a = 42 \text{ \AA}$) entails inherent problems during X-ray data acquisition since the volume of the unit cell occupied by the spheres equals the volume occupied by solvents, and the crystal packing provides channels for the solvent evacuation. Hence, crystals of this structure type are extremely unstable during sample handling as soon as they are taken from the mother liquor. This presents an additional challenge for reliable X-ray structure determination.

Compounds **7@3*** crystallize in the monoclinic non-centrosymmetric space group Cc and are isostructural to **2@3*-Cl**.^[21] X-ray structure analyses reveal the presence of nano-bowl shaped host molecules comprising an idealized scaffold $[(\text{Cp}^*\text{Fe}(\eta^5\text{-P}_5))_{11}\{\text{CuX}\}_{15-n}]$ encapsulating one molecule of $[(\text{CpMo})_2(\mu, \eta^{3:3}\text{-P}_3)(\mu, \eta^{2:2}\text{-PS})]$ (**7**, Figure 5a). The host scaffolds can conceptually be derived from the well-known 80-vertex spherical hosts $[(\text{Cp}^*\text{Fe}(\eta^5\text{-P}_5))_{12}\{\text{CuX}\}_{20-n}]$ (host type **B**)^[14b,c,e,f,g] by cutting off a $[(\text{Cp}^*\text{Fe}(\eta^5\text{-P}_5))\{\text{CuX}\}_5]$ moiety, resulting in truncated, open-structured bowls. Both compounds display solid solutions of host-guest aggregates with differing CuX contents (average: **7@3*-Cl**: 13.35; **7@3*-Br**: 14.55) and CHCl_3 solvate molecules are found to point into the positions of the $\{\text{CuX}\}$ vacancies (Figure 5b). Remarkably, in **7@3*-Cl**, one $\{\text{CuCl}\}$ position is left completely vacant, so that the presence of “complete bowls” with 15 CuCl can be excluded for this crystal.

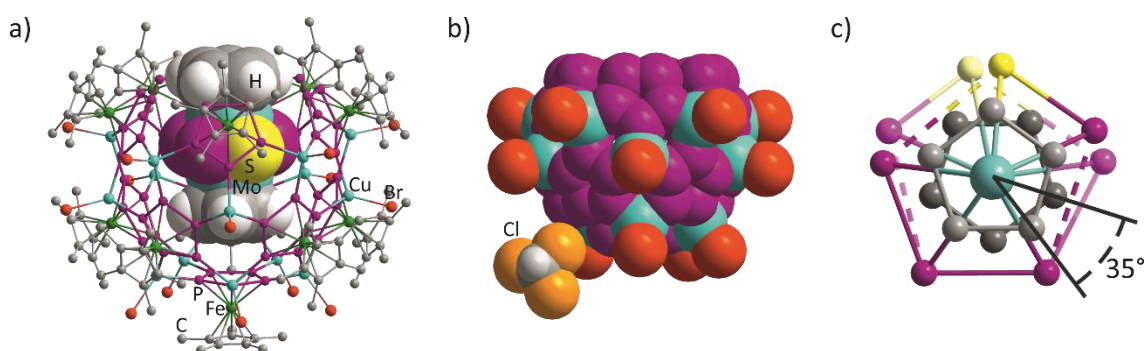


Figure 5. a) Molecular structure of **7@3*-Br** with hydrogen atoms and minor parts of disorder omitted for clarity; the template is shown in the space-filling model; b) CHCl_3 molecule pointing into a CuBr vacancy; c) disorder of the P_4S middle deck in the template with second orientation highlighted by a brighter color and conformation of the Cp ligands in the template.

Due to the open-core structure of the host aggregate, the triple decker guest molecule **7** with a length of $10.071(4) \text{ \AA}$ can protrude from the core of the host being $7.92 - 7.95 \text{ \AA}$ deep.^[40] With a width of 7.77 \AA , **7** fits well within the void of the host aggregates comprising diameters of 8.38

(**7@3^x-Cl**) and 8.39 Å (**7@3^x-Br**).^[41] The top Cp ligand and the P₄S middle deck of the guest molecule are more or less eclipsed and oriented such that steric repulsion with the inner surface of the host molecule is minimized. The middle deck of the guest molecule **7** is thereby disordered over two positions in a ratio of 80:20 (Figure 5c). In contrast, the bottom Cp ligand is staggered with respect to the P₄S middle deck and the top Cp ligand by about 35° and thus at the same time being in an eclipsed conformation towards the bottom P₅ ring of the host. The respective Cp⋯P₅ distances amount to 3.580(5) – 3.591(4) Å (**7@3^x-Cl**) and 3.556(4) – 3.565(4) Å (**7@3^x-Br**) indicating π-π host-guest interactions. These orientations of the top, middle and bottom ligands with respect to one another and the host are found similarly in **2@3^x** and differ from free **2** and **7**, which both comprise a nearly eclipsed conformation of all three ligands.^[21]

Another commonality of compounds **2@3^x** and **7@3^x** is the presence of intramolecular host-guest interactions. The Cp ligand protruding from the core of the host participates in Cp⋯Cp* π-π interactions (**7@3^x-Cl**: 3.235(6) – 3.267(6) Å, **7@3^x-Br**: 3.217(5) – 3.255(5) Å) with the Cp* of the opposite side of the next host-guest assembly (Figure 6a). The so formed head-to-tail columns are further interconnected by a network of X⋯Cp* σ-π specific interactions and Cp*⋯Cp* π-π interactions (Figure 6b-c), as already found for compounds **2@3^x**.^[21]

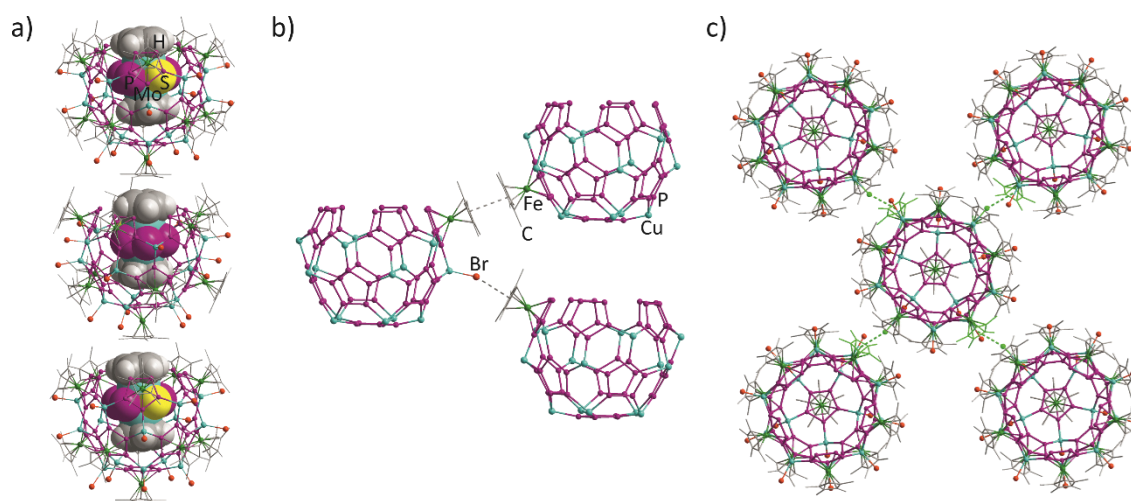


Figure 6. a) head-to-tail column of **7@3^x-Br** formed by intermolecular Cp⋯Cp* host-guest interactions; b) intermolecular Cp*⋯Cp* interaction and a σ-π supramolecular synthon based on Br⋯Cp* interactions; c) packing of the columns interconnected by σ-π synthons highlighted in green.

Compounds **2@3^x-Cl** and **7@3^x** crystallize in the monoclinic non-centrosymmetric space group *Cc* and are isotypic to **2@3^x-Br**.^[21] Compounds **2@3^x-Br** crystallize in the non-centrosymmetric monoclinic space groups *Pc* (from CH₂Cl₂ / CH₃CN, **2@3^x-Br**) or *C2* (from toluene / CH₃CN, **2@3^x-Br'**). Again, in all compounds, nano-bowl shaped host molecules comprising a scaffold [$\{\text{Cp}^x\text{Fe}(\eta^5\text{-P}_5)\}_{11}\{\text{CuX}\}_{15-n}$] are found, which act as hosts for the applied triple decker molecules. Except for **7@3^x-Br**, all these nano-bowls based on **1^x** are disordered over two positions, with apertures of both positions being opposed to each other. Thus, also the

triple decker guest molecule is disordered over two partly overlapping positions. Moreover, although structural refinement is not completed yet and thus total CuX (X = Cl, Br) contents are not yet finally refined to the best fit to the diffraction data, it is nevertheless already clear, that compounds **2@3^x-Cl**, **2@3^x-Br**, **7@3^x-Cl** and **7@3^x-Br** provide some {CuX} vacancies, and CH₂Cl₂ molecules partly occupy these positions instead. This has not yet been found for **2@3^x-Br'**, which was crystallized from C₇H₈ / CH₃CN in the absence of CH₂Cl₂, although C₇H₈ may occupy vacant CuX positions in such spherical compounds as well.^[14g] Independent of the triple decker guest molecule **2** or **7**, the Cp ligand protruding from the core of the host and located at its “bottle-neck” takes in an eclipsed conformation with respect to the As₅ (**2@3^x**) or P₄S (**7@3^x**) middle deck, so that both ligands best prevent steric repulsion towards the inner surface and “bottle-neck” atoms of the host. The P₄S middle decks in compounds **7@3^x** are additionally disordered over at least two positions. As for the Cp* analogues, this additional disorder can predominantly be traced back to the deviation from five-fold symmetry in the P₄S middle deck, which is better explained as a PS dumbbell interacting with a P₃ ligand. The Cp ligand located within the core of the host is staggered with respect to the middle deck and the Cp ligand at the “bottle neck”, thus taking in an eclipsed orientation towards the P₅ ring of the bowl-shaped host with Cp...P₅ distances of 3.61 Å (**2@3^x-Cl**), 3.57 and 3.61 Å (**2@3^x-Br**), 3.58 Å (**7@3^x-Br**) and 3.62 Å (**7@3^x-Br**) indicating π-π host-guest interactions. In **2@3^x-Br'**, however, the respective Cp ligand is disordered over two positions and exhibits a larger Cp...P₅ distance of 3.68 Å (major position) or 3.75 Å (minor position of disorder), suggesting weaker π-π interactions.

Similarly to the **1*** based aggregates, the **1*** based compounds **2@3^x-Cl**, **2@3^x-Br**, **7@3^x-Cl** and **7@3^x-Br** additionally exhibit intermolecular host-guest interactions between the Cp ligand at the open “bottle neck” and the Cp^x ligand of the next host molecule opposed to the aperture, hence leading to head-to-tail columns. However, the Cp...Cp^x distances amount to 3.53 – 3.54 Å (**2@3^x-Cl**), 3.48 – 3.55 Å (**2@3^x-Br**), 3.51 – 3.52 Å (**7@3^x-Br**) and 3.49 – 3.53 Å (**7@3^x-Br**) and are distinctly larger than the Cp...Cp* distances in analogous **1*** based compounds **2@3*** (3.23 and 3.17 Å)^[21] and **7@3*** (3.21 – 3.27 Å, *vide supra*). This can be caused by an adjustment to the steric demand of the Et group, which also causes a non-parallel arrangement of the C₅ planes of the Cp and the Cp^x ligands with plane-to-plane angles of roughly 8 to 11°, while in the Cp* analogues these angles only amount to a maximum of 3.9(4)° (found in **2@3*-Cl**).^[21] Therefore, the columns of **3^x** host molecules show a slight zigzag arrangement. Another consequence thereof is that in contrast to most other Cp^x ligands in the host the respective Cp^x ligand is not disordered since this would require a parallel arrangement of the Cp and Cp^x ligands.

Compound **2@3^x-Br'** once more displays an exception, as toluene molecules are located in between the Cp ligand at the “bottle neck” of one aggregate and the Cp^x ligand at the opposed

side of the next aggregate, expanding the Cp to Cp^x distance to roughly 6.9 Å. Hence, presumably indirect Cp^{...}C₇H₈^{...}Cp^x contacts build up the 1D columns in **2@3^x-Br'**, and the Cp^x ligand is disordered. Moreover, while columns in **2@3^x** and **7@3^x** are arranged parallel to each other, the angle between the columns in **2@3^x-Br'** amounts to about 70° since they are not parallel to the 2-fold axes of the C₂ space group.

X^{...}Cp^x σ-π synthons are found interconnecting the columns in all **1^x** based nano-bowls, analogically to the **1*** based aggregates. However, instead of additional Cp^{*}^{...}Cp^{*} π-π interactions, in **2@3^x-Cl**, **2@3^x-Br**, **7@3^x-Cl** and **7@3^x-Br** only CH^{...}π interactions are present, and in **2@3^x-Br'** even these are not found.

To sum up, the structures of the individual host-guest aggregates **2@3^x** and **7@3^x** barely differ from their Cp^{*} analogues. By contrast, decisive differences are found in the intermolecular interactions. Presumably, next to the presence of CH^{...}π instead of π-π inter-column interactions, the decisively weaker Cp^{...}Cp^x intermolecular host-guest interactions within the columns account for the exceedingly higher solubility of compounds **2@3^x** and **7@3^x** compared to the Cp^{*} analogues.

Supramolecules: Solubilities

Compounds **2@3^{*}**^[21] and **7@3^{*}** are insoluble in hexane, pentane, toluene and CH₃CN, while they are sparsely soluble in CH₂Cl₂ and THF and moderately soluble in CHCl₃. The Cl derivative exhibits a slightly higher solubility than the Br derivative. The analogues based on **1^x** profit from enhanced solubilities especially in CH₂Cl₂ and CHCl₃. While compounds **2@3^x** are insoluble in pentane and CH₃CN, they are moderately soluble in toluene and THF. In CH₂Cl₂ they are well soluble and in CHCl₃ they are very well soluble, enabling detailed NMR spectroscopic investigations in solution. Compounds **7@3^x** are insoluble in pentane and CH₃CN, and surprisingly also insoluble in toluene and THF. However, they exhibit good solubilities in CH₂Cl₂ and CHCl₃. Compounds "**4@5^{*}**" are insoluble in pentane, hexane, toluene and CH₃CN but moderately soluble in THF and CH₂Cl₂ (for "**4@5^{*}-Cl**" cf. reference [21]). Again, the Cl compound benefits from higher solubilities than the Br analogue, thus being soluble enough in CH₂Cl₂ for detection of guest species by NMR spectroscopy. For the Br compound, this is better achieved from CHCl₃ solutions. As reported for other 90-vertex spheres,^[13] compounds **2@6^{*}** are merely soluble in mixtures of CH₂Cl₂ and CH₃CN.^[14c] Moreover, all of the aforementioned compounds exhibit good solubility in pyridine under complete disaggregation of the host and concomitant release of the guest molecule.

Supramolecules: Mass spectrometry

In the negative ion ESI mass spectra in CH₂Cl₂ / CH₃CN mixtures, barely copper halide fragments are detected, with the largest fragments being [Cu₆X₇]⁻. In the positive ion ESI mass spectra, in all cases numerous pentaphosphaferrocene-containing fragments are found. The largest fragment detected is [(Cp^RFeP₅)₄Cu₁₃Cl₁₂]⁺ (*m/z* = 2635.4). Surprisingly, for the compounds “4@5*-Br” and 2@3^x also a peak attributed to [(CpCr)₂(μ,η^{5:5}-As₅)]⁺ (*m/z* = 608.6) is present. For the compounds 7@3*-Cl, 7@3^x-Cl and 7@3^x-Br [(CpMo)₂P₄S]-containing fragments are found, in which the triple decker **7** acts as a neutral ligand complex next to 1* or 1^x, with [(CpMo)₂P₄S]{Cp^RFeP₅}Cu₃X₂]⁺ being the largest of such fragments detected.

The EI mass spectra of all compounds show peaks corresponding to [Cp^RFeP₅] and [(Cp^RFeP₅)-P₂]. In the spectra of 7@3^x, additionally [(CpMo)₂P₄S]⁺ (and [(CpMo)₂P₄S]-P₂)⁺ for 7@3^x-Cl) is detected, hence corroborating the presence of the template **7**. Likewise, the spectra of compounds 2@3*^[21] and 2@3^x additionally exhibit peaks attributed to [(CpCr)₂(μ,η^{5:5}-As₅)]⁺, [As₄]⁺ and sometimes also [(CpCr)₂(μ,η^{5:5}-As₅)-As₂]⁺ and [As₂]⁺, confirming the presence of the template **2**. In contrast, next to the aforementioned 1* derived peaks, the EI mass spectra of “4@5*-Cl” and “4@5*-Br” each only exhibit a peak for [As₄]⁺ with high intensity (84% (Cl) or 68% (Br) relative to 1*), but [(CpCr)₂(μ,η^{5:5}-As₅)]⁺ is not detected. Therefore, it is suggested that the triple decker **2** is not encapsulated as such and the structural interpretation as a disordered nano-bowl 2@3* (borderline case b) becomes highly unlikely.

Supramolecules: NMR and EPR spectroscopy

As found for poorly soluble compound 2@3*-Cl,^[21] the ³¹P{¹H} NMR spectra of 2@3^x, 7@3* and 7@3^x in CD₂Cl₂ or CDCl₃ all show broad signals in the range of about 60 – 130 ppm, which is similar to the respective spectra of 80-vertex spheres. Since for 80-vertex spheres obtained from [Cp^{Bn}Fe(η⁵-P₅)] (Cp^{Bn} = C₅(CH₂Ph)₅) the different signals obtained were traced back to spherical aggregates of different porosities,^[42] and such CuX vacancies are also found in the course of X-ray structure investigation for compounds 2@3^x, 7@3* and 7@3^x, a similar interpretation is suggested. Moreover, uncoordinated 1* or 1^x are additionally detected in the ³¹P{¹H} and ¹H NMR spectra indicating some degree of disaggregation of the hosts in solution.

The ¹H NMR spectra of compounds 7@3* also exhibit signals attributed to the building blocks 1* of the host molecules. These signals are shifted to lower field (δ = 2.05 – 2.36 ppm for Cl, δ = 2.08 – 2.41 ppm for Br) in comparison to free 1* (δ = 1.44 ppm), are broadened and further splitting is presumably caused by the presence of hosts with different CuX contents. For comparison, in the ¹H NMR spectra of compounds 2@3* additional host signals are detected at higher (δ = 1.4 – 1.5 ppm) and lower (δ = 3.2 – 3.4 ppm) field though the molecular structure of

the hosts does not differ.^[21] Hence, these additional signals must be due to the proximity of the Cp* ligands to the paramagnetic guest molecule in compounds **2@3***. This effect was found to be more pronounced in the solid state ¹H MAS NMR spectra ($\delta = 1.4$ and 6.7 ppm).^[21]

The same features are found for the host signals in the ¹H NMR spectra of compounds **2@3^x** and **7@3^x**, although the spectra are impliedly more complicated due to the magnetically inequivalent protons of the Cp^x ligand. For **7@3^x**, the ethyl protons resonate at chemical shifts of 0.98 – 1.09 (CH₃) and 2.73 – 3.20 ppm (CH₂), as compared to 0.75 and 1.94 ppm for free **1^x**, and are thus shifted to lower field. Assignments were confirmed by ¹H,¹H-COSY NMR spectroscopy. Similarly, the signals of the methyl protons are shifted to 2.06 – 2.40 ppm while the respective signals of free **1^x** are found at 1.43 and 1.45 ppm. For **2@3^x**, the ¹H NMR spectra show additional signals at higher ($\delta = 0.67$ - 0.69 (CH₂CH₃), 1.45-1.48 (CH₃), 2.09-2.22 (CH₂CH₃) ppm) and lower field ($\delta = 1.78$ - 1.79 (CH₂CH₃), 3.20-3.41 (CH₃), 4.11-4.33 (CH₂CH₃) ppm) due to the proximity to the paramagnetic guest molecule.

In the ³¹P{¹H} NMR spectra of compounds **7@3*-Cl** and **7@3^x-Cl**, the guest molecule is detected as four very small signals at -397, -150, 332 and 351 ppm, which are shifted compared to free **7** (-403.8, -168.6, 318.9 and 336.6 ppm). However, the signals are not sufficiently resolved for further conclusions. For the Br analogues, no signals for encapsulated **7** are detected in the ³¹P{¹H} NMR spectra. In contrast, the ¹H NMR spectra of compounds **7@3*** and **7@3^x** show up to four signals for the encapsulated triple decker **7** in the range from about 4.4 – 4.9 ppm for the Cl analogues and 4.6 – 5.1 ppm for the Br analogues. The presence of up to four instead of only two signals, as expected, is most probably due to the presence of CuX vacancies. Additionally, a singlet for free **7** is also detected at 5.21 or 5.22 ppm in the ¹H NMR spectra of **7@3*** and **7@3^x-Cl**, which is in accordance with some disaggregation of the hosts in solution already detected by ³¹P{¹H} NMR spectroscopy.

Remarkably, compounds **2@3^x** are soluble enough to detect even the broadened signals of the paramagnetic guest molecule in solution. For **2@3^x-Cl**, a small broad signal at 23.9 ppm is observed for free **2**, which is in line with the observation of some disaggregation of the host in solution. Upon encapsulation, the signals for **2** are shifted to higher field and further split up. Two sets of signals are observed at 19 and 21 ppm with an integral ratio of 1:1. This is surprising, since in the ¹H MAS NMR spectra of the Cp* analogues **2@3*** signals at 16 and 21 ppm are detected.^[21] For a better consistency, crystals of **2@3*-Cl** were isolated, this time without drying in order to guarantee a better solubility, and the ¹H NMR spectrum of the dissolved crystals of **2@3*-Cl** in CDCl₃ was recorded. Thereby, indeed also signals at 19 and 21 ppm are detected. Hence, the signals at 19 ppm in the solution ¹H NMR spectra of **2@3*-Cl** and **2@3^x** can be assigned to the Cp protons at the “bottle neck” of the nano-bowl. In the solid state ¹H MAS NMR

spectrum of **2@3*-Cl** this signal is high-field shifted to 16 ppm supposedly caused by the π -stacking interactions to the Cp* protons of the next host guest aggregate (cf. X-ray structure). Therefore, the signals at 21 ppm are attributed to the Cp protons within the core of the host **3**, having a similar environment as the Cp protons of $[(\text{CpCr})_2(\mu, \eta^{5:5}\text{-As}_5)]@[\{\text{Cp}^*\text{Fe}(\eta^5\text{-P}_5)\}_{12}\{\text{CuBr}\}_{25}\{\text{CH}_3\text{CN}\}_{10}]$ (**2@6*-Br**, host type **A**) which resonate at 20.5 ppm.^[14c] As already found for the signals of encapsulated **7** in compounds **7@3*** and **7@3^x**, the signals for encapsulated **2** in compounds **2@3*-Cl** and **2@3^x** also further split up due to the presence of host molecules with differing CuX contents.

Compounds **2@3^x**, **7@3*** and **7@3^x** are also soluble in pyridine-*d*₅ under complete disaggregation of the host molecules. Hence, in the ¹H and ³¹P{¹H} NMR spectra uncoordinated **1*** or **1^x** is detected next to released triple decker templates **2** or **7**.

With the enhanced solubility of nano-bowls **2@3^x**, it was hence possible to shed light onto the assignments of the signals for encapsulated **2** in **2@3***. With this knowledge in hand, the NMR spectra of proposed compound "**4@5*-Cl**"^[14c] can be reconsidered critically and compared to the novel Br analogue "**4@5*-Br**". An overview of selected analytical data is given in table 1.

Table 1. Comparison of selected analytical data obtained from nano-bowls **2@3*** and compounds "**4@5***".

Compound	2@3*-Cl ^[21]	2@3*-Br ^[21]	" 4@5*-Cl " ^[14c, 21]	" 4@5*-Br "
δ_{H} (guest) in solid state [ppm]	16.4, 21.3	16.2, 21.3	19	—
δ_{H} (guest) in CD ₂ Cl ₂ or CDCl ₃ [ppm]	19.4, 21.5 ^[a]	—	19.8, 21.3	19.8, 21.4
δ_{H} (guest) in pyridine- <i>d</i> ₅ [ppm]	23.9	24.0	6 (br), 23.9	23.9
Fragments detected in the EI-MS	2⁺ , [As ₄] ⁺⁺	2⁺ , [As ₄] ⁺⁺ , [As ₂] ⁺⁺	[As ₄] ⁺⁺ ^[a]	[As ₄] ⁺⁺ , [As ₂] ⁺⁺
Fragments detected in the ESI-MS	—	—	—	2⁺
Half-field signal in the EPR spectrum	no	no	yes	yes

[a] Additional data reported herein.

Since the ³¹P{¹H} NMR spectra of nano-bowls **3*** (*vide supra*) and 80-vertex spheres of **1*** do not differ significantly, the ³¹P{¹H} NMR spectra of both compounds "**4@5***" cannot give any hint on the nature of the formed host aggregate. In the ¹H NMR spectra in CD₂Cl₂ or CDCl₃, signals at 19 and 21 ppm are detected next to the signals assigned to the host molecules. The latter show shifts to higher ($\delta = 1.43 - 1.47$ ppm) and lower ($\delta = 3.26 - 3.44$ ppm) field due to the proximity to the paramagnetic guest molecule, as already found for compounds **2@3*** and **2@3^x** (host type **C**). Previously, it was reasoned that the signal at 19 ppm in the NMR spectra of "**4@5*-Cl**"

is attributed to $[\text{CpCr}(\eta^5\text{-As}_5)]$ encapsulated into an 80-vertex sphere $[\{\text{Cp}^*\text{Fe}(\eta^5\text{-P}_5)\}_{12}\{\text{CuCl}\}_{20-n}]$ (**4@5*-Cl**, host type **B**, borderline case a), while the signal at 21 ppm was assigned to co-crystallizing $[(\text{CpCr})_2(\mu, \eta^{5:5}\text{-As}_5)]@[\{\text{Cp}^*\text{Fe}(\eta^5\text{-P}_5)\}_{12}\{\text{CuBr}\}_{25}\{\text{CH}_3\text{CN}\}_{10}]$ (**2@6*-Br**, host type **A**)^[14c] or $[(\text{CpCr})_2(\mu, \eta^{5:5}\text{-As}_5)]@[\{\text{Cp}^*\text{Fe}(\eta^5\text{-P}_5)\}_{11}\{\text{CuCl}\}_{15-n}]$ (**2@3*-Cl**, host type **C**, borderline case b).^[21] With the herein presented solution ¹H NMR spectra of **2@3*-Cl** and **2@3*** (host type **C**) exhibiting both signals at 19 and 21 ppm, at first glance it seems now more likely that the similar signals in proposed compounds “**4@5***” are solely due to **2@3*** instead. Free template **2** ($\delta_{\text{H}} = 24$ ppm) is also detected in the ¹H NMR spectra of “**4@5***” in pyridine-*d*₅ further supporting this hypothesis. However, in the EPR spectra of “**4@5***” a large signal next to a smaller signal at half-field is detected, being characteristic for a molecule in a triplet state (for “**4@5-Cl**” cf. ref. [21], for “**4@5-Cl**” cf. Figure 7 in the Experimental Part). The EPR spectra of **2@3***^[21] and **2@3*** in contrast do not exhibit any signal at all. Hence, a different species with triplet ground state must be present in “**4@5***”, which could be NMR inactive. On the one hand, this species might be the proposed $[\text{CpCr}(\eta^5\text{-As}_5)]$ fragment encapsulated (**4@5***, borderline case a) with 16 valence electrons, or, on the other hand also oxidation of the triple decker **2** to give $[(\text{CpCr})_2(\mu, \eta^{5:5}\text{-As}_5)]^+$ as a 26 VE molecule encapsulated (**2⁺@3***, borderline case c) may be conceivable. The counterion in the latter case might be a single Cl⁻ or Br⁻ anion, which could neither be excluded nor verified by X-ray crystallography due to potential disorder, by mass spectrometry or even elemental analysis (cf. Experimental Part). Interestingly, the ¹H MAS NMR spectrum of “**4@5*-Br**” does not exhibit any signals in the region for **2** (16 – 24 ppm, depending on encapsulation and solid-state packing). Moreover, the EI mass spectra obtained from crystals of both compounds “**4@5***” each do not reveal a molecular peak for $[(\text{CpCr})_2(\mu, \eta^{5:5}\text{-As}_5)]^+$ ($m/z = 608.6$) although an intense peak for As₄⁺ is detected. This speaks against the presence of **2@3*** in the solid state. Instead, it is more probable that **2@3*** is formed from “**4@5***” upon dissolving. This points to borderline case c with an oxidized triple decker **2⁺** encapsulated into a nano-bowl **3***. Furthermore, for “**4@5*-Br**”, although $[(\text{CpCr})_2(\mu, \eta^{5:5}\text{-As}_5)]^+$ is not detected in the EI mass spectrum, it is detected in the cationic ESI mass spectrum. Nevertheless, for an unambiguous conclusion, further investigations are necessary:

- 1.) Do DFT calculations on the proposed molecule **2⁺** support the theory of its triplet ground state with 26 valence electrons?
- 2.) May **2** be selectively oxidized into **2⁺**? If so, does the EPR spectrum of **2⁺** show a half-field signal indicating a triplet ground state and is **2⁺** unstable in (Cu^I-containing) solution so that it is re-reduced into **2**?
- 3.) Is the nano-bowl **2@3*-Br'** obtained from toluene / CH₃CN (analogous conditions to the synthesis of “**4@5***”) in fact also rather to be described as **2⁺@3*-Br'**?

Interestingly, the oxidation of $[(\text{Cp}^*\text{Cr})_2(\mu, \eta^{5:5}\text{-P}_5)]$ by $[\text{FeCp}_2]\text{SbF}_6$ leads to $[(\text{Cp}^*\text{Cr})_2(\mu, \eta^{5:5}\text{-P}_5)]^+\text{SbF}_6^-$, which exhibits a triplet ground state at temperatures above 150 K with two non-interacting d^4 Cr^{II} centers separated by $3.185(8)$ Å,^[43] as opposed to $2.727(5)$ Å in neutral $[(\text{Cp}^*\text{Cr})_2(\mu, \eta^{5:5}\text{-P}_5)]$.^[44] Between 150 K and 23 K the Cr...Cr distance decreases, below 23 K only diamagnetic behavior is observed while the Cr...Cr distance is decreased to $2.782(2)$ Å at 12 K.^[43,45] In the molecular structure of **2@3^x-Br^r**, the Cr...Cr distance amounts to about 2.76 Å, which is similar to the Cr...Cr distances in **2@3^{*}** ($2.739(2)$ Å; $2.7461(10)$ Å) and to free **2** ($2.7791(19)$ Å).^[21] Hence no hint for similar behavior or presence of **2⁺@3^x-Br^r** can be drawn from the X-ray structure data so far. Also, no conclusion can be drawn concerning the presence of one extra Br^- anion, which would be required for charge balance in **2⁺@3^x-Br^r**. EPR spectroscopy and solid state ^1H MAS NMR spectroscopy hence are to be performed.

5.3 Conclusion

The capability of triple decker complexes to act as a template in the self-assembly of pentaphosphaferrocenes with copper halides was investigated. For this, the parent compound $[(\text{CpMo})_2(\mu, \eta^{3:3}\text{-P}_3)(\mu, \eta^{2:2}\text{-PS})]$ (**7**) was synthesized by using the higher-boiling solvent *m*-diisopropylbenzene.^[14g] **7** bears two unsubstituted Cp end decks and a mixed group 15/16 middle deck. Moreover, the template properties of the triple decker complex $[(\text{CpCr})_2(\mu, \eta^{5:5}\text{-As}_5)]$ (**2**) were further examined.

When carried out in a $\text{CH}_2\text{Cl}_2 / \text{CH}_3\text{CN}$ layering reaction, self-assembly of $[\text{Cp}^*\text{Fe}(\eta^5\text{-P}_5)]$ (**1^{*}**) with CuX ($X = \text{Cl}, \text{Br}$) in the presence of **2** leads to the formation of nano-bowls $[(\text{CpCr})_2(\mu, \eta^{5:5}\text{-As}_5)]@[\{\text{Cp}^*\text{Fe}(\eta^5\text{-P}_5)\}_{11}\{\text{CuX}\}_{15-n}]$ (**2@3^{*}**, host type **C**) with the triple decker complex encapsulated in an opened host aggregate.^[21] In contrast, when the reaction is carried out in toluene / CH_3CN , the outcome is dependent on the concentration applied. Under diluted conditions 90-vertex spheres (host type **A**) are obtained. While for $X = \text{Br}$ encapsulation of **2** was proven from X-ray diffraction data,^[14c] for $X = \text{Cl}$ this was not possible and NMR spectroscopy revealed only a minor amount of **2**, so that well-known **1^{*}@6^{*}-Cl** must have been the major product. Under more concentrated conditions, the proposed 80-vertex spherical (host type **B**) compounds "**4@5^{*}**" are formed independent of the nature of the halide. New possibilities in understanding of the X-ray data are introduced, and all three conceivable interpretations are discussed and re-examined with the help of additional methods. For this, the synthesis of more soluble nano-bowls $[(\text{CpCr})_2(\mu, \eta^{5:5}\text{-As}_5)]@[\{\text{Cp}^*\text{Fe}(\eta^5\text{-P}_5)\}_{11}\{\text{CuX}\}_{15-n}]$ (**2@3^x**, host type **C**) from $\text{CH}_2\text{Cl}_2 / \text{CH}_3\text{CN}$ layering reactions was crucial, leading to more insight into the NMR spectroscopic behavior of the template. Changing solvents to toluene / CH_3CN interestingly did

not result in Cp^x analogues of proposed 80-vertex spheres “4@5*” (host type B), but to crystallization of another phase of nano-bowl 2@3^x-Br (host type C).

Application of the novel triple decker complex **7** as a template in the 1* / CuX (X = Cl, Br) system leads to nano-bowls [(CpMo)₂(μ,η^{3:3}-P₃)(μ,η^{2:2}-PS)]@[(Cp*Fe(η⁵-P₅))₁₁{CuX}_{15-n}] (**7@3***, host type C) with a change of solvents to CHCl₃ / CH₃CN being crucial for their X-ray structure determination. On the contrary, in the reaction with CuBr in toluene / CH₃CN the nano-bowl **7@3*-Br** (host type C) is crystallized in a disordered fashion. Furthermore, a range of 90-vertex spheres (host type A) with CuCl or CuBr are obtained crystallizing as new phases. These 90-vertex spheres again were found to mainly encapsulate 1* instead of the triple decker **7**.

When [Cp^xFe(η⁵-P₅)] (1^x) is applied as a building block, nano-bowls [(CpMo)₂(μ,η^{3:3}-P₃)(μ,η^{2:2}-PS)]@[(Cp^xFe(η⁵-P₅))₁₁{CuX}_{15-n}] (**7@3^x**, host type C) are obtained, which already crystallize in an ordered fashion from CH₂Cl₂ / CH₃CN, reflecting their enhanced solubility when compared to the Cp* analogues. These reactions were found to be highly dependent on the stoichiometry applied. With a 12 : 18 stoichiometric ratio of 1^x : CuBr (excess of CuBr), a novel phase of 90-vertex spheres **6^x-Br** (host type A) is obtained with 1^x encapsulated in most spheres. **1^x@6^x-Br** is also the only characterized product of the reaction of 1^x, CuBr and **7** in toluene / CH₃CN. For CuCl, the application of a 12:20 stoichiometric ratio of 1^x : CuCl (excess of CuCl) in CH₂Cl₂ / CH₃CN leads to the sole crystallization of the novel 2D polymer [(CpMo)₂(μ₄,η^{3:3:1:1}-P₃)(μ₃,η^{2:2:1}-PS))CuCl]_n (**8**) next to soluble spheres of (CHCl₃)_m@[(Cp^xFe(η⁵-P₅))₁₂{CuCl}_{20-n}] (host type B). The same polymer **8** was obtained as the only crystalline product in the analogous reaction in toluene / CH₃CN, and can be directly synthesized by self-assembly of **7** and CuCl.

In the course of these studies, also the first 3D coordination polymer based on 1* polymer [(Cp*Fe(η^{5:1:1:1}-P₅))₂{Cp*Fe(η^{5:1:1}-P₅)}Cu₄(μ-I)₄]_n (**9**)^[14g] is obtained by the attempt to synthesize a CuI-containing nano-bowl.

All nano-bowls **2@3***,^[21] **2@3^x**, **7@3*** and **7@3^x** (host type C) have been comprehensively characterized by X-ray crystallography, NMR spectroscopy, mass spectrometry and elemental analysis. Thereby, striking differences have been found. The enhanced solubility of 1^x based host-guest aggregates compared to the Cp* analogues could be traced back to the distinctly different intermolecular interactions in the solid state. The ¹H NMR signals attributed to the hosts of nano-bowls are partially shifted upon encapsulation of the paramagnetic triple decker complex **2** compared to the diamagnetic triple decker complex **7**. The ¹H NMR signals of the Cp ligands of **2** and **7** split into two sets of signals upon encapsulation, further split up by the presence of CuX vacancies. Moreover, comparison of the ¹H NMR signals of **2@3^x** in solution with those of **2@3*** in the solid state^[21] enabled assignments of the Cp signals of encapsulated

2, and the effect of π -stacking interactions in the solid state on the chemical shift of the “bottle neck” Cp ligand were proven.

With these new insights, the ambiguous structures of proposed 80-vertex spheres “**4@5*** (host type **B**)” were (re-)investigated. Based on solid state MAS NMR investigations and EI mass spectrometry the interpretation as a disordered phase of **2@3*** (host type **C**) becomes highly unlikely. The presence of a half-field signal in the EPR spectra suggests that **2** undergoes either cleavage to 16VE [CpCr(η^5 -As₅)] or oxidation to 26VE [(CpCr)₂(μ , $\eta^{5:5}$ -As₅)]⁺ upon encapsulation.

5.4 Experimental Part

General Remarks

All reactions were performed under an inert atmosphere of dry nitrogen or argon with standard vacuum, Schlenk and glove-box techniques. Solvents were purified, dried and degassed prior to use by standard procedures. [Cp*Fe(η^5 -P₅)] (**1***)^[11], [Cp^xFe(η^5 -P₅)] (**1^x**)^[46] and [(CpCr)₂(μ , $\eta^{5:5}$ -As₅)] (**2**)^[20] were synthesized following reported procedures, although yields were improved to 75%, 56% and 52% by the use of higher-boiling solvents meta-diisopropylbenzene (*m*-DIB, for **1*** and **1^x**) and decalin (for **2**), respectively. CuCl, CuBr and CuI are available commercially and were used without further purification. [CpMo(CO)₂]₂ and P₄S₃ were available in-house. Solution NMR spectra were recorded on a BRUKER Avance 400 spectrometer. MAS NMR spectra were acquired on a Bruker Avance 300 spectrometer. Chemical shifts δ are given in [ppm] referring to external standards of tetramethylsilane (¹H NMR and ¹³C{¹H} NMR spectra), 85% phosphoric acid (³¹P{¹H} NMR spectra) or NaH₂PO₄ (³¹P{¹H} MAS NMR spectra). ESI-MS spectra were recorded on a ThermoQuest Finnigan MAT TSQ 7000 spectrometer and EI-MS spectra were recorded on a Finnigan MAT 95 mass spectrometer. Elemental analyses were performed on a Vario EL III apparatus.

Synthesis of [(CpCr)₂(μ , $\eta^{5:5}$ -As₅)]@[{Cp*Fe(η^5 -P₅)}]₁₁(CuCl)_{13.5} · 8 CH₂Cl₂ · 0.5 CH₃CN (**2@3*-Cl**)^[21]

[Cp*Fe(η^5 -P₅)] (**1***, 102 mg, 0.30 mmol) and [(CpCr)₂(μ , $\eta^{5:5}$ -As₅)] (**2**, 19 mg, 0.031 mmol) were dissolved in CH₂Cl₂ (22 mL). After treatment in a warm ultrasonic bath (1 h, 60°C, 35 kHz), the dark green solution was filtered into a thick Schlenk tube and carefully layered with a colorless solution of CuCl (64 mg, 0.65 mmol) in CH₃CN (22 mL). After 1-2 weeks, the mother liquor was decanted, and the crystals were washed three times each with CH₂Cl₂/CH₃CN (2:1) and pentane and dried.

Analytical Data of **2@3*-Cl**:

Yield:^[21] 72 mg (11 μ mol, 42%).

¹H MAS NMR:^[21] δ [ppm] = -13.6 (br), 1.4 (s, br), 6.7 (s, br), 16.4 (br, Cp_{bottle-neck} of **2**), 21.3 (s, br, Cp_{bowl} of **2**).

³¹P{¹H} MAS NMR:^[21] δ [ppm] = 74 (br), 125 (br); a small shoulder at 150 ppm was detected, which can most probably be assigned to free **1***.

¹H NMR (CD₂Cl₂):^[21] δ [ppm] = 1.42 (s, br), 1.43 (s, br), 1.97 (s, CH₃CN), 2.08 (s, br), 2.18 (s, br), 2.20 (s, br), 3.26 (s, br), 3.33 (s, br).

³¹P{¹H} NMR (CD₂Cl₂):^[21] δ [ppm] = 60 (br), 120 (br), 152.2 (s, **1***_{free}); signals almost below noise floor.

¹H NMR (CDCl₃, not dried crystals): δ [ppm] = 1.44 (s, br), 2.00 (s, br), 2.09 (s, br), 2.19 (s, br), 2.22 (s, br), 3.18 (s, br), 3.21 (s, br), 3.29 (s, br), 3.36 (s, br), 19.4 (m, br, Cp_{bottle-neck} of **2**), 21.5 (m, br, Cp_{bowl} of **2**), 24.0 (s, **2**_{free}).

³¹P{¹H} NMR (CDCl₃, not dried crystals): δ [ppm] = 67 (m, br), 120 (br), 131 (br), 152.8 (s, **1***_{free}).

¹H NMR (pyridine-d₅):^[21] δ [ppm] = 1.33 (s, [Cp*Fe(η^5 -P₅)]), 1.87 (s, CH₃CN), 23.9 (s, br, **2**_{free}).

³¹P{¹H} NMR (pyridine-d₅):^[21] δ [ppm] = 150.5 (s, **1***_{free}).

EPR-spectrum (crystals, quartz tube):^[21] no signal detected.

EI-MS (70 eV):^[21] m/z = 608.5645 [(CpCr)₂(μ , $\eta^{5:5}$ -As₅)]⁺, 345.9187 [Cp*Fe(η^5 -P₅)]⁺, 299.6829 [As₄]⁺, 283.9715 [{Cp*Fe(η^5 -P₅)}-P₂]⁺.

Positive ion ESI-MS (CH₂Cl₂/CH₃CN):^[21] m/z = 2635.3742 [{Cp*FeP₅}₄Cu₁₃Cl₁₂]⁺, 2535.4794 [{Cp*FeP₅}₄Cu₁₂Cl₁₁]⁺, 2437.5809 [{Cp*FeP₅}₄Cu₁₁Cl₁₀]⁺, 2337.6845 [{Cp*FeP₅}₄Cu₁₀Cl₉]⁺, 1793.9710 [{Cp*FeP₅}₃Cu₈Cl₇]⁺, 1744.0238 [{Cp*FeP₅}₄Cu₄Cl₃]⁺, 1694.0742 [(Cp*FeP₅)₃Cu₇Cl₆]⁺, 1596.1752 [{Cp*FeP₅}₃Cu₆Cl₅]⁺, 952.5663 [{Cp*FeP₅}₂Cu₃Cl₂]⁺, 854.6687 [{Cp*FeP₅}₂Cu₂Cl]⁺, 754.7722 [(Cp*FeP₅)₂Cu]⁺, 490.9028 [Cp*FeP₅]₂Cu(CH₃CN)₂⁺, 449.8772 [Cp*FeP₅]₂Cu(CH₃CN)⁺, 408.8500 [Cp*FeP₅]₂Cu⁺.

Negative ion ESI-MS (CH₂Cl₂/CH₃CN):^[21] m/z = 232.7628 [Cu₂Cl₃]⁻.

Elemental Analysis:^[21] Calculated (%) for [(CpCr)₂As₅]@[{Cp*FeP₅}₁₁{CuCl}_{13.5}].8CH₂Cl₂.0.5CH₃CN (6451 g/mol): C 24.02, H 3.01, N 0.11, Cu 13.30, P 26.41; found (%): C 23.88, H 3.35, N 0.07, Cu 13.40, P 26.81.

Synthesis of $[(\text{CpCr})_2(\mu, \eta^{5:5}\text{-As}_5)]@[\{\text{Cp}^*\text{Fe}(\eta^5\text{-P}_5)\}_{11}(\text{CuBr})_{12.5}] \cdot 2 \text{CH}_2\text{Cl}_2$ (2@3*-Br**)^[21]**

1* (106 mg, 0.31 mmol) and **2** (21 mg, 0.034 mmol) were dissolved in CH_2Cl_2 (21 mL). After treatment in a warm ultrasonic bath (1 h, 60°C, 35 kHz), the dark green solution was filtered into a thick Schlenk tube and carefully layered with a colorless solution of CuBr (87 mg, 0.61 mmol) in CH_3CN (21 mL). After 1-2 weeks, the mother liquor was decanted, and the crystals were washed three times each with $\text{CH}_2\text{Cl}_2/\text{CH}_3\text{CN}$ (2:1) and pentane and dried.

Analytical Data of **2@3*-Br** taken from ref. [21]:

Yield: 122 mg (19 μmol , 69%).

^1H MAS NMR: δ [ppm] = -13.4 (br), 1.4 (s, br), 6.8 (s, br), 16.2 (br, $\text{Cp}_{\text{bottle-neck}}$ of **2**), 21.3 (s, br, Cp_{bowl} of **2**).

$^{31}\text{P}\{^1\text{H}\}$ MAS NMR: δ [ppm] = 70 (br), 126 (br).

^1H NMR (CDCl_3): δ [ppm] = 1.44 (s, br), 1.48 (s, br), 1.49 (s, br), 2.13 (s, br), 2.14 (s, CH_3CN), 2.25 (s, br), 3.32 (s, br), 3.40 (s, br).

$^{31}\text{P}\{^1\text{H}\}$ NMR (CDCl_3): δ [ppm] = 152.8 (s, **1*_{free}**).

^1H NMR (pyridine- d_5): δ [ppm] = 1.33 (s, **1*_{free}**), 1.87 (s, CH_3CN), 5.69 (s, CH_2Cl_2), 24.0 (s, br, **2_{free}**).

$^{31}\text{P}\{^1\text{H}\}$ NMR (pyridine- d_5): δ [ppm] = 150.5 (s, **1*_{free}**).

EPR-spectrum (crystals, quartz tube): no signal detected.

EI-MS (70 eV): m/z = 608.5667 $[(\text{CpCr})_2(\mu, \eta^{5:5}\text{-As}_5)]^+$, 345.9197 $[\text{Cp}^*\text{Fe}(\eta^5\text{-P}_5)]^+$, 299.6853 $[\text{As}_4]^{2+}$, 283.9724 $[\{\text{Cp}^*\text{Fe}(\eta^5\text{-P}_5)\}\text{-P}_2]^{2+}$, 149.8517 $[\text{As}_2]^{2+}$.

Positive ion ESI-MS ($\text{CH}_2\text{Cl}_2/\text{CHCl}_3/\text{CH}_3\text{CN}$): m/z = 1042.4600 $[\{\text{Cp}^*\text{Fe}(\eta^5\text{-P}_5)\}_2\text{Cu}_3\text{Br}_2]^+$, 898.6152 $[\{\text{Cp}^*\text{Fe}(\eta^5\text{-P}_5)\}_2\text{Cu}_2\text{Br}]^+$, 754.7710 $[\{\text{Cp}^*\text{Fe}(\eta^5\text{-P}_5)\}_2\text{Cu}]^+$, 449.8758 $[\{\text{Cp}^*\text{Fe}(\eta^5\text{-P}_5)\}\text{Cu}(\text{CH}_3\text{CN})]^+$.

Negative ion ESI-MS ($\text{CH}_2\text{Cl}_2/\text{CHCl}_3/\text{CH}_3\text{CN}$): m/z = 322.6601 $[\text{Cu}_2\text{ClBr}_2]^-$, 222.7643 $[\text{CuBr}_2]^-$, 178.8144 $[\text{CuClBr}]^-$, 134.8649 $[\text{CuCl}_2]^-$.

Elemental analysis: Calculated (%) for $[(\text{CpCr})_2(\mu, \eta^{5:5}\text{-As}_5)]@[\{\text{Cp}^*\text{Fe}(\eta^5\text{-P}_5)\}_{11}(\text{CuBr})_{12.5}] \cdot 2 \text{CH}_2\text{Cl}_2$ (6377 g/mol): C 22.98, H 2.83, N 0, Cu 12.46, P 26.71; found (%): C 23.01, H 2.90, N 0, Cu 12.44, P 26.77.

Reaction of 1* with 2 and CuCl in toluene/CH₃CN under concentrated conditions:**Synthesis of “[CpCr(μ,η⁵-As₅)]@[{Cp*Fe(η⁵-P₅)}₁₂(CuCl)₂₀]” (“4@5*-Cl”)^[14c,21]**

1* (105 mg, 0.30 mmol) and 2 (23 mg, 0.038 mmol) were dissolved in toluene (26 mL). After treatment in a warm ultrasonic bath (1 h, 50°C, 35 kHz), the dark green solution was filtered into a thick Schlenk tube and carefully layered with a colorless solution of CuCl (58 mg, 0.59 mmol) in CH₃CN (20 mL). After 2-3 weeks, the mother liquor was decanted, and the crystals were washed twice with toluene/CH₃CN (1:1) and dried.

Analytical Data of “4@5*-Cl”:

Yield:^[21] 44 mg (6.6 μmol, 26% (interpretation a: 4@5*-Cl) or 7.4 μmol, 27% (interpretation c: 2⁺@3*-Cl).

¹H NMR (CD₂Cl₂):^[21] δ [ppm] = 1.42 (s, br), 1.43 (s, br), 2.08 (s, br), 2.17 (s, br), 2.34 (s, C₇H₈), 3.26 (s, br), 3.33 (s, br), 7.14 – 7.26 (m, C₇H₈), 19.8 (s, br, Cp_{bottle-neck} of 2@3*-Cl), 21.3 (s, br, Cp_{bowli} of 2@3*-Cl).

³¹P{¹H} NMR (CD₂Cl₂):^[21] δ [ppm] = 69 (br), 120 (br), 151.5 (s, 1*_{free}); signals almost below noise floor.

¹H NMR (pyridine-d₅):^[21] δ [ppm] = 1.34 (s, 1*_{free}), 1.83 (s, CH₃CN), 2.22 (s, C₇H₈), 6.0 (br), 7.16 – 7.30 (m, C₇H₈), 23.9 (s, br, 2_{free}).

³¹P{¹H} NMR (pyridine-d₅):^[21] δ [ppm] = 147.2 (s, 1*_{free}).

EPR-spectrum (crystals, quartz tube):^[21] half-field signal detected (cf. chapter 4).

EI-MS (70 eV): *m/z* = 345.9202 [Cp*Fe(η⁵-P₅)⁺], 299.6857 [As₄]⁺, 283.9726 [{Cp*Fe(η⁵-P₅)}-P₂]⁺.

Positive ion ESI-MS (CH₂Cl₂/CH₃CN): *m/z* = 952.5648 [{Cp*FeP₅]₂Cu₃Cl₂]⁺, 854.6673 [{Cp*FeP₅]₂Cu₂Cl]⁺, 754.7722 [(Cp*FeP₅)₂Cu]⁺, 490.9035 [{Cp*FeP₅}Cu(CH₃CN)₂]⁺, 449.8776 [{Cp*FeP₅}Cu(CH₃CN)]⁺.

Negative ion ESI-MS (CH₂Cl₂/CH₃CN): *m/z* = 332.6604 [Cu₃Cl₄]⁻, 232.7645 [Cu₂Cl₃]⁻, 134.8661 [CuCl₂]⁻.

Elemental analysis: Calculated (%) for [CpCr(η⁵-As₅)]@[{Cp*Fe(η⁵-P₅)}₁₂(CuCl)₁₇] · 4 C₇H₈ (6695 g/mol): C 27.45, H 3.27, N 0; calculated (%) for [(CpCr)₂(μ,η^{5:5}-As₅)]@[{Cp*Fe(η⁵-P₅)}₁₁(CuCl)₁₃] · 2 C₇H₈ (5885 g/mol): C 27.35, H 3.27, N 0; calculated (%) for [(CpCr)₂(μ,η^{5:5}-As₅)]⁺@[{Cp*Fe(η⁵-P₅)}₁₁Cu₁₃Cl₁₄]⁻ · 2.2 C₇H₈ (5939 g/mol): C 27.38, H 3.27, N 0; found (%): C 27.38, H 3.24, N 0.

Reaction of 1* with 2 and CuBr in toluene/CH₃CN under concentrated conditions:**Synthesis of “[CpCr(μ,η⁵-As₅)]@[{Cp*Fe(η⁵-P₅)}₁₂(CuBr)_{20-n}]” (“4@5*-Br”)**

1* (51 mg, 0.15 mmol) and 2 (19 mg, 0.031 mmol) were dissolved in toluene (8 mL) and sonicated for one hour at 60°C. After filtration, the dark green solution was carefully layered with a solution of CuBr (29 mg, 0.20 mmol) in CH₃CN (8 mL). Already after two days, the formation of dark brown cubes of ‘[CpCrAs₅]]@[{Cp*FeP₅}₁₂{CuBr}_{20-x}]’ was observed. After complete diffusion, the mother liquor was shaken up and decanted together with the precipitate. The crystals were washed first with a mixture of toluene / CH₃CN (2:1, 3x5 mL), then with pentane (3x5 mL) and dried *in vacuo*.

Analytical Data of “4@5*-Br”:

Yield: 49 mg (6.6 μmol, 55% (interpretation a: 4@5*-Br) or 7.5 μmol, 56% (interpretation c: 2* @ 3*-Br))

¹H MAS NMR: δ [ppm] = -14 (br), * 1.5 (br), 6.6 (br). *Signal almost below noise floor.

³¹P{¹H} MAS NMR: δ [ppm] = 72 (br), 123 (br), 151.7 (s, 1*_{free}).

¹H NMR (CD₂Cl₂): δ [ppm] = 1.44 (s, br), 1.47 (s, br), 1.51 (s, br), 2.12 (s, br), 2.23 (s, br), 2.34 (s, C₇H₈), 3.30 (s, br), 3.38 (s, br), 7.14 – 7.26 (m, C₇H₈), 19.8 (s, br, Cp_{bottle-neck} of 2@3*-Br), 21.2 (s, br, Cp_{bow}l of 2@3*-Br).

¹H NMR (CDCl₃): δ [ppm] = 1.49 (s, br), 1.53 (s, br), 1.57 (s, br), 2.19 (s, br), 2.29 (s, br), 2.40 (s, C₇H₈), 3.36 (s, br), 3.44 (s, br), 7.14 – 7.26 (m, C₇H₈), 19.8 (s, br, Cp_{bottle-neck} of 2@3*-Br), 21.4 (s, br, Cp_{bow}l of 2@3*-Br).

³¹P{¹H} NMR (CDCl₃): δ [ppm] = 60 (br), 70 (br), 122 (br), 125 (br), 152.8 (s, 1*_{free}); signals almost below noise floor.

¹H NMR (pyridine-d₅): δ [ppm] = 1.32 (s, 1*_{free}), 1.86 (s, CH₃CN), 2.23 (s, C₇H₈), 7.16 – 7.30 (m, C₇H₈), 23.9 (s, br, 2_{free}).

³¹P{¹H} NMR (pyridine-d₅): δ [ppm] = 150.5 (s, 1*_{free}).

EI-MS (70 eV): *m/z* = 345.9263 [Cp*Fe(η⁵-P₅)]⁺, 299.6905 [As₄]⁺, 283.9775 [{Cp*Fe(η⁵-P₅)}-P₂]⁺, 149.8468 [As₂]⁺.

Positive ion ESI-MS (CH₂Cl₂/CH₃CN): *m/z* = 1042.4639 [{Cp*Fe(η⁵-P₅)}₂Cu₃Br₂]⁺, 898.6184 [{Cp*Fe(η⁵-P₅)}₂Cu₂Br]⁺, 754.7731 [{Cp*Fe(η⁵-P₅)}₂Cu]⁺, 696.5418 [{Cp*Fe(η⁵-P₅)}Cu₃Br₂]⁺, 608.5666 [(CpCr)₂(μ,η^{5:5}-As₅)]⁺, 552.6964 [{Cp*Fe(η⁵-P₅)}Cu₂Br]⁺, 490.9040 [{Cp*Fe(η⁵-P₅)}Cu(CH₃CN)₂]⁺, 449.8779 [{Cp*Fe(η⁵-P₅)}Cu(CH₃CN)]⁺.

Negative ion ESI-MS ($\text{CH}_2\text{Cl}_2/\text{CH}_3\text{CN}$): $m/z = 939.9944$ $[\text{Cu}_6\text{Br}_7]^-$, 796.1492 $[\text{Cu}_5\text{Br}_4]^-$, 654.3017 $[\text{Cu}_4\text{Br}_5]^-$, 510.4561 $[\text{Cu}_3\text{Br}_4]^-$, 366.6107 $[\text{Cu}_2\text{Br}_3]^-$, 322.6610 $[\text{Cu}_2\text{ClBr}_2]^-$, 222.7651 $[\text{CuBr}_2]^-$, 178.8153 $[\text{CuClBr}]^-$.

Elemental analysis: Calculated (%) for $[\text{CpCr}(\eta^5\text{-As}_5)]@[\{\text{Cp}^*\text{Fe}(\eta^5\text{-P}_5)\}_{12}(\text{CuBr})_{17}] \cdot 4 \text{C}_7\text{H}_8$ (7450 g/mol): C 24.67, H 2.94, N 0; calculated (%) for $[(\text{CpCr})_2(\mu, \eta^{5:5}\text{-As}_5)]@[\{\text{Cp}^*\text{Fe}(\eta^5\text{-P}_5)\}_{11}(\text{CuBr})_{13.5}] \cdot 2 \text{C}_7\text{H}_8$ (6535 g/mol): C 24.63, H 2.95, N 0; calculated (%) for $[(\text{CpCr})_2(\mu, \eta^{5:5}\text{-As}_5)]^+@[\{\text{Cp}^*\text{Fe}(\eta^5\text{-P}_5)\}_{11}\text{Cu}_{13}\text{Br}_{14}]^- \cdot 2 \text{C}_7\text{H}_8$ (6543 g/mol): C 24.60, H 2.94, N 0; found (%): C 24.55, H 2.95, N 0.

EPR-spectrum (crystals, quartz tube, r.t.):

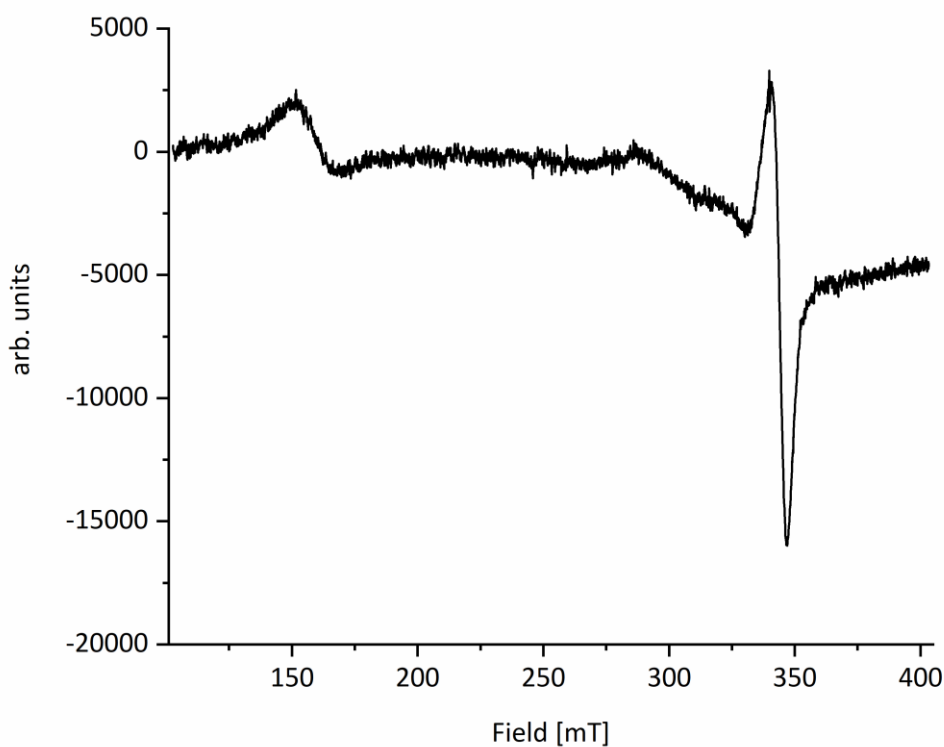


Figure 7. EPR spectrum of crystals of “4@5*-Br” in a quartz tube at r.t.

Synthesis of $[(\text{CpCr})_2(\mu, \eta^{5:5}\text{-As}_5)]@[(\text{Cp}^x\text{FeP}_5)_{11}(\text{CuCl})_{15-n}]$ ($2@3^x\text{-Cl}$)

$[\text{Cp}^x\text{Fe}(\eta^5\text{-P}_5)]$ (1^x , 30 mg, 0.83 mmol) and **2** (9 mg, 0.015 mmol) were dissolved in CH_2Cl_2 (7 mL). After treatment in a warm ultrasonic bath (2 h, 60°C , 35 kHz), the dark green solution was filtered into a thick Schlenk tube and carefully layered with a colorless solution of CuCl (11 mg, 0.11 mmol) in CH_3CN (6 mL). After 1-2 weeks, crystals of $2@3^x\text{-Cl}$ have formed. After complete diffusion, the mother liquor was decanted, and the crystals were washed with $\text{CH}_2\text{Cl}_2/\text{CH}_3\text{CN}$ (2:1, 5 x 5-10 mL) and pentane (3 x 5 mL) and dried.

Analytical Data of $2@3^x\text{-Cl}$:

Yield: 12 mg (2.0 μmol , 27%).

$^1\text{H NMR}$ (CDCl_3): δ [ppm] = 0.67 (br, $-\text{CH}_2\text{CH}_3$ of 1^x_a), 0.75 (t, $^3J_{\text{HH}} = 7.5$ Hz, 3H, $-\text{CH}_2\text{CH}_3$ of 1^x_{free}), 0.98 (br, $-\text{CH}_2\text{CH}_3$ of 1^x_b), 1.45 (br, $-\text{CH}_3$ of 1^x_a and 1^x_{free}), 1.79 (br, $-\text{CH}_2\text{CH}_3$ of 1^x_c), 1.96 (q, $^3J_{\text{HH}} = 7.6$ Hz, 2H, $-\text{CH}_2\text{CH}_3$ of 1^x_{free}), 2.09 – 2.22 (br, $-\text{CH}_3$ of 1^x_b and $-\text{CH}_2\text{CH}_3$ of 1^x_a), 2.91 (br, $-\text{CH}_2\text{CH}_3$ of 1^x_b), 3.20 – 3.36 (br, $-\text{CH}_3$ of 1^x_c), 4.11 – 4.21 (br, $-\text{CH}_2\text{CH}_3$ of 1^x_c), 5.30 (s, CH_2Cl_2), 19.2 (br, $\text{Cp}_{\text{bottle-neck}}$ of **2**), 19.5 (br, $\text{Cp}_{\text{bottle-neck}}$ of **2**), 21.2 (br, Cp_{bowl} of **2**), 21.4 (br, Cp_{bowl} of **2**), 23.9 (br, 2_{free}).

$^{31}\text{P}\{^1\text{H}\}$ NMR (CDCl_3): δ [ppm] = 66 (br), 119 (br), 130 (br), 152.4 (s, 1^x_{free}); signals almost below noise floor.

$^1\text{H NMR}$ (pyridine- d_5): δ [ppm] = 0.66 (t, $^3J_{\text{HH}} = 7.6$ Hz, 3H, $-\text{CH}_2\text{CH}_3$ of 1^x_{free}), 1.39 (s, 6H, $-\text{CH}_3$ of 1^x_{free}), 1.42 (s, 6H, $-\text{CH}_3$ of 1^x_{free}), 1.87 (s, CH_3CN), 1.94 (q, $^3J_{\text{HH}} = 7.6$ Hz, 2H, $-\text{CH}_2\text{CH}_3$ of 1^x_{free}), 15.6 (s, 10H, $(\text{CpCr})_2\text{AsO}_5$),^[47] 23.8 (s, br, 10H, 2_{free}).

$^{31}\text{P}\{^1\text{H}\}$ NMR (pyridine- d_5): δ [ppm] = 145.2 (s, 1^x_{free}).

EI-MS (70 eV): m/z = 608.5691 $[(\text{CpCr})_2(\mu, \eta^{5:5}\text{-As}_5)]^+$, 458.7259 $\{[(\text{CpCr})_2(\mu, \eta^{5:5}\text{-As}_5)]\text{-As}_2\}^+$, 359.9370 $[\text{Cp}^x\text{Fe}(\eta^5\text{-P}_5)]^+$, 299.6876 $[\text{As}_4]^+$, 297.9890 $\{[\text{Cp}^x\text{Fe}(\eta^5\text{-P}_5)]\text{-P}_2\}^+$, 149.8531 $[\text{As}_2]^+$.

Positive ion ESI-MS ($\text{CH}_2\text{Cl}_2/\text{CH}_3\text{CN}$): m/z = 980.5971 $\{[\text{Cp}^x\text{FeP}_5]_2\text{Cu}_3\text{Cl}_2\}^+$, 882.6990 $\{[\text{Cp}^x\text{FeP}_5]_2\text{Cu}_2\text{Cl}\}^+$, 782.8034 $[(\text{Cp}^x\text{FeP}_5)_2\text{Cu}]^+$, 608.5660 $[(\text{CpCr})_2(\mu, \eta^{5:5}\text{-As}_5)]^+$, 563.7886 $\{[\text{Cp}^x\text{FeP}_5]\text{Cu}_2\text{Cl}(\text{CH}_3\text{CN})\}^+$, 522.7620 $\{[\text{Cp}^x\text{FeP}_5]\text{Cu}_2\text{Cl}\}^+$, 504.9190 $\{[\text{Cp}^x\text{FeP}_5]\text{Cu}(\text{CH}_3\text{CN})_2\}^+$, 463.8933 $\{[\text{Cp}^x\text{FeP}_5]\text{Cu}(\text{CH}_3\text{CN})\}^+$, 422.8658 $\{[\text{Cp}^x\text{FeP}_5]\text{Cu}\}^+$.

Negative ion ESI-MS ($\text{CH}_2\text{Cl}_2/\text{CH}_3\text{CN}$): m/z = 232.7644 $[\text{Cu}_2\text{Cl}_3]^-$, 134.8658 $[\text{CuCl}_2]^-$.

Elemental Analysis: Calculated (%) for $[(\text{CpCr})_2\text{As}_5]@[(\text{Cp}^x\text{FeP}_5)_{11}\{\text{CuCl}\}_{15}]$ (6053 g/mol): C 25.99, H 3.28, N 0; found (%): C 26.14, H 3.37, N 0.

Synthesis of $[(\text{CpCr})_2(\mu, \eta^{5:5}\text{-As}_5)]@[(\text{Cp}^x\text{FeP}_5)_{11}(\text{CuBr})_{15-n}] (\mathbf{2@3^x}\text{-Br})$

$\mathbf{1^x}$ (31 mg, 0.86 mmol) and $\mathbf{2}$ (10 mg, 0.016 mmol) were dissolved in CH_2Cl_2 (6 mL). After treatment in a warm ultrasonic bath (2 h, 60°C, 35 kHz), the dark green solution was filtered into a Schlenk tube and carefully layered with a colorless solution of CuBr (18 mg, 0.13 mmol) in CH_3CN (6 mL). After 1-2 weeks, crystals of $\mathbf{2@3^x}\text{-Br}$ have formed. After complete diffusion, the mother liquor was decanted, and the crystals were washed with $\text{CH}_2\text{Cl}_2/\text{CH}_3\text{CN}$ (2:1, 5 x 5-10 mL) and pentane (3 x 3 mL) and dried.

Analytical Data of $\mathbf{2@3^x}\text{-Br}$:

Yield: 30 mg (4.7 μmol , 60%).

$^1\text{H NMR (CDCl}_3)$: δ [ppm] = 0.69 (br, $-\text{CH}_2\text{CH}_3$ of $\mathbf{1^x_a}$), 0.75 (t, $^3J_{\text{HH}} = 7.6$ Hz, 3H, $-\text{CH}_2\text{CH}_3$ of $\mathbf{1^x_{free}}$), 0.98 (br, $-\text{CH}_2\text{CH}_3$ of $\mathbf{1^x_b}$), 1.44 (s, 6H, $-\text{CH}_3$ of $\mathbf{1^x_{free}}$), 1.45 (s, 6H, $-\text{CH}_3$ of $\mathbf{1^x_{free}}$), 1.48 (br, $-\text{CH}_3$ of $\mathbf{1^x_a}$), 1.78 (br, $-\text{CH}_2\text{CH}_3$ of $\mathbf{1^x_c}$), 1.96 (q, $^3J_{\text{HH}} = 7.7$ Hz, 2H, $-\text{CH}_2\text{CH}_3$ of $\mathbf{1^x_{free}}$), 2.15 (br, $-\text{CH}_2\text{CH}_3$ of $\mathbf{1^x_a}$), 2.15 – 2.26 (br, $-\text{CH}_3$ of $\mathbf{1^x_b}$), 2.80 – 3.01 (br, $-\text{CH}_2\text{CH}_3$ of $\mathbf{1^x_b}$), 3.24 – 3.41 (br, $-\text{CH}_3$ of $\mathbf{1^x_c}$), 4.18 – 4.33 (br, $-\text{CH}_2\text{CH}_3$ of $\mathbf{1^x_c}$), 5.30 (s, CH_2Cl_2), 19.3 (br, $\text{Cp}_{\text{bottle-neck}}$ of $\mathbf{2}$), 19.6 (br, $\text{Cp}_{\text{bottle-neck}}$ of $\mathbf{2}$), 21.1 (br, Cp_{bowl} of $\mathbf{2}$), 21.3 (br, Cp_{bowl} of $\mathbf{2}$), 21.5 (br, $\mathbf{2_{free}}$).

$^{31}\text{P}\{^1\text{H}\}$ NMR (CDCl_3): δ [ppm] = 60 (br), 69 (br), 121 (br), 125 (br), 152.5 (s, $\mathbf{1^x_{free}}$).

$^1\text{H NMR (pyridine-}d_5)$: δ [ppm] = 0.66 (t, $^3J_{\text{HH}} = 7.6$ Hz, 3H, $-\text{CH}_2\text{CH}_3$ of $\mathbf{1^x_{free}}$), 1.40 (s, 6H, $-\text{CH}_3$ of $\mathbf{1^x_{free}}$), 1.43 (s, 6H, $-\text{CH}_3$ of $\mathbf{1^x_{free}}$), 1.95 (q, $^3J_{\text{HH}} = 7.6$ Hz, 2H, $-\text{CH}_2\text{CH}_3$ of $\mathbf{1^x_{free}}$), 5.69 (s, CH_2Cl_2), 23.9 (s, br, 10H, $\mathbf{2_{free}}$).

$^{31}\text{P}\{^1\text{H}\}$ NMR (pyridine- d_5): δ [ppm] = 143.9 (s, $\mathbf{1^x_{free}}$).

EI-MS (70 eV): m/z = 608.5719 $[(\text{CpCr})_2(\mu, \eta^{5:5}\text{-As}_5)]^+$, 458.7274 $[(\text{CpCr})_2(\mu, \eta^{5:5}\text{-As}_5)\text{-As}_2]^+$, 359.9384 $[\text{Cp}^x\text{Fe}(\eta^5\text{-P}_5)]^+$, 299.6896 $[\text{As}_4]^+$, 297.9902 $[\{\text{Cp}^x\text{Fe}(\eta^5\text{-P}_5)\text{-P}_2\}]^+$, 182.0165 $[\text{Cp}_2\text{Cr}]^+$, 149.8557 $[\text{As}_2]^+$.

Positive ion ESI-MS ($\text{CH}_2\text{Cl}_2/\text{CH}_3\text{CN}$): m/z = 1070.4943 $[\{\text{Cp}^x\text{FeP}_5\}_2\text{Cu}_3\text{Br}_2]^+$, 1026.5439 $[\{\text{Cp}^x\text{FeP}_5\}_2\text{Cu}_3\text{ClBr}]^+$, 926.6489 $[\{\text{Cp}^x\text{FeP}_5\}_2\text{Cu}_2\text{Br}]^+$, 782.8032 $[(\text{Cp}^x\text{FeP}_5)_2\text{Cu}]^+$, 608.5657 $[(\text{CpCr})_2(\mu, \eta^{5:5}\text{-As}_5)]^+$, 566.7114 $[\{\text{Cp}^x\text{FeP}_5\}_2\text{Cu}_2\text{Br}]^+$, 504.9188 $[\{\text{Cp}^x\text{FeP}_5\}\text{Cu}(\text{CH}_3\text{CN})_2]^+$, 463.8929 $[\{\text{Cp}^x\text{FeP}_5\}\text{Cu}(\text{CH}_3\text{CN})]^+$, 422.8656 $[\{\text{Cp}^x\text{FeP}_5\}\text{Cu}]^+$.

Negative ion ESI-MS ($\text{CH}_2\text{Cl}_2/\text{CH}_3\text{CN}$): m/z = 939.9954 $[\text{Cu}_6\text{Br}_7]^-$, 796.1500 $[\text{Cu}_5\text{Br}_6]^-$, 654.3023 $[\text{Cu}_4\text{Br}_5]^-$, 510.4566 $[\text{Cu}_3\text{Br}_4]^-$, 366.6109 $[\text{Cu}_2\text{Br}_3]^-$, 322.6613 $[\text{Cu}_2\text{ClBr}_2]^-$, 222.7656 $[\text{CuBr}_2]^-$, 178.8154 $[\text{CuClBr}]^-$, 134.8654 $[\text{CuCl}_2]^-$.

Elemental Analysis: Calculated (%) for $[(\text{CpCr})_2\text{As}_5]@[(\text{Cp}^x\text{FeP}_5)_{11}\{\text{CuCl}\}_{12.8}]$ (6405 g/mol): C 24.57, H 3.10, N 0; found (%): C 24.59, H 3.18, N 0.

Synthesis of $[(\text{CpCr})_2(\mu, \eta^{5:5}\text{-As}_5)]@[(\text{Cp}^x\text{FeP}_5)_{11}(\text{CuBr})_{15-n}]$ (**2@3^x-Br'**)

1^x (29 mg, 0.081 mmol) and **2** (10 mg, 0.016 mmol) were dissolved in toluene (8 mL). After treatment in a warm ultrasonic bath (2 h, 60°C, 35 kHz), the dark green solution was filtered into a Schlenk tube and carefully layered with a colorless solution of CuBr (22 mg, 0.15 mmol) in CH₃CN (8 mL). After one month, crystals of **2@3^x-Br'** have formed.

Synthesis of $[(\text{CpMo})_2(\mu, \eta^{3:3}\text{-P}_3)(\mu, \eta^{2:2}\text{-PS})]$ (**7**)^[14g]

$[\text{CpMo}(\text{CO})_2]_2$ (1.0 g, 2.30 mmol) and P₄S₃ (506 g, 2.30 mmol) were dissolved in 1,3-diisopropylbenzene (*m*-DIB, bp = 203 °C, 150 mL) and refluxed for 20 hours. The solvent was removed, and the dark residue was dissolved in toluene. Subsequently, this solution was filtered over celite and the solvent was again removed. The solid was adsorbed on silica and loaded onto a column filled with silica and hexane (20 cm x 3 cm). Compound **7** could be eluted as a red band using a hexane/toluene (1:1) solvent mixture. The solvent was removed and pure **7** could be isolated as dark red powder. Crystals suitable for X-ray diffraction analysis were obtained by layering a solution of **7** in CH₂Cl₂ with CH₃CN.

Analytical data of **7**:

Yield: 200 mg (crystalline yield, 0.42 mmol, 18%).

¹H NMR (C₆D₆): δ [ppm] = 4.73 (s, C₅H₅).

¹H NMR (CDCl₃): δ [ppm] = 5.21 (s, C₅H₅).

¹H NMR (pyridine-d₅): δ [ppm] = 5.23 (s, C₅H₅).

¹³C{¹H} NMR (C₆D₆): δ [ppm] = 91.2 (s, C₅H₅).

³¹P{¹H} NMR (C₆D₆): δ [ppm] = 336.6 (ddd, P_A), 318.9 (ddd, P_B), -168.6 (ddd, P_M), -403.8 (ddd, P_X); J_{PP}(AB) = 19 Hz, J_{PP}(AM) = 59 Hz, J_{PP}(AX) = 376 Hz, J_{PP}(BM) = 6 Hz, J_{PP}(BX) = 376 Hz, J_{PP}(MX) = 20 Hz.

FD-MS (toluene): *m/z* = 479.9 (M⁺).

Elemental analysis: Calculated (%) for [C₁₀H₁₀Mo₂P₄S] (478.0 g/mol): C 25.13, H 2.11, S 6.71; found: C 24.81, H 2.10, S 7.19.

Synthesis of $[(\text{CpMo})_2(\mu, \eta^{3:3}\text{-P}_3)(\mu, \eta^{2:2}\text{-PS})]@[(\text{Cp}^*\text{FeP}_5)_{11}(\text{CuCl})_{13.3}] \cdot 5.325 \text{CHCl}_3 \cdot 0.7 \text{C}_7\text{H}_8$ (7@3*-Cl**)**

1* (53 mg, 0.15 mmol) and **7** (6 mg, 13 μmol) were dissolved in CHCl_3 (9 mL) and sonicated for one hour at 60°C. After filtration, the dark green solution was carefully layered with a solution of CuCl (29 mg, 0.29 mmol) in CH_3CN (9 mL). After one week, the formation of dark brown rods of **7@3*-Cl** was observed. After complete diffusion, the mother liquor was shaken up and decanted together with the precipitate. The crystals were washed first with a mixture of $\text{CH}_2\text{Cl}_2 / \text{CH}_3\text{CN}$ (2:1, 2 x 10 mL), then with pentane (3 x 5 mL) and dried *in vacuo*.

Analytical Data of **7@3*-Cl**:

Yield: 28 mg (5.0 μmol , 40%).

$^1\text{H NMR}$ (CDCl_3): δ [ppm] = 1.44 (s, **1***_{free}), 2.05 (s, br), 2.06 (s, br), 2.13 (s), 2.20 (s), 2.22 (s), 2.28 (s, br), 2.36 (s), 2.36 (s), 4.47 (s, Cp_{bottle-neck} of **7**), 4.51 (s, Cp_{bottle-neck} of **7**), 4.85 (s, Cp_{bowl} of **7**), 4.89 (s, Cp_{bowl} of **7**), 5.22 (s, **7**_{free}).

$^{31}\text{P}\{^1\text{H}\}$ NMR (CDCl_3): δ [ppm] = -396.8 (m, P_x of **7**), -149.8 (m, P_M of **7**), 67 (br), 70 (br), 79 (br), 112 (br), 124 (br), 152.7 (s, **1***_{free}), 332.9 (m, P_B of **7**), 352.6 (m, P_A of **7**); signals almost below noise floor.

$^1\text{H NMR}$ (pyridine- d_5): δ [ppm] = 1.37 (s, **1***_{free}), 1.84 (s, CH_3CN), 5.26 (s, **7**_{free}), 5.68 (s, CH_2Cl_2), 8.54 (s, CHCl_3).

$^{31}\text{P}\{^1\text{H}\}$ NMR (pyridine- d_5): δ [ppm] = -407.8 (m, P_x of **7**_{free}), -168.7 (m, P_M of **7**_{free}), 143.0 (s, **1***_{free}), 306.2 (m, P_B of **7**_{free}), 325.8 (m, P_A of **7**_{free}).

EI-MS (70 eV): m/z = 345.9202 [$\text{Cp}^*\text{Fe}(\eta^5\text{-P}_5)]^+$, 283.9734 [$\{\text{Cp}^*\text{Fe}(\eta^5\text{-P}_5)\text{-P}_2\}^+$.

Positive ion ESI-MS ($\text{CH}_2\text{Cl}_2/\text{CH}_3\text{CN}$): m/z = 1694.0696 [$\{\text{Cp}^*\text{FeP}_5\}_3\text{Cu}_7\text{Cl}_6\}^+$, 1596.1709 [$\{\text{Cp}^*\text{FeP}_5\}_3\text{Cu}_6\text{Cl}_5\}^+$, 1398.5842 [$\{\text{Cp}^*\text{FeP}_5\}_3\text{Cu}_4\text{Cl}_3\}^+$, 1086.3965 [$\{(\text{CpMo})_2\text{P}_4\text{S}\}\{\text{Cp}^*\text{FeP}_5\}\text{Cu}_3\text{Cl}_2\}^+$, 986.4999 [$\{(\text{CpMo})_2\text{P}_4\text{S}\}\{\text{Cp}^*\text{FeP}_5\}\text{Cu}_2\text{Cl}\}^+$, 952.5632 [$\{\text{Cp}^*\text{FeP}_5\}_2\text{Cu}_3\text{Cl}_2\}^+$, 854.6662 [$\{\text{Cp}^*\text{FeP}_5\}_2\text{Cu}_2\text{Cl}\}^+$, 754.7698 [$(\text{Cp}^*\text{FeP}_5)_2\text{Cu}\}^+$, 549.7709 [$\{\text{Cp}^*\text{FeP}_5\}\text{Cu}_2\text{Cl}(\text{CH}_3\text{CN})\}^+$, 490.9023 [$\{\text{Cp}^*\text{FeP}_5\}\text{Cu}(\text{CH}_3\text{CN})_2\}^+$, 449.8757 [$\{\text{Cp}^*\text{FeP}_5\}\text{Cu}(\text{CH}_3\text{CN})\}^+$, 408.8495 [$\{\text{Cp}^*\text{FeP}_5\}\text{Cu}\}^+$.

Negative ion ESI-MS ($\text{CH}_2\text{Cl}_2/\text{CH}_3\text{CN}$): m/z = 232.77631 [$\text{Cu}_2\text{Cl}_3\}^-$, 134.8654 [$\text{CuCl}_2\}^-$.

Elemental Analysis: Calculated (%) for $[(\text{CpMo})_2\text{P}_4\text{S}]@[\{\text{Cp}^*\text{FeP}_5\}_{11}(\text{CuCl})_{13}]$ (5570 g/mol): C 25.87, H 3.17, N 0, S 0.58; found (%): C 25.63, H 3.34, N traces, S 0.26.

Synthesis of $[(\text{CpMo})_2(\mu, \eta^{3:3}\text{-P}_3)(\mu, \eta^{2:2}\text{-PS})]@[(\text{Cp}^*\text{FeP}_5)_{11}(\text{CuBr})_{13,235}] \cdot 5.55 \text{CHCl}_3 \cdot 2.4 \text{C}_7\text{H}_8$ (7@3^{*}-Br**)**

1* (53 mg, 0.15 mmol) and **7** (11 mg, 23 μmol) were dissolved in CHCl_3 (6 mL) and sonicated for two hours at 60°C . After filtration, the dark green solution was carefully layered with a solution of CuBr (41 mg, 0.29 mmol) in CH_3CN (6 mL). After one week, the formation of dark brown rods of **7@3^{*}-Br** was observed. After complete diffusion, the mother liquor was shaken up and decanted together with the precipitate. The crystals were washed first with a mixture of $\text{CH}_2\text{Cl}_2 / \text{CH}_3\text{CN}$ (2:1, 5 x 5 mL), then with pentane (3 x 3 mL) and dried *in vacuo*.

Analytical Data of **7@3^{*}-Br**:

Yield: 32 mg (5.4 μmol , 39%).

$^1\text{H NMR}$ (CDCl_3): δ [ppm] = 1.44 (s, **1^{*}_{free}**), 2.08 (br), 2.15 (br), 2.24 (br), 2.25 (br), 2.34 (br), 2.40 (s), 2.41 (s), 4.71 (s, $\text{Cp}_{\text{bottle-neck}}$ of **7**), 4.75 (s, $\text{Cp}_{\text{bottle-neck}}$ of **7**), 5.04 (s, Cp_{bowl} of **7**), 5.08 (s, Cp_{bowl} of **7**), 5.21 (s, **7_{free}**).

$^{31}\text{P}\{^1\text{H}\}$ NMR (CDCl_3): δ [ppm] = 67 (br), 74 (br), 108 (br), 152.8 (s, **1^{*}_{free}**).

$^1\text{H NMR}$ (pyridine- d_5): δ [ppm] = 1.37 (s, **1^{*}_{free}**), 1.87 (s, CH_3CN), 5.29 (s, **7_{free}**), 5.69 (s, CH_2Cl_2), 8.56 (s, CHCl_3).

$^{31}\text{P}\{^1\text{H}\}$ NMR (pyridine- d_5): δ [ppm] = -408.3 (m, P_x of **7_{free}**), -168.5 (m, P_M of **7_{free}**), 145.2 (s, **1^{*}_{free}**), 306.4 (m, P_B of **7_{free}**), 324.9 (m, P_A of **7_{free}**).

EI-MS (70 eV): m/z = 345.9200 $[\text{Cp}^*\text{Fe}(\eta^5\text{-P}_5)]^+$, 283.9736 $[\{\text{Cp}^*\text{Fe}(\eta^5\text{-P}_5)\text{-P}_2\}]^+$.

Positive ion ESI-MS ($\text{CHCl}_3/\text{CH}_3\text{CN}$): m/z = 1042.4586 $[\{\text{Cp}^*\text{FeP}_5\}_2\text{Cu}_3\text{Br}_2]^+$, 898.6140 $[\{\text{Cp}^*\text{FeP}_5\}_2\text{Cu}_2\text{Br}]^+$, 754.7703 $[\{\text{Cp}^*\text{FeP}_5\}_2\text{Cu}]^+$, 449.8754 $[\{\text{Cp}^*\text{FeP}_5\}\text{Cu}(\text{CH}_3\text{CN})]^+$.

Negative ion ESI-MS ($\text{CHCl}_3/\text{CH}_3\text{CN}$): m/z = 322.6599 $[\text{Cu}_2\text{Br}_2\text{Cl}]^-$, 222.7640 $[\text{CuBr}_2]^-$.

Elemental Analysis: Calculated (%) for $[(\text{CpMo})_2\text{P}_4\text{S}]@[\{\text{Cp}^*\text{FeP}_5\}_{11}\{\text{CuBr}\}_{11.3}]$ (5904 g/mol): C 24.41, H 2.99, N 0, S 0.54; found (%): C 24.41, H 3.03, N 0, S 0.48.

Synthesis of $[(\text{CpMo})_2(\mu, \eta^{3:3}\text{-P}_3)(\mu, \eta^{2:2}\text{-PS})]@[(\text{Cp}^*\text{FeP}_5)_{11}(\text{CuCl})_{15-n}]$ (7@3^x-Cl**)**

1^x (32 mg, 0.089 mmol) and **7** (7 mg, 0.015 mmol) were dissolved in CH_2Cl_2 (7 mL). After treatment in a warm ultrasonic bath (1 h, 60°C , 35 kHz), the dark green solution was filtered into a thick Schlenk tube and carefully layered with a colorless solution of CuCl (12 mg, 0.12 mmol) in CH_3CN (7 mL). After three days, crystals of **7@3^x-Cl** have formed. After complete diffusion,

the mother liquor was decanted, and the crystals were washed with CH₂Cl₂/CH₃CN (2:1, 4 x 3-10 mL) and pentane (3 x 3 mL) and dried.

Analytical Data of **7@3^x-Cl**:

Yield: 23 mg (3.9 μmol, 48%).

¹H NMR (CDCl₃): δ [ppm] = 0.75 (t, ³J_{HH} = 7.6 Hz, 3H, -CH₂CH₃ of **1^x_{free}**), 0.98 (br, -CH₂CH₃ of **1^x_a**), 1.09 (br, -CH₂CH₃ of **1^x_b**), 1.45 (s, 6H, -CH₃ of **1^x_{free}**), 1.45 (s, 6H, -CH₃ of **1^x_{free}**), 1.96 (q, ³J_{HH} = 7.6 Hz, 2H, -CH₂CH₃ of **1^x_{free}**), 2.06 (br, -CH₃ of **1^x_a**), 2.15 – 2.37 (br, -CH₃ of **1^x_b**), 2.73 (br, -CH₂CH₃ of **1^x_a**), 2.87 – 3.13 (br, -CH₂CH₃ of **1^x_b**), 4.43 (s, Cp_{bottle-neck} of **7**), 4.48 (s, Cp_{bottle-neck} of **7**), 4.80 (s, Cp_{bowl} of **7**), 4.84 (s, Cp_{bowl} of **7**), 5.22 (s, **7_{free}**), 5.30 (s, CH₂Cl₂).

³¹P{¹H} NMR (CDCl₃): δ [ppm] = -396.6 (m, P_x of **7**), -149.6 (m, P_M of **7**), 66 (br), 69 (br), 78 (br), 112 (br), 123 (br), 152.3 (s, **1^{*}_{free}**), 331.6 (m, P_B of **7**), 350.8 (m, P_A of **7**); Signals almost below noise floor.

¹H NMR (pyridine-d₅): δ [ppm] = 0.66 (t, ³J_{HH} = 7.7 Hz, 3H, -CH₂CH₃ of **1^x_{free}**), 1.37 (s, 6H, -CH₃ of **1^x_{free}**), 1.39 (s, 6H, -CH₃ of **1^x_{free}**), 1.86 (s, CH₃CN), 1.91 (q, ³J_{HH} = 7.6 Hz, 2H, -CH₂CH₃ of **1^x_{free}**), 5.24 (s, **7_{free}**), 5.69 (s, CH₂Cl₂).

³¹P{¹H} NMR (pyridine-d₅): δ [ppm] = -405.5 (m, P_x of **7_{free}**), -168.3 (m, P_M of **7_{free}**), 148.4 (s, **1^{*}_{free}**), 312.6 (m, P_B of **7_{free}**), 331.5 (m, P_A of **7_{free}**).

EI-MS (70 eV): *m/z* = 477.7595 [(CpMo)₂P₄S]⁺, 415.8142 [{(CpMo)₂P₄S}-P₂]⁺, 359.9409 [Cp^xFe(η⁵-P₅)]⁺, 297.9928 [{Cp^xFe(η⁵-P₅)-P₂]⁺.

Positive ion ESI-MS (CH₂Cl₂/CH₃CN): *m/z* = 1098.4162 [{(CpMo)₂P₄S}{Cp^xFeP₅}Cu₃Cl₂]⁺, 1000.5189 [{(CpMo)₂P₄S}{Cp^xFeP₅}Cu₂Cl]⁺, 980.5982 [{Cp^xFeP₅}₂Cu₃Cl₂]⁺, 902.6214 [{(CpMo)₂P₄S}{Cp^xFeP₅}Cu]⁺, 882.6999 [{Cp^xFeP₅}₂Cu₂Cl]⁺, 782.8035 [(Cp^xFeP₅)₂Cu]⁺, 563.7888 [{Cp^xFeP₅}Cu₂Cl(CH₃CN)]⁺, 522.7622 [{Cp^xFeP₅}Cu₂Cl]⁺, 504.9191 [{Cp^xFeP₅}Cu(CH₃CN)₂]⁺, 463.8930 [{Cp^xFeP₅}Cu(CH₃CN)]⁺.

Negative ion ESI-MS (CH₂Cl₂/CH₃CN): *m/z* = 332.6601 [Cu₃Cl₄]⁻, 232.7641 [Cu₂Cl₃]⁻, 134.8657 [CuCl₂]⁻.

Elemental Analysis: Calculated (%) for [(CpMo)₂P₄S]@[{Cp^xFeP₅}₁₁{CuCl}]₁₅ (5923 g/mol): C 26.57, H 3.35, N 0, S 0.54; calculated (%) for [(CpMo)₂P₄S]@[{Cp^xFeP₅}₁₁{CuCl}]₁₃·3CH₂Cl₂ (6064 g/mol): C 26.74, H 3.41, N 0, S 0.53; found (%): C 26.81, H 3.25, N 0, S 0.62.

Synthesis of $[(\text{CpMo})_2(\mu, \eta^{3:3}\text{-P}_3)(\mu, \eta^{2:2}\text{-PS})]@[(\text{Cp}^x\text{FeP}_5)_{11}(\text{CuBr})_{15-n}]$ ($7@3^x\text{-Br}$)

1^x (32 mg, 0.089 mmol) and **7** (7 mg, 0.015 mmol) were dissolved in CH_2Cl_2 (11 mL). After treatment in a warm ultrasonic bath (1 h, 60°C , 35 kHz), the dark green solution was filtered into a Schlenk tube and carefully layered first with an intermediate layer of $\text{CH}_2\text{Cl}_2/\text{CH}_3\text{CN}$ (2:1, 1 mL), subsequently with a colorless solution of CuBr (17 mg, 0.12 mmol) in CH_3CN (1 mL). After three weeks, crystals of $7@3^x\text{-Br}$ have formed. After complete diffusion, the mother liquor was decanted, and the crystals were washed with $\text{CH}_2\text{Cl}_2/\text{CH}_3\text{CN}$ (2:1, 3 x 10 mL) and pentane (3 x 5 mL) and dried. After further two months, a second crop of crystals could be isolated from the mother liquor.

Analytical Data of $7@3^x\text{-Br}$:

Yield: 11 mg (1.8 μmol , 22%).

$^1\text{H NMR}$ (CDCl_3): δ [ppm] = 0.75 (t, $^3J_{\text{HH}} = 7.6$ Hz, 3H, $-\text{CH}_2\text{CH}_3$ of 1^x_{free}), 1.06 (br, $-\text{CH}_2\text{CH}_3$ of 1^x_{a}), 1.44 (s, 6H, $-\text{CH}_3$ of 1^x_{free}), 1.45 (s, 6H, $-\text{CH}_3$ of 1^x_{free}), 1.95 (q, $^3J_{\text{HH}} = 7.7$ Hz, 2H, $-\text{CH}_2\text{CH}_3$ of 1^x_{free}), 2.16 – 2.34 (br, $-\text{CH}_3$ of 1^x_{a}), 2.94 – 3.10 (br, $-\text{CH}_2\text{CH}_3$ of 1^x_{a}), 5.30 (s, CH_2Cl_2).

$^{31}\text{P}\{^1\text{H}\}$ NMR (CDCl_3): δ [ppm] = 66 (br), 109 (br), 152.4 (s, 1^x_{free}); Signals almost below noise floor.

$^1\text{H NMR}$ (mother liquor, CD_2Cl_2): δ [ppm] = 0.75 (t, $^3J_{\text{HH}} = 7.6$ Hz, 3H, $-\text{CH}_2\text{CH}_3$ of 1^x_{free}), 0.98 (br, $-\text{CH}_2\text{CH}_3$ of 1^x_{a}), 1.06 (br, $-\text{CH}_2\text{CH}_3$ of 1^x_{b}), 1.44 (s, 6H, $-\text{CH}_3$ of 1^x_{free}), 1.45 (s, 6H, $-\text{CH}_3$ of 1^x_{free}), 1.94 (q, $^3J_{\text{HH}} = 7.6$ Hz, 2H, $-\text{CH}_2\text{CH}_3$ of 1^x_{free}), 2.07 (br, $-\text{CH}_3$ of 1^x_{a}), 2.13 – 2.40 (br, $-\text{CH}_3$ of 1^x_{b}), 2.76 (br, $-\text{CH}_2\text{CH}_3$ of 1^x_{a}), 2.94 – 3.20 (br, $-\text{CH}_2\text{CH}_3$ of 1^x_{b}), 4.66 (s, $\text{Cp}_{\text{bottle-neck}}$ of **7**), 4.69 (s, $\text{Cp}_{\text{bottle-neck}}$ of **7**), 5.01 (s, Cp_{bowl} of **7**), 5.05 (s, Cp_{bowl} of **7**), 5.32 (s, CH_2Cl_2).

$^{31}\text{P}\{^1\text{H}\}$ NMR (mother liquor, CD_2Cl_2): δ [ppm] = 66 (br), 74 (br), 107 (br), 114 (br), 124 (br), 151.8 (s, 1^x_{free}); Signals almost below noise floor.

$^1\text{H NMR}$ (pyridine- d_5): δ [ppm] = 0.66 (t, $^3J_{\text{HH}} = 7.6$ Hz, 3H, $-\text{CH}_2\text{CH}_3$ of 1^x_{free}), 1.35 (s, 6H, $-\text{CH}_3$ of 1^x_{free}), 1.38 (s, 6H, $-\text{CH}_3$ of 1^x_{free}), 1.89 (q, $^3J_{\text{HH}} = 7.6$ Hz, 2H, $-\text{CH}_2\text{CH}_3$ of 1^x_{free}), 5.24 (s, 7_{free}), 5.71 (s, CH_2Cl_2).

$^{31}\text{P}\{^1\text{H}\}$ NMR (pyridine- d_5): δ [ppm] = 151.5 (s, $[\text{Cp}^x\text{Fe}(\eta^5\text{-P}_5)]$).

EI-MS (70 eV): m/z = 477.7775 $[(\text{CpMo})_2\text{P}_4\text{S}]^+$, 359.9353 $[\text{Cp}^x\text{Fe}(\eta^5\text{-P}_5)]^+$, 297.9876 $[\{\text{Cp}^x\text{Fe}(\eta^5\text{-P}_5)\}\text{-P}_2]^+$, 123.89545 $[\text{P}_4]^+$.

Positive ion ESI-MS ($\text{CH}_2\text{Cl}_2/\text{CH}_3\text{CN}$): m/z = 2147.6684 $[\{\text{Cp}^x\text{FeP}_5\}_3\text{Cu}_8\text{Br}_7]^+$, 2003.8194 $[\{\text{Cp}^x\text{FeP}_5\}_3\text{Cu}_7\text{Br}_6]^+$, 1959.8668 $[\{\text{Cp}^x\text{FeP}_5\}_3\text{Cu}_7\text{ClBr}_5]^+$, 1859.9709 $[\{\text{Cp}^x\text{FeP}_5\}_3\text{Cu}_6\text{Br}_5]^+$, 1816.0199 $[\{\text{Cp}^x\text{FeP}_5\}_3\text{Cu}_6\text{ClBr}_4]^+$, 1188.3135 $[\{(\text{CpMo})_2\text{P}_4\text{S}\}\{\text{Cp}^x\text{FeP}_5\}\text{Cu}_3\text{Br}_2]^+$, 1070.4956

$[(\text{Cp}^*\text{FeP}_5)_2\text{Cu}_3\text{Br}_2]^+$, 1024.5470 $[(\text{Cp}^*\text{FeP}_5)_2\text{Cu}_3\text{ClBr}]^+$, 926.6505 $[(\text{Cp}^*\text{FeP}_5)_2\text{Cu}_2\text{Br}]^+$, 782.8036 $[(\text{Cp}^*\text{FeP}_5)_2\text{Cu}]^+$, 463.8933 $[(\text{Cp}^*\text{FeP}_5)\text{Cu}(\text{CH}_3\text{CN})]^+$, 422.8661 $[(\text{Cp}^*\text{FeP}_5)\text{Cu}]^+$.

Negative ion ESI-MS ($\text{CH}_2\text{Cl}_2/\text{CH}_3\text{CN}$): $m/z = 896.0711$ $[\text{Cu}_6\text{ClBr}_6]^-$, 796.1748 $[\text{Cu}_5\text{Br}_6]^-$, 654.3247 $[\text{Cu}_4\text{Br}_5]^-$, 608.3756 $[\text{Cu}_4\text{ClBr}_4]^-$, 510.4763 $[\text{Cu}_3\text{Br}_4]^-$, 366.6282 $[\text{Cu}_2\text{Br}_3]^-$, 322.6776 $[\text{Cu}_2\text{ClBr}_2]^-$, 222.7798 $[\text{CuBr}_2]^-$, 178.8288 $[\text{CuClBr}]^-$, 134.8769 $[\text{CuCl}_2]^-$.

Elemental Analysis: Calculated (%) for $[(\text{CpMo})_2\text{P}_4\text{S}]\text{@[}(\text{Cp}^*\text{FeP}_5)_{11}\{\text{CuBr}\}_{12.3}\text{]}$ (6202 g/mol): C 25.37, H 3.20, N 0, S 0.52; calculated (%) for $[(\text{CpMo})_2\text{P}_4\text{S}]\text{@[}(\text{Cp}^*\text{FeP}_5)_{11}\{\text{CuBr}\}_{11.5}\text{}]\cdot 3\text{CH}_2\text{Cl}_2$ (6342 g/mol): C 25.38, H 3.23, N 0, S 0.51; found (%): C 25.40, H 3.38, N traces, S 0.40.

Synthesis of $[(\text{CpMo})_2\text{P}_4\text{S}]\{\text{CuCl}\}_n$ (**8**)

7 (11 mg, 0.023 mmol) was dissolved in toluene (10 mL). After treatment in a warm ultrasonic bath (1 h, 60°C, 35 kHz), the solution was filtered into a Schlenk tube and carefully layered with a colorless solution of CuCl (3 mg, 0.03 mmol) in CH_3CN (10 mL). After one day, crystals of **8** have formed. After complete diffusion, the mother liquor was decanted, and the crystals were washed with toluene (3 x 5 mL) and pentane (3 x 5 mL) and dried. Alternatively, **7** could also be dissolved in CH_2Cl_2 and layered with a solution of CuCl in CH_3CN to give **8**.

Analytical Data of **8**:

Yield: 5 mg (8.7 μmol , 38%).

^1H NMR (pyridine- d_5): δ [ppm] = 1.87 (s, CH_3CN), 2.23 (s, C_7H_8), 5.25 (s, **7**_{free}), 7.17 – 7.31 (m, C_7H_8).

$^{31}\text{P}\{^1\text{H}\}$ NMR (pyridine- d_5): δ [ppm] = -405.8 (m, P_x of **7**_{free}), -168.4 (m, P_M of **7**_{free}), 312.0 (m, P_B of **7**_{free}), 331.1 (m, P_A of **7**_{free}).

Positive ion ESI-MS ($\text{CH}_2\text{Cl}_2/\text{CH}_3\text{CN}$):^[48] $m/z = 1597.0937$ $[(\text{CpMo})_2\text{P}_4\text{S}]_3\text{Cu}_2\text{Cl}^+$, 1118.3383 $[(\text{CpMo})_2\text{P}_4\text{S}]_2\text{Cu}_2\text{Cl}^+$, 1020.4412 $[(\text{CpMo})_2\text{P}_4\text{S}]_2\text{Cu}^+$.

Negative ion ESI-MS ($\text{CH}_2\text{Cl}_2/\text{CH}_3\text{CN}$):^[48] $m/z = 232.7640$ $[\text{Cu}_2\text{Cl}_3]^-$, 134.8658 $[\text{CuCl}_2]^-$.

Elemental Analysis: Calculated (%) for $[(\text{CpMo})_2\text{P}_4\text{S}]\{\text{CuCl}\}_n$ (577.0 g/mol): C 20.82, H 1.75, N 0, S 5.56; found (%): C 21.38, H 1.83, N traces, S 5.15.

Synthesis of $[(\text{Cp}^*\text{Fe}(\eta^{5:1:1:1}\text{-P}_5))_2\{\text{Cp}^*\text{Fe}(\eta^{5:1:1}\text{-P}_5)\}\text{Cu}_4(\mu\text{-I})_4]_n$ (**9**)^[14g]

In a Schlenk tube a dark green solution of **1*** (30 mg, 0.087 mmol) and $[(\text{CpMo})_2(\mu, \eta^{6:6}\text{-P}_6)]$ (15 mg, 0.030 mmol) in CH_2Cl_2 (10 mL) was carefully layered with a colorless solution of CuI

(33 mg, 0.17 mmol) in CH₃CN (10 mL). Thereby, the phase boundary turned yellow-brownish and got turbid. After complete diffusion, black brownish-red needles of **9** as well as brown plates of $[\{\text{Cp}^*\text{Fe}(\eta^5\text{-P}_5)\}(\text{CuI})]_n$ ^[12] could be observed. The mother liquor was decanted, the crystals were washed with hexane (3 x 10 mL) and dried *in vacuo*. Unfortunately, attempts to reproduce **9**, with and without the addition of $[(\text{CpMo})_2(\mu, \eta^{6:6}\text{-P}_6)]$, mostly failed. In total, **9** was observed only twice (both times when the triple decker complex $[(\text{CpMo})_2(\mu, \eta^{6:6}\text{-P}_6)]$ was present).

Analytical data of **9** and $[\{\text{Cp}^*\text{Fe}(\eta^5\text{-P}_5)\}(\text{CuI})]_n$:

Yield: 30 mg

³¹P{¹H} NMR (pyridine, C₆D₆ capillary): δ [ppm] = 152.0 (s, **1***_{free}).

Elemental analysis: Calculated (%) for $[\{\text{Cp}^*\text{Fe}(\eta^5\text{-P}_5)\}_3(\text{CuI})_4]$ (**9**, 1800 g/mol): C 20.02, H 2.52; calculated (%) for $[\text{Cp}^*\text{Fe}(\eta^5\text{-P}_5)\text{CuI}]$ (536 g/mol): C 22.39, H 2.82; found: C 21.94, H 2.84.

5.5 Crystallographic Details

Crystals of **2@3^x-Cl**, **2@3^x-Br**, **2@3^x-Br'**, **7**, **7@3^{*}-Cl**, **7@3^{*}-Br**, **7@3^x-Cl**, **7@3^x-Br**, **8** and **9** were taken from a Schlenk flask under a stream of argon and quickly covered with mineral oil (**7**, **9**) or perfluorinated oil Fomblin[®] to prevent decomposition and a loss of solvent. The quickly chosen single crystals covered by a drop of the oil were directly positioned in a stream of cold nitrogen on pre-centered goniometer head with CryoMount[®] at the goniometer of a diffractometer.

The data for **7** and **9** were collected using 1° ω scans on an Agilent Technologies diffractometer equipped with Atlas CCD detector and a SuperNova CuK α microfocus source at 123 K. The data for **8** were collected on an Agilent Technologies diffractometer equipped with Titan^{S2} CCD detector and a SuperNova CuK α microfocus source using 0.5° ω scans at 123 K. Absorption correction for **7**, **8** and **9** was applied based on crystal faces. The molecule (CpMo)₂(P₃)(PS) in **7** lies on 2-fold axis, and the ligand μ,η^2 -PS is represented by one crystallographically independent atom. To refine the disordered ligand both the coordinates and displacement parameters of P and S atom were equated.

To collect diffraction data at helium temperature, the crystals of **2@3^x**, **7@3^{*}** and **7@3^x** were carefully selected, mounted on magnetic holders, checked for quality and placed into a Dewar vessel with liquid nitrogen using standard cryocrystallography tools. After a few weeks it was taken to the DESY PETRA III synchrotron. Using standard procedures, the crystals are placed into a special Dewar vessel filled with liquid nitrogen. A robotic mounting/demounting was used for further manipulations in the P11 beamline hutch.^[49] X-ray diffraction experiments for **2@3^x**, **7@3^{*}** and **7@3^x** were measured using one-circle goniostat and DECTRIS PILATUS 6M pixel array detector at 6(2) K using open-flow helium cryo system Cryocool-LHe (CRYO Industries of America, Inc.). The data were acquired by 360° shutterless ϕ -rotation with 0.2° readouts and exposure 0.8 s per frame at a wavelength $\lambda = 0.6888 \text{ \AA}$ (18 keV) or 0.7085 \AA (17.5 keV). Data reduction for all data sets was performed with CrysAlisPro software.^[50] Empirical absorption correction using equivalent reflections was applied.

All structures were solved with *SHELXT*^[51] and refined by full-matrix least-squares method against F^2 in anisotropic approximation using multi-processor variable memory versions of *SHELXL* (2014-2018). For the refinement of isostructural compounds, the same model was used and adapted to the specific features of every structure. The structure refinement for the supramolecular compounds **2@3^x**, **7@3^{*}** and **7@3^x** is made complicated by disorder of the heavy atoms, by the disorder of the guest triple decker complexes, and solvent molecules CH₃CN, CHCl₃ or CH₂Cl₂. The occupation factors for disordered positions of heavy atoms were refined with fixed isotropic U_{iso} similar to the average U_{iso} for the fully occupied heavy atoms in

the corresponding structure (usually $\sim 0.025\text{--}0.030 \text{ \AA}^2$). The molecular site occupancy factors (equal s.o.f.'s for all atoms of a solvent molecule) were refined using the FVAR instruction of SHELX with isotropic displacement parameters fixed at $U_{\text{iso}} = 0.050 \text{ \AA}^2$ for compounds measured at $T = 80\text{--}90 \text{ K}$ and to $U_{\text{iso}} = 0.035$ for compounds measured at $T = 6 \text{ K}$. The resulting occupancies were fixed, and the light (C and N) atoms with occupancies of more than 0.5 were refined in anisotropic approximation. Some minor positions of the solvent molecules were refined with restraint geometry. Most of the restraints were removed at the final stage of the refinement when possible.

The refinement of the 3D polymer **9** is not yet complete, since not all solvent molecules could be localized. The framework represents a new topological type of 3-connected 3-periodic net. In this structure, the Cu atoms and the 1,2,4-coordinated $[\text{Cp}^*\text{Fe}(\eta^5\text{-P}_5)]$ molecules form nodes of the polymeric framework, connected by 1,3-coordinated $[\text{Cp}^*\text{Fe}(\eta^5\text{-P}_5)]$ spacers (Figure 8).

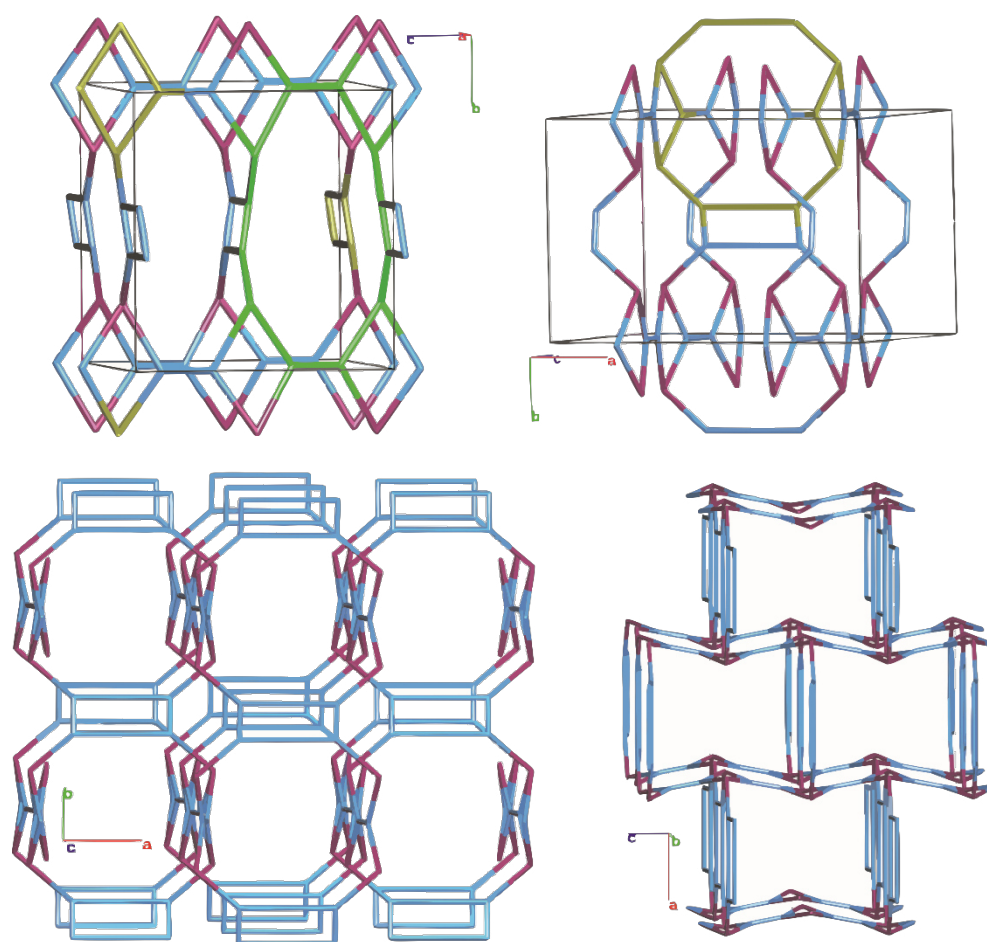


Figure 8. The 3-connected net of the new topology in **9**, containing 4, 10 (yellow highlighted) and 12-membered rings (green highlighted). Blue nodes correspond to Cu, purple ones to pentaphosphaferrocene.

Table 2. Experimental details for compounds **2@3^x-Cl** (preliminary data) and **2@3^x-Br** (preliminary data).

Crystal data	2@3^x-Cl	2@3^x-Br
Structural formula	{Cp ₂ Cr ₂ As ₅ }@[(Cp ^x FeP ₅) ₁₁ (CuCl) ₁₅] ·mCH ₂ Cl ₂ ·nCH ₃ CN	{Cp ₂ Cr ₂ As ₅ }@[(Cp ^x FeP ₅) ₁₁ (CuBr) ₁₅] ·mCHCl ₃ ·nCH ₃ CN
Chemical formula	C ₁₃₁ H ₁₉₇ As ₅ Cl ₁₅ Cr ₂ Cu ₁₅ Fe ₁₁ P ₅₅	C ₁₄₅ H ₂₁₉ As ₅ Br ₁₅ Cl ₂ Cr ₂ Cu ₁₅ Fe ₁₁ NP ₆₀
<i>M_r</i>	> 6053.02	> 7150.00
Crystal system, space group	Monoclinic, <i>Cc</i>	Monoclinic, <i>Pc</i>
Temperature (K)	90(2)	80.0(2)
<i>a, b, c</i> (Å)	26.9617(4), 32.9241(3), 25.9870(3)	35.88143(12), 22.59511(4), 33.62902(13)
<i>β</i> (°)	101.6419(13)	116.2262(4)
<i>V</i> (Å ³)	22593.8(5)	24457.84(13)
<i>Z</i>	4	4
<i>F</i> (000)	> 11988	> 13956
<i>D_x</i> (Mg m ⁻³)	> 1.779	> 1.942
Radiation type	Cu <i>Kα</i>	Synchrotron, <i>λ</i> = 0.6888 Å
<i>μ</i> (mm ⁻¹)	14.13	> 5.098
Crystal colour and shape	Dark brown prism	Dark brown flattened prism
Crystal size (mm)	0.20 × 0.14 × 0.11	0.18 × 0.18 × 0.12
Data collection		
Diffractometer	SuperNova, Titan ^{S2}	P11 beamline, PETRA III, DESY, Dectris PILATUS 6M
Absorption correction	Gaussian	multi-scan
<i>T_{min}</i> , <i>T_{max}</i>	0.161, 0.316	0.574, 1.000
No. of measured, independent and observed [<i>I</i> > 2σ(<i>I</i>)] reflections	116171, 37304, 31307	354161, 140658, 133566
<i>R_{int}</i>	0.0429	0.0430
Range of <i>h, k, l</i>	<i>h</i> = -33→28, <i>k</i> = -39→40, <i>l</i> = -28→32	<i>h</i> = -49→49, <i>k</i> = -33→33, <i>l</i> = -50→50
Refinement		
<i>R</i> [<i>F</i> ² > 2σ(<i>F</i> ²)], <i>wR</i> (<i>F</i> ²), <i>S</i>	0.0639, 0.1880, 1.063	0.0822,
No. of reflections	37304	140658
No. of parameters	2313	3897
No. of restraints	3	2
H-atom treatment	H-atom parameters constrained	H-atom parameters constrained
Δ _{max} , Δ _{min} (e Å ⁻³)	2.461, -2.129	5.246, -4.733
Absolute structure parameter	Refined as an inversion twin	Refined as an inversion twin
Absolute structure parameter	0.019(5)	0.679(6)

Computer programs: SHELXT2018/5 (Sheldrick, 2018), SHELXL2018/3 (Sheldrick, 2018), for **2@3^x-Cl**: CrysAlisPro 1.171.40.18c (Rigaku OD, 2018) and **2@3^x-Br**: CrysAlisPro 1.171.41.21a (Rigaku OD, 2019).

Table 3. Experimental details for compounds **2@3^x-Br'** (preliminary data) and **7**.

Crystal data	2@3^x-Br'	7
Structural formula	{Cp ₂ Cr ₂ As ₅ }@[(Cp ^x FeP ₅) ₁₁ (CuBr) ₁₅] ·nTol·mCH ₃ CN	Cp ₂ Mo ₂ (P ₃)(PS)
Chemical formula	C ₁₃₁ H ₁₉₇ As ₅ Br ₁₅ ClCr ₂ Cu ₁₅ Fe ₁₁ N _{1.50} P ₅₅ *	C ₁₀ H ₁₀ Mo ₂ P ₄ S
<i>M_r</i>	6776.39	478.00
Crystal system, space group	Monoclinic, C2	Monoclinic, C2/c
Temperature (K)	80.0(2)	123.0(2)
<i>a</i> , <i>b</i> , <i>c</i> (Å)	32.27794(13), 25.29490(8), 33.48555(12)	11.4167 (5), 10.9669 (3), 12.1695 (6)
<i>β</i> (°)	103.3508(4)	117.231 (6)
<i>V</i> (Å ³)	26600.98(17)	1354.82 (10)
<i>Z</i>	4	4
<i>F</i> (000)	> 13178	920
<i>D_x</i> (Mg m ⁻³)	> 1.692	2.343
Radiation type	Synchrotron, λ = 0.6888 Å	Cu Kα
μ (mm ⁻¹)	> 4.65	20.84
Crystal color and shape	Dark brown prism	Dark red rhombohedron
Crystal size (mm)	0.15 × 0.10 × 0.10	0.13 × 0.07 × 0.06
Data collection		
Diffractometer	P11 beamline, PETRA III, DESY, Dectris PILATUS 6M	SuperNova, Single source at offset, Atlas diffractometer
Absorption correction	multi-scan	Multi-scan
<i>T_{min}</i> , <i>T_{max}</i>	0.565, 1.000	0.356, 1.000
No. of measured, independent and observed [<i>I</i> > 2σ(<i>I</i>)] reflections	201103, 76440, 65058	3339, 1345, 1243
<i>R_{int}</i>	0.0392	0.013
(sin θ/λ) _{max} (Å ⁻¹)		0.624
Range of <i>h</i> , <i>k</i> , <i>l</i>	<i>h</i> = -45→45, <i>k</i> = -37→38, <i>l</i> = -47→47	<i>h</i> = -14→11, <i>k</i> = -12→13, <i>l</i> = -14→13
Refinement		
<i>R</i> [<i>F</i> ² > 2σ(<i>F</i> ²)], <i>wR</i> (<i>F</i> ²), <i>S</i>	0.0513, 0.1553, 0.936	0.021, 0.058, 1.07
No. of reflections	76440	1345
No. of parameters	1796	78
No. of restraints	1	0
H-atom treatment	H-atom parameters constrained	H-atom parameters constrained
Δ _{max} , Δ _{min} (e Å ⁻³)	1.86, -0.98	1.09, -1.20
Absolute structure parameter	Refined as an inversion twin	-
Absolute structure parameter	0.636(5)	-

Computer programs for **2@3^x-Br'**: CrysAlis PRO 1.171.41.21a (Rigaku OD, 2019), SHELXT2018/5 (Sheldrick, 2018), SHELXL2018/3 (Sheldrick, 2018); for **7**: CrysAlis PRO, Agilent Technologies, SHELXL97 (Sheldrick, 1997), SHELXL2013 (Sheldrick, 2013).

Table 4. Experimental details for compounds **7@3*-Cl** and **7@3*-Br**.

Crystal data	7@3*-Cl	7@3*-Br
Structural formula	{Cp ₂ Mo ₂ (P ₃)(PS)}@ [(Cp*FeP ₅) ₁₁ (CuCl) _{13.3}] ·5.325CHCl ₃ ·0.7CH ₃ CN	{Cp ₂ Mo ₂ (P ₃)(PS)}@ [(Cp*FeP ₅) ₁₁ (CuBr) _{13.235}] ·5.55CHCl ₃ ·2.4CH ₃ CN
Chemical formula	C ₁₀ H ₁₀ Mo ₂ P ₄ S·C ₁₁₀ H ₁₆₅ Cl _{13.3} Cu _{13.30} Fe ₁₁ Mo ₂ P ₅₉ S·(CH ₃ CN) _{0.70} ·(CH ₂ Cl ₂) _{5.325}	C ₁₂₀ H ₁₇₅ Br _{13.24} Cu _{13.24} Fe ₁₁ Mo ₂ S·5.55(C HCl ₃)·2.4(CH ₃ CN)
<i>M_r</i>	6264.05	6942.69
Crystal system, space group	Monoclinic, <i>Cc</i>	Monoclinic, <i>Cc</i>
Temperature (K)	80	80
<i>a, b, c</i> (Å)	30.1530(3), 29.8661(2), 29.2349(3)	30.3708(3), 29.7220(4), 29.3586(3)
<i>β</i> (°)	111.3759(14)	112.1079(12)
<i>V</i> (Å ³)	24516.5(5)	24552.9(5)
<i>Z</i>	4	4
<i>F</i> (000)	12408	13551
<i>D_x</i> (Mg m ⁻³)	1.697	1.878
Radiation type	Synchrotron, λ = 0.7085 Å	Synchrotron, λ = 0.6888 Å
μ (mm ⁻¹)	2.60	4.23
Crystal color and shape	Dark brown rod	Dark brown rod
Crystal size (mm)	0.10 × 0.04 × 0.03	0.20 × 0.05 × 0.05
Data collection		
Diffractometer	P11 beamline, PETRA III, DESY, Dectris PILATUS 6M	P11 beamline, PETRA III, DESY, Dectris PILATUS 6M
Absorption correction	Multi-scan	Multi-scan
<i>T_{min}</i> , <i>T_{max}</i>	0.590, 1.000	0.433, 1.000
No. of measured and independent reflections	97627, 46625, 42445	78866, 44582, 41972
<i>R_{int}</i>	0.040	0.030
(sin θ/λ) _{max} (Å ⁻¹)	0.625	0.625
Range of <i>h, k, l</i>	<i>h</i> = -37→37, <i>k</i> = -37→37, <i>l</i> = -36→36	<i>h</i> = -39→37, <i>k</i> = -36→37, <i>l</i> = -36→36
Refinement		
<i>R</i> [<i>F</i> ² > 2σ(<i>F</i> ²)], <i>wR</i> (<i>F</i> ²), <i>S</i>	0.056, 0.165, 1.05	0.045, 0.130, 1.13
No. of reflections	46617	44582
No. of parameters	2543	2725
No. of restraints	77	79
H-atom treatment	H-atom parameters constrained	H-atom parameters constrained
Δ _{max} , Δ _{min} (e Å ⁻³)	2.31, -0.94	1.324, -1.438
Absolute structure parameter	Refined as an inversion twin 0.126(10)	Refined as an inversion twin 0.018(6)

Computer programs: SHELXT2018/5 (Sheldrick, 2018), SHELXL2018/3 (Sheldrick, 2018); for **7@3*-Cl**: CrysAlis PRO 1.171.41.21a (Rigaku OD, 2019); for **7@3*-Br**: CrysAlis PRO 1.171.40.6a (Rigaku OD, 2018).

Table 5. Experimental details for compounds **7@3^x-Cl** (preliminary data) and **7@3^x-Br** (preliminary data).

Crystal data	7@3^x-Cl	7@3^x-Br
Structural formula	{Cp ₂ Mo ₂ (P ₃)(PS)}@ [(Cp ^x FeP ₅) ₁₁ (CuCl) ₁₅] ·nCH ₂ Cl ₂ ·mCH ₃ CN	{Cp ₂ Mo ₂ (P ₃)(PS)}@ [(Cp ^x FeP ₅) ₁₁ (CuBr) _{13.35}] ·nCH ₂ Cl ₂ ·mCH ₃ CN
Chemical formula	C ₁₃₁ H ₁₉₇ Cl ₁₅ Cu ₁₅ Fe ₁₁ Mo ₂ N _{7.50} P ₅₉ S	C _{138.50} H ₁₈₀ Br _{13.35} Cl ₂ Cu _{13.35} Fe ₁₁ Mo ₂ N _{0.75} P ₅₉ S
<i>M_r</i>	> 6027.32	> 6506.80
Crystal system, space group	Monoclinic, Cc	Monoclinic, Cc
Temperature (K)	6(2)	80(2)
<i>a</i> , <i>b</i> , <i>c</i> (Å)	26.9077(3), 32.82882(14), 26.1506(2)	26.80940(10), 33.08595(9), 26.64631(12)
<i>β</i> (°)	100.9568(10)	101.3496(4)
<i>V</i> (Å ³)	22679.0(3)	23173.46(15)
<i>Z</i>	4	4
<i>F</i> (000)	> 11986	> 12703
<i>D_x</i> (Mg m ⁻³)	> 1.765	> 1.865
Radiation type	Synchrotron, λ = 0.6888 Å	Synchrotron, λ = 0.6888 Å
μ (mm ⁻¹)	> 2.57	> 4.349
Crystal color and shape	Dark brown rod	Dark brown prism
Crystal size (mm)	0.15 × 0.15 × 0.05	0.10 × 0.07 × 0.05
Data collection		
Diffractometer	P11 beamline, PETRA III, DESY, Dectris PILATUS 6M	P11 beamline, PETRA III, DESY, Dectris PILATUS 6M
Absorption correction	multi-scan	multi-scan
<i>T_{min}</i> , <i>T_{max}</i>	0.612, 1.000	
No. of measured, independent and observed [<i>I</i> > 2σ(<i>I</i>)] reflections	182872, 59310, 37111	178098, 60060, 50776
<i>R_{int}</i>	0.0335	0.0348
Range of <i>h</i> , <i>k</i> , <i>l</i>	<i>h</i> = -40→40, <i>k</i> = -43→43, <i>l</i> = -39→39	<i>h</i> = -39→39, <i>k</i> = -44→44, <i>l</i> = -34→31
Refinement		
<i>R</i> [<i>F</i> ² > 2σ(<i>F</i> ²)], <i>wR</i> (<i>F</i> ²), <i>S</i>	0.0482, 0.1292, 0.807	0.0499, 0.1295, 1.304
No. of reflections	59310	60060
No. of parameters	2449	2377
No. of restraints	5	5
H-atom treatment	H-atom parameters constrained	H-atom parameters constrained
Δ _{max} , Δ _{min} (e Å ⁻³)	1.539, -1.383	2.278, -0.886
Absolute structure	Refined as an inversion twin	Refined as an inversion twin
Absolute structure parameter	0.781(9)	0.020(3)

Computer programs for **7@3^x-Cl** and **7@3^x-Br**: CrysAlis PRO 1.171.41.21a (Rigaku OD, 2019), SHELXT2018/5 (Sheldrick, 2018), SHELXL2018/3 (Sheldrick, 2018).

Table 6. Experimental details for compounds **8** and **9**.

Crystal data	8	9
Structural formula	$[(\text{CpMo})_2(\text{P}_3)(\text{PS})](\text{CuCl})$	$[(\text{Cp}^*\text{FeP}_5)_2](\text{Cp}^*\text{FeP}_5)\text{Cu}_4\text{I}_4 \cdot n\text{Solvent}$
Chemical formula	$\text{C}_{10}\text{H}_{10}\text{ClCuMo}_2\text{P}_4\text{S}$	$\text{C}_{35}\text{H}_{52.5}\text{Cu}_4\text{Fe}_3\text{I}_4\text{N}_{2.5}\text{P}_{15}^*$
M_r	576.99	> 1902.16
Crystal system, space group	Monoclinic, $P2_1/c$	orthorhombic, $Pnma$
Temperature (K)	123(2)	123(2)
a, b, c (Å)	10.0744(2), 15.4903(2), 10.8048(3)	25.1960(5), 16.1506(3), 15.0851(3)
β (°)	112.862 (3)	90, 90, 90
V (Å ³)	1553.70 (6)	6138.6(5)
Z	4	4
$F(000)$	1104	> 3732
D_x (Mg m ⁻³)	2.467	>
Radiation type	Cu $K\alpha$	Cu $K\alpha$
μ (mm ⁻¹)	21.18	> 26.95
Crystal color and shape	Black plate	brown needle
Crystal size (mm)	0.16 × 0.08 × 0.03	0.24 × 0.02 × 0.01
Data collection		
Diffractometer	SuperNova, Titan ^{S2}	SuperNova, Single source at offset, Atlas diffractometer
Absorption correction	Gaussian	gaussian
T_{\min}, T_{\max}	0.162, 0.609	0.141, 0.770
No. of measured, independent and observed [$I > 2\sigma(I)$] reflections	13802, 3109, 2986	25789, 6541, 5457
R_{int}	0.036	0.0443
$(\sin \theta/\lambda)_{\text{max}}$ (Å ⁻¹)	0.624	0.792
Range of h, k, l	$h = -12 \rightarrow 12,$ $k = -19 \rightarrow 19,$ $l = -13 \rightarrow 13$	$h = -31 \rightarrow 30,$ $k = -19 \rightarrow 20,$ $l = -18 \rightarrow 18$
Refinement		
$R[F^2 > 2\sigma(F^2)], wR(F^2), S$	0.027, 0.070, 1.09	0.0378, 0.1137, 1.045
No. of reflections	3109	6541
No. of parameters	172	320
No. of restraints	0	0
H-atom treatment	H-atom constrained	parameters H atom parameters constrained
$\Delta_{\text{max}}, \Delta_{\text{min}}$ (e Å ⁻³)	0.77, -0.84	2.139, -0.955
Absolute structure	-	-
Absolute structure parameter	-	-

Computer programs for **8**: CrysAlis PRO 1.171.39.45g (Rigaku OD, 2018), SHELXT (Sheldrick, 2015), SHELXL2014/7 (Sheldrick, 2014), Olex2 (Dolomanov et al., 2009); for **9**: CrysAlis PRO 1.171.41.21a (Rigaku OD, 2019), SHELXT2018/5 (Sheldrick, 2018), SHELXL2018/3 (Sheldrick, 2018).

5.6 Author Contributions

- The synthesis of compounds **2@3*-Cl** and **2@3*-Br** were performed by Dr. Claudia Heindl; the characterization was performed by Helena Brake, the MAS NMR spectroscopy was performed by Prof. Dr. Werner Kremer
- The synthesis and characterization of **2@6*-Br** was performed by Dr. Andrea Schindler and is also part of her dissertation (University of Regensburg, **2010**)
- The synthesis and characterization of "**4@5-Cl**" was performed by Dr. Andrea Schindler and is also part of her dissertation (University of Regensburg, **2010**); further characterization of "**4@5-Cl**" was performed by Helena Brake and has partly already been presented in chapter 4.
- Synthesis and characterization of compounds **2@3*-Cl**, **2@3*-Br**, "**4@5-Cl**" and **2@6*-Br** are also subject to chapter 4 of this thesis
- The synthesis and characterization of compounds **2@3^x-Cl**, **2@3^x-Br**, **2@3^x-Br'**, "**4@5*-Br**", **7@3*-Cl**, **7@3*-Br**, **7@3^x-Cl**, **7@3^x-Br** and **8** were performed by Helena Brake
- The synthesis and characterizations of compounds **7** and **9** were performed by Dr. Claudia Heindl and are also part of her dissertation (University of Regensburg, **2015**).
- X-ray structural analyses of **2@3^x-Cl**, **2@3^x-Br**, **2@3^x-Br'**, "**4@5*-Br**", **7@3*-Cl**, **7@3*-Br**, **7@3^x-Cl**, **7@3^x-Br** and **8** were performed by Dr. Eugenia Peresyphkina, Dr. Sc. Alexander V. Virovets and Helena Brake. Parts of this research were carried out at PETRAIII at DESY, a member of the Helmholtz Association (HGF), by Dr. Eugenia Peresyphkina and Dr. Sc. Alexander V. Virovets. EP and AV are grateful to the P11 beamline team for their assistance.
- X-ray structural analyses of **7** and **9** were performed by Dr. Eugenia Peresyphkina, Dr. Sc. Alexander V. Virovets and Dr. Claudia Heindl
- MAS NMR spectroscopy of compound "**4@5*-Br**" was performed by Prof. Dr. Werner Kremer
- The manuscript (introduction, results and discussion, experimental part, conclusion; including figures and graphical abstract) was written by Helena Brake with the exception of the discussion and experimental part concerning compounds **7** and **9**, which were written by Dr. Claudia Heindl and are also part of her dissertation (University of Regensburg, **2015**).
- The section 'crystallographic details' was written by Dr. Eugenia Peresyphkina

5.7 References

- [1] a) H. W. Kroto, J. R. Heath, S. C. O'Brien, R. F. Curl, R. E. Smalley, *Nature* **1985**, *318*, 162-163; b) "The Nobel Prize in Chemistry 1996". *NobelPrize.org*. Nobel Media AB 2020. Tue. 1 Sep 2020. <https://www.nobelprize.org/prizes/chemistry/1996/summary/>
- [2] J. M. Hawkins, A. Meyer, T. A. Lewis, S. Loren, F. J. Hollander, *Science* **1991**, *252*, 312.
- [3] a) J. R. Heath, S. C. O'Brien, Q. Zhang, Y. Liu, R. F. Curl, F. K. Tittel, R. E. Smalley, *J. Am. Chem. Soc.* **1985**, *107*, 7779-7780; b) T. Almeida Murphy, T. Pawlik, A. Weidinger, M. Höhne, R. Alcalá, J. M. Spaeth, *Phys. Rev. Lett.* **1996**, *77*, 1075-1078; c) S. Stevenson, G. Rice, T. Glass, K. Harich, F. Cromer, M. R. Jordan, J. Craft, E. Hadju, R. Bible, M. M. Olmstead, K. Maitra, A. J. Fisher, A. L. Balch, H. C. Dorn, *Nature* **1999**, *401*, 55-57; d) K. Komatsu, M. Murata, Y. Murata, *Science* **2005**, *307*, 238.
- [4] R. Chakrabarty, P. S. Mukherjee, P. J. Stang, *Chem. Rev.* **2011**, *111*, 6810-6918.
- [5] D. Zhang, T. K. Ronson, J. R. Nitschke, *Acc. Chem. Res.* **2018**, *51*, 2423-2436.
- [6] T. L. Mako, J. M. Racicot, M. Levine, *Chem. Rev.* **2019**, *119*, 322-477.
- [7] Y. Fang, J. A. Powell, E. Li, Q. Wang, Z. Perry, A. Kirchon, X. Yang, Z. Xiao, C. Zhu, L. Zhang, F. Huang, H.-C. Zhou, *Chem. Soc. Rev.* **2019**, *48*, 4707-4730.
- [8] a) C. J. Brown, F. D. Toste, R. G. Bergman, K. N. Raymond, *Chem. Rev.* **2015**, *115*, 3012-3035; b) M. Han, D. M. Engelhard, G. H. Clever, *Chem. Soc. Rev.* **2014**, *43*, 1848-1860; c) T. R. Cook, Y.-R. Zheng, P. J. Stang, *Chem. Rev.* **2013**, *113*, 734-777.
- [9] a) J.-M. Lehn, *Supramol. Chem.* **1995**, 139-197; b) E. C. Constable, *Pure Appl. Chem.* **1996**, *68*, 253-260.
- [10] a) A. Górczyński, J. M. Harrowfield, V. Patroniak, A. R. Stefankiewicz, *Chem. Rev.* **2016**, *116*, 14620-14674; b) S. Chakraborty, G. R. Newkome, *Chem. Soc. Rev.* **2018**, *47*, 3991-4016; c) Y. Sun, C. Chen, J. Liu, P. J. Stang, *Chem. Soc. Rev.* **2020**, *49*, 3889-3919.
- [11] O. J. Scherer, T. Brück, *Angew. Chem. Int. Ed. Engl.* **1987**, *26*, 59.
- [12] a) J. Bai, A. V. Virovets, M. Scheer, *Angew. Chem. Int. Ed.* **2002**, *41*, 1737-1740; b) S. Welsch, C. Gröger, M. Sierka, M. Scheer, *Angew. Chem. Int. Ed.* **2011**, *50*, 1435-1438; c) F. Dielmann, A. Schindler, S. Scheuermayer, J. Bai, R. Merkle, M. Zabel, A. V. Virovets, E. V. Peresyapkina, G. Brunklaus, H. Eckert, M. Scheer, *Chem. Eur. J.* **2012**, *18*, 1168-1179.
- [13] J. Bai, A. V. Virovets, M. Scheer, *Science* **2003**, *300*, 781-783; b) M. Scheer, J. Bai, B. P. Johnson, R. Merkle, A. V. Virovets, C. E. Anson, *Eur. J. Inorg. Chem.* **2005**, 4023-4026; c) M. Scheer, A. Schindler, J. Bai, B. P. Johnson, R. Merkle, R. Winter, A. V. Virovets, E. V. Peresyapkina, V. A. Blatov, M. Sierka, H. Eckert, *Chem. Eur. J.* **2010**, *16*, 2092-2107.

- [14] a) M. Scheer, A. Schindler, R. Merkle, B. P. Johnson, M. Linseis, R. Winter, C. E. Anson, A. V. Virovets, *J. Am. Chem. Soc.* **2007**, *129*, 13386-13387; b) M. Scheer, A. Schindler, C. Gröger, A. V. Virovets, E. V. Peresyphkina, *Angew. Chem. Int. Ed.* **2009**, *48*, 5046-5049; c) A. Schindler, C. Heindl, G. Balázs, C. Gröger, A. V. Virovets, E. V. Peresyphkina, M. Scheer, *Chem. Eur. J.* **2012**, *18*, 829-835; d) C. Schwarzmaier, A. Schindler, C. Heindl, S. Scheuermayer, E. V. Peresyphkina, A. V. Virovets, M. Neumeier, R. Gschwind, M. Scheer, *Angew. Chem. Int. Ed.* **2013**, *52*, 10896-10899; e) E. V. Peresyphkina, C. Heindl, A. Schindler, M. Bodensteiner, A. V. Virovets, M. Scheer, *Z. Kristallogr. - Cryst. Mater.* **2014**, *229*, 735-740; f) E. Peresyphkina, C. Heindl, A. Virovets, H. Brake, E. Mädl, M. Scheer, *Chem. Eur. J.* **2018**, *24*, 2503-2508; g) C. Heindl, *Dissertation (University of Regensburg)*, **2015**.
- [15] P. Seiler, J. D. Dunitz, *Acta Cryst. Sect. B.* **1980**, *B36*, 2255-2260.
- [16] Calculated by the distance of two furthestmost H atoms (5.675(6) Å) taken from ref. [15] plus twice the van-der-Waals radius of H (1.10 Å), as reported in ref. [17].
- [17] M. Mantina, A. C. Chamberlin, R. Valero, C. J. Cramer, D. G. Truhlar, *J. Phys. Chem. A* **209**, *113*, 5806-5812; and references therein.
- [18] Calculated by the distance of two furthestmost C atoms (7.086(4) Å) taken from ref. [19] plus twice the van-der-Waals radius of C (1.70 Å), as reported in ref. [17].
- [19] A. O'Neil, C. Wilson, J. M. Webster, F. J. Allison, J. A. K. Howard, and M. Poliakoff, *Angew. Chem. Int. Ed.* **2002**, *41*, 3796.
- [20] O. J. Scherer, W. Wiedemann, G. Wolmershäuser, *J. Organomet. Chem.* **1989**, *361*, C11-C14.
- [21] H. Brake, E. Peresyphkina, C. Heindl, A. V. Virovets, W. Kremer, M. Scheer, *Chem. Sci.* **2019**, *10*, 2940-2944.
- [22] Calculated by the distance of two furthestmost H atoms (7.84859(13) Å) taken from ref. [21] plus twice the van-der-Waals radius of H (1.10 Å), as reported in ref. [17].
- [23] Unit cell parameters:
aP, a = 25.98 Å, b = 34.24 Å, c = 42.65 Å, $\alpha = 93.6^\circ$, $\beta = 106.4^\circ$, $\gamma = 90.8^\circ$, V = 36259 Å³, identified as **1*@6*-Cl** by preliminary X-ray diffraction data.
- [24] Hereby, the percentage of **2@6*-Cl** is calculated by the formula $\frac{195 \times f(TD)}{10 \times f(1^*) + 15 \times f(TD)}$, since every 90-vertex spherical host not encapsulating a triple decker molecule is instead encapsulating another molecule of **1***. This formula holds true for every triple decker guest molecule with 10 H atoms and every 90-vertex sphere based on **1***.

- [25] Unit cell parameters:
cP 31.6 Å, $V = 31554 \text{ \AA}^3$ or mC 41.2 Å, 42.3 Å, 29.9 Å; $\beta \approx 90^\circ$; $V = 52108 \text{ \AA}^3$ identified as 80-vertex sphere according to our unpublished data.
- [26] cf. Chapter 3.
- [27] H. Brunner, U. Klement, W. Meier, J. Wachter, O. Serhadle, M. L. Ziegler, *J. Organomet. Chem.* **1987**, 335, 339-352.
- [28] C. Gröger, H. R. Kalbitzer, M. Pronold, D. Piryazev, M. Scheer, J. Wachter, A. Virovets, M. Zabel, *Eur. J. Inorg. Chem.* **2011**, 785-793.
- [29] a) L. J. Gregoriades, G. Balázs, E. Brunner, C. Gröger, J. Wachter, M. Zabel, M. Scheer, *Angew. Chem. Int. Ed.* **2007**, 46, 5966-5970; b) M. Fleischmann, S. Welsch, L. J. Gregoriades, C. Gröger, M. Scheer, *Z. Naturforsch., B: J. Chem. Sci.* **2014**, 69, 1348-1356.
- [30] a) P. Pyykkoe, M. Atsumi, *Chem. Eur. J.* **2009**, 15, 186-197; b) P. Pyykkoe, M. Atsumi, *Chem. Eur. J.* **2009**, 15, 12770-12779.
- [31] Unit cell parameters:
oC 68.7 Å, 37.8 Å, 36.5 Å, $V = 95500 \text{ \AA}^3$ identified as **1*@6*-Cl** by preliminary X-ray diffraction data.
- [32] Unit cell parameters (from toluene / CH₃CN):
aP, a = 25.8 Å, b = 34.3 Å, c = 40.7 Å, $\alpha = 95.6^\circ$, $\beta = 102.6^\circ$, $\gamma = 90.7^\circ$, $V = 34961 \text{ \AA}^3$ identified as ion pair of 90-vertex spheres by comparison to unpublished data.
aP, a = 26.0 Å, b = 34.1 Å, c = 42.7 Å, $\alpha = 93.7^\circ$, $\beta = 106.5^\circ$, $\gamma = 90.6^\circ$, $V = 36318 \text{ \AA}^3$ identified as neutral 90-vertex sphere **6*-Cl** by comparison to unpublished data.
Unit cell parameters (from xylene / CH₃CN):
mC, a = 36.6 Å, b = 26.1 Å, c = 21.6 Å, $\beta = 126.5^\circ$, $V = 16618 \text{ \AA}^3$ identified as anionic 90-vertex sphere $[\text{Cu}(\text{CH}_3\text{CN})_4]^+[\mathbf{1}@\{(\mathbf{1}^*)_{12}(\text{Cu}_{24}\text{Cl}_{25})(\text{CH}_3\text{CN})_8\}]^-$ by preliminary X-ray diffraction data.
Unit cell parameters (from o-DFB / CH₃CN):
mI, a = 49 Å, b = 26 Å, c = 79 Å, $\beta = 102.6^\circ$, $V = 100714 \text{ \AA}^3$ identified as **1*@6*-Cl** by preliminary X-ray diffraction data.
- [33] Unit cell parameters (from xylene / CH₃CN):
aP, a = 22.21 Å, b = 39.22 Å, c = 43.57 Å, $\alpha = 84.8^\circ$, $\beta = 89.98^\circ$, $\gamma = 89.7^\circ$, $V = 37804 \text{ \AA}^3$ identified as **1*@6*-Br** by preliminary X-ray diffraction data.
Unit cell parameters (from o-DFB / CH₃CN):
oI, a = 41.9 Å, b = 49.6 Å, c = 57.3 Å, $V = 119000 \text{ \AA}^3$ identified as **1*@6*-Br** by preliminary X-ray diffraction data.

- [34] Unit cell parameters (from toluene / CH₃CN):
tP, a = 42 Å, b = 42 Å, c = 30 Å, V = 53000 Å³ and hR, a = 42 Å, b = 42 Å, c = 52 Å; V = 80000 Å³.
- [35] Unit cell parameters:
oC, a = 24.1 Å, b = 37.3 Å, c = 72.8 Å, V = 65600 Å³ identified as 90-vertex spheres **6^x-Br** by comparison to unpublished data.
- [36] Hereby, the percentage of **7@6^x-Br** is calculated by the formula $\frac{156 \times f(TD)}{10 \times f(\text{Me groups of } 1^x) + 12 \times f(TD)}$, since every 90-vertex spherical host not encapsulating a triple decker molecule is instead encapsulating another molecule of **1^x**. This formula holds true for every triple decker guest molecule with 10 H atoms and every 90-vertex sphere based on **1^x**.
- [37] Unit cell parameters:
mP, a = 33.76 Å, b = 24.68 Å, c = 34.23 Å, β = 93°, V = 28429 Å³ and mC, a = 33 Å, b = 24 Å, c = 34.3 Å; β = 102.8°, V = 26516 Å³ both identified as (CHCl₃)_m@[{Cp^xFe(η⁵-P₅)}]₁₂{CuCl}_{20-n}] by preliminary X-ray diffraction data.
- [38] M. Fleischmann, C. Heindl, M. Seidl, G. Balázs, A. V. Virovets, E. V. Peresykina, M. Tsunoda, F. P. Gabbai, M. Scheer, *Angew. Chem. Int. Ed.* **2012**, *51*, 9918-9921.
- [39] C. Janiak, *J. Chem. Soc., Dalton Trans.* **2000**, 3885-3896.
- [40] The height of free **7** is calculated by the distance of the Cp planes (6.671(4) Å) plus twice the van-der-Waals radius of C (1.70 Å) as found in ref. [17]. The height of the host core is calculated by the distance of the centroids of the bottom P₅ plane and the top rim of 10 P atoms (**7@3*-Cl**: 9.7392(13) – 9.7517(13) Å, **7@3*-Br**: 9.7195(12) – 9.7337(11) Å) minus the van-der-Waals radius of P (1.80 Å) as found in ref. [17].
- [41] The width of free **7** is calculated by the maximum distance of a P atom and a P/S atom (4.1729(10) Å) plus twice the van-der-Waals radius of P (or S) (1.80 Å). The width of the void of the host aggregates is calculated by the average P...P distance of two opposing P atoms (**7@3*-Cl**: 11.98; **7@3*-Br**: 11.99 Å) minus twice the van-der-Waals radius of P (1.80 Å). Van-der-Waals radii are taken from ref. [17].
- [42] F. Dielmann, M. Fleischmann, C. Heindl, E. V. Peresykina, A. V. Virovets, R. M. Gschwind, M. Scheer, *Chem. Eur. J.* **2015**, *21*, 6208-6214.
- [43] A. K. Hughes, V. J. Murphy, D. O'Hare, *J. Chem. Soc., Chem. Commun.* **1994**, 163-164.
- [44] O. J. Scherer, J. Schwalb, G. Wolmershäuser, W. Kaim, R. Gross, *Angew. Chem. Int. Ed. Engl.* **1986**, *25*, 363-364.

- [45] A. E. Goeta, J. A. K. Howard, A. K. Hughes, D. O'Hare, R. C. B. Copley, *J. Mater. Chem.* **2007**, *17*, 485-492.
- [46] O. J. Scherer, T. Brück, G. Wolmershäuser, *Chem. Ber.* **1988**, *121*, 935-938.
- [47] L. Y. Goh, R. C. S. Wong, W. H. Yip, T. C. W. Mak, *Organometallics* **1991**, *10*, 875-879.
- [48] Pyridine was added in order to dissolve the polymer under disaggregation. After removal of the solvent the products were dissolved in CH₂Cl₂ / CH₃CN.
- [49] A. Burkhardt, T. Pakendorf, B. Reime et al., *Eur. Phys. J. Plus* **2016**, *131*, 56-64.
- [50] *CrysAlisPRO*, different versions **2006-2020**, Rigaku Oxford Diffraction.
- [51] G. M. Sheldrick. *Acta Cryst.* **2015**, *C71*, 3-8.

6 The first Au-containing Coordination Polymers based on Polyphosphorus Ligand Complexes

H. Brake, E. V. Peresykina, A. V. Virovets, W. Kremer, C. Klimas, C. Schwarzmaier, M. Scheer

Abstract:

Whereas the self-assembly of pentaphosphaferrocenes [$\text{Cp}^{\text{R}}\text{Fe}(\eta^5\text{-P}_5)$] ($\text{Cp}^{\text{R}} = \text{Cp}^*$, Cp^{\times} , Cp^{Bn}) with Cu and Ag salts has been well studied in the past, the coordination chemistry towards Au complexes has been left untouched so far. Herein, the results of self-assembly processes of [$\text{Cp}^{\text{R}}\text{Fe}(\eta^5\text{-P}_5)$] with Au salts of different anions (GaCl_4^- , SbF_6^- , TEF^-) are reported. Next to a variety of molecular coordination products, also the first coordination polymers based on polyphosphorus ligand complexes and Au salts are obtained. Thereby, an unprecedented 2D coordination polymer comprising metal vacancies is isolated. In all products, the Au centers are coordinated in a planar fashion. In solution, highly dynamic processes are observed. NMR spectroscopy at variable temperatures, solid state NMR spectroscopy and X-ray powder diffraction were applied to gain further insight in selected coordination compounds.

6.1 Introduction

Coordination-driven self-assembly is a powerful tool for the construction of intricate structures.^[1] On the one hand, a combination of divergent building blocks leads to extended coordination polymers, such as MOFs, finding applications in catalysis^[2] or sensing,^[3] amongst others.^[4] On the other hand, convergent self-assembly may result in discrete aggregates spanning 2D helicates,^[5] grids^[6] and macrocycles^[7] as well as 3D polyhedra,^[8] often resembling Platonic or Archimedean solids. The donor building blocks typically bear N or O donor atoms,^[9] while P or S donor sites are rare.^[10] In recent years, our group focused on coordination-driven self-assembly employing pentaphosphaferrocene-derivatives [$\text{Cp}^R\text{Fe}(\eta^5\text{-P}_5)$] ($\text{Cp}^R = \text{Cp}, \text{Cp}^*, \text{Cp}^\times, \text{Cp}^{\text{Bn}}, \text{Cp}^{\text{BiG}}$) as outstanding organometallic five-fold symmetric donor components. In combination with group 13 metal salts $\text{M}[\text{TEF}]$ ($\text{M} = \text{Ga}, \text{In}, \text{Tl}$; $\text{TEF} = \text{Al}(\text{OC}(\text{CF}_3)_3)_4$) a series of isostructural 1D polymers was obtained.^[11] When using Cu(I) salts of halides or weakly coordinating anions (WCAs) instead, a myriad of 1D to 3D coordination polymers become accessible.^[12] However, depending on the reaction conditions employed, also spherical assemblies are obtained, which partially act as hosts for smaller molecules.^[12b,d,g,h,13] The application of WCAs is of special importance, when aggregates with Ag cations are targeted, since Ag(I) halides are poorly soluble. Thus, also polymeric and spherical assemblies of pentaphosphaferrocenes and Ag cations have been reported.^[12e,14] Thereby, the coinage metal ion is not coordinatively saturated by the anion anymore, but instead, either all coordination sites are occupied by the *cyclo*- P_5 ligand complex or additional coordination of a labile ligand (e.g. by benzyl groups or acetonitrile) is observed. However, instead of acetonitrile, also ditopic flexible dinitriles may act as a third component in self-assembly. With ditopic dinitrile linkers, even polymeric assemblies of spherical supramolecules have been obtained for the first time.^[14b,15] Despite this versatility of the supramolecular chemistry of pentaphosphaferrocenes with Cu and Ag, remarkably, no supramolecular assemblies based on pentaphosphaferrocenes and Au have been reported so far.

In general, coordination polymers have been obtained from multitopic phosphines^[16] or phospholes^[17] and Au precursors. On the contrary, concerning P_4 and polyphosphorus (P_n) complexes, less Au coordination compounds are known. Reactions of Au(I)Cl species with a chloride abstractor (e.g. GaCl_3 or LiTEF) and P_4 led to discrete coordination compounds.^[18] Interestingly, Forfar et al. performed similar reactions with Cu and Ag salts as well.^[18a] While the reactions of CuCl and AgOTf (OTf = O_3SCF_3), respectively, with GaCl_3 and P_4 led to the formation of coordination polymers based on coordinating GaCl_4 units and/or Cu- P_4 coordination bonds,

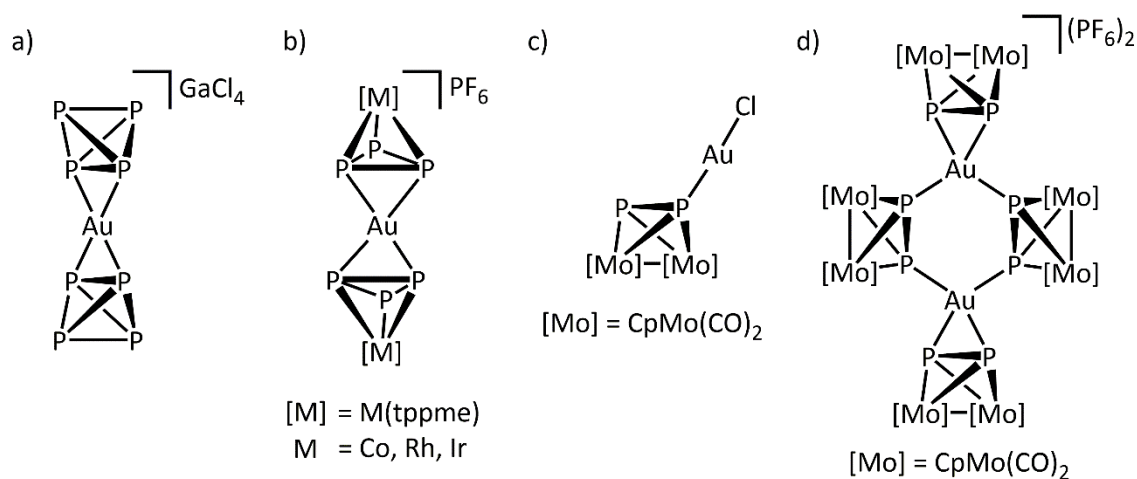


Figure 1. Examples of coordination complexes in which P_4 or a P_n ligand complex coordinates to Au.

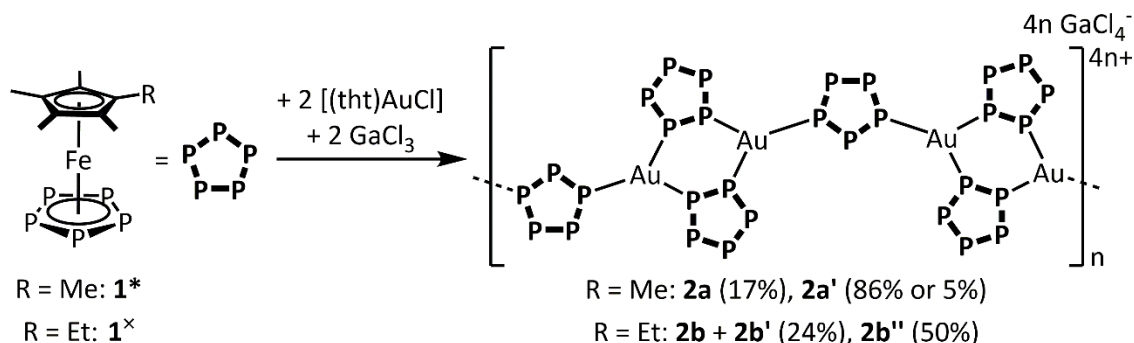
the analogous reaction with AuCl gave the homoleptic complex $[\text{Au}(\text{P}_4)_2]^+$ with a non-coordinating GaCl_4 counterion (Figure 1a). Stoppioni and Peruzzini have reported on the first examples of Au coordination to P_n ligand complexes.^[19] The reactions of $[\text{M}(\text{tppme})\text{P}_3]$ ($\text{M} = \text{Co, Rh, Ir}$; tppme = 1,1,1-tris(diphenylphosphinomethyl)ethane) with $[(\text{L})\text{AuCl}]_n$ ($\text{L} = \text{PMe}_3, \text{PPh}_3, n = 1$; $\text{R} = \{\text{Ph}_2\text{P}(\text{CH}_2)_x\text{PPh}_2\}_{0.5}$ with $x = 1, 2, n = 2$) and TIPF_6 as a Cl^- abstractor yielded isomeric mononuclear complexes (Figure 1b). Therein, two P_3 complexes each act as terminal ligands to an Au cation resulting in a discrete cationic coordination compound. Later, our group reported on the reactions of the P_2 ligand complex $[\{\text{CpMo}(\text{CO})_2\}_2(\mu, \eta^2\text{-P}_2)]$ with Au precursors.^[20] While the reactions with $[\text{LAuCl}]$ ($\text{L} = \text{CO}$ or tetrahydrothiophene (tht)) led to the end-on coordination of the P_2 complex to a $\{\text{AuCl}\}$ moiety (Figure 1c), the reaction with $[(\text{PPh}_3)\text{Au}(\text{thf})]\text{PF}_6$ (generated *in situ* from $[(\text{PPh}_3)\text{AuCl}]$, TIPF_6 and tetrahydrofuran) yielded a dicationic supramolecular coordination compound (Figure 1d), in which for the first time a P_n ligand complex bridges two Au centers.

Since the supramolecular chemistry of pentaphosphaferrocenes $[\text{Cp}^{\text{R}}\text{Fe}(\eta^5\text{-P}_5)]$ ($\text{Cp}^{\text{R}} = \text{Cp}^*$ ($\mathbf{1}^*$), Cp^\times ($\mathbf{1}^\times$), Cp^{Bn} ($\mathbf{1}^{\text{Bn}}$))^[21] with Cu and Ag salts is exceedingly versatile, the question arises, as to whether supramolecular aggregates can also be obtained with Au. Herein, we report on the self-assembly of $\mathbf{1}^*$, $\mathbf{1}^\times$ and $\mathbf{1}^{\text{Bn}}$ with Au salts of GaCl_4^- , SbF_6^- and TEF^- . Thereby, next to monomeric and dimeric coordination compounds, a series of supramolecular coordination polymers (1D and 2D) is obtained. These represent the first examples of coordination polymers based on polyphosphorus ligand complexes and Au. All products were extensively characterized by single crystal X-ray diffraction analysis, NMR spectroscopy, mass spectrometry and elemental analysis. Where appropriate, X-ray powder diffraction, MAS- and VT-NMR spectroscopy were applied as well.

6.2 Results and Discussion

Coordination Behavior of **1** towards AuGaCl₄

Following the synthesis of [(P₄)₂Au]GaCl₄ (Figure 1a),^[18a] when a mixture of [Cp*Fe(η⁵-P₅)] (**1***),^[21a] [(tth)AuCl] and GaCl₃ is stirred in CH₂Cl₂ and layered with toluene (method A), yellow-brown crystals of 1D polymeric [(Cp*Fe(η⁵-P₅))₃Au₂]_n(GaCl₄)_{2n} · 0.5n C₇H₈ · 0.15n CH₂Cl₂ (**2a**) are formed in 17% yield (Scheme 1).



Scheme 1. Reactions of **1*** and **1**^x, respectively, with [(tth)AuCl] and GaCl₃. The 1D polymeric products are represented by two repeating units without solvate molecules.

Astonishingly, **2a** constitutes the first coordination polymer based on a P_n ligand complex and Au. It is built up from {Cp*Fe(η⁵-P₅)}₂Au₂ moieties with 1,2-coordinated units of **1*** interconnected by the third, 1,3-coordinated moiety of **1***. This is similar to the structure of the 1D polymers [(Cp*Fe(η⁵-P₅))₄Cu₂]_n(WCA)_{2n} (WCA = TEF, FAI; FAI = FAI{OC₆F₁₀(C₆F₅)₃}), in which an additional 1,2-coordinated unit of **1*** leads {Cp*Fe(η⁵-P₅)}₃Cu₂ moieties interconnected by 1,3-coordinated units of **1*** and thus to a tetrahedral coordination environment of Cu.^[12f] In the analogous reaction with [Cp^xFe(η⁵-P₅)] (**1**^x),^[21b] the isotypic compound [(Cp^xFe(η⁵-P₅))₃Au₂]_n(GaCl₄)_{2n} · 0.5n C₇H₈ · 0.35n CH₂Cl₂ (**2b**) crystallizes at first, while after few days also a polymorph **2b'** is formed, with a combined yield of 24%. The yields in both cases are underestimated since the isolation of pure **2a** or **2b/2b'** is only feasible by taking the crystals from the Schlenk wall with a spatula before complete diffusion. Otherwise, an insoluble precipitate is formed which cannot be separated from the product and leads to a higher S content according to elemental analysis.^[22] However, the isolable yields may be increased by changing the synthesis methods. After addition of one equivalent of THT to [(tth)AuCl] and GaCl₃ and subsequent stirring in *o*-difluorobenzene (*o*-DFB), this reaction mixture is filtered and layered with a toluene solution of **1*** (method B). Then, **2a** crystallizes as a solvatomorph [(Cp*Fe(η⁵-P₅))₃Au₂]_n(GaCl₄)_{2n} · 1.6n C₇H₈ · 0.4n *o*-C₆H₄F₂ (**2a'**) in up to 86% yield. Furthermore, **2a'** is accessible by a third method though in lower yields. One equivalent of THT is added to a mixture of [(tth)AuCl], GaCl₃ and **1***, reacted in *o*-DFB and layered with toluene (method C). With **1**^x, crystals of **2b''** with similar unit cell constants as **2b'** are formed by method B in 50% yield,^[23]

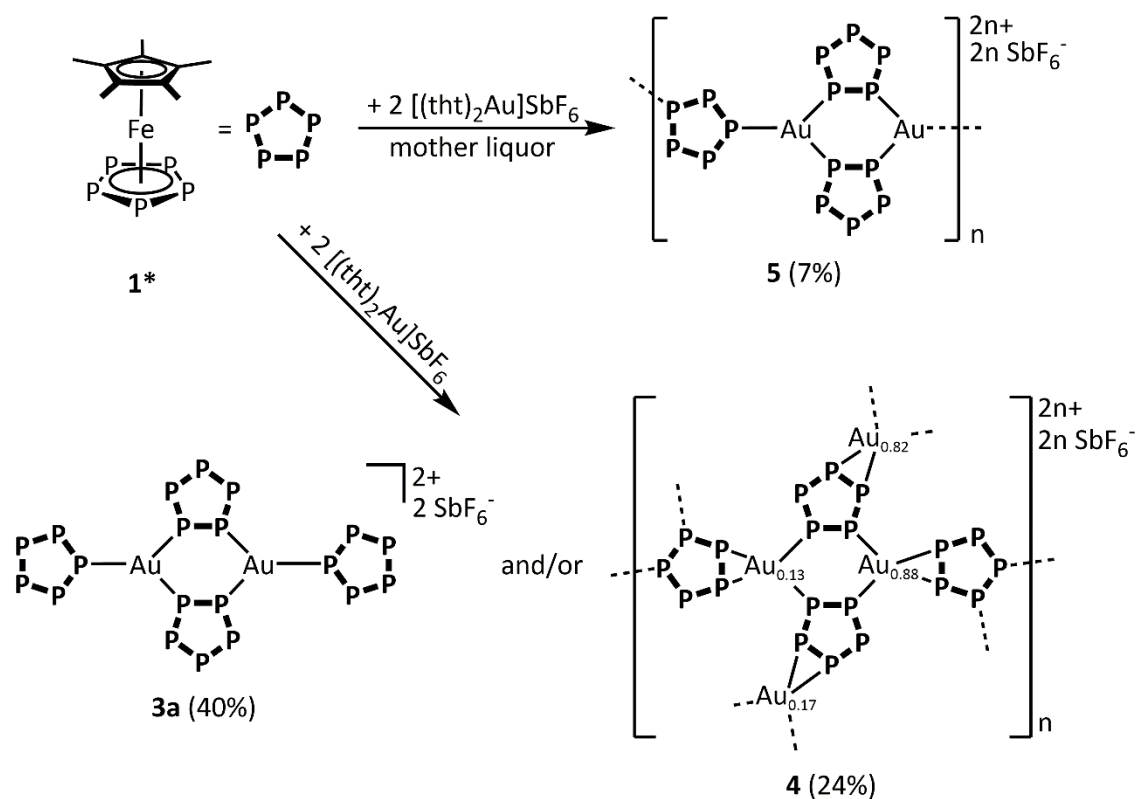
thus presumably constituting a solvatomorph of **2b'**. Again yields are underestimated due to incomplete crystallization as indicated by the $^{31}\text{P}\{\text{H}\}$ NMR spectra of the mother liquors, which show broad signals at 115 ppm (in reactions with **1***) and 117 ppm (in reactions with **1^x**) attributed to coordinated **1*** and **1^x**, respectively. The products may contain THT as solvate molecules which can be removed by washing with CH_2Cl_2 .

In an attempt to synthesize spherical assemblies with **1^x** and Au, the reactions were also carried out in the presence of *o*- $\text{C}_2\text{B}_{10}\text{H}_{12}$ or $[\text{CoCp}_2]\text{PF}_6$. Both compounds have been applied successfully as templates for spherical assemblies based on Cu(I)halides and **1*** or **1^x** and do not bear the risk to reduce Au(I) to Au(0).^[13d,h,i] Still, the only characterizable products were **2b** and **2b'**. Since the ratio of **1^x** to Au in compounds **2** only amounts to 3:2, the question arose whether different products are formed in case 4 or 6 equivalents of Au salt were applied, but again only **2b** and **2b'** crystallized.

Coordination Behavior of **1** towards AuSbF_6

When a solution of *in situ* generated $[(\text{tth})_2\text{Au}]\text{SbF}_6$ ^[24] in CH_2Cl_2 is layered with a solution of **1*** in toluene, brown prisms and plates of $[\{\text{Cp}^*\text{Fe}(\eta^5\text{-P}_5)\}_4\text{Au}_2](\text{SbF}_6)_2$ crystallize concomitantly as a dimer (**3a**) and a 2D polymer (**4**) being structural isomers (Scheme 2, for yields *vide infra*). After few days, also brown rods of the 1D polymer $[\{\text{Cp}^*\text{Fe}(\eta^5\text{-P}_5)\}_3\text{Au}_2]_n(\text{SbF}_6)_{2n} \cdot 2n \text{C}_7\text{H}_8$ (**5**) crystallize. Crystals of **5** are selectively obtained when layering the mother liquor again with toluene to give 7% yield. Compound **3a** is built up from $\{\text{Cp}^*\text{Fe}(\eta^5\text{-P}_5)\}_2\text{Au}_2$ moieties similarly to the abovementioned polymers **2**. However, terminally coordinating **1*** moieties impede further aggregation and are reminiscent of the structure of the dimeric $[\{\text{CpMo}(\text{CO})_2\}_2(\mu, \eta^2\text{-P}_2)]$ based compound in Figure 1d. With compound **4**, also the synthesis of a two-dimensional coordination polymer of a P_n ligand complex and Au is achieved for the first time. Moreover, the structure of compound **5** is reminiscent of the 1D polymers **2**.

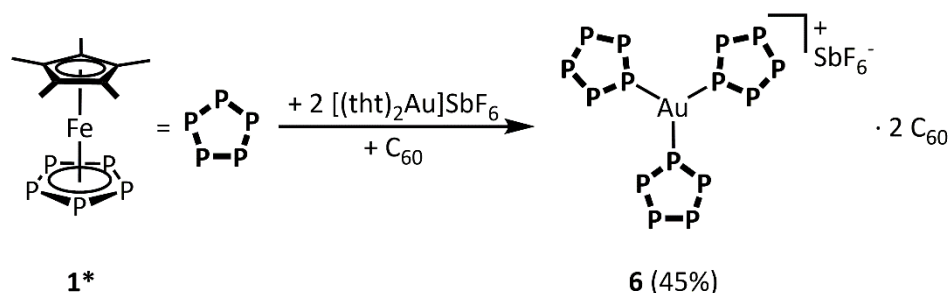
Compounds **3a** and **4** cannot be separated due to similar crystal habits and solubilities. However, while **3a** and **4** are soluble in CH_2Cl_2 and insoluble in CH_3CN , for compound **5** the opposite is the case. Hence, **5** can be dissolved to get a mixture of **3a** and **4**, or the latter two are dissolved to give pure **5**. Since **5** is always obtained by further crystallization from the mother liquors, its deliberate direct synthesis was also targeted by applying more diluted reaction conditions, but still **4** was obtained at first. Moreover, as in the 2D polymer **4** four Au positions are occupied by a total of two Au atoms, the question arose whether **4** can also be synthesized with more Au incorporated into the polymeric network. Thus, the reaction was carried out in a **1***:Au ratio of 1:4, but surprisingly only the dimer **3a** and subsequently the 1D polymer **5** are



Scheme 2. Reaction of **1*** with 2 eq. of $[(tth)_2Au]SbF_6$. The polymeric structures are represented by one (**4**) or two (**5**) repeating units without solvate molecules.

formed. The formation of **3a** vs. **4** could neither be controlled by variation of the concentration. Luckily, the pure crystallization of **3a** was observed once in 40% yield. Also, the pure crystallization of **4** (with minor amounts of **5** sorted out under the microscope) was achieved once in 24% yield. Remarkably, the elemental analysis of crystals of **4** also fits to an overall sum formula of $\{[Cp^*Fe(\eta^5-P_5)]_4Au_2\}(SbF_6)_2$, thus no variation of the Au content seems to be possible.

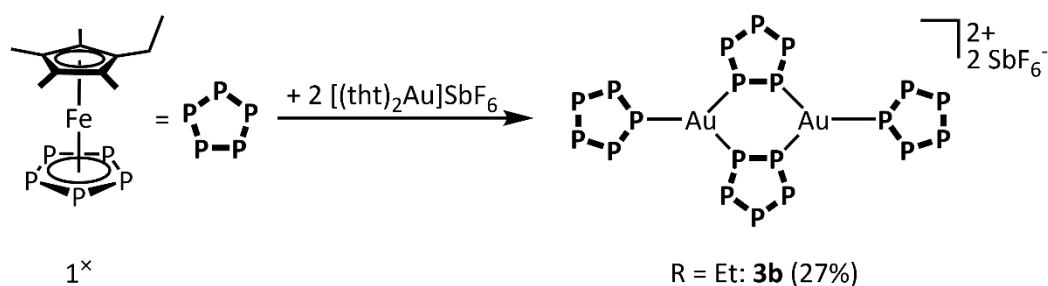
Again, also the synthesis of spherical assemblies was aimed at by adding a potential template. Reactions of **1*** and $[(tth)_2Au]SbF_6$ in the presence of $o\text{-C}_2\text{B}_{10}\text{H}_{12}$ or P_4S_3 only led to the formation of **3a** and **4**. In a further attempt, the choice fell on C_{60} as potential template, since it represents the largest species successfully encapsulated by a spherical assembly of **1*** and Cu(I) halides so far.^[13c] A potentially formed larger host sphere of **1*** and Au would require less deviation from an intrinsic planar coordination environment of both building blocks. Hence, **1*** and C_{60} were dissolved in *o*-dichlorobenzene (*o*-DCB). Toluene was added to change the density and enable layering onto a solution of freshly prepared $[(tth)_2Au]SbF_6$ ^[24] in CH_2Cl_2 . Thereby, large black prisms of $\{[Cp^*Fe(\eta^5-P_5)]_3Au\}(SbF_6) \cdot 2 C_{60}$ (**6**) crystallize in very low yield (Scheme 3). Subsequently layering the concentrated mother liquor with toluene only resulted in the crystallization of the 1D polymer **5**. Instead, the yield of **6** can be improved by increasing the concentration of the layering experiment in the first place, whereby the solubility of C_{60} is the



Scheme 3. Reaction of **1*** with 2 eq. of $[(tth)_2Au]SbF_6$ in the presence of C_{60} .

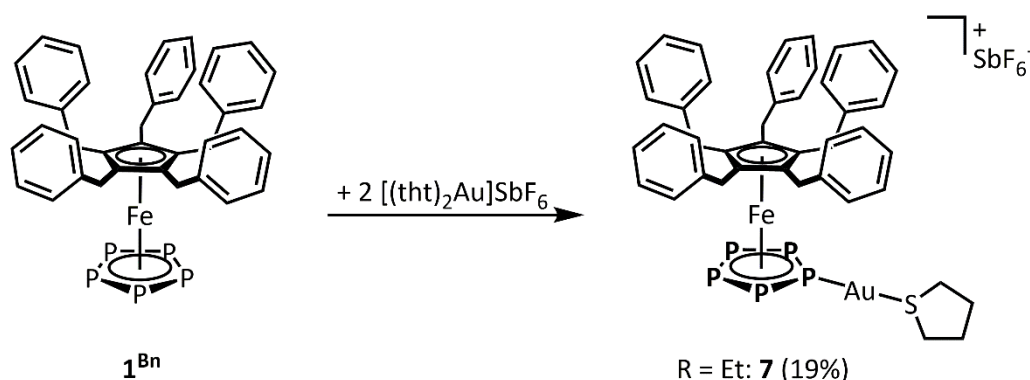
limiting factor. Hence, **1*** and C_{60} were dissolved in a minimum of *o*-dichlorobenzene (*o*-DCB) with the aid of sonication and only a minor amount of xylenes (which is known to be a good solvent for C_{60} as well)^[25] was applied for adjustment of the density instead of toluene. As a result, the yield was improved to 45%. In compound **6** only one Au center is coordinated by three units of **1***, each acting as a terminal ligand. The resulting coordination complex co-crystallizes with two molecules C_{60} .

Moreover, the self-assembly of **1*** with $[(tth)_2Au]SbF_6$ was studied. Layering a freshly prepared solution of $[(tth)_2Au]SbF_6$ in CH_2Cl_2 with a solution of **1*** in toluene, leads to the crystallization of orange-brown plates of $\{[Cp^xFe(\eta^5-P_5)]_4Au_2\}(SbF_6)_2$ (**3b**) in 27% yield (Scheme 4), comprising a dimeric structure similar to that of **3a**. Again the yield is underestimated due to incomplete crystallization as shown by the presence of a broad signal at 115 ppm in the $^{31}P\{^1H\}$ NMR spectrum of the mother liquor, corresponding to coordinated **1***. Remarkably, the synthesis is much more selective than the reaction starting from **1*** and no polymeric products like **4** or **5** are found. This might be due to the better solubility of **1***, rather leading to molecular products than polymers.



Scheme 4. Reaction of **1*** with 2 eq. of $[(tth)_2Au]SbF_6$.

For the reaction with **1^{Bn}**, a solution of $[(tth)_2Au]SbF_6$ in CH_2Cl_2 was added to a solution of **1^{Bn}** in CH_2Cl_2 and stirred. After layering with pentane, greenish-brown rods of $\{[Cp^{Bn}Fe(\eta^5-P_5)]Au(tth)\}(SbF_6) \cdot 0.625 CH_2Cl_2$ (**7**) crystallized from the red-brown mother liquor in 19% yield (Scheme 5).

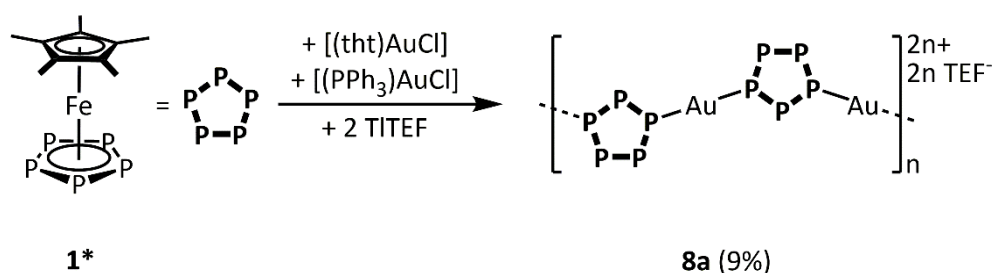


Scheme 5. Reaction of 1^{Bn} with 2 eq. of $[(tth)_2Au]SbF_6$.

In the $^{31}\text{P}\{^1\text{H}\}$ NMR spectrum of the mother liquor, only a sharp singlet at 162 ppm corresponding to uncoordinated 1^{Bn} is observed. The low yield can be rationalized by the additional formation of red oil, settling at the bottom of the Schlenk, and in more diluted reactions even lower yields and more oil are obtained. In this case, the ^1H and $^{31}\text{P}\{^1\text{H}\}$ NMR spectra of the reaction mixture (incl. oil) are reminiscent of the spectra of the dissolved crystals of **7**, thus suggesting its quantitative formation. In contrast to the reactions with 1^* and 1^x , only one of the tht ligands in $[(tth)_2Au]SbF_6$ is replaced by the P_n ligand complex. With 1^{Bn} acting as a terminal ligand, the Au atom is only two-coordinate. The Bn residues of 1^{Bn} also lead to an enhanced solubility of the product, which is why it can only be crystallized by layering with pentane instead of toluene.

Coordination Behavior of **1** towards AuTEF

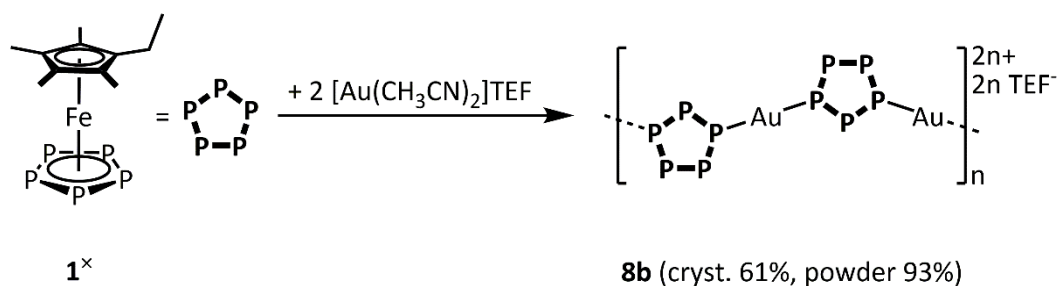
When $[(tth)AuCl]$, $[(PPh_3)AuCl]$, TITEF and 1^* are reacted in CH_2Cl_2 , layered with hexane and stored at -30°C , yellow-brown needles of 1D polymeric $[\{Cp^*Fe(\eta^5-P_5)\}Au]_n(TEF)_n$ (**8a**) crystallize reproducibly in 9% yield (Scheme 6). In contrast to the 1D polymers with $GaCl_4^-$ and SbF_6^- counterions (**2a**, **2b**, **5**), **8a** comprises only 1,3-coordinated pentaphosphaferrocene units and only two-coordinate Au centers. This may be caused by the steric demand of the large TEF $^-$ counterion.



Scheme 6. Reaction of 1^* with $[(tth)AuCl]$, $[(PPh_3)AuCl]$ and 2eq. TITEF.

In order to increase the yield of **8a**, **1*** should be directly reacted with isolable, room temperature stable $[\text{Au}(\text{CH}_3\text{CN})_2]\text{TEF}$.^[26] Therefore, the synthesis of $[\text{Au}(\text{CH}_3\text{CN})_2]\text{TEF}$ was altered with respect to the applied ratio of Au(0) powder to NOTEF. When an excess of NOTEF is applied as described in literature, or the conversion is incomplete with unreacted NOTEF still in solution, it cannot be separated from the desired $[\text{Au}(\text{CH}_3\text{CN})_2]\text{TEF}$ salt due to similar solubility. Hence, only 0.75 equivalents of NOTEF were reacted with Au(0) powder for several weeks, leading to the isolation of pure $[\text{Au}(\text{CH}_3\text{CN})_2]\text{TEF}$.

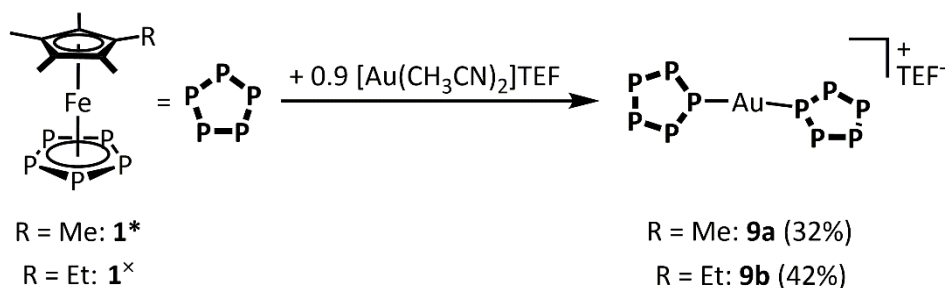
When **1*** was reacted with $[\text{Au}(\text{CH}_3\text{CN})_2]\text{TEF}$ in CH_2Cl_2 , unfortunately, rapid precipitation was observed. The precipitate was merely soluble in CH_3CN , but all attempts to recrystallize from this solution remained unfruitful. Since supramolecular products of **1*** tend to be more soluble than the often isostructural **1*** based counterparts, the analogous reaction was performed with **1^x**. The reaction mixture is filtered quickly after stirring for only ten minutes to avoid precipitation. Layering with pentane indeed results in the crystallization of yellow-orange rods of $\{[\text{Cp}^x\text{Fe}(\eta^5\text{-P}_5)]\text{Au}_n(\text{TEF})_n$ (**8b**), a 1D polymer isotypic to **8a**, in 61% yield (Scheme 7).



Scheme 7. Reaction of **1^x** with 2 eq. of $[\text{Au}(\text{CH}_3\text{CN})_2]\text{TEF}$.

Nevertheless, most attempts to reproduce the synthesis of crystalline **8b** were hampered due to rapid precipitation from the reaction mixture. The precipitate was analyzed exemplarily from the reaction with **1^x** and was shown to be 1D polymer **8b** by NMR, elemental analysis and X-ray powder diffraction. Hence, **8b** is accessible as a precipitate in an astonishing 93% yield.

Precipitation of **8a** and **8b** is avoided, when the reactions of **1*** and **1^x** with $[\text{Au}(\text{CH}_3\text{CN})_2]\text{TEF}$ are performed more concentrated and with a deficiency of $[\text{Au}(\text{CH}_3\text{CN})_2]\text{TEF}$ (<1eq.). Then, the red solution can be stirred even for one day without significant precipitation. Layering with pentane leads to crystallization of brown rods of $\{[\text{Cp}^*\text{Fe}(\eta^5\text{-P}_5)]_2\text{Au}\}(\text{TEF})$ (**9a**, 32% yield) and isotypic compound $\{[\text{Cp}^x\text{Fe}(\eta^5\text{-P}_5)]_2\text{Au}\}(\text{TEF})$ (**9b**, 42% yield), respectively (Scheme 8).



Scheme 8. Reactions of **1*** and **1^x** with <1 eq. of $[\text{Au}(\text{CH}_3\text{CN})_2]\text{TEF}$.

In contrast to dimeric compounds **3a** and **3b** obtained with SbF_6^- counterions, the structure of **9a** rather can be described as two weakly interacting, nearly linear $\{\text{Cp}^{\text{R}}\text{Fe}(\eta^5\text{-P}_5)\}_2\text{Au}$ units. Crystals of **9b** were of insufficient quality for single crystal X-ray characterization but were nevertheless identified by similar unit cell constants as **9a**.^[27] Its identity is further confirmed by elemental analysis and similar solubility properties as **9a** while featuring different solubility than the 1D polymer **8b**. For both **9a** and **9b**, yields are underestimated due to incomplete crystallization, as shown by the presence of a broad signal at 130 ppm and 125 ppm in the $^{31}\text{P}\{^1\text{H}\}$ NMR spectra of the mother liquors, corresponding to coordinated **1*** and **1^x**, respectively.

Solid state characterization of the Coordination Compounds

In the following, the solid-state structures of compounds **2a** – **9a** will be described sorted by their dimensionality. Selected bond lengths and angular sums around Au centers are given in table 1. Table 1 also lists short intermolecular $\text{Au}\cdots\text{P}$ contacts found in **9a**. In all structures, the Au-P bond lengths are close to the sum of the covalent radii (2.43 Å),^[28] and the P-P bond lengths are similar to the ones reported for uncoordinated complexes **1***,^[14a] **1^x**,^[21b] and **1^{Bn}**,^[21c] if not described otherwise. The coordination geometry around the Au centers is nearly linear (**7**, **8a**, **8b**, **9a**) or trigonal planar (**2a**, **2a'**, **2b**, **2b'**, **3a**, **3b**, **5**, **6**) with an angular sum close to 360°, thereby being more or less distorted trigonal (individual bond angles may deviate from 120°). The only exception thereof is compound **4** and its structure will be discussed separately. Moreover, in most compounds (**2a'**, **2b'**, **3a**, **4**, **5**, **7**, **8a**, **8b**, **9a**) short $\text{Au}\cdots\text{H}$ contacts in the range of 2.51 – 2.98 Å are found,^[29] partially accompanied by a tilt of the P_5 ligand complex towards the respective Au-P bond, leading to out-of-(P_5)plane coordination of Au.

Table 1. Selected bond lengths in compounds **2** – **9** compared to reported bond lengths of **1***, **1^x**, **1^{Bn}**. Angular sums for threefold coordinated Au centers (**2** – **6**) or bond angles for twofold coordinated Au centers (**7** – **9**).

Compound	P-P bond lengths [Å]	Au-P bond lengths [Å] (Au-S bond lengths [Å])	angular sums or bond angles
1* [14a]	2.116(2) – 2.127(2)	-	-
1^x [21b]	2.088(3) – 2.108(3)	-	-
1^{Bn} [21c]	2.1083(3) – 2.1121(8)	-	-
2a	2.100(2) – 2.125(2)	2.3218(17) – 2.3971(17)	359.91(12)° (Au1) 359.89(12)° (Au2)
2a'	2.0996(13) – 2.1235(17)	2.3273(9) – 2.3737(10)	359.78(9)° (Au1) 359.70(9)° (Au2)
2b	2.1007(16) – 2.1281(18)	2.3255(11) – 2.3948(11)	359.82(12)° (Au1) 359.94(12)° (Au2)
2b'	2.096(2) – 2.128(2)	2.3146(14) – 2.3984(14)	359.91(15)° (Au1) 359.86(15)° (Au2)
3a	2.103(2) – 2.121(3)	2.3475(16) – 2.3739(14)	359.46(15)° (Au1) 359.44(16)° (Au2)
3b	2.105(2) – 2.127(2)	2.3505(13) – 2.3890(15)	359.49(15)°
4	2.0985(17) – 2.1368(16) 2.142(2) – 2.2633(16) ^[a]	2.3016(18) – 2.5560(18) 2.2710(17) – 2.5146(18) ^[b]	-
5	2.090(3) – 2.138(12)	2.3238(16) – 2.3882(15)	359.49(15)° (Au1) 359.13(18)° (Au2)
6	2.1051(16) – 2.130(3)	2.3062(14) – 2.3687(10)	359.28(11)°
7	2.102(3) – 2.119(3)	2.242(2) – 2.338(3) (2.327(4) – 2.332(7))	170.04(10)° (Au1) 175.0(2)° (Au1A)
8a	2.103(3) – 2.116(4)	2.288(2) – 2.291(2)	175.67(10)°
8b	2.097(3) – 2.115(2)	2.2827(15) – 2.2875(14)	176.11(6)° (Au1) 177.18(6)° (Au2)
9a	2.094(2) – 2.1235(17)	2.2886(11) – 2.3058(11) 2.9903(13) – 3.262 ^[c]	165.06(4)° (Au1) 163.17(5)° (Au2)

[a] η^2 -coordinated P-P bonds (cf. Table 2 for more details); [b] η^2 -(P-Au) bonds lengths; [c] distances of short Au...P contacts.

Monomeric and dimeric compounds (**3a**, **3b**, **6**, **7**, **9a**)

The dimeric compound **3a** crystallizes in the triclinic space group $P\bar{1}$ with two crystallographically unique molecules in the centers of symmetry. In contrast, the similar **1^x**-based compound **3b** crystallizes in the monoclinic space group $P2_1/c$ with one unique molecule in the inversion center. Both compounds are built up from $\{\text{Cp}^R\text{Fe}(\eta^5\text{-P}_5)\}_2\text{Au}_2$ ($\text{Cp}^R = \text{Cp}^*$, Cp^x) moieties with 1,2-coordinated pentaphosphaferrocenes, thus forming $\{\text{P}_4\text{Au}_2\}$ six-membered rings (Figure 2a, b). This motif is well known for Cu or Ag.^[12,13,14] The Au atoms are further coordinated by terminal, η^1 -coordinating **1*** or **1^x** units. This is in contrast to the structure of the $[\{\text{CpMo}(\text{CO})_2\}_2(\mu, \eta^2\text{-P}_2)]$ based compound shown in Figure 1d,^[20] where the

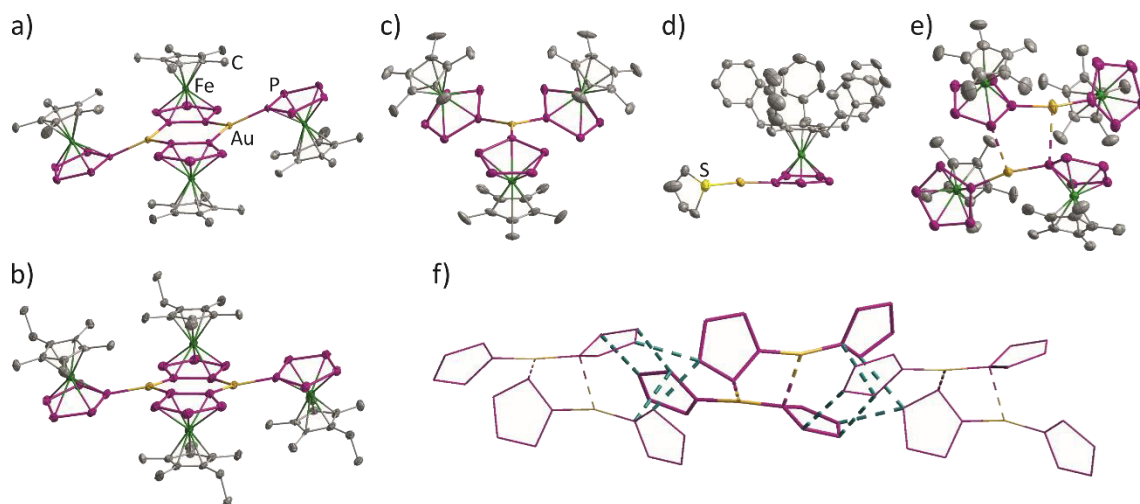


Figure 2. Molecular structures of **3a** (a), **3b** (b), **6** (c), **7** (d) and **9a** (e) in the solid state. H atoms, solvent and C_{60} molecules, counterions and minor parts of disorder omitted for clarity. Dashed lines in e) and f) illustrate the short Au...P (yellow-pink) and P...P interactions (turquoise) interconnecting the monomers.

terminal P_2 ligand complexes coordinate in a side-on η^2 -fashion. In **3b**, the P_5 planes of 1,2-coordinating 1^* are 7.5° tilted towards the P_4Au_2 plane. In one unique molecule of **3a**, the bridging 1^* units are tilted more towards the P_4Au_2 plane (angle P_5 plane – P_4Au_2 plane: 10.6°), enabling close Au...H contacts (Au1...H20C: 2.97 \AA) to Cp^* protons of the bridging 1^* units. In the second unique molecule of **3a**, additionally, close Au2...H39A contacts (2.91 \AA) to the terminal 1^* units are formed, which are not twisted around the Au-P bond anymore. This leads to a more pronounced chair conformation of the $\{P_4Au_2\}$ ring (Figure 1a), presumably to avoid steric repulsion between the Cp^* ligands of terminal and bridging units of 1^* . The coordination geometry of the Au atoms in **3a** and **3b** is best described as trigonal planar with angles merely deviating from 120° and an angular sum very close to 360° (cf. table 1).

The monomeric compound **6** crystallizes in the orthorhombic space group $Pnma$ with half a formula unit in the asymmetric unit. The molecule lies on a mirror plane as well as both co-crystallizing molecules of C_{60} and the major part of the SbF_6^- counterion. Three units of 1^* coordinate terminally in an η^1 -fashion to the central Au atom (Figure 2c). While the two symmetry-related ligand complexes coordinate in-plane (distance Au... P_5 plane: $0.102(2) \text{ \AA}$), the third P_5 complex is tilted (distance Au... P_5 plane: $0.585(2) \text{ \AA}$), although no close Au...H contacts are found. The P-Au-P bond angles amount to $129.85(3)^\circ$ and $99.58(5)^\circ$, the latter being the angle between the symmetry-related units of 1^* . Nevertheless, the coordination geometry around the Au center is nearly planar with an angular sum of $359.28(11)^\circ$ (cf. table 1). The two C_{60} molecules are disordered over four and eight positions, respectively, and only few of the P...C distances ($> 3.38 \text{ \AA}$, as found for P11-C320) fall below the sum of the van der Waals radii (3.50 \AA).^[30] Hence, the absence of significant π -interactions allows for the rotational disorder of the C_{60} molecules even at 14 K.

Compound **7** crystallizes in the monoclinic space group $P2_1/n$ with one crystallographically unique molecule in general position. Here, the Au atom is only coordinated by one tht ligand and one unit of 1^{Bn} (Figure 2d). The Au(tht) moiety is disordered over two positions with resulting P-Au-S bond angles amounting to $170.04(10)^\circ$ or $175.0(2)^\circ$. Moreover, the Au(tht) unit is also tilted towards the Cp^{Bn} ligand resulting in an out-of-plane P-Au coordination (distances Au \cdots P₅ plane: 0.102(3) and 0.421(4) Å). This is more pronounced for the minor Au(tht) position, which hence exhibits a short Au \cdots H contact (Au1A \cdots H13A: 2.797 Å) to one of the CH₂ protons of the Cp^{Bn} ligand. The Au-P (2.242(2) and 2.338(3) Å) and Au-S (2.327(4) and 2.332(7) Å) bond lengths are close to the sum of the covalent radii (Au-P: 2.43 Å, Au-S 2.41 Å).^[28]

Compound **9a** crystallizes in the monoclinic space group $C2/c$. In the asymmetric unit, two nearly linear ($165.06(4)^\circ$ and $163.17(5)^\circ$) monocations $\{Cp^*Fe(\eta^5-P_5)\}_2Au$ are found (Figure 2e). The monomers comprise short intermolecular Au \cdots P contacts (2.9903(13) and 3.262(1) Å; Table 1), that considerably exceed the sum of the covalent radii (Au-P: 2.43 Å)^[28] and can at best be described as weak interactions, leading to a dimeric structure. Also taking these Au \cdots P interactions into account, the coordination geometry around the Au atoms is still almost planar (Table 1). Additionally, a short Au \cdots H contact (Au1 \cdots H18A: 2.89 Å) is found for one of the 1^* units, which exhibits the largest deviation from in-plane coordination of Au (distance Au \cdots P₅ plane: 0.556(2) Å). Furthermore, short P \cdots P contacts are found with distances 3.291(2) – 3.561(2) Å falling below the sum of the van der Waals radii (3.60 Å),^[30] through which the dimers are interconnected to 1D strands (Figure 2f).

1D polymeric compounds (**2a**, **2a'**, **2b**, **2b'**, **5**, **8a**, **8b**)

Compound **2a** crystallizes in the triclinic space group $P\bar{1}$ with one $\{Cp^*Fe(\eta^5-P_5)\}_3Au_2$ repeating unit, two GaCl₄ counterions and disordered solvent molecules toluene and CH₂Cl₂ with partial occupancies (0.5 and 0.15) per asymmetric unit (Figure 3a). With 1^* , the isotypic compound **2b** crystallizes with 0.5 toluene and 0.35 CH₂Cl₂ solvent molecules per formula unit instead. Moreover, a polymorph **2b'** is obtained after longer diffusion times, merely differing in the positions of the Et groups and the solvate molecules. **2b'** crystallizes in the monoclinic space group $P2_1/c$. From *o*-DFB reactions with 1^* , **2a'** crystallizes as a solvatomorph of **2a** in the orthorhombic space group $Pbca$. Compound **5** is isotypic to **2a'**, with SbF₆⁻ counterions instead of GaCl₄⁻ counterions and 2 toluene solvate molecules instead of 1.6 toluene and 0.4 *o*-DFB per formula unit (Figure 3d). All five structures of **2** and **5** constitute waved 1D polymeric chains. In the structures of **2a**, **2b** and **2b'** the polymer chains stack in a similar manner (Figure 3b,c), but different to the ones in **2a'** and **5** (Figure 3e,f). The strands are comprised of $\{Cp^RFe(\eta^5-P_5)\}_2Au_2$

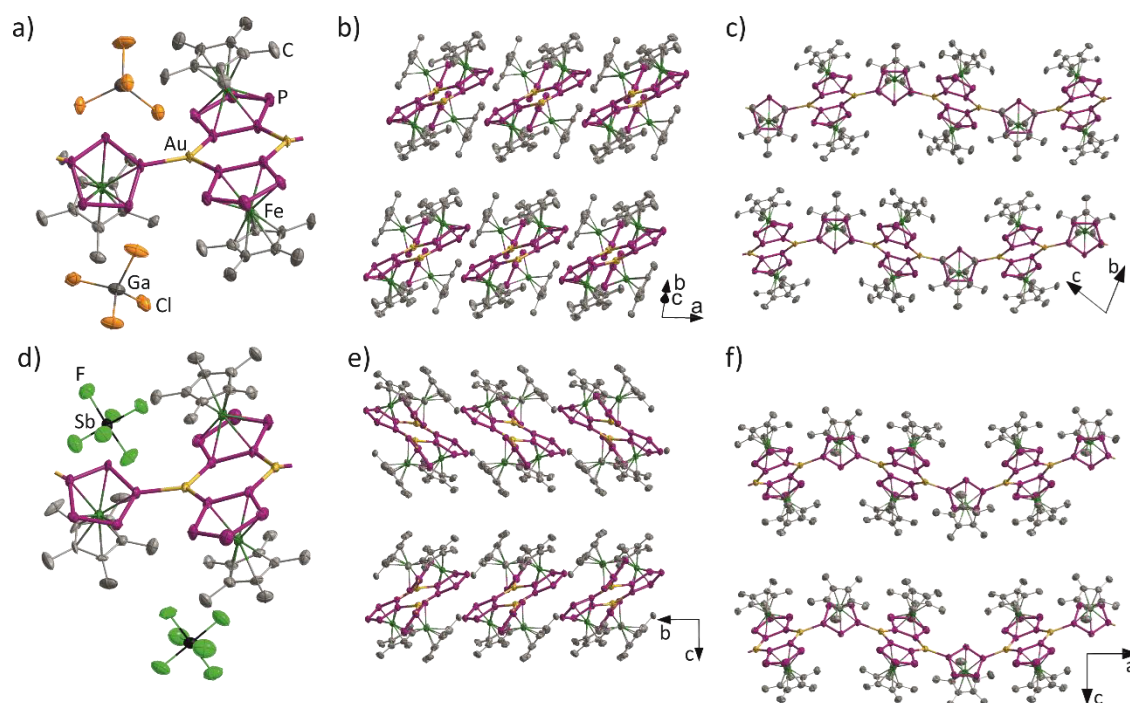


Figure 3. Repeating units of the 1D polymers **2a** (a) and **5** (d) with solvate molecules and H atoms omitted for clarity. Packing of the 1D chains in **2a** (b and c) and **2a'** (e and f) without counterions.

moieties with 1,2-coordinated units of **1*** or **1^x**, thus forming $\{P_4Au_2\}$ six-membered rings in a more or less pronounced chair conformation, as already found in dimeric compounds **3** (Figure 3). The $\{Cp^RFe\}$ moieties are arranged opposed to each other. Again, a further unit of **1*** or **1^x** additionally coordinates to the Au centers, however this time not as a terminal ligand as in compounds **3**, but as a bridging unit connecting $\{Cp^RFe(\eta^5-P_5)\}_2Au_2$ moieties in a 1,3-coordination mode. This bridging P_5 complex is tilted with respect to the $\{P_4Au_2\}$ ring by about 34.98 to 47.71° due to the steric repulsion of the $\{Cp^RFe\}$ fragments.^[31] All Au centers are three-coordinate with P-Au-P angles in the range of 106.60(4) to 135.25(4)°, thus deviating from a trigonal coordination geometry. Nevertheless, all Au centers are coordinated in a nearly perfect planar environment, with angular sums very close to 360°.

Compared to the aforementioned compounds, the 1D polymeric structures of **8a** and **8b** differ. Compound **8a** crystallizes in the space group $P2_1/c$ with one repeating unit $\{Cp^RFe(\eta^5-P_5)\}Au$ per asymmetric unit (Figure 4a). Compound **8b** crystallizes in the space group $P2_1/n$ with two repeating units in the asymmetric unit, showing a certain similarity in the metrics of the unit cell, which can be approximately described as a pseudo structure-superstructure relation ($a' \rightarrow 2a$). Both polymers are built up from 1,3-coordinated moieties of **1*** or **1^x**, while the Au centers in turn are only coordinated by two P_5 complexes (Figure 4b). This results in a nearly linear coordination geometry around the Au centers with P-Au-P angles of 175.67(10)°

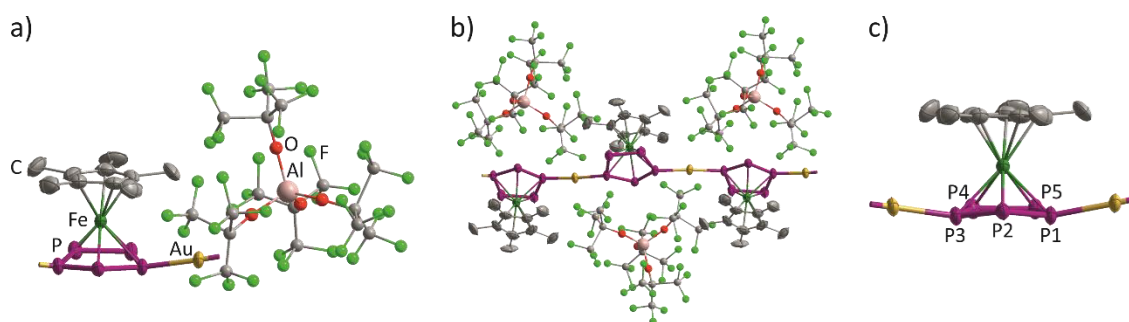


Figure 4. a) Repeating unit and b) section of the polymeric structure of **8a**. c) Numbering scheme of the distorted P_5 cycles in **8a**. H atoms and minor parts of disorder are omitted for clarity. TEF^- anions are depicted in the ball-and-sticks model.

(in **8a**) or $176.11(6)^\circ$ and $177.18(6)^\circ$ (in **8b**). The P_5 complexes coordinate Au with large out-of-plane angles ranging from 17.19° to 24.67° ,^[32] and at the same time exhibit a deviation from planarity within the P_5 ring (Figure 4c). While the Au-P bonds are tilted towards the Cp^R ligands, thus participating in short Au \cdots H contacts ($2.57 - 2.94 \text{ \AA}$), the coordinating P atoms are bent in the opposite direction with an angle of 8.63° to 11.40° between the planes of P2P4P5 and P2P3P4 or P2P1P5. The structural difference between polymers **8** and polymers **2** and **5** are most probably due to the large TEF^- counterions separating the 1D strands in compounds **8**. The Au \cdots Au distances within one strand of **8** are about 7.5 \AA , while in polymers **2** and **5** the repeating unit containing two Au atoms only spans 12 \AA . Therefore, in **2** and **5** also two anions must pack within this 12 \AA period, which is presumably only possible with the smaller anions ($GaCl_4^-$ and SbF_6^-) but not with the large TEF^- counterion.

Rapid precipitation from the respective reaction mixtures is observed when reacting **1*** or **1 \times** with $[Au(CH_3CN)_2]TEF$. Hence, the solid was isolated from the reaction with **1 \times** and analyzed by powder X-ray diffraction (Figure 5).

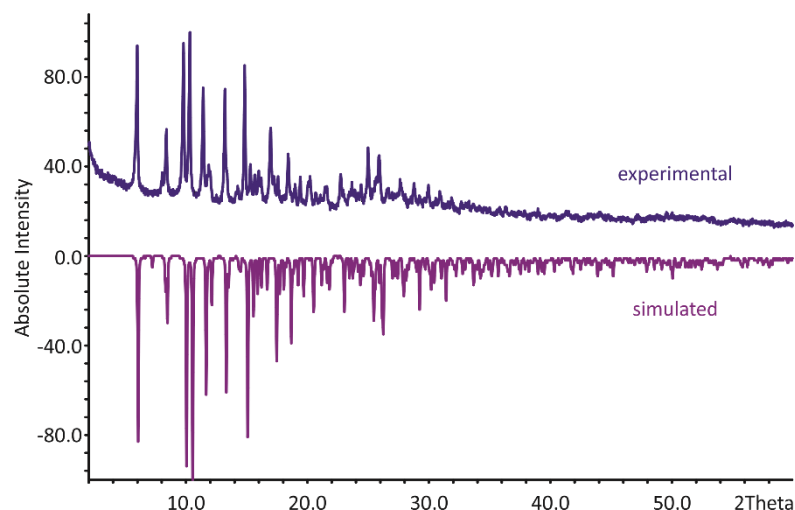


Figure 5. Experimental (top) X-ray powder diffraction pattern of the precipitate in comparison with the diffraction pattern simulated from the single-crystal X-ray data of **8b** (bottom).

Since the measured diffraction pattern fits well to the diffraction pattern simulated from the single crystal X-ray data of **8b** discussed above, its identity is confirmed.

2D polymeric compound (**4**)

Compound **4** crystallizes in the triclinic space group $P\bar{1}$ with one repeating unit $[\{\text{Cp}^*\text{Fe}(\eta^5\text{-P}_5)\}_4\text{Au}_{4-2}](\text{SbF}_6)_2$ per asymmetric unit (Figure 6a). The structure is built up from $\{\text{Cp}^*\text{Fe}(\eta^5\text{-P}_5)\}_2\text{Au}_{2-x}$ units with 1,2-coordinated **1***, thus again forming $\{\text{P}_4\text{Au}_{2-x}\}$ six-membered rings. The Au atoms are further coordinated in an η^2 -fashion by the **1*** moiety of the next $\{\text{Cp}^*\text{Fe}(\eta^5\text{-P}_5)\}_2\text{Au}_{2-x}$ unit thus forming a 2D polymeric network with puckered layers (Figure 6b).

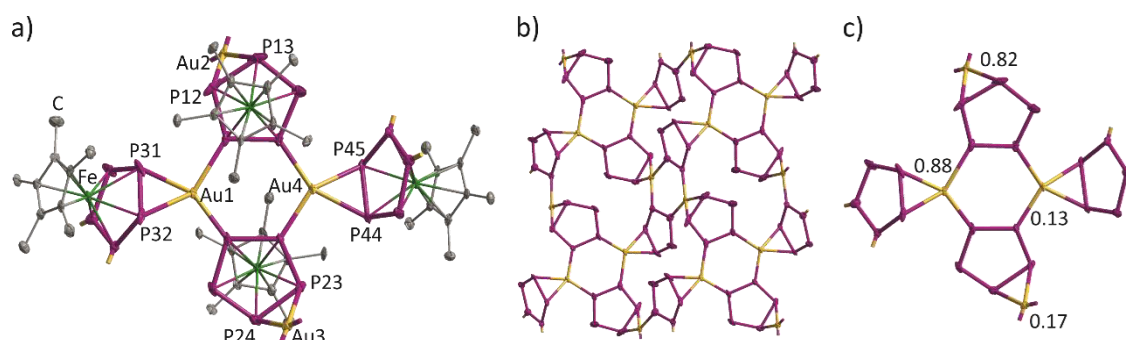


Figure 6. a) Repeating unit with numbering scheme and b) section of the 2D polymeric network **4**. c) Site occupancy factors for the Au atoms. H atoms, counterions and in b) and c) $\{\text{Cp}^*\text{Fe}\}$ units omitted for clarity.

Hence, every Au atom is coordinated by four P atoms. In contrast to the $[\{\text{CpMo}(\text{CO})_2\}_2(\mu, \eta^2\text{-P}_2)]$ coordination dimer in Figure 1d, the η^2 -coordinated P_2 edges in **4** are only twisted by up to 24.6° with respect to the plane of the coordinated Au and the two η^1 -coordinating P atoms and thus, the coordination geometry of Au in **4** may rather be described as distorted square planar. As a remarkable feature, the four Au positions found in the asymmetric unit are not completely occupied. Site occupancy factors (S.O.F.) vary from 0.13 to 0.88, but in sum amount to exactly 2 (Figure 6c). This is also in accordance with the elemental analysis of the bulk phase of isolated **4**, showing no deviation from this ratio. Interestingly, the η^2 -coordinating P-P bonds are elongated significantly up to $2.2633(16)$ Å (compared to $2.116(2) - 2.127(2)$ Å in **1***),^[14a] thus being even longer than a normal P-P single bond (2.22 Å).^[33] Moreover, this elongation is more pronounced, the higher the occupancy of the coordinated Au atom position is (Table 2).

Table 2. Comparison of the site occupancy factors (S.O.F.) for Au sites and coordinated P-P bond lengths.

Au site	S.O.F.	P-P bond	bond length [Å]
Au1	0.88	P31-P32	2.2633(16)
Au2	0.82	P12-P13	2.2369(15)
Au3	0.17	P23-P24	2.157(2)
Au4	0.13	P44-P45	2.142(2)

The Au-P bond lengths are in the normal range for η^1 -coordinated P atoms (2.3016(18) – 2.5560(18) Å) and η^2 -coordinated P atoms (2.2710(17) – 2.5146(18) Å) as well.

Characterization in Solution: Solubilities and Mass spectrometry

All 1D polymeric compounds (**2a**, **2a'**, **2b''**, **5**, **8b**) are completely insoluble in non-coordinating solvents like pentane, toluene and CH_2Cl_2 . While polymer **2a** is only soluble in pyridine under complete depolymerization (cf. NMR spectra in the Experimental Part) and completely insoluble in other coordinating solvents like CH_3CN and THF, on the contrary, the solvatomorph **2a'** is sparsely soluble in CH_3CN and THF. Likewise, compound **2b''** is sparsely soluble in CH_3CN and THF. Surprisingly, the similar SbF_6^- containing 1D polymer **5** is only soluble in CH_3CN , but insoluble in THF. The TEF^- containing 1D polymer **8b** is well soluble in CH_3CN , THF and even *o*-DFB. Hence, characterization of the 1D polymers (**2a**, **2a'**, **2b''**, **5**, **8b**) was predominantly carried out in CH_3CN solution. Next to peaks for the respective counterions, the ESI mass spectra of 1D polymeric compounds **2a'**, **2b''**, **5**, **8b** in CH_3CN merely display peaks corresponding to respective monomeric $[(\text{Cp}^R\text{FeP}_5)_2\text{Au}]^+$ fragments. The isotope pattern clearly proves the monomeric and thus monocationic nature of the detected fragment, excluding oligomeric $[(\text{Cp}^R\text{FeP}_5)_2\text{Au}]_n^{n+}$ fragments. For compound **2a'**, an extra peak attributed to the presence of THT is detected. For compound **8b**, the spectrum additionally displays a peak corresponding to $[(\text{Cp}^X\text{FeP}_5)\text{Au}(\text{CH}_3\text{CN})]^+$. The insolubility of **2a'** is further supported by the positive ion ESI mass spectrum of **2a'** in CH_2Cl_2 , which displays no product signals.

Dimeric compounds **3a** and **3b** are moderately soluble in CH_2Cl_2 , whereas they are insoluble in other common solvents such as pentane, toluene, CH_3CN and THF. Since the 2D polymeric compound **4** possesses similar solubilities, a separation of **3a** and **4** by washing is challenging. However, since the solubility of 1D polymer **5** in CH_2Cl_2 and CH_3CN is opposed to that of **3a** and **4**, the latter compounds can be freed of **5** by washing with CH_3CN . Compounds **3a**, **3b** and **4** are characterized in CH_2Cl_2 . The ESI mass spectra in CH_2Cl_2 or $\text{CH}_2\text{Cl}_2/\text{CH}_3\text{CN}$ mixtures again merely display peaks attributed to the respective monomeric $[(\text{Cp}^R\text{FeP}_5)_2\text{Au}]^+$ fragments and the SbF_6^- counterions, sometimes accompanied by the detection of $[\text{SC}_4\text{H}_8]^+$. Also, the insolubility of **4** in CH_3CN is supported by the absence of product-related fragment peaks in the positive ion ESI mass spectrum in CH_3CN .

The monomeric compound **6** is completely insoluble in common solvents like pentane, toluene, CH_2Cl_2 , CH_3CN , THF. It is also insoluble in *o*-dichlorobenzene (*o*-DCB), *o*-DCB/ CH_3CN mixtures, pyridine and pyridine/THT mixtures. Merely in CS_2 a quite pale, reddish solution was obtained over a high amount of undissolved compound **6**. ^1H and $^{31}\text{P}\{^1\text{H}\}$ NMR spectra only showed signals of uncoordinated **1***, while surprisingly no C_{60} was detected despite its reportedly good solubility in CS_2 .^[25] This confirms the low solubility of **6** and the resulting too

low concentration for $^{13}\text{C}\{^1\text{H}\}$ NMR spectroscopy. Hence, compound **6** was further characterized in the solid state.

The monomeric compound **7** is well soluble in CH_2Cl_2 , CH_3CN and THF, while being insoluble in pentane and toluene. Its high solubility is most probably due to the benzyl groups in the $\mathbf{1}^{\text{Bn}}$ moiety. Likewise, compounds **9a** and **9b** exhibit high solubilities in CH_2Cl_2 , CH_3CN and THF, this time rather due to the large weakly-coordinating TEF^- counterions. The ESI mass spectra of **9a** and **9b** in CH_3CN or $\text{CH}_2\text{Cl}_2/\text{CH}_3\text{CN}$ mixtures display peaks for the monomeric $[(\text{Cp}^{\text{R}}\text{FeP}_5)_2\text{Au}]^+$ fragments and TEF^- counterions. While in the negative ion ESI mass spectrum of **7** only the SbF_6^- anion is detected, in the positive ion ESI mass spectrum next to $[(\text{Cp}^{\text{Bn}}\text{FeP}_5)\text{Au}(\text{tht})]^+$ also $[(\text{Cp}^{\text{Bn}}\text{FeP}_5)_2\text{Au}]^+$ and $[(\text{tht})_2\text{Au}]^+$ are detected, indicating scrambling of the $\mathbf{1}^{\text{Bn}}$ and tht ligands.

Characterization in Solution: NMR spectroscopy

When **5** is dissolved in CD_3CN , only free $\mathbf{1}^*$ is detected as sharp singlets in the ^1H and $^{31}\text{P}\{^1\text{H}\}$ NMR spectra at chemical shifts of 1.43 ppm and 151.8 ppm, respectively, thus indicating complete disaggregation. In contrast, the $^{31}\text{P}\{^1\text{H}\}$ NMR spectra of 1D polymers **2a'** and **2b''** in CD_3CN each exhibit a broad singlet at 143.5 and 144.6 ppm, respectively. In addition to the broadening of the signal, the high-field shift compared to free $\mathbf{1}^*$ (153.0 ppm)^[21a] or $\mathbf{1}^{\times}$ (152.8 ppm)^[21b] indicates the presence of some coordinated pentaphosphaferrocene species. This is further supported by the ^1H NMR spectra, in which the signals are broadened and slightly shifted to lower field compared to free $\mathbf{1}^*$ or $\mathbf{1}^{\times}$.^[34] Hence, **2a'** and **2b''** undergo only a partial disaggregation in CD_3CN , while in contrast pyridine- d_5 as a highly coordinating solvent causes complete disaggregation of **2a** (cf. Experimental Part). The same effect is observed for **8b**. The $^{31}\text{P}\{^1\text{H}\}$ NMR spectrum of **8b** in CD_3CN only exhibits a very small but broad signal at 135 ppm. The low resolution is most probably attributed to the dynamic behavior of Au- $\mathbf{1}^{\times}$ coordination bonds in solution rather than a too diluted sample, since the corresponding $^{19}\text{F}\{^1\text{H}\}$ NMR spectrum nevertheless exhibits a pronounced, sharp singlet for the TEF^- counterions and **8b** was found to be highly soluble in CH_3CN . When **8b** is dissolved in pyridine- d_5 , however, only signals of uncoordinated $\mathbf{1}^{\times}$ are observed in the ^1H and $^{31}\text{P}\{^1\text{H}\}$ NMR spectra.

Moreover, in the $^{19}\text{F}\{^1\text{H}\}$ NMR spectra of **8b** in CD_3CN as well as in pyridine- d_5 a small amount of $\text{HOC}(\text{CF}_3)_3$ is detected next to TEF^- , which may either be left-over starting material of the synthesis of the TEF^- salts^[35] or formed by partial decomposition of the TEF^- salt. This is known to occur when the reaction of Au powder with NOTEF was performed in CH_2Cl_2 instead of CH_3CN ,²⁶ and the $[\text{Au}(\text{CH}_3\text{CN})_2]\text{TEF}$ salt seems to be unstable in CH_2Cl_2 over time according to our own observations.^[36] In the $^{19}\text{F}\{^1\text{H}\}$ NMR spectra of compounds **9a** and **9b** in CD_2Cl_2 , next to the

TEF⁻ anion also a small singlet at -139.3 ppm is detected, which might be due to partial decomposition of the TEF⁻ anion as well.

The ³¹P{¹H} NMR spectra of compounds **9a** and **9b** in CD₂Cl₂ each exhibit a broad singlet at 123.0 and 122.6 ppm, respectively, which is again shifted to higher field compared to free **1*** or **1^x** and indicates highly dynamic Au-P coordination bonds (Table 3). In the corresponding ¹H NMR spectra, the Cp* and Cp^x protons are detected at lower field (**9a**: δ = 1.67 ppm; **9b**: δ = 0.90 (t), 1.67 (s), 1.69 (s), 2.19 (q) ppm) compared to free **1*** or **1^x**.^[37] The ¹H and ³¹P{¹H} NMR spectra of the dimeric compounds **3a**, **3b** as well as 2D polymeric **4** in CD₂Cl₂ merely differ from the spectra of compounds **9** (Table 3). This corroborates the presence of highly dynamic processes in solution. In the ¹⁹F{¹H} NMR spectra of SbF₆⁻ containing products **3a**, **3b** and **4** no signal is detected, which might be due to their moderate solubility in CD₂Cl₂ in combination with the expected low intensities of the signals resulting from coupling to the ¹²¹Sb (*I* = 5/2, 57%) and ¹²³Sb (*I* = 7/2, 43%) nuclei.^[38] However, the absence of the SbF₆⁻ signal in the ¹⁹F{¹H} NMR spectra is even observed for compound **7**, which is very well soluble in CD₂Cl₂. The ³¹P{¹H} NMR spectrum of **7** shows a broad singlet at 128.8 ppm attributed to coordinated **1^{Bn}** (Table 3), which is clearly shifted to higher field compared to free **1^{Bn}** (δ = 162.2 ppm).^[21c] In the ¹H NMR spectrum of **7** in CD₂Cl₂ the signals for the Cp^{Bn} ligand are shifted to lower field compared to free **1^{Bn}**. Additionally, two broad multiplets are observed attributed to the tht protons. These are as well shifted to lower field compared to free THT (δ = 1.42 (m) and 2.49 (m) ppm in CDCl₃)^[39] but similar to [(tht)₂Au]SbF₆ (δ = 2.21 (m) and 3.47 (m) ppm in CDCl₃).^[24]

Table 3. ³¹P{¹H} NMR chemical shifts and peak widths at half-height compared for compounds **3a**, **3b**, **4**, **7**, **9a** and **9b** in CD₂Cl₂ at r.t.

Compound	3a	3b	4	7	9a	9b
δ _p [ppm]	123.1	124.1	123.1	128.8	123.0	122.6
ω _{1/2} [Hz]	20	24	26	55	62	35

Since dynamic processes involving the Au-P coordination contacts are assumed to cause line broadening in the aforementioned ³¹P{¹H} NMR spectra (Table 3), NMR spectroscopy was carried out at variable temperatures for **7**, exemplarily, due to its high solubility and the large peak width at half-height observed already at room temperature. Figure 7 shows the ³¹P{¹H} NMR spectra of **7**, in which the signal is broadened significantly when cooled down to 213 K. At 193 K, splitting into two broad signals is observed, which still partially overlap and reveal an integral ratio of roughly 4:1. This reflects the ratio of uncoordinated vs. coordinated P atoms in **7** upon freezing of the dynamics, while the coordinated P atom is expected to resonate at higher fields. Thus, it is suggested that the {Au(tht)} fragment circumambulates from one P atom to another at r.t.,

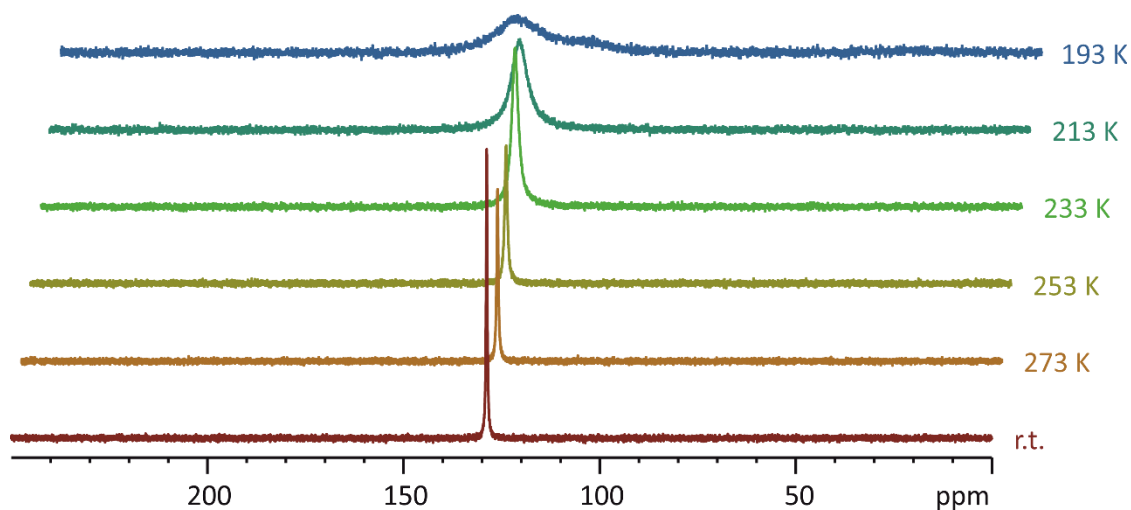


Figure 7. $^{31}\text{P}\{^1\text{H}\}$ NMR spectrum of **7** in CD_2Cl_2 at variable temperatures.

while being held in position at low temperatures. However, cooling to 193 K did not seem to freeze the dynamics entirely. Hence, further conclusions cannot be drawn, and no P-P couplings can be derived.

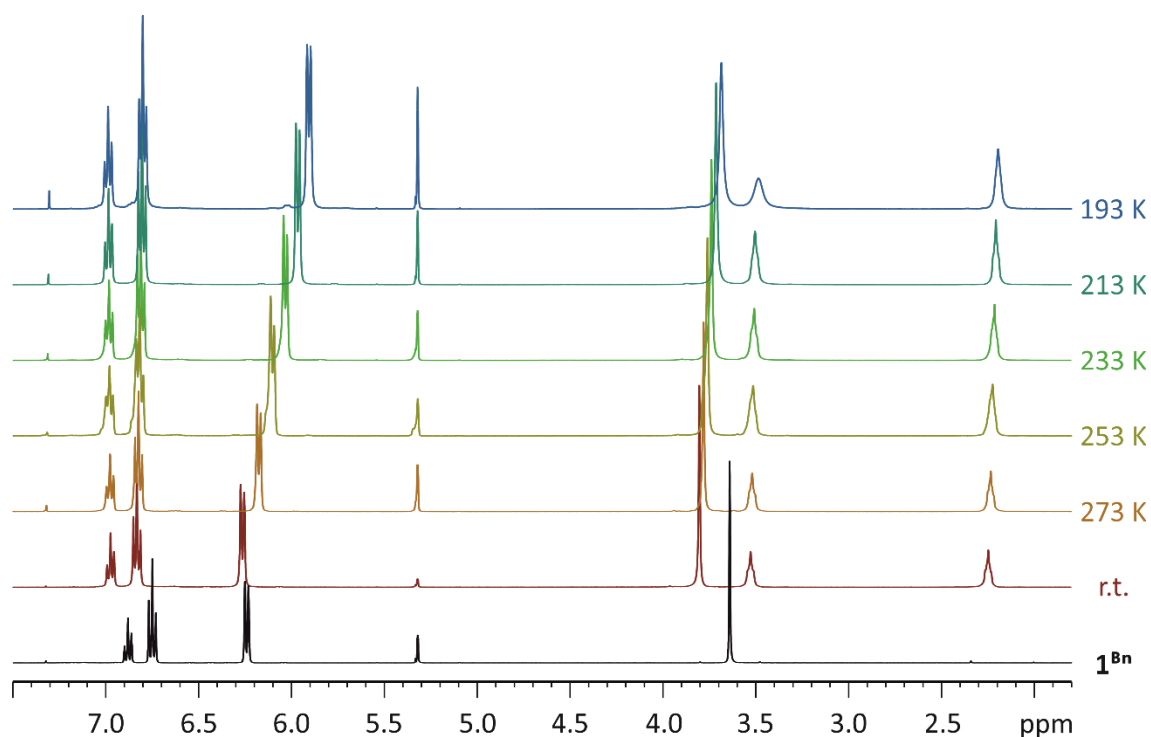


Figure 8. ^1H NMR spectrum of **7** in CD_2Cl_2 at variable temperatures in comparison to the ^1H NMR spectrum of **1^{Bn}** (black) in CD_2Cl_2 at r.t.

The corresponding ^1H NMR spectra of **7** in CD_2Cl_2 at variable temperatures are depicted in Figure 8, next to the spectrum of **1^{Bn}** at r.t. Upon cooling to 193 K, the chemical shift of the *meta*- and *para*-CH protons of the Cp^{Bn} ligand merely change. The same is true for the signals of the tht ligand, thus supporting the proposed shift of the entire $\{\text{Au}(\text{tht})\}$ fragment. In contrast,

the CH₂ protons and especially the *ortho*-CH protons of the Cp^{Bn} ligand resonate at higher field when cooled to 193 K. This is presumably caused by their proximity to the {Au(tht)} fragment, even though in the crystal structure only one close Au⋯H contact to a CH₂ proton is observed. However, in solution further Au⋯H contacts might be conceivable also for the *ortho*-CH protons due to rotation of the Bn groups. In any case, these interactions apparently are too weak to lock the {Au(tht)} fragment in one position within the NMR time scale since no splitting of the CH₂ and *ortho*-CH protons is observed.

Since compound **6** is completely insoluble, solid-state magic angle spinning (MAS) NMR spectroscopy was carried out. In the ³¹P{¹H} NMR spectrum (Figure 9), at least two broad signals overlap in the region of 120 to 170 ppm. The small signal at 132 ppm exhibits a ¹J_{P,P} coupling of 300 Hz and is presumably attributed to the three P atoms coordinating to Au. Unfortunately, no other couplings are resolved.

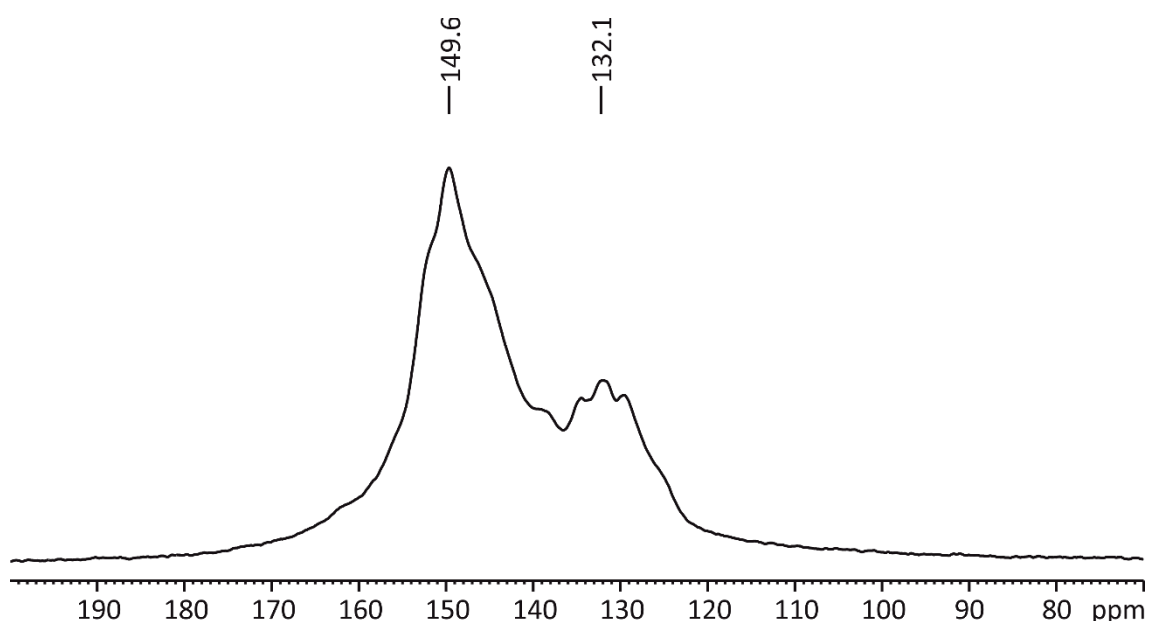


Figure 9. ³¹P{¹H} MAS NMR spectrum of compound **6**.

In the ¹³C{¹H} MAS NMR spectrum of **6** (Figure 10), C₆₀ is detected as two close singlets at δ = 143.4 and 144.0 ppm. Since free C₆₀ resonates at 144.1 ppm,^[13c] most probably the latter signal is due to C₆₀ not interacting with the units of **1***, while the singlet at 143.4 ppm might be shifted to higher field due to π-interactions. However, only few close P⋯C contacts were found in the crystal structure. Hence, the presence of two distinct signals for C₆₀ probably is merely caused by the fact that two crystallographically unique C₆₀ molecules co-crystallize. Moreover, the ¹³C{¹H} MAS NMR spectrum shows two sets of resonances at 13.0 and 16.3 ppm (methyl groups) and 95.6 and 97.3 ppm (Cp* ring). The integral ratio amounts to approximately 2:1 for both sets, being in line with the ratio of crystallographically unique Cp* rings. Hence, the low-field shifted,

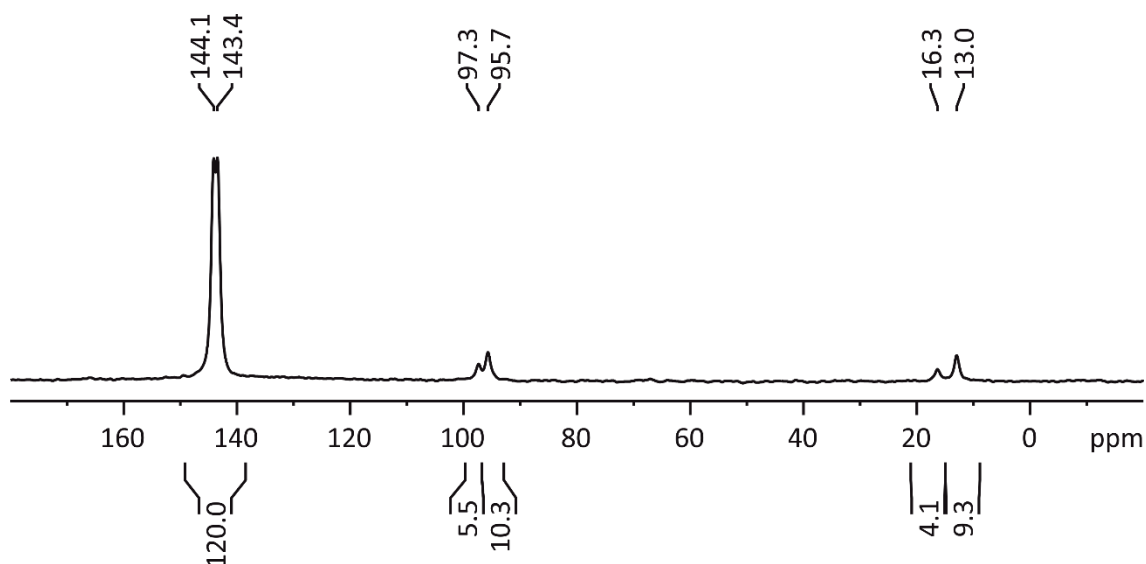


Figure 10. $^{13}\text{C}\{^1\text{H}\}$ MAS NMR spectrum of compound **6**.

smaller signals may be assigned to the C atoms of the single **1*** unit lying on the mirror plane, while the high-field shifted, larger signals may be attributed to the C atoms of the two symmetry-related **1*** moieties in **6**.

6.3 Conclusion

In summary, a variety of unprecedented coordination products of *cyclo*- P_5 ligand complexes **1***, **1^x** and **1^{Bn}** and Au are reported herein. Remarkably, a series of 1D and even 2D polymers was obtained, constituting the first coordination polymers based on P_n ligand complexes and Au in general. Thus, we successfully extended the supramolecular chemistry of pentaphosphaferrocenes from Cu and Ag now to Au. For the synthesis of AuGaCl_4 containing products, the application of $[(\text{tht})\text{AuCl}]$ and GaCl_3 proved beneficial. SbF_6^- containing products were obtained from *in situ* generated $[(\text{tht})_2\text{Au}]\text{SbF}_6$. Even larger TEF^- counterions were implemented by reactions with the isolable $[\text{Au}(\text{CH}_3\text{CN})_2]\text{TEF}$ salt. Starting from AuGaCl_4 , 1D polymers are obtained as a series of polymorphs and solvatomorphs. With AuSbF_6 , the reaction outcome depends on the Cp^R ligand of the pentaphosphaferrocene. **1*** gives a dimer and a 2D polymer as structural isomers, as well as a 1D polymer obtained by further crystallization from the mother liquor. **1^x** reacts more selectively with AuSbF_6 to give a dimer similar to that obtained from **1***. With **1^{Bn}**, only one *tht* ligand is replaced from $[(\text{tht})_2\text{Au}]\text{SbF}_6$ to give a monomer exhibiting a highly dynamic behavior in solution. Hence, the increase in solubility of the building blocks from **1*** to **1^x** to **1^{Bn}** appears to correlate with the formation of polymeric (**1***) vs. oligomeric (**1^x**) vs. monomeric (**1^{Bn}**) products. With AuTEF , 1D polymers or monomers are obtained depending on the stoichiometry applied. The molecular products as well as partially disaggregated polymeric products exhibit highly dynamic behavior in solution even at low

temperatures. These results offer an incentive for further investigations concerning the potential of the molecular coordination products in Au catalysis. Moreover, all obtained products comprise Au centers with an either linear or planar coordination environment, impeding the formation of spherical aggregates. Therefore, in future investigations, Au salts are to be reacted with further P_n and As_n ligand complexes known to coordinate in an out-of-plane fashion, such as $[CpMo(CO)_2(\eta^3-P_3)]^{[40]}$ and $[Cp^*Fe(\eta^5-As_5)]^{[41]}$.

6.4 Experimental Part

General Remarks

All reactions were performed under an inert atmosphere of dry nitrogen or argon with standard vacuum, Schlenk and glove-box techniques in the dark. Solvents and THT were purified, dried and degassed prior to use by standard procedures. $[Cp^*Fe(\eta^5-P_5)]$ (**1***), $[Cp^xFe(\eta^5-P_5)]$ (**1^x**) and $[Cp^{Bn}Fe(\eta^5-P_5)]$ (**1^{Bn}**) were synthesized following reported procedures,^[21] although the syntheses of **1*** and **1^x** were performed in *meta*-diisopropylbenzene with an improved yield of 75% and 56%, respectively. $[(tth)_2Au]SbF_6$ ^[24] was synthesized freshly in analogy to the reported method and added *in situ* to the respective syntheses. $[Au(CH_3CN)_2]TEF$ ^[26] was synthesized by an improved method based on the reported one. $[(tth)AuCl]$, $[PPh_3AuCl]$, TITEF, and C_{60} were available in-house. $GaCl_3$ is commercially available and was sublimed prior to use. Solution NMR spectra were recorded on a BRUKER Avance 400 spectrometer. MAS NMR spectra were acquired on a Bruker Avance 300 spectrometer. Chemical shifts δ are given in [ppm] referring to external standards of tetramethylsilane (1H NMR and $^{13}C\{^1H\}$ NMR spectra), adamantane ($^{13}C\{^1H\}$ MAS NMR spectra), 85% phosphoric acid ($^{31}P\{^1H\}$ NMR spectra), NaH_2PO_4 ($^{31}P\{^1H\}$ MAS NMR spectra) or $CFCl_3$ ($^{19}F\{^1H\}$ NMR spectra). ESI-MS spectra were recorded on a ThermoQuest Finnigan MAT TSQ 7000 spectrometer and EI-MS spectra were recorded on a Finnigan MAT 95 mass spectrometer. Elemental analyses were performed on a Vario EL III apparatus.

Synthesis of $[(Cp^*Fe(\eta^5-P_5))_3Au_2]_n(GaCl_4)_{2n}$ (**2a**, **2a'**)

Method A:

$[(tth)AuCl]$ (31 mg, 0.097 mmol) and $GaCl_3$ (15 mg, 0.085 mmol) were dissolved in CH_2Cl_2 (3 mL) and stirred for 15 minutes. $[Cp^*Fe(\eta^5-P_5)]$ (16 mg, 0.046 mmol) was dissolved in CH_2Cl_2 (5 mL) and added. After stirring 15 minutes, the red-brown solution was filtered into a thin Schlenk tube, concentrated (to 3 mL), and layered with toluene (6 mL). Already after one day, brown prisms of **2a** crystallized. After complete diffusion, the crystals were taken from the

Schlenk wall with a spatula and quickly dipped into a Schlenk tube with toluene. The crystals were washed with toluene (3 x 3 mL) and pentane (3 x 3 mL) and dried.

Analytical Data of **2a**:

Yield: 5 mg (2.7 μ mol, 17%)

^1H NMR (pyridine- d_5): δ [ppm] = 1.28 (s, $[\text{Cp}^*\text{Fe}(\eta^5\text{-P}_5)]_{\text{free}}$), 1.66 (m, SC_4H_8), 2.20 (s, C_7H_8), 2.67 (m, SC_4H_8), 5.66 (s, CH_2Cl_2), 7.12 – 7.28 (m, C_7H_8).

$^{31}\text{P}\{^1\text{H}\}$ NMR (pyridine- d_5): δ [ppm] = 152.3 (s, $[\text{Cp}^*\text{Fe}(\eta^5\text{-P}_5)]_{\text{free}}$).

Elemental Analysis: Calculated (%) for $(\text{C}_{10}\text{H}_{15}\text{FeP}_5)_3(\text{AuGaCl}_4)_2 \cdot 0.18 \text{C}_7\text{H}_8$ (1871 g/mol): C 20.06, H 2.50, N 0, S 0; found (%): C 20.06, H 2.41, N traces, S 0.

Method B:

To a mixture of $[(\text{tht})\text{AuCl}]$ (59 mg, 0.18 mmol) and GaCl_3 (33 mg, 0.19 mmol), SC_4H_8 (THT, 0.015 mL, 0.17 mmol) was added. Then, *o*-difluorobenzene (*o*-DFB, 4 mL) was added and the mixture was stirred for 30 minutes. After filtration, the yellowish solution was layered with a solution of $[\text{Cp}^*\text{Fe}(\eta^5\text{-P}_5)]$ (33 mg, 0.095 mmol) in toluene (6 mL) in a thin Schlenk tube. After complete diffusion, the mother liquor was decanted, the brown plates of **2a'** washed with toluene (3 x 5 mL) and pentane (3 x 5 mL) and dried.

Analytical Data of **2a'**:

Yield: 52 mg (27 μ mol, 86%)

Elemental Analysis: Calculated (%) for $(\text{C}_{10}\text{H}_{15}\text{FeP}_5)_3(\text{AuGaCl}_4)_2 \cdot 0.5 \text{SC}_4\text{H}_8$ (1899 g/mol): C 20.24, H 2.60, N 0, S 0.84; found (%): C 19.75, H 2.45, N 0, S 0.80.

Method B (upscale):

To a mixture of $[(\text{tht})\text{AuCl}]$ (119 mg, 0.37 mmol) and GaCl_3 (70 mg, 0.40 mmol), SC_4H_8 (THT, 0.03 mL, 0.34 mmol) was added. Then, *o*-difluorobenzene (*o*-DFB, 10 mL) was added and the mixture was stirred for 45 minutes. After filtration, the yellowish solution was layered with a solution of $[\text{Cp}^*\text{Fe}(\eta^5\text{-P}_5)]$ (69 mg, 0.20 mmol) in toluene (10 mL) in a thin Schlenk tube. Already after one day, thin brown plates of **2a'** crystallized. Unfortunately, the thin plates grew at the interface so that further diffusion was hampered. Hence, from time to time the crystals were loosened with a spatula letting them sink to the bottom of the Schlenk. After complete diffusion, yellow-brown plates of **2a'** were taken from the Schlenk wall with a spatula and quickly dipped into a Schlenk tube with *o*-DFB (3 mL). The crystals were washed with CH_2Cl_2 (3 x 5 mL) and dried. However, smaller yellow plates of **2a'** could not be isolated by this method. Instead, the fluffy yellow plates were transferred with the mother liquor into a new Schlenk tube and washed with

CH₂Cl₂ (5 x 5 mL), whereby the crystals were left to settle each time. Thus, after drying a second crop of crystals could be isolated.

Analytical Data of **2a'**:

Yields: 30 mg (16 μmol, 23%, first crop), 38 mg (second crop)

¹H NMR (CD₃CN): δ [ppm] = 1.51 (s, [Cp*Fe(η⁵-P₅)]), 2.32 (s, C₇H₈), 2.91 (br, H₂O), 5.44 (s, CH₂Cl₂), 7.14 – 7.26 (m, C₇H₈).

³¹P{¹H} NMR (CD₃CN): δ [ppm] = 143.5 (s, ω_{1/2} = 102 Hz, [Cp*Fe(η⁵-P₅)]).

Elemental Analysis of the first crop: Calculated (%) for (C₁₀H₁₅FeP₅)₃(AuGaCl₄)₂ · 0.65 C₆H₄F₂ (1929 g/mol): C 21.11, H 2.49, S 0; found (%): C 21.10, H 2.05, S 0.

Elemental Analysis of the second crop: Calculated (%) for (C₁₀H₁₅FeP₅)₃(AuGaCl₄)₂ (1855 g/mol): C 19.43, H 2.45, S 0; found (%): C 18.30, H 1.76, S traces.

Analytical Data of the mother liquor:

³¹P{¹H} NMR (C₆D₆-cap.): δ [ppm] = 115.0 (br, ω_{1/2} = 19 Hz, [Cp*Fe(η⁵-P₅)]_{coord.}).

Method C:

To a mixture of [(tht)AuCl] (59 mg, 0.18 mmol) and GaCl₃ (33 mg, 0.19 mmol), SC₄H₈ (THT, 0.015 mL, 0.17 mmol) was added. Then, *o*-difluorobenzene (*o*-DFB, 4 mL) was added and the mixture was stirred for 30 minutes. [Cp*Fe(η⁵-P₅)] (33 mg, 0.095 mmol) was added to the yellow-grey suspension and stirred for further 10 minutes. The rust-red suspension was filtered into a thin Schlenk tube and layered with toluene (4 mL). Already after one day, brown plates of **2a'** crystallized. After complete diffusion, the crystals were taken from the Schlenk wall with a spatula and quickly dipped into a Schlenk tube with toluene. The crystals were washed with toluene (3 x 5 mL) and pentane (3 x 5 mL) and dried.

Analytical Data of **2a'**:

Yield: 3 mg (1.6 μmol, 5%)

Positive ion ESI-MS (CH₂Cl₂): *m/z* = 88.0755 [SC₄H₈]⁺.

Negative ion ESI-MS (CH₂Cl₂): *m/z* = 210.7997 [GaCl₄]⁻.

Positive ion ESI-MS (CH₃CN): *m/z* = 888.8070 [(Cp*FeP₅)₂Au]⁺, 88.0755 [SC₄H₈]⁺.

Negative ion ESI-MS (CH₃CN): *m/z* = 210.7995 [GaCl₄]⁻.

Elemental Analysis: Calculated (%) for (C₁₀H₁₅FeP₅)₃(AuGaCl₄)₂ (1855 g/mol): C 19.43, H 2.45, N 0, S 0; found (%): C 19.25, H 2.29, N 0, S 0.

Synthesis of $[(\text{Cp}^*\text{Fe}(\eta^5\text{-P}_5))_3\text{Au}_2]_n(\text{GaCl}_4)_{2n}$ (**2b**, **2b'**, **2b''**)

Method A:

$[(\text{tth})\text{AuCl}]$ (125 mg, 0.390 mmol) and GaCl_3 (72 mg, 0.41 mmol) were dissolved in CH_2Cl_2 (10 mL) and stirred for 20 minutes. $[\text{Cp}^*\text{Fe}(\eta^5\text{-P}_5)]$ (68 mg, 0.19 mmol) was dissolved in CH_2Cl_2 (7 mL) and added. After stirring for further two hours, the red-brown solution was filtered into a thin Schlenk tube and layered with toluene (17 mL). Already after one day, yellow-brown plates of **2b** crystallized, while later also crystals of the polymorph **2b'** were formed. After two weeks, the formation of some precipitate was observed. Hence, despite incomplete diffusion, the crystals were isolated. Therefore, the mother liquor was shaken to suspend the precipitate and crystals. The crystals were left to settle, and the suspended precipitate was decanted with the mother liquor. The crystals were washed with CH_2Cl_2 (5 x 5 mL), thereby suspending residual precipitate each time, and dried.

Analytical Data of **2b** and **2b'**:

Yield: 29 mg (15 μmol , 24%)

Elemental Analysis: Calculated (%) for $(\text{C}_{10}\text{H}_{15}\text{FeP}_5)_3(\text{AuGaCl}_4)_2$ (1897 g/mol): C 20.90, H 2.71, S 0; found (%): C 21.02, H 2.53, S 0.

Analytical Data of the mother liquor:

$^{31}\text{P}\{^1\text{H}\}$ NMR ($\text{C}_6\text{D}_6\text{-cap.}$): δ [ppm] = 116.8 (br, $\omega_{1/2}$ = 51 Hz, $[\text{Cp}^*\text{Fe}(\eta^5\text{-P}_5)]_{\text{coord.}}$).

Method B:

To a mixture of $[(\text{tth})\text{AuCl}]$ (119 mg, 0.37 mmol) and GaCl_3 (70 mg, 0.40 mmol), SC_4H_8 (THT, 0.03 mL, 0.34 mmol) was added. Then, *o*-DFB (10 mL) was added and the mixture was stirred for 45 minutes. After filtration, the yellowish solution was layered with a solution of $[\text{Cp}^*\text{Fe}(\eta^5\text{-P}_5)]$ (68 mg, 0.19 mmol) in toluene (10 mL) in a thin Schlenk tube. Already after one day, thin yellow-orange plates of **2b''** (unit cell constants: monoclinic P, $a = 9.1209(6)$ Å, $b = 24.187(2)$ Å, $c = 29.543(3)$ Å; $\beta = 98.175(7)^\circ$; $V = 6451.2(9)$ Å³), presumably a solvatomorph of **2b'**, crystallized. After complete diffusion, bigger crystals were taken from the Schlenk wall with a spatula and quickly dipped into a Schlenk tube with *o*-DFB. The crystals were washed with *o*-DFB (3 x 5 mL) and toluene (3 x 3 mL) and dried. However, smaller yellow plates of **2b''** could not be isolated by this method. Instead, the mother liquor was decanted after the fluffy yellow plates had settled. The crystals were then suspended in CH_2Cl_2 (10 mL), transferred into a new Schlenk tube, washed with CH_2Cl_2 (3 x 10 mL) and dried.

Analytical Data of **2b''**:

Yields: 43 mg (22 μmol , 35%, first crop), 18 mg (9.5 μmol , 15%, second crop)

^1H NMR (CD_3CN): δ [ppm] = 0.78 (t, br, 3 H, Cp^*FeP_5), 1.51-1.52 (2 x s, 12 H, Cp^*FeP_5), 2.03 (br, 2 H, Cp^*FeP_5), 2.32 (s, C_7H_8), 3.02 (br, H_2O), 5.44 (s, CH_2Cl_2), 7.14 – 7.26 (m, C_7H_8).

$^{31}\text{P}\{^1\text{H}\}$ NMR (CD_3CN): δ [ppm] = 144.6 (br, $\omega_{1/2}$ = 66 Hz, $[\text{Cp}^*\text{Fe}(\eta^5\text{-P}_5)]$).

Positive ion ESI-MS (CH_3CN): m/z = 916.8405 $[(\text{Cp}^*\text{FeP}_5)_2\text{Au}]^+$.

Negative ion ESI-MS (CH_3CN): m/z = 210.7998 $[\text{GaCl}_4]^-$.

Elemental Analysis (first crop): Calculated (%) for $(\text{C}_{11}\text{H}_{17}\text{FeP}_5)_3(\text{AuGaCl}_4)_2 \cdot 0.36 \text{C}_7\text{H}_8$ (1930 g/mol): C 22.10, H 2.81, N 0, S 0; found (%): C 22.10, H 2.49, N 0, S 0.

Elemental Analysis (second crop): Calculated (%) for $(\text{C}_{11}\text{H}_{17}\text{FeP}_5)_3(\text{AuGaCl}_4)_2$ (1897 g/mol): C 20.90, H 2.71, N 0, S 0; found (%): C 21.34, H 2.50, N 0, S 0.

Analytical Data of the mother liquor:

$^{31}\text{P}\{^1\text{H}\}$ NMR ($\text{C}_6\text{D}_6\text{-cap.}$): δ [ppm] = 116.7 (br, $\omega_{1/2}$ = 18 Hz, $[\text{Cp}^*\text{Fe}(\eta^5\text{-P}_5)]_{\text{coord.}}$).

Synthesis of $[(\text{Cp}^*\text{Fe}(\eta^5\text{-P}_5))_4\text{Au}_2](\text{SbF}_6)_2$ (**3a**)

To a mixture of $[(\text{tth})\text{AuCl}]$ (31 mg, 0.097 mmol) and AgSbF_6 (34 mg, 0.099 mmol), SC_4H_8 (THT, 0.009 mL, 0.1 mmol) and CH_2Cl_2 (3 mL) were added and the mixture was stirred for 30 minutes. After filtration from the grey precipitate (AgCl), the yellowish solution of *in situ* generated $[(\text{tth})_2\text{Au}]\text{SbF}_6$ was layered with the solution of $[\text{Cp}^*\text{Fe}(\eta^5\text{-P}_5)]$ (15 mg, 0.043 mmol) in toluene (3 mL) in a thin Schlenk tube. Already after one day, yellow-brown plates of **3a** crystallized. After complete diffusion, the mother liquor was decanted and the crystals were washed with toluene (2 x 10 mL), thereby transferred into a new Schlenk tube and washed again with toluene (2 x 5 mL) and pentane (3 x 5 mL) and dried.

Analytical Data of **3a**:

Yield: 10 mg (4.4 μmol , 40%)

^1H NMR (CD_2Cl_2): δ [ppm] = 1.67 (s, 15 H, $[\text{Cp}^*\text{Fe}(\eta^5\text{-P}_5)]$), 2.13 (m, SC_4H_8), 3.23 (m, SC_4H_8), 5.32 (s, CD_2Cl_2), 7.32 (s, CDCl_3).

$^{31}\text{P}\{^1\text{H}\}$ NMR (CD_2Cl_2): δ [ppm] = 123.1 (s, $\omega_{1/2}$ = 20 Hz, $[\text{Cp}^*\text{Fe}(\eta^5\text{-P}_5)]_{\text{coord.}}$).

$^{19}\text{F}\{^1\text{H}\}$ NMR (CD_2Cl_2): no signal detected.

Positive ion ESI-MS (CH_2Cl_2 / CH_3CN): m/z = 888.8075 $[(\text{Cp}^*\text{FeP}_5)_2\text{Au}]^+$, 88.07540 $[\text{SC}_4\text{H}_8]^+$.

Negative ion ESI-MS (CH_2Cl_2 / CH_3CN): m/z = 234.8958 $[\text{SbF}_6]^-$.

Elemental Analysis: Calculated (%) for $(\text{C}_{10}\text{H}_{15}\text{FeP}_5)_4(\text{AuSbF}_6)_2 \cdot 0.4 \text{SC}_4\text{H}_8$ (2284 g/mol): C 21.87, H 2.79, N 0, S 0.56; found (%): C 21.64, H 2.53, N 0, S 0.55.

The reaction sometimes gave **4** instead or in addition to **3a**, after longer crystallization times also crystals of **5** were formed. A dependence on stoichiometry or concentration could not be found.

Synthesis of $[\{\text{Cp}^*\text{Fe}(\eta^5\text{-P}_5)\}_4\text{Au}_2]_n(\text{SbF}_6)_{2n}$ (**4**)

To a mixture of $[(\text{tht})\text{AuCl}]$ (132 mg, 0.412 mmol) and AgSbF_6 (138 mg, 0.402 mmol), SC_4H_8 (THT, 0.036 mL, 0.41 mmol) and CH_2Cl_2 (14 mL) were added and the mixture was stirred for 1h. After filtration from the grey precipitate (AgCl), the yellowish solution of *in situ* generated $[(\text{tht})_2\text{Au}]\text{SbF}_6$ was layered with the solution of $[\text{Cp}^*\text{Fe}(\eta^5\text{-P}_5)]$ (62 mg, 0.18 mmol) in toluene (28 mL) in a thin Schlenk tube. Already after one day, large brown prisms of **4** crystallized. After complete diffusion, also few brown rods of **5** started to crystallize. Hence, the crystals were taken from the Schlenk wall with a spatula, quickly dipped into mineral oil and sorted under the microscope. The crystals of **4** were transferred with mineral oil into a Schlenk tube, washed with pentane (20 x 5 mL) and dried. Analogously, the crystals of **5** were transferred with mineral oil into a Schlenk tube, washed with pentane (4 x 3 mL) and dried.

Analytical Data of **4**:

Yield: 24 mg (11 μmol , 24%)

$^1\text{H NMR}$ (CD_2Cl_2): δ [ppm] = 1.68 (s, 15 H, $[\text{Cp}^*\text{Fe}(\eta^5\text{-P}_5)]_{\text{coord.}}$), 2.34 (s, C_7H_8), 5.32 (s, CD_2Cl_2), 7.16 – 7.25 (m, C_7H_8), 7.32 (s, CDCl_3).

$^{31}\text{P}\{^1\text{H}\}$ NMR (CD_2Cl_2): δ [ppm] = 123.1 (s, $\omega_{1/2}$ = 26 Hz, $[\text{Cp}^*\text{Fe}(\eta^5\text{-P}_5)]_{\text{coord.}}$).

$^{19}\text{F}\{^1\text{H}\}$ NMR (CD_2Cl_2): no signal detected.

Positive ion ESI-MS (CH_3CN): no corresponding signals are detected.

Negative ion ESI-MS (CH_3CN): m/z = 234.8940 $[\text{SbF}_6]^-$.

Positive ion ESI-MS (CH_2Cl_2): m/z = 888.8099 $[(\text{Cp}^*\text{FeP}_5)_2\text{Au}]^+$.

Negative ion ESI-MS (CH_2Cl_2): m/z = 234.8941 $[\text{SbF}_6]^-$.

Elemental Analysis: Calculated (%) for $(\text{C}_{10}\text{H}_{15}\text{FeP}_5)_4(\text{AuSbF}_6)_2$ (2249 g/mol): C 21.36, H 2.69, N 0, S 0; found (%): C 21.44, H 2.31, N 0, S 0.

Analytical Data of **5**:

Yield: few crystals

The reaction sometimes gave **3a** instead or in addition to **4**, after longer crystallization times also crystals of **5** were formed (further crystals of **5** were found in the mother liquor). A dependence on stoichiometry or concentration could not be found.

Synthesis of $[\{\text{Cp}^*\text{Fe}(\eta^5\text{-P}_5)\}_4\text{Au}_2](\text{SbF}_6)_2$ (**3a**), $[\{\text{Cp}^*\text{Fe}(\eta^5\text{-P}_5)\}_4\text{Au}_2]_n(\text{SbF}_6)_{2n}$ (**4**) and $[\{\text{Cp}^*\text{Fe}(\eta^5\text{-P}_5)\}_3\text{Au}_2]_n(\text{SbF}_6)_{2n}$ (**5**)

To a mixture of $[(\text{tht})\text{AuCl}]$ (109 mg, 0.412 mmol) and AgSbF_6 (119 mg, 0.402 mmol), SC_4H_8 (THT, 0.03 mL, 0.41 mmol) and CH_2Cl_2 (12 mL) were added and the mixture was stirred for 15 minutes. After filtration from the grey precipitate (AgCl), the yellowish solution of *in situ* generated $[(\text{tht})_2\text{Au}]\text{SbF}_6$ was layered with the solution of $[\text{Cp}^*\text{Fe}(\eta^5\text{-P}_5)]$ (60 mg, 0.18 mmol) in

toluene (12 mL) in a thin Schlenk tube. Already after one day, brown crystals of **3a** and **4** had formed. After complete diffusion, the mother liquor was decanted. The crystals (mixture of **3a**, **4** and **5**) were washed with toluene (3 x 10 mL), thereby loosened from the Schlenk wall with a spatula and then transferred into a new Schlenk tube. The crystals were again washed with toluene (1 x 5 mL) and pentane (3 x 5 mL) and dried.

The mother liquor was layered with toluene (10 mL) and crystals of **5** had grown within two weeks. The crystals were taken from the Schlenk wall with a spatula and quickly dipped into a Schlenk tube with toluene, washed with toluene (3 x 5 mL), pentane (3 x 5 mL) and dried.

Analytical Data of **3a**, **4** and **5**:

Yield: 47 mg

Elemental Analysis: Calculated (%) for $(C_{10}H_{15}FeP_5)_{3.2}(AuSbF_6)_2 \cdot (SC_4H_8)_{0.48}$ (2015 g/mol): C 20.22, H 2.59, N 0, S 0.76; found (%): C 20.10, H 2.48, N 0, S 0.89.

Elemental Analysis (after washing with CH_2Cl_2): Calculated (%) for $(C_{10}H_{15}FeP_5)_3(AuSbF_6)_2 \cdot 0.25 SC_4H_8$ (1903 g/mol): C 19.34, H 2.46, N 0, S 0.42; found (%): C 19.10, H 2.31, N 0, S 0.65.

Elemental Analysis (after washing with CH_3CN): Calculated (%) for $(C_{10}H_{15}FeP_5)_4(AuSbF_6)_2$ (2249 g/mol): C 21.36, H 2.69, N 0, S 0; found (%): C 21.28, H 2.24, N 0, S 0.

Analytical Data of **5**:

Yield: 8 mg (4 μ mol, 7%)

1H NMR (CD_3CN): δ [ppm] = 1.43 (s, 15 H, $[Cp^*Fe(\eta^5-P_5)]_{free}$), 1.94 (CD_3CN), 2.13 (s, H_2O), 5.44 (s, CD_2Cl_2).

$^{31}P\{^1H\}$ NMR (CD_3CN): δ [ppm] = 151.8 (s, $[Cp^*Fe(\eta^5-P_5)]_{free}$).

$^{19}F\{^1H\}$ NMR (CD_3CN): no signal detected.

Positive ion ESI-MS (CH_3CN): m/z = 888.8086 $[(Cp^*FeP_5)_2Au]^+$.

Negative ion ESI-MS (CH_3CN): m/z = 234.8945 $[SbF_6]^-$.

Elemental Analysis: Calculated (%) for $(C_{10}H_{15}FeP_5)_3(AuSbF_6)_2 \cdot 0.67 SC_4H_8 \cdot 0.1 C_7H_8$ (1972 g/mol): C 20.34, H 2.62, N 0, S 1.09; found (%): C 20.33, H 2.52, N traces, S 1.07.

Elemental Analysis (after washing with CH_2Cl_2): Calculated (%) for $(C_{10}H_{15}FeP_5)_3(AuSbF_6)_2$ (1903 g/mol): C 18.93, H 2.38, N 0, S 0; found (%): C 18.70, H 2.27, N 0, S 0.

Synthesis of $[(Cp^*Fe(\eta^5-P_5))_4Au_2](SbF_6)_2$ (**3b**)

To a mixture of $[(tth)AuCl]$ (119 mg, 0.371 mmol) and $AgSbF_6$ (127 mg, 0.370 mmol), SC_4H_8 (THT, 0.04 mL, 0.5 mmol) and CH_2Cl_2 (13 mL) were added and the mixture was stirred for 1h. After filtration from the grey precipitate ($AgCl$), the yellowish solution of *in situ* generated $[(tth)_2Au]SbF_6$ was layered with the solution of $[Cp^*Fe(\eta^5-P_5)]$ (63 mg, 0.18 mmol) in toluene

(13 mL) in a thin Schlenk tube. Already after two days, orange-brown plates of **3b** crystallized. After complete diffusion, the crystals were taken from the Schlenk wall with a spatula and quickly dipped into a Schlenk tube with a mixture of toluene / CH₂Cl₂ (1:1). The crystals were washed with toluene (3 x 3 mL), pentane (3 x 3 mL) and dried.

Analytical Data of **3b**:

Yield: 27 mg (12 μmol, 27%)

¹H NMR (CD₂Cl₂): δ [ppm] = 0.90 (t, ³J_{HH} = 7.6 Hz, 3 H, [Cp^{*}Fe(η⁵-P₅)]_{coord.}), 1.54 (s, H₂O), 1.67 (s, 6 H, [Cp^{*}Fe(η⁵-P₅)]_{coord.}), 1.69 (s, 6 H, [Cp^{*}Fe(η⁵-P₅)]_{coord.}), 2.19 (q, ³J_{HH} = 7.6 Hz, 2 H, [Cp^{*}Fe(η⁵-P₅)]_{coord.}), 2.34 (s, C₇H₈), 5.32 (s, CD₂Cl₂), 7.09 – 7.26 (m, C₇H₈), 7.32 (CDCl₃).

³¹P{¹H} NMR (CD₂Cl₂): δ [ppm] = 124.1 (s, ω_{1/2} = 24 Hz, [Cp^{*}Fe(η⁵-P₅)]_{coord.}).

¹⁹F{¹H} NMR (CD₂Cl₂): no signal detected.

Positive ion ESI-MS (CH₂Cl₂ / CH₃CN): *m/z* = 916.8411 [(Cp^{*}FeP₅)₂Au]⁺.

Negative ion ESI-MS (CH₂Cl₂ / CH₃CN): *m/z* = 234.8937 [SbF₆]⁻.

Elemental Analysis: Calculated (%) for (C₁₁H₁₇FeP₅)₄(AuSbF₆)₂ (2305 g/mol): C 22.92, H 2.97, N 0, S 0; found (%): C 23.24, H 2.84, N 0, S 0.

Analytical Data of the mother liquor:

³¹P{¹H} NMR (C₆D₆-cap.): δ [ppm] = 114.8 (s, ω_{1/2} = 14 Hz, [Cp^{*}Fe(η⁵-P₅)]_{coord.}).

¹⁹F{¹H} NMR (C₆D₆-cap.): no signal detected.

Synthesis of [(Cp^{*}Fe(η⁵-P₅))₃Au](SbF₆) · 2 C₆₀ (**6**)

[Cp^{*}Fe(η⁵-P₅)] (58 mg, 0.17 mmol) and C₆₀ (82 mg, 0.11 mmol) were dissolved in *o*-dichlorobenzene (*o*-DCB, 11 mL) by treatment in the ultrasonic bath for 15 minutes, and xylenes (4 mL) were added. To a mixture of [(tht)AuCl] (132 mg, 0.412 mmol) and AgSbF₆ (138 mg, 0.402 mmol), SC₄H₈ (THT, 0.036 mL, 0.41 mmol) and CH₂Cl₂ (14 mL) were added and the mixture was stirred for 1h. After filtration from the grey precipitate (AgCl), the yellowish solution of *in situ* generated [(tht)₂Au]SbF₆ was layered with the solution of [Cp^{*}Fe(η⁵-P₅)] and C₆₀ in a thick Schlenk tube. Already after two days, large black prisms of **6** crystallized. After complete diffusion, the crystals were taken from the Schlenk wall with a spatula and quickly dipped into a Schlenk tube with toluene. The crystals were washed with toluene (3 x 5 mL) and pentane (3 x 5 mL) and dried.

Analytical Data of **6**:

Yield: 74 mg (25 μmol, 45%)

¹H NMR (CS₂, C₆D₆-cap.): δ [ppm] = 0.38 (br, H₂O), 1.77 (s, [Cp^{*}Fe(η⁵-P₅)]_{free}), 7.16 (s, C₆D₆), 7.56 (s).

³¹P{¹H} NMR (CS₂, C₆D₆-cap.): δ [ppm] = 156.1 (s, [Cp^{*}Fe(η⁵-P₅)]_{free}).

$^{13}\text{C}\{^1\text{H}\}$ NMR (CS_2 , C_6D_6 -cap.): δ [ppm] = 127.69 (t, C_6D_6), 193.23 (s, CS_2).

$^{31}\text{P}\{^1\text{H}\}$ MAS NMR: δ [ppm] = 120 – 170 (br).

$^{13}\text{C}\{^1\text{H}\}$ MAS NMR: δ [ppm] = 12.9 (s, 10 C, $-\text{C}_5\text{Me}_5$), 16.3 (s, 5 C, $-\text{C}_5\text{Me}_5$), 95.7 (s, 10 C, $-\text{C}_5\text{Me}_5$), 97.3 (s, 5 C, $-\text{C}_5\text{Me}_5$), 143.4 (s, 60 C, C_{60}), 144.1 (s, 60 C, C_{60}).

EI-MS (70 eV): no signal detected.

Elemental Analysis: Calculated (%) for $(\text{C}_{10}\text{H}_{15}\text{FeP}_5)_3(\text{AuSbF}_6) \cdot 2 \text{C}_{60}$ (2912 g/mol): C 61.87, H 1.56, N 0, S 0; found (%): C 61.89, H 1.60, N 0, S 0.

Analytical Data of the mother liquor:

$^{31}\text{P}\{^1\text{H}\}$ NMR (C_6D_6 -cap.): no signal detected.

$^{13}\text{C}\{^1\text{H}\}$ NMR (C_6D_6 -cap.): δ [ppm] = 143.3 (s, C_{60}), 144.5 (s, C_{60}).

$^{19}\text{F}\{^1\text{H}\}$ NMR (C_6D_6 -cap.): no signal detected.

When the reaction was performed more diluted the yield decreased. The attempt to obtain additional crystals of **6** from the diluted reaction mixture by concentrating the mother liquor and layering with toluene only resulted in the formation of **5** instead.

Synthesis of $[(\text{Cp}^{\text{Bn}}\text{Fe}(\eta^5\text{-P}_5))\text{Au}(\text{SC}_4\text{H}_8)](\text{SbF}_6)$ (**7**)

To a mixture of $[(\text{tht})\text{AuCl}]$ (66 mg, 0.21 mmol) and AgSbF_6 (69 mg, 0.20 mmol), SC_4H_8 (THT, 0.02 mL, 0.2 mmol) and CH_2Cl_2 (7 mL) were added and the mixture was stirred for 1h. After filtration from the grey precipitate (AgCl), the yellowish solution of *in situ* generated $[(\text{tht})_2\text{Au}]\text{SbF}_6$ was added to a solution of $[\text{Cp}^{\text{Bn}}\text{Fe}(\eta^5\text{-P}_5)]$ (62 mg, 0.085 mmol) in CH_2Cl_2 (2 mL). After stirring for 15 minutes, the red-brown solution was filtered into a thin Schlenk tube and layered with pentane (14 mL). Already after two days, greenish-brown rods of **7** crystallized and red oil drops formed at the bottom of the Schlenk. After complete diffusion, the sticky crystals were taken from the Schlenk wall with a spatula and quickly dipped into a Schlenk tube with toluene. The crystals were washed with toluene (3 x 5 mL), pentane (3 x 5 mL) and dried.

Analytical Data of **7**:

Yield: 20 mg (16 μmol , 19%)

^1H NMR (CD_2Cl_2 , r.t.): δ [ppm] = 2.25 (m, 4 H, $\text{CH}_2(3,4)$, $(\text{tht})_{\text{coord.}}$), 3.53 (m, 4 H, $\text{CH}_2(2,5)$, $(\text{tht})_{\text{coord.}}$), 3.80 (s, 10 H, CH_2 , $[\text{Cp}^{\text{Bn}}\text{Fe}(\eta^5\text{-P}_5)]_{\text{coord.}}$), 5.32 (s, CD_2Cl_2), 6.26 (d, 10 H, $^3J_{\text{HH}} = 7.5$ Hz, *o*- CH_{aryl} , $[\text{Cp}^{\text{Bn}}\text{Fe}(\eta^5\text{-P}_5)]_{\text{coord.}}$), 6.83 (pst, 10 H, $^3J_{\text{HH}} = 7.7$ Hz, *m*- CH_{aryl} , $[\text{Cp}^{\text{Bn}}\text{Fe}(\eta^5\text{-P}_5)]_{\text{coord.}}$), 6.97 (t, 5 H, $^3J_{\text{HH}} = 7.4$ Hz, *p*- CH_{aryl} , $[\text{Cp}^{\text{Bn}}\text{Fe}(\eta^5\text{-P}_5)]_{\text{coord.}}$), 7.32 (CDCl_3).

$^{31}\text{P}\{^1\text{H}\}$ NMR (CD_2Cl_2 , r.t.): δ [ppm] = 128.8 (s, $\omega_{1/2} = 55$ Hz, $[\text{Cp}^{\text{Bn}}\text{Fe}(\eta^5\text{-P}_5)]_{\text{coord.}}$).

$^{19}\text{F}\{^1\text{H}\}$ NMR (CD_2Cl_2): no signal detected.

Positive ion ESI-MS (CH_2Cl_2): $m/z = 1649.1274$ $[(\text{Cp}^{\text{Bn}}\text{FeP}_5)_2\text{Au}]^+$, 1011.0800 $[(\text{Cp}^{\text{Bn}}\text{FeP}_5)\text{Au}(\text{tht})]^+$, 531.2687 $[\text{Cp}^{\text{Bn}}\text{O}]^+$, 373.0359 $[(\text{tht})_2\text{Au}]^+$.

Negative ion ESI-MS (CH₂Cl₂): $m/z = 234.8954$ [SbF₆].

Elemental Analysis: Calculated (%) for [(C₄₀H₃₅FeP₅)Au(SC₄H₈)]SbF₆ (1247 g/mol): C 42.37, H 3.47, N 0, S 2.57; found (%): C 42.52, H 3.45, N 0, S 2.59.

Analytical Data of the mother liquor:

³¹P{¹H} NMR (C₆D₆-cap.): δ [ppm] = 161.7 (s, [Cp^{Bn}Fe(η^5 -P₅)]_{free}).

¹⁹F{¹H} NMR (C₆D₆-cap.): no signal detected.

Improved synthesis of [Au(CH₃CN)₂]TEF

Au powder (0.16 g, 0.81 mmol) and NOTEF (0.60 g, 0.60 mmol, 0.75 eq.) were dissolved in CH₃CN (15 mL) in a double Schlenk tube equipped with a G₄ frit and a pressure relief valve. After stirring in the dark for six weeks, the solution was filtered to the other Schlenk tube side and dried.

Analytical Data of [Au(CH₃CN)₂]TEF:

Yield: 575 mg (0.461 mmol, 77%)

The applied excess of Au powder as well as the enhanced reaction time compared to the reported procedure^[26] were crucial for the isolation of pure [Au(CH₃CN)₂]TEF, since the separation of unreacted NOTEF was unsuccessful due to similar solubility.

Synthesis of [{Cp*Fe(η^5 -P₅)}Au]_n(TEF)_n (**8a**)

[(t^ht)AuCl] (93 mg, 0.14 mmol), [(PPh₃)AuCl] (143 mg, 0.14 mmol) and [Cp*Fe(η^5 -P₅)] (100 mg, 0.14 mmol) were dissolved in CH₂Cl₂ (20 mL). A solution of TITEF (677 mg, 0.26 mmol) in CH₂Cl₂ (20 mL) was slowly added and the mixture was stirred for 15 minutes. The brown solution was concentrated and decanted from an oily residue. The solution was layered with hexane and stored at -30 °C after complete diffusion. After three days yellow-brown needles of **8a** had crystallized.

Analytical Data of **8b**:

Yield: 38 mg (25 μ mol, 9%)

Attempts to reproduce the formation of **8a** by reaction of [Cp*Fe(η^5 -P₅)] with [Au(CH₃CN)₂]TEF (>1 eq.) only led to a) oil in case the reaction was performed by layering using CH₃CN as solvent for the Au salt or b) to rapid precipitation in case the reactants were stirred in CH₂Cl₂. The precipitate was characterized exemplarily for the analogous reaction with [Cp^xFe(η^5 -P₅)] (**8b**).

Synthesis of $[(\text{Cp}^*\text{Fe}(\eta^5\text{-P}_5))\text{Au}]_n(\text{TEF})_n$ (8b**)**

$[\text{Cp}^*\text{Fe}(\eta^5\text{-P}_5)]$ (13 mg, 0.036 mmol) and $[\text{Au}(\text{CH}_3\text{CN})_2]\text{TEF}$ (108 mg, 0.087 mmol) were dissolved in CH_2Cl_2 (8 mL) and stirred for 10 minutes. After filtration into a thin Schlenk tube the orange solution was layered with pentane (8 mL). Already after one day, yellow-orange rods of **8b** had crystallized. After complete diffusion, the mother liquor was decanted and the crystals were washed with toluene (3 x 10 mL), transferred to a new Schlenk tube, washed again with toluene (1 x 5 mL), pentane (3 x 5 mL) and dried.

Analytical Data of **8b**:

Yield: 44 mg (22 μmol , 61%)

Positive ion ESI-MS (CH_3CN): $m/z = 916.8392$ $[(\text{Cp}^*\text{FeP}_5)_2\text{Au}]^+$, 597.9296 $[(\text{Cp}^*\text{FeP}_5)\text{Au}(\text{CH}_3\text{CN})]^+$.

Negative ion ESI-MS (CH_3CN): $m/z = 966.9058$ $[\text{TEF}]^-$.

Elemental Analysis: Calculated (%) for $(\text{C}_{11}\text{H}_{17}\text{FeP}_5\text{AuAlO}_4\text{C}_{16}\text{F}_{36}) \cdot \text{CH}_3\text{CN} \cdot 5 \text{CH}_2\text{Cl}_2$ (1990 g/mol): C 20.52, H 1.52, N 0.70; found (%): C 20.30, H 1.03, N 0.76.

Unfortunately, most reproductions led to rapid precipitation of **8b** in the reaction mixture.

$[\text{Cp}^*\text{Fe}(\eta^5\text{-P}_5)]$ (14 mg, 0.039 mmol) and $[\text{Au}(\text{CH}_3\text{CN})_2]\text{TEF}$ (104 mg, 0.080 mmol) were dissolved in CH_2Cl_2 (5 mL) and stirred for one day, while precipitation was already observed immediately. The orange suspension was filtered over a G_4 frit and the precipitate was washed with CH_2Cl_2 (3 x 5 mL) and dried.

Analytical Data of **8b** (precipitated):

Yield: 55 mg (36 μmol , 93%)

$^{31}\text{P}\{^1\text{H}\}$ NMR (CD_3CN): δ [ppm] = 135.2 (br, $[\text{Cp}^*\text{Fe}(\eta^5\text{-P}_5)]_{\text{coord.}}$). *Signal almost below noise floor.*

$^{19}\text{F}\{^1\text{H}\}$ NMR (CD_3CN): δ [ppm] = -73.6 ($\text{HOC}(\text{CF}_3)_3$), -74.8 (s, TEF^-).

^1H NMR (pyridine- d_5): δ [ppm] = 0.62 (t, $^3J_{\text{HH}} = 7.6$ Hz, 3 H, $[\text{Cp}^*\text{Fe}(\eta^5\text{-P}_5)]_{\text{free}}$), 1.30 (s, 6 H, $[\text{Cp}^*\text{Fe}(\eta^5\text{-P}_5)]_{\text{free}}$), 1.33 (s, 6 H, $[\text{Cp}^*\text{Fe}(\eta^5\text{-P}_5)]_{\text{free}}$), 1.84 (q, $^3J_{\text{HH}} = 7.6$ Hz, 2 H, $[\text{Cp}^*\text{Fe}(\eta^5\text{-P}_5)]_{\text{free}}$), 2.20 (s, C_7H_8), 5.67 (s, CH_2Cl_2), 7.23 (m, C_7H_8).

$^{31}\text{P}\{^1\text{H}\}$ NMR (pyridine- d_5): δ [ppm] = 152.4 (s, $[\text{Cp}^*\text{Fe}(\eta^5\text{-P}_5)]_{\text{free}}$).

$^{19}\text{F}\{^1\text{H}\}$ NMR (pyridine- d_5): δ [ppm] = -75.7 ($\text{HOC}(\text{CF}_3)_3$), -76.7 (s, TEF^-).

Elemental Analysis: Calculated (%) for $\text{C}_{11}\text{H}_{17}\text{FeP}_5\text{AuAlO}_4\text{C}_{16}\text{F}_{36}$ (1524 g/mol): C 21.28, H 1.12, N 0; found (%): C 21.12, H 0.84, N 0.

Synthesis of $[(\text{Cp}^*\text{Fe}(\eta^5\text{-P}_5))_2\text{Au}](\text{TEF})$ (9a**)**

$[\text{Cp}^*\text{Fe}(\eta^5\text{-P}_5)]$ (35 mg, 0.10 mmol) and $[\text{Au}(\text{CH}_3\text{CN})_2]\text{TEF}$ (110 mg, 0.088 mmol) were dissolved in CH_2Cl_2 (5 mL) and stirred for one day. After filtration into a thin Schlenk tube the orange solution was layered with pentane (8 mL). Already after one day, brown rods of **9a** had

crystallized. After complete diffusion, the crystals were taken from the Schlenk wall with a spatula and quickly dipped into a Schlenk tube with CH₂Cl₂ / pentane (1:1). The crystals were washed with pentane (3 x 5 mL) and dried.

Analytical Data of **9a**:

Yield: 30 mg (16 μmol, 32%)

¹H NMR (CD₂Cl₂): δ [ppm] = 0.88 (t, ³J_{HH} = 7.0 Hz, C₅H₁₂), 1.24 – 1.31 (m, C₅H₁₂), 1.67 (s, 15 H, [Cp*Fe(η⁵-P₅)]_{coord.}), 2.34 (s, C₇H₈), 5.32 (s, CD₂Cl₂), 7.11 – 7.24 (m, C₇H₈), 7.32 (s, CDCl₃).

³¹P{¹H} NMR (CD₂Cl₂): δ [ppm] = 123.0 (s, ω_{1/2} = 62 Hz, [Cp*Fe(η⁵-P₅)]_{coord.}).

¹⁹F{¹H} NMR (CD₂Cl₂): δ [ppm] = -75.6 (s, TEF⁻), -139.3 (s).

Positive ion ESI-MS (CH₃CN): *m/z* = 888.8115 [(Cp*FeP₅)₂Au]⁺.

Negative ion ESI-MS (CH₃CN): *m/z* = 966.9085 [TEF]⁻.

Elemental Analysis: Calculated (%) for (C₁₀H₁₅FeP₅)₂AuAlO₄C₁₆F₃₆ · 0.3 C₅H₁₂ (1878 g/mol): C 23.99, H 1.80, N 0; found (%): C 24.25, H 1.54, N traces.

Analytical Data of the mother liquor:

³¹P{¹H} NMR (C₆D₆-cap.): δ [ppm] = 130.4 (br, ω_{1/2} = 7 Hz, [Cp*Fe(η⁵-P₅)]_{coord.}).

¹⁹F{¹H} NMR (C₆D₆-cap.): δ [ppm] = -74.8 (HOC(CF₃)₃), -75.5 (s, TEF⁻).

Synthesis of [{Cp*Fe(η⁵-P₅)₂Au}(TEF) (**9b**)

[Cp*Fe(η⁵-P₅)] (27 mg, 0.075 mmol) and [Au(CH₃CN)₂TEF (98 mg, <0.079 mmol)^[42] were dissolved in CH₂Cl₂ (5 mL) and stirred for five minutes. After filtration into a thin Schlenk tube the orange-red solution was layered with pentane (10 mL). After three days, brown rods of **9b** had crystallized. After complete diffusion, the crystals were taken from the Schlenk wall with a spatula and quickly dipped into a Schlenk tube with CH₂Cl₂ / pentane (1:1). The crystals were washed with pentane (3 x 5 mL) and dried.

Analytical Data of **9b**:

Yield: 30 mg (16 μmol, 42%)

¹H NMR (CD₂Cl₂): δ [ppm] = 0.90 (t, ³J_{HH} = 7.6 Hz, 3 H, [Cp*Fe(η⁵-P₅)]_{coord.}), 1.67 (s, 6 H, [Cp*Fe(η⁵-P₅)]_{coord.}), 1.69 (s, 6 H, [Cp*Fe(η⁵-P₅)]_{coord.}), 2.19 (q, ³J_{HH} = 7.6 Hz, 2 H, [Cp*Fe(η⁵-P₅)]_{coord.}), 2.34 (s, C₇H₈), 5.32 (s, CD₂Cl₂), 7.12 – 7.24 (m, C₇H₈), 7.32 (s, CDCl₃).

³¹P{¹H} NMR (CD₂Cl₂): δ [ppm] = 122.6 (s, ω_{1/2} = 35 Hz, [Cp*Fe(η⁵-P₅)]_{coord.}).

¹⁹F{¹H} NMR (CD₂Cl₂): δ [ppm] = -75.6 (s, TEF⁻), -139.3 (s).

Positive ion ESI-MS (CH₂Cl₂ / CH₃CN): *m/z* = 916.8410 [(Cp*FeP₅)₂Au]⁺.

Negative ion ESI-MS (CH₂Cl₂ / CH₃CN): *m/z* = 966.9082 [TEF]⁻.

Elemental Analysis: Calculated (%) for $(C_{11}H_{17}FeP_5)_2(AuAlO_4C_{16}F_{36})$ (1884 g/mol): C 24.23, H 1.82, N 0; found (%): C 24.73, H 1.58, N 0.

Analytical Data of the mother liquor:

$^{31}P\{^1H\}$ NMR (C_6D_6 -cap.): δ [ppm] = 124.9 (br, $\omega_{1/2}$ = 23 Hz, $[Cp^*Fe(\eta^5-P_5)]_{coord.}$).

$^{19}F\{^1H\}$ NMR (C_6D_6 -cap.): δ [ppm] = -74.8 (HOC(CF₃)₃), -75.5 (s, TEF).

6.5 Crystallographic Details

Crystals of **2a**, **2a'**, **2b**, **2b'**, **3a**, **3b**, **4-7**, **8a**, **8b** or **9a** were taken from a Schlenk flask under a stream of argon and immediately covered with mineral oil to prevent decomposition and a loss of solvent. The quickly chosen single crystals covered by a protective layer of the oil were directly placed on a magnetic base and into a stream of cold nitrogen with a pre-centered goniometer head with a CryoMount[®] and attached to the goniometer of a diffractometer.

The diffraction data for **2a**, **2a'**, **2b**, **2b'**, **3a**, **3b**, **4**, **5**, **7**, **8a** or **8b** were collected at 90, 100 (for **4**) or 123 K (for **2b** and **7**) on an Agilent Technologies diffractometer equipped with a Titan^{S2} CCD detector and a SuperNova CuK α microfocus source using ω scans with 0.5° frame width.

The data for **8a** were measured on an Agilent Technologies Gemini diffractometer equipped with Ruby CCD detector and a microfocus CuK α source using 0.5° ω scans at 100 K.

X-ray diffraction experiments for **6** and **9a** were measured at 14 and 23 K, respectively, at DESY PETRA III synchrotron (beamline P24)^[43] equipped with Huber 3-cycle diffractometer and MAR165 CCD (in case of **6**) or PILATUS CdTe 1M (**9a**) detectors and an open-flow He LT system. Data collection for **6** and **9a** was performed by 360° ϕ -rotation with 0.2° scan width and exposure 1 s per frame at a wavelength λ = 0.56076 Å (22.11 keV).

Data reduction and absorption correction for all experiments was performed with CrysAlisPro software.^[44] The structures were solved by direct methods with *SHELXS* or *SHELXT* and were refined by full-matrix least-squares method against F^2 in anisotropic approximation using multiprocessor variable memory versions of *SHELXL* (1997-2018).^[45] All non-hydrogen atoms with occupancies higher than 0.5 were refined anisotropically, while the hydrogen atoms were refined riding on pivot atoms.

In the structures, various types of disorder were encountered; for SbF₆⁻ or TEF⁻ counter-anions, solvent molecules, Cp* or Cp^{Bn} ligands, etc. The occupation factors for disordered positions of atoms were refined with fixed isotropic U_{iso} similar to the average U_{iso} for the fully occupied heavy atoms in the corresponding structure (usually 0.025-0.035 for heavy and 0.05 Å² for light atoms also with respect to the temperature). The resulting occupancies were fixed and

the structures were refined in anisotropic approximation. Some minor positions of the solvent molecules of disordered TEF⁻ anions were refined with restraint geometry. The restraints were removed at the final stage of the refinement when possible. In **6**, the disorder of C₆₀ was not suppressed by extremely low temperatures. The fullerene molecule was refined in a rigid body approximation; the model for the refinement was taken from Cambridge Structural Database (CSD^[46]) LUGKUT01.^[47] In each of two crystallographically unique positions the model of C₆₀ was generated in two orientations with the best fit to the electron density and the respective molecular occupation factor was refined and fixed in the resulting value.

Table 4. Experimental details for **2a** and **2a'**.

Crystal data	2a	2a'
Structural formula	$[(C_{10}H_{15}FeP_5)_3Au_2](GaCl_4)_2 \cdot 0.5(C_7H_8) \cdot 0.15(CH_2Cl_2)$	$[(C_{10}H_{15}FeP_5)_3Au_2](GaCl_4)_2 \cdot 1.6C_7H_8 \cdot 0.4C_6H_4F_2$
Chemical formula	$C_{33.65}H_{49.30}Au_2Cl_{8.30}Fe_3Ga_2P_{15}$	$C_{43.60}H_{59.40}Au_2Cl_{8F_{0.80}}Fe_3Ga_2P_{15}$
M_r	1913.54	2047.78
Crystal system, space group	Triclinic, $P\bar{1}$	Orthorhombic, $Pbca$
Temperature (K)	90	90
a, b, c (Å)	9.0101(3), 15.6107(5), 23.6681(6)	23.4813(2), 18.4552(2), 31.2969(3)
α, β, γ (°)	72.829(3), 86.028(2), 82.643(2)	90, 90, 90
V (Å ³)	3152.71 (17)	13562.6 (2)
Z	2	8
$F(000)$	1831	7898
D_x (Mg m ⁻³)	2.016	2.006
Radiation type	Cu $K\alpha$	Cu $K\alpha$
μ (mm ⁻¹)	21.90	20.33
Crystal shape and colour	Brown prism	Brown plate
Crystal size (mm)	0.06 × 0.04 × 0.03	0.18 × 0.09 × 0.05
Data collection		
Diffractometer	SuperNova, Titan ^{S2}	SuperNova, Titan ^{S2}
Absorption correction	Gaussian	Gaussian
T_{min}, T_{max}	0.460, 0.739	0.124, 0.449
No. of measured, independent and observed [$I > 2\sigma(I)$] reflections	20802, 12216, 8991	42537, 13503, 10347
R_{int}	0.054	0.029
$(\sin \theta/\lambda)_{max}$ (Å ⁻¹)	0.624	0.624
Range of h, k, l	$h = -10 \rightarrow 11,$ $k = -19 \rightarrow 18,$ $l = -21 \rightarrow 29$	$h = -20 \rightarrow 27,$ $k = -22 \rightarrow 22,$ $l = -37 \rightarrow 38$
Refinement		
$R[F^2 > 2\sigma(F^2)], wR(F^2), S$	0.040, 0.091, 0.94	0.031, 0.078, 0.93
No. of reflections	12216	13503
No. of parameters	645	794
No. of restraints	2	0
H-atom treatment	H-atom constrained	parameters H-atom parameters constrained
$\Delta_{max}, \Delta_{min}$ (e Å ⁻³)	1.90, -2.69	1.97, -1.08

Computer programs for **2a**: *CrysAlis PRO* 1.171.40.18c (Rigaku OD, 2018), *SHELXT2014/7* (Sheldrick, 2015), *SHELXL2014/7* (Sheldrick, 2014); for **2a'**: *CrysAlis PRO* 1.171.40.18c (Rigaku OD, 2018), *SHELXL2015/3* (Sheldrick, 2014), *SHELXL2014/7* (Sheldrick, 2014).

Table 5. Experimental details for **2b** and **2b'**.

Crystal data	2b	2b'
Structural formula	$[(C_{10}H_{15}FeP_5)_3Au_2](GaCl_4)_2 \cdot 0.5C_7H_8 \cdot 0.35CH_2Cl_2$	$[(C_{10}H_{15}FeP_5)_3Au_2](GaCl_4)_2 \cdot 0.5C_7H_8 \cdot 0.35CH_2Cl_2$
Chemical formula	$C_{36.85}H_{55.70}Au_2Cl_{8.70}Fe_3Ga_2P_{15}$	$C_{36.85}H_{55.70}Au_2Cl_{8.70}Fe_3Ga_2P_{15}$
M_r	1972.60	1972.60
Crystal system, space group	Triclinic, $P1$	Monoclinic, $P2_1/c$
Temperature (K)	123	90
a, b, c (Å)	9.0881(3), 15.8675(6), 23.8644(7)	9.07128(12), 24.2492(3), 29.5646(4)
α, β, γ (°)	72.027(3), 86.009(3), 81.599(3)	90, 98.2189(12), 90
V (Å ³)	3237.2 (2)	6436.55 (14)
Z	2	4
$F(000)$	1895	3791
D_x (Mg m ⁻³)	2.024	2.036
Radiation type	Cu $K\alpha$	Cu $K\alpha$
μ (mm ⁻¹)	22.02	21.63
Crystal shape	Dark brown plate	Dark yellow plank
Crystal size (mm)	0.16 × 0.13 × 0.03	0.12 × 0.05 × 0.03
Data collection		
Diffractometer	SuperNova, Titan ^{S2}	SuperNova, Titan ^{S2}
Absorption correction	Gaussian	Gaussian
T_{min}, T_{max}	0.141, 0.660	0.255, 0.603
No. of measured, independent and observed [$I > 2\sigma(I)$] reflections	20557, 12431, 11250	21873, 12565, 9816
R_{int}	0.022	0.034
$(\sin \theta/\lambda)_{max}$ (Å ⁻¹)	0.624	0.627
Range of h, k, l	$h = -11 \rightarrow 6,$ $k = -19 \rightarrow 18,$ $l = -29 \rightarrow 27$	$h = -11 \rightarrow 8,$ $k = -17 \rightarrow 29,$ $l = -34 \rightarrow 35$
Refinement		
$R[F^2 > 2\sigma(F^2)], wR(F^2), S$	0.035, 0.102, 1.10	0.036, 0.091, 0.99
No. of reflections	12431	12565
No. of parameters	655	632
No. of restraints	0	1
H-atom treatment	H-atom constrained	parameters H-atom parameters constrained
$\Delta_{max}, \Delta_{min}$ (e Å ⁻³)	1.91, -2.79	2.61, -1.87

Computer programs for **2b**: CrysAlisPro 1.171.38.46 (Rigaku OD, 2018), SHELXT-2018/5 (Sheldrick, 2018), SHELXL2014/7 (Sheldrick, 2014); for **2b'**: CrysAlis PRO 1.171.39.45g (Rigaku OD, 2018), SHELXL2015/3 (Sheldrick, 2015), SHELXL2014/7 (Sheldrick, 2014).

Table 6. Experimental details for **3a** and **3b**.

Crystal data	3a	3b
Structural formula	$[(C_{10}H_{15}FeP_5)_4Au_2](SbF_6)_2$	$[(C_{11}H_{17}FeP_5)_2Au](SbF_6)$
Chemical formula	$C_{40}H_{60}Au_2F_{12}Fe_4P_{20}Sb_2$	$C_{22}H_{34}AuF_6Fe_2P_{10}Sb$
M_r	2249.11	1152.61
Crystal system, space group	Triclinic, $P\bar{1}$	Monoclinic, $P2_1/c$
Temperature (K)	90	90
a, b, c (Å)	8.22240(19), 16.7022(3), 24.6249(6)	14.1340(2), 22.6968(3), 11.84522(19)
α, β, γ (°)	88.0033(17), 86.2346(19), 86.6611(17)	110.1048 (16)
V (Å ³)	3367.13 (13)	3568.37 (9)
Z	2	4
$F(000)$	2144	2208
D_x (Mg m ⁻³)	2.218	2.145
Radiation type	Cu $K\alpha$	Cu $K\alpha$
μ (mm ⁻¹)	26.00	24.56
Crystal shape and colour	Brown plate	Brown plate
Crystal size (mm)	0.16 × 0.07 × 0.03	0.09 × 0.03 × 0.02
Data collection		
Diffractometer	SuperNova, Titan ^{S2}	SuperNova, Titan ^{S2}
Absorption correction	Gaussian	Gaussian
T_{min}, T_{max}	0.166, 0.619	0.330, 0.689
No. of measured, independent and observed [$I > 2\sigma(I)$] reflections	22214, 13072, 10085	15403, 7099, 5602
R_{int}	0.043	0.055
$(\sin \theta/\lambda)_{max}$ (Å ⁻¹)	0.624	0.624
Range of h, k, l	$h = -10 \rightarrow 9,$ $k = -13 \rightarrow 20,$ $l = -30 \rightarrow 29$	$h = -17 \rightarrow 14,$ $k = -23 \rightarrow 28,$ $l = -14 \rightarrow 14$
Refinement		
$R[F^2 > 2\sigma(F^2)], wR(F^2), S$	0.036, 0.089, 0.93	0.039, 0.094, 0.97
No. of reflections	13072	7099
No. of parameters	741	389
No. of restraints	0	0
H-atom treatment	H-atom constrained	H-atom constrained
$\Delta_{max}, \Delta_{min}$ (e Å ⁻³)	3.35, -2.75	2.65, -2.43

Computer programs for **3a**: *CrysAlis PRO* 1.171.40.6a (Rigaku OD, 2018), *SHELXT2014/7* (Sheldrick, 2014), *SHELXL2014/7* (Sheldrick, 2014); for **3b**: *CrysAlis PRO* 1.171.40.18c (Rigaku OD, 2018), *SHELXS2018/3* (Sheldrick, 2018), *SHELXL2018/3* (Sheldrick, 2018).

Table 7. Experimental details for 4 and 5.

Crystal data	4	5
Structural formula	$[(C_{10}H_{15}FeP_5)_2Au](SbF_6)$	$[(C_{10}H_{15}FeP_5)_3Au_2](SbF_6)_2 \cdot 2C_7H_8$
Chemical formula	$C_{20}H_{30}AuF_6Fe_2P_{10}Sb$	$C_{44}H_{61}Au_2F_{12}Fe_3P_{15}Sb_2$
M_r	1124.55	2087.46
Crystal system, space group	Triclinic, $P\bar{1}$	Orthorhombic, $Pbca$
Temperature (K)	100	90
a, b, c (Å)	14.37678(12), 15.90521(16), 15.91187(15)	23.4741(3), 17.5218(2), 31.4779(3)
α, β, γ (°)	89.5405(8), 72.3082(8), 72.2996(8)	90, 90, 90
V (Å ³)	3288.01 (6)	12947.1 (3)
Z	4	8
$F(000)$	2144	7968
D_x (Mg m ⁻³)	2.272	2.142
Radiation type	Cu $K\alpha$	Cu $K\alpha$
μ (mm ⁻¹)	26.64	24.16
Crystal shape and colour	Dark brown prism	Brown rod
Crystal size (mm)	0.07 × 0.05 × 0.03	0.07 × 0.05 × 0.03
Data collection		
Diffractometer	SuperNova, Titan ^{S2}	SuperNova, Titan ^{S2}
Absorption correction	Gaussian	Gaussian
T_{min}, T_{max}	0.302, 0.576	0.248, 0.620
No. of measured, independent and observed [$I > 2\sigma(I)$] reflections	37137, 13047, 12561	30038, 12753, 8396
R_{int}	0.024	0.033
$(\sin \theta/\lambda)_{max}$ (Å ⁻¹)	0.624	0.624
Range of h, k, l	$h = -15 \rightarrow 17$, $k = -19 \rightarrow 19$, $l = -19 \rightarrow 19$	$h = -18 \rightarrow 28$, $k = -21 \rightarrow 18$, $l = -38 \rightarrow 35$
Refinement		
$R[F^2 > 2\sigma(F^2)], wR(F^2), S$	0.022, 0.056, 1.09	0.036, 0.087, 0.88
No. of reflections	13047	12753
No. of parameters	760	789
No. of restraints	0	0
H-atom treatment	H-atom parameters constrained	H-atom parameters constrained
$\Delta_{max}, \Delta_{min}$ (e Å ⁻³)	1.43, -1.06	1.50, -1.87

Computer programs for 4: *CrysAlis PRO* 1.171.40.66a (Rigaku OD, 2019), *SHELXT2018/3* (Sheldrick, 2018), *SHELXL2014/7* (Sheldrick, 2014); for 5: *CrysAlis PRO* 1.171.40.18c (Rigaku OD, 2018), *SHELXT2015/3* (Sheldrick, 2013), *SHELXL2014/7* (Sheldrick, 2014).

Table 8. Experimental details for **6** and **7**.

Crystal data	6	7
Structural formula	$[(C_{10}H_{15}FeP_5)_3Au](SbF_6) \cdot 2C_{60}$	$[(C_{11}H_{17}FeP_5)Au(SC_4H_8)](SbF_6) \cdot 0.625CH_2Cl_2$
Chemical formula	$C_{150}H_{45}AuF_6Fe_3P_{15}Sb$	$C_{44.62}H_{44.25}AuCl_{1.25}F_6FeP_5Sb$
M_r	2911.67	1300.34
Crystal system, space group	Orthorhombic, $Pnma$	Monoclinic, $P2_1/n$
Temperature (K)	14	123
a, b, c (Å)	27.59546(6), 16.35584(4), 22.32253(5)	17.4517(3), 10.4554(2), 26.1943(5)
β (°)	90	99.7084 (17)
V (Å ³)	10075.20 (4)	4711.06 (15)
Z	4	4
$F(000)$	5728	2537
D_x (Mg m ⁻³)	1.920	1.833
Radiation type	Synchrotron, $\lambda = 0.56076$ Å	Cu $K\alpha$
μ (mm ⁻¹)	1.32	15.84
Crystal shape	Prism	Plate
Colour	Black	Dark brown
Crystal size (mm)	0.3 × 0.3 × 0.2	0.15 × 0.09 × 0.07
Data collection		
Diffractometer	P24 beamline, PETRA III, DESY, Huber diffractometer, MAR165 CCD	SuperNova, Titan ^{S2}
Absorption correction	Multi-scan	Gaussian
T_{min}, T_{max}	0.725, 1.000	0.252, 0.458
No. of measured, independent and observed [$I > 2\sigma(I)$] reflections	217843, 17987, 15694	16343, 9122, 7314
R_{int}	0.053	0.034
$(\sin \theta/\lambda)_{max}$ (Å ⁻¹)	0.746	0.624
Range of h, k, l	$h = -41 \rightarrow 41$, $k = -24 \rightarrow 24$, $l = -33 \rightarrow 33$	$h = -18 \rightarrow 21$, $k = -12 \rightarrow 8$, $l = -32 \rightarrow 29$
Refinement		
$R[F^2 > 2\sigma(F^2)], wR(F^2), S$	0.066, 0.182, 1.05	0.051, 0.142, 1.07
No. of reflections	17986	9122
No. of parameters	501	722
No. of restraints	24	2
H-atom treatment	H-atom parameters constrained	H-atom parameters constrained
$\Delta_{max}, \Delta_{min}$ (e Å ⁻³)	2.58, -2.82	1.90, -0.78

Computer programs for **6**: *CrysAlis PRO* 1.171.41.21a (Rigaku OD, 2019), *SHELXT2018/5* (Sheldrick, 2018), *SHELXL2018/3* (Sheldrick, 2018); for **7**: *CrysAlis PRO* 1.171.40.18c (Rigaku OD, 2018), *SHELXT2014/7* (Sheldrick, 2014), *SHELXL2014/7* (Sheldrick, 2014).

Table 9. Experimental details for **8a** and **8b**.

Crystal data	8a	8b
Structural formula	$[(C_{10}H_{15}FeP_5)Au](AlO_4C_{16}F_{36})$	$[(C_{11}H_{17}FeP_5)Au](AlO_4C_{16}F_{36})$
Chemical formula	$C_{26}H_{15}AlAuF_{36}FeO_4P_5$	$C_{37}H_{17}O_4F_{36}AlAuFeP_5$
M_r	1510.03	1524.05
Crystal system, space group	Monoclinic, $P2_1/c$	Monoclinic, $P2_1/n$
Temperature (K)	100	90
a, b, c (Å)	10.5454(3), 14.9339(3), 28.9423(9)	29.1772 (5), 14.9185 (2), 21.2608 (3)
β (°)	92.395(4)	92.938 (2)
V (Å ³)	4554.0(2)	9242.2 (2)
Z	4	8
$F(000)$	2880	5824
D_x (Mg m ⁻³)	2.202	2.191
Radiation type	Cu $K\alpha$	Cu $K\alpha$
μ (mm ⁻¹)	12.12	11.95
Crystal shape and colour	yellow needle	Orange rod
Crystal size (mm)	0.45 × 0.04 × 0.02	0.36 × 0.05 × 0.04
Data collection		
Diffractometer	Gemini R-Ultra, Ruby	SuperNova, Titan ^{S2}
Absorption correction	multi-scan	Gaussian
T_{min}, T_{max}	0.524, 0.785	0.193, 0.894
No. of measured, independent and observed [$I > 2\sigma(I)$] reflections	25688, 7871, 5959	33837, 18010, 10513
R_{int}	0.0739	0.043
$(\sin \theta/\lambda)_{max}$ (Å ⁻¹)	0.597	0.624
Range of h, k, l	$h = -12 \rightarrow 12,$ $k = -14 \rightarrow 17,$ $l = -34 \rightarrow 32$	$h = -35 \rightarrow 32,$ $k = -16 \rightarrow 18,$ $l = -25 \rightarrow 26$
Refinement		
$R[F^2 > 2\sigma(F^2)], wR(F^2), S$	0.067, 0.218, 1.11	0.050, 0.139, 0.89
No. of reflections	7871	18010
No. of parameters	819	1745
No. of restraints	0	45
H-atom treatment	H-atom constrained	parameters H-atom parameters constrained
$\Delta\rho_{max}, \Delta\rho_{min}$ (e Å ⁻³)	2.87, -2.27	1.50, -1.56

Computer programs for **8a**: CrysAlis CCD, Oxford Diffraction Ltd., Version 1.171.32.15, CrysAlis RED, SHELXS97 (Sheldrick, 1990), SHELXL97 (Sheldrick, 1997); for **8b** CrysAlis PRO 1.171.40.18c (Rigaku OD, 2018), SHELXT 2014/5 (Sheldrick, 2014), SHELXL2018/3 (Sheldrick, 2018).

Table 10. Experimental details for **9a**.

Crystal data	9a
Structural formula	$[(C_{10}H_{15}FeP_5)_4Au_2](TEF)_2 \cdot 0.625(CH_2Cl_2)$
Chemical formula	$C_{72.62}H_{61.25}Al_2Au_2Cl_{1.25}F_{72}Fe_4O_8P_{20}$
M_r	3764.97
Crystal system, space group	Monoclinic, $C2/c$
Temperature (K)	23
a, b, c (Å)	37.5584 (5), 21.24925 (19), 35.8922 (3)
β (°)	117.3677 (12)
V (Å ³)	25439.0 (5)
Z	8
$F(000)$	14546
D_x (Mg m ⁻³)	1.966
Radiation type	Synchrotron, $\lambda = 0.56076$ Å
μ (mm ⁻¹)	1.71
Crystal shape	Rod
Colour	Light brown
Crystal size (mm)	0.2 × 0.1 × 0.1
Data collection	
Diffractometer	P24 beamline, PETRA III, DESY, Huber diffractometer, PILATUS CdTe 1M
Absorption correction	Multi-scan
T_{min}, T_{max}	0.578, 1.000
No. of measured, independent and observed [$I > 2\sigma(I)$] reflections	169600, 28477, 24010
R_{int}	0.052
$(\sin \theta/\lambda)_{max}$ (Å ⁻¹)	0.658
Range of h, k, l	$h = -49 \rightarrow 49$, $k = -26 \rightarrow 26$, $l = -47 \rightarrow 47$
Refinement	
$R[F^2 > 2\sigma(F^2)], wR(F^2), S$	0.047, 0.147, 1.13
No. of reflections	28477
No. of parameters	2189
No. of restraints	24
H-atom treatment	H-atom parameters constrained
$\Delta\rho_{max}, \Delta\rho_{min}$ (e Å ⁻³)	1.71, -2.86

Computer programs for **9a**: *CrysAlis PRO* 1.171.41.21a (Rigaku OD, 2019), *SHELXT2018/5* (Sheldrick, 2018), *SHELXL2018/3* (Sheldrick, 2018).

6.6 Author Contributions

- The synthesis and characterization of compounds **2a** – **9b** (except for crystalline **8a**) were performed by Helena Brake
- The synthesis of crystalline compound **8a** was performed by Dr. Christoph Schwarzmaier and are also part of his diploma thesis (University of Regensburg, **2008**).
- X-ray structural analyses of **2a** – **9b** were performed by Dr. Eugenia Peresykina, Dr. Sc. Alexander V. Virovets and Helena Brake. Parts of this research were carried out at PETRAIII at DESY, a member of the Helmholtz Association (HGF), by Dr. Eugenia Peresykina and Dr. Sc. Alexander V. Virovets. EP and AV are grateful to the P24 beamline team for their assistance.
- X-ray structural analysis of **8a** was performed by Dr. Eugenia Peresykina, Dr. Sc. Alexander V. Virovets and Dr. Christoph Schwarzmaier
- The X-ray powder diffraction of compound **8b** was performed by Dr. Christian Klimas (group of Prof. Dr. Arno Pfitzner)
- The MAS NMR spectra of compound **6** were recorded by Prof. Dr. Werner Kremer
- The manuscript (introduction, results and discussion, experimental part, conclusion; including figures and schemes) was written by Helena Brake
- The section ‘crystallographic details’ was written by Dr. Eugenia Peresykina

6.7 References

- [1] a) S. Chakraborty, G. R. Newkome, *Chem. Soc. Rev.* **2018**, *47*, 3991-4016; b) W. Wang, Y.-X. Wang, H.-B. Yang, *Chem. Soc. Rev.* **2016**, *45*, 2656-2693; c) T. R. Cook, Y.-R. Zheng, P. J. Stang, *Chem. Rev.* **2013**, *113*, 734-777.
- [2] a) A. Bavykina, N. Kolobov, I. S. Khan, J. A. Bau, A. Ramirez, J. Gascon, *Chem. Rev.* **2020**, *120*, 8468-8353; b) Y.-S. Wei, M. Zhang, R. Zou, Q. Xu, *Chem. Rev.* **2020**, *120*, 12089-12174.
- [3] L. E. Kreno, K. Leong, O. K. Farha, M. Allendorf, R. P. Van Duyne, J. T. Hupp, *Chem. Rev.* **2012**, *112*, 1105-1125.
- [4] a) L. S. Xie, G. Skorupskii, M. Dincă, *Chem. Rev.* **2020**, *120*, 8536-8580; b) A. E. Thorarinsdottir, T. D. Harris, *Chem. Rev.* **2020**, *120*, 8716-8789; c) Y.-X. Tan, F. Wang, J. Zhang, *Chem. Soc. Rev.* **2018**, *47*, 2130-2144; d) K. Rissanen, *Chem. Soc. Rev.* **2017**, *46*, 2638-2648; e) Y. Inokuma, S. Yoshioka, J. Ariyoshi, T. Arai, Y. Hitora, K. Takada, S. Matsunaga, K. Rissanen, M. Fujita, *Nature* **2013**, *495*, 461-466.
- [5] a) J. M. Lehn, A. Rigault, J. Siegel, J. Harrowfield, B. Chevrier, D. Moras, *Proc. Natl. Acad. Sci. USA* **1987**, *84*, 2565-2569; b) J.-M. Lehn, A. Rigault, *Angew. Chem. Int. Ed. Engl.* **1988**, *27*, 1095-1097; c) H. S. Sahoo, D. K. Chand, *Dalton Trans.* **2010**, *39*, 7223-7225.
- [6] a) M. Ruben, J. Rojo, F. J. Romero-Salguero, L. H. Uppadine, J.-M. Lehn, *Angew. Chem. Int. Ed.* **2004**, *43*, 3644-3662; b) P. N. W. Baxter, J.-M. Lehn, G. Baum, D. Fenske, *Chem. Eur. J.* **2000**, *6*, 4510-4517; c) J. Rojo, J.-M. Lehn, G. Baum, D. Fenske, O. Waldmann, P. Müller, *Eur. J. Inorg. Chem.* **1999**, 517-522; d) P. N. W. Baxter, J.-M. Lehn, J. Fischer, M.-T. Youinou, *Angew. Chem. Int. Ed. Engl.* **1994**, *33*, 2284-2287.
- [7] a) M.-M. Gan, J.-Q. Liu, L. Zhang, Y.-Y. Wang, F. E. Hahn, Y.-F. Han, *Chem. Rev.* **2018**, *118*, 9587-9641; b) S. Chakraborty, G. R. Newkome, *Chem. Soc. Rev.* **2018**, *47*, 3991-4016; c) L. Xu, Y.-X. Wang, L.-J. Chen, H.-B. Yang, *Chem. Soc. Rev.* **2015**, *44*, 2148-2167.
- [8] a) E.-S. M. El-Sayed, D. Yuan, *Chem. Lett.* **2019**, *49*, 28-53; b) T. R. Cook, P. J. Stang, *Chem. Rev.* **2015**, *115*, 7001-7045.
- [9] a) S. Peng, Q. He, G. I. Vargas-Zúñiga, L. Qin, I. Hwang, S. K. Kim, N. J. Heo, C.-H. Lee, R. Dutta, J. L. Sessler, *Chem. Soc. Rev.* **2020**, *49*, 865-907; b) C. E. Housecroft, E. C. Constable, *J. Inorg. Organomet. Polym.* **2018**, *28*, 414-427; c) A. Gorczyński, J. M. Harrowfield, V. Patroniak, A. R. Stefankiewicz, *Chem. Rev.* **2016**, *116*, 14620-14674; d) C. J. Brown, F. D. Toste, R. G. Bergman, K. N. Raymond, *Chem. Rev.* **2015**, *115*, 3012-3035; e) M. Han, D. M. Engelhard, G. H. Clever, *Chem. Soc. Rev.* **2014**, *43*, 1848-1860.

- [10] a) Z. Ji, C. Trickett, X. Pei, O. M. Yaghi, *J. Am. Chem. Soc.* **2018**, *140*, 13618–13622; b) A. J. Clough, J. W. Yoo, M. H. Mecklenburg, S. C. Marinescu, *J. Am. Chem. Soc.* **2015**, *137*, 118–121; c) X. Huang, P. Sheng, Z. Tu, F. Zhang, J. Wang, H. Geng, Y. Zou, C.-a. Di, Y. Yi, Y. Sun, W. Xu, D. Zhu, *Nat. Commun.* **2015**, *6*, 7408; d) Y. Jiang, B. Li, Y. Wang, D. Liu, X. Song, X. Chang, *J. Organomet. Chem.* **2014**, *759*, 37-45.
- [11] a) S. Welsch, L. J. Gregoriades, M. Sierka, M. Zabel, A. V. Virovets, M. Scheer, *Angew. Chem. Int. Ed.* **2007**, *46*, 9323-9326; b) M. Fleischmann, S. Welsch, H. Krauss, M. Schmidt, M. Bodensteiner, E. V. Peresykina, M. Sierka, C. Gröger, M. Scheer, *Chem. Eur. J.* **2014**, *20*, 3759-3768.
- [12] a) J. Bai, A. V. Virovets, M. Scheer, *Angew. Chem. Int. Ed.* **2002**, *41*, 1737-1740; b) S. Welsch, C. Gröger, M. Sierka, M. Scheer, *Angew. Chem. Int. Ed.* **2011**, *50*, 1435-1438; c) F. Dielmann, A. Schindler, S. Scheuermayer, J. Bai, R. Merkle, M. Zabel, A. V. Virovets, E. V. Peresykina, G. Brunklaus, H. Eckert, M. Scheer, *Chem. Eur. J.* **2012**, *18*, 1168-1179; d) F. Dielmann, C. Heindl, F. Hastreiter, E. V. Peresykina, A. V. Virovets, R. M. Gschwind, M. Scheer, *Angew. Chem. Int. Ed.* **2014**, *53*, 13605-13608; e) C. Heindl, S. Heini, D. Lüdeker, G. Brunklaus, W. Kremer, M. Scheer, *Inorg. Chim. Acta* **2014**, *422*, 218-223; f) M. Fleischmann, S. Welsch, E. V. Peresykina, A. V. Virovets, M. Scheer, *Chem. Eur. J.* **2015**, *21*, 14332-14336; g) C. Heindl, *Dissertation (University of Regensburg)* **2015**; h) C. Heindl, E. Peresykina, A. V. Virovets, I. S. Bushmarinov, M. G. Medvedev, B. Krämer, B. Dittrich, M. Scheer, *Angew. Chem. Int. Ed.* **2017**, *56*, 13237-13243.
- [13] a) J. Bai, A. V. Virovets, M. Scheer, *Science* **2003**, *300*, 781-783; b) M. Scheer, J. Bai, B. P. Johnson, R. Merkle, A. V. Virovets, C. E. Anson, *Eur. J. Inorg. Chem.* **2005**, 4023-4026; c) M. Scheer, A. Schindler, R. Merkle, B. P. Johnson, M. Linseis, R. Winter, C. E. Anson, A. V. Virovets, *J. Am. Chem. Soc.* **2007**, *129*, 13386-13387; d) M. Scheer, A. Schindler, C. Gröger, A. V. Virovets, E. V. Peresykina, *Angew. Chem. Int. Ed.* **2009**, *48*, 5046-5049; e) M. Scheer, A. Schindler, J. Bai, B. P. Johnson, R. Merkle, R. Winter, A. V. Virovets, E. V. Peresykina, V. A. Blatov, M. Sierka, H. Eckert, *Chem. Eur. J.* **2010**, *16*, 2092-2107; f) A. Schindler, C. Heindl, G. Balázs, C. Gröger, A. V. Virovets, E. V. Peresykina, M. Scheer, *Chem. Eur. J.* **2012**, *18*, 829-835; g) C. Schwarzmaier, A. Schindler, C. Heindl, S. Scheuermayer, E. V. Peresykina, A. V. Virovets, M. Neumeier, R. Gschwind, M. Scheer, *Angew. Chem. Int. Ed.* **2013**, *52*, 10896-10899; h) E. V. Peresykina, C. Heindl, A. Schindler, M. Bodensteiner, A. V. Virovets, M. Scheer, *Z. Kristallogr. - Cryst. Mater.* **2014**, *229*, 735-740; i) F. Dielmann, M. Fleischmann, C. Heindl, E. V. Peresykina, A. V. Virovets, R. M. Gschwind, M. Scheer, *Chem. Eur. J.* **2015**, *21*, 6208-6214; j) C. Heindl, E. V. Peresykina, A. V. Virovets, W. Kremer, M. Scheer, *J. Am. Chem. Soc.* **2015**, *137*, 10938-10941; k) S. Heini, E. Peresykina,

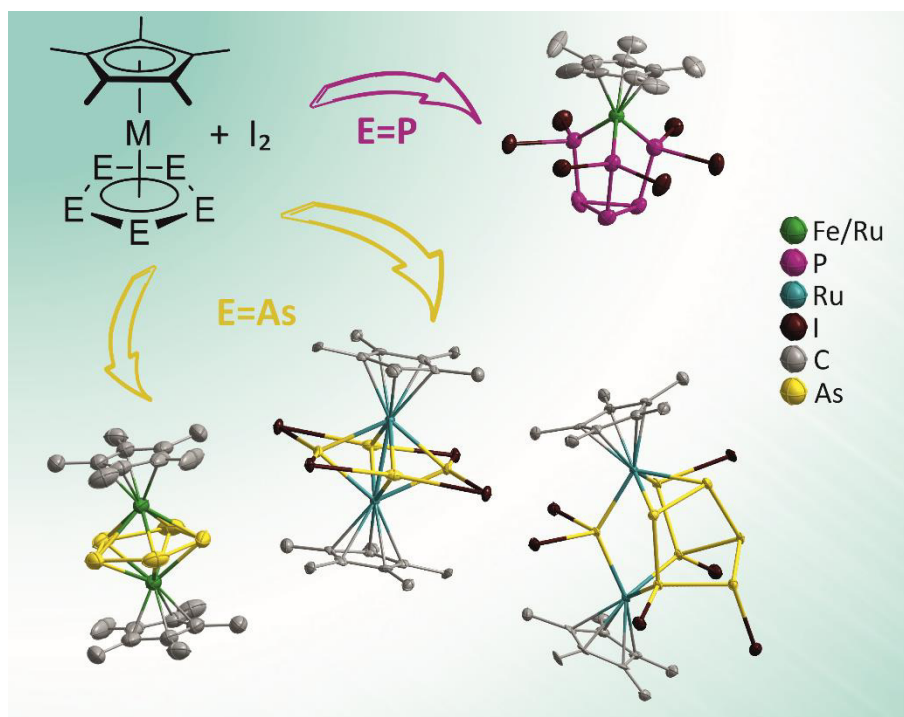
- J. Sutter, M. Scheer, *Angew. Chem. Int. Ed.* **2015**, *54*, 13431-13435; l) E. Peresykina, C. Heindl, A. Virovets, H. Brake, E. Mädl, M. Scheer, *Chem. Eur. J.* **2018**, *24*, 2503-2508; m) H. Brake, E. Peresykina, C. Heindl, A. V. Virovets, W. Kremer, M. Scheer, *Chem. Sci.* **2019**, *10*, 2940-2944; n) J. Schiller, E. Peresykina, A. V. Virovets, M. Scheer, *Angew. Chem. Int. Ed.* **2020**, *59*, 13647-13650.
- [14] a) M. Scheer, L. J. Gregoriades, A. V. Virovets, W. Kunz, R. Neueder, I. Krossing, *Angew. Chem. Int. Ed.* **2006**, *45*, 5689-5693; b) B. Hiltl, *Dissertation (University of Regensburg)* **2018**.
- [15] E. Peresykina, M. Bielmeier, A. Virovets, M. Scheer, *Chem. Sci.* **2020**, *11*, 9067-9071.
- [16] a) V. J. Catalano, M. A. Malwitz, S. J. Horner, J. Vasquez, *Inorg. Chem.* **2003**, *42*, 2141-2148; b) M.-C. Brandys, R. J. Puddephatt, *J. Am. Chem. Soc.* **2001**, *123*, 4839-4840; c) M. J. Irwin, J. J. Vittal, G. P. A. Yap, R. J. Puddephatt, *J. Am. Chem. Soc.* **1996**, *118*, 13101-13102.
- [17] R. Hoy, P. Lönnecke, E. Hey-Hawkins, *Dalton Trans.* **2018**, *47*, 14515-14520.
- [18] a) L. C. Forfar, T. J. Clark, M. Green, S. M. Mansell, C. A. Russell, R. A. Sanguramath, J. M. Slattery, *Chem. Commun.* **2012**, *48*, 1970-1972; b) J. E. Borger, M. S. Bakker, A. W. Ehlers, M. Lutz, J. Chris Slootweg, K. Lammertsma, *Chem. Commun.* **2016**, *52*, 3284-3287.
- [19] M. Di Vaira, P. Stoppioni, M. Peruzzini, *J. Chem. Soc., Dalton Trans.* **1990**, 109-113.
- [20] M. Scheer, L. J. Gregoriades, M. Zabel, J. Bai, I. Krossing, G. Bruncklaus, H. Eckert, *Chem. Eur. J.* **2008**, *14*, 282-295.
- [21] a) O. J. Scherer, T. Brück, *Angew. Chem. Int. Ed. Engl.* **1987**, *26*, 59; b) O. J. Scherer, T. Brück, G. Wolmershäuser, *Chem. Ber.* **1988**, *121*, 935-938; c) F. Dielmann, R. Merkle, S. Heindl, M. Scheer, *Z. Naturforsch. B: J. Chem. Sci.* **2009**, *64*, 3-10.
- [22] The S content found in the elemental analysis could not be explained by the mere presence of THT. Thus, it is proposed that the precipitate is formed from an unknown S containing reaction product of THT.
- [23] Unit cell parameters: monoclinic P, $a = 9.1209(6) \text{ \AA}$, $b = 24.187(2) \text{ \AA}$, $c = 29.543(3) \text{ \AA}$; $\beta = 98.175(7)^\circ$; $V = 6451.2(9) \text{ \AA}^3$. Unfortunately, the crystal quality was not sufficient for X-ray structural analysis of **2b''**. However, the unit cell parameters are similar to those of **2b'**. While the structure of **2b'** contains CH_2Cl_2 solvate molecules, this is not possible for **2b''** obtained in the absence of CH_2Cl_2 . Hence, it is suggested that **2b''** displays a solvatomorph of **2b'**.
- [24] N. Savjani, S. P. Bew, D. L. Hughes, S. J. Lancaster, M. Bochmann, *Organometallics* **2012**, *31*, 2534-2537.
- [25] R. S. Ruoff, D. S. Tse, R. Malhotra, D. C. Lorents, *J. Phys. Chem.* **1993**, *97*, 3379-3383.

- [26] T. A. Engesser, C. Friedmann, A. Martens, D. Kratzert, P. J. Malinowski, I. Krossing, *Chem. Eur. J.* **2016**, *22*, 15085-15094.
- [27] Unit cell parameters: monoclinic C, $a \approx 37 \text{ \AA}$, $b \approx 21 \text{ \AA}$, $c \approx 36 \text{ \AA}$, $\beta \approx 118^\circ$; $V \approx 25000 \text{ \AA}^3$.
- [28] B. Cordero, V. Gomez, A. E. Platero-Prats, M. Reves, J. Echeverria, E. Cremades, F. Barragan, S. Alvarez, *Dalton Trans.* **2008**, 2832-2838.
- [29] H. Schmidbaur, H. G. Raubenheimer, L. Dobrzańska, *Chem. Soc. Rev.* **2014**, *43*, 345-380.
- [30] A. Bondi, *J. Phys. Chem.* **1964**, *68*, 441-451.
- [31] The tilting angle is measured between the P_5 plane of the 1,3-coordinating $[\text{Cp}^R\text{Fe}(\eta^5\text{-P}_5)]$ ligand complex and the P_4 plane within the $\{\text{P}_4\text{Au}_2\}$ rings of the $\{\text{Cp}^R\text{Fe}(\eta^5\text{-P}_5)\}_2\text{Au}_2$ unit.
- [32] The out-of-plane (oop) angles here are determined by the angle between the Au-P bond and the plane drawn through the coordinating P atom and the two neighboring ones within the P_5 cycle.
- [33] P. Pyykkoe, M. Atsumi, *Chem. Eur. J.* **2009**, *15*, 12770-12779.
- [34] **1***: ^1H NMR (CD_3CN): δ [ppm] = 1.36 (s).
1*: ^1H NMR ($\text{CD}_2\text{Cl}_2 + \text{CD}_3\text{CN}$): δ [ppm] = 0.70 (t), 1.39 (s), 1.41 (s), 1.91 (m, $\text{CD}_3\text{CN} + \mathbf{1}^*$).
- [35] I. Krossing, *Chem. Eur. J.* **2001**, *7*, 490-502.
- [36] Stirring of $[\text{Au}(\text{CH}_3\text{CN})_2]\text{TEF}$ in CH_2Cl_2 results in a pale pink solution after one hour, while after one day the color had intensified and a Au^0 mirror had formed.
- [37] **1***: ^1H NMR (CD_2Cl_2): δ [ppm] = 1.43 (s).
1*: ^1H NMR (CD_2Cl_2): δ [ppm] = 0.75 (t, $^3J_{\text{HH}} = 7.6 \text{ Hz}$, 3 H, $-\text{CH}_2\text{CH}_3$), 1.43 (s, 6 H, $-\text{CH}_3$), 1.45 (s, 6 H, $-\text{CH}_3$), 1.94 (q, $^3J_{\text{HH}} = 7.6 \text{ Hz}$, 2 H, $-\text{CH}_2\text{CH}_3$).
- [38] K. H. Robin, D. B. Edwin, M. C. d. M. Sonia, G. Robin, G. Pierre, *Pure Appl. Chem.* **2001**, *73*, 1795-1818.
- [39] S. Enthaler, M. Weidauer, *Catal. Lett.* **2011**, *141*, 833-838.
- [40] O. J. Scherer, H. Sitzmann, G. Wolmershäuser, *J. Organomet. Chem.* **1984**, *268*, C9-C12.
- [41] O. J. Scherer, C. Blath, G. Wolmershäuser, *J. Organomet. Chem.* **1990**, *387*, C21-C24.
- [42] The $[\text{Au}(\text{CH}_3\text{CN})_2]\text{TEF}$ applied was synthesized by stirring only for three weeks instead of six and contained some impurities as shown by elemental analysis. Hence, the applied molar amount is overestimated and presumably falls below 1 eq.
- [43] https://photon-science.desy.de/facilities/petra_iii/beamlines/p24_chemical_crystallography/eh2/index_eng.html
- [44] *CrysAlisPRO*, different versions 2006-2020, Rigaku Oxford Diffraction.
- [45] G. M. Sheldrick. *Acta Cryst.* **2015**, *C71*, 3-8; G. M. Sheldrick. *Acta Cryst.* **2015**, *A71*, 3-8.
- [46] C. R. Groom, I. J. Bruno, M. P. Lightfoot and S. C. Ward, *Acta Cryst.* **2016**, *B72*, 171-179.

- [47] A. O'Neil, C. Wilson, J. M. Webster, F. J. Allison, J. A. K. Howard, and M. Poliakoff. *Angew. Chem. Int. Ed.* **2002**, *41*, 3796.

7 Iodination of *cyclo*-E₅-Complexes (E = P, As)

H. Brake, E. Peresyphkina, A. V. Virovets, M. Piesch, W. Kremer, L. Zimmermann, C. Klimas, M. Scheer, *Angew. Chem. Int. Ed.* **2020**, *59*, 16241-16246. ([view online](#))

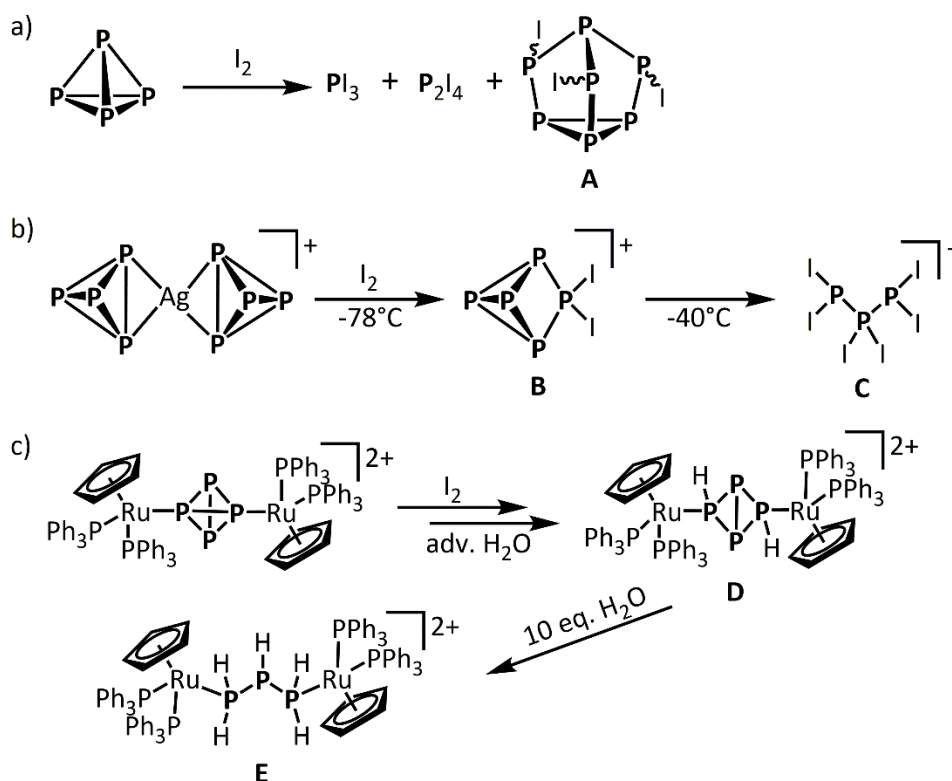


Abstract:

In a high-yield one-pot synthesis, the reactions of $[\text{Cp}^*\text{M}(\eta^5\text{-P}_5)]$ ($\text{M} = \text{Fe}$ (**1**), Ru (**2**)) with I_2 resulted in the selective formation of $[\text{Cp}^*\text{MP}_6\text{I}_6]^+$ salts (**3**, **4**). The products comprise unprecedented all-*cis* tripodal triphosphino-cyclotriphosphine ligands. The iodination of $[\text{Cp}^*\text{Fe}(\eta^5\text{-As}_5)]$ (**6**) gave, in addition to $[\text{Fe}(\text{CH}_3\text{CN})_6]^{2+}$ salts of the rare $[\text{As}_6\text{I}_8]^{2-}$ (in **7**) and $[\text{As}_4\text{I}_{14}]^{2-}$ (in **8**) anions, the first di-cationic Fe-As triple decker complex $[(\text{Cp}^*\text{Fe})_2(\mu, \eta^{5:5}\text{-As}_5)][\text{As}_6\text{I}_8]$ (**9**). In contrast, the iodination of $[\text{Cp}^*\text{Ru}(\eta^5\text{-As}_5)]$ (**10**) did not result in the full cleavage of the M-As bonds. Instead, a number of dinuclear complexes were obtained: $[(\text{Cp}^*\text{Ru})_2(\mu, \eta^{5:5}\text{-As}_5)][\text{As}_6\text{I}_8]_{0.5}$ (**11**) represents the first Ru-As₅ triple decker complex, thus completing the series of monocationic complexes $[(\text{Cp}^*\text{M})_2(\mu, \eta^{5:5}\text{-E}_5)]^+$ ($\text{M} = \text{Fe}, \text{Ru}$; $\text{E} = \text{P}, \text{As}$). $[(\text{Cp}^*\text{Ru})_2\text{As}_8\text{I}_6]$ (**12**) crystallizes as a racemic mixture of both enantiomers, while $[(\text{Cp}^*\text{Ru})_2\text{As}_4\text{I}_4]$ (**13**) crystallizes as a symmetric and an asymmetric isomer and features a unique tetramer of $\{\text{AsI}\}$ arsinidene units as a middle deck.

7.1 Introduction

As a step in the synthesis of organophosphorus compounds, the chlorination of white phosphorus (P₄) still is an industrially relevant process, in which PCl₃ or PCl₅ are formed and subsequently derivatized to give the desired products that act for example, as additives in fertilizers, detergents and food.^[1] Very recently, the detailed mechanism of the complete iodination of P₄ to four equivalents of PI₃ was postulated based on DFT analyses, describing each step as a concerted reaction rather than a redox reaction.^[2] Before, Tattershall and Kendall had studied halogenations of white phosphorus thoroughly by performing ³¹P NMR investigations on the reaction mixtures.^[3] In those reactions of P₄ with Br₂ or I₂, besides larger amounts of PX₃ and P₂X₄, also P₄Br₂ and P₇X₃ (X = Br, I (**A**)) are formed (Scheme 1a). In general, while P₄X₂ butterfly compounds were detected only for X = Cl, Br, the P₇X₃ cage compound was rather formed for X = I. However, the products were merely detected spectroscopically, and a synthetic access was not given. Moreover, iodine is not only known to accelerate the transformation of white phosphorus to red phosphorus, but also to contribute to the transformation of red phosphorus to its black allotrope.^[4] In both the formation of the P₇I₃ cage and the allotropic transformations of phosphorus, besides the cleavage, also the recombination of the P-P bonds must take place.



Scheme 1. Selected examples of iodination reactions as a route to novel polyphosphorus frameworks.

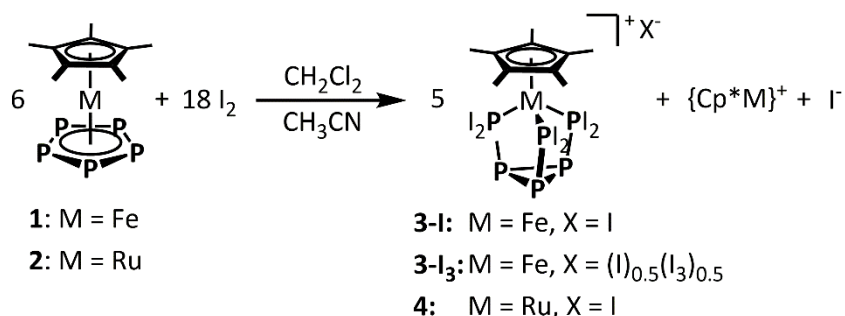
Hence, the question arises if novel polyphosphorus frameworks can also be synthesized by reactions of polyphosphorus complexes with I₂. Nevertheless, such investigations are rare and limited to P₄ complexes. While the reaction of an η¹-P₄ complex with I₂ gives four equivalents of

PI₃, one of which stays coordinated to the metal center,^[5] the reaction of [Ag(η²-P₄)₂][TEF] (TEF⁻ = Al{OC(CF₃)₃}₄⁻) with I₂ at -78°C affords the binary phosphorus-rich cation [P₅I₂]⁺ (**B**), which reacts further above -40°C to give P₃I₆⁺ (**C**) as the first subvalent binary P-X cation (Scheme 1b).^[6] In 2012, Stoppioni et al. reported on the synthesis of a bridging P₄H₂ butterfly ligand complex **D** from a bridging P₄ complex by reaction with I₂ and adventitious water. Further hydrolysis afforded a bridging P₃H₅ ligand in **E**, releasing phosphorous acid (Scheme 1c). Both the P₄H₂ butterfly and the linear P₃H₅ ligand had until then been unprecedented.^[7] These examples clearly show the potential of iodinating P₄ and its complexes for the synthesis of unprecedented polyphosphorus moieties. Thus, the question arises as to what interesting new products may be expected when polypnictogen complexes other than P₄ complexes are iodinated. Surprisingly, such investigations have been left untouched so far.

Herein, we report on the iodination of the *cyclo*-E₅ complexes [Cp*M(η⁵-E₅)] (M = Fe, Ru; E = P, As) to establish iodination reactions as a general method in polypnictogen chemistry to obtain unprecedented E-I-containing cage compounds and ligands.

7.2 Results and Discussion

Layering a CH₂Cl₂ solution of [Cp*Fe(η⁵-P₅)]^[8] (**1**) with three equivalents of I₂ dissolved in CH₃CN afforded small black needles of [Cp*FeP₆I₆]I (**3-I**) and [Cp*FeP₆I₆](I)_{0.5}(I₃)_{0.5} (**3-I₃**) (Scheme 2). Upon drying of **3-I₃** or mixtures thereof, I₂ was evaporated out of the crystals leaving pure **3-I** in 79% yield. Applying an excess of I₂ (9 equiv.) affords PI₃ in addition to crystalline **3-I₃**. Analogously, the layering reaction of [Cp*Ru(η⁵-P₅)]^[9] (**2**) with three equivalents of I₂ resulted in [Cp*RuP₆I₆]I (**4**) as metallic black needles in 84% yield (Scheme 2).



Scheme 2. Reactions of [Cp*Fe(η⁵-P₅)] (M = Fe (**1**), Ru (**2**)) with I₂.

The fate of the respective {Cp*M} fragments could not be clarified, even though [FeCp*₂]⁺ was detected in the ESI-MS spectrum of the mother liquor of the reaction with M = Fe. Furthermore, the interception of the {Cp*M} fragments by another equivalent of [Cp*M(η⁵-P₅)] (**1** or **2**) to form the triple decker cations [(Cp*M)₂(μ,η^{5:5}-P₅)]⁺ is conceivable. In fact, in the ³¹P{¹H} NMR spectrum of the mother liquor of the reaction with M = Fe, a signal at -18.6 ppm

was detected, comprising a chemical shift similar to that of other known $[(\text{Cp}^R\text{Fe})_2(\mu, \eta^{5:5}\text{-P}_5)]^+$ salts ($[(\text{Cp}^*\text{Fe})_2(\mu, \eta^{5:5}\text{-P}_5)][\text{BF}_4]^{[10]}$; $\delta_{\text{P}} = -23.0$ ppm; $[\text{CpFe}(\mu, \eta^{5:5}\text{-P}_5)\text{FeCp}^*][\text{PF}_6]^{[11]}$; $\delta_{\text{P}} = -15.8$ ppm).

Alternatively, **3-I** can be synthesized more easily by stirring both starting materials pre-dissolved in CH_2Cl_2 and CH_3CN , where the $[\text{Cp}^*\text{FeP}_6\text{I}_6]^+$ salts (**3**) precipitated immediately as an insoluble black microcrystalline powder. After drying, its composition and purity were confirmed by elemental analysis and X-ray powder diffraction, respectively (Figure 1).

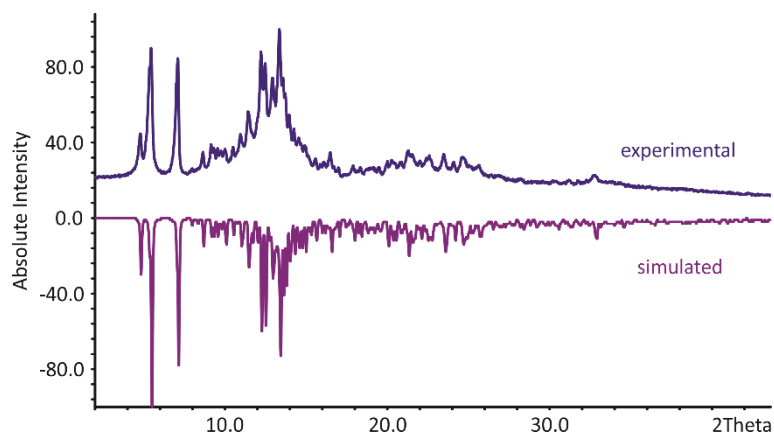


Figure 1. Experimental (top) X-ray powder diffraction pattern of precipitated $[\text{Cp}^*\text{FeP}_6\text{I}]$ (**3-I**) in comparison to the diffraction pattern (bottom) simulated from the single-crystal X-ray data of **3-I**.

The molecular structures of **3-I**, **3-I₃** and **4** (Figure 2) each reveal a tripodal *cyclo*-P₃(PI₂)₃ ligand coordinating to the {Cp*M} fragment thus capping the three PI₂-groups, with the resulting MP₆ core resembling the nortricyclane structure of P₇³⁻.^[12] Interestingly, a related *cyclo*-P₃(P^tBu₂)₃ ligand was reported by Fritz et al., acting as a bridging ligand towards two Ni centers.^[13] However, in contrast to **3** and **4**, the phosphino-substituents in *cyclo*-P₃(P^tBu₂)₃ are not arranged all-*cis*, thus impeding the formation of mononuclear complexes. Moreover, Fenske reported on the cluster $[(\text{Cp}^*\text{Fe})_3\{(\eta^3\text{-P}_3)\text{Fe}\}\text{P}_6]$ comprising an all-*cis* arranged *cyclo*-P₃(P)₃ core but with capping Cp*Fe units.^[14] Therefore, compounds **3** and **4** represent unprecedented examples of free metallo-nortricyclane derivatives.

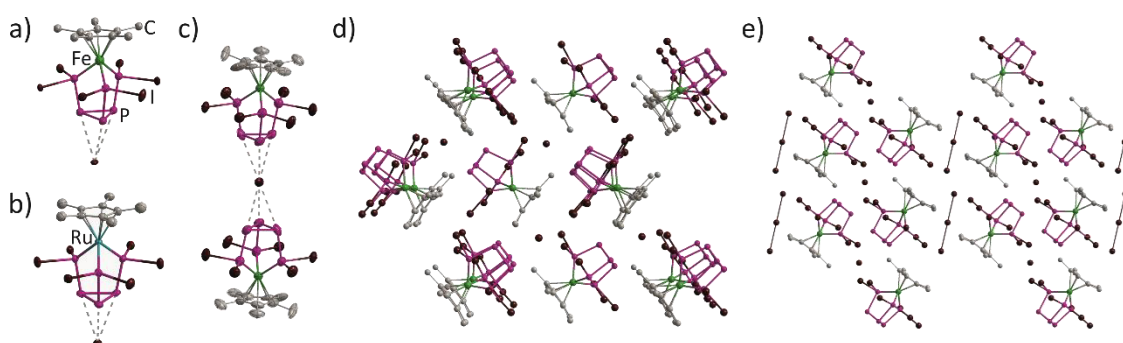


Figure 2. Molecular structures with shortened P...I contacts of a) $[\text{Cp}^*\text{FeP}_6\text{I}]$ (**3-I**); b) $[\text{Cp}^*\text{RuP}_6\text{I}]$ (**4**); c) $[\text{Cp}^*\text{FeP}_6\text{I}]_{0.5}(\text{I}_3)_{0.5}$ (**3-I₃**). A.d.p. ellipsoids at 50% probability level and H atoms omitted for clarity. Crystal packing in d) $[\text{Cp}^*\text{FeP}_6\text{I}]$ (**3-I**) and e) $[\text{Cp}^*\text{FeP}_6\text{I}]_{0.5}(\text{I}_3)_{0.5}$ (**3-I₃**) drawn in the ball-and-sticks model with view along the crystallographic *b* axis.

The P-P bond lengths in **3-I**, **3-I₃** and **4** each are in the range of P-P single bonds (2.22 Å),^[15] with the endocyclic bonds (2.160(6) Å – 2.234(9) Å) being somewhat shorter than the exocyclic ones (2.245(4) Å – 2.281(7) Å). The exocyclic P-P bonds in **3** and **4** are also longer than the P-P bonds between the basal and the equatorial P atoms in C₃ symmetric P₇R₃-nortricyclan structures (2.1709(4) – 2.229(1) Å),^[16a,b] but comparable to the exocyclic P-P bond lengths in the *cyclo*-P₃(P^tBu₂)₃ ligand (2.259(1) – 2.276(1) Å).^[13d] While the endocyclic P-P bond lengths for **3-I** and **4** (2.199(9) – 2.234(9) Å) are comparable to the bond lengths between the basal P atoms of P₇R₃ nortricyclan structures (2.2021(7) – 2.244(11) Å)^[16c,d] and to the endocyclic P-P bond lengths of the *cyclo*-P₃(P^tBu₂)₃ ligand (2.199(1) – 2.208(1) Å),^[13d] two of the endocyclic P-P bond lengths of **3-I₃** are shorter (2.160(6), 2.187(7) and 2.210(6) Å). Interestingly, in all three structures, close P...I⁻ contacts between the I⁻ counterions and P atoms of the P₃ cycles are found with distances of 3.395(3) Å to 3.666(5) Å being smaller than the sum of the van-der-Waals radii (3.78 Å).^[17] While for **3-I** and **4** the average distances are especially short, in **3-I₃** it is slightly longer and the I⁻ counterion interacts with P atoms of two P₃ cycles compared to one as in **3-I** and **4** (Figure 2a-c). Similar P...I⁻ distances (3.426(1) Å) are also found for a *P*-Iodo-substituted N-heterocyclic phosphine (I-NHP), in which the P...I interaction was described as predominantly ionic.^[18] The significantly shortened I⁻...I specific contacts between the I⁻ counterion and two iodine atoms of the PI₂ ligands of two different [Cp*FeP₆I₆]⁺ cations (3.3523(9) and 3.535(1) Å (**3-I**); 3.336(2) and 3.508(2) Å (**4**); cf. sum of the van-der-Waals radii 3.96 Å)^[17] give rise to different 3D networks for **3-I** and **4** in the solid state. In a similar way, the [Cp*FeP₆I₆]⁺ cations in **3-I₃** participate in I⁻...I specific contacts of 3.545(1) Å with terminal atoms of the I₃⁻ counter anion.

Compounds **3** and **4** are insoluble in all common solvents (pentane, toluene, CH₂Cl₂, CH₃CN and thf). Moreover, **3** is insoluble in 1,4-dioxane, dme, CS₂, liquid SO₂, whereas it is soluble under decomposition in dmsO, DMF, NMP, HMPA (PI₃ and **1** detected in the ³¹P{¹H} NMR spectra). Attempts to obtain a soluble [Cp^RFeP₆I₆]⁺ salt by a) anion exchange of **3-I** with TITEF and b) reaction of [Cp^{BIG}Fe(η⁵-P₅)]^[19] (Cp^{BIG} = C₅(*p*-C₆H₄ⁿBu)₅) with I₂ only resulted in the formation of PI₃. These facts suggest that the [Cp*FeP₆I₆]⁺ cation might be unstable in solution.

Therefore, solid state ³¹P{¹H} NMR magic angle spinning (MAS) spectroscopy was carried out on **3** and **4** (Figure 3). For **3**, two signals are detected at chemical shifts of about +75 ppm (PI₂ groups) and -60 ppm (P₃ cycle) next to rotational sidebands (*, ♦). In the Ru analogue **4**, the corresponding signals are slightly shifted to higher field (+58 ppm and -67 ppm). For a sample of **4**, the spinning frequency was exemplarily adjusted from 11400 Hz (Figure 3d) to 25000 Hz (Figure 3e) allowing the clear assignment of signals vs. rotational sidebands. Furthermore, the crystal packing does not seem to influence the ³¹P{¹H} MAS NMR spectrum. While for a) crystals of **3-I₃** were isolated and dried to give **3-I**, in b) powder of **3-I** was used and in c) crystals of **3-I₃**

were isolated without significant drying. Nevertheless, the resulting spectra do not exhibit any substantial differences.

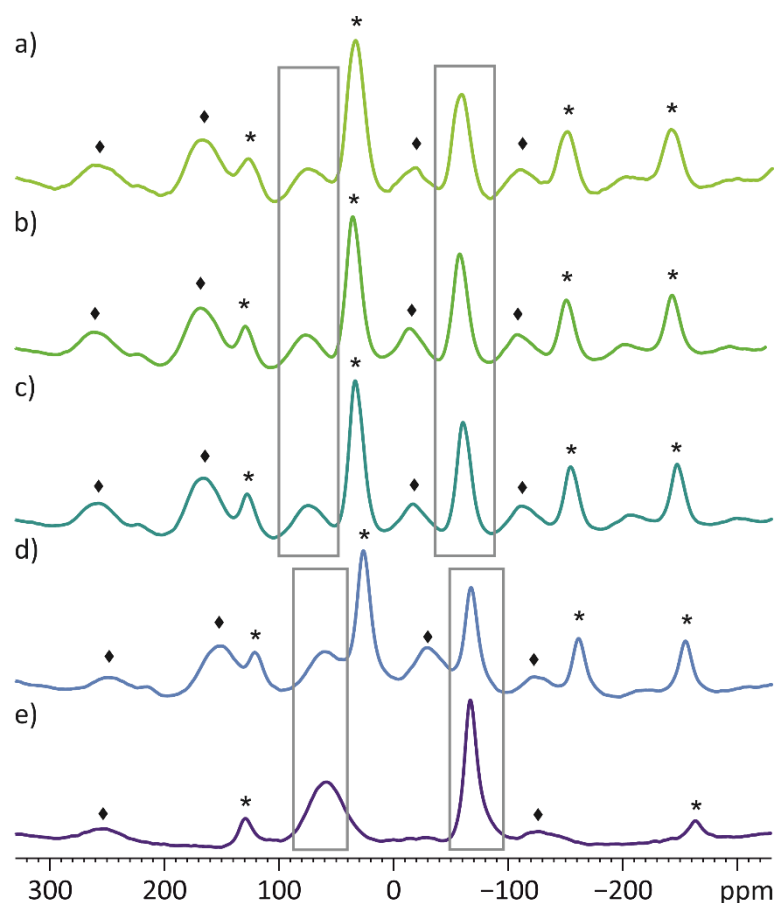


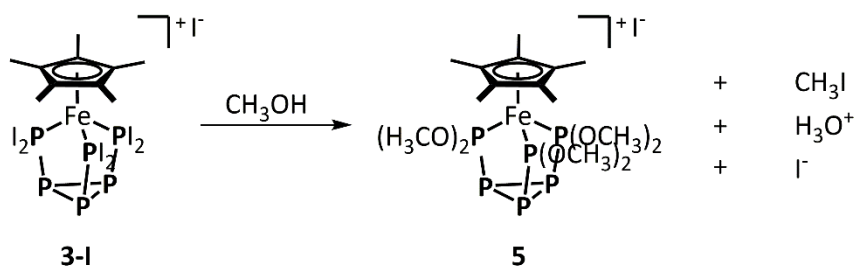
Figure 3. $^{31}\text{P}\{^1\text{H}\}$ MAS NMR spectra of a) dried crystals of **3-I₃**; b) powder of **3-I**; c) undried crystals of **3-I₃**; d) powder of **4**, each recorded at 14000 Hz MAS frequency and e) $^{31}\text{P}\{^1\text{H}\}$ MAS NMR spectrum of powder of **4** recorded at 25000 Hz MAS frequency. Rotational sidebands are marked with * or ◆, signals are highlighted by grey boxes.

In the solid state EI-MS spectrum of **3-I** and **4**, only the respective pentaphosmetalocenenes **1⁺** and **2⁺** as well as **I₂⁺** were detected, besides **HI⁺**, **I⁺**, **PI₃⁺** and **P₂I₄⁺**, thus further confirming the high sensibility of the $[\text{Cp}^*\text{MP}_6\text{I}_6]^+$ cations.

DFT computations of the frontier molecular orbitals of **3-I** (B3LYP/def2-SVP level of theory, Computational Details, Figure 10) show that the HOMO as well as the LUMO are mainly located on the P_6I_6 ligand. The HOMO displays formally a linear combination of p orbitals of the iodine substituents, while the LUMO predominantly shows antibonding character between the P and I atoms (formally σ^*). Therefore, a nucleophilic attack on the P-I bonds becomes conceivable.

So far, subsequent reactions of **3-I** have mostly led to the re-reduction of the $[\text{Cp}^*\text{FeP}_6\text{I}_6]^+$ cation, as $[\text{Cp}^*\text{Fe}(\eta^5\text{-P}_5)]$ (**1**) was detected in the $^{31}\text{P}\{^1\text{H}\}$ NMR spectra of the reactions with KC_8 , $[\text{CoCp}_2]$, NaCp , LiCp^* , LiAlH_4 , NaBH_4 , KH , RLi (R = Me, ⁿBu, ^tBu), $[\text{Cp}''_2\text{Zr}(\eta^{1:1}\text{-P}_4)]$. Cyclovoltammetry measurements in the solid state confirmed the possibility of reducing **3-I** (cf. Experimental Part, Figure 6).

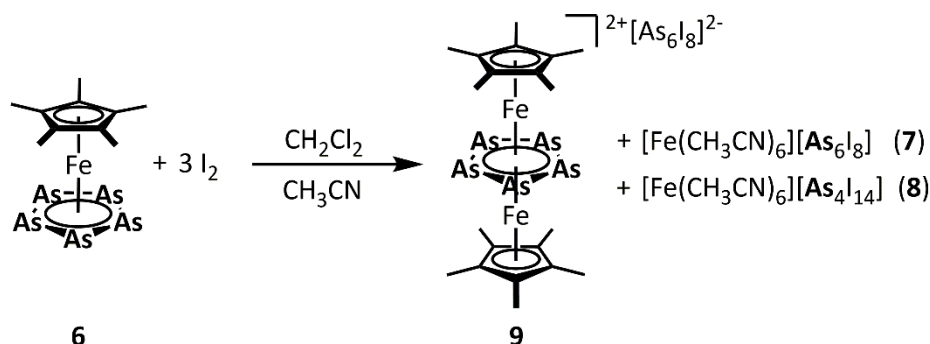
Halogen exchange reactions of **3-I** with KF or AgF resulted in disproportionation to give **1** and the PF₆⁻ anion. Interestingly, **3-I** is soluble in CH₃OH but a reaction occurs. The ESI-MS spectrum of the resulting solution suggests the formation of [Cp*FeP₆(OCH₃)₆]I (**5**, Scheme 3), with [Cp*FeP₆(OCH₃)_{6-x}H_x]⁺ (x = 1-3) fragments being detected as well, which could be side-products or just as well fragmentation products of **5** (cleavage of 1-3 molecules of CH₂O) under mass spectrometric conditions.



Scheme 3. Reaction of [Cp*FeP₆I₆] (**3-I**) with CH₃OH.

The ³¹P{¹H} NMR spectrum of the reaction mixture shows two multiplets at 285 ppm and -152 ppm. **5** is formed faster (30 minutes instead of overnight stirring) when **3-I** is reacted with NaOCH₃ in CH₃OH, and the subsequent extraction with CH₂Cl₂ leaves a colorless precipitate (presumably NaI). Unfortunately, this reaction is less selective and numerous attempts to crystallize **5** failed.

After exploring the iodination reactions of the P-containing complexes, the question arose as to what would happen when As-containing complexes were used instead. The heavier homologue of pentaphosphaferrocene, [Cp*Fe(η⁵-As₅)]^[20] (**6**), shows similar redox events in the cyclic voltammogram, with, however, its reactivity towards KH differing significantly.^[21] Hence, similarly to the synthesis of **3-I**, the iodination reaction of the arsenic analogue [Cp*Fe(η⁵-As₅)] (**6**) was carried out. The obtained single crystals, as products of a concomitant crystallization, were characterized by X-ray diffraction revealing the structures of [Fe(CH₃CN)₆][As₆I₈] (**7**), [Fe(CH₃CN)₆][As₄I₁₄] (**8**) and [(Cp*Fe)₂(μ,η^{5:5}-As₅)]₂[As₆I₈] (**9**) (Scheme 4).



Scheme 4. Reaction of [Cp*Fe(η⁵-As₅)] (**6**) with I₂.

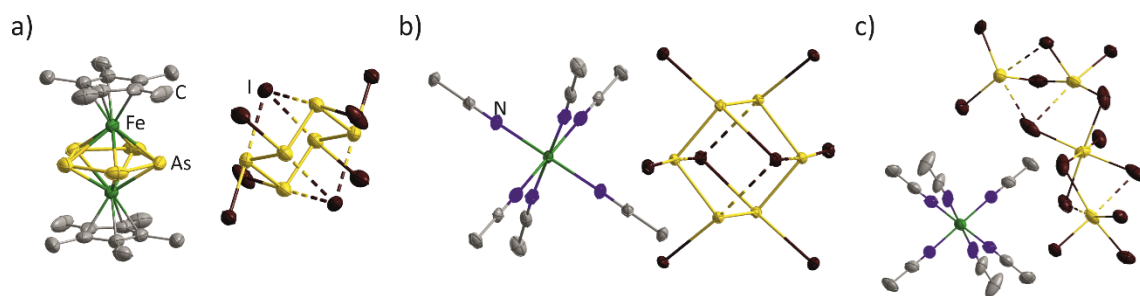


Figure 4. Molecular structures of a) **9** (including counterion); b) **7** and c) **8**. A.d.p. ellipsoids at 50% probability level. H atoms and minor positions of disorder omitted for clarity.

While, during the formation of **7** and **8**, a complete cleavage of the Fe-As bonds must have taken place, **9** is notably the first example of a di-cationic Fe-As triple decker complex (Figure 4). The As-As bond lengths within the 29 VE triple decker di-cation of **9** (2.380(5) Å – 2.392(6) Å) range between a normal single (2.42 Å) and a double bond (2.28 Å).^[15] When compared to the monocationic triple decker complexes [CpFe($\mu, \eta^{5:5}$ -As₅)FeCp*][PF₆]^[20] (av. 2.328 Å) and [(Cp^{Bn}Fe)₂($\mu, \eta^{5:5}$ -As₅)] [BF₄]^[22] (av. 2.34 Å), the As-As bonds in **9** are slightly elongated. The Fe...Fe distance in **9** (2.795(4) Å) is still longer than the sum of the covalent radii (2.64 Å),^[23] but significantly smaller than in the comparable monocations (3.074(3) Å,^[20] 3.125(1) Å and 3.1207(9) Å^[22]), thus indicating some Fe...Fe bonding interactions. This is further confirmed by a Wiberg bond index (WBI) of 0.38. Moreover, ESR spectroscopy was carried out on crystals of **9**, showing an axial signal with *g* values of 1.98691 (*g*(*z*)) and 1.93421 (*g*(*x,y*)), roughly corresponding to one unpaired electron (Experimental Part, Figure 7).

The [Fe(CH₃CN)₆]²⁺ complex cation as well as the [As₆I₈]²⁻ and [As₄I₁₄]²⁻ anions were already structurally characterized as salts with other respective counterions.^[24] Therefore, the structures of **7** and **8** will not be discussed hereafter. Remarkably, [As₆I₈]²⁻ has so far only been synthesized by the reduction of AsI₃ (either directly or via another As^I iodide reagent),^[24b,d] so the reaction according to Scheme 4 represents, for the first time, a formal oxidation of (As₅)⁻ to this anion. [As₄I₁₄]²⁻ was previously only synthesized by the reaction of grey As and phthalonitrile at 493 K under a stream of I₂ vapor under much harsher conditions.^[24c]

In order to prevent the cleavage of the arsenic ligand from the metal center during iodination, I₂ was also allowed to react with [Cp*Ru(η^5 -As₅)]^[25] (**10**, Scheme 5), with, again, three concomitant crystallization products.

as compared to **13-sym**. Nevertheless, all As-I distances are still close to the bond distances in other As-I-As bridges.^[27] The Ru-Ru distances in both isomers are similar within experimental error and amount to 2.6594(6) Å (**13-sym**) and 2.6595(7) Å (**13-asym**), being smaller than the sum of the covalent radii (2.92 Å)^[23] and close to other reported Ru-Ru bonds.^[28] The Ru-As distances (2.4655(6) Å – 2.4840(5) Å) are in the range of a single bond (2.46 Å).^[15] The As...As distances, ranging from 2.9411(8) Å to 2.9558(8) Å, are smaller than the sum of the van-der-Waals radii (3.70 Å)^[17] and the WBIs of 0.21-0.22 (**13-sym**) and 0.20-0.21 (**13-asym**) also suggest weak As...As interactions. Interestingly, no significant I...I intermolecular interactions are found in the solid state and therefore the difference in the structure of the isomers cannot be traced back to this factor. DFT computations were carried out in order to determine which structure of **13** is energetically favored, however, the outcome of the geometry optimization is strongly dependent on the used functional and no clear conclusions can be drawn (cf. Computational Details).

Compound **11** crystallizes as red rods in the triclinic space group $P\bar{1}$. Being the first monocationic Ru-As₅ triple decker complex reported, it thus completes the series of monocationic complexes $[(Cp^R M)_2(\mu, \eta^{5:5}-E_5)]^+$ (M = Fe, Ru; E = P, As). The Ru...Ru distance in **11** (3.3378(9) Å) is larger than the sum of the covalent radii (2.92 Å)^[23] and similar to the distance reported for $[(Cp^* Ru)_2(\mu, \eta^{5:5}-P_5)]^+$ (3.352(1) Å).^[29] The As-As distances (2.3649(9) Å – 2.3830(8) Å) are in-between a single and a double bond.

Compound **12** crystallizes as a racemic mixture of both enantiomers in the monoclinic space group $P2_1/c$ and is found as a minor phase. It comprises two separate bridging ligands {AsI₂} and {As₇I₄}. All As-I bonds lengths (2.5821(9) Å – 2.6703(9) Å) are in accordance with As-I single bonds (2.54 Å).^[15] The As-As bonds lengths range between 2.397(1) Å and 2.481(1) Å and are also in agreement with the expected single bond length (2.42 Å).^[15] This is also rather true for the Ru-As bonds (2.375(1) Å – 2.542(1) Å; lit.: 2.46 Å).^[15]

7.3 Conclusion

We showed that the iodination of polypnictogen complexes is a powerful tool for the synthesis of novel types of polypnictogen complexes. The iodination of *cyclo*-As₅ complexes resulted in numerous novel complexes. Of these, the first di-cationic Fe-As triple decker was characterized, revealing further potential in the redox chemistry of polypnictogen complexes. Moreover, for the first time, a monocationic Ru-As₅ triple decker was obtained, thus completing the series of 30VE triple decker complexes $[(Cp^R M)_2(\mu, \eta^{5:5}-E_5)]^+$ (M = Fe, Ru; E = P, As). Much more remarkable, it was also possible to structurally characterize two different isomers of a complex with a unique tetramer of bridging iodoarsinidene ligands. The iodination of the

homologous *cyclo*-P₅ complexes takes place selectively, leading to unprecedented all-*cis* triphosphino-cyclotriphosphine complexes in a high-yield one-pot synthesis. Future investigations will be directed on the halogenation of other polypnictogen complexes, varying the number of heteroatoms in the ligand, the nature of the metal center, the halogen, and its source.

7.4 Experimental Part

General Remarks

All reactions were performed under an inert atmosphere of dry nitrogen or argon with standard vacuum, Schlenk and glove-box techniques. Solvents were purified, dried, and degassed prior to use by standard procedures. [Cp*Fe(η^5 -P₅)] (**1**),^[30] [Cp*Ru(η^5 -P₅)] (**2**),^[31] [Cp*Fe(η^5 -As₅)] (**6**),^[20] [Cp*Ru(η^5 -As₅)] (**10**),^[25] Tl[TEF],^[32] [Cp^{BiG}Fe(η^5 -P₅)],^[19] KC₈,^[33] [CoCp₂],^[34] NaCp,^[35] LiCp*,^[36] [Cp''₂Zr($\eta^{1:1}$ -P₄)]^[37] were synthesized following reported procedures. I₂, LiAlH₄, NaBH₄, KH, CH₃Li, ⁿBuLi, ^tBuLi, KF, AgF and NaOCH₃ are commercially available and were used without further purification. Solution NMR spectra were recorded on a BRUKER Avance 400. Chemical shifts δ are given in [ppm] referring to external standards of tetramethylsilane (¹H NMR spectra), 85% phosphoric acid (³¹P{¹H} NMR spectra) or CFCl₃ (¹⁹F{¹H} NMR spectra). MAS NMR spectra were acquired on a Bruker Avance 300 spectrometer and chemical shifts δ are given in [ppm] referring to an external standard of NaH₂PO₄ (³¹P{¹H} MAS NMR spectra). ESI-MS spectra were recorded on a ThermoQuest Finnigan MAT TSQ 7000 and EI-MS and FD-MS spectra were recorded on a Finnigan MAT 95 mass spectrometer. Elemental analyses were performed on a Vario EL III apparatus. ESR spectroscopy was carried out on a MiniScope MS400 device with a frequency of 9.44 GHz.

Synthesis of [Cp*FeP₆I₆]I (**3-I**) by layering

A solution of [Cp*Fe(η^5 -P₅)] (**1**, 77 mg, 0.22 mmol) in 50 mL CH₂Cl₂ was layered first with a mixture of CH₂Cl₂/CH₃CN (2:1, 10 mL), then with a solution of I₂ (190 mg, 0.749 mmol) in CH₃CN. After one day already grey-black solid precipitated, while black needles of **3-I₃** crystallized only after a few days. After complete diffusion, the mother liquor was decanted together with the crystals of **3-I₃**, which were then again washed with CH₂Cl₂ (20 mL). The precipitate was washed with CH₂Cl₂ (20 mL) as well. Both solids were dried and analyzed separately.

Analytical data of **3-I**:

Yield: 107 mg (84.6 μ mol, 46%) crystals, 79 mg (62 μ mol, 34%) powder.

Elemental analysis: calculated (%) for [C₁₀H₁₅FeP₆I₆](I)_{0.5}(I₃)_{0.5} (**3-I₃**): C 8.63, H 1.09; calculated (%) for [C₁₀H₁₅FeP₆I₆]I (**3-I**): C 9.49, H 1.19; found (%) for crystals: C 9.67, H 1.06; found (%) for powder: C 9.87, H 1.14.

³¹P{¹H} MAS NMR:^[38] δ [ppm] = -58.8 (P₃(PI₂)₃), 74.8 (P₃(PI₂)₃).

Synthesis of [Cp*FeP₆I₆](I)_{0.5}(I₃)_{0.5} (**3-I₃**)

A solution of [Cp*Fe(η⁵-P₅)] (**1**, 77 mg, 0.22 mmol) in 50 mL CH₂Cl₂ was layered first with a mixture of CH₂Cl₂/CH₃CN (2:1, 10 mL), then with a solution of I₂ (258 mg, 1.02 mmol) in CH₃CN. After complete diffusion, the mother liquor and the black crystals of **3-I₃** were decanted from the grey-black precipitate at the bottom of the Schlenk tube. The crystals were then washed with CH₃CN (3 x 20 mL) and CH₂Cl₂ (3 x 20 mL) and dried only marginally until pourable.

Analytical data of **3-I₃**:

Yield: 52 mg (37 μmol, 20%).

Elemental Analysis: Calculated (%) for [C₁₀H₁₅FeP₆I₆](I)_{0.5}(I₃)_{0.5} · 5 CH₂Cl₂ · 0.1 CH₃CN: C 10.03, H 1.40, N 0.08; Found (%): C 10.08, H 1.18, N in traces.

³¹P{¹H} MAS NMR:^[38] δ [ppm] = -60.7 (P₃(PI₂)₃), 74.3 (P₃(PI₂)₃).

Reaction of [Cp*Fe(η⁵-P₅)] (**1**) with 9eq. I₂

A solution of [Cp*Fe(η⁵-P₅)] (**1**, 10 mg, 29 μmol) in 15 mL CH₂Cl₂ was layered first with a solution of I₂ (65 mg, 0.26 mmol) in CH₃CN. After one day, black crystals of **3-I₃** formed. After complete diffusion, the mother liquor was decanted.

³¹P{¹H} NMR (C₆D₆-cap.): δ [ppm] = 172.2 (PI₃).

Synthesis of [Cp*FeP₆I₆]I (**3-I**) by stirring

To a solution of [Cp*Fe(η⁵-P₅)] (**1**, 180 mg, 0.52 mmol) in 60 mL CH₂Cl₂ a solution of I₂ (396 mg, 1.56 mmol) in 90 mL CH₃CN was added under stirring at r.t. The mixture was stirred for three days before filtered over a G4 frit. The solid residue was washed with CH₂Cl₂ (10 mL) and CH₃CN (10 mL) and dried.

Analytical data for **3-I**:

Yield: 371 mg (0.293 mmol, 68%).

Elemental Analysis: Calculated (%) for [C₁₀H₁₅FeP₆I₆]: C 9.49, H 1.19; found (%): C 9.49, H 1.32.

³¹P{¹H} NMR (C₆D₆-cap. in dmsO): δ [ppm] = -11.8 (s), 0.2 (s), 2.7 (s), 7.6 (s), 169.7 (PI₃).

³¹P{¹H} NMR (C₆D₆-cap. in DMF): δ [ppm] = 152.2 ([Cp*Fe(η⁵-P₅)]), 168.9 (s), 172.8 (PI₃).

³¹P{¹H} NMR (C₆D₆-cap. in NMP): δ [ppm] = 172.6 (PI₃).

³¹P{¹H} NMR (C₆D₆-cap. in HMPA): δ [ppm] = 152.2 ([Cp*Fe(η⁵-P₅)]), 170.8 (PI₃).

EI-MS (solid): *m/z* = 411.6360 (PI₃⁺), 345.8771 ([Cp*Fe(η⁵-P₅)⁺], 253.7751 (I₂⁺), 127.8930 (HI⁺), 126.8856 (I⁺).

Analytical data for the mother liquor:

³¹P{¹H} NMR (CD₂Cl₂): δ [ppm] = -18.6 (s), 152.7 ([Cp*Fe(η⁵-P₅)]).

FD-MS (CH₂Cl₂/CH₃CN): no ions detected.

Positive ion ESI-MS (CH₂Cl₂/CH₃CN): *m/z* = 326.1695 ([FeCp₂)⁺).

Negative ion ESI-MS (CH₂Cl₂/CH₃CN): *m/z* = 126.9057 (I⁻).

Cyclic voltammetry:

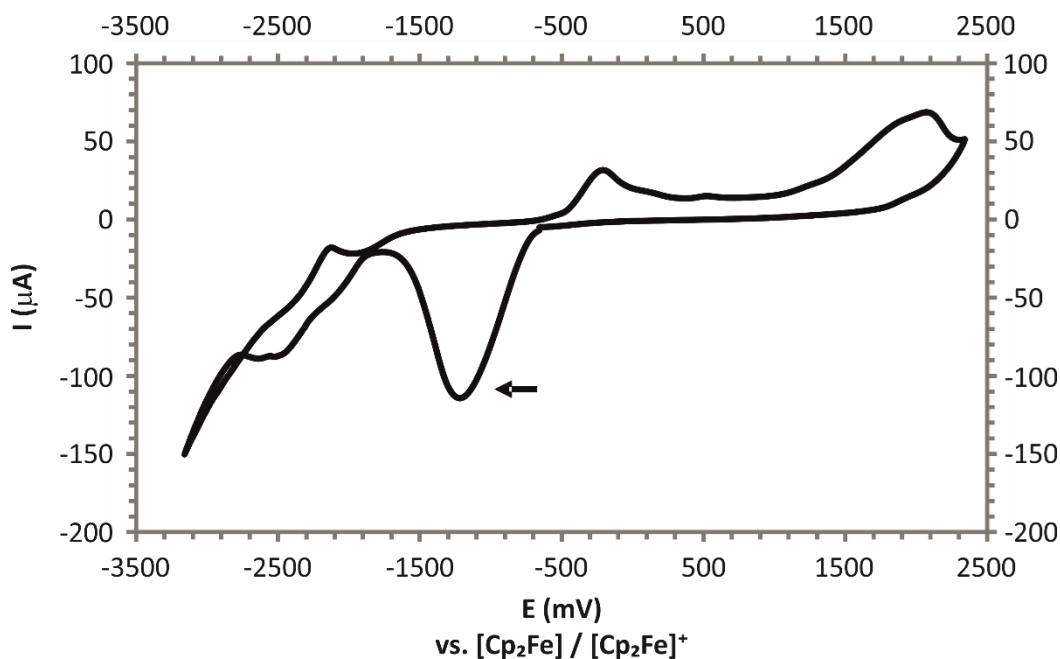


Figure 6. Cyclic voltammogram of solid **3-I** applied onto an Ag electrode, recorded at a scan rate of 0.1 V s⁻¹ in CH₂Cl₂ referenced against Fc/Fc⁺ with [tBu₄N][PF₆] as supporting electrolyte.

For the cyclic voltammetry measurements, a suspension of [Cp*FeP₆I₆] (**3-I**) in CH₂Cl₂ was applied onto a Ag electrode and carefully dried. The covered electrode was carefully set into the cell filled with a solution of [tBu₄N][PF₆] (and Fc) in CH₂Cl₂. The thus obtained cyclic voltammetry data of solid [Cp*FeP₆I₆] (**3-I**) in CH₂Cl₂ revealed an irreversible reduction (E = -1.21 V). This

observation is in line with the experimental results, since the degradation of the P₆ motif and formation of [Cp*Fe(η⁵-P₅)] (**1**) is observed in the chemical reduction of **3-I** with e.g. [CoCp₂]. Further redox events detected (E = -2.53 V, -2.64 V, -2.12 V, -0.208 V) are tentatively suggested to correspond to the subsequent reduction and re-oxidations of [Cp*Fe(η⁵-P₅)] (**1**), which are reported to occur at E = -2.05 V, -1.34 V and 0.57 V.^[39] It must be noted that the electrode was still covered with solids during this measurement. However, the separation of the measured oxidation and reduction potentials is similar to the values reported for [Cp*Fe(η⁵-P₅)] (**1**).

Synthesis of [Cp*RuP₆I] (**4**)

A solution of [Cp*Ru(η⁵-P₅)] (**2**, 9 mg, 23 μmol) in 4 mL CH₂Cl₂ was layered with a solution of I₂ (24 mg, 95 μmol) in 6 mL CH₃CN. After complete diffusion the mother liquor was decanted. The crystals were washed with a mixture of CH₂Cl₂/CH₃CN (2:1, 5 mL), CH₃CN (5 mL) and CH₂Cl₂ (5 mL) and dried.

Analytical data of **4**:

Yield: 21 mg (16 μmol, 84%).

Elemental Analysis: Calculated (%) for [C₁₀H₁₅RuP₆I]: C 9.17, H 1.15; found (%): C 9.15 H 1.11.

³¹P{¹H} MAS NMR: δ [ppm] = -67.1 (P₃(Pl₂)₃), 58.3 (P₃(Pl₂)₃).

EI-MS (solid): *m/z* = 569.4585 (P₂I₄⁺), 411.6546 (Pl₃⁺), 391.8598 ([Cp*Ru(η⁵-P₅)]⁺), 253.7871 (I₂⁺), 126.8923 (I⁺).

Positive ion ESI-MS (CH₃CN): no cations detected.

Negative ion ESI-MS (CH₃CN): *m/z* = 380.7146 (I₃⁻), 126.9055 (I⁻).

Synthesis of [Fe(CH₃CN)₆][As₆I₈] (**7**), [Fe(CH₃CN)₆][As₄I₁₄] (**8**) and [(Cp*Fe)₂(μ,η^{5:5}-As₅)] [As₆I₈] (**9**)

In the dark, a solution of [Cp*Fe(η⁵-As₅)] (**6**, 30 mg, 53 μmol) in 9 mL CH₂Cl₂ was layered first with a mixture of CH₂Cl₂/CH₃CN (2:1, 2 mL), then with a solution of I₂ (50 mg, 0.20 mmol) in 11 mL CH₃CN. After complete diffusion, the mother liquor and the precipitate were decanted. The crystals were washed with toluene (3 x 5 mL) and pentane (3 x 5 mL) and dried. The only way to get pure **7** was to take the crystals from the Schlenk wall with a spatula, quickly dip them into a Schlenk tube with toluene, wash them with toluene (3 x 5 mL) and pentane (3 x 5 mL) and dry them. Pure **9** could only be obtained by taking crystals from the Schlenk wall into a microscope dish with mineral oil and selecting the dark red crystals under the microscope. The

crystals were then put back into a Schlenk tube, washed with hexane (20 x 5 mL) and dried. Unfortunately, **9** is insoluble in CH₂Cl₂ or CH₃CN, impeding paramagnetic ¹H NMR spectroscopy and Evans NMR spectroscopy.

Analytical data of **7**, **8** and **9**:

Yield: 12 mg (mixture of **7** and **8**); few crystals (**9**).

7: ¹H NMR (CD₃CN): δ [ppm] = 1.95 (CH₃CN), 2.17 (br).

7: Positive ion ESI-MS (CH₃CN): *m/z* = 151.0467 ([Fe(CH₃CN)₆]²⁺).

7: Negative ion ESI-MS (CH₃CN): *m/z* = 1337.858 (As₆I₇⁻), 934.2045 (As₄I₅⁻), 784.3642 (As₂I₅⁻), 582.5392 (AsI₄⁻), 126.9049 (I⁻).

7+8: Positive ion ESI-MS (CH₂Cl₂/CH₃CN): no cations detected.

7+8: Negative ion ESI-MS (CH₂Cl₂/CH₃CN): *m/z* = 1337.8604 (As₆I₇⁻), 934.2083 (As₄I₅⁻), 784.3676 (As₂I₅⁻), 732.3811 (As₆I₈²⁻ or any {As₃I₄⁻}_n), 380.7144 (I₃⁻), 126.9054 (I⁻).

EPR spectroscopy of 9:

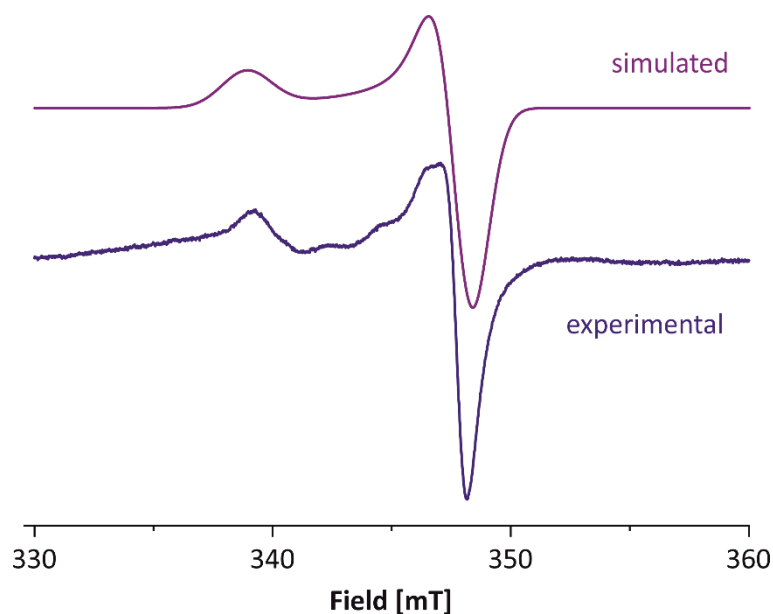


Figure 7. Simulated (top, violet) and experimental (bottom, blue) ESR spectra of **9** at 293 K.

The experimental EPR spectrum was acquired from crystals of **9** washed with CH₂Cl₂ (to dissolve residual impurities of **7** and **8**) and suspended in CH₂Cl₂. It shows an axial signal without significant hyperfine splitting. Apparently, minor paramagnetic impurities are still present despite washing the crystals. According to spin computations (cf. Computational Details, Figure 11), the spin density is mainly located at the Fe atoms. Hence, coupling to the ⁷⁵As atoms is expected to be negligible small. On the other hand, ⁵⁴Fe (n = 5.8%, I = 0) and ⁵⁶Fe (n = 91.8%, I = 0), the main isotopes of Fe, are NMR inactive.^[40] Thus, the observed signal fits nicely to what

is expected for the [(Cp*Fe)₂As₅]²⁺ dication of **9**. Simulation was performed with the program EasySpin.^[41] Parameters used for fitting: $g(z) = 1.98691$; $g(x,y) = 1.93421$.

Unfortunately, compounds **7**, **8** and **9** could not be further characterized. Compounds **7** and **8** have a similar solubilities and colors, impeding separation under the microscope or by extraction. Compound **9** is insoluble in CH₂Cl₂ and CH₃CN. However, washing the mixture of **7**, **8** and **9** with CH₂Cl₂ did not remove all impurities of **7** and **8** (cf. Figure 7). Crystals of **9** can be selected as dark red crystals under the microscope, while compounds **7** and **8** are yellow to orange in color. However, its insolubility impedes NMR spectroscopy and mass spectrometry.

Synthesis of [(Cp*Ru)₂(μ,η⁵⁻⁵-As₅)] [As₆I₈]_{0.5} (**11**), [(Cp*Ru)₂As₈I₆] (**12**), [(Cp*Ru)₂As₄I₄] (**13-sym** and **13-asym**)

In the dark, a solution of [Cp*Ru(η⁵-As₅)] (**10**, 27 mg, 44 μmol) in 12 mL CH₂Cl₂ was layered first with a mixture of CH₂Cl₂/CH₃CN (2:1, 3 mL), then with a solution of I₂ (38 mg, 0.150 mmol) in 12 mL CH₃CN. After complete diffusion, the crystals were taken with a spatula from the Schlenk wall and quickly dipped into a mixture of CH₂Cl₂/CH₃CN (1:1), washed three further times with this mixture (5 mL each), washed with CH₃CN (3 x 5 mL) and dried.

Analytical data of **11**, **12**, **13-sym** and **13-asym**:

Yield: 13 mg

¹H NMR (CDCl₃): δ [ppm] = 1.53, 1.70, 1.95 (s, CH₃CN).

FD-MS (pentane): $m/z = 1009.7430$ ([[(Cp*Ru)₃As₄]⁺).

FD-MS (toluene): $m/z = 847.6576$ ([[(Cp*Ru)₂As₅]⁺)

Positive ion ESI-MS (CH₂Cl₂/CH₃CN): $m/z = 847.6545$ ([[(Cp*Ru)₂As₅]⁺).

Negative ion ESI-MS (CH₂Cl₂/CH₃CN): $m/z = 126.9054$ (I⁻).

Unfortunately, compounds **11**, **12**, **13-sym** and **13-asym** could not be further characterized. Crystals of **11** and **13** are not clearly distinguishable by color or shape, impeding their separation under the microscope. Attempts to extract pure compounds from the mixture were made, however, neither ¹H NMR spectroscopy nor mass spectrometry are suitable for tracing the extractions. Since compounds **11**, **12** and **13** only contain Cp* protons, a clear assignment in ¹H NMR spectroscopy is not possible. On the other hand, mass spectrometry of the pentane and toluene extracts was performed. In pentane solution, [(Cp*Ru)₃As₄]⁺ was found, which was not present in the crystalline mixture and thus must have been formed under mass spectrometric conditions. In toluene solution, [(Cp*Ru)₂As₅]⁺ was found, while **11** is not expected to be soluble

in toluene, so it is assumed to be formed under mass spectrometric conditions as well. Compound **12** (black crystals) is distinguishable from **11** and **13** (red crystals) by color. However, it was only observed once, presumably since they re-dissolve quickly in the mother liquor.

Reaction of [Cp*FeP₆I] (**3-I**) with TI[TEF] (TEF⁻ = Al(OC(CF₃)₃)₄⁻)

[Cp*FeP₆I] (**3-I**, 14 mg, 11 μmol) and TI[TEF] (13 mg, 11 μmol) were dissolved in 10 mL CH₂Cl₂ and stirred for 29 hours, then treated in the ultrasonic bath for another 3 hours. The resulting suspension was filtered and washed with another 2 mL CH₂Cl₂. The orange filtrate was concentrated to 7 mL.

³¹P{¹H} NMR (C₆D₆-cap.): δ [ppm] = 174 (s, P₁₃).

¹⁹F{¹H} NMR (C₆D₆-cap.): δ [ppm] = -75.8 (s, TEF⁻).

Reaction of [Cp^{BIG}Fe(η⁵-P₅)] with I₂

A solution of [Cp^{BIG}Fe(η⁵-P₅)] (30 mg, 32 μmol) in 8 mL CH₂Cl₂ was layered with a solution of I₂ (25 mg, 99 μmol) in 8 mL CH₃CN. The orange-brown solution was filtered from the insoluble precipitate and concentrated.

³¹P{¹H} NMR (CD₂Cl₂): δ [ppm] = 102.8 (s, P_{2I4}), 171.8 (s, [Cp^{BIG}Fe(η⁵-P₅)]), 174.7 (s, P₁₃).

Reaction of [Cp*FeP₆I] (**3-I**) with KC₈

[Cp*FeP₆I] (**3-I**, 30 mg, 24 μmol) and KC₈ (20 mg, 0.15 mmol, 6 eq.) were dissolved in 10 mL toluene and stirred overnight. The black suspension was filtered to give a yellowish filtrate.

³¹P{¹H} NMR (C₆D₆-cap.): δ [ppm] = 153.0 ([Cp*Fe(η⁵-P₅)]).

Reaction of [Cp*FeP₆I] (**3-I**) with [CoCp₂]

[Cp*FeP₆I] (**3-I**, 32 mg, 25 μmol) and [CoCp₂] (29 mg, 0.15 mmol, 6 eq.) were dissolved in 10 mL toluene and stirred for three days. The solvent was removed, and the residue dissolved in 5 mL CH₃CN to give a yellow-green solution after filtration. The solvent was removed again and the remaining solid analyzed.

¹H NMR (D₂O): δ [ppm] = 2.08 (CH₃CN), 5.77 ([CoCp₂]⁺).

³¹P{¹H} NMR (C₆D₆-cap. in CH₂Cl₂ solution): δ [ppm] = 152.2 ([Cp*Fe(η⁵-P₅)]).

Reaction of [Cp*FeP₆I₆]I (3-I) with NaCp

[Cp*FeP₆I₆]I (3-I, 15 mg, 12 μmol) and NaCp (6 mg, 68 μmol) were dissolved in 10 mL thf and stirred for 17 hours. After removal of the solvent the residue was extracted with toluene (3 x 3 mL) to give a yellow solution.

¹H NMR (CD₂Cl₂): δ [ppm] = 1.43 (s, 15 H, [Cp*Fe(η⁵-P₅)]), 1.64 (m, 2H, IC₂H₄-CH₂-CH₂OH), 1.91 (m, 2H, ICH₂-CH₂-C₂H₄OH), 3.24 (t, ³J_{H,H} = 7.0 Hz, 2H, ICH₂-C₃H₆OH), 3.64 (t, ³J_{H,H} = 6.3 Hz, 2 H, IC₃H₆-CH₂OH).

³¹P{¹H} NMR (CD₂Cl₂): δ [ppm] = 152.2 ([Cp*Fe(η⁵-P₅)]).

Reaction of [Cp*FeP₆I₆]I (3-I) with LiCp*

[Cp*FeP₆I₆]I (3-I, 15 mg, 12 μmol) and LiCp* (4 mg, 28 μmol) were dissolved in 10 mL thf, stirred for 18 hours and treated in the ultrasonic bath for another six hours. After removal of the solvent the residue was extracted with 20 mL CH₂Cl₂ to give a pinkish solution.

¹H NMR (CD₂Cl₂): δ [ppm] = 1.43 (s, 15 H, [Cp*Fe(η⁵-P₅)]), 1.65 (m, 2H, IC₂H₄-CH₂-CH₂OH), 1.91 (m, 2H, ICH₂-CH₂-C₂H₄OH), 3.24 (t, ³J_{H,H} = 7.0 Hz, 2H, ICH₂-C₃H₆OH), 3.66 (br, 2 H, IC₃H₆-CH₂OH).

³¹P{¹H} NMR (CD₂Cl₂): δ [ppm] = 152.2 ([Cp*Fe(η⁵-P₅)]), signal almost below noise floor.

Reaction of [Cp*FeP₆I₆]I (3-I) with LiAlH₄

[Cp*FeP₆I₆]I (3-I, 30 mg, 24 μmol) and LiAlH₄ (1 mg, 26 μmol) were dissolved in 10 mL thf and stirred for six days. The suspension was concentrated to 1 mL.

³¹P{¹H} NMR (C₆D₆-cap.): δ [ppm] = 152.4 ([Cp*Fe(η⁵-P₅)]).

Reaction of [Cp*FeP₆I₆]I (3-I) with NaBH₄

[Cp*FeP₆I₆]I (3-I, 30 mg, 24 μmol) and NaBH₄ (1 mg, 26 μmol) were dissolved in 10 mL thf and stirred overnight to give a red solution over a black precipitate. The suspension was concentrated to 5 mL.

³¹P{¹H} NMR (C₆D₆-cap.): δ [ppm] = 152.4 ([Cp*Fe(η⁵-P₅)]).

Reaction of [Cp*FeP₆I₆]I (3-I) with KH

[Cp*FeP₆I₆]I (3-I, 30 mg, 24 μmol) and KH (6 mg, 0.15 mmol) were dissolved in 10 mL thf and stirred for six days. The suspension was concentrated to 1 mL.

³¹P{¹H} NMR (C₆D₆-cap.): δ [ppm] = 152.4 ([Cp*Fe(η⁵-P₅)]).

Reaction of [Cp*FeP₆I₆]I (3-I) with MeLi

[Cp*FeP₆I₆]I (3-I, 30 mg, 24 μmol) was dissolved in 5 mL toluene and CH₃Li (0.14 mL, 1.0312 M solution in Et₂O, 0.14 mmol) was added. The resulting red-brown suspension was stirred for 20 hours.

³¹P{¹H} NMR (C₆D₆-cap.): δ [ppm] = 153.0 ([Cp*Fe(η⁵-P₅)]).

Reaction of [Cp*FeP₆I₆]I (3-I) with ⁿBuLi

[Cp*FeP₆I₆]I (3-I, 30 mg, 24 μmol) was dissolved in 5 mL toluene and ⁿBuLi (0.09 mL, 1.6 M solution in hexane, 0.14 mmol) was added. The resulting red-brown suspension was stirred for 20 hours.

³¹P{¹H} NMR (C₆D₆-cap.): δ [ppm] = 153.0 ([Cp*Fe(η⁵-P₅)]).

Reaction of [Cp*FeP₆I₆]I (3-I) with ^tBuLi

[Cp*FeP₆I₆]I (3-I, 30 mg, 24 μmol) was dissolved in 5 mL toluene and ^tBuLi (0.3 mL, 0.473 M solution in pentane, 0.14 mmol) was added. The resulting red-brown suspension was stirred for 26 hours.

³¹P{¹H} NMR (C₆D₆-cap.): δ [ppm] = 153.1 ([Cp*Fe(η⁵-P₅)]), signal almost below noise floor.

Reaction of [Cp*FeP₆I₆]I (3-I) with [Cp''₂Zr(η^{1:1}-P₄)]

[Cp*FeP₆I₆]I (3-I, 30 mg, 24 μmol) and [Cp''₂Zr(η^{1:1}-P₄)] (40 mg, 70 μmol) was dissolved in 10 mL toluene. The greenish suspension was stirred for 21 hours, filtered and concentrated to 5 mL.

¹H NMR (C₆D₆): δ [ppm] = 1.23 (s, [Cp*Fe(η⁵-P₅)]), 1.32 (s, 36H, [Cp''₂ZrI₂]), 5.74 (d, ⁴J_{H,H} = 2.5 Hz, 4H, [Cp''₂ZrI₂]), 7.36 (t, ⁴J_{H,H} = 2.5 Hz, 2H, [Cp''₂ZrI₂]).

³¹P{¹H} NMR (C₆D₆): δ [ppm] = -520.4 (s, P₄), 152.8 (s, [Cp*Fe(η⁵-P₅)]).

Reaction of [Cp*FeP₆I₆]I (3-I) with KF

[Cp*FeP₆I₆]I (**3-I**, 30 mg, 24 μmol) and KF (10 mg, 0.17 mmol) were dissolved in 5 mL CH₃CN and stirred overnight. After removal of the solvent, the residue was dissolved in 1 mL CD₃CN and filtered.

¹H NMR (CD₃CN): δ [ppm] = 1.42 (s, [Cp*Fe(η⁵-P₅)]).

³¹P{¹H} NMR (CD₃CN): δ [ppm] = -143.1 (PF₆⁻), 151.9 ([Cp*Fe(η⁵-P₅)]).

¹⁹F{¹H} NMR (CD₃CN): δ [ppm] = -6.26 (dt), -71.7 (d, PF₆⁻).

Reaction of [Cp*FeP₆I₆]I (3-I) with AgF

[Cp*FeP₆I₆]I (**3-I**, 30 mg, 24 μmol) and AgF (21 mg, 0.17 mmol) were dissolved in 5 mL CH₃CN. The mixture was stirred overnight and filtered to give a yellow solution.

¹H NMR (CD₃CN): δ [ppm] = 1.42 (s, [Cp*Fe(η⁵-P₅)]).

³¹P{¹H} NMR (CD₃CN): δ [ppm] = -143.1 (sept, PF₆⁻), 151.8 ([Cp*Fe(η⁵-P₅)]).

¹⁹F{¹H} NMR (CD₃CN): δ [ppm] = -71.7 (d, PF₆⁻).

Reaction of [Cp*FeP₆I₆]I (3-I) with CH₃OH

[Cp*FeP₆I₆]I (**3-I**, 14 mg, 11 μmol) were dissolved in 4 mL CH₃OH and stirred overnight. The solvent was removed to give an oily, orange residue of [Cp*FeP₆(OCH₃)₆]I (**5**).

¹H NMR (CD₃OD): δ [ppm] = 1.62 (s, Cp* of **5**), 1.68 (s), 3.34 (CH₃OH), 3.6-3.8 (m), 3.96 (m, -OCH₃ of **5**).

³¹P{¹H} NMR (CD₃OD): δ [ppm] = -152 (m, **5**), 25.7 (s), 171.2 (s), 284 (m, **5**).

Positive ion ESI-MS (CH₃OH): *m/z* (%) = 563.0069 (100, [Cp*FeP₆(OCH₃)₆]⁺), 532.0059 (11, [Cp*FeP₆(OCH₃)₅H]⁺), 503.1187 (9, [Cp*FeP₆(OCH₃)₄H₂]⁺), 473.1078 (6, [Cp*FeP₆(OCH₃)₃H₃]⁺).

Negative ion ESI-MS (CH₃OH): *m/z* (%) = 126.9071 (100, I⁻), 380.7147 (0.1, I₃⁻).

Reaction of [Cp*FeP₆I₆]I (3-I) with NaOCH₃ in CH₃OH

NaOCH₃ (10 mg, 0.19 mmol) was dissolved in 5 mL CH₃OH and added to solid [Cp*FeP₆I₆]I (**3-I**, 31 mg, 25 μmol) under stirring. After 30 minutes, the grey-black solid of **3-I** was completely dissolved to give an orange solution. The solvent was removed, and the residue extracted with

CH₂Cl₂ (5 mL in total). The colorless precipitate (NaI) was disposed. The solvent was removed from the extract to give an oily, orange residue of [Cp*FeP₆(OCH₃)₆]I (**5**).

¹H NMR (extract, CD₂Cl₂): δ [ppm] = 1.6-1.8 (m, Cp* of **5**), 2.15 (s, CH₃l), 3.6-4.0 (m, -OCH₃ of **5**).

³¹P{¹H} NMR (extract, CD₂Cl₂): δ [ppm] = -164 to -138 (m, **5**), 11.2 (s), 152.2 (s), 174.8 (s), 181.5 (s), 284 (m, **5**), 289 (d, br).

7.5 Crystallographic Details

Crystals of **3-I**, **3-I₃**, **4**, **7**, **8**, **9**, **11**, **12**, **13-sym** and **13-asym** were taken from a Schlenk flask under a stream of argon and immediately placed in a mineral oil to prevent decomposition. The quickly chosen single crystals covered by a drop of the oil were directly placed into a stream of cold nitrogen with the pre-centered goniometer head with CryoMount[®] and attached to the goniometer of a diffractometer.

The diffraction data for **3-I₃**, **7**, **8**, **9**, **11**, **12**, **13-sym** and **13-asym** were collected on a Rigaku Oxford Diffraction diffractometer equipped with a Titan^{S2} CCD detector and a SuperNova CuK α microfocus sources using narrow 0.5° ω scans. The diffraction data for **3-I₃** were collected on a Rigaku Oxford Diffraction diffractometer equipped with an Eos CCD detector and a SuperNova MoK α microfocus sources using 0.5° ω scans. Analytical absorption correction or empirical (for **12**) was applied using CrysAlis software.^[42] Due to high absorbing powder of the compounds, an attempt was made to measure them at DESY PETRA III light source (P11 beamline) with shorter wavelengths.^[43] The crystals of **3-I** were carefully selected, mounted on the magnetic holders, checked for quality and placed into a Dewar vessel with liquid nitrogen using standard cryocrystallography tools. Using standard procedures, they were placed into a special Dewar vessel filled with liquid nitrogen among other crystals. A robotic mounting/demounting was used for further manipulations in the P11 beamline hutch. Unfortunately, **3-I₃**, **7**, **8** and **9** proved to be prone to fast radiolysis. The diffraction data undamaged by crystal decay in these cases proved incomplete; therefore, the data obtained in-house were used for structure refinement. Only the X-ray diffraction data for **3-I** were collected using one-circle diffractometer and DECTRIS PILATUS 6M pixel array detector at 80(2) K.^[43] The data were acquired by 360° ϕ -rotation with 0.3° scan width and exposure of 0.1 s per frame at wavelength $\lambda = 0.6199 \text{ \AA}$ (20 keV) and the beam attenuated to 10%. Data reduction for all data sets was performed with CrysAlisPro software.^[42] Due to partial radiolysis only those frames were taken into integration, which were least affected by decomposition of the crystal. Empirical absorption correction using equivalent reflections was applied.

The structures were solved by direct methods with *SHELXT*^[44] and refined by full-matrix least-squares method against F^2 in anisotropic approximation using multi-processor variable memory versions of *SHELXL (2014-2018)*. In the structure of [(Cp*Fe)₂As₅](As₆I₈) (**9**), the middle deck of the cationic triple decker complex is disordered by center of symmetry. In the [Fe(CH₃CN)₆][As₄I₁₄] (**8**) diffuse reflections suggest doubled unit cell parameter b ($b' = 16.1004(3) \text{ \AA}$). However, the superstructural model in $P2_1/c$ gives neither reasonable crystallochemical interpretation (suggesting unreasonable disorder) nor good quality factors ($R_1 \sim 0.18$). Therefore, we surmised that these superstructural reflections with different

morphology (both sharp and smeared) most probably have non-Bragg nature and they are caused by diffuse scattering (Figure 8). This structural effect can originate from the disorder (most probably negatively correlated) of the disordered partly occupied terminal {AsI₂} groups including atoms As3, I7 and I8. In the presented average structural model these groups are related by a 2-fold axis of the *C2/c* space group.

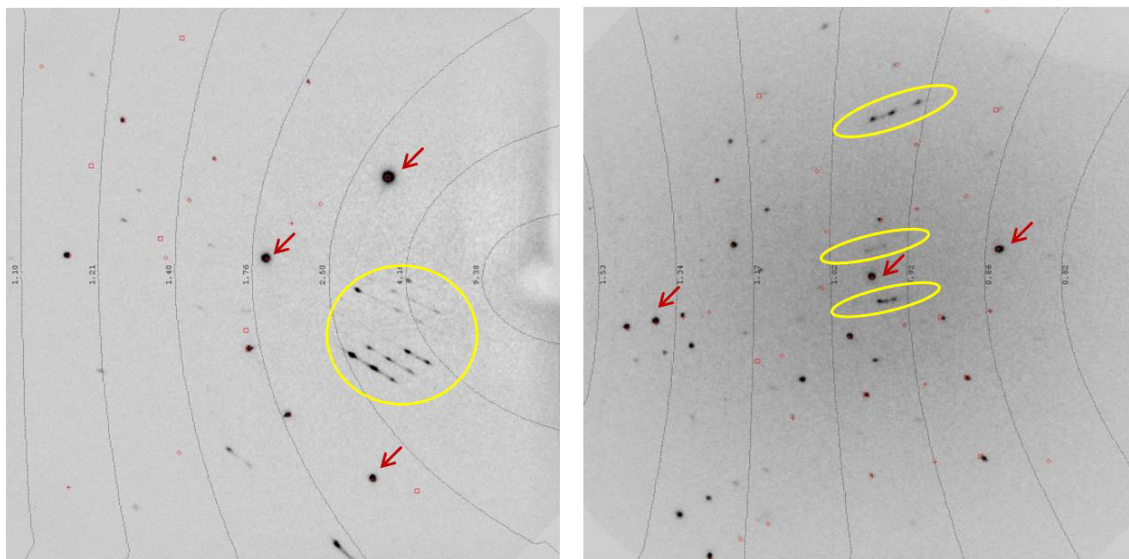


Figure 8. A view of the diffraction pattern of **8**. Red signs point out Bragg reflections indexed in the chosen small unit cell (Table 2). Yellow signs encircle some of the smeared supposedly non-Bragg reflections.

CIF files with comprehensive information on the details of the diffraction experiments and full tables of bond lengths and angles for **3-I**, **3-I₃**, **4**, **7**, **8**, **9**, **11**, **12**, **13-sym** and **13-asm** are deposited in the Cambridge Crystallographic Data Centre under the deposition codes CCDC 1985257 – CCDC 1985266, respectively.

Table 1. Experimental details for compounds **3-I**, **3-I₃** and **4**.

Crystal data	3-I	3-I₃	4
CCDC Codes	CCDC-1985266	CCDC-1985259	CCDC-1985265
Structural formula	[Cp*FeI ₆ P ₆]I	[Cp*FeI ₆ P ₆] ₂ (I ₃)(I)	[Cp*RuP ₆ I ₆]I
Chemical formula	C ₁₀ H ₁₅ FeI ₇ P ₆	C ₂₀ H ₃₀ Fe ₂ I ₁₆ P ₁₂	C ₁₀ H ₁₅ I ₇ P ₆ Ru
<i>M_r</i>	1265.19	2784.18	1310.41
Crystal system, space group	Orthorhombic, <i>Pna</i> 2 ₁	Monoclinic, <i>C2/c</i>	Orthorhombic, <i>Pna</i> 2 ₁
Temperature (K)	80	90	100
<i>a</i> , <i>b</i> , <i>c</i> (Å)	16.79985(9), 10.17539(5), 15.42831(7)	34.4141(9), 10.1665(3), 16.2059(5)	17.0620(6), 10.1848(5), 15.4991(6)
α , β , γ (°)	90, 90, 90	90, 94.140(3), 90	90, 90, 90
<i>V</i> (Å ³)	2637.39 (2)	5655.2 (3)	2693.34(19)
<i>Z</i>	4	4	4
<i>F</i> (000)	2248	4920	2320
<i>D_x</i> (Mg m ⁻³)	3.186	3.270	3.232
Radiation type	Synchrotron, $\lambda = 0.6199$ Å	Cu <i>K</i> α	Mo <i>K</i> α
μ (mm ⁻¹)	6.32	76.08	8.96
Crystal shape and color	Black needle	Black needle	Metallic black needle
Crystal size (mm)	0.05 × 0.01 × 0.01	0.18 × 0.03 × 0.01	0.28 × 0.01 × 0.01
Data collection			
Diffractometer	1-cycle diffractometer	Supernova, Titan ^{S2}	SuperMova, Eos
Absorption correction	Multi-scan	Gaussian	Gaussian
<i>T_{min}</i> , <i>T_{max}</i>	0.667, 1.000	0.047, 0.575	0.356, 1.000
No. of measured, independent and observed [<i>I</i> > 2 σ (<i>I</i>)] reflections	50761, 8364, 6805	13384, 5614, 3689	8634, 5308, 3531
<i>R_{int}</i>	0.051	0.070	0.055
(<i>sin</i> θ / λ) _{max} (Å ⁻¹)	0.725	0.623	0.649
Range of <i>h</i> , <i>k</i> , <i>l</i>	<i>h</i> = -24→24, <i>k</i> = -14→14, <i>l</i> = -22→22	<i>h</i> = -42→31, <i>k</i> = -12→10, <i>l</i> = -20→19	<i>h</i> = -22→9, <i>k</i> = -13→7, <i>l</i> = -20→19
Refinement			
<i>R</i> [<i>F</i> ² > 2 σ (<i>F</i> ²)], <i>wR</i> (<i>F</i> ²), <i>S</i>	0.035, 0.083, 0.99	0.066, 0.176, 0.95	0.051, 0.116, 0.89
No. of reflections	8364	5614	5308
No. of parameters	223	233	222
No. of restraints	1	0	61
H-atom treatment	H-atom parameters constrained	H-atom parameters constrained	H-atom parameters constrained
Δ _{max} , Δ _{min} (e Å ⁻³)	2.44, -2.80	3.78, -2.18	1.88, -1.74
Twin batch	inversion twin; 0.49 (4)	-	0.04 (6)

Computer programs: P11 beamline software, CrysAlis PRO (Rigaku OD, 2015), SHELXT, SHELXL2014-2018 (Sheldrick, 2018).

Table 2. Experimental details for compounds 7, 8 and 9.

Crystal data	7	8	9
CCDC Codes	CCDC-1985257	CCDC-1985262	CCDC-1985261
Structural formula	[Fe(CH ₃ CN) ₆](As ₆ I ₈)	[Fe(CH ₃ CN) ₆](As ₄ I ₁₄)	[(CpFe) ₂ As ₅](As ₆ I ₈)
Chemical formula	C ₁₂ H ₁₈ As ₆ FeI ₈ N ₆	C ₁₂ H ₁₈ FeN ₆ As ₄ I ₁₄	C ₂₀ H ₃₀ As ₁₁ Fe ₂ I ₈
<i>M_r</i>	1766.89	2378.45	2221.46
Crystal system, space group	Triclinic, <i>P</i> 1	Monoclinic, <i>C</i> 2/ <i>c</i>	Triclinic, <i>P</i> 1
Temperature (K)	90	90	123
<i>a</i> , <i>b</i> , <i>c</i> (Å)	8.24209(17), 9.5666(2), 12.2385(3)	27.1423(7), 8.05281(17), 24.9066(7)	10.7570(12), 10.7611(14), 11.9570(16)
α , β , γ (°)	88.7874(17), 81.4347(17), 82.0433(18)	90, 110.724(3), 90	63.956(13), 73.254(11), 65.839(11)
<i>V</i> (Å ³)	945.04(3)	5091.7(2)	1124.7 (3)
<i>Z</i>	1	4	1
<i>F</i> (000)	780	4128	989
<i>D_x</i> (Mg m ⁻³)	3.105	3.103	3.280
Radiation type	Cu <i>K</i> α	Cu <i>K</i> α	Cu <i>K</i> α
μ (mm ⁻¹)	60.25	72.05	57.41
Crystal shape and colour	Yellow polyhedron	Orange plate	Dark red elongated plate
Crystal size (mm)	0.06 × 0.04 × 0.02	0.10 × 0.05 × 0.02	0.14 × 0.09 × 0.03
Data collection			
Diffractometer	SuperNova, Titan ^{S2}	SuperNova, Titan ^{S2}	SuperNova, Titan ^{S2}
Absorption correction	Gaussian	Gaussian	Empirical
<i>T_{min}</i> , <i>T_{max}</i>	0.112, 0.468	0.045, 0.374	0.068, 0.167
No. of measured, independent and observed [<i>I</i> > 2σ(<i>I</i>)] reflections	23686, 3806, 3619	14306, 5044, 4227	7308, 4331, 3661
<i>R_{int}</i>	0.030	0.043	0.038
(sin θ/λ) _{max} (Å ⁻¹)	0.624	0.623	0.623
Range of <i>h</i> , <i>k</i> , <i>l</i>	<i>h</i> = -10→10, <i>k</i> = -11→11, <i>l</i> = -15→15	<i>h</i> = -33→29, <i>k</i> = -7→9, <i>l</i> = -30→30	<i>h</i> = -13→9, <i>k</i> = -13→12, <i>l</i> = -14→12
Refinement			
<i>R</i> [<i>F</i> ² > 2σ(<i>F</i> ²)], <i>wR</i> (<i>F</i> ²), <i>S</i>	0.018, 0.042, 1.05	0.083, 0.242, 1.06	0.050, 0.139, 1.02
No. Of reflections	3806	5044	4331
No. Of parameters	154	186	213
No. Of restraints	0	0	0
H-atom treatment	H-atom parameters constrained	H-atom parameters constrained	H-atom parameters constrained
Δ _{max} , Δ _{min} (e Å ⁻³)	0.48, -0.92	4.58, -5.01	2.40, -2.62

Computer programs: *CrysAlis PRO 1.171.38.42b* (Rigaku OD, 2015), *SHELXS2014/7* (Sheldrick, 2014), *SHELXL2018/3* (Sheldrick, 2018).

Table 3. Experimental details for compounds **11** and **12**.

Crystal data	11	12
CCDC Codes	CCDC-1985263	CCDC-1985260
Structural formula	[(Cp*Ru) ₂ As ₅] ₂ (As ₆ I ₆)(I) ₂	[(Cp*Ru) ₂ As ₈ I ₆]
Chemical formula	C ₄₀ H ₆₀ As ₁₆ I ₈ Ru ₄	C ₂₀ H ₃₀ As ₈ I ₆ Ru ₂
<i>M_r</i>	3159.08	1833.34
Crystal system, space group	Triclinic, <i>P</i> 1	Monoclinic, <i>P</i> 2 ₁ / <i>c</i>
Temperature (K)	90	90
<i>a</i> , <i>b</i> , <i>c</i> (Å)	11.4880(3), 12.3989(3), 15.1541(4)	17.8758(3), 12.51878(19), 17.3531(3)
α , β , γ (°)	66.141(2), 69.808(3), 66.057(3)	90, 9 8.6149(16), 90
<i>V</i> (Å ³)	1761.38(10)	3839.51(11)
<i>Z</i>	1	4
<i>F</i> (000)	1428	3280
<i>D_x</i> (Mg m ⁻³)	2.978	3.172
Radiation type	Cu <i>K</i> α	Cu <i>K</i> α
μ (mm ⁻¹)	42.88	52.02
Crystal shape and colour	Red rod	Black plate
Crystal size (mm)	0.07 × 0.02 × 0.01	0.16 × 0.06 × 0.02
Data collection		
Diffractometer	SuperNova, Titan ^{S2}	SuperNova, Titan ^{S2}
Absorption correction	Gaussian	Multi-scan
<i>T_{min}</i> , <i>T_{max}</i>	0.268, 0.780	0.208, 1.000
No. of measured, independent and observed [<i>I</i> > 2σ(<i>I</i>)] reflections	13650, 6941, 5635	15097, 7488, 6453
<i>R_{int}</i>	0.031	0.046
(sin θ/λ) _{max} (Å ⁻¹)	0.623	0.624
Range of <i>h</i> , <i>k</i> , <i>l</i>	<i>h</i> = -14→13, <i>k</i> = -15→15, <i>l</i> = -18→18	<i>h</i> = -21→22, <i>k</i> = -15→9, <i>l</i> = -19→21
Refinement		
<i>R</i> [<i>F</i> ² > 2σ(<i>F</i> ²)], <i>wR</i> (<i>F</i> ²), <i>S</i>	0.027, 0.058, 0.94	0.039, 0.102, 1.02
No. of reflections	6941	7488
No. of parameters	317	335
No. of restraints	0	12
H-atom treatment	H-atom parameters constrained	H-atom parameters constrained
Δ _{max} , Δ _{min} (e Å ⁻³)	1.35, -1.15	2.16, -2.12

Computer programs: CrysAlis PRO 1.171.38.42b (Rigaku OD, 2015), SHELXS2014/7 (Sheldrick, 2014), SHELXL2018/3 (Sheldrick, 2018).

Table 4. Experimental details for compounds **13-sym** and **13-asym**.

Crystal data	13-sym	13-asym
CCDC Codes	CCDC-1985258	CCDC-1985264
Structural formula	[(Cp* <i>Ru</i>) ₂ As ₄ I ₄]	[(Cp* <i>Ru</i>) ₂ As ₄ I ₄]
Chemical formula	C ₂₀ H ₃₀ As ₄ I ₄ Ru ₂	C ₂₀ H ₃₀ As ₄ I ₄ Ru ₂
<i>M_r</i>	1279.86	1279.86
Crystal system, space group	Monoclinic, <i>P</i> 2 ₁ / <i>n</i>	Monoclinic, <i>C</i> 2/ <i>c</i>
Temperature (K)	90	90
<i>a</i> , <i>b</i> , <i>c</i> (Å)	9.1063(2), 15.3410(3), 10.9574(2)	14.42612(18), 11.41304(16), 17.5300(3)
α , β , γ (°)	90, 106.869(2), 90	90, 94.1351(13), 90
<i>V</i> (Å ³)	1464.88(5)	2878.73(7)
<i>Z</i>	2	4
<i>F</i> (000)	1164	2328
<i>D_x</i> (Mg m ⁻³)	2.902	2.953
Radiation type	Cu <i>K</i> α	Cu <i>K</i> α
μ (mm ⁻¹)	46.54	47.37
Crystal shape and colour	Dark red prism	Dark red plate
Crystal size (mm)	0.07 × 0.04 × 0.03	0.05 × 0.04 × 0.03
Data collection		
Diffractometer	SuperNova, Titan ^{S2}	SuperNova, Titan ^{S2}
Absorption correction	Gaussian	Gaussian
<i>T_{min}</i> , <i>T_{max}</i>	0.161, 0.406	0.222, 0.445
No. of measured, independent and observed [<i>l</i> > 2σ(<i>l</i>)] reflections	9561, 2928, 2469	5451, 2820, 2542
<i>R_{int}</i>	0.039	0.019
(sin θ/λ) _{max} (Å ⁻¹)	0.624	0.623
Range of <i>h</i> , <i>k</i> , <i>l</i>	<i>h</i> = -11→10, <i>k</i> = -13→18, <i>l</i> = -12→13	<i>h</i> = -17→11, <i>k</i> = -12→14, <i>l</i> = -21→21
Refinement		
<i>R</i> [<i>F</i> ² > 2σ(<i>F</i> ²)], <i>wR</i> (<i>F</i> ²), <i>S</i>	0.021, 0.045, 0.92	0.021, 0.051, 0.98
No. of reflections	2928	2820
No. of parameters	141	141
No. of restraints	0	0
H-atom treatment	H-atom parameters constrained	H-atom parameters constrained
Δ _{max} , Δ _{min} (e Å ⁻³)	0.64, -0.66	0.73, -1.08

Computer programs: *CrysAlis PRO* 1.171.38.42b (Rigaku OD, 2015), *SHELXS2014/7* (Sheldrick, 2014), *SHELXL2018/3* (Sheldrick, 2018).

7.6 Computational Details

Gaussian 09 program^[45] was used throughout. Density functional theory (DFT) in form of Becke's three-parameter hybrid functional B3LYP^[46] with def2-SVP all electron basis set,^[47] BP86^[48] (Becke's exchange and Perdew 86 correlation functional) with def2-TZVP all electron basis set or wB97XD^[49] with def2-TZVP all electron basis set was employed. Solvents effects were accounted by using continuous polarizable continuum model (CPM).^[50] The dielectric constant of water ($\epsilon = 78.3553$) has been used in the calculations of the cations **3**, the dielectric constant of thf ($\epsilon = 7.4257$) has been used in the calculations of **13_B3LYP_D**, **13_B3LYP_F**, **13_BP86_B**, **13_BP86_D**, **13_wB97XD_B** and **13_wB97XD_D** and the dielectric constant of hexane ($\epsilon = 1.8819$) was used for the calculations of **13_B3LYP_C**, **13_B3LYP_E**, **13_BP86_A**, **13_BP86_C**, **13_wB97XD_A** and **13_wB97XD_C**. The Natural Bond Orbital (NBO) analysis has been performed with the NBO6 program.^[51] The dispersion correction GD3BJ was applied (except for **3**, **13_B3LYP_A**, **13_B3LYP_B**, **13_wB97XD_A-D**).^[52] The figures for the supporting information concerning the DFT calculations were created with Chemcraft.^[53]

Geometry optimization were started from atomic coordinates of **13-sym** obtained from X-ray diffractions for **13_B3LYP_A**, **13_B3LYP_C**, **13_B3LYP_D**, **13_BP86_A**, **13_BP86_B**, **13_wB97XD_A**, **13_wB97XD_B**. Geometry optimization were started from atomic coordinates of **13-asym** obtained from X-ray diffractions for **13_B3LYP_B**, **13_B3LYP_E**, **13_B3LYP_F**, **13_BP86_C**, **13_BP86_D**, **13_wB97XD_C**, **13_wB97XD_D**.

The initial target of the DFT calculations concerning complex **13** (**13-sym** and **13-asym**) was to determine which isomer is energetically favored. The outcome of the geometry optimization is strongly dependent on the used functional (B3LYP, BP86, wB97XD) while the use of the empirical dispersion correction GD3BJ, solvent effects (SCRF) and basis set (def2-SVP or def2-TZVP) play only a minor role in the obtained geometries. The kind of the solvent used within CPM has only an influence on the energy but not on the geometry. The outcome of the geometry optimizations is independent whether the geometry optimization is started from the atomic coordinates of **13-sym** or **13-asym** (cf. Tables 7-10). Using B3LYP or wB97XD delivers geometries similar to **13-asym** (obtained from X-ray diffraction data), while the short As-I contacts are shorter than those in **13-asym** and the long As-I contacts are longer than those in **13-asym** (cf. Tables 7, 8 and 10). When BP86 is used a symmetric geometry of the As₄I₄ ligand analog to **13-sym** is obtained (cf. Table 9). Finally, no clear answer can be given which isomer is energetically favored. Possibly, the different geometries of **13-asym** and **13-sym** are due to different packing in the solid state (cf. Figure 9).

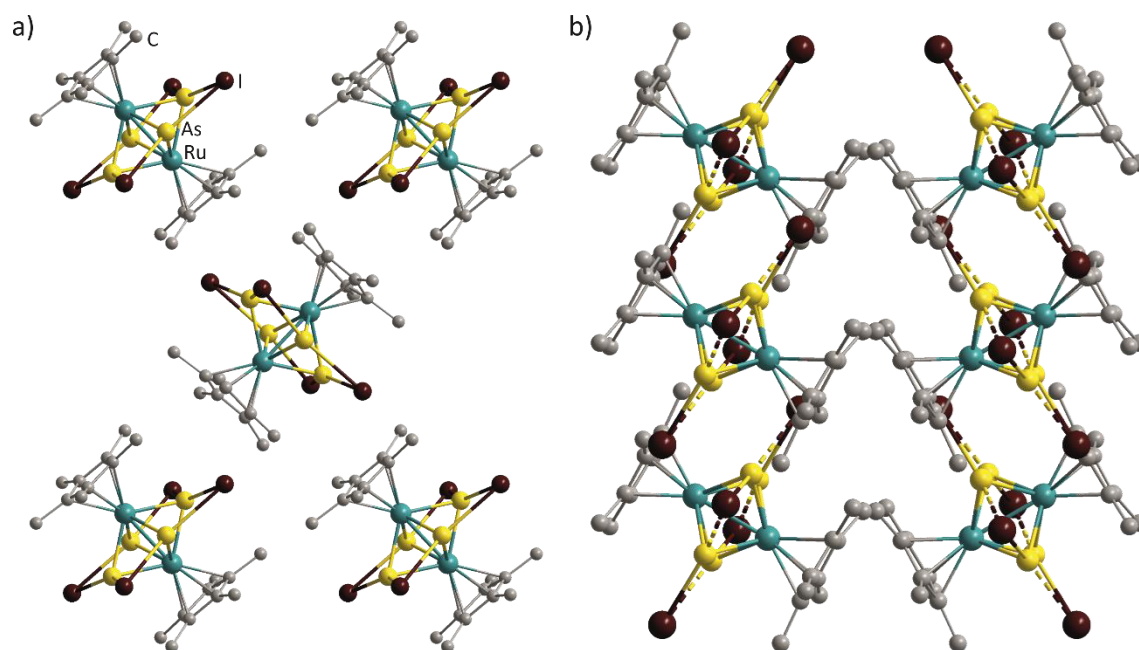


Figure 9. Crystal packing in a) **13-sym** and b) **13-asm** drawn in the ball-and-sticks model with view along the crystallographic *a* axis.

Table 5. Total energies for all optimized geometries. a) B3LYP/def2-SVP without SCRF and GD3BJ, b) B3LYP/def2-SVP including SCRF and GD3BJ, c) BP86/def2-TZVP including SCRF and GD3BJ, d) wB97XD including SCRF.

		total energy [Ha]
a	3 [Cp*Fe(P ₆ I ₆)] ⁺	-5487.80369448
a	9 [(Cp*Fe) ₂ As ₅] ²⁺	-14484.7160854
a	13_B3LYP_A	-11103.6304934
a	13_B3LYP_B	-11103.6304472
b	13_B3LYP_C	-11103.9040607
b	13_B3LYP_D	-11103.9102778
b	13_B3LYP_E	-11103.9039161
b	13_B3LYP_F	-11103.9101377
c	13_BP86_A	-11107.2904620
c	13_BP86_B	-11107.2960443
c	13_BP86_C	-11107.2903013
c	13_BP86_D	-11107.2958880
d	13_wB97XD_A	-11105.5026631
d	13_wB97XD_B	-11105.5096565
d	13_wB97XD_C	-11105.5025180
d	13_wB97XD_D	-11105.5096038

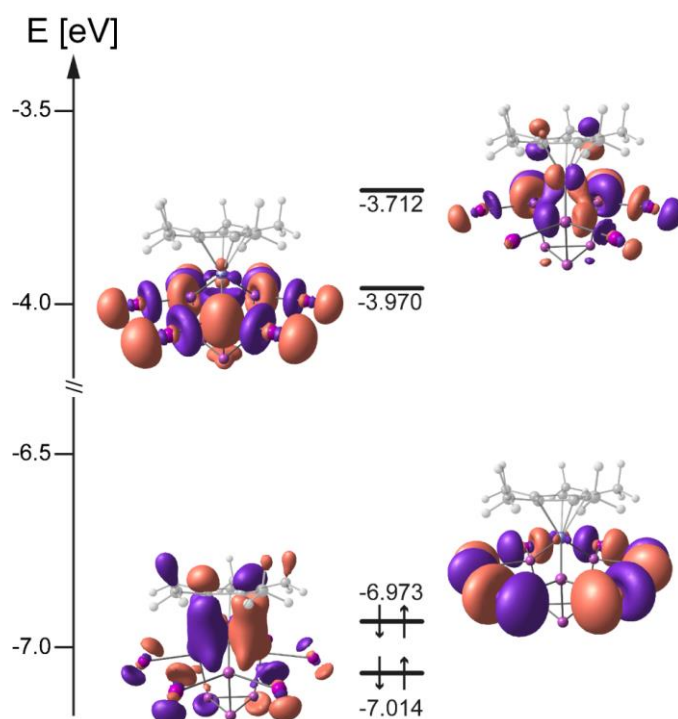


Figure 10. Frontier molecular orbitals of **3** (B3LYP/def2-SVP level of theory).

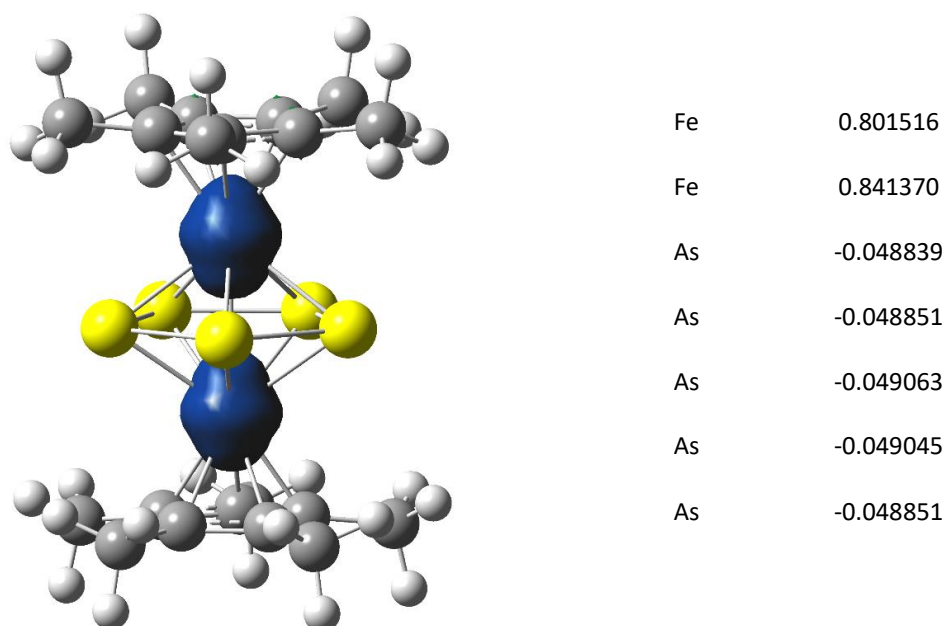
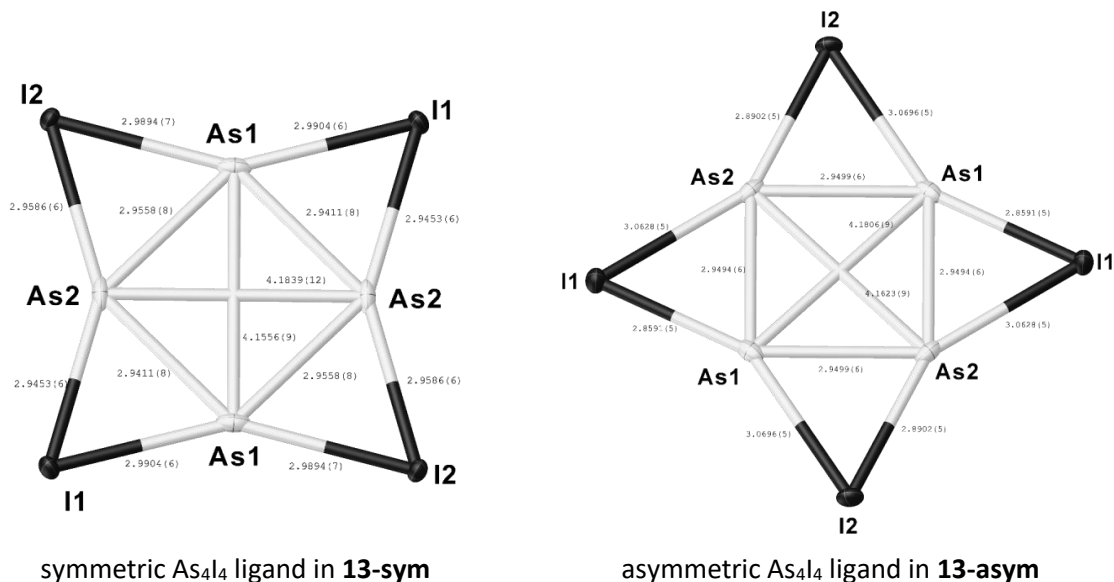


Figure 11. Isosurface of the spin density in the cation of **9** (B3LYP/def2-SVP level of theory, cut off value of 0.006, left) and spin densities of the heavy atoms (right).

Table 6. Data obtained from X-ray diffraction experiments.



	13-sym	13-asym
d (Ru-Ru) / Å	2.6594(6)	2.6595(7)
d (As-I) (longer) / Å	2.9894(7)	3.0696(5)
	2.9904(6)	3.0628(5)
d (As-I) (shorter) / Å	2.9586(6)	2.8902(5)
	2.9453(6)	2.8591(5)

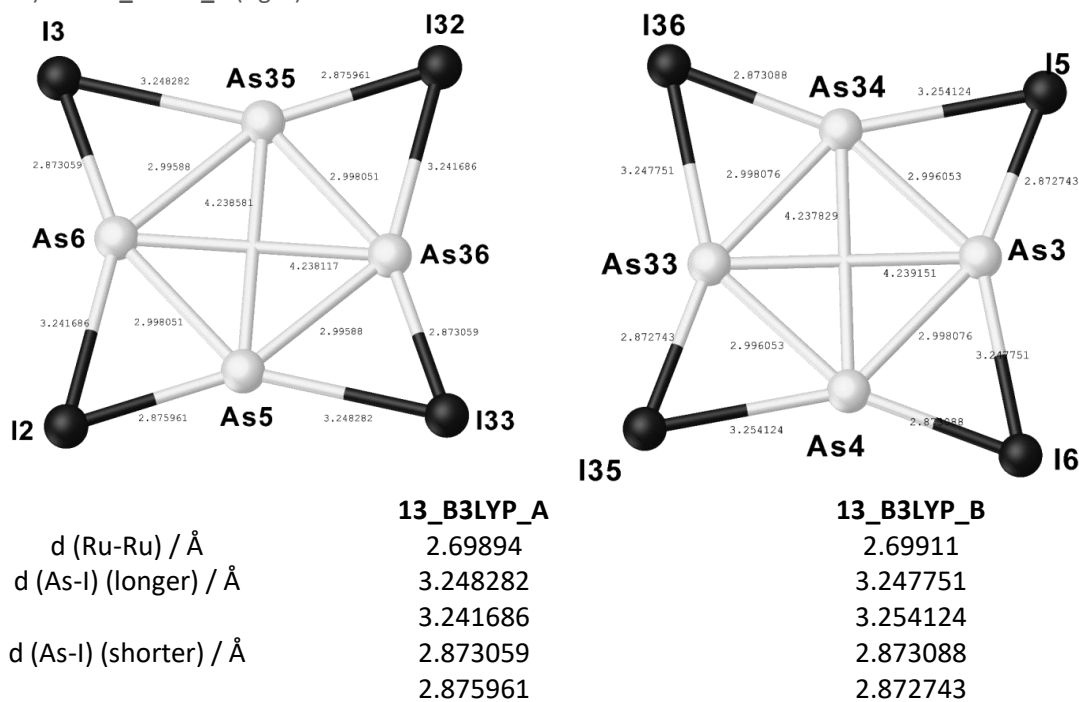
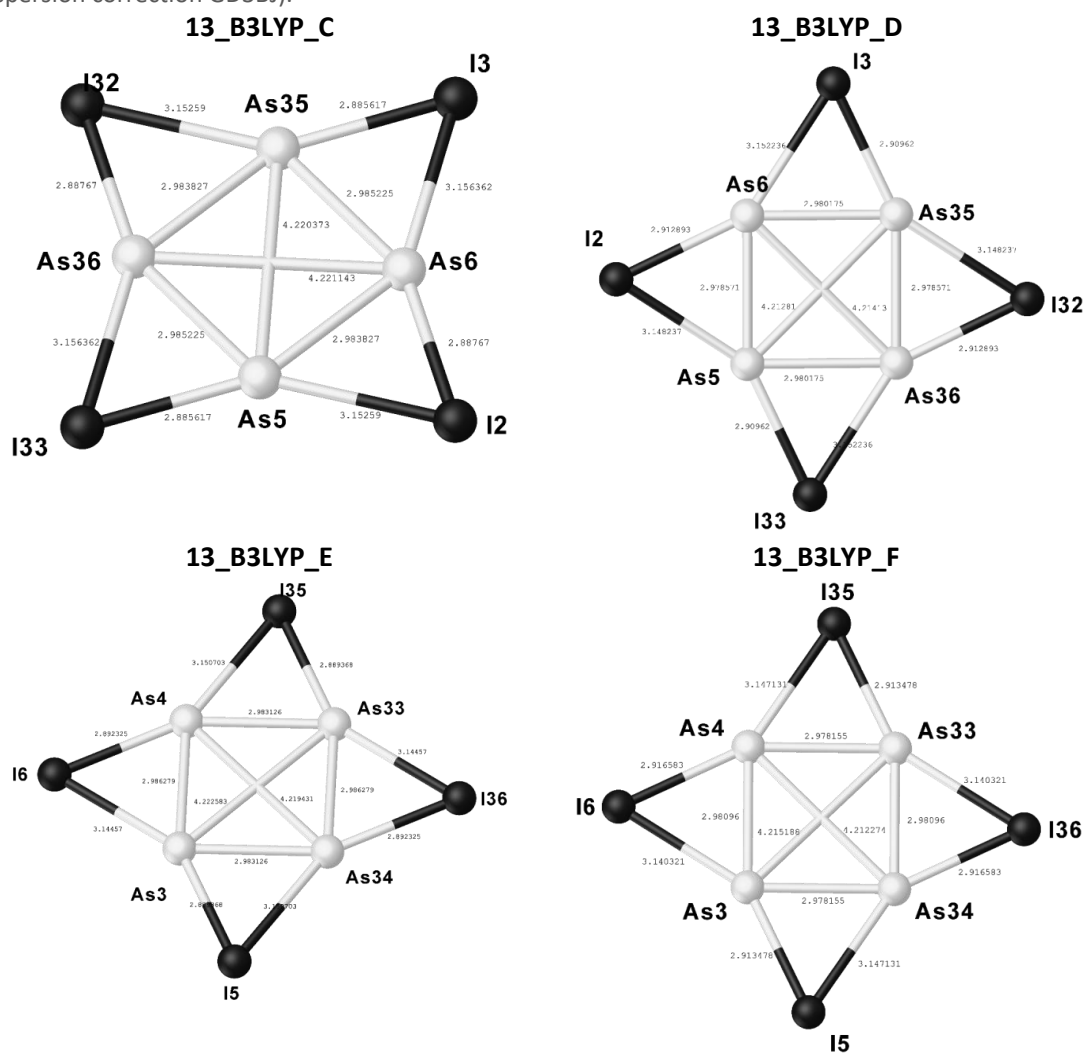
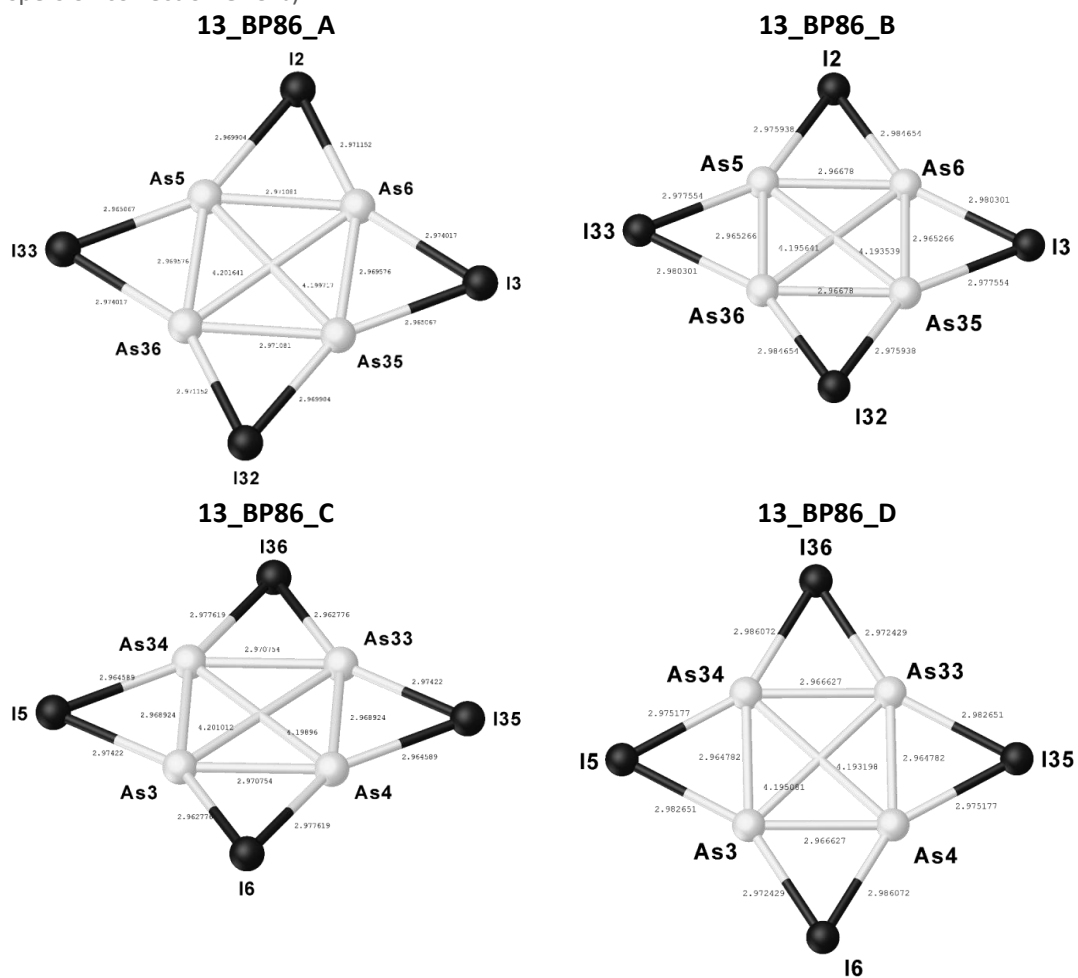
Table 7. Data obtained from DFT calculations (B3LYP/def2-SVP without SCRF and GD3BJ) **13_B3LYP_A** (left) and **13_B3LYP_B** (right).

Table 8. Data obtained from DFT calculations (B3LYP/def2-SVP with SCRf (hexane and thf) and empirical dispersion correction GD3BJ).



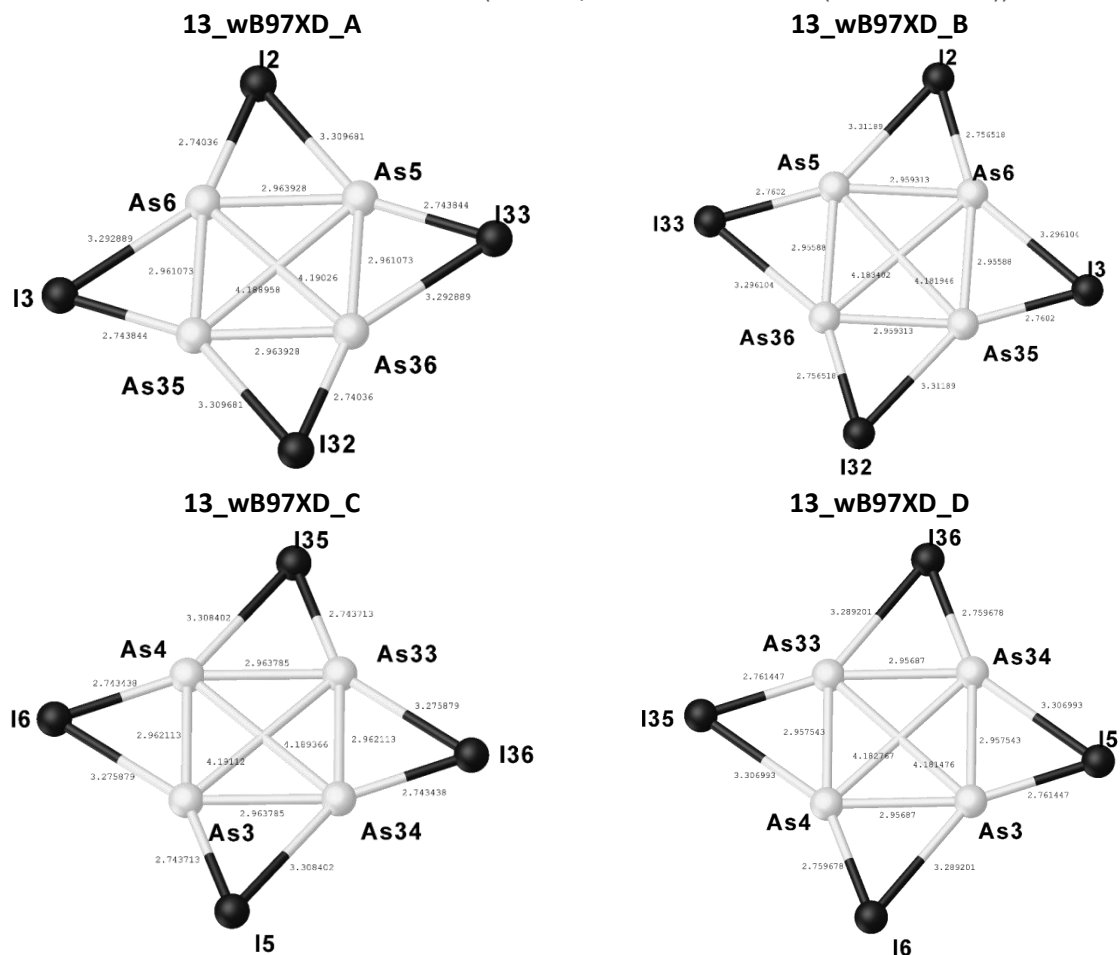
	13_B3LYP_C	13_B3LYP_D	13_B3LYP_E	13_B3LYP_F
d (Ru-Ru) / Å	2.66104	2.66112	2.66131	2.66136
d (As-I) (longer) / Å	3.15259	3.152236	3.150703	3.147131
d (As-I) (shorter) / Å	3.156362	3.148237	3.14457	3.140321
	2.88767	2.90962	2.889368	2.913478
	2.885617	2.912893	2.892325	2.913478

Table 9. Data obtained from DFT calculations (BP86/def2-TZVP with SCRf (hexane and thf) and empirical dispersion correction GD3BJ).



	13_BP86_A	13_BP86_B	13_BP86_C	13_BP86_D
d (Ru-Ru) / Å	2.66214	2.66240	2.66329	2.66336
d (As-I) (longer) / Å	2.971152	2.984654	2.977619	2.986072
d (As-I) (shorter) / Å	2.974017	2.980301	2.97422	2.982651
	2.969904	2.975938	2.962776	2.972429
	2.965067	2.977554	2.964589	2.975177

Table 10. Data obtained from DFT calculations (wB97XD/def2-TZVP with SCRF (hexane and thf)).



	13_wB97XD_A	13_wB97XD_B	13_wB97XD_C	13_wB97XD_D
d (Ru-Ru) / Å	2.67665	2.67608	2.67599	2.67594
d (As-I) (longer) / Å	3.309681	3.31189	3.308402	3.289201
d (As-I) (shorter) / Å	2.74036 2.743844	2.756518 2.7602	2.743713 2.759678	2.759678 2.761447

Table 11. Optimized geometry of 3. XYZ coordinates in angstroms. B3LYP/def2-SVP level of theory.

Fe	5.864947000	4.858787000	7.665417000	H	5.855380000	7.482087000	10.280737000
P	3.785562000	5.251785000	4.530305000	H	6.988691000	6.652209000	11.357412000
P	2.448101000	5.725269000	6.286008000	H	5.337078000	6.032866000	11.186923000
P	2.875735000	3.576738000	5.739559000	C	6.151166000	3.339178000	10.659412000
P	5.840994000	5.393156000	5.513370000	H	5.166256000	3.680710000	11.006082000
P	4.010473000	6.039112000	7.917645000	H	6.841719000	3.400059000	11.518573000
P	4.594025000	3.100347000	7.168683000	H	6.067964000	2.282107000	10.378875000
I	7.082236000	4.072960000	3.764338000	C	8.033328000	2.346135000	8.259185000
I	6.439236000	7.691155000	4.694512000	H	8.252814000	2.138299000	7.203865000
I	4.022132000	8.551831000	7.880711000	H	7.327986000	1.587468000	8.621379000
I	2.480730000	5.717598000	9.888315000	H	8.973091000	2.216971000	8.824340000
I	3.214576000	1.866160000	8.870277000	C	9.132182000	4.906723000	6.777796000
I	5.433382000	1.082971000	5.918216000	H	9.067392000	5.759109000	6.088186000
C	6.688340000	5.616697000	9.540724000	H	9.164910000	3.981374000	6.189609000
C	6.688339000	4.186867000	9.549083000	H	10.095724000	4.992750000	7.310283000
C	7.539943000	3.741916000	8.469568000	C	7.923656000	7.478498000	8.212301000
C	8.036874000	4.898367000	7.795849000	H	8.356863000	7.628523000	7.216251000
C	7.483560000	6.065286000	8.433929000	H	8.702217000	7.728001000	8.954267000
C	6.167794000	6.491276000	10.636285000	H	7.104707000	8.198556000	8.342732000

Table 12. Optimized geometry of 9. XYZ coordinates in angstroms. B3LYP/def2-SVP level of theory.

Fe	-1.446961000	0.000294000	-0.000298000	As	-0.000193000	1.814633000	-0.953812000
C	-3.216683000	0.271154000	1.192542000	As	-0.003441000	1.468273000	1.430019000
C	-3.216395000	-1.051193000	0.627066000	As	-0.000538000	-0.906506000	1.837475000
C	-3.217158000	-0.921866000	-0.805351000	C	3.209223000	-0.285517000	-1.189709000
C	-3.217963000	0.480374000	-1.125154000	C	3.209636000	1.043396000	-0.638152000
C	-3.218064000	1.217675000	0.109573000	C	3.208606000	0.929429000	0.796072000
C	-3.375885000	0.601706000	2.643279000	C	3.207861000	-0.469682000	1.130839000
H	-2.946614000	1.579292000	2.902730000	C	3.208250000	-1.220653000	-0.096344000
H	-4.452737000	0.648439000	2.883858000	C	3.392611000	-0.632216000	-2.634353000
H	-2.932669000	-0.158946000	3.300685000	H	2.961319000	-1.608970000	-2.892838000
C	-3.374896000	-2.328556000	1.390015000	H	4.474093000	-0.690551000	-2.851792000
H	-2.937749000	-3.189896000	0.866479000	H	2.971479000	0.125966000	-3.308701000
H	-2.939068000	-2.274859000	2.397179000	C	3.393278000	2.310212000	-1.414019000
H	-4.451672000	-2.539556000	1.515460000	H	2.976121000	3.186193000	-0.898756000
C	-3.376231000	-2.042074000	-1.784471000	H	2.958087000	2.255954000	-2.421236000
H	-2.940095000	-2.983624000	-1.423085000	H	4.474752000	2.496573000	-1.540505000
H	-4.453118000	-2.226437000	-1.945798000	C	3.389645000	2.058619000	1.761754000
H	-2.939718000	-1.809879000	-2.765609000	H	2.951994000	2.999011000	1.399816000
C	-3.377845000	1.066104000	-2.492742000	H	4.470642000	2.239091000	1.900292000
H	-2.936561000	2.068845000	-2.576182000	H	2.972776000	1.837229000	2.753782000
H	-2.946819000	0.429421000	-3.277622000	C	3.386997000	-1.038320000	2.503778000
H	-4.454797000	1.167849000	-2.715252000	H	2.973691000	-2.051721000	2.598627000
C	-3.378353000	2.699286000	0.244641000	H	2.944059000	-0.404819000	3.284451000
H	-2.934603000	3.088605000	1.171282000	H	4.467528000	-1.109996000	2.721943000
H	-2.950435000	3.249566000	-0.604608000	C	3.389040000	-2.701974000	-0.212581000
H	-4.455383000	2.941590000	0.276011000	H	2.973993000	-3.106619000	-1.145741000
Fe	1.438975000	0.000161000	-0.000476000	H	2.949472000	-3.249230000	0.632541000
As	-0.002052000	-2.027719000	-0.294904000	H	4.469974000	-2.929753000	-0.215782000
As	-0.001787000	-0.345832000	-2.020039000				

Table 13. Optimized geometry of 13_B3LYP_A. XYZ coordinates in angstroms. B3LYP/def2-SVP level of theory.

I	3.753774000	1.692320000	0.594254000	I	-3.753774000	-1.692320000	-0.594254000
I	1.570117000	-2.395189000	-3.023652000	I	-1.570117000	2.395189000	3.023652000
Ru	0.258688000	-0.965267000	0.906866000	Ru	-0.258688000	0.965267000	-0.906866000
As	0.965489000	1.418645000	1.243652000	As	-0.965489000	-1.418645000	-1.243652000
As	1.843784000	-0.418051000	-0.957133000	As	-1.843784000	0.418051000	0.957133000
C	-0.118186000	-3.152798000	1.578204000	C	0.118186000	3.152798000	-1.578204000
C	-0.562806000	-2.269439000	2.623551000	C	0.562806000	2.269439000	-2.623551000
C	0.579109000	-1.529173000	3.098563000	C	-0.579109000	1.529173000	-3.098563000
C	1.729835000	-1.951223000	2.337465000	C	-1.729835000	1.951223000	-2.337465000
C	1.296816000	-2.956938000	1.399471000	C	-1.296816000	2.956938000	-1.399471000
C	-0.938920000	-4.234195000	0.945014000	C	0.938920000	4.234195000	-0.945014000
H	-1.985253000	-3.928716000	0.809774000	H	1.985253000	3.928716000	-0.809774000
H	-0.929940000	-5.129185000	1.592898000	H	0.929940000	5.129185000	-1.592898000
H	-0.541285000	-4.528385000	-0.035684000	H	0.541285000	4.528385000	0.035684000
C	-1.925260000	-2.284602000	3.249077000	C	1.925260000	2.284602000	-3.249077000
H	-2.148441000	-1.342789000	3.767902000	H	2.148441000	1.342789000	-3.767902000
H	-1.979845000	-3.099237000	3.993508000	H	1.979845000	3.099237000	-3.993508000
H	-2.715021000	-2.458307000	2.505192000	H	2.715021000	2.458307000	-2.505192000
C	0.606206000	-0.661756000	4.319320000	C	-0.606206000	0.661756000	-4.319320000
H	1.454065000	0.036137000	4.307278000	H	-1.454065000	-0.036137000	-4.307278000
H	0.704941000	-1.295154000	5.218980000	H	-0.704941000	1.295154000	-5.218980000
H	-0.310250000	-0.066176000	4.424690000	H	0.310250000	0.066176000	-4.424690000
C	3.153420000	-1.593053000	2.634938000	C	-3.153420000	1.593053000	-2.634938000
H	3.791070000	-1.659660000	1.743756000	H	-3.791070000	1.659660000	-1.743756000
H	3.558773000	-2.287200000	3.392691000	H	-3.558773000	2.287200000	-3.392691000
H	3.249956000	-0.572463000	3.026795000	H	-3.249956000	0.572463000	-3.026795000
C	2.191154000	-3.810570000	0.554866000	C	-2.191154000	3.810570000	-0.554866000
H	1.711228000	-4.108799000	-0.386712000	H	-1.711228000	4.108799000	0.386712000
H	2.455317000	-4.729514000	1.108159000	H	-2.455317000	4.729514000	-1.108159000
H	3.125260000	-3.294478000	0.296321000	H	-3.125260000	3.294478000	-0.296321000

Table 14. Optimized geometry of **13_B3LYP_B**. XYZ coordinates in angstroms. B3LYP/def2-SVP level of theory.

Ru	-0.111404000	0.680889000	1.159859000	H	3.521242000	-1.545589000	-2.141071000	Ru	0.111404000	-	
As	-1.538141000	-1.320659000	0.618532000	0.680889000	-1.159859000			As	1.538141000	1.320659000	-0.618532000
As	1.448174000	-1.272480000	0.879423000	As	-1.448174000	1.272480000	-0.879423000	As	-1.448174000	1.272480000	-0.879423000
I	-4.146771000	-0.391514000	-0.145922000	I	4.146771000	0.391514000	0.145922000	I	4.146771000	0.391514000	0.145922000
I	0.248809000	-3.528567000	2.193283000	I	-0.248809000	3.528567000	-2.193283000	C	0.249235000	-2.682697000	-2.236464000
C	-0.249235000	2.682697000	2.236464000	C	0.249235000	-2.682697000	-2.236464000	C	0.420216000	0.784690000	3.413625000
C	0.892979000	1.980944000	2.767050000	C	-0.892979000	-1.980944000	-2.767050000	C	-0.420216000	-0.784690000	-3.413625000
C	0.420216000	0.784690000	3.413625000	C	-0.420216000	-0.784690000	-3.413625000	C	1.012059000	-0.742716000	-3.282558000
C	-0.102059000	0.742716000	3.282558000	C	1.012059000	-0.742716000	-3.282558000	C	1.429213000	-1.918543000	-2.560724000
C	-1.429213000	1.918543000	2.560724000	C	1.429213000	-1.918543000	-2.560724000	C	0.232941000	-4.069202000	-1.670347000
C	-0.232941000	4.069202000	1.670347000	C	0.232941000	-4.069202000	-1.670347000	H	0.700418000	4.284250000	1.133715000
H	0.700418000	4.284250000	1.133715000	H	-0.700418000	-4.284250000	-1.133715000	H	-0.329533000	4.804666000	2.488881000
H	-0.329533000	4.804666000	2.488881000	H	0.329533000	-4.804666000	-2.488881000	H	-1.057095000	4.238648000	0.965632000
H	-1.057095000	4.238648000	0.965632000	H	1.057095000	-4.238648000	-0.965632000	C	2.290705000	2.512185000	2.844907000
C	2.290705000	2.512185000	2.844907000	C	-2.290705000	-2.512185000	-2.844907000	H	3.041090000	1.712173000	2.793041000
H	3.041090000	1.712173000	2.793041000	H	-3.041090000	-1.712173000	-2.793041000	H	2.429255000	3.046444000	3.801891000
H	2.429255000	3.046444000	3.801891000	H	2.429255000	-3.046444000	-3.801891000	C	2.507906000	3.218332000	2.032652000
C	2.507906000	3.218332000	2.032652000	H	-2.507906000	3.218332000	2.032652000	C	1.243733000	-0.135631000	4.261928000
C	1.243733000	-0.135631000	4.261928000	C	1.243733000	0.135631000	-4.261928000	H	0.864974000	-1.166536000	4.237577000
H	0.864974000	-1.166536000	4.237577000	H	-0.864974000	1.166536000	-4.237577000	H	1.215399000	0.209444000	5.311186000
H	1.215399000	0.209444000	5.311186000	H	1.215399000	-0.209444000	-5.311186000	H	2.295292000	-0.153174000	3.945117000
H	2.295292000	-0.153174000	3.945117000	C	-2.295292000	0.153174000	-3.945117000	C	-1.917989000	-0.236990000	3.965330000
C	-1.917989000	-0.236990000	3.965330000	C	1.917989000	0.236990000	-3.965330000	H	-2.894241000	-0.306822000	5.467085000
H	-2.894241000	-0.306822000	5.467085000	H	2.894241000	0.306822000	-5.467085000	H	-2.094392000	0.086837000	3.006865000
H	-2.094392000	0.086837000	3.006865000	H	-2.094392000	-0.086837000	-3.006865000	C	-1.478887000	-1.243574000	3.997639000
C	-1.478887000	-1.243574000	3.997639000	H	1.478887000	1.243574000	-3.997639000	C	-2.845461000	2.375079000	2.389566000
C	-2.845461000	2.375079000	2.389566000	H	2.845461000	-2.375079000	-2.389566000	H	-2.938177000	3.127922000	1.595380000
H	-2.938177000	3.127922000	1.595380000	C	2.938177000	-3.127922000	-1.595380000	H	-3.201885000	2.832672000	3.329589000
H	-3.201885000	2.832672000	3.329589000	H	3.201885000	2.832672000	-3.329589000	H	-3.521242000	1.545589000	2.141071000
H	-3.521242000	1.545589000	2.141071000								

Table 15. Optimized geometry of **13_B3LYP_C**. XYZ coordinates in angstroms. B3LYP/def2-SVP level of theory.

I	3.331568000	2.010222000	1.344613000	I	-3.331568000	-2.010222000	-1.344613000	I	-3.331568000	-2.010222000	-1.344613000
I	2.282324000	-1.885128000	-2.859091000	I	2.282324000	1.885128000	2.859091000	I	-2.282324000	1.885128000	2.859091000
Ru	0.240584000	-0.967053000	0.881597000	Ru	-0.240584000	0.967053000	-0.881597000	Ru	0.240584000	-0.967053000	0.881597000
As	0.233744000	1.450434000	1.514758000	As	-0.233744000	-1.450434000	-1.514758000	As	-0.233744000	-1.450434000	-1.514758000
As	2.063792000	0.114565000	-0.426789000	As	-2.063792000	-0.114565000	0.426789000	As	2.063792000	0.114565000	-0.426789000
C	-0.187706000	-3.069034000	1.571398000	C	0.187706000	3.069034000	-1.571398000	C	0.187706000	3.069034000	-1.571398000
C	-0.551437000	-2.173700000	2.639239000	C	0.551437000	2.173700000	-2.639239000	C	0.551437000	2.173700000	-2.639239000
C	0.637305000	-1.489931000	3.070951000	C	-0.637305000	1.489931000	-3.070951000	C	-0.637305000	1.489931000	-3.070951000
C	1.736966000	-1.962246000	2.274253000	C	1.736966000	1.962246000	-2.274253000	C	-1.736966000	-1.962246000	2.274253000
C	1.228272000	-2.933821000	1.341729000	C	-1.228272000	2.933821000	-1.341729000	C	-1.228272000	2.933821000	-1.341729000
C	-1.083163000	-4.088289000	0.949764000	C	1.083163000	4.088289000	-0.949764000	C	1.083163000	4.088289000	-0.949764000
H	-2.109562000	-3.716420000	0.843628000	H	2.109562000	3.716420000	-0.843628000	H	2.109562000	3.716420000	-0.843628000
H	-1.107918000	-4.993950000	1.579775000	H	1.107918000	4.993950000	-1.579775000	H	1.107918000	4.993950000	-1.579775000
H	-0.734454000	-4.378410000	-0.049651000	H	0.734454000	4.378410000	0.049651000	H	0.734454000	4.378410000	0.049651000
C	-1.888481000	-2.093393000	3.300507000	C	1.888481000	2.093393000	-3.300507000	C	1.888481000	2.093393000	-3.300507000
H	-2.107064000	-1.073257000	3.641879000	H	2.107064000	1.073257000	-3.641879000	H	2.107064000	1.073257000	-3.641879000
H	-1.906571000	-2.759413000	4.180446000	H	1.906571000	2.759413000	-4.180446000	H	1.906571000	2.759413000	-4.180446000
H	-2.693395000	-2.405071000	2.622234000	H	2.693395000	2.405071000	-2.622234000	H	2.693395000	2.405071000	-2.622234000
C	0.744123000	-0.577731000	4.249964000	C	-0.744123000	0.577731000	-4.249964000	C	-0.744123000	0.577731000	-4.249964000
H	1.564692000	0.141837000	4.128945000	H	-1.564692000	-0.141837000	-4.128945000	H	-1.564692000	-0.141837000	-4.128945000
H	0.944139000	-1.171504000	5.158804000	H	-0.944139000	1.171504000	-5.158804000	H	-0.944139000	1.171504000	-5.158804000
H	-0.184036000	-0.014046000	4.410297000	H	0.184036000	0.014046000	-4.410297000	H	0.184036000	0.014046000	-4.410297000
C	3.176086000	-1.643149000	2.508448000	C	-3.176086000	1.643149000	-2.508448000	C	-3.176086000	1.643149000	-2.508448000
H	3.779069000	-1.798189000	1.604370000	H	-3.779069000	1.798189000	-1.604370000	H	-3.779069000	1.798189000	-1.604370000
H	3.574256000	-2.300528000	3.300645000	H	-3.574256000	2.300528000	-3.300645000	H	-3.574256000	2.300528000	-3.300645000
H	3.315064000	-0.602537000	2.827348000	H	-3.315064000	0.602537000	-2.827348000	H	-3.315064000	0.602537000	-2.827348000
C	2.059061000	-3.788449000	0.442039000	C	-2.059061000	3.788449000	-0.442039000	C	-2.059061000	3.788449000	-0.442039000
H	1.480944000	-4.165246000	0.410870000	H	-1.480944000	4.165246000	-0.410870000	H	-1.480944000	4.165246000	-0.410870000
H	2.442755000	-4.656038000	-1.005838000	H	-2.442755000	4.656038000	1.005838000	H	-2.442755000	4.656038000	1.005838000
H	2.918131000	-3.239313000	0.036216000	H	-2.918131000	3.239313000	-0.036216000	H	-2.918131000	3.239313000	-0.036216000

Table 16. Optimized geometry of **13_B3LYP_D**. XYZ coordinates in angstroms. B3LYP/def2-SVP level of theory.

I	3.329418000	2.023380000	1.364619000	I	-3.329418000	-2.023380000	-1.364619000	I	-3.329418000	-2.023380000	-1.364619000
I	2.304445000	-1.882654000	-2.858255000	I	2.304445000	1.882654000	2.858255000	I	-2.304445000	1.882654000	2.858255000
Ru	0.240452000	-0.967128000	0.881609000	Ru	-0.240452000	0.967128000	-0.881609000	Ru	0.240452000	-0.967128000	0.881609000
As	0.237665000	1.448064000	1.511148000	As	-0.237665000	-1.448064000	-1.511148000	As	-0.237665000	-1.448064000	-1.511148000
As	2.059836000	0.111627000	-0.429345000	As	-2.059836000	-0.111627000	0.429345000	As	2.059836000	0.111627000	-0.429345000
C	-0.188513000	-3.069545000	1.573311000	C	0.188513000	3.069545000	-1.573311000	C	0.188513000	3.069545000	-1.573311000
C	-0.550903000	-2.173806000	2.640972000	C	0.550903000	2.173806000	-2.640972000	C	-0.550903000	-2.173806000	2.640972000
C	0.638329000	-1.490146000	3.071205000	C	-0.638329000	1.490146000	-3.071205000	C	-0.638329000	1.490146000	-3.071205000
C	1.737112000	-1.963118000	2.273656000	C	-1.737112000	1.963118000	-2.273656000	C	-1.737112000	1.963118000	-2.273656000
C	1.227111000	-2.935166000	1.342314000	C	1.227111000	2.935166000	-1.342314000	C	-1.227111000	2.935166000	-1.342314000
C	-1.083865000	-4.090834000	0.956293000	C	1.083865000	4.090834000	-0.956293000	C	1.083865000	4.090834000	-0.956293000
H	-2.111550000	-3.721245000	0.856266000	H	2.111550000	3.721245000	-0.856266000	H	2.111550000	3.721245000	-0.856266000
H	-1.102723000	-4.993712000	1.589954000	H	1.102723000	4.993712000	-1.589954000	H	1.102723000	4.993712000	-1.589954000
H	-0.736861000	-4.383688000	-0.042817000	H	0.736861000	4.383688000					

H	1.569671000	0.135151000	4.135493000	H	-1.569671000	-0.135151000	-4.135493000
H	0.944038000	-1.181195000	5.157484000	H	-0.944038000	1.181195000	-5.157484000
H	-0.181241000	-0.018111000	4.414789000	H	0.181241000	0.018111000	-4.414789000
C	3.176318000	-1.647289000	2.508309000	C	-3.176318000	1.647289000	-2.508309000
H	3.778736000	-1.798756000	1.603371000	H	-3.778736000	1.798756000	-1.603371000
H	3.571249000	-2.311652000	3.295837000	H	-3.571249000	2.311652000	-3.295837000
H	3.315494000	-0.609818000	2.836532000	H	-3.315494000	0.609818000	-2.836532000
C	2.056369000	-3.793836000	0.445977000	C	-2.056369000	3.793836000	-0.445977000
H	1.479592000	-4.166525000	-0.409578000	H	-1.479592000	4.166525000	0.409578000
H	2.428241000	-4.664008000	1.013102000	H	-2.428241000	4.664008000	-1.013102000
H	2.923469000	-3.251021000	0.049181000	H	-2.923469000	3.251021000	-0.049181000

Table 17. Optimized geometry of **13_B3LYP_E**. XYZ coordinates in angstroms. B3LYP/def2-SVP level of theory.

Ru	-0.111054000	0.669333000	1.144682000	Ru	0.111054000	-0.669333000	-1.144682000
As	-1.533878000	-1.315558000	0.611618000	As	1.533878000	1.315558000	-0.611618000
As	1.440450000	-1.269360000	0.874487000	As	-1.440450000	1.269360000	-0.874487000
I	-4.101376000	-0.287777000	-0.225084000	I	4.101376000	0.287777000	0.225084000
I	0.116256000	-3.484266000	2.180720000	I	-0.116256000	3.484266000	-2.180720000
C	-0.252595000	2.651344000	2.190716000	C	0.252595000	-2.651344000	-2.190716000
C	0.892820000	1.956040000	2.718379000	C	-0.892820000	-1.956040000	-2.718379000
C	0.427922000	0.758586000	3.365143000	C	-0.427922000	-0.758586000	-3.365143000
C	-1.003059000	0.711220000	3.239381000	C	1.003059000	-0.711220000	-3.239381000
C	-1.427047000	1.884224000	2.519990000	C	1.427047000	-1.884224000	-2.519990000
C	-0.238939000	4.016230000	1.586110000	C	0.238939000	-4.016230000	-1.586110000
H	0.679173000	4.197859000	1.013228000	H	-0.679173000	-4.197859000	-1.013228000
H	-0.301976000	4.777084000	2.382956000	H	0.301976000	-4.777084000	-2.382956000
H	-1.083368000	4.166867000	0.902396000	H	1.083368000	-4.166867000	-0.902396000
C	2.289625000	2.479467000	2.763849000	C	-2.289625000	-2.479467000	-2.763849000
H	3.028946000	1.669411000	2.738685000	H	-3.028946000	-1.669411000	-2.738685000
H	2.438173000	3.051195000	3.696187000	H	-2.438173000	-3.051195000	-3.696187000
H	2.501314000	3.147374000	1.918975000	H	-2.501314000	-3.147374000	-1.918975000
C	1.262392000	-0.179858000	4.174391000	C	-1.262392000	0.179858000	-4.174391000
H	0.870650000	-1.204681000	4.136023000	H	-0.870650000	1.204681000	-4.136023000
H	1.263506000	0.145676000	5.229155000	H	-1.263506000	-0.145676000	-5.229155000
H	2.303120000	-0.198822000	3.825172000	H	-2.303120000	0.198822000	-3.825172000
C	-1.898610000	-0.292364000	3.890331000	C	1.898610000	0.292364000	-3.890331000
H	-2.867572000	-0.359877000	3.378911000	H	2.867572000	0.359877000	-3.378911000
H	-2.085421000	0.001867000	4.937637000	H	2.085421000	-0.001867000	-4.937637000
H	-1.443212000	-1.291376000	3.894244000	H	1.443212000	1.291376000	-3.894244000
C	-2.841599000	2.318874000	2.324021000	C	2.841599000	-2.318874000	-2.324021000
H	-2.937014000	3.020526000	1.485260000	H	2.937014000	-3.020526000	-1.485260000
H	-3.201182000	2.826295000	3.235681000	H	3.201182000	-2.826295000	-3.235681000
H	-3.505316000	1.468769000	2.122580000	H	3.505316000	-1.468769000	-2.122580000

Table 18. Optimized geometry of **13_B3LYP_F**. XYZ coordinates in angstroms. B3LYP/def2-SVP level of theory.

Ru	-0.111376000	0.669108000	1.144813000	Ru	0.111376000	-0.669108000	-1.144813000
As	-1.521857000	-1.321680000	0.615683000	As	1.521857000	1.321680000	-0.615683000
As	1.447685000	-1.259108000	0.868716000	As	-1.447685000	1.259108000	-0.868716000
I	-4.112266000	-0.287168000	-0.225696000	I	4.112266000	0.287168000	0.225696000
I	0.114697000	-3.495128000	2.183941000	I	-0.114697000	3.495128000	-2.183941000
C	-0.253198000	2.651720000	2.192032000	C	0.253198000	-2.651720000	-2.192032000
C	0.892254000	1.955779000	2.718644000	C	-0.892254000	-1.955779000	-2.718644000
C	0.427083000	0.758413000	3.365399000	C	-0.427083000	-0.758413000	-3.365399000
C	-1.003989000	0.712046000	3.240636000	C	1.003989000	-0.712046000	-3.240636000
C	-1.427620000	1.885146000	2.521706000	C	1.427620000	-1.885146000	-2.521706000
C	-0.240430000	4.018425000	1.592982000	C	0.240430000	-4.018425000	-1.592982000
H	0.682502000	4.206491000	1.030233000	H	-0.682502000	-4.206491000	-1.030233000
H	-0.312122000	4.772729000	2.394891000	H	0.312122000	-4.772729000	-2.394891000
H	-1.082273000	4.169300000	0.906242000	H	1.082273000	-4.169300000	-0.906242000
C	2.287947000	2.480481000	2.766242000	C	-2.287947000	-2.480481000	-2.766242000
H	3.027480000	1.670641000	2.748873000	H	-3.027480000	-1.670641000	-2.748873000
H	2.429844000	3.054798000	3.697632000	H	-2.429844000	-3.054798000	-3.697632000
H	2.500747000	3.147324000	1.920911000	H	-2.500747000	-3.147324000	-1.920911000
C	1.259799000	-0.178102000	4.177549000	C	-1.259799000	0.178102000	-4.177549000
H	0.868443000	-1.202890000	4.139212000	H	-0.868443000	1.202890000	-4.139212000
H	1.254013000	0.149865000	5.231171000	H	-1.254013000	-0.149865000	-5.231171000
H	2.302310000	-0.194368000	3.834063000	H	-2.302310000	0.194368000	-3.834063000
C	-1.899694000	-0.286915000	3.896995000	C	1.899694000	0.286915000	-3.896995000
H	-2.868004000	-0.359080000	3.385274000	H	2.868004000	0.359080000	-3.385274000
H	-2.087566000	0.018652000	4.940510000	H	2.087566000	-0.018652000	-4.940510000
H	-1.442251000	-1.284651000	3.912780000	H	1.442251000	1.284651000	-3.912780000
C	-2.841317000	2.323090000	2.330776000	C	2.841317000	-2.323090000	-2.330776000
H	-2.939132000	3.022048000	1.490145000	H	2.939132000	-3.022048000	-1.490145000
H	-3.190848000	2.836112000	3.242858000	H	3.190848000	-2.836112000	-3.242858000
H	-3.508928000	1.473557000	2.141068000	H	3.508928000	-1.473557000	-2.141068000

Table 19. Optimized geometry of **13_BP86_A**. XYZ coordinates in angstroms. BP86/def2-TZVP level of theory.

I	3.246934000	2.013206000	1.365543000	I	-3.246934000	-2.013206000	-1.365543000
I	2.296864000	-1.829901000	-2.797847000	I	-2.296864000	1.829901000	2.797847000
Ru	0.240869000	-0.968042000	0.881264000	Ru	-0.240869000	0.968042000	-0.881264000
As	0.334301000	1.445427000	1.486065000	As	-0.334301000	-1.445427000	-1.486065000
As	2.039783000	0.041762000	-0.500988000	As	-2.039783000	-0.041762000	0.500988000
C	-0.191818000	-3.072069000	1.568442000	C	0.191818000	3.072069000	-1.568442000
C	-0.556221000	-2.174546000	2.637289000	C	0.556221000	2.174546000	-2.637289000
C	0.632849000	-1.483131000	3.065069000	C	-0.632849000	1.483131000	-3.065069000
C	1.735236000	-1.952772000	2.263609000	C	-1.735236000	1.952772000	-2.263609000
C	1.225776000	-2.931155000	1.332029000	C	-1.225776000	2.931155000	-1.332029000

C	-1.088217000	-4.086783000	0.945702000	C	1.088217000	4.086783000	-0.945702000
H	-2.108207000	-3.702829000	0.817994000	H	2.108207000	3.702829000	-0.817994000
H	-1.135494000	-4.984031000	1.584982000	H	1.135494000	4.984031000	-1.584982000
H	-0.725710000	-4.392245000	-0.043657000	H	0.725710000	4.392245000	0.043657000
C	-1.894261000	-2.090740000	3.292081000	C	1.894261000	2.090740000	-3.292081000
H	-2.106449000	-1.070880000	3.639051000	H	2.106449000	1.070880000	-3.639051000
H	-1.922353000	-2.762139000	4.166603000	H	1.922353000	2.762139000	-4.166603000
H	-2.696186000	-2.392061000	2.606315000	H	2.696186000	2.392061000	-2.606315000
C	0.732570000	-0.558087000	4.232777000	C	-0.732570000	0.558087000	-4.232777000
H	1.556571000	0.156514000	4.109301000	H	-1.556571000	-0.156514000	-4.109301000
H	0.920713000	-1.139283000	5.151158000	H	-0.920713000	1.139283000	-5.151158000
H	-0.195681000	0.010488000	4.375200000	H	0.195681000	-0.010488000	-4.375200000
C	3.171524000	-1.620260000	2.485776000	C	-3.171524000	1.620260000	-2.485776000
H	3.764312000	-1.757642000	1.572811000	H	-3.764312000	1.757642000	-1.572811000
H	3.587396000	-2.279999000	3.265579000	H	-3.587396000	2.279999000	-3.265579000
H	3.301534000	-0.580988000	2.813417000	H	-3.301534000	0.580988000	-2.813417000
C	2.051796000	-3.778915000	0.424732000	C	-2.051796000	3.778915000	-0.424732000
H	1.479003000	-4.122128000	-0.445450000	H	-1.479003000	4.122128000	0.445450000
H	2.411022000	-4.667291000	0.970466000	H	-2.411022000	4.667291000	-0.970466000
H	2.925845000	-3.235767000	0.044754000	H	-2.925845000	3.235767000	-0.044754000

Table 20. Optimized geometry of **13_BP86_B**. XYZ coordinates in angstroms. BP86/def2-TZVP level of theory.

I	3.248778000	2.022502000	1.378125000	I	-3.248778000	-2.022502000	-1.378125000
I	2.311212000	-1.830704000	-2.799981000	I	-2.311212000	1.830704000	2.799981000
Ru	0.240891000	-0.968092000	0.881395000	Ru	-0.240891000	0.968092000	-0.881395000
As	0.331689000	1.443272000	1.484382000	As	-0.331689000	-1.443272000	-1.484382000
As	2.037130000	0.043546000	-0.499055000	As	-2.037130000	-0.043546000	0.499055000
C	-0.191758000	-3.072457000	1.570249000	C	0.191758000	3.072457000	-1.570249000
C	-0.555456000	-2.174363000	2.638681000	C	0.555456000	2.174363000	-2.638681000
C	0.633992000	-1.483267000	3.065724000	C	-0.633992000	1.483267000	-3.065724000
C	1.735815000	-1.953744000	2.264123000	C	-1.735815000	1.953744000	-2.264123000
C	1.225651000	-2.932375000	1.333338000	C	-1.225651000	2.932375000	-1.333338000
C	-1.087820000	-4.089191000	0.951695000	C	1.087820000	4.089191000	-0.951695000
H	-2.109632000	-3.708033000	0.832011000	H	2.109632000	3.708033000	-0.832011000
H	-1.127715000	-4.984709000	1.593432000	H	1.127715000	4.984709000	-1.593432000
H	-0.728258000	-4.395481000	-0.038381000	H	0.728258000	4.395481000	0.038381000
C	-1.891129000	-2.094396000	3.297261000	C	1.891129000	2.094396000	-3.297261000
H	-2.101021000	-1.077333000	3.652913000	H	2.101021000	1.077333000	-3.652913000
H	-1.913646000	-2.771995000	4.166775000	H	1.913646000	2.771995000	-4.166775000
C	-2.695358000	-2.392770000	2.613071000	C	2.695358000	2.392770000	-2.613071000
C	0.735192000	-0.562619000	4.236018000	C	-0.735192000	0.562619000	-4.236018000
H	1.560342000	0.151009000	4.115848000	H	-1.560342000	-0.151009000	-4.115848000
H	0.923558000	-1.149825000	5.150135000	H	-0.923558000	1.149825000	-5.150135000
H	-0.193131000	0.004441000	4.382694000	H	0.193131000	-0.004441000	-4.382694000
C	3.172081000	-1.624895000	2.488251000	C	-3.172081000	1.624895000	-2.488251000
H	3.765782000	-1.761190000	1.575822000	H	-3.765782000	1.761190000	-1.575822000
H	3.583038000	-2.290013000	3.265683000	H	-3.583038000	2.290013000	-3.265683000
H	3.302534000	-0.588175000	2.823126000	H	-3.302534000	0.588175000	-2.823126000
C	2.051085000	-3.783880000	0.429873000	C	-2.051085000	3.783880000	-0.429873000
H	1.478829000	-4.127899000	-0.440303000	H	-1.478829000	4.127899000	0.440303000
H	2.403299000	-4.671599000	0.980660000	H	-2.403299000	4.671599000	-0.980660000
H	2.929867000	-3.245102000	0.054848000	H	-2.929867000	3.245102000	-0.054848000

Table 21. Optimized geometry of **13_BP86_C**. XYZ coordinates in angstroms. BP86/def2-TZVP level of theory.

Ru	-0.113125000	0.669766000	1.145382000	Ru	0.113125000	-0.669766000	-1.145382000
As	-1.477205000	-1.350189000	0.637951000	As	1.477205000	1.350189000	-0.637951000
As	1.483077000	-1.219031000	0.849860000	As	-1.483077000	1.219031000	-0.849860000
I	-4.042101000	-0.173793000	-0.301934000	I	4.042101000	0.173793000	0.301934000
I	-0.017002000	-3.439502000	2.148123000	I	0.017002000	3.439502000	-2.148123000
C	-0.260664000	2.651005000	2.182014000	C	0.260664000	-2.651005000	-2.182014000
C	0.892302000	1.955971000	2.704425000	C	-0.892302000	-1.955971000	-2.704425000
C	0.430814000	0.754370000	3.354917000	C	-0.430814000	-0.754370000	-3.354917000
C	-1.004045000	0.706706000	3.238824000	C	1.004045000	-0.706706000	-3.238824000
C	-1.434297000	1.881036000	2.520729000	C	1.434297000	-1.881036000	-2.520729000
C	-0.258848000	4.009415000	1.567723000	C	0.258848000	-4.009415000	-1.567723000
H	0.675631000	4.209714000	1.029514000	H	-0.675631000	-4.209714000	-1.029514000
H	-0.373398000	4.775021000	2.353061000	H	0.373398000	-4.775021000	-2.353061000
H	-1.079723000	4.129994000	0.849956000	H	1.079723000	-4.129994000	-0.849956000
C	2.289277000	2.475002000	2.731081000	C	-2.289277000	-2.475002000	-2.731081000
H	3.025170000	1.662243000	2.688097000	H	-3.025170000	-1.662243000	-2.688097000
H	2.456401000	3.041257000	3.662493000	H	-2.456401000	-3.041257000	-3.662493000
H	2.487395000	3.145230000	1.885251000	H	-2.487395000	-3.145230000	-1.885251000
C	1.270283000	-0.195839000	4.142483000	C	-1.270283000	0.195839000	-4.142483000
H	0.884478000	-1.221984000	4.075242000	H	-0.884478000	1.221984000	-4.075242000
H	1.267595000	0.100708000	5.204787000	H	-1.267595000	-0.100708000	-5.204787000
C	2.310745000	-0.197515000	3.793517000	C	-2.310745000	0.197515000	-3.793517000
H	-1.895565000	-0.299782000	3.886725000	C	1.895565000	0.299782000	-3.886725000
H	-2.855368000	-0.383051000	3.361297000	H	2.855368000	0.383051000	-3.361297000
H	-2.101484000	0.002157000	4.927324000	H	2.101484000	-0.002157000	-4.927324000
H	-1.427735000	-1.292904000	3.906891000	H	1.427735000	1.292904000	-3.906891000
C	-2.847900000	2.313185000	3.2328117000	C	2.847900000	-2.313185000	-3.2328117000
H	-2.946261000	3.004562000	1.481834000	H	2.946261000	-3.004562000	-1.481834000
H	-3.201998000	2.831504000	3.234866000	H	3.201998000	-2.831504000	-3.234866000
H	-3.513761000	1.461309000	2.141126000	H	3.513761000	-1.461309000	-2.141126000

Table 22. Optimized geometry of **13_BP86_D**. XYZ coordinates in angstroms. BP86/def2-TZVP level of theory.

Ru	-0.113058000	0.669640000	1.145499000	Ru	0.113058000	-0.669640000	-1.145499000
As	-1.472003000	-1.350847000	0.638824000	As	1.472003000	1.350847000	-0.638824000
As	1.484180000	-1.214730000	0.846976000	As	-1.484180000	1.214730000	0.846976000
I	-4.052383000	-0.182179000	-0.295018000	I	4.052383000	0.182179000	0.295018000
I	-0.007169000	-3.448386000	2.152075000	I	0.007169000	3.448386000	-2.152075000
C	-0.260421000	2.651563000	2.183601000	C	0.260421000	-2.651563000	-2.183601000
C	0.892116000	1.955894000	2.705726000	C	-0.892116000	-1.955894000	-2.705726000
C	0.430116000	0.754380000	3.355807000	C	-0.430116000	-0.754380000	-3.355807000
C	-1.004688000	0.707386000	3.239565000	C	1.004688000	-0.707386000	-3.239565000
C	-1.434264000	1.881979000	2.521774000	C	1.434264000	-1.881979000	-2.521774000
C	-0.258324000	4.011757000	1.574589000	C	0.258324000	-4.011757000	-1.574589000
H	0.679312000	4.216063000	1.043588000	H	-0.679312000	-4.216063000	-1.043588000
H	-0.377301000	4.771229000	2.364831000	H	0.377301000	-4.771229000	-2.364831000
H	-1.078279000	4.134533000	0.856238000	H	1.078279000	-4.134533000	-0.856238000
C	2.288037000	2.476025000	2.735971000	C	-2.288037000	-2.476025000	-2.735971000
H	3.023828000	1.662959000	2.703271000	H	-3.023828000	-1.662959000	-2.703271000
H	2.447272000	3.046106000	3.666095000	H	-2.447272000	-3.046106000	-3.666095000
H	2.489176000	3.143828000	1.889032000	H	-2.489176000	-3.143828000	-1.889032000
C	1.267603000	-0.193173000	4.147460000	C	-1.267603000	0.193173000	-4.147460000
H	0.881762000	-1.219261000	4.082223000	H	-0.881762000	1.219261000	-4.082223000
H	1.258948000	0.107653000	5.208192000	H	-1.258948000	-0.107653000	-5.208192000
H	2.309605000	-0.193766000	3.803595000	H	-2.309605000	0.193766000	-3.803595000
C	-1.896462000	-0.294834000	3.892288000	C	1.896462000	0.294834000	-3.892288000
H	-2.856598000	-0.380656000	3.368156000	H	2.856598000	0.380656000	-3.368156000
H	-2.101231000	0.016181000	4.930113000	H	2.101231000	-0.016181000	-4.930113000
H	-1.427790000	-1.287101000	3.921089000	H	1.427790000	1.287101000	-3.921089000
C	-2.847068000	2.316696000	2.333082000	C	2.847068000	-2.316696000	-2.333082000
H	-2.947601000	3.005736000	1.485252000	H	2.947601000	-3.005736000	-1.485252000
H	-3.192652000	2.839561000	3.240175000	H	3.192652000	-2.839561000	-3.240175000
H	-3.515576000	1.464920000	2.156308000	H	3.515576000	-1.464920000	-2.156308000

Table 23. Optimized geometry of **13_wB97XD_A**. XYZ coordinates in angstroms. wB97XD/def2-TZVP level of theory.

I	3.665278000	1.703652000	0.742992000	I	-3.665278000	-1.703652000	-0.742992000
I	1.675534000	-2.243003000	-3.001275000	I	-1.675534000	2.243003000	3.001275000
Ru	0.248114000	-0.965371000	0.893089000	Ru	-0.248114000	0.965371000	-0.893089000
As	0.440792000	1.450761000	1.444935000	As	-0.440792000	-1.450761000	-1.444935000
As	2.012463000	-0.035043000	-0.581665000	As	-2.012463000	0.035043000	0.581665000
C	-0.155229000	-3.066261000	1.547450000	C	0.155229000	3.066261000	-1.547450000
C	-0.563210000	-2.193535000	2.604108000	C	0.563210000	2.193535000	-2.604108000
C	0.590512000	-1.492718000	3.068962000	C	-0.590512000	1.492718000	-3.068962000
C	1.711291000	-1.920842000	2.295485000	C	-1.711291000	1.920842000	-2.295485000
C	1.252227000	-2.893312000	1.352310000	C	-1.252227000	2.893312000	-1.352310000
C	-1.004250000	-4.111806000	0.910141000	C	1.004250000	4.111806000	-0.910141000
H	-2.032041000	-3.775043000	0.791068000	H	2.032041000	3.775043000	-0.791068000
H	-1.007420000	-5.006256000	1.538721000	H	1.007420000	5.006256000	-1.538721000
H	-0.627664000	-4.389773000	-0.072686000	H	0.627664000	4.389773000	0.072686000
C	-1.911909000	-2.157198000	3.240164000	C	1.911909000	2.157198000	-3.240164000
H	-2.142113000	-1.166372000	3.629277000	H	2.142113000	1.166372000	-3.629277000
H	-1.936349000	-2.864039000	4.073911000	H	1.936349000	2.864039000	-4.073911000
H	-2.693492000	-2.438549000	2.536206000	H	2.693492000	2.438549000	-2.536206000
C	0.654574000	-0.633777000	4.284998000	C	-0.654574000	0.633777000	-4.284998000
H	1.444692000	0.111856000	4.210939000	H	-1.444692000	-0.111856000	-4.210939000
H	0.864076000	-1.262688000	5.154597000	H	-0.864076000	1.262688000	-5.154597000
H	-0.284764000	-0.113912000	4.460255000	H	0.284764000	0.113912000	-4.460255000
C	3.133902000	-1.588418000	2.584382000	C	-3.133902000	1.588418000	-2.584382000
H	3.761448000	-1.692376000	1.701272000	H	-3.761448000	1.692376000	-1.701272000
H	3.510624000	-2.270859000	3.351136000	H	-3.510624000	2.270859000	-3.351136000
H	3.244575000	-0.570083000	2.951643000	H	-3.244575000	0.570083000	-2.951643000
C	2.125786000	-3.737939000	0.490424000	C	-2.125786000	3.737939000	-0.490424000
H	1.589148000	-4.125665000	-0.372383000	H	-1.589148000	4.125665000	0.372383000
H	2.494385000	-4.586125000	1.073376000	H	-2.494385000	4.586125000	-1.073376000
H	2.985302000	-3.182261000	0.119186000	H	-2.985302000	3.182261000	-0.119186000

Table 24. Optimized geometry of **13_wB97XD_B**. XYZ coordinates in angstroms. wB97XD/def2-TZVP level of theory.

I	3.670861000	1.710964000	0.751463000	I	-3.670861000	-1.710964000	-0.751463000
I	1.686071000	-2.245748000	-3.007848000	I	-1.686071000	2.245748000	3.007848000
Ru	0.247921000	-0.965175000	0.892926000	Ru	-0.247921000	0.965175000	-0.892926000
As	0.442322000	1.448552000	1.441602000	As	-0.442322000	-1.448552000	-1.441602000
As	2.008619000	-0.037162000	-0.582479000	As	-2.008619000	0.037162000	0.582479000
C	-0.154936000	-3.067152000	1.548270000	C	0.154936000	3.067152000	-1.548270000
C	-0.563018000	-2.194264000	2.604611000	C	0.563018000	2.194264000	-2.604611000
C	0.590582000	-1.493443000	3.069491000	C	-0.590582000	1.493443000	-3.069491000
C	1.711341000	-1.921670000	2.296105000	C	-1.711341000	1.921670000	-2.296105000
C	1.252353000	-2.894386000	1.353346000	C	-1.252353000	2.894386000	-1.353346000
H	-1.002760000	-4.115410000	0.915158000	C	1.002760000	4.115410000	-0.915158000
H	-2.032231000	-3.782186000	0.801704000	H	2.032231000	3.782186000	-0.801704000
H	-0.999486000	-5.007082000	1.547143000	H	0.999486000	5.007082000	-1.547143000
H	-0.628059000	-4.395372000	-0.067754000	H	0.628059000	4.395372000	0.067754000
C	-1.909586000	-2.162965000	3.243908000	C	1.909586000	2.162965000	-3.243908000
H	-2.140204000	-1.174908000	3.639422000	H	2.140204000	1.174908000	-3.639422000
H	-1.927200000	-2.873808000	4.073969000	H	1.927200000	2.873808000	-4.073969000
H	-2.692418000	-2.444912000	2.541748000	H	2.692418000	2.444912000	-2.541748000
C	0.655920000	-0.639470000	4.288269000	C	-0.655920000	0.639470000	-4.288269000
H	1.444317000	0.108040000	4.216038000	H	-1.444317000	-0.108040000	-4.216038000
H	0.870978000	-1.274379000	5.151773000	H	-0.870978000	1.274379000	-5.151773000
H	-0.285620000	-0.126436000	4.470773000	H	0.285620000	0.126436000	-4.470773000

C	3.133762000	-1.593052000	2.587340000	C	-3.133762000	1.593052000	-2.587340000
H	3.762628000	-1.700354000	1.705625000	H	-3.762628000	1.700354000	-1.705625000
H	3.504156000	-2.278609000	3.353974000	H	-3.504156000	2.278609000	-3.353974000
H	3.245592000	-0.576258000	2.958323000	H	-3.245592000	0.576258000	-2.958323000
C	2.126616000	-3.742193000	0.496232000	C	-2.126616000	3.742193000	-0.496232000
H	1.587897000	-4.141847000	-0.359664000	H	-1.587897000	4.141847000	0.359664000
H	2.498164000	-4.582376000	1.088311000	H	-2.498164000	4.582376000	-1.088311000
H	2.984398000	-3.187114000	0.120247000	H	-2.984398000	3.187114000	-0.120247000

Table 25. Optimized geometry of **13_wB97XD_C**. XYZ coordinates in angstroms. wB97XD/def2-TZVP level of theory.

Ru	-0.109777000	0.669556000	1.153200000	Ru	0.109777000	-0.669556000	-1.153200000
As	-1.464901000	-1.355893000	0.637958000	As	1.464901000	1.355893000	-0.637958000
As	1.486489000	-1.210819000	0.843780000	As	-1.486489000	1.210819000	-0.843780000
I	-4.057375000	-0.660944000	0.068674000	I	4.057375000	0.660944000	-0.068674000
I	0.561593000	-3.439929000	2.148422000	I	-0.561593000	3.439929000	-2.148422000
C	-0.230450000	2.634925000	2.186598000	C	0.230450000	-2.634925000	-2.186598000
C	0.888534000	1.922508000	2.719958000	C	-0.888534000	-1.922508000	-2.719958000
C	0.398534000	0.742901000	3.358113000	C	-0.398534000	-0.742901000	-3.358113000
C	-1.021825000	0.719758000	3.217298000	C	1.021825000	-0.719758000	-3.217298000
C	-1.413826000	1.892210000	2.497710000	C	1.413826000	-1.892210000	-2.497710000
C	-0.183288000	4.009624000	1.614610000	C	0.183288000	-4.009624000	-1.614610000
H	0.732221000	4.178426000	1.050227000	H	-0.732221000	-4.178426000	-1.050227000
H	-0.222046000	4.740379000	2.426713000	H	0.222046000	-4.740379000	-2.426713000
H	-1.019582000	4.199232000	0.945694000	H	1.019582000	-4.199232000	-0.945694000
C	2.286982000	2.426648000	2.807621000	C	-2.286982000	-2.426648000	-2.807621000
H	3.011854000	1.615908000	2.771336000	H	-3.011854000	-1.615908000	-2.771336000
H	2.416666000	2.956474000	3.755237000	H	-2.416666000	-2.956474000	-3.755237000
H	2.521040000	3.115837000	1.998502000	H	-2.521040000	-3.115837000	-1.998502000
C	1.209112000	-0.171805000	4.211039000	C	-1.209112000	0.171805000	-4.211039000
H	0.755646000	-1.157193000	4.292207000	H	-0.755646000	1.157193000	-4.292207000
H	1.283015000	0.254131000	5.215419000	H	-1.283015000	-0.254131000	-5.215419000
C	2.219512000	-0.294555000	3.823724000	C	-2.219512000	0.294555000	-3.823724000
C	-1.940596000	-0.258840000	3.867838000	C	1.940596000	0.258840000	-3.867838000
H	-2.896892000	-0.315771000	3.350401000	H	2.896892000	0.315771000	-3.350401000
H	-2.129943000	0.052292000	4.898669000	H	2.129943000	-0.052292000	-4.898669000
H	-1.505237000	-1.257103000	3.891007000	H	1.505237000	1.257103000	-3.891007000
C	-2.814439000	2.361006000	2.298766000	C	2.814439000	-2.361006000	-2.298766000
H	-2.887012000	3.065835000	1.472337000	H	2.887012000	-3.065835000	-1.472337000
H	-3.156608000	2.865668000	3.206100000	H	3.156608000	-2.865668000	-3.206100000
H	-3.492308000	1.534788000	2.094116000	H	3.492308000	-1.534788000	-2.094116000

Table 26. Optimized geometry of **13_wB97XD_D**. XYZ coordinates in angstroms. wB97XD/def2-TZVP level of theory.

Ru	-0.105359000	0.667648000	1.154691000	Ru	0.105359000	-0.667648000	-1.154691000
As	-1.368014000	-1.422129000	0.690849000	As	1.368014000	1.422129000	-0.690849000
As	1.572054000	-1.125782000	0.796961000	As	-1.572054000	1.125782000	-0.796961000
I	-4.026683000	-0.843447000	0.219473000	I	4.026683000	0.843447000	-0.219473000
I	0.813973000	-3.425872000	2.120110000	I	-0.813973000	3.425872000	-2.120110000
C	-0.215890000	2.634398000	2.188207000	C	0.215890000	-2.634398000	-2.188207000
C	0.892216000	1.906342000	2.724647000	C	-0.892216000	-1.906342000	-2.724647000
C	0.383526000	0.734204000	3.362630000	C	-0.383526000	-0.734204000	-3.362630000
C	-1.036215000	0.730604000	3.216299000	C	1.036215000	-0.730604000	-3.216299000
C	-1.409425000	1.905629000	2.492847000	C	1.409425000	-1.905629000	-2.492847000
C	-0.151878000	4.010534000	1.622981000	C	0.151878000	-4.010534000	-1.622981000
H	0.779069000	4.180363000	1.085015000	H	-0.779069000	-4.180363000	-1.085015000
H	-0.209935000	4.735255000	2.438943000	H	0.209935000	-4.735255000	-2.438943000
H	-0.972297000	4.204138000	0.936174000	H	0.972297000	-4.204138000	-0.936174000
C	2.296576000	2.391073000	2.818817000	C	-2.296576000	-2.391073000	-2.818817000
H	3.009159000	1.569343000	2.784770000	H	-3.009159000	-1.569343000	-2.784770000
H	2.427713000	2.914668000	3.769300000	H	-2.427713000	-2.914668000	-3.769300000
H	2.542128000	3.081106000	2.014169000	H	-2.542128000	-3.081106000	-2.014169000
C	1.173393000	-0.185454000	4.227847000	C	-1.173393000	0.185454000	-4.227847000
H	0.715015000	-1.169201000	4.297996000	H	-0.715015000	1.169201000	-4.297996000
H	1.224579000	0.239579000	5.233709000	H	-1.224579000	-0.239579000	-5.233709000
H	2.192121000	-0.308801000	3.863931000	H	-2.192121000	0.308801000	-3.863931000
C	-1.971355000	-0.226602000	3.873389000	C	1.971355000	0.226602000	-3.873389000
H	-2.922051000	-0.285528000	3.346416000	H	2.922051000	0.285528000	-3.346416000
H	-2.169130000	0.112183000	4.893625000	H	2.169130000	-0.112183000	-4.893625000
H	-1.544538000	-1.227089000	3.927513000	H	1.544538000	1.227089000	-3.927513000
C	-2.804708000	2.384995000	2.283177000	C	2.804708000	-2.384995000	-2.283177000
H	-2.859492000	3.115969000	1.478546000	H	2.859492000	-3.115969000	-1.478546000
H	-3.160500000	2.861558000	3.200055000	H	3.160500000	-2.861558000	-3.200055000
H	-3.479538000	1.565127000	2.043745000	H	3.479538000	-1.565127000	-2.043745000

7.7 Author Contributions

- The synthesis and characterization of compounds **3-I**, **3-I₃**, **7**, **8**, **9**, **11**, **12**, **13-sym** and **13-asym** was performed by Helena Brake
- The synthesis of compound **4** and the synthesis and characterization of **5** was performed by Helena Brake and Lisa Zimmermann and is also part of her Bachelor thesis; the characterization of **4** was performed by Helena Brake
- The reaction behavior of **3-I** was investigated by Helena Brake and Lisa Zimmermann and is also part of her Bachelor thesis
- The reactions of [Cp^{BiG}Fe(η⁵-P₅)] with I₂ and the reaction of **3-I** with [CoCp₂] was performed by Helena Brake
- X-ray structure analyses of compounds **3-I**, **3-I₃**, **4**, **7**, **8**, **9**, **11**, **12**, **13-sym** and **13-asym** were performed by Dr. Eugenia Peresyphkina, Dr. Sc. Alexander Virovets with Helena Brake. Parts of this research (project I-20160654) were carried out at PETRA III at DESY, a member of the Helmholtz Association (HGF), by Dr. Eugenia Peresyphkina and Dr. Sc. Alexander V. Virovets. EP and AV are grateful to Dr. A. Burkhardt for the assistance regarding the use of the beamline P11.
- DFT computations on **3-I**, **9**, **13-sym** and **13-asym** were performed by Dr. Martin Piesch
- Solid-state MAS NMR spectroscopy of compounds **3-I**, **3-I₃** and **4** was performed by Prof. Dr. W. Kremer
- X-ray powder diffraction of **3-I** was performed by Dr. Christian Klimas (group of Prof. Dr. Arno Pfitzner)
- ESR spectroscopy of compound **8** was performed by Helena Brake with the aid of Dr. Gábor Balázs
- The manuscript (introduction, results and discussion, experimental part, conclusion; including figures and graphical abstract) was written by Helena Brake
- The section ‘crystallographic details’ was written by Dr. Eugenia Peresyphkina
- The section ‘computational details’ was written by Dr. Martin Piesch

7.8 References

- [1] F. Scalambra, M. Peruzzini, A. Romerosa, in *Adv. Organomet. Chem.*, Vol. 72 (Ed.: P. J. Pérez), Academic Press, **2019**, pp. 173-222.
- [2] C. Mealli, A. Ienco, M. Peruzzini, G. Manca, *Dalton Transactions* **2018**, 47, 394-408.
- [3] B. W. Tattershall, N. L. Kendall, *Polyhedron* **1994**, 13, 1517-1521.
- [4] a) R. Boulouch, *Compt. rend.* **1905**, 141, 256-258; b) N. Wiberg, E. Wiberg, A. F. Hollemann, *Anorganische Chemie, 103rd edition, Vol. 1*, Walter de Gruyter GmbH **2017**, pp. 849 and 853; c) S. Lange, P. Schmidt, T. Nilges, *Inorg. Chem.* **2007**, 46, 4028-4035; d) Z. Zhang, X. Xin, Q. Yan, Q. Li, Y. Yang, T.-L. Ren, *Sci. China Mater.* **2016**, 59, 122-134.
- [5] I. De los Rios, J.-R. Hamon, P. Hamon, C. Lapinte, L. Toupet, A. Romerosa, M. Peruzzini, *Angew. Chem. Int. Ed.* **2001**, 40, 3910-3912.
- [6] I. Krossing, *J. Chem. Soc., Dalton Trans.* **2002**, 500-512.
- [7] P. Barbaro, C. Bazzicalupi, M. Peruzzini, S. Seniori Costantini, P. Stoppioni, *Angew. Chem. Int. Ed.* **2012**, 51, 8628-8631.
- [8] O. J. Scherer, T. Brück, *Angew. Chem. Int. Ed. Engl.* **1987**, 26, 59.
- [9] O. J. Scherer, T. Brück, G. Wolmershäuser, *Chem. Ber.* **1988**, 121, 935-938.
- [10] A. R. Kudinov, D. A. Loginov, P. V. Petrovskii, M. I. Rybinskaya, *Russ. Chem. Bull.* **1998**, 47, 1583-1584.
- [11] O. J. Scherer, T. Brück, G. Wolmershäuser, *Chem. Ber.* **1989**, 122, 2049-2054.
- [12] W. Dahlmann, H. G. Von Schnering, *Naturwissenschaften* **1972**, 59, 420.
- [13] a) G. Fritz, T. Vaahs, *Z. Anorg. Allg. Chem.* **1987**, 553, 85-89; b) G. Fritz, T. Vaahs, H. Fleischer, E. Matern, *Z. Anorg. Allg. Chem.* **1989**, 570, 54-66; c) G. Fritz, T. Vaahs, H. Fleischer, E. Matern, *Angew. Chem.* **1989**, 101, 324-325; d) H. Krautscheid, E. Matern, J. Olkowska-Oetzel, J. Pikies, G. Fritz, *Z. Anorg. Allg. Chem.* **2001**, 627, 999-1002.
- [14] R. Ahlrichs, D. Fenske, K. Fromm, H. Krautscheid, U. Krautscheid, O. Treutler, *Chem. Eur. J.* **1996**, 2, 238-244.
- [15] P. Pyykkoe, M. Atsumi, *Chem. Eur. J.* **2009**, 15, 12770-12779.
- [16] a) D. Weber, C. Mujica, H. G. von Schnering, *Angew. Chem. Int. Ed. Engl.* **1982**, 21, 863; b) G. Fritz, E. Layher, H. Goesmann, D. Hanke, C. Persau, *Z. Anorg. Allg. Chem.* **1991**, 594, 36-46; c) K. Schwedtmann, J. Haberstroh, S. Roediger, A. Bauzá, A. Frontera, F. Hennersdorf, J. J. Weigand, *Chem. Sci.* **2019**, 10, 6868-6875; d) G. Fritz, K. D. Hoppe, W. Höhle, D. Weber, C. Mujica, V. Manriquez, H. G. v. Schnering, *J. Organomet. Chem.* **1983**, 249, 63-80.
- [17] A. Bondi, *J. Phys. Chem.* **1964**, 68, 441-451.

- [18] S. Burck, D. Gudat, M. Nieger, Z. Benkő, L. Nyulászi, D. Szieberth, *Z. Anorg. Allg. Chem.* **2009**, *635*, 245-252.
- [19] S. Heini, G. Balázs, M. Scheer, *Phosphorus, Sulfur Silicon Relat. Elem.* **2014**, *189*, 924-932.
- [20] O. J. Scherer, C. Blath, G. Wolmershäuser, *J. Organomet. Chem.* **1990**, *387*, C21-C24.
- [21] M. Schmidt, D. Konieczny, E. V. Peresyphkina, A. V. Virovets, G. Balázs, M. Bodensteiner, F. Riedlberger, H. Krauss, M. Scheer, *Angew. Chem. Int. Ed.* **2017**, *56*, 7307-7311.
- [22] M. Schmidt, A. E. Seitz, M. Eckhardt, G. Balázs, E. V. Peresyphkina, A. V. Virovets, F. Riedlberger, M. Bodensteiner, E. M. Zolnhofer, K. Meyer, M. Scheer, *J. Am. Chem. Soc.* **2017**, *139*, 13981-13984.
- [23] B. Cordero, V. Gomez, A. E. Platero-Prats, M. Reves, J. Echeverria, E. Cremades, F. Barragan, S. Alvarez, *Dalton Trans.* **2008**, 2832-2838.
- [24] a) B. A. Stork-Blaisse, G. C. Verschoor, C. Romers, *Acta Cryst. sect. B* **1972**, *28*, 2445-2453; b) C. A. Ghilardi, S. Midollini, S. Moneti, A. Orlandini, *J. Chem. Soc., Chem. Commun.* **1988**, 1241-1242; c) J. Janczak, R. Kubiak, *Acta Cryst. sect. C* **2003**, *C59*, m70-m72; d) B. D. Ellis, C. L. B. Macdonald, *Inorg. Chem.* **2004**, *43*, 5981-5986.
- [25] O. J. Scherer, C. Blath, G. Heckmann, G. Wolmershäuser, *J. Organomet. Chem.* **1991**, *409*, C15-C18.
- [26] a) A. Strube, G. Huttner, L. Zsolnai, W. Imhof, *J. Organomet. Chem.* **1990**, *399*, 281-290; b) I. Y. Ilyin, S. N. Konchenko, N. A. Pushkarevsky, *J. Cluster Sci.* **2015**, *26*, 257-268.
- [27] A survey in the Cambridge Crystal Structure Database (CCSD), version 5.40 update 3, 08/2019, revealed 19 As-I-As bridging compounds with a mean As-I distance of 3.043 Å (median 3.077 Å).
- [28] a) H. Brunner, B. Nuber, L. Poll, G. Roidl, J. Wachter, *Chem. Eur. J.* **1997**, *3*, 57-61; b) D. Carmichael, F. Mathey, L. Ricard, N. Seeboth, *Chem. Commun.* **2002**, 2976-2977; c) X. Zhang, Q. Guo, Y. Zhang, Y. Zhang, W. Zheng, *Dalton Trans.* **2018**, *47*, 13332-13336.
- [29] A. R. Kudinov, D. A. Loginov, Z. A. Starikova, P. V. Petrovskii, M. Corsini, P. Zanello, *Eur. J. Inorg. Chem.* **2002**, 3018-3027.
- [30] M. Detzel, G. Friedrich, O. J. Scherer, G. Wolmershäuser, *Angew. Chem. Int. Ed. Engl.* **1995**, *34*, 1321.
(Thermolysis was performed in *meta*-Diisopropylbenzene delivering an improved yield of 80%).
- [31] B. Rink, O. J. Scherer, G. Wolmershäuser, *Chem. Ber.* **1995**, *128*, 71-74.
(Thermolysis was performed in *meta*-Diisopropylbenzene delivering a similar yield of 16%).
- [32] M. Gonsior, I. Krossing, N. Mitzel, *Z. Anorg. Allg. Chem.* **2002**, *628*, 1821.
- [33] M. A. Schwindt, T. Lejon, L. S. Hegedus, *Organometallics* **1990**, *9*, 2814-2819.

- [34] J. F. Cordes, *Chem. Ber.* **1962**, *95*, 3084.
- [35] K. Ziegler, H. Froitzheim-Kühlhorn, K. Hafner, *Chem. Ber.* **1956**, *89*, 434.
- [36] O. T. Beachley, Jr., R. Blom, M. R. Churchill, K. Faegri, Jr., J. C. Fettinger, J. C. Pazik, L. Victoriano, *Organometallics* **1989**, *8*, 346-356.
- [37] O. J. Scherer, M. Swarowsky, H. Swarowsky, G. Wolmershäuser, *Angew. Chem. Int. Ed. Engl.* **1988**, *27*, 694–695; *Angew. Chem.* **1988**, *100*, 738-739.
- [38] Due to the resemblance of the spectra of **3** and **4** at 11400 Hz and the similarity of their structures, the assignment of the signals of **3** was undertaken.
- [39] R. F. Winter, W. E. Geiger, *Organometallics* **1999**, *18*, 1827-1833.
- [40] E.R. Cohen, T. Cvitas, J.G. Frey, B. Holmstrom, K. Kuchitsu, R. Marquardt, I. Mills, F. Pavese, M. Quack, J. Stohner, H. Strauss, M. Takami, A.J. Thor, *Quantities, Units, and Symbols in Physical Chemistry, IUPAC Green Book, 3rd edition*, RSC Publishing, **2007**, p. 123.
- [41] S. Stoll, A. Schweiger, *J. Magn. Reson.* **2006**, *178*(1), 42-55.
- [42] *CrysAlisPRO*, different versions **2006-2018**, Rigaku Oxford Diffraction.
- [43] A. Burkhardt, T. Pakendorf, B. Reime et al, *Eur. Phys. J. Plus* **2016**, *131*, 56-64.
- [44] G. M. Sheldrick. *Acta Cryst. Sect. C* **2015**, *C71*, 3-8.
- [45] M. J. Frisch, G. W. Trucks, H. B. Schlegel, G. E. Scuseria, M. A. Robb, J. R. Cheeseman, G. Scalmani, V. Barone, B. Mennucci, G. A. Petersson, H. Nakatsuji, M. Caricato, X. Li, H. P. Hratchian, A. F. Izmaylov, J. Bloino, G. Zheng, J. L. Sonnenberg, M. Hada, M. Ehara, K. Toyota, R. Fukuda, J. Hasegawa, M. Ishida, T. Nakajima, Y. Honda, O. Kitao, H. Nakai, T. Vreven, J. A. Montgomery, Jr., J. E. Peralta, F. Ogliaro, M. Bearpark, J. J. Heyd, E. Brothers, K. N. Kudin, V. N. Staroverov, T. Keith, R. Kobayashi, J. Normand, K. Raghavachari, A. Rendell, J. C. Burant, S. S. Iyengar, J. Tomasi, M. Cossi, N. Rega, J. M. Millam, M. Klene, J. E. Knox, J. B. Cross, V. Bakken, C. Adamo, J. Jaramillo, R. Gomperts, R. E. Stratmann, O. Yazyev, A. J. Austin, R. Cammi, C. Pomelli, J. W. Ochterski, R. L. Martin, K. Morokuma, V. G. Zakrzewski, G. A. Voth, P. Salvador, J. J. Dannenberg, S. Dapprich, A. D. Daniels, O. Farkas, J. B. Foresman, J. V. Ortiz, J. Cioslowski, and D. J. Fox, Gaussian, Inc., Wallingford CT, 2013.
- [46] a) A. D. Becke, *J. Chem. Phys.* **1993**, *98*, 5648–5652; b) C. Lee, W. Yang, R. G. Parr, *Phys. Rev. B* **1988**, *37*, 785–789.
- [47] a) F. Weigend, R. Ahlrichs, *Phys. Chem. Chem. Phys.* **2005**, *7*, 3297–3305; b) D. Andrae, U. Häußermann, M. Dolg, H. Stoll, H. Preuß, *Theor. Chim. Acta* **1990**, *77*, 123–141.
- [48] a) J. P. Perdew, *Phys. Rev. B*, **1986**, 8822; b) A. D. Becke, *Phys. Rev. A*, **1988**, 3098.
- [49] a) J.-D. Chai, M. Head-Gordon, *J. Chem. Phys.* **2008**, *128*, 84106; b) J.-D. Chai, M. Head-Gordon, *Phys. Chem. Chem. Phys.* **2008**, *10*, 6615–6620.

- [50] a) G. Scalmani, M. J. Frisch, *J. Chem. Phys.* **2010**, *132*, 114110; b) J. Tomasi, B. Mennucci, R. Cammi, *Chem. Rev.* **2005**, *105*, 2999–3094.
- [51] NBO 6.0. E. D. Glendening, J. K. Badenhoop, A. E. Reed, J. E. Carpenter, J. A. Bohmann, C. M. Morales, C. R. Landis, and F. Weinhold (Theoretical Chemistry Institute, University of Wisconsin, Madison, WI, 2013), <http://nbo6.chem.wisc.edu>.
- [52] a) S. Grimme, J. Antony, S. Ehrlich, H. Krieg, *J. Chem. Phys.* **2010**, *132*, 154104; b) S. Grimme, S. Ehrlich, L. Goerigk, *J. Comp. Chem.* **2011**, *32*, 1456–1465.
- [53] Chemcraft - graphical software for visualization of quantum chemistry computations. <https://www.chemcraftprog.com>.

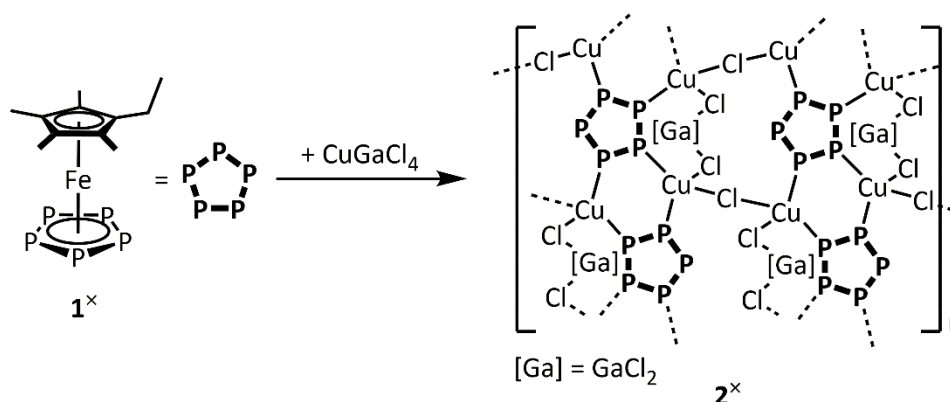
8 Thesis Treasury

In the following chapter, preliminary results are presented that provide an incentive for further investigations. For the presented compounds, preliminary structural models or complete data of the single-crystal X-ray structural characterizations are available and/or other characterization is still due. However, all obtained data and syntheses will be presented.

8.1 Self-Assembly of $[\text{Cp}^{\text{R}}\text{Fe}(\eta^5\text{-P}_5)]$ ($\text{Cp}^{\text{R}} = \text{Cp}^*, \text{Cp}^{\text{x}}$) with CuGaCl_4

The reactions of pentaphosphaferrocenes with CuGaCl_4 are mostly unexplored. Merely one polymer (**A**, cf. Scheme 2) has been obtained by self-assembly of **1*** with 2 eq. CuGaCl_4 so far,^[1] and neither a variation of the pentaphosphaferrocene or of the applied stoichiometries nor addition of a template have been investigated.

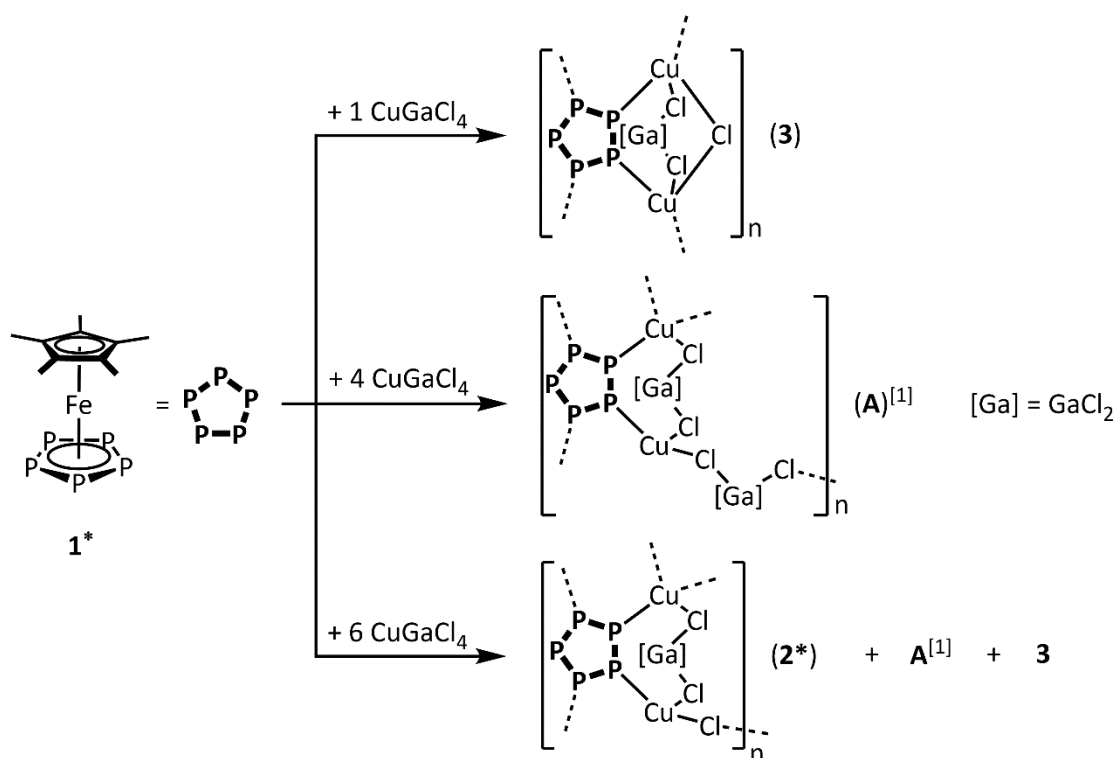
Therefore, **1*** was reacted with CuGaCl_4 in a 1:1 stoichiometry (Scheme 1) to give a novel 2D polymer $[\{\text{Cp}^{\text{x}}\text{Fe}(\mu_5, \eta^{5:1:1:1:1}\text{-P}_5)\}\text{Cu}_2(\mu\text{-Cl})(\mu, \eta^{1:1}\text{-GaCl}_4)]_n$ (**2***).



Scheme 1. Self-assembly of **1*** with 1 eq. CuGaCl_4 to give 2D polymer **2***.

In contrast, applying a 1:2, 1:4 or 1:6 (**1***: CuGaCl_4) stoichiometry did not furnish any crystalline products. For the 1:4 reaction, the precipitate was re-dissolved in CH_3CN and the solution was layered with toluene to give 2D polymers $[\{\text{1}^*\}_2\{\text{CuCl}\}_6\{\text{CH}_3\text{CN}\}]_n \cdot n\text{CH}_3\text{CN}$ and $[\{\text{1}^*\}\{\text{CuCl}\}_3]_n$, which have already been described in chapter 3 (compound **4-Cl** and **4-Cl-CH₃CN**) and in which no GaCl_4 unit is present.

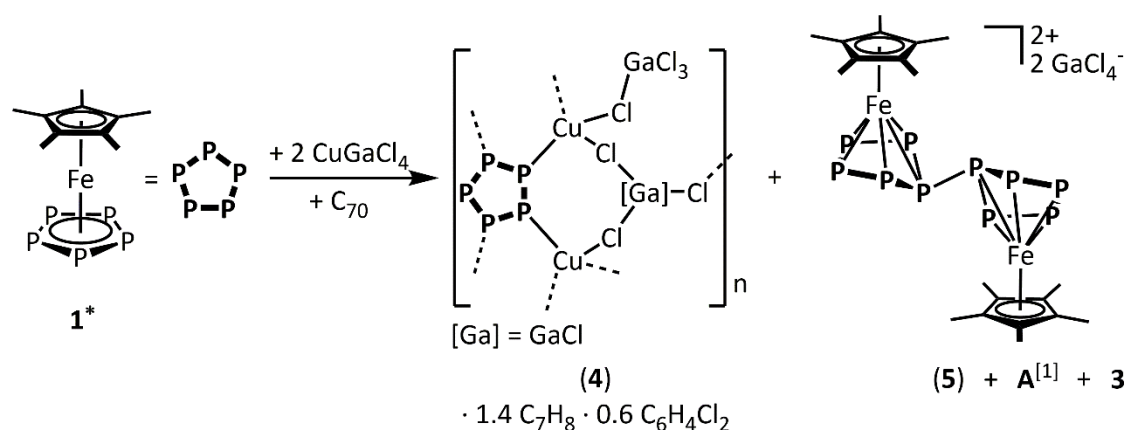
Furthermore, **1*** was reacted with CuGaCl_4 in molar ratios of 1:1, 1:4 and 1:6 (Scheme 2). In a 1:4 ratio, the reported polymer **A**^[1] was reproduced. Applying a 1:1 stoichiometry led reproducibly to the novel 2D polymer $[\{\text{Cp}^*\text{Fe}(\mu_5, \eta^{5:1:1:1:1}\text{-P}_5)\}\text{Cu}_2(\mu\text{-Cl})(\mu, \eta^{1:1}\text{-GaCl}_4)]_n$ (**3**) besides amorphous byproducts. In contrast, by applying 6 eq. CuGaCl_4 polymer **3** was obtained in addition to the reported polymer **A**,^[1] as well as another species (**2***) with similar unit cell parameters (oP, $a = 11.9 \text{ \AA}$, $b = 12.5 \text{ \AA}$, $c = 15.9 \text{ \AA}$; $V = 2365 \text{ \AA}^3$) as the **1***-based polymer **2***, thus



Scheme 2. Self-assembly of **1*** with 1, 4 or 6 eq. of CuGaCl_4 .

suggesting an isotopic structure. Noticeably, all obtained products exhibit a **1***:Cu ratio of 1:2, independently of the stoichiometry applied.

Since the GaCl_4^- counterions in the previously discussed structures were found to coordinate in a bridging mode, the question arose whether they can also support the formation of spherical assemblies. For instance, self-assembly of $[\text{Cp}^{\text{Bn}}\text{Fe}(\eta^5\text{-P}_5)]$ (**1^{Bn}**) with CuOTf or AgOTf ($\text{OTf} = \text{O}_3\text{SCF}_3$) leads to large spherical products with bridging OTf ligands. As the formation of spherical aggregates from **1*** is template-driven, the reaction of **1*** with CuGaCl_4 was additionally performed in the presence of $[\text{FeCp}_2]$, C_{60} or C_{70} as potential templates, using *o*-dichlorobenzene and toluene as solvents. Thereby, the new 2D polymer $[\{\text{Cp}^*\text{Fe}(\mu_5, \eta^{5:1:1:1:1}\text{-P}_5)\}\text{Cu}_2(\mu_3, \eta^{1:1:1}\text{-GaCl}_4)(\eta^1\text{-GaCl}_4)]_n \cdot 1.4 \text{ C}_7\text{H}_8 \cdot 0.6 \text{ C}_6\text{H}_4\text{Cl}_2$ (**4**) crystallized. Although compound **4** was the only crystalline product in the reactions with $[\text{FeCp}_2]$ or C_{60} , the elemental analysis of the isolated material did not furnish the expected results. In the reaction with C_{70} , also three other phases crystallized: the known 2D polymer **A**,^[1] polymer **3** and dimeric compound $[(\text{Cp}^*\text{Fe})_2(\mu, \eta^{5:5}\text{-P}_{10})](\text{GaCl}_4)_2$ (**5**, Scheme 3).



Scheme 3. Self-assembly of **1*** with 2 eq. CuGaCl_4 in the presence of C_{70} .

The 2D polymer $[\{\text{Cp}^x\text{Fe}(\mu_5, \eta^{5:1:1:1:1}\text{-P}_5)\}\text{Cu}_2(\mu\text{-Cl})(\mu, \eta^{1:1}\text{-GaCl}_2)]_n$ (**2***) crystallized as yellow needles in the orthorhombic space group *Pbcm* (Figure 1). It is built up in a similar manner as $[\{\text{Cp}^x\text{Fe}(\eta^5\text{-P}_5)\}\{\text{CuCl}\}_3]_n$ (compound **4-Cl** from chapter 3), with formally every $\{\text{CuCl}_2\}$ with a threefold coordinated Cu atom exchanged by a $\mu, \eta^{1:1}\text{-GaCl}_2$ unit additionally bound to two terminal Cl atoms. Hence, instead of $\{\text{CuCl}\}$ infinite helices, in **2*** infinite “-Cu-(Cl)-Cu-(Cl-Ga-Cl)-” helices are formed, interconnecting the units of **1***. Thus, **1*** is not pentacoordinating but only tetracoordinating in **2***. In contrast to the reported 2D polymer **A**,^[1] no short $\text{Cl}\cdots\text{H}$ contacts are found in between the layers which allows the Et groups of the Cp^x ligands to be disordered over three positions. However, $\text{Cl}\cdots\text{H}$ contacts of $2.8231(12) - 2.8494(8)$ Å (sum of the van-der-Waals radii: 2.85 Å)^[2] are found between the methyl or methylene protons and the bridging Cl atom within one layer.

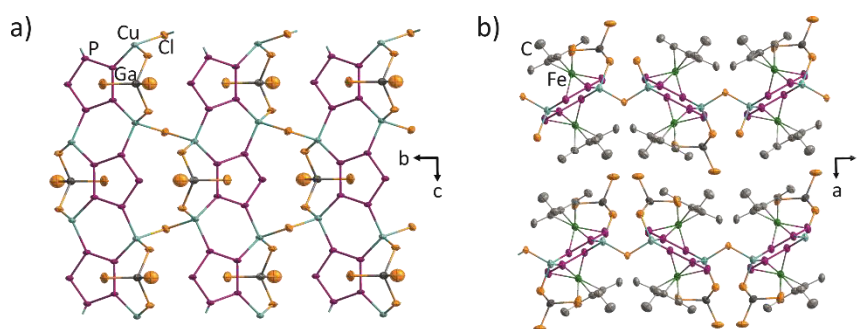


Figure 1. Section of the 2D polymeric structure of **2*** with $\{\text{Cp}^x\text{Fe}\}$ moieties (a), H atoms and minor parts of disorder omitted for clarity.

X-ray structure analysis of **3**, crystallizing in the orthorhombic space group *Pnma*, reveals a 2D coordination network, again with tetracoordinating units of **1*** (Figure 2). Although **3** has a similar sum formula as **2*** (except for the additional Me group) and proposed compound **2***, its connectivity is different. While the bridging Cl atoms in **2*** are decisive for the formation of the 2D layers, in compound **3** they only bridge two Cu atoms connected to the same **1*** moiety.

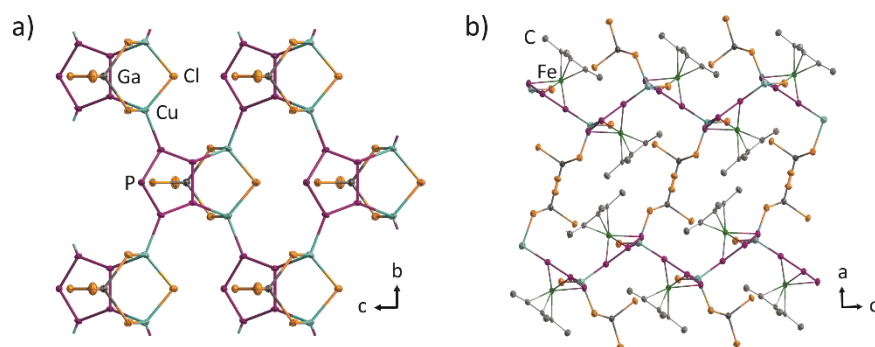


Figure 2. Section of the 2D polymeric structure of **3** with {Cp*Fe} moieties (a) and H atoms omitted for clarity.

Hence, the 2D network of **3** remains intact when conceptually removing all Cl and GaCl₄ units. Also, since no two P₅ complexes are connected by more than one Cu atom, no {P₄Cu₂} six-membered rings are formed. Instead, larger {P₇Cu₄Cl} rings are found.

Moreover, the structure of **4** was elucidated by X-ray crystallography (Figure 3). The sum formula is similar to that of 2D polymer **A**,^[1] however, again the connectivity is different (Figure 3a). Instead of only η²-coordinating bridging GaCl₄ units, in **4**, half of the GaCl₄ units coordinates terminally in an η¹-fashion, while the other half coordinates in a μ₃,η^{1:1:1}-fashion. The P₅ rings are 1,2,3,4-coordinated, and the Cu atoms comprise a distorted tetrahedral environment coordinated by 2 P atoms and 2 Cl atoms of the GaCl₄ units. For half of the Cu atoms, both coordinating Cl atoms are from μ₃-bridging GaCl₄ units. Thus, eight-membered Cu₂Ga₂Cl₄ rings are formed. The 1D strands built up from **1*** and Cu atoms exhibit {P₄Cu₂} six-membered rings, but describe waved strands (Figure 3b) instead of mostly planar ones as in **A**.^[1] The 2D layers are separated by toluene molecules, which participate in short H⋯Cl contacts of 2.7742(15) – 2.8021(12) Å (sum of the van-der-Waals radii: 2.85 Å)^[2] with the terminal Cl atom of each μ₃-bridging GaCl₄ unit of both adjacent layers (Figure 3c).

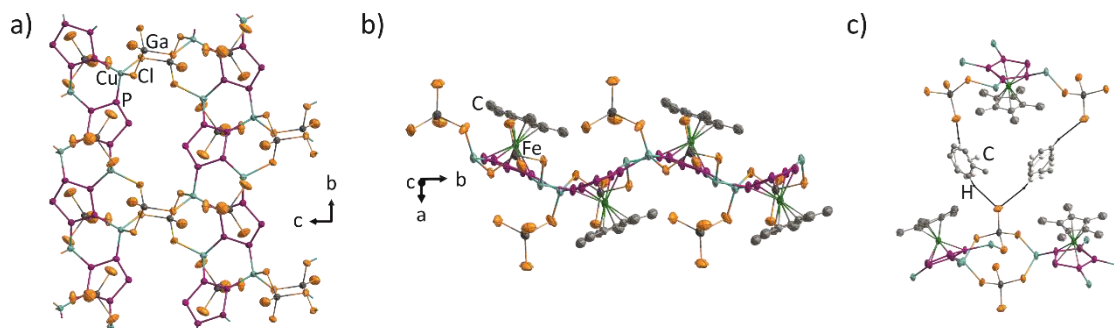


Figure 3. a) and b) Section of the 2D polymeric structure of **4** with {Cp*Fe} fragments or H atoms as well as solvate molecules omitted for clarity. c) H⋯Cl contacts of toluene and the adjacent polymeric layers.

Crystal structure analysis of **5** revealed a [(Cp*Fe)₂(μ,η^{5:5}-P₁₀)]²⁺ cation, which has already been reported as a SbF₆-salt obtained by the reaction of **1*** with thianthrenium hexafluoroantimonate ([C₁₂H₈S₂][SbF₆]) as an oxidizing agent.^[3] Hence, in *o*-DCB / toluene

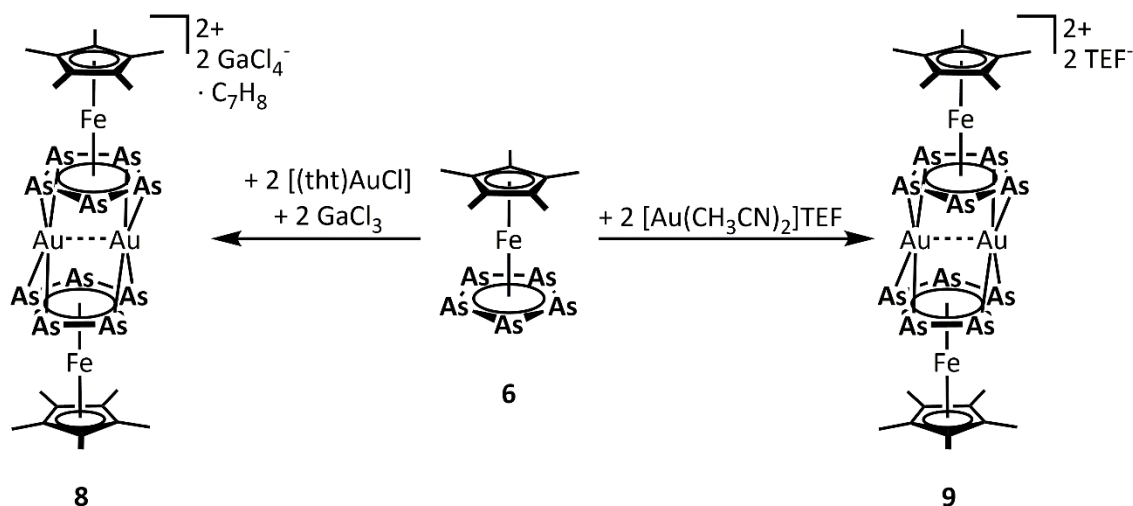
mixtures, either Cu^I or C₇₀ might have been reduced while oxidizing **1***. Both structures merely differ in their structural characteristics, so the structure is not further discussed herein.

Since in all aforementioned reactions, polymers with Cl atoms are formed, the origin of these Cl atoms has to be questioned. An obvious explanation might be, that CuGaCl₄ contained residual CuCl from its synthesis with GaCl₃. Another possibility is the partial hydrolysis of the GaCl₄⁻ anions, or a Cl abstraction from CH₂Cl₂ or GaCl₄⁻. As the synthesis of all described compounds was highly unselective and not controllable by stoichiometry (compounds **2*** and **3** are even constitutional isomers), a detailed further investigation was hampered.

8.2 Self-Assembly of $[\text{Cp}^*\text{Fe}(\eta^5\text{-As}_5)]$ and $[\text{CpMo}(\text{CO})_2(\eta^3\text{-P}_3)]$ with Au Salts

In Chapter 6, the self-assembly of pentaphosphaferrocenes $[\text{Cp}^*\text{Fe}(\eta^5\text{-P}_5)]$ (**1***), $[\text{Cp}^x\text{Fe}(\eta^5\text{-P}_5)]$ (**1^x**) and $[\text{Cp}^{\text{Bn}}\text{Fe}(\eta^5\text{-P}_5)]$ (**1^{Bn}**) with Au salts was examined. In the course of these investigations, molecular products as well as coordination polymers were obtained. However, the formation of spherical products was hampered, presumably due to the preferred planar coordination environment of Au in combination with the preferred in-plane σ -coordination of pentaphosphaferrocenes **1** leading to divergent self-assembly. Hence, when spherical assemblies are targeted, the application of convergently coordinating E_n ligand complexes ($E = \text{P}, \text{As}$) should be considered as building blocks instead of **1**. The *cyclo*- As_5 complex $[\text{Cp}^*\text{Fe}(\eta^5\text{-As}_5)]$ (**6**)^[4] comes to mind, since arsoly ligands prefer π -coordination over in-plane σ -coordination, even when coordinated to late transition metal like Cu or Hg.^[5] Moreover, the *cyclo*- P_3 complex $[\text{CpMo}(\text{CO})_2(\eta^3\text{-P}_3)]$ (**7**)^[6] is known to exhibit an out-of-plane σ -coordination mode with P-M bonds bent by approximately 40° with respect to the *cyclo*- P_3 plane.^[7] Hence, the question arose whether spherical assemblies of Au can be obtained by applying **6** or **7** as convergent building blocks.

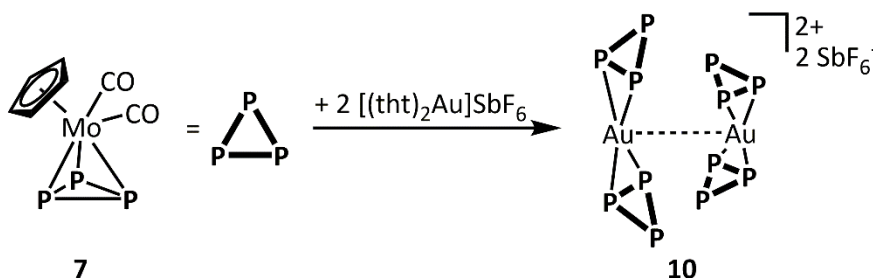
The reaction of $[\text{Cp}^*\text{Fe}(\eta^5\text{-As}_5)]$ (**6**) with a mixture of $[(\text{tth})\text{AuCl}]$ and GaCl_3 in CH_2Cl_2 gave a red suspension. After filtration and crystallization with toluene, brown crystals of $\{[\text{Cp}^*\text{Fe}(\mu_3, \eta^{5:2:2}\text{-As}_5)]_2\text{Au}_2\}(\text{GaCl}_4)_2 \cdot \text{C}_7\text{H}_8$ (**8**) were obtained (Scheme 4, left). The reaction mixture as well as the product seemed to be very light- and air-sensitive. The formation of a Au^0 mirror leads to low yields (few crystals) and the mother liquor turns intensely violet in contact with air. This impeded the isolation of practicable amounts of **8**. Moreover, the crystals rapidly undergo radiolysis when exposed to synchrotron radiation, but fortunately X-ray crystallographic characterization was possible using $\text{Cu } K\alpha$ irradiation.



Scheme 4. Self-assembly of $[\text{Cp}^*\text{Fe}(\eta^5\text{-As}_5)]$ (**6**) with $[(\text{tth})\text{AuCl}]$ and GaCl_3 (left) or $[\text{Au}(\text{CH}_3\text{CN})_2]\text{TEF}$ (right).

Moreover, by stirring $[\text{Cp}^*\text{Fe}(\eta^5\text{-As}_5)]$ (**6**) and $[\text{Au}(\text{CH}_3\text{CN})_2]\text{TEF}^{[8]}$ in CH_2Cl_2 and layering the filtrate with pentane, next to the formation of a Au^0 mirror also dark red prisms of $[\{\text{Cp}^*\text{Fe}(\mu_3, \eta^{5:2:2}\text{-As}_5)\}_2\text{Au}_2](\text{TEF})_2$ (**9**) crystallized in the triclinic system,^[9] with one formula unit occupying the center of symmetry (Scheme 4, right). **9** exhibits a similar structure to compound **8** but structural characterization was hampered due to systematic twinning and X-ray sensitivity. Thus, only the atom connectivity could be derived and was found to be similar to that of compound **8**.

The self-assembly of $[\text{CpMo}(\text{CO})_2(\eta^3\text{-P}_3)]$ (**7**) with $[(\text{tht})_2\text{Au}]\text{SbF}_6^{[10]}$ yielded orange crystals. Preliminary data suggest a dimeric structure of $[\{\text{CpMo}(\text{CO})_2(\mu, \eta^{3:2}\text{-P}_3)\}_2\text{Au}]_2(\text{SbF}_6)$ (**10**, Scheme 5), however, again systematic twinning and rapid radiolysis complicated X-ray crystallographic characterization and only allowed the atom connectivity to be deduced so far. Compound **10** was also obtained from similar reactions in the presence of P_4S_3 or with $o\text{-C}_2\text{B}_{10}\text{H}_{12}$ as potential templates.



Scheme 5. Self-assembly of $[\text{CpMo}(\text{CO})_2(\eta^3\text{-P}_3)]$ (**7**) with $[(\text{tht})_2\text{Au}]\text{SbF}_6$.

Compound **8** crystallizes in the monoclinic space group $C2/c$ with one formula unit in a general position. Both units of **6** coordinate through their π -system in an η^2 -fashion (Figure 4a). The Au ions are pairwise disordered over a total of five positions in between the two parallel As_5 cycles (angle between As_5 planes: 0.66°). One orientation of the Au_2 dumbbell is occupied by 9% with a close $\text{Au}3\cdots\text{Au}4$ contact of $2.863(8)$ Å, being in the range of aurophilic $\text{Au}\cdots\text{Au}$ distances ($2.85 - 3.50$ Å).^[11] Another orientation of the Au_2 dumbbell is rotated by 89° , thus being almost perpendicular, and is occupied by 91% with a close $\text{Au}1\cdots\text{Au}2$ contact of $2.8785(8)$ Å and an additional disorder of the Au2 position with a minor occupancy of 3%. Disregarding this minor position (Au2A), the Au-As bond lengths range from $2.514(7)$ Å to $2.863(8)$ Å, with most of them being longer than the Au-As bonds in $[(\text{PPh}_3)\text{Au}(\eta^2\text{-As}_4)]\text{TEF}$ ($2.5358(6)$ and $2.5514(5)$ Å)^[12] and one being even longer than the Au-As bonds in a $\{\text{AuAs}_2\text{B}_9\}$ cluster ($< 2.7094(12)$ Å),^[13] which are the only other reported compounds with an As_2 unit side-on coordinated to Au. The coordination geometry of the Au centers is best described as linear (taking the center of the As-As edges with centroid-Au-centroid angles $> 170^\circ$) or distorted square planar (taking each As

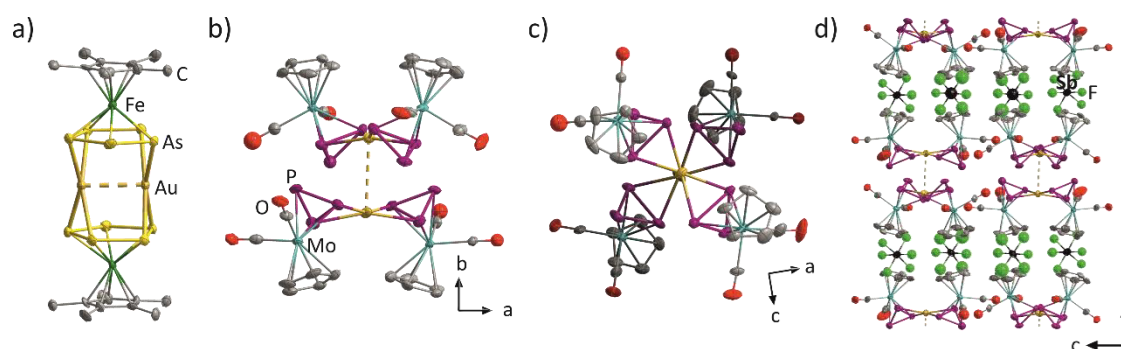


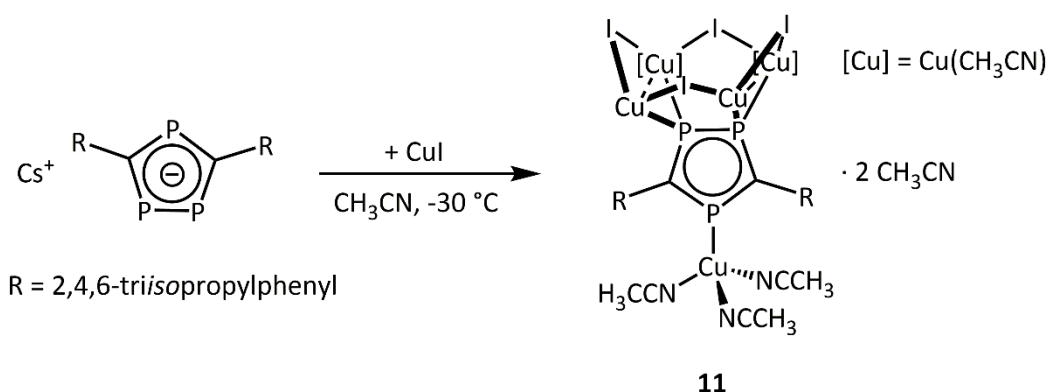
Figure 4. Molecular structure of a) the cation of **8**; b) and c) the dimer in **10**. d) 2D layers of the dimers in **10** separated by SbF_6^- counterions. A.d.p. ellipsoids at 50% probability level. H atoms and minor positions of disorder omitted for clarity.

atom individually) for Au1-4. In the latter description, the deviation from the planar environment is mainly due to the staggered conformation of the two As_5 rings leading to the non-parallel arrangement of the coordinating As-As bonds. Moreover, the As_5 rings are shifted by 0.98 Å. The As-As bonds are elongated from 2.312(2) – 2.319(2) Å in **6**^[4] to 2.3473(19) – 2.447(2) Å in **8**, an effect which has already been observed to a lesser extent for π -coordination of **6** to Cu.^[5a]

Preliminary data suggest that in **10**, two *cyclo*- P_3 complexes coordinate in an out-of-plane η^2 -fashion to one Au atom comprising a distorted square planar (taking all bound P atoms into account) or linear (taking the centroids of the coordinating P_2 bonds) coordination environment (Figure 4b,c). This is similar to the reported structures of $[\{\text{M}(\text{tppme})(\text{P}_3)\}_2\text{Au}]\text{PF}_6$ (M = Co, Rh, Ir; tppme = 1,1,1-tris(diphenylphosphinomethyl)ethane).^[14] However, in **10**, additional short Au...Au contacts (≈ 3.4 Å) to the neighboring cation are found, leading to a dimeric structure through aurophilic interactions.^[11] In $[\{\text{M}(\text{tppme})(\text{P}_3)\}_2\text{Au}]\text{PF}_6$, these might be prevented by the steric bulk of the large tppme ligand. While the Au_2 dumbbells in **8** are formed by ligand-supported aurophilic interactions, this is not true for compound **10**, probably as a result of the smaller *cyclo*- P_3 ligand compared to the *cyclo*- As_5 ligand. Moreover, the dimers in **10** are arranged in 2D layers, which are separated by the SbF_6^- counterions (Figure 4d). Due to the provisional nature of the structural model, no further details can be given at this point and some residual electron density still has to be assigned.

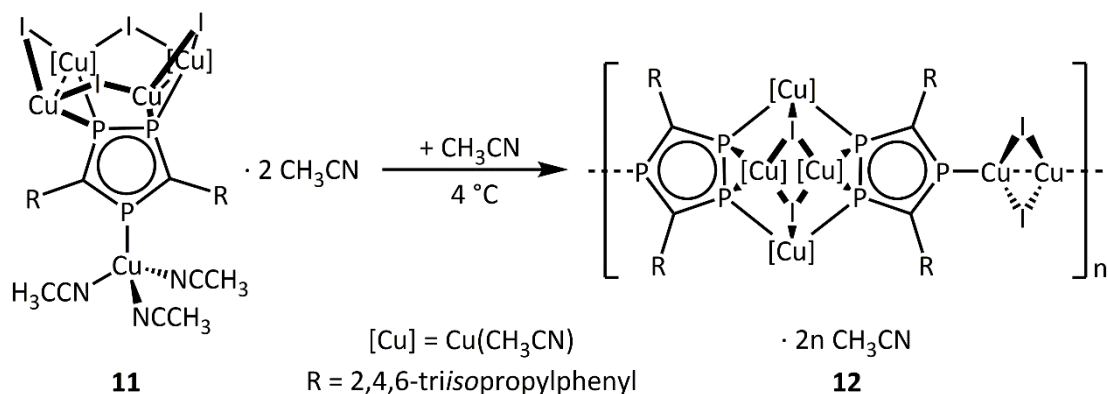
8.3 Supramolecular Chemistry of Polyphospholyl Salts

Self-assembly of $\text{Cs}[\text{P}_3\text{C}_2(\text{trip})_2]$ ($\text{trip} = 2,4,6\text{-tri-}i\text{-propylphenyl}$)^[15] with CuI results in the formation of $[(\mu, \eta^{1:2:2}\text{-P}_3\text{C}_2(\text{trip})_2)\{\text{Cu}(\text{CH}_3\text{CN})_3\}\{\text{Cu}(\text{CH}_3\text{CN})(\mu\text{-I})_2\}\{\text{Cu}(\mu\text{-I})_2\}] \cdot 2 \text{CH}_3\text{CN}$ (**11**) at -30°C (Scheme 6).



Scheme 6. Self-assembly of $\text{Cs}[\text{P}_3\text{C}_2(\text{trip})_2]$ and CuI to give monomeric compound **11**.

When **11** is recrystallized from concentrated CH_3CN solution at 4°C , instead the 1D polymer $[(\mu_4, \eta^{1:1:1:2}\text{-P}_3\text{C}_2\text{trip}_2)_2\{\text{Cu}(\text{CH}_3\text{CN})(\mu_3\text{-I})_2\}\{\text{Cu}(\text{CH}_3\text{CN})_2\}\{\text{Cu}(\mu_2\text{-I})_2\}]_n \cdot 2n \text{CH}_3\text{CN}$ (**12**) crystallizes (Scheme 7).



Scheme 7. Recrystallization of the monomer **11** at 4°C leading to the 1D polymer **12**.

Compound **11** crystallizes in the orthorhombic space group $Pna2_1$ as a racemic twin. Its structure (Figure 5) resembles the structure of a monomer obtained by self-assembly of CuI and $[\text{Cp}^*\text{Fe}(\eta^5\text{-P}_3\text{C}_2\text{Mes}_2)]$ ($\text{Mes} = 2,4,6\text{-trimethylphenyl}$), where the Cp^*Fe fragment is split off and the triphospholyl ligand self-assembles with CuI .^[16] Thus, **11** is built up from one planar (rms: 0.012 \AA) P_3C_2 ligand, which coordinates with all three P atoms. The isolated P atom is coordinated to a $\text{Cu}(\text{CH}_3\text{CN})_3$ unit. The adjacent P atoms are coordinated to a distorted $\{\text{Cu}_4\text{I}_4(\text{CH}_3\text{CN})_2\}$ crown motif. Here, the main difference to the monomer obtained with the $\text{P}_3\text{C}_2\text{Mes}_2$ -ligand is, that only two instead of four CH_3CN ligands are coordinated to the Cu_4I_4 motif. This most probably is due to the enhanced steric bulk of the trip substituents compared

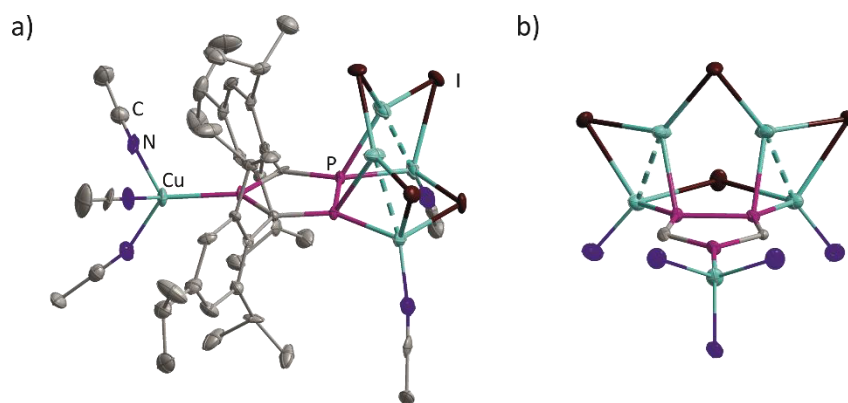


Figure 5. a) Molecular structure of compound **11** with solvate molecules and H atoms omitted. b) Core structural motif of **11** with solvate molecules, trip residues and CCH₃ moieties of CH₃CN ligands omitted.

to the Mes substituents in the reported compound. Therefore, the “bottom” Cu atoms are coordinated in a distorted tetrahedral fashion, while the “top” Cu atoms are coordinated in a nearly trigonal planar manner (distances Cu⋯I₂P plane: 0.24 and 0.13 Å). To avoid steric repulsion between the coordinated CH₃CN ligands and the trip substituents, the {Cu₄I₄} crown in **11** is not coordinated symmetrically by the adjacent P atoms but is tilted so that the CH₃CN-bearing Cu atoms are almost in plane with the P₃C₂trip₂ ligand (distances Cu⋯P₃C₂ plane: 0.22 and 0.29 Å). The other two Cu atoms are located well above the plane (distances Cu⋯P₃C₂ plane: 2.00 and 2.04 Å). Moreover, the “bottom” and “top” Cu atoms form close Cu⋯Cu contacts with distances of 2.50 Å, thus being within the expected range,^[17] similarly to the reported Mes analogue. In contrast, however, these Cu₂ dimers are not arranged parallel to one another, but the “top” Cu atoms are only separated by 2.845(3) Å, while the “bottom” Cu atoms are separated by 4.31 Å.

Compound **12** crystallizes in the monoclinic space group *C2/c*. The repeating unit is built up from two planar (rms: 0.006 Å) P₃C₂ ligands that coordinate to Cu in different modes (Figure 6). The adjacent P atoms are coordinated each in an η¹-fashion to Cu (2.25 Å), which connects to the next phospholyl ligand, thus building a {P₄Cu₂} six-membered ring. This motif is capped by

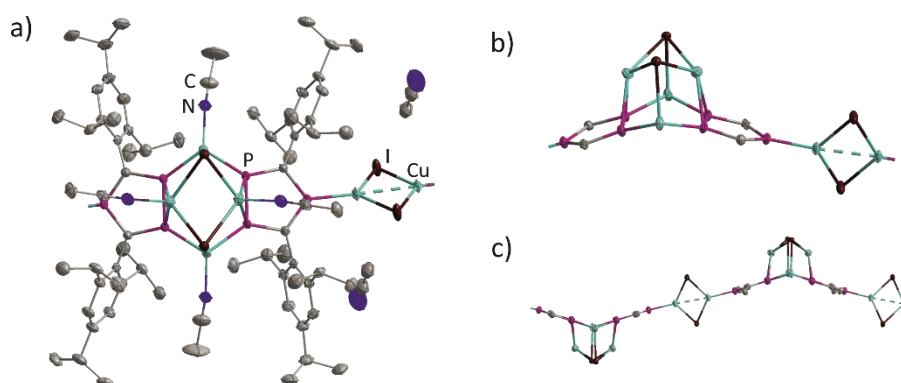


Figure 6. a) Repeating unit of 1D polymer **12** with H atoms omitted and b) with trip residues, solvate molecules and coordinated CH₃CN ligands omitted. c) Section of the waved 1D polymeric structure of **12**.

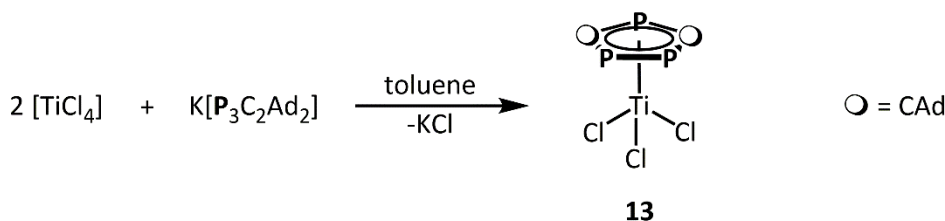
{Cu₂I₂} four-membered ring, with its Cu atoms being η²-coordinated by the phospholyl ligands (2.4717(6) – 2.5324(6) Å), and the I atoms additionally coordinating to the Cu atoms of the six-membered ring. The Cu atoms within this Cu₄I₂P₂ motif are coordinatively saturated by one CH₃CN ligand each, thus exhibiting a distorted pseudo-tetrahedral coordination environment (the η²-coordination is thereby regarded as one coordination site). The isolated P atoms of the triphospholyl ligands are η¹-coordinated to {Cu₂I₂} rings (2.20 Å), which connect to the isolated P atom of the phospholyl ligand in the next repeating unit. Thus, these Cu atoms are coordinated in a trigonal planar geometry (I-Cu-P angles: 124.71(2)°, 115.790(12)°, 119.41(2)°). The I atoms are either bridging two (Cu₂I₂ ring) or three (Cu₄I₂P₄ motif) Cu atoms with Cu-I-Cu angles of 64.212(12)° to 71.736(10)°. Moreover, short Cu⋯Cu contacts are found between the Cu atoms of the {Cu₂I₂} units bridging the repeating units, with a Cu⋯Cu distance of 2.7229(6) Å being in the expected range.^[17] In contrast, the Cu⋯Cu distance within the Cu₂I₂ ring capping the P₄Cu₂ motif amounts to 3.0123(7) Å.

In the ¹H NMR spectrum of the monomer **11**, the expected signals for the trip residue are observed. Thereby, not only the *ortho*- and *para*-ⁱPr groups are distinguishable, but this time also the *ortho*-CH(CH₃) protons split into two signals with an integral ratio of 12:12. This is most probably due to the unsymmetrical arrangement of the Cu₄I₄ crown, leading to magnetic inequivalence of the ⁱPr groups above and below the P₃C₂ ligand plane. Additionally, a singlet at 1.95 ppm is attributed to the five coordinated CH₃CN ligands in **11**. Interestingly, crystals of **11** are bright orange, but upon drying decompose to a microcrystalline reddish powder. With addition of CH₃CN this color shift is reversible and again orange microcrystalline material is obtained. The elemental analysis fits to (P₃C₃₂H₄₆)(Cu₅I₄)(CH₃CN), containing only one instead of five (coordinated) plus two (uncoordinated) CH₃CN ligands.

8.4 Early Transition Metal Complexes of Polyphospholyl Ligands

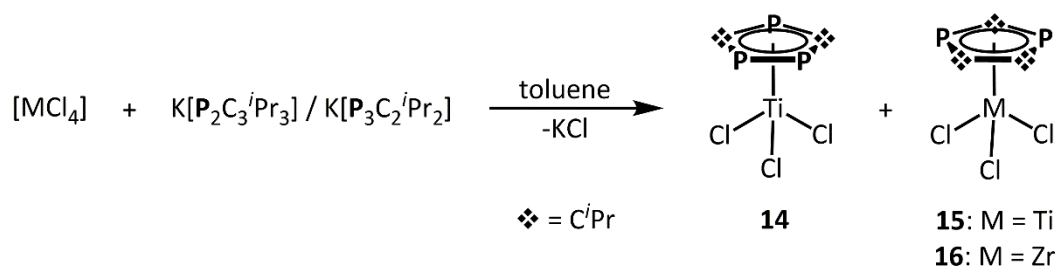
Homogeneous early transition metal catalysts often comprise Cp-ligands and are applied in various reactions such as olefin polymerization and dehydropolymerization.^[18] Thereby, enhanced electrophilicity of the metal center often comes along with enhanced catalytic activity.^[19] Interestingly, phospholyl ligands are isolobal to Cp ligands but constitute better π -acceptor properties. Thus, the formal exchange of Cp ligands by phospholyl ligands is thought to be a promising approach towards more active early transition metal catalysts. Indeed, the application of monophospholyl ligands $[\text{PC}_4\text{R}_4]^-$ in Zr complexes has been thoroughly investigated and brought forth some patented catalysts.^[20] The effect of incorporation of polyphospholyl ligands into early transition metal catalysts on their activity has in contrast only been sparsely investigated.^[21] Hence, the question arose, whether further polyphospholyl complexes of early transition metals are accessible.

Therefore, polyphospholyl salts were reacted with early transition metal halides in salt metathesis reactions. The reactions of $\text{Cs}[1,2,4\text{-P}_3\text{C}_2\text{trip}_2]$ (trip = 1,3,5-tri-*isopropylphenyl*) with $[\text{Cp}_2\text{TiCl}_2]$, $[\text{VCl}_3(\text{thf})_3]$, $[\text{CrCl}_3(\text{thf})_3]$, $[\text{Cp}^*\text{TiCl}_3]$, $[\text{Cp}_2\text{ZrCl}_2]$, $[\text{TiCl}_4(\text{thf})_2]$ and $[\text{ZrCl}_4]$, respectively, each gave $(\text{HP}_3\text{C}_2\text{trip}_2)_2$, the dimerization product of the protonated phosphole ligand.^[22] Its structure and characterization have already been discussed elsewhere.^[22] In contrast, target coordination product $[(\eta^5\text{-}1,2,4\text{-P}_3\text{C}_2\text{Ad}_2)\text{TiCl}_3]$ (**12**) could be detected $^{31}\text{P}\{^1\text{H}\}$ NMR spectroscopically from the reaction of $[\text{TiCl}_4]$ with $\text{K}(1,2,4\text{-P}_3\text{C}_2\text{Ad}_2)$ (Ad = adamantyl, Scheme 8).

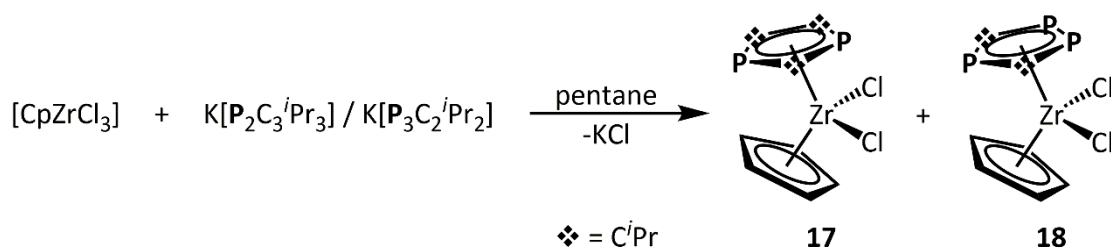


Scheme 8. Reaction of $[\text{TiCl}_4]$ with $\text{K}[\text{P}_3\text{C}_2\text{Ad}_2]$.

Unfortunately, the synthesis of the *i*Pr substituted phospholyl ligands often furnishes a mixture of di- and triphospholyl salts and the selective synthesis of the diphospholyl salt has not been accomplished yet.^[23] Hence, $[(\eta^5\text{-}1,2,4\text{-P}_3\text{C}_2^i\text{Pr}_2)\text{TiCl}_3]$ (**14**) and $[(\eta^5\text{-}1,3\text{-P}_2\text{C}_3^i\text{Pr}_3)\text{TiCl}_3]$ (**15**) were obtained by reaction of a mixture of $\text{K}(1,3\text{-P}_2\text{C}_3^i\text{Pr}_3)$ and $\text{K}(1,2,4\text{-P}_3\text{C}_2^i\text{Pr}_2)$ with $[\text{TiCl}_4]$ (Scheme 9). While **13** is stable at room temperature, its less kinetically stabilized *i*Pr analogue **14** proved to be thermally unstable and decomposed at r.t. Therefore, from the mixture of **14** and **15**, only **15** could be crystallized so far. The analogous Zr complex $[(\eta^5\text{-}1,3\text{-P}_2\text{C}_3^i\text{Pr}_3)\text{ZrCl}_3]$ (**16**) was detected ^1H and $^{31}\text{P}\{^1\text{H}\}$ NMR spectroscopically from the reaction of $[\text{ZrCl}_4]$ with $\text{K}(1,2,4\text{-P}_3\text{C}_2^i\text{Pr}_2)$ / $\text{K}(1,3\text{-P}_2\text{C}_3^i\text{Pr}_3)$, while its triphospholyl analogue was not detected at room temperature (Scheme 9).

Scheme 9. Reaction of $[\text{MCl}_4]$ ($\text{M} = \text{Ti}, \text{Zr}$) with a mixture of $\text{K}[\text{P}_2\text{C}_3^i\text{Pr}_3]$ and $\text{K}[\text{P}_3\text{C}_2^i\text{Pr}_2]$.

Moreover, the reaction of $\text{K}(\eta^5\text{-}1,2,4\text{-P}_3\text{C}_2^i\text{Pr}_2) / \text{K}(\eta^5\text{-}1,3\text{-P}_2\text{C}_3^i\text{Pr}_3)$ with $[\text{CpZrCl}_3]$ furnished the sandwich complexes $[\text{Cp}(\eta^5\text{-}1,3\text{-P}_2\text{C}_3^i\text{Pr}_3)\text{ZrCl}_2]$ (**17**) and $[\text{Cp}(\eta^5\text{-}1,2,4\text{-P}_3\text{C}_2^i\text{Pr}_2)\text{ZrCl}_2]$ (**18**) according to ^1H and $^{31}\text{P}\{^1\text{H}\}$ NMR spectroscopy with both compounds being stable at room temperature (Scheme 10).

Scheme 10. Reactions of $[\text{CpZrCl}_3]$ with a mixture of $\text{K}[\text{P}_2\text{C}_3^i\text{Pr}_3]$ and $\text{K}[\text{P}_3\text{C}_2^i\text{Pr}_2]$.

The half-sandwich triphospholyl compounds **13** and **14** were detected by $^{31}\text{P}\{^1\text{H}\}$ NMR spectroscopy as a triplet at 302.8 or 299.7 ppm and a doublet at 338.0 or 345.7 ppm with a coupling constant of about 50 Hz. This is in accordance with the spectrum of the reported ^tBu analogue $[(\eta^5\text{-}1,2,4\text{-P}_3\text{C}_2^t\text{Bu}_2)\text{TiCl}_3]$ exhibiting a triplet at 305.1 and a doublet at 346.8 ppm.^[21a] In contrast to **14**, the ^tBu ^[21a] and Ad analogue **13** are stable at r.t. Interestingly, the ^tBu derivative proved up to four times more active in ethylene polymerization with methylaluminoxane (MAO) as cocatalyst than its carbon analogue $[\text{CpTiCl}_3]$.^[21a] The proposed Zr analogue of **14**, $[(\eta^5\text{-}1,2,4\text{-P}_3\text{C}_2^i\text{Pr}_2)\text{ZrCl}_3]$, was not detected at r.t. Zenneck reported that the ^tBu analogue $[(\eta^5\text{-}1,2,4\text{-P}_3\text{C}_2^t\text{Bu}_2)\text{ZrCl}_3]$ was too reactive or unstable to handle and could only be detected spectroscopically.^[21b] Therefore, it is not surprising that the less kinetically stabilized ^iPr analogue could not be obtained.

The half-sandwich diphospholyl compounds **15** ($\text{M} = \text{Ti}$) and **16** ($\text{M} = \text{Zr}$) are more stable. The $^{31}\text{P}\{^1\text{H}\}$ NMR spectra show singlets at 254.7 and 225.9 ppm, respectively. The ^tBu analogue of **16** resonates at 260.3 ppm and was characterized by X-ray crystallography.^[21b] A Ti analogue like **15** has not been reported so far. The ^1H NMR spectra each show a septet or multiplet for the adjacent and the isolated $-\text{CH}(\text{CH}_3)_2$ atoms. Surprisingly, the doublets assigned to the Me groups split into three instead of two signals with an integral ratio of 6:6:6. Since the $-\text{CH}(\text{CH}_3)_2$ protons of the adjacent ^iPr groups seem to be magnetically equivalent, the inequivalence of the Me

protons seems to stem from hindered rotation of the adjacent ⁱPr groups so that the Me groups above and below the P₂C₃ plane split into two signals.

This effect has already been observed for [Cp*Fe(η⁵-1,3-P₂C₃ⁱPr₃)]^[23] and also applies to the diphospholyl sandwich complex **17**. The ¹H NMR spectra of the sandwich complexes **17** and **18** additionally exhibit a singlet assigned to the Cp ligand. Interestingly, in [Cp(η⁵-1,2,4-P₃C₂^tBu₂)ZrCl₂], the rotation of the Cp ligand is hindered leading to two singlets in the ¹H NMR spectrum.^[21b] This was not found for the herein reported ⁱPr analogue **18**. The ³¹P{¹H} NMR spectrum of the sandwich complex **18** reveals a triplet at 289.1 ppm and a doublet at 248.2 ppm with a coupling constant of 51 Hz, again in accordance with the reported ^tBu analogue (282.5 and 260.2 ppm).^[21a,b] The latter could be characterized by X-ray crystal structure analysis despite its thermal lability/instability.^[21b] The respective diphospholyl complex **17** resonates at 215.9 ppm in the ³¹P{¹H} NMR spectrum, similarly to the ^tBu analogue (236.7 ppm) which was also characterized by means of X-ray crystallography.^[21b]

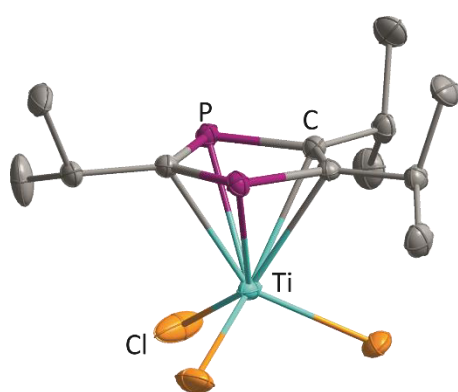


Figure 7. Molecular structure of **15** with H atoms omitted for clarity.

Remarkably, compound **15** displays the first structurally characterized Ti diphospholyl complex (Figure 7). It crystallizes in the triclinic space group $P\bar{1}$ with two crystallographically unique molecules in the asymmetric unit. All P-C (1.7448(12) – 1.7794(12) Å) and C-C (1.4095(16) – 1.4101(16) Å) bond lengths within the P₂C₃ ring are in between single and double bonds (P-C 1.86 Å, P=C 1.69 Å, C-C 1.50 Å, C=C 1.34 Å).^[24] The Ti-Cl bond lengths (2.2287(4) – 2.2429(4) Å) are in agreement with single bonds (2.25 Å).^[24]

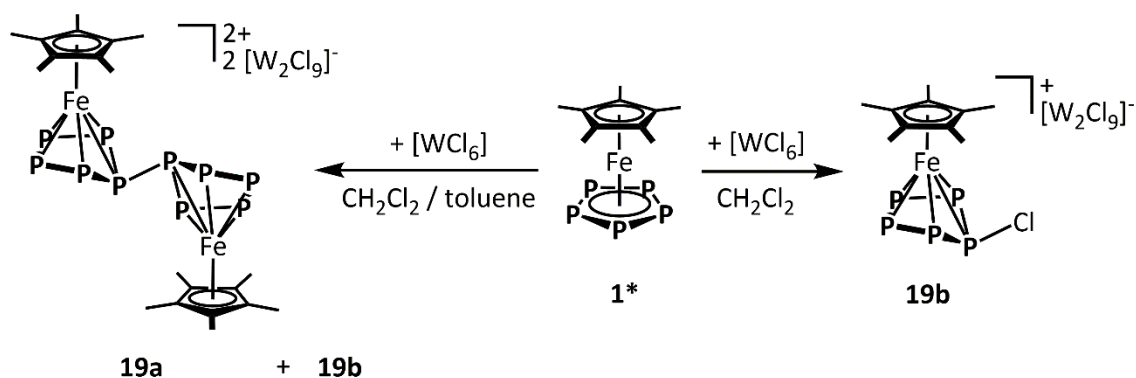
8.5 Halogenations of [Cp*Fe(η^5 -P₅)]

In Chapter 7, the iodination of [Cp*Fe(η^5 -P₅)] (**1***) and its heavier congeners [Cp*M(η^5 -E₅)] (M = Fe, E = As (**6**); M = Ru, E = P, As) giving a number of unprecedented complexes, such as [Cp*FeP₆I], was described. The question arose, which new compounds might be formed by fluorination, chlorination or bromination reactions.

Stirring [Cp*Fe(η^5 -P₅)] (**1***) with CoF₃, [FNC₅H₅]BF₄ and [FeCp₂]PF₆ (in the presence of CsF), respectively, did not lead to any reaction. However, when [Cp*Fe(η^5 -P₅)] (**1***) is reacted with 3 eq. of XeF₂ in CH₃CN in a plastic vial, only the formation of PF₆⁻ is observed by ³¹P{¹H} and ¹⁹F{¹H} NMR spectroscopy of the mother liquor.

With FeCl₃ or C₂Cl₆, again no reaction with **1*** was observed. In contrast, CuCl₂ reacts with **1*** under formation of the 90-vertex sphere [Cp*Fe(η^5 -P₅)]@[Cp*Fe(η^5 -P₅)]₁₂{CuCl}₂₅{CH₃CN}₁₀,^[25] wherein Cu^{II} is reduced to Cu^I. When **1*** was reacted with PCl₅, primarily PCl₃ and P₂Cl₄ were formed. The control experiment with 8 eq. PCl₅ resulted in almost exclusive formation of PCl₃ and only trace amounts of **1*** were detected in the ³¹P{¹H} NMR spectrum, thus indicating that PCl₃ is not only formed from PCl₅ but also from **1*** in a comproportionation reaction. Astonishingly, also P₄ was detected in the reaction mixtures of **1*** and PCl₅. Hence, ³¹P{¹H} NMR spectroscopy of the reaction mixture prepared at -78 °C was carried out at variable temperatures from 193 K to r.t., proving that P₄ is indeed formed as an intermediate between 253 and 273 K.

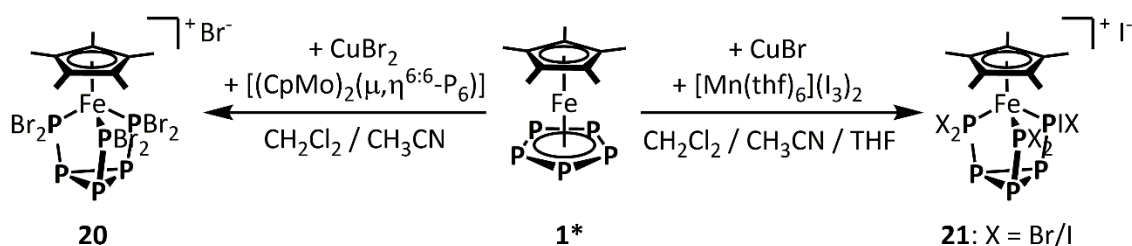
Moreover, layering a solution of **1*** in CH₂Cl₂ with a solution of WCl₆ in toluene lead to the crystallization of black crystals of [(Cp*Fe)₂(μ , $\eta^{5:5}$ -P₁₀)]₂[W₂Cl₉]₂ (**19a**, Scheme 11, left).^[26] The structure of the cation has already been reported as a SbF₆⁻-salt obtained by the oxidation of **1*** with thianthrenium hexafluoroantimonate ([C₁₂H₈S₂]⁺SbF₆⁻).^[3] In the crystal structure, however, residual electron density is found, suggesting to co-crystallization of **19a** with [Cp*Fe(η^5 -P₅Cl)]₂[W₂Cl₉]₂ (**19b**) in a 85:30 ratio. Unfortunately, the crystal quality was insufficient for an appropriate X-ray structure determination.



Scheme 11. Reactions of **1*** with [WCl₆] under varying conditions.

Interestingly, $^{31}\text{P}\{^1\text{H}\}$ NMR spectroscopy of the mother liquor again proved the presence of P_4 in the reaction mixture. Compound **19b** can be purely crystallized when **1*** is reacted with WCl_6 by stirring in CH_2Cl_2 (Scheme 11, right), but again the quality of the crystals only gave poor data. Hence, the structure interpretation of the X-ray data of **19a** and **19b** have to be regarded with caution. In both reactions the crystals decomposed and thus no product could be isolated. Likewise, $[(\text{Cp}^*\text{Fe})_2(\mu, \eta^{5:5}\text{-P}_{10})][\text{SbF}_6]_2$, the SbF_6^- analogue of **19a**, is reported to be unstable in various solvents.^[3]

When **1*** is reacted with CuBr_2 in the presence of $[(\text{CpMo})_2(\mu, \eta^{6:6}\text{-P}_6)]$, few crystals of $[\text{Cp}^*\text{FeP}_6\text{Br}_6]\text{Br}$ (**20**) are formed (Scheme 12, left). **20** is the bromine analogue of $[\text{Cp}^*\text{FeP}_6\text{I}_6]\text{I}$ (chapter 7, compound **3-I**), which was obtained reproducibly and selectively from the reaction of **1*** and I_2 . In contrast, all attempts to reproduce **20** by this method failed and reactions of **1*** with CuBr_2 also only resulted in the formation of $[\{\text{Cp}^*\text{Fe}(\eta^5\text{-P}_5)\}\text{CuBr}]_n$,^[27] next to PBr_3 and P_2Br_4 . In order to favor oxidation over coordination, **1*** and CuBr_2 were additionally reacted in pyridine / CH_3CN . Blue prisms of $[\text{Cu}(\text{NC}_5\text{H}_5)_4]\text{Br}_2 \cdot 2 \text{CH}_3\text{CN}$ had crystallized, as shown by preliminary X-ray diffraction data.^[28] The reactions of PBr_5 or Br_2 with **1*** resulted in the sole formation of PBr_3 and P_2Br_4 . With 8eq. Br_2 , the reaction takes place selectively forming PBr_3 and quantitatively, since no residual **1*** is detected in the $^{31}\text{P}\{^1\text{H}\}$ NMR spectrum of the reaction mixture anymore.



Scheme 12. Bromination (left) and mixed bromination / iodination (right) of **1***.

In the reaction of **1*** with CuCl in the presence of *in situ* generated $[\text{Mn}(\text{thf})_6](\text{I}_3)_2$,^[29] the CuI containing polymer $[\{\text{Cp}^*\text{Fe}(\eta^5\text{-P}_5)\}\text{CuI}]_n$ ^[30] is formed as only crystalline product. X-ray structure determination of the polymer was repeated, this time at 100 K instead of 150 K. In contrast, when the same reaction was performed with CuBr , crystals of $[\{\text{Cp}^*\text{Fe}(\eta^5\text{-P}_5)\}\text{CuI}]_n$ ^[31] and tiny black needles of $[\text{Cp}^*\text{FeP}_6\text{Br}_{2.47}\text{I}_{3.53}]\text{I}$ (**21**) were obtained (Scheme 12, right). Unfortunately, the isolation of pure **21** failed due to the contamination with other insoluble solids, wherefore elemental analysis did not furnish the expected results.

The preliminary X-ray structure data of **19b** suggest the formation of a $[\text{Cp}^*\text{Fe}(\eta^5\text{-P}_5\text{Cl})]^+$ cation and a $[\text{W}_2\text{Cl}_9]^-$ anion (Figure 8a). In the cation, one P atom of the P_5 ring is bent out of the plane and is bound to the Cl atom. The Cl atom is oriented in the endo-position of the P_5 ring motif. Due to the provisional nature of the structural model, no further details can be given at this point and some residual electron density still has to be assigned.

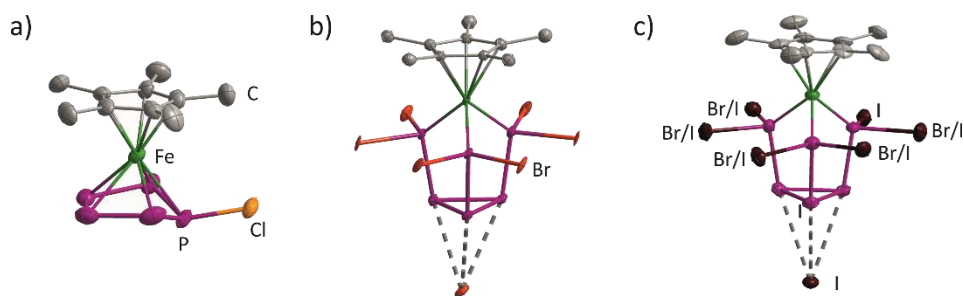


Figure 8. Molecular structure of a) the cation of **19b**; b) and c) the cations of **20** and **21** with close P...X contacts to the Br⁻ (**20**) and I⁻ (**21**) counterions indicated by grey dashed lines. A.d.p. ellipsoids at 50% probability level and H atoms omitted for clarity.

Compound **21** (Figure 8c) is isostructural to the irreproducible Br-compound **20** (Figure 8b) and the I-analogue [Cp*FeP₆I₆]I (chapter 7, compound **3-I**) and comprises an intermediary composition. The crystal of **21** can be regarded as solid solution of compounds [Cp*FeP₆Br_xI_{6-x}]I with a maximum Br content of $x = 5$ since no mixed Br/I occupancy is found for one of the six bound halide positions and for the I⁻ counterion. Interestingly, this I atom exhibits a specific I...I contact to the counterion with a distance of 3.3435(12) Å (sum of the van-der-Waals radii: 3.96 Å).^[32] The mixed sites show Br contents ranging from 17% to 71%. Similarly to [Cp*FeP₆I₆]I (cf. chapter 6) and **21**, also the Br analogue exhibits specific contacts, however this time as Br...Br⁻ contact of 3.4534(18) Å (sum of the van-der-Waals-radii: 3.70 Å).^[32] Moreover, the solid state structures of **20** and **21** both reveal short P...X⁻ (**20**: X = Br; **21**: X = I) contacts between the P₃ cycles and the counterions with distances of 3.088(3) – 3.254(3) Å (**20**, sum of the r_{vdW} : 3.65 Å)^[32] and 3.389(3) – 3.564(3) Å (**21**, sum of the r_{vdW} : 3.78 Å).^[32]

8.6 Experimental Part

General Remarks

All reactions were performed under an inert atmosphere of dry nitrogen or argon with standard vacuum, Schlenk and glove-box techniques. Solvents and THT were purified, dried and degassed prior to use by standard procedures. $[\text{Cp}^*\text{Fe}(\eta^5\text{-P}_5)]$ (**1***) and $[\text{Cp}^\times\text{Fe}(\eta^5\text{-P}_5)]$ (**1^x**) were synthesized following reported procedures,^[33] although the syntheses of **1*** and **1^x** were performed in *meta*-diisopropylbenzene with an improved yield of 75% and 56%, respectively. $[(\text{tht})_2\text{Au}]\text{SbF}_6$ ^[10] was synthesized freshly in analogy to the reported method and added *in situ* to the respective syntheses. $[\text{Au}(\text{CH}_3\text{CN})_2]\text{TEF}$ ^[8] was synthesized by an improved method based on the reported one (cf. chapter 6). $\text{Cs}[\text{P}_3\text{C}_2(\text{trip})_2]$ ^[34] and the mixture of $\text{K}[\text{P}_2\text{C}_3'\text{Pr}_3]$ / $\text{K}[\text{P}_3\text{C}_2'\text{Pr}_2]$ ^[23] were synthesized following reported procedures. $\text{K}[\text{P}_3\text{C}_2\text{Ad}_2]$ was synthesized analogously to the *t*-Bu derivative^[35] starting from the respective phosphalkene $\text{Me}_3\text{SiO}(\text{Ad})\text{C}=\text{P}(\text{SiMe}_3)$ ^[36] and $\text{KP}(\text{SiMe}_3)_2$.^[37] $[\text{Cp}^*\text{Fe}(\eta^5\text{-As}_5)]$ (**6**), $[\text{CpMo}(\text{CO})_2(\eta^3\text{-P}_3)]$ (**7**) and $[(\text{tht})\text{AuCl}]$ were kindly provided by Dr. M. Piesch, A. Garbagnati and Dr. M. Elsayed Moussa. GaCl_3 and PCl_5 are commercially available and were sublimed prior to use. All other chemicals are commercially available and used without further purification or were available in-house. Solution NMR spectra were recorded on a BRUKER Avance 300 or 400 spectrometer. Chemical shifts δ are given in [ppm] referring to external standards of tetramethylsilane (¹H NMR spectra), 85% phosphoric acid (³¹P{¹H} NMR spectra) or CFCl_3 (¹⁹F{¹H} NMR spectra).

Chapter 8.1

Synthesis of $[\{\text{Cp}^\times\text{Fe}(\eta^{5:1:1:1:1}\text{-P}_5)\text{Cu}_2(\mu\text{-Cl})(\mu,\eta^{1:1}\text{-GaCl}_4)]_n$ (**2^x**)

CuGaCl_4 (22 mg, 0.080 mmol) was dissolved in toluene (5 mL) and layered onto a solution of $[\text{Cp}^\times\text{Fe}(\eta^5\text{-P}_5)]$ (**1^x**, 30 mg, 0.083 mmol) in CH_2Cl_2 (6 mL). After three days, yellow needles of **2^x** had crystallized.

Synthesis of $[\{\text{Cp}^*\text{Fe}(\eta^{5:1:1:1:1}\text{-P}_5)\text{Cu}_2(\mu\text{-Cl})(\mu,\eta^{1:1}\text{-GaCl}_4)]_n$ (**3**)

CuGaCl_4 (40 mg, 0.15 mmol) was dissolved in CH_2Cl_2 (10 mL) and toluene (1 mL). A solution of $[\text{Cp}^*\text{Fe}(\eta^5\text{-P}_5)]$ (**1***, 49 mg, 0.14 mmol) in toluene (10 mL) was layered on top. After five days, yellow-brown plates of **3** had crystallized.

Synthesis of $[\{\text{Cp}^*\text{Fe}(\eta^{5:1:1:1:1}\text{-P}_5)\text{Cu}_2(\mu\text{-Cl})(\mu,\eta^{1:1}\text{-GaCl}_4)]_n$ (**2***)

CuGaCl_4 (82 mg, 0.30 mmol) was dissolved in CH_2Cl_2 (12 mL) and toluene (1 mL). A solution of $[\text{Cp}^*\text{Fe}(\eta^5\text{-P}_5)]$ (**1***, 17 mg, 0.049 mmol) in toluene (10 mL) was layered on top. After five days, yellow needles of **2*** had crystallized besides yellow rods of **A**^[1] and yellow-green plates of **3**.

Synthesis of $[(\text{Cp}^*\text{Fe}(\eta^{5:1:1:1:1}\text{-P}_5))\text{Cu}_2(\mu_3, \eta^{1:1:1}\text{-GaCl}_4)(\eta^1\text{-GaCl}_4)]_n \cdot 1.4 \text{C}_7\text{H}_8 \cdot 0.6 \text{C}_6\text{H}_4\text{Cl}_2$ (4**) and $[(\text{Cp}^*\text{Fe})_2(\mu, \eta^{5:5}\text{-P}_{10})](\text{GaCl}_4)_2$ (**5**)**

CuGaCl_4 (80 mg, 0.29 mmol) was dissolved in toluene (15 mL) and layered onto a solution of $[(\text{Cp}^*\text{Fe}(\eta^5\text{-P}_5))]$ (**1***, 50 mg, 0.14 mmol) and C_{70} (42 mg, 0.050 mmol) in CH_2Cl_2 (10 mL) and *o*-DCB (10 mL). After one day already, yellow plates of **4** had crystallized, in addition to brown plates of **5**, yellow rods of **A**^[1] and yellow-brown plates of **3**.

Chapter 8.2

Synthesis of $[(\text{Cp}^*\text{Fe}(\mu_3, \eta^{5:2:2}\text{-As}_5))_2\text{Au}_2](\text{GaCl}_4)_2 \cdot \text{C}_7\text{H}_8$ (8**)**

$[(\text{tht})\text{AuCl}]$ (36 mg, 0.11 mmol) and GaCl_3 (21 mg, 0.12 mmol) were dissolved in CH_2Cl_2 (3 mL) and stirred for 15 minutes. $[(\text{Cp}^*\text{Fe}(\eta^5\text{-As}_5))]$ (**6**, 32 mg, 0.06 mmol) was dissolved in CH_2Cl_2 (5 mL) and added under stirring. The red suspension was filtered into a thin Schlenk tube, concentrated (to 3 mL), and layered with toluene (6 mL). After four days, besides a Au^0 mirror, also few red-brown crystals of **8** had formed.

Analytical data of **8**:

Yield: few crystals

Synthesis of $[(\text{Cp}^*\text{Fe}(\mu_3, \eta^{5:2:2}\text{-As}_5))_2\text{Au}_2](\text{TEF})_2$ (9**)**

$[(\text{Cp}^*\text{Fe}(\eta^5\text{-As}_5))]$ (**6**, 12 mg, 0.021 mmol) and $[\text{Au}(\text{CH}_3\text{CN})_2]\text{TEF}$ (49 mg, 0.039 mmol) were dissolved in CH_2Cl_2 (4 mL) under stirring and the reaction mixture was immediately filtrated into a thin Schlenk tube. After layering with pentane (8 mL), besides a Au^0 mirror, also red-brown prisms of **9** had formed.

Analytical data of **9**:

Yield: few crystals

Synthesis of $[(\text{CpMo}(\text{CO})_2(\mu, \eta^{3:2}\text{-P}_3))_2\text{Au}_2](\text{SbF}_6)_2$ (10**)**

To a mixture of $[(\text{tht})\text{AuCl}]$ (31 mg, 0.097 mmol) and AgSbF_6 (36 mg, 0.10 mmol), SC_4H_8 (THT, 0.01 mL, 0.1 mmol) and CH_2Cl_2 (3 mL) were added and the mixture was stirred for 30 minutes. After filtration from the grey precipitate (AgCl), the yellowish solution of *in situ* generated $[(\text{tht})_2\text{Au}]\text{SbF}_6$ was layered with the solution of $[(\text{CpMo}(\text{CO})_2(\eta^3\text{-P}_3))]$ (**7**, 13 mg, 0.042 mmol) in toluene (3 mL) in a thin Schlenk tube. Immediately, an orange precipitate formed and after one day, orange prisms of **10** crystallized. After complete diffusion, the mother liquor was decanted and the solids were washed with toluene (3 x 10 mL), thereby suspended and transferred to another Schlenk tube, washed again with toluene (1 x 5 mL) and pentane (3 x 5 mL) and dried.

Analytical Data of the solids (**10** + precipitate):

Yield: 20 mg

Elemental Analysis: Calculated (%) for $(C_7H_5O_2MoP_5)_4(AuSbF_6)_2$ (2105 g/mol): C 15.97, H 0.96, S 0; found (%): C 14.34, H 1.28, S 1.35.

Chapter 8.3

Synthesis of $[P_3C_2(trip)_2](Cu_5I_4)(CH_3CN)_5 \cdot 2 CH_3CN$ (11) and $[P_3C_2(trip)_2]_2(Cu_6I_4)(CH_3CN)_4 \cdot 2n CH_3CN$ (12)

$Cs[P_3C_2(trip)_2]$ (81 mg, 0.098 mmol) was dissolved in DME (15 mL) and added to a solution of CuI (226 mg, 1.2 mmol) in CH_3CN (15 mL). After stirring for 24 hours, the solution was concentrated (to 15 mL) and layered with Et_2O (30 mL). Thereby, a grey precipitate was formed. After complete diffusion, the mother liquor was decanted, and the precipitate was dissolved in CH_3CN (10 mL). After six weeks at $-30\text{ }^\circ\text{C}$, orange prisms of **11** had formed. The crystals were washed with small amounts of CH_3CN and dried to give a red microcrystalline powder. Crystals of **11** were re-dissolved in CH_3CN (1 mL) and the solution was stored at $4\text{ }^\circ\text{C}$. After few months, yellow blocks of **12** had crystallized.

Analytical data of **11**:

Yield: 7 mg (5 μmol , 5%).

$^1\text{H NMR (CD}_3\text{CN):}$ δ [ppm] = 1.11 (d, $^3J_{\text{H,H}} = 6.9\text{ Hz}$, 12 H, $-\text{CH}(\text{CH}_3)_2$), 1.20 (d, $^3J_{\text{H,H}} = 6.8\text{ Hz}$, 12 H, $-\text{CH}(\text{CH}_3)_2$), 1.26 (d, $^3J_{\text{H,H}} = 7.0\text{ Hz}$, 12 H, $-\text{CH}(\text{CH}_3)_2$), 1.95 (s, 15 H, CH_3CN), 2.90 (sept, $^3J_{\text{H,H}} = 6.9\text{ Hz}$, 2 H, $p\text{-CH}(\text{CH}_3)_2$), 3.18 (sept, $^3J_{\text{H,H}} = 6.9\text{ Hz}$, 4 H, $o\text{-CH}(\text{CH}_3)_2$), 7.07 (s, 4 H, $m\text{-CH}_{\text{aryl}}$).

$^{31}\text{P}\{^1\text{H}\}$ NMR (CD_3CN): no signal detected.

Elemental Analysis: Calculated (%) for $(P_3C_3_2H_{46})(Cu_5I_4)(CH_3CN)$ (1390 g/mol): C 29.38, H 3.55, N 1.01; found (%): C 29.07, H 3.55, N 1.00.

Chapter 8.4

Synthesis of $[(\eta^5\text{-1,2,4-P}_3\text{C}_3\text{Ad}_2)\text{TiCl}_3]$ (13)

$K[1,2,4\text{-P}_3\text{C}_3\text{Ad}_2]$ (128 mg, 0.3 mmol) was taken up in toluene (5 mL) and added dropwise to a solution of $[\text{TiCl}_4]$ in toluene (2.7 mL, $c = 0.22\text{ mol/L}$, 0.6 mmol) at $-78\text{ }^\circ\text{C}$. While stirring overnight, the mixture was allowed to warm to room temperature. After removal of the solvent, the solid was washed with pentane (10 mL) and extracted with toluene.

Analytical data of **13**:

$^{31}\text{P}\{^1\text{H}\}$ NMR (C_6D_6): δ [ppm] = 302.8* (t, $^2J_{\text{P,P}} = 50\text{ Hz}$, 1 P), 338.0 (d, $^2J_{\text{P,P}} = 49\text{ Hz}$, 2 P). *Signal almost below noise floor.

Synthesis of $[(\eta^5\text{-}1,2,4\text{-P}_3\text{C}_2^i\text{Pr}_2)\text{TiCl}_3]$ (14**) and $[(\eta^5\text{-}1,3\text{-P}_2\text{C}_3^i\text{Pr}_3)\text{TiCl}_3]$ (**15**)**

A solution of $[\text{TiCl}_4]$ in toluene (1.4 mL, $c = 0.22$ mol/L, 0.3 mmol) was quickly added to a mixture of $\text{K}[1,3\text{-P}_2\text{C}_2^i\text{Pr}_3]$ and $\text{K}[1,2,4\text{-P}_3\text{C}_3^i\text{Pr}_2]$ (77 mg, 0.3 mmol) in toluene (5 mL) at -78°C . After stirring for 7 hours at -78°C , the solution was decanted from the precipitate and analyzed by $^{31}\text{P}\{^1\text{H}\}$ NMR spectroscopy. The mixture was allowed to warm to r.t. and after removal of the solvent, the solid was extracted with pentane (5 mL) and toluene (5 mL). Crystals of **15** were obtained from concentrated pentane solution within one week.

Analytical data of the reaction mixture kept at -78°C :

$^{31}\text{P}\{^1\text{H}\}$ NMR (C_6D_6): δ [ppm] = 253.1 (s, 2 P, **15**), 299.7* (t, $^2J_{\text{P,P}} = 51$ Hz, 1 P, **14**), 345.7 (d, $^2J_{\text{P,P}} = 50$ Hz, 2 P, **14**). *Signal almost below noise floor.

Analytical data of **15**:

^1H NMR (C_6D_6): δ [ppm] = 0.90 (d, $^3J_{\text{H,H}} = 6.8$ Hz, 6 H, $-\text{CH}(\text{CH}_3)_2$, **15**), 1.26 (d, $^3J_{\text{H,H}} = 6.8$ Hz, 6 H, $-\text{CH}(\text{CH}_3)_2$, **15**), 1.50 (d, $^3J_{\text{H,H}} = 6.6$ Hz, 6 H, $-\text{CH}(\text{CH}_3)_2$, **15**), 3.15 (m, 2 H, $-\text{CH}(\text{CH}_3)_2$, **15**), 3.39 (m, 1 H, $-\text{CH}(\text{CH}_3)_2$, **15**).

$^{31}\text{P}\{^1\text{H}\}$ NMR (C_6D_6): δ [ppm] = 254.7 (s, 2 P, **15**),

Synthesis of $[(\eta^5\text{-}1,3\text{-P}_2\text{C}_3^i\text{Pr}_3)\text{ZrCl}_3]$ (16**)**

A mixture of $\text{K}[1,3\text{-P}_2\text{C}_2^i\text{Pr}_3]$ and $\text{K}[1,2,4\text{-P}_3\text{C}_3^i\text{Pr}_2]$ (78 mg, 0.3 mmol) was taken up in toluene (3 mL) and added dropwise to a suspension of $[\text{ZrCl}_4]$ (74 mg, 0.3 mmol) in toluene (3 mL). After stirring for 2.5 days at room temperature, the mixture was filtered and washed with toluene (2 mL). After removal of the solvent, the products were dissolved in C_6D_6 (1 mL).

Analytical data of **16**:

^1H NMR (C_6D_6): δ [ppm] = 0.94 (d, $^3J_{\text{H,H}} = 6.8$ Hz, 6 H, $-\text{CH}(\text{CH}_3)_2$), 1.26 (d, $^3J_{\text{H,H}} = 6.8$ Hz, 6 H, $-\text{CH}(\text{CH}_3)_2$), 1.46 (d, $^3J_{\text{H,H}} = 6.7$ Hz, 6 H, isolated $-\text{CH}(\text{CH}_3)_2$), 3.07 (m, 2 H, $-\text{CH}(\text{CH}_3)_2$), 3.31 (sept, $^3J_{\text{H,H}} = 6.8$ Hz, 1 H, isolated $-\text{CH}(\text{CH}_3)_2$).

$^{31}\text{P}\{^1\text{H}\}$ NMR (C_6D_6): δ [ppm] = 225.9 (s, 2 P).

Synthesis of $[\text{Cp}(\eta^5\text{-}1,3\text{-P}_2\text{C}_3^i\text{Pr}_3)\text{ZrCl}_2]$ (17**) and $[\text{Cp}(\eta^5\text{-}1,2,4\text{-P}_3\text{C}_2^i\text{Pr}_2)\text{ZrCl}_2]$ (**18**)**

A mixture of $\text{K}[1,3\text{-P}_2\text{C}_2^i\text{Pr}_3]$ and $\text{K}[1,2,4\text{-P}_3\text{C}_3^i\text{Pr}_2]$ (14 mg, 0.05 mmol) was taken up in pentane (6 mL) and added dropwise to a suspension of $[\text{CpZrCl}_2]$ (15 mg, 0.05 mmol) in pentane (2 mL). After stirring for 5 hours at room temperature, the mixture was filtered and washed with hexane (4 mL). After removal of the solvent, the products were dissolved in C_6D_6 (1 mL).

Analytical data of **17** and **18**:

$^1\text{H NMR (C}_6\text{D}_6)$: δ [ppm] = 1.08 (d, $^3J_{\text{H,H}} = 6.8$ Hz, 6 H, $-\text{CH}(\text{CH}_3)_2$, **17**), 1.19 (d, $^3J_{\text{H,H}} = 6.7$ Hz, 6 H, $-\text{CH}(\text{CH}_3)_2$, **17**), 1.34 (d, $^3J_{\text{H,H}} = 6.9$ Hz, 12 H, $-\text{CH}(\text{CH}_3)_2$, **18**), 1.61 (d, $^3J_{\text{H,H}} = 6.7$ Hz, 6 H, $-\text{CH}(\text{CH}_3)_2$, **17**), 2.79 (sept, $^3J_{\text{H,H}} = 7.3$ Hz, 1 H, $-\text{CH}(\text{CH}_3)_2$, **17**), 3.25 (m, 2 H, $-\text{CH}(\text{CH}_3)_2$, **17**), 4.10 (m, 2 H, $-\text{CH}(\text{CH}_3)_2$, **18**), 6.09 (s, 5 H, $-\text{C}_5\text{H}_5$, **18**), 6.20 (s, 5 H, $-\text{C}_5\text{H}_5$, **17**).

$^{31}\text{P}\{^1\text{H}\}$ NMR (C_6D_6): δ [ppm] = 215.9 (s, 2 P, **17**), 248.2 (d, $^2J_{\text{P,P}} = 51$ Hz, 2 P, **18**), 289.1 (t, $^2J_{\text{P,P}} = 51$ Hz, 1 P, **18**).

Chapter 8.5

Reaction of $[\text{Cp}^*\text{Fe}(\eta^5\text{-P}_5)]$ (**1***) with XeF_2

$[\text{Cp}^*\text{Fe}(\eta^5\text{-P}_5)]$ (**1***, 30 mg, 0.087 mmol) was taken up in CH_3CN (10 mL), cooled to 4 °C and added to XeF_2 (44 mg, 0.26 mmol) in a plastic vial in the dark. The mixture was stirred in the dark for two days to give a yellow supernatant over a green solid of unreacted **1***.

$^1\text{H NMR (CD}_3\text{CN)}$: δ [ppm] = 1.36 (s, 15 H, **1***).

$^{31}\text{P}\{^1\text{H}\}$ NMR (CD_3CN): δ [ppm] = -143.2 (sept, $^1J_{\text{P,F}} = 706.4$ Hz, 1 P, PF_6^-), 151.8 (s, 5 P, **1***).

Ratio **1*** : PF_6^- = 1 : 14.

$^{19}\text{F}\{^1\text{H}\}$ NMR (CD_3CN): δ [ppm] = -71.7 (d, $^1J_{\text{P,F}} = 706.6$ Hz, 6 F, PF_6^-).

$^1\text{H NMR (CD}_2\text{Cl}_2)$: δ [ppm] = 1.43 (s, 15 H, **1***).

$^{31}\text{P}\{^1\text{H}\}$ NMR (CD_2Cl_2): δ [ppm] = -143.6 (sept, $^1J_{\text{P,F}} = 712.1$ Hz, 1 P, PF_6^-), 152.2 (s, 5 P, **1***).

Ratio **1*** : PF_6^- = 19 : 1.

$^{19}\text{F}\{^1\text{H}\}$ NMR (CD_2Cl_2): δ [ppm] = -71.7 (d, $^1J_{\text{P,F}} = 706.8$ Hz, 6 F, PF_6^-).

Reaction of $[\text{Cp}^*\text{Fe}(\eta^5\text{-P}_5)]$ (**1***) with PCl_5

$[\text{Cp}^*\text{Fe}(\eta^5\text{-P}_5)]$ (**1***, 19 mg, 0.055 mmol) and PCl_5 (28 mg, 0.13 mmol) were dissolved in CH_2Cl_2 (10 mL) and stirred for 1 hour. After concentrating to 2 mL, NMR spectroscopy was performed.

$^{31}\text{P}\{^1\text{H}\}$ NMR ($\text{C}_6\text{D}_6\text{-cap.}$): δ [ppm] = -521 (s, 4 P, P_4), 152.8 (s, 5 P, **1***), 222.3 (s, PCl_3).

Reaction of $[\text{Cp}^*\text{Fe}(\eta^5\text{-P}_5)]$ (**1***) with $[\text{WCl}_6]$

$[\text{Cp}^*\text{Fe}(\eta^5\text{-P}_5)]$ (**1***, 30 mg, 0.087 mmol) was dissolved in CH_2Cl_2 (13 mL) and layered with a solution of $[\text{WCl}_6]$ (101 mg, 0.25 mmol) in toluene (13 mL). Thereby, black intergrown crystals of **19** formed besides a brown precipitate.

Analytical data of the mother liquor:

$^{31}\text{P}\{^1\text{H}\}$ NMR ($\text{C}_6\text{D}_6\text{-cap.}$): δ [ppm] = -522.4* (s, 4 P, P_4), 152.7 (s, 5 P, **1***), 220.1 (s, 1 P, PCl_3).

*Signal almost below noise floor.

Synthesis of [Cp*Fe(η^5 -P₅Cl)] (19b)

[WCl₆] (100 mg, 0.25 mmol) was dissolved in CH₂Cl₂ (20 mL) and added to a solution of [Cp*Fe(η^5 -P₅)] (**1***, 30 mg, 0.087 mmol) in CH₂Cl₂ (10 mL). Thereby, a brown precipitate was formed. After two weeks, few crystals of **19b** had formed.

Synthesis of [Cp*FeP₆Br₆]Br (20)

[Cp*Fe(η^5 -P₅)] (**1***, 30 mg, 0.087 mmol) was dissolved in CH₂Cl₂ (10 mL) and layered with a solution of [(CpMo)₂(μ , $\eta^{6:6}$ -P₆)] (7 mg, 0.014 mmol) and CuBr₂ (39 mg, 0.17 mmol) in a mixture of CH₃CN (10 mL) and CH₂Cl₂ (3 mL). After complete diffusion, crystals of **20** had formed.

Synthesis of [Cp*FeP₆Br_{2.47}I_{3.53}]I (21)

A freshly prepared suspension of [Mn(thf)₆](I₃)₂^[29] in THF (1 mL) was added to a solution of CuBr (42 mg, 0.29 mmol) in CH₃CN (10 mL). The resulting clear red solution was layered onto a solution of [Cp*Fe(η^5 -P₅)] (**1***, 50 mg, 0.14 mmol) in CH₂Cl₂ (10 mL). Within one day, brown-black crystals of [(Cp*Fe(η^5 -P₅))CuI]_n^[31] and **21** had formed besides a red precipitate. After complete diffusion, the mother liquor was decanted and the solids were washed with a mixture of CH₂Cl₂ / CH₃CN (2:1, 3 x 5 mL) and dried. The solids were insoluble even in CH₃CN preventing further purification.

Analytical data of the solids:

Yield: 12 mg

Elemental analysis: Calculated (%) for [C₁₀H₁₅FeP₆Br_{2.47}I_{3.53}]I (1149 g/mol): C 10.45, 1.32 H; found (%): C 22.67, H 2.77.

8.7 Crystallographic Details

Crystals of all investigated compounds were taken from a Schlenk flask under a stream of nitrogen and immediately covered with mineral oil. The quickly chosen single crystals covered by a thin layer of oil were taken to the pre-centered goniometer head with suitable CryoMount® and directly mounted on the goniometer into a stream of cold nitrogen.

The data for **2^x**, **3-5**, **8**, **11**, **12**, **19b** and **20** were collected on a Rigaku Oxford Diffraction diffractometer equipped with a Titan⁵² CCD detector and a SuperNova CuK α microfocus source using ϕ -scans of 0.5 or 1° frames depending on the unit cell constants. The data for **15** were collected on a Bruker APEX-II diffractometer equipped with a CCD detector and a MoK α microfocus sealed tube using combined ϕ and ω scans of 0.5° frames. The X-ray experiments for **2^x**, **3-5**, **8** were performed at 90 K, for **11**, **12**, **19b** and **20** at 123 K, for **15** at 100 K.

The data processing and reduction of **2^x**, **4**, **5**, **8**, **10**, **11**, **12**, **19b** and **20** were performed with CrysAlisPRO software.^[38] Numerical absorption correction based on gaussian integration over a multifaceted crystal model and an empirical absorption correction using spherical harmonics as implemented in SCALE3 ABSPACK were applied for **11** and **12**. For **15**, data processing and reduction were performed with Bruker APEX3 and Bruker SAINT software and multi-scan absorption correction was applied using SADABS program.^[39]

The single crystals of **10** and **21** were carefully selected, mounted on a magnetic holder, checked for quality, and placed into a Dewar vessel in liquid nitrogen using standard cryocrystallography tools. Then they were transported to DESY PETRA III synchrotron. Using standard procedures, they were placed into a Dewar vessel filled with liquid nitrogen among other crystals. A robotic mounting/demounting was used for further manipulations in the P11 beamline hutch.^[40] X-ray diffraction experiment measured using one-circle diffractometer and DECTRIS PILATUS 6M pixel array detector at 80.0(2) K. The data were acquired by 360° ϕ -rotation with 0.3° scan width and exposure 0.13 s per frame at the wavelengths $\lambda = 0.68880$ Å (18 keV for **10**) and $\lambda = 0.619919$ Å (20 keV for **21**), respectively.

The structures were solved with SHELXT^[41] and least-square refinements on F^2 were carried out with SHELXL.^[42] Crystal structures of **11** and **21** were refined as inversion twins. Crystals of **10** were systematically twinned according to a twin matrix [0 1 0, -1 0 0, 0 0 1]. The de-twin procedure in CrysAlis did not give good separation of the diffraction maxima, and the preliminary structure refinement was performed using the reflections of the major twin component only. The hydrogen atoms were located in idealized positions and refined isotropically with a riding model.

CIF files with comprehensive information on the details of the diffraction experiments and full tables of bond lengths and angles for **2^x**, **3** and **4** are deposited in Cambridge Crystallographic

Data Center under the deposition codes CCDC 2038696, CCDC 2038695 and CCDC 2038693, respectively. These data are provided free of charge by The Cambridge Crystallographic Data Centre (<https://www.ccdc.cam.ac.uk/>). Crystallographic data and details of the diffraction experiments of compounds **5** – **21** are given in tables 1 – 6.

Table 1. Experimental details for **2^x** and **3**.

Crystal data	2^x	3
CCDC codes	CCDC-2038696	CCDC-2038695
Structural formula	(C ₁₁ H ₁₇ FeP ₅)Cu ₂ Cl(GaCl ₄)	[(C ₁₀ H ₁₅ FeP ₅)Cu ₂ Cl(GaCl ₄)]
Chemical formula	C ₁₁ H ₁₇ Cl ₅ Cu ₂ FeGaP ₅	C ₁₀ H ₁₅ Cl ₅ Cu ₂ FeGaP ₅
<i>M_r</i>	733.99	719.97
Crystal system, space group	Orthorhombic, <i>Pbcm</i>	Orthorhombic, <i>Pnma</i>
Temperature (K)	90	90
<i>a</i> , <i>b</i> , <i>c</i> (Å)	12.0704 (5), 15.9084 (4), 12.5439 (4)	22.7939(4) 10.9858(3) 8.54325(19)
<i>V</i> (Å ³)	2408.68 (13)	2139.33 (8)
<i>Z</i>	4	4
<i>F</i> (000)	1432	1400
<i>D_x</i> (Mg m ⁻³)	2.024	2.235
Radiation type	Cu <i>K</i> α	Cu <i>K</i> α
μ (mm ⁻¹)	16.23	18.23
Crystal shape and colour	Yellow needle	Yellow-brown rhombic plate
Crystal size (mm)	0.17 × 0.03 × 0.02	0.11 × 0.08 × 0.02
Data collection		
Diffractometer	SuperNova, Titan ^{S2}	SuperNova, Titan ^{S2}
Absorption correction	Gaussian	Gaussian
<i>T_{min}</i> , <i>T_{max}</i>	0.214, 0.809	0.328, 0.738
No. of measured, independent and observed [<i>I</i> > 2σ(<i>I</i>)] reflections	7011, 2506, 1927	5323, 2274, 1803
<i>R_{int}</i>	0.046	0.034
(sin θ/λ) _{max} (Å ⁻¹)	0.628	0.627
Range of <i>h</i> , <i>k</i> , <i>l</i>	<i>h</i> = -10→14, <i>k</i> = -19→14, <i>l</i> = -15→15	<i>h</i> = -27→28, <i>k</i> = -13→11, <i>l</i> = -10→4
Refinement		
<i>R</i> [<i>F</i> ² > 2σ(<i>F</i> ²)], <i>wR</i> (<i>F</i> ²), <i>S</i>	0.039, 0.096, 0.98	0.034, 0.090, 0.98
No. of reflections	2505	2274
No. of parameters	137	123
No. of restraints	0	0
H-atom treatment	H-atom constrained	parameters H-atom parameters constrained
Δ _{max} , Δ _{min} (e Å ⁻³)	0.68, -0.60	0.86, -0.85

Computer programs for **2^x**: *CrysAlis PRO* 1.171.39.37b (Rigaku OD, 2017), *SHELXT2014/7* (Sheldrick, 2014), *SHELXL2014/7* (Sheldrick, 2014); for **3**: *CrysAlis PRO* 1.171.39.37b (Rigaku OD, 2017), *SHELXL2014/7* (Sheldrick, 2014), *SHELXL2014/7* (Sheldrick, 2014).

Table 2. Experimental details of 4 and 5.

Crystal data	4	5
CCDC codes	CCDC-2038693	-
Structural formula	$[(C_{10}H_{15}FeP_5)Cu_2(GaCl_4)_2] \cdot 1.4(C_7H_8) \cdot 0.6(C_6H_4Cl_2)$	$[(C_{10}H_{15}FeP_5)_2](GaCl_4)_2$
Chemical formula	$C_{23.4}H_{28.6}Cl_{9.2}Cu_2FeGa_2P_5$	$C_{20}H_{30}Cl_8Fe_2Ga_2P_{10}$
M_r	1113.22	1114.88
Crystal system, space group	Monoclinic, $C2/c$	Monoclinic, $P2_1/n$
Temperature (K)	90	90
a, b, c (Å)	33.4184 (5), 11.63537 (14), 20.3494 (3)	12.7280 (6), 11.5415 (6), 13.0786 (8)
β (°)	103.7343 (15)	94.133 (5)
V (Å ³)	7686.32 (19)	1916.25 (17)
Z	8	2
$F(000)$	4371	1100
D_x (Mg m ⁻³)	1.924	1.932
Radiation type	Cu $K\alpha$	Cu $K\alpha$
μ (mm ⁻¹)	13.77	16.80
Crystal shape and colour	Yellow plate	Brown plate
Crystal size (mm)	0.22 × 0.16 × 0.03	0.07 × 0.03 × 0.02
Data collection		
Diffractometer	SuperNova, Titan ^{S2}	SuperNova, Titan ^{S2}
Absorption correction	Gaussian	Gaussian
T_{min}, T_{max}	0.169, 0.832	0.505, 0.752
No. of measured, independent and observed [$I > 2\sigma(I)$] reflections	17828, 7801, 7411	6618, 3746, 2515
R_{int}	0.029	0.064
$(\sin \theta/\lambda)_{max}$ (Å ⁻¹)	0.627	0.628
Range of h, k, l	$h = -35 \rightarrow 41,$ $k = -12 \rightarrow 14,$ $l = -25 \rightarrow 17$	$h = -15 \rightarrow 11,$ $k = -14 \rightarrow 12,$ $l = -15 \rightarrow 15$
Refinement		
$R[F^2 > 2\sigma(F^2)], wR(F^2), S$	0.048, 0.130, 1.03	0.045, 0.107, 0.94
No. of reflections	7801	3746
No. of parameters	405	195
No. of restraints	0	0
H-atom treatment	H-atom constrained	H-atom parameters constrained
$\Delta_{max}, \Delta_{min}$ (e Å ⁻³)	2.41, -1.29	0.59, -0.57

Computer programs for 4: *CrysAlis PRO* 1.171.39.37b (Rigaku OD, 2017), *SHELXT2014/7* (Sheldrick, 2014), *SHELXL2014/7* (Sheldrick, 2014); for 5: *CrysAlis PRO* 1.171.39.37b (Rigaku OD, 2017), *SHELXT2014/7* (Sheldrick, 2014), *SHELXL2014/7* (Sheldrick, 2014).

Table 3. Experimental details for **8** and preliminary experimental details for **10** (* = preliminary data).

Crystal data	8	10 *
Structural formula	$[(C_{10}H_{15}FeAs_5)_2Au_2](GaCl_4)_2 \cdot (C_7H_8)$	$\{[(C_5H_5)Mo(CO)_2(P_3)]_2Au\}(SbF_6)$
Chemical formula	$C_{27}H_{38}As_{10}Au_2Cl_8Fe_2Ga_2$	$C_{14}H_{10}O_4F_6P_6Mo_2SbAu$
M_r	2040.44	> 742.68
Crystal system, space group	Monoclinic, $C2/c$	Orthorhombic, $Pban$
Temperature (K)	90	80
a, b, c (Å)	34.5179 (9), 18.4540 (3), 16.3182 (4)	19.54839(9), 27.10855(17), 29.3776(2)
β (°)	113.076 (3)	90
V (Å ³)	9562.9 (4)	15568.03(18)
Z	8	16
$F(000)$	7504	> 5344
D_x (Mg m ⁻³)	2.834	> 1.267
Radiation type	Cu $K\alpha$	Synchrotron, $\lambda = 0.68880$ Å
μ (mm ⁻¹)	29.18	> 4.512
Crystal shape and colour	Brown prism	brown prism
Crystal size (mm)	0.09 × 0.05 × 0.02	0.20 × 0.10 × 0.10
Data collection		
Diffractometer	SuperNova, Titan ^{S2}	P11 beamline, PETRA III DESY, PILATUS 6M pixel array detector
Absorption correction	Gaussian	multi-scan
T_{min}, T_{max}	0.189, 0.640	0.796, 1.000
No. of measured, independent and observed [$I > 2\sigma(I)$] reflections	17714, 9243, 6685	101074, 21240, 16623
R_{int}	0.048	0.0986
$(\sin \theta/\lambda)_{max}$ (Å ⁻¹)	0.624	0.762
Range of h, k, l	$h = -40 \rightarrow 42,$ $k = -22 \rightarrow 16,$ $l = -20 \rightarrow 18$	$h = -25 \rightarrow 26,$ $k = -31 \rightarrow 37,$ $l = -39 \rightarrow 38$
Refinement		
$R[F^2 > 2\sigma(F^2)], wR(F^2), S$	0.057, 0.168, 1.09	0.0900, 0.2739, 1.117
No. of reflections	9243	21240
No. of parameters	511	782
No. of restraints	52	0
H-atom treatment	H-atom constrained	parameters not refined
$\Delta_{max}, \Delta_{min}$ (e Å ⁻³)	2.91, -1.65	8.88, -5.74

Computer programs for **8**: *CrysAlis PRO* 1.171.39.45g (Rigaku OD, 2018), *SHELXT2015/3* (Sheldrick, 2015), *SHELXL2014/7* (Sheldrick, 2014); for **10**: Computer programs: *CrysAlisPro* 1.171.41.21a (Rigaku OD, 2019), *'SHELXL-2018/3* (Sheldrick, 2018)'.

Table 4. Experimental details for **11** and **12**.

Crystal data	11	12
Structural formula	$[\{P_3C_2(C_{15}H_{23})_2\}Cu_5I_4(CH_3CN)_5] \cdot 2CH_3CN$	$[\{P_3C_2(C_{15}H_{23})_2\}Cu_3I_2(CH_3CN)_2] \cdot CH_3CN$
Chemical formula	$C_{42}H_{61}Cu_5I_4N_5P_3 \cdot 2(C_2H_3N)$	$C_{36}H_{52}Cu_3I_2N_2P_3 \cdot CH_3CN$
M_r	1636.27	1091.18
Crystal system, space group	Orthorhombic, $Pna2_1$	Monoclinic, $C2/c$
Temperature (K)	123	123
a, b, c (Å)	20.8549 (4), 13.3221 (2), 21.5088 (4)	28.5800 (4), 10.52543 (14), 31.5396 (5)
β (°)	90	90 106.7896 (15) 90
V (Å ³)	5975.84 (17)	9083.2 (2)
Z	4	8
$F(000)$	3176	4336
D_x (Mg m ⁻³)	1.819	1.596
Radiation type	Cu $K\alpha$	Cu $K\alpha$
μ (mm ⁻¹)	19.22	13.51
Crystal shape and colour	Orange prism	Yellow truncated prism
Crystal size (mm)	0.23 × 0.18 × 0.07	0.14 × 0.10 × 0.06
Data collection		
Diffractometer	SuperNova, Titan ^{S2}	SuperNova, Titan ^{S2}
Absorption correction	Gaussian	Gaussian
T_{min}, T_{max}	0.550, 0.834	0.218, 0.548
No. of measured, independent and observed [$I > 2\sigma(I)$] reflections	12569, 5169, 4953	49339, 9072, 8774
R_{int}	0.029	0.024
$(\sin \theta/\lambda)_{max}$ (Å ⁻¹)	0.549	0.623
Range of h, k, l	$h = -9 \rightarrow 22,$ $k = -14 \rightarrow 13,$ $l = -23 \rightarrow 12$	$h = -35 \rightarrow 35,$ $k = -12 \rightarrow 12,$ $l = -37 \rightarrow 38$
Refinement		
$R[F^2 > 2\sigma(F^2)], wR(F^2), S$	0.026, 0.062, 1.02	0.021, 0.051, 1.02
No. of reflections	5169	9072
No. of parameters	596	457
No. of restraints	1	0
H-atom treatment	H-atom constrained	parameters H-atom parameters constrained
$\Delta_{max}, \Delta_{min}$ (e Å ⁻³)	0.89, -0.48	1.26, -0.93
Absolute structure	Refined as an inversion twin	-
Absolute structure parameter	0.498 (6)	-

Computer programs for **11**: Computer programs: *CrysAlis PRO* 1.171.39.8e (Rigaku OD, 2015), *SHELXT2018/5* (Sheldrick, 2018), *SHELXL2018/3* (Sheldrick, 2018); for **12**: *CrysAlis PRO* 1.171.39.8e (Rigaku OD, 2015), *SHELXL2018/3* (Sheldrick, 2018).

Table 5. Experimental details for **15** and preliminary experimental details for **19b** (* = preliminary data).

Crystal data	15	19b *
Structural formula	[(P ₂ C ₃ (C ₃ H ₇) ₃)TiCl ₃]	[C ₁₀ H ₁₅ FeP ₅ Cl][W ₂ Cl ₉]
Chemical formula	C ₁₂ H ₂₁ Cl ₃ P ₂ Ti	C ₁₀ H ₁₅ FeP ₅ Cl ₁₀ W ₂
<i>M_r</i>	381.48	8544.95
Crystal system, space group	Triclinic, <i>P</i> $\bar{1}$	Monoclinic, <i>C2/c</i>
Temperature (K)	100	123
<i>a</i> , <i>b</i> , <i>c</i> (Å)	8.2370 (3)	24.363(2)
	14.0216 (5)	16.3684(6)
	15.6986 (6)	17.928(3)
α , β , γ (°)	98.601 (2), 105.0720 (10), 90.448 (2)	90, 131.518(17), 90
<i>V</i> (Å ³)	1728.99 (11)	5353.0(17)
<i>Z</i>	4	8
<i>F</i> (000)	784.0	3952
<i>D_x</i> (Mg m ⁻³)	1.465	2.651
Radiation type	Mo <i>K</i> α	Cu <i>K</i> α
μ (mm ⁻¹)	1.126	32.81
Crystal shape and colour	Red block	black block
Crystal size (mm)	0.07 × 0.07 × 0.03	0.125 × 0.093 × 0.047
Data collection		
Diffractometer	Bruker APEX-II, CCD	SuperNova, Atlas
Absorption correction	Multi-scan	gaussian
<i>T_{min}</i> , <i>T_{max}</i>	0.679, 0.715	0.103, 0.380
No. of measured, independent and observed [<i>I</i> > 2 σ (<i>I</i>)] reflections	26010, 9893, 8819	15773, 5335, 4907
<i>R_{int}</i>	0.026	0.0479
(<i>sin</i> θ / λ) _{max} (Å ⁻¹)	0.704	0.600
Range of <i>h</i> , <i>k</i> , <i>l</i>	<i>h</i> = -11→11, <i>k</i> = -19→17, <i>l</i> = -19→22	<i>h</i> = -29→30, <i>k</i> = -14 → 20, <i>l</i> = -21→21
Refinement		
<i>R</i> [<i>F</i> ² > 2 σ (<i>F</i> ²)], <i>wR</i> (<i>F</i> ²), <i>S</i>	0.026, 0.069, 1.08	0.0537, 0.1286, 1.076
No. of reflections	9893	5335
No. of parameters	337	298
No. of restraints	0	0
H-atom treatment	H-atom constrained	parameters H-atom parameters constrained
Δ _{max} , Δ _{min} (e Å ⁻³)	0.75, -0.94	1.835, -2.11

Computer programs for **15**: Bruker APEX3 (v2016.1-0), Bruker SAINT V8.35A, SHELXT-2014/4 (Sheldrick 2014), SHELXL-2014/7 (Sheldrick 2014); for **19b**: CrysAlisPro 1.171.39.45g (Rigaku OD, 2018), SHELXL-2018/3 (Sheldrick, 2018).

Table 6. Experimental details for **20** and **21**.

Crystal data	20	21
Structural formula	[C ₁₀ H ₁₅ FeP ₆ Br ₆]Br	[C ₁₀ H ₁₅ FeP ₆ Br _{2.47} I _{3.53}]
Chemical formula	C ₁₀ H ₁₅ Br ₇ FeP ₆	C ₁₀ H ₁₅ Br _{2.47} FeI _{4.53} P ₆
M_r	936.26	1149.12
Crystal system, space group	Orthorhombic, <i>Pna</i> 2 ₁	Orthorhombic, <i>Pna</i> 2 ₁
Temperature (K)	123	80
a, b, c (Å)	16.2829 (3), 9.58590 (15), 14.8033 (2)	16.75252 (12) 10.02378 (7) 15.26967 (11)
V (Å ³)	2310.58 (6)	2564.14 (3)
Z	4	4
$F(000)$	1744	2070
D_x (Mg m ⁻³)	2.691	2.977
Radiation type	Cu $K\alpha$	Synchrotron $\lambda = 0.6199$ Å
μ (mm ⁻¹)	23.33	7.124
Crystal shape and colour	dark prism	Black needle
Crystal size (mm)	0.28 × 0.12 × 0.06	0.07 × 0.02 × 0.02
Data collection		
Diffractometer	SuperNova, Titan ^{S2}	P11 beamline, PETRA III DESY, pixel array detector
Absorption correction	Gaussian	Multi scan
T_{\min}, T_{\max}	0.058, 0.396	0.56927, 1.00000
No. of measured, independent and observed [$I > 2\sigma(I)$] reflections	4694, 2995, 2881	39394, 6368, 5013
R_{int}	0.029	0.059
$(\sin \theta/\lambda)_{\text{max}}$ (Å ⁻¹)	0.623	0.667
Range of h, k, l	$h = -5 \rightarrow 19,$ $k = -11 \rightarrow 11,$ $l = -10 \rightarrow 18$	$h = -22 \rightarrow 22,$ $k = -13 \rightarrow 13,$ $l = -20 \rightarrow 20$
Refinement		
$R[F^2 > 2\sigma(F^2)], wR(F^2), S$	0.050, 0.132, 1.06	0.034, 0.084, 0.92
No. of reflections	2995	6368
No. of parameters	222	223
No. of restraints	115	1
H-atom treatment	H-atom parameters constrained	H-atom parameters constrained
$\Delta_{\text{max}}, \Delta_{\text{min}}$ (e Å ⁻³)	1.63, -2.36	2.83, -0.83
Absolute structure	Classical Flack preferred over because s.u. lower.	Refined as a 2-component inversion twin
Absolute structure parameter/ twin batch	0.010 (14)	0.61 (3)

Computer programs for **20**: *CrysAlis PRO* 1.171.38.41 (Rigaku OD, 2015), *SHELXT*, *SHELXL2018/3* (Sheldrick, 2018); for **21**: *CrysAlis PRO* 1.171.38.46 (Rigaku OD, 2015), *SHELXL-2016/6* (Sheldrick, 2016).

8.8 Author Contributions

- The synthesis of compounds **2^x**, **2^{*}**, **3**, **4** and **5** was performed by Helena Brake and by Robert Szlosek under supervision of Helena Brake and are also part of his Bachelor thesis.
- The synthesis and characterization of compounds **8 – 21** (with exception of compound **20**) was performed by Helena Brake. The synthesis and characterization of compounds **13 – 18** was performed by Helena Brake during a research stay in the group of Prof. T. Don Tilley (University of California, Berkeley, USA).
- The synthesis of **20** was performed by Dr. Claudia Heindl.
- The reaction of **1^{*}** with XeF₂ was performed by Helena Brake and by Lisa Zimmermann under supervision of Helena Brake and is also part of her Bachelor thesis.
- X-ray structural analysis of **2^x**, **2^{*}**, **3**, **4**, **5**, **8**, **20** and **21** was performed by Dr. Eugenia Peresykina and Dr. Sc. Alexander V. Virovets. The crystal of compound **21** was measured at DESY PETRA III synchrotron. EP and AV are grateful to the P11 beamline team for their assistance.
- X-ray structural analysis of **9 – 12**, **19** and **19b** was performed by Helena Brake, Dr. Eugenia Peresykina and Dr. Sc. Alexander V. Virovets.
- X-ray structural analysis of **15** was performed by Dr. Micah Ziegler (group of Prof. T. Don Tilley, University of California, Berkeley, USA).
- The manuscript was written by Helena Brake.
- The section ‘Crystallographic Details’ was written by Dr. Eugenia Peresykina and Helena Brake.

8.9 References

- [1] C. Heindl, S. Heintl, D. Lüdeker, G. Brunklaus, W. Kremer, M. Scheer, *Inorg. Chim. Acta* **2014**, *422*, 218-223.
- [2] M. Mantina, A. C. Chamberlin, R. Valero, C. J. Cramer, D. G. Truhlar, *J. Phys. Chem. A* **2009**, *113*, 5806-5812; and references therein.
- [3] M. V. Butovskiy, G. Balázs, M. Bodensteiner, E. V. Peresyphkina, A. V. Virovets, J. Sutter, M. Scheer, *Angew. Chem. Int. Ed.* **2013**, *52*, 2972-2976.
- [4] O. J. Scherer, C. Blath, G. Wolmershäuser, *J. Organomet. Chem.* **1990**, *387*, C21-C24.
- [5] a) H. Krauss, G. Balázs, M. Bodensteiner, M. Scheer, *Chem. Sci.* **2010**, *1*, 337-342; b) M. Fleischmann, J. S. Jones, F. P. Gabbai, M. Scheer, *Chem. Sci.* **2015**, *6*, 132-139.
- [6] O. J. Scherer, H. Sitzmann, G. Wolmershäuser, *J. Organomet. Chem.* **1984**, *268*, C9-C12.
- [7] L. J. Gregoriades, B. K. Wegley, M. Sierka, E. Brunner, C. Gröger, E. V. Peresyphkina, A. V. Virovets, M. Zabel, M. Scheer, *Chem. Asian J.* **2009**, *4*, 1578-1587.
- [8] T. A. Engesser, C. Friedmann, A. Martens, D. Kratzert, P. J. Malinowski, I. Krossing, *Chem. Eur. J.* **2016**, *22*, 15085-15094.
- [9] Unit cell parameters: aP, a = 11.50 Å, b = 13.53 Å, c = 17.24 Å, $\alpha = 68.7^\circ$, $\beta = 86.3^\circ$, $\gamma = 89.8^\circ$, V = 2494 Å³ or aP, a = 17.24 Å, b = 17.74 Å, c = 17.74 Å, $\alpha = 80.39^\circ$, $\beta = 71.75^\circ$, $\gamma = 76.11^\circ$, V = 4977 Å³.
- [10] N. Savjani, S. P. Bew, D. L. Hughes, S. J. Lancaster, M. Bochmann, *Organometallics* **2012**, *31*, 2534-2537.
- [11] H. Schmidbaur, A. Schier, *Chem. Soc. Rev.* **2012**, *41*, 370-412.
- [12] C. Schwarzmaier, M. Sierka, M. Scheer, *Angew. Chem. Int. Ed.* **2013**, *52*, 858-861.
- [13] G. Ferguson, J. F. Gallagher, J. D. Kennedy, A.-M. Kelleher, T. R. Spalding, *Dalton Transactions* **2006**, 2133-2139.
- [14] M. Di Vaira, P. Stoppioni, M. Peruzzini, *J. Chem. Soc., Dalton Trans.* **1990**, 109-113.
- [15] C. Heindl, E. V. Peresyphkina, A. V. Virovets, G. Balázs, M. Scheer, *Chem. Eur. J.* **2016**, *22*, 1944-1948.
- [16] C. Heindl, A. Kuntz, E. V. Peresyphkina, A. V. Virovets, M. Zabel, D. Lüdeker, G. Brunklaus, M. Scheer, *Dalton Trans.* **2015**, *44*, 6502-6509.
- [17] C.-M. Che, S.-W. Lai, *Coord. Chem. Rev.* **2005**, *249*, 1296-1309.
- [18] a) T. D. Tilley, *Acc. Chem. Res.* **1993**, *26*, 22-29; b) T. Imori, T. D. Tilley, *Chem. Commun.* **1993**, 1607-1609.

- [19] a) A. D. Sadow, T. D. Tilley, *Organometallics* **2003**, *22*, 3577-3585; b) N. R. Neale, T. D. Tilley, *J. Am. Chem. Soc.* **2002**, *124*, 3802-3803; c) N. R. Neale, T. D. Tilley, *Tetrahedron* **2004**, *60*, 7247-7260; d) N. R. Neale, T. D. Tilley, *J. Am. Chem. Soc.* **2005**, *127*, 14745-14755.
- [20] a) C. Janiak, U. Versteeg, K. C. H. Lange, R. Weimann, E. Hahn, *J. Organomet. Chem.* **1995**, *501*, 219-234; b) C. Janiak, K. C. H. Lange, U. Versteeg, D. Lentz, P. H. M. Budzelaar, *Chem. Ber.* **1996**, *129*, 1517-1529; c) E. J. M. de Boer, I. J. Gilmore, F. M. Korndorffer, A. D. Horton, A. van der Linden, B. W. Royan, B. J. Ruisch, L. Schoon, R. W. Shaw, *J. Mol. Catal. A: Chem.* **1998**, *128*, 155-165; d) W. P. Freeman, Y. J. Ahn, T. K. Hollis, J. A. Whitaker, V. C. Vargas, R. J. Rubio, K. D. Alingog, E. B. Bauer, F. S. Tham, *J. Organomet. Chem.* **2008**, *693*, 2415-2423; e) K. Yokota, Kiyohiko. *Eur. Pat. Appl.* **1994**, EP 590486 A2 19940406; f) J.A.M. Van Beek, G.H.J. Doremaele, K.A. Vandewiele, Y. Van Den Winkel, Yvar, *Belg. Pat. Appl.* **1995**, BE 1007262 A3 19950502; g) E.J.M. De Boer, H.J. Heeres, H.J.R. De Boer, *Eur. Pat. Appl.* **1995**, EP 638593 A1 19950215; h) E.J.M. De Boer, H.J.R. De Boer, H.J. Heeres, (Union Carbide) *U.S. Pat.* **1998**, 5756417; i) M. Sone, O. Yoshida, M. Sato, (Tosoh) *Jpn. Kokai Tokkyo Koho* **2000**, JP 2000273114 A 20001003.
- [21] a) S. S. Rodrigues, J. A. Fernandes, S. Fernandes, M. M. Marques, *Inorg. Chim. Acta* **2009**, *362*, 1275-1281; b) J. Panhans, F. W. Heinemann, U. Zenneck, *J. Organomet. Chem.* **2009**, *694*, 1223-1234; c) T. Aoki, S. Kanejima, (Asahi Chemical Ind) *Jpn. Kokai Tokkyo Koho* **1995**, JP 07070224 A 19950314.
- [22] H. Brake, *Master thesis* (University of Regensburg, **2015**).
- [23] C. Heindl, S. Reisinger, C. Schwarzmaier, L. Rummel, A. V. Virovets, E. V. Peresyphkina, M. Scheer, *Eur. J. Inorg. Chem.* **2016**, *5*, 743-753.
- [24] P. Pyykkoe, M. Atsumi, *Chem. Eur. J.* **2009**, *15*, 12770-12779.
- [25] M. Scheer, A. Schindler, J. Bai, B. P. Johnson, R. Merkle, R. Winter, A. V. Virovets, E. V. Peresyphkina, V. A. Blatov, M. Sierka, H. Eckert, *Chem. Eur. J.* **2010**, *16*, 2092-2107.
- [26] Unit cell parameters: mP, $a = 8.74 \text{ \AA}$, $b = 23.91 \text{ \AA}$, $c = 12.32 \text{ \AA}$, $\beta = 94.48^\circ$, $V = 2567 \text{ \AA}^3$.
- [27] J. Bai, A. V. Virovets, M. Scheer, *Angew. Chem. Int. Ed.* **2002**, *41*, 1737-1740.
- [28] Unit cell parameters: oP; $a = 10.55 \text{ \AA}$, $b = 15.21 \text{ \AA}$, $c = 16.02 \text{ \AA}$, $V = 2571 \text{ \AA}^3$.
- [29] P. Stolz, S. Pohl, *Z. Naturforsch. B: Chem. Sci.* **1988**, *43*, 175-181.
- [30] F. Dielmann, A. Schindler, S. Scheuermayer, J. Bai, R. Merkle, M. Zabel, A. V. Virovets, E. V. Peresyphkina, G. Brunklaus, H. Eckert, M. Scheer, *Chem. - Eur. J.* **2012**, *18*, 1168-1179. X-ray structural determination was reported for $T = 150 \text{ K}$ (cf. ref.) and was performed again at $T = 100 \text{ K}$. The latter CIF file with comprehensive information on the details of the

diffraction experiment and full tables of bond lengths and angles is deposited in Cambridge Crystallographic Data Centre under the deposition code CCDC-2038694.

- [31] According to preliminary data the I analogue of $[\{\text{Cp}^*\text{Fe}(\eta^5\text{-P}_5)\}\text{CuBr}]_n$ (ref. 27) had crystallized.
- [32] A. Bondi, *J. Phys. Chem.* **1964**, *68*, 441-451.
- [33] a) O. J. Scherer, T. Brück, *Angew. Chem. Int. Ed. Engl.* **1987**, *26*, 59; b) O. J. Scherer, T. Brück, G. Wolmershäuser, *Chem. Ber.* **1988**, *121*, 935-938.
- [34] C. Heindl, E. V. Peresykina, A. V. Virovets, G. Balázs, M. Scheer, *Chem. Eur. J.* **2016**, *22*, 1944-1948.
- [35] a) C. S. J. Callaghan, P. B. Hitchcock, J. F. Nixon, *J. Organomet. Chem.* **1999**, *584*, 87; b) G. Becker, W. Becker, R. Knebl, H. Schmidt, U. Weeber, M. Westerhausen, *Nova Acta Leopold.* **1985**, *59*, 55.
- [36] T. Allspach, M. Regitz, G. Becker, W. Becker, *Synthesis* **1986**, 31-36.
- [37] F. Uhlig, R. Hummeltenberg, *J. Organomet. Chem.* **1993**, *452*, C9.
- [38] *CrysAlis PRO* different versions (Rigaku OD).
- [39] G. M. Sheldrick, SADABS, Bruker AXS, Madison, USA, **2007**.
- [40] A. Burkhardt, T. Pakendorf, B. Reime, et al, *Eur. Phys. J. Plus* **2016**, *131*, 56-64.
- [41] G. M. Sheldrick, *Acta Cryst. A* **2015**, *A71*, 3-8.
- [42] G. M. Sheldrick, *Acta Cryst. A* **2008**, *64*, 112–122.

9 Conclusion

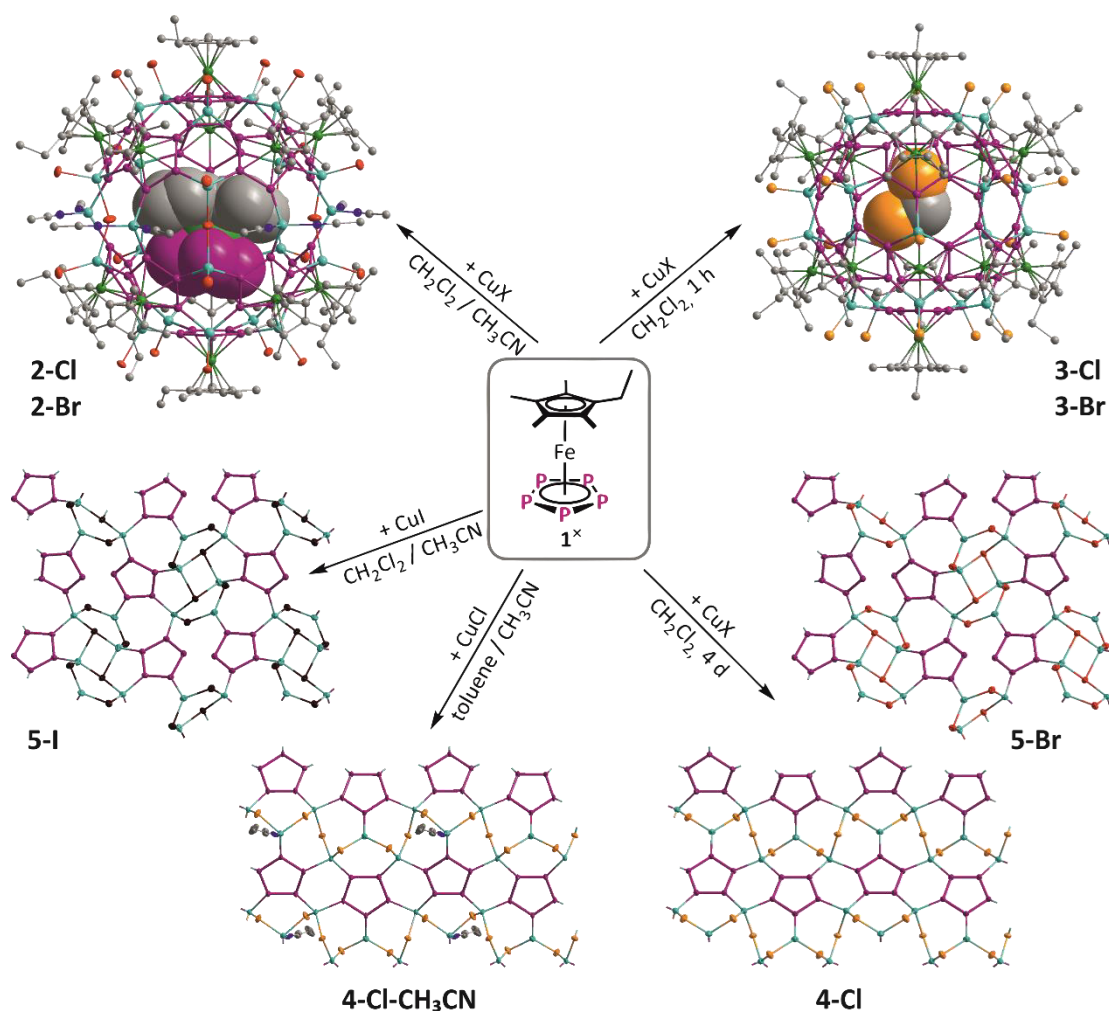
This work deals with the supramolecular chemistry and halogenation reactions of pentaphosphaferrocenes. The introduction (chapter 1) outlines fundamental concepts of supramolecular chemistry and focuses on the polymeric assemblies and discrete spherical aggregates obtained by polyphosphorus complexes as building blocks. The consequential research objectives are delineated in chapter 2. The results obtained are presented in the self-contained chapters 3 – 7 as well as in the thesis treasury (chapter 8).

The primary objective was the investigation of the coordination behavior of pentaphosphaferrocenes $[\text{Cp}^{\text{R}}\text{Fe}(\eta^5\text{-P}_5)]$ towards Cu(I) salts with variation of the Cp^{R} ligand (Chapter 3), the triple decker template (Chapter 4 and 5) and the counterion of the metal salt (Chapter 8.1). The second part of this thesis concerns the transfer of the supramolecular chemistry of polyphosphorus complexes to Au (Chapter 6 and Chapter 8.2). The coordination behavior of di- or triphospholyl ligands towards Cu salts and early transition metals is investigated in Chapters 8.3 and 8.4. Finally, the iodination of $[\text{Cp}^*\text{Fe}(\eta^5\text{-P}_5)]$ and its heavier congeners is dealt with in Chapter 7, further halogenation studies of $[\text{Cp}^*\text{Fe}(\eta^5\text{-P}_5)]$ are described in Chapter 8.5.

Self-Assembly of Pentaphosphaferrocenes $[\text{Cp}^{\text{R}}\text{Fe}(\eta^5\text{-P}_5)]$ and Cu Salts

Pentaphosphaferrocenes $[\text{Cp}^{\text{R}}\text{Fe}(\eta^5\text{-P}_5)]$ display remarkable building blocks for the construction of spherical aggregates *via* self-assembly with coinage metal salts. The most thoroughly investigated systems include the derivatives $[\text{Cp}^*\text{Fe}(\eta^5\text{-P}_5)]$ (**1***) and $[\text{Cp}^{\text{Bn}}\text{Fe}(\eta^5\text{-P}_5)]$ (**1^{Bn}**). Both polyphosphorus complexes are capable of constructing fullerene-like 80-vertex spheres which can act as hosts for small molecules. For **1***, also a variety of polymeric assemblies and a slightly larger 90-vertex sphere is accessible. Unfortunately, both systems suffer from disadvantages concerning either limited solubility of the spherical products and unselective self-assembly (**1***) or limited versatility and low-quality crystallization (**1^{Bn}**). Therefore, the self-assembly of $[\text{Cp}^{\text{x}}\text{Fe}(\eta^5\text{-P}_5)]$ (**1^x**) with Cu(I) halides was investigated.

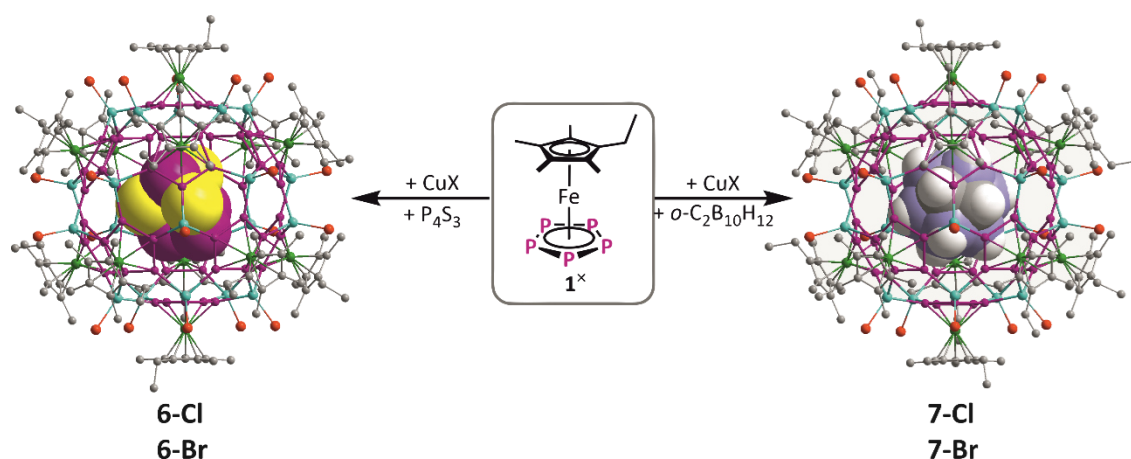
Surprisingly, the outcome of the reactions is not only easily controllable by the reaction conditions applied, but the products each are also formed selectively. In the presence of CH_3CN , the two-component reactions of **1^x** and CuCl or CuBr give 90-vertex spheres $[\text{Cp}^{\text{x}}\text{Fe}(\eta^5\text{-P}_5)]_{12}@\{[\text{Cp}^{\text{x}}\text{Fe}(\eta^5\text{-P}_5)]_{12}\{[\text{CuX}]_{25}\{\text{CH}_3\text{CN}\}_{10}\}$ (**2**, X = Cl, Br, Scheme 1). The analogous



Scheme 1. Polymeric and spherical assemblies obtained from self-assembly of 1^* and Cu(I) halides.

reaction with CuI exclusively yielded the novel 2D polymer $[(Cp^*Fe(\eta^5-P_5))\{CuI\}_3]$ (**5-I**). By avoiding CH_3CN , instead the $(80-n)$ -vertex spheres $(CH_2Cl_2)_m@[(Cp^*Fe(\eta^5-P_5))_{12}\{CuX\}_{20-n}]$ (**3**, $X = Cl$: $m \geq 0.84$, $n = 1.20$; $X = Br$) are accessible. Crystals of **3** are solid solutions of $(80-n)$ -vertex spheres with varying CuX contents. The void of these spheres is occupied by solvent molecules. These spherical aggregates rearrange in the presence of crystallization seeds to give 2D polymers $[(Cp^*Fe(\eta^5-P_5))\{CuX\}_3]$ ($X = Cl$: **4-Cl**; $X = Br$: **5-Br**). Compound **4-Cl** constitutes the first example of a polymer in which the pentaphosphaferrocene building block is coordinated to five Cu atoms by σ -coordination through all five P atom lone pairs. This mode has only been observed in spherical compounds so far. In the presence of CH_3CN , also a derivative, $[(1^*)_2\{CuCl\}_6\{CH_3CN\}]_n \cdot nCH_3CN$ (**4-Cl-CH₃CN**), was obtained, in which some of the Cu atoms additionally coordinate to CH_3CN . In contrast, isostructural polymers **5-Br** and **5-I** comprise 1,2,3,4-coordinating building blocks of 1^* . All polymers were characterized by $^{31}P\{^1H\}$ MAS NMR spectroscopy, thus complementing an earlier NMR study on pentaphosphaferrocene-based polymers limited to other coordination modes.

In order to prevent the rearrangement of spherical assemblies to polymers, P_4S_3 and $o\text{-C}_2\text{B}_{10}\text{H}_{12}$ were added as templates and as a third component to the self-assembly process. Again, (80- n)-vertex spheres are formed, this time acting as hosts for the respective template (Scheme 2). Interestingly, in the presence of the templates, the outcome of the reaction is independent on the reaction conditions applied. Thus, different crystalline phases of $(P_4S_3)_m@[\{1^x\}_{12}\{\text{CuX}\}_{20-n}]$ (**6-Cl** and **6-Br**; $0.68 < m < 1$; $2.8 > n > 1.4$) or $(o\text{-C}_2\text{B}_{10}\text{H}_{12})_m@[\{1^x\}_{12}\{\text{CuX}\}_{20-n}]$ (**7-Cl** and **7-Br**; $0.5 < m < 1$; $2.52 > n > 1.52$) are accessible. The voids of the more or less metal-deficient spheres are occupied by up to one molecule of P_4S_3 or $o\text{-C}_2\text{B}_{10}\text{H}_{12}$.



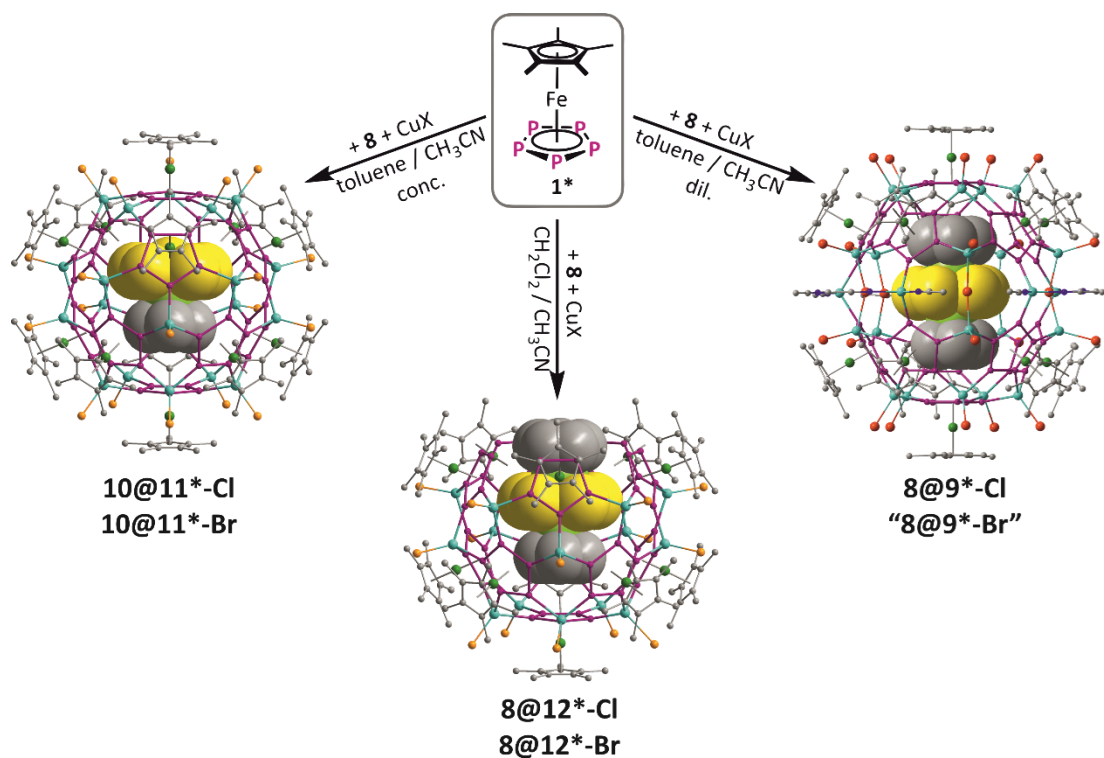
Scheme 2. Host-guest assemblies obtained from self-assembly of 1^x and Cu(I) halides in the presence of a template.

Next to the highly directional self-assembly of the 1^x / Cu(I) halide system, the obtained (80- n)-vertex spheres also show surprisingly high solubility in CH_2Cl_2 . This enabled thorough NMR investigations in solution. Thereby, a transformation of the (80- n)-vertex spheres **3** into 90-vertex spheres **2** could be observed for the first time, by addition of the respective Cu(I) halide dissolved in CH_3CN . Moreover, mixed-halide 90-vertex spheres are accessible by this approach. Furthermore, post-synthetic addition of $o\text{-C}_2\text{B}_{10}\text{H}_{12}$ to solutions of **3** lead to its encapsulation as evidenced by $^{11}\text{B}\{^1\text{H}\}$ NMR spectroscopy.

In conclusion, 1^x combines all advantages of 1^* and 1^{Bn} as a supramolecular building block. The self-assembly of 1^x results in versatile products spanning polymers, 90-vertex spheres, (80- n)-vertex spheres and guest stabilized (80- n)-vertex spheres. The obtained spherical assemblies are highly soluble, all products are formed selectively, the crystals are of sufficient quality for X-ray crystallographic characterization and host-guest aggregates are obtainable by different synthetic routes, thus opening further opportunities to this chemistry.

A variety of small molecules has already been encapsulated as guests into 80-vertex spherical assemblies of **1***. With $[\text{CoCp}_2]^+$ as cationic guest, P_4 or As_4 as exceedingly small guests and C_{60} as very large guest, different spherical host molecules are formed describing prism- or cube-shaped, ellipsoid-shaped or barrel-like aggregates. It was of special interest to apply large, non-spherical molecules as templates in the self-assembly of **1*** with Cu(I) halides. Therefore, the triple decker complex $[(\text{CpCr})_2(\mu, \eta^{5:5}\text{-As}_5)]$ (**8**) with rather rod-like shape came to mind. In a previous work, the self-assembly of **1***, **8** and CuX ($\text{X} = \text{Cl}, \text{Br}$) in toluene / CH_3CN was investigated. Thereby, encapsulation of **8** into a 90-vertex sphere to give $[(\text{CpCr})_2(\mu, \eta^{5:5}\text{-As}_5)]@[\{\text{Cp}^*\text{Fe}(\eta^5\text{-P}_5)\}_{12}\{\text{CuBr}\}_{25}\{\text{CH}_3\text{CN}\}_{10}]$ (**8@9*-Br**) was observed for $\text{X} = \text{Br}$, while for $\text{X} = \text{Cl}$, the cleavage of **8** into $[\text{CpCr}(\eta^5\text{-As}_5)]$ upon encapsulation into an 80-vertex sphere to give $[\text{CpCr}(\eta^5\text{-As}_5)]@[\{\text{Cp}^*\text{Fe}(\eta^5\text{-P}_5)\}_{12}\{\text{CuCl}\}_{20}]$ (**10@11*-Cl**) was proposed.

Within the scope of the collaboration with Dr. Claudia Heindl, this self-assembly reaction was repeated in CH_2Cl_2 / CH_3CN , leading to host-guest aggregates $[(\text{CpCr})_2(\mu, \eta^{5:5}\text{-As}_5)]@[\{\text{Cp}^*\text{Fe}(\eta^5\text{-P}_5)\}_{11}\{\text{CuX}\}_{15-n}]$ (**8@12***, Scheme 3) with an unprecedented bowl-like host encapsulating the intact triple decker molecule **8**. The host scaffold can be derived from the well-known (80- n)-vertex spheres by conceptually removing one $[\{\text{Cp}^*\text{Fe}(\eta^5\text{-P}_5)\}\{\text{CuX}\}_5]$ moiety, leaving a truncated, open host shell from whose core the triple decker guest may protrude.



Scheme 3. Host-guest aggregates obtained from self-assembly of **1*** with Cu(I) halides and **8**.

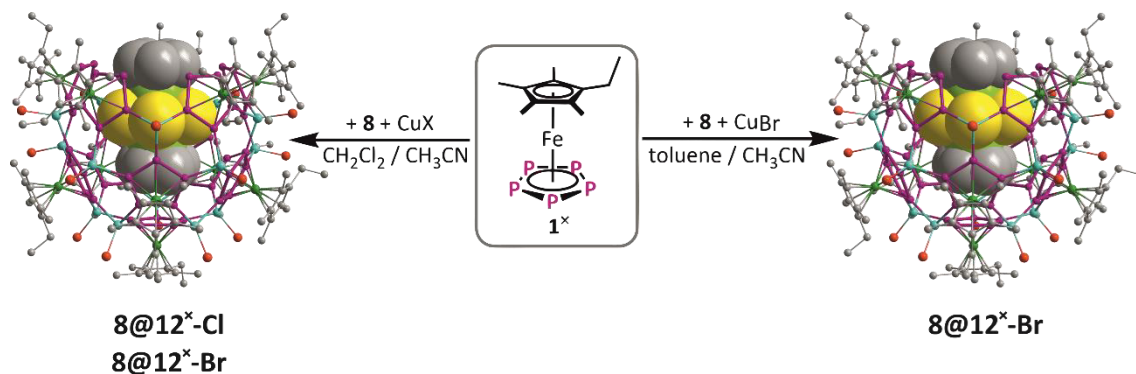
The self-assembly in toluene / CH_3CN was thereupon reinvestigated. The formation of "80"- vs. 90-vertex spheres was found to depend on the concentration rather than the halide

(Scheme 3). While encapsulation of **8** into the Cl analogue 90-vertex sphere could not be proven by X-ray crystallography, the Br analogue 80-vertex sphere “[CpCr(η^5 -As₅)]@{[Cp*Fe(η^5 -P₅)]₁₂{CuBr}_{20-n}” (“**10@11*-Br**”) was accessed. Both proposed 80-vertex spheres “**10@11***” were thoroughly characterized by solid state MAS and solution NMR spectroscopy, ESI and EI mass spectrometry, EPR spectroscopy and elemental analysis. This was of special interest since the structure determination from X-ray data is unfortunately quite ambiguous in these cases. As a result, three borderline cases for interpretation of the X-ray data are presented.

- Cleavage of **8** and encapsulation into an (80-n)-vertex sphere (“**10@11***”)
- Encapsulation of intact **8** into a disorderedly crystallizing nano-bowl (**8@12***)
- Oxidation and encapsulation of **8**⁺ into a disorderedly crystallizing, anionic nano-bowl (**8⁺@12***)

Taking all data of the questionable compounds “**10@11***” into account and comparing these to the data obtained from **8@12*** (crystallized unambiguously from CH₂Cl₂ / CH₃CN), at least the borderline interpretation b) as sole product could be ruled out.

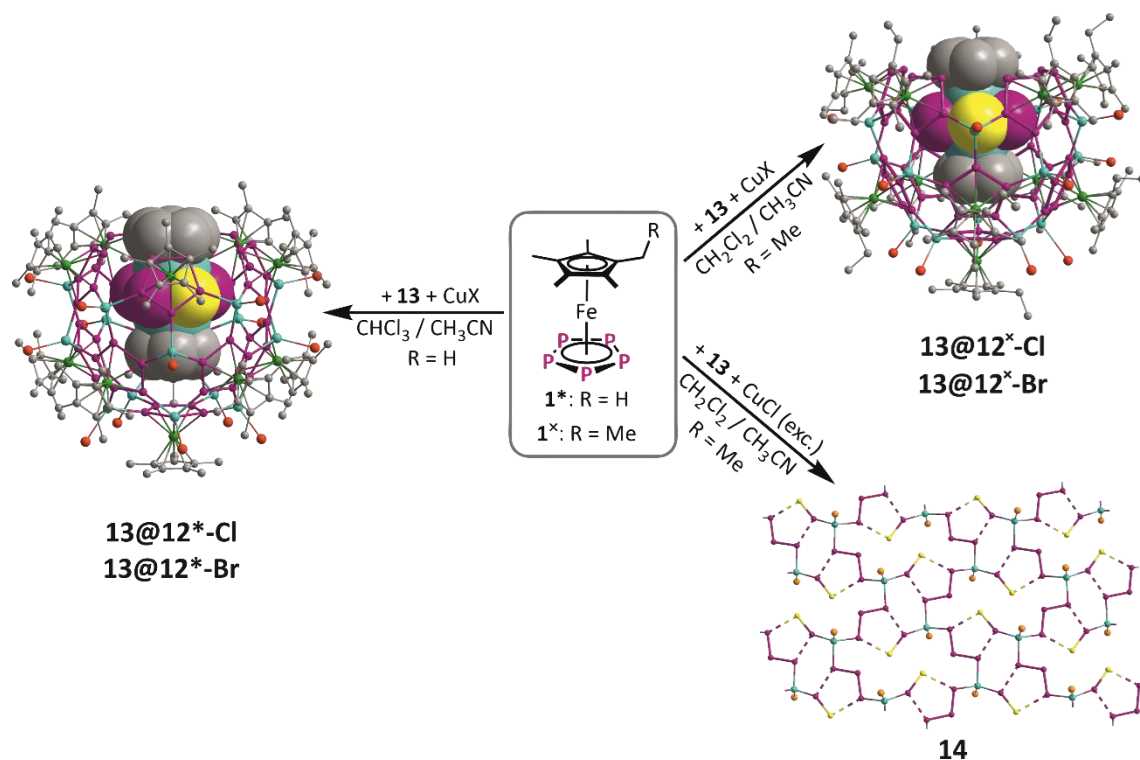
Compounds **8@12*** were thoroughly characterized, though their limited solubility impeded spectroscopic investigations in solution. Hence, **1^x** was applied as a building block instead of **1*** since it previously proved beneficial *inter alia* in terms of solubility of the spherical products. The self-assembly of **1^x** with CuX (X = Cl, Br) and **8** indeed gave nano-bowls [(CpCr)₂(μ , $\eta^{5:5}$ -As₅)]@{[Cp^xFe(η^5 -P₅)]₁₁{CuX}_{15-n}} (**8@12^x**) showing enhanced solubility (Scheme 4). By comparison of the ¹H MAS NMR spectra of **8@12^x** with the ¹H NMR spectra of solutions of **8@12^x**, a reliable assignment of the signals to the Cp ligands of encapsulated **8** was enabled. Thereby, the signals of the Cp ligands located at the ‘bottle-neck’ of the host are shifted in solid-state due to the presence of π -stacking interactions to the next host-guest assembly, which is not observed in solution.



Scheme 4. Host-guest aggregates obtained from self-assembly of **1^x** with Cu(I) halides and **8**.

Within the scope of the dissertation of Dr. Claudia Heindl, a synthetic approach towards the novel triple decker [(CpMo)₂(μ , $\eta^{3:3}$ -P₃)(μ , $\eta^{2:2}$ -PS)] (**13**) was given. Therefore, the application of

this triple decker molecule as diamagnetic template was investigated. While the analogous reaction with **1*** and CuCl/Br in CH₂Cl₂ / CH₃CN did not provide unambiguous X-ray data due to disorder, slower crystallization was targeted to overcome this problem. This was achieved on the one hand by a switch of solvents to CHCl₃ / CH₃CN, on the other hand by again applying **1^x** instead of **1***. In both cases, the nano-bowls [(CpMo)₂(μ,η^{3:3}-P₃)(μ,η^{2:2}-PS)]@[{Cp^RFe(η⁵-P₅)₁₁{CuX}_{15-n}] (Cp^R = Cp*: **13@12***, Cp^R = Cp^x: **13@12^x**) were obtained (Scheme 5). In contrast to the reactions with **1*** and triple decker **8**, applying toluene / CH₃CN as solvents this time did not change the outcome of the reaction, but **13@12*-Br** was obtained in a new crystalline phase instead. The reactions with **1^x** proved to be highly dependent on the stoichiometry. Changing from a stoichiometric ratio of 11:15 (**1***:Cu) to higher Cu contents, instead of nano-bowls this time 80- (X = Cl) or 90-vertex spheres (X = Br) are obtained. Unfortunately, the triple decker **13** or a reaction product thereof is not encapsulated this time, but solvent molecules or **1^x** itself act as a guest. For X = Cl, triple decker **13** instead acted as ligand complex towards Cu, resulting in the formation of the novel 2D polymer [{(CpMo)₂(μ₄,η^{3:3:1:1}-P₃)(μ₃,η^{2:2:1}-PS)}CuCl]_n (**14**). Compound **14** can be directly synthesized from triple decker **13** and CuCl as well.



Scheme 5. Host-guest aggregates and polymers obtained from self-assembly of **1*** (R = H) or **1^x** (R = Me) with Cu(I) halides and **13**.

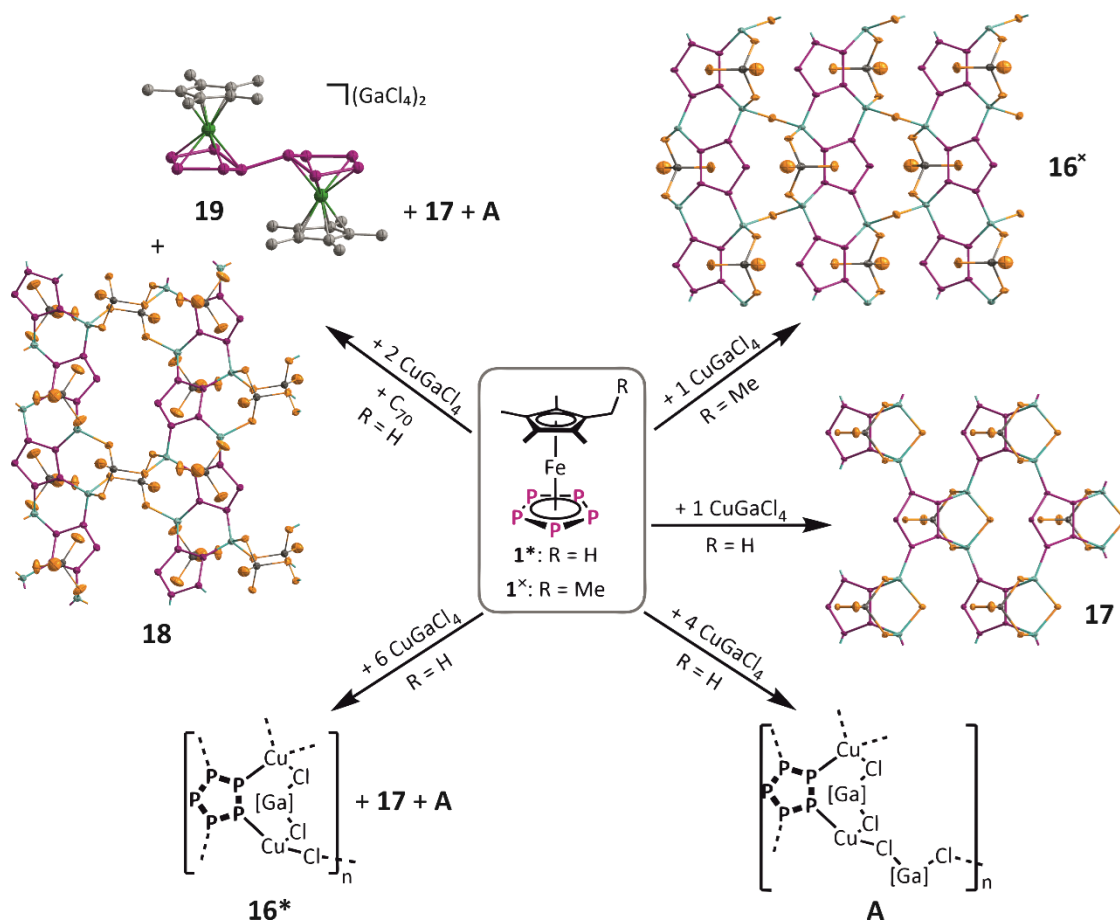
Attempts to obtain CuI-containing nano-bowls merely lead to the formation of the 3D polymer [{Cp*Fe(η^{5:1:1}-P₅)₂{Cp*Fe(η^{5:1:1}-P₅)Cu₄(μ-I)₄]_n (**15**), which was described in the

dissertation of Dr. Claudia Heindl, and remarkably constitutes the first 3D polymer based on pentaphosphaferrocenes.

In the course of these studies, also a variety of novel crystalline phases of 90-vertex spheres were investigated. Unluckily, the encapsulation of triple decker complexes **8** or **13** could not be verifiably observed and the majority of 90-vertex spheres rather hosts molecules of **1*** or **1^x**.

The enhanced solubilities of **8@12^x** and **13@12^x** compared to the **1*** based counterparts **8@12*** and **13@12*** can partly be traced back to fewer or weaker intermolecular interactions in the solid state. By comparison of the NMR spectroscopic data of the nano-bowls **8@12***, **8@12^x**, **13@12*** and **13@12^x**, it was proven that the ¹H NMR signals of the hosts are partly shifted upon encapsulation of the paramagnetic triple decker complex **8**. Furthermore, the Cp ligands of **8** and **13** become magnetically inequivalent upon encapsulation into the nano-bowls, and further splitting of the two signals is caused by the presence of CuX vacancies in the host.

In the self-assembly reactions of pentaphosphaferrocenes and Cu(I) salts, another variable is the nature of the counterion. Not only Cu(I) salts of coordinating halides have been used in these reactions, but also a series of salts of weakly coordinating anions (WCAs).



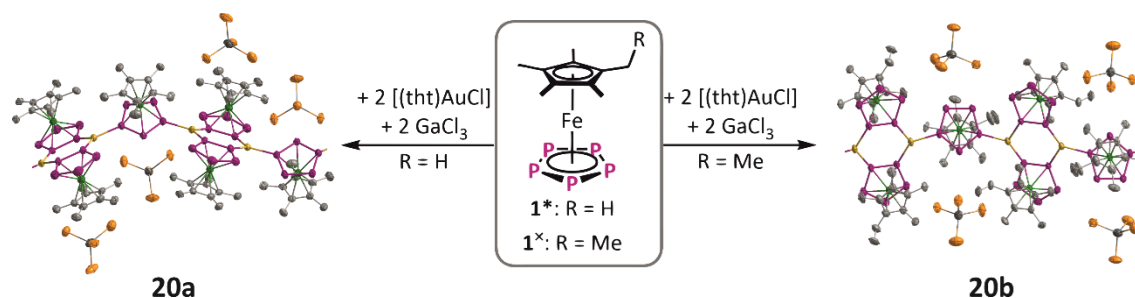
Scheme 6. Polymers obtained from the self-assembly of **1*** or **1^x** and CuGaCl_4 .

Thereby, the GaCl_4^- anion is an interesting intermediary case, as it may act coordinating or not. However, the self-assembly of CuGaCl_4 with pentaphosphaferrocenes is largely unexplored. Therefore, the *cyclo*- P_5 ligand complexes were reacted with CuGaCl_4 , thereby varying the Cp ligand of the pentaphosphaferrocene, applied stoichiometries and the presence of potential templates. As a result, a series of novel polymers (**16** – **18**) was obtained besides the only reported polymer (**A**) and the dimer $[(\text{Cp}^*\text{Fe})_2(\mu, \eta^{5,5}\text{-P}_{10})](\text{GaCl}_4)_2$ (**19**, Scheme 6). The latter displays the oxidation product of **1*** and has already been reported as SbF_6^- salt. The polymers **16** – **18** are 2D coordination networks with coordinating GaCl_4 units and encompass a **1** : Cu ratio of 1:2 despite the differing stoichiometric ratios applied in the reactions. Compound **18** is a constitutional isomer to the reported polymer. In contrast to these, compounds **16** and **17** comprise coordinating Cl atoms. Unfortunately, the reactions were highly unselective and could not be controlled by stoichiometry, so that a further investigation was hampered.

Self-Assembly of Polyphosphorus Complexes and Au Salts

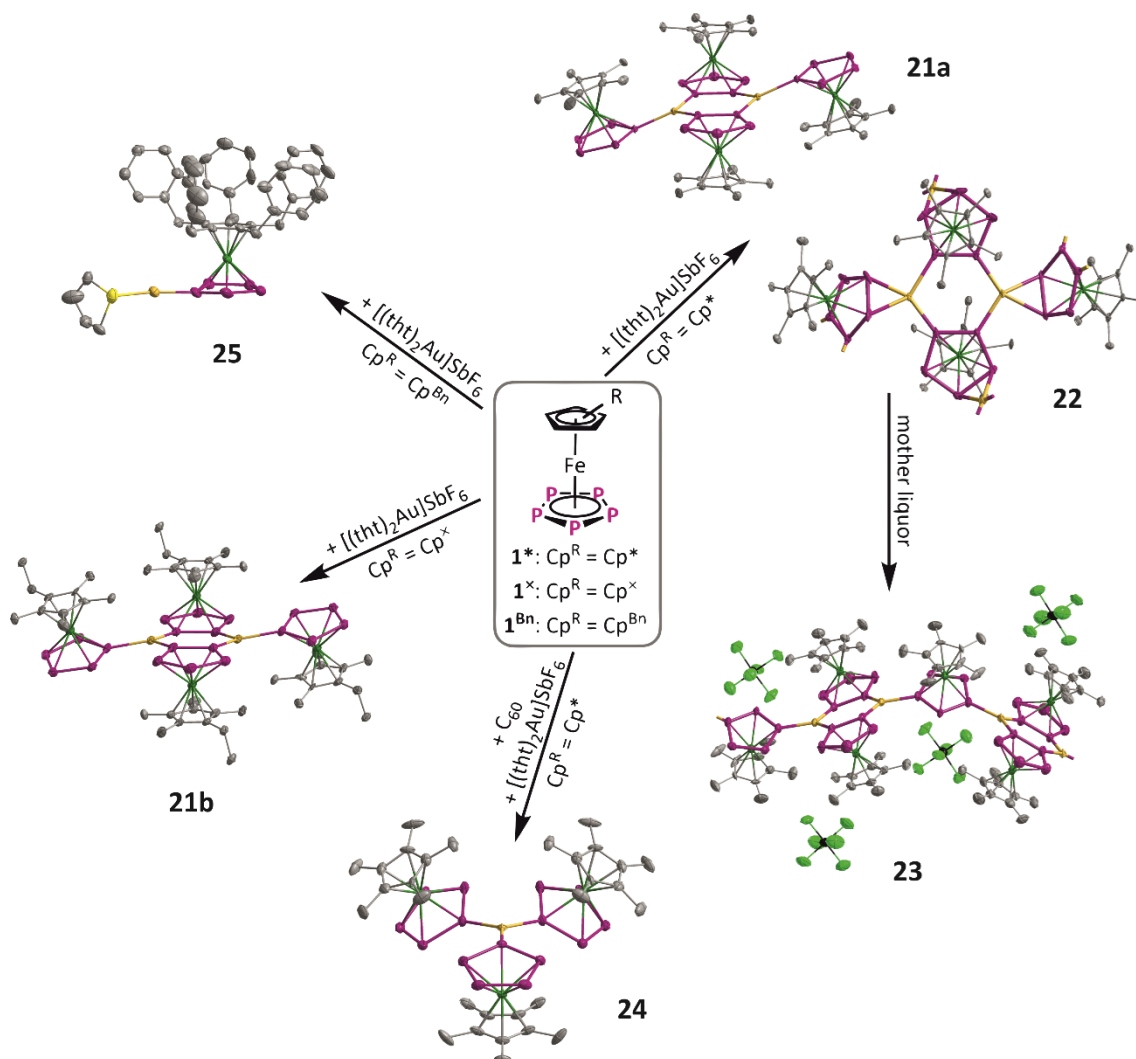
The self-assembly of polyphosphorus complexes and coinage metal salts has so far been mostly limited to Cu and Ag. Merely two examples have been reported where a polyphosphorus complex coordinates to Au, both applying $[(\text{CpMo}(\text{CO})_2)_2(\mu, \eta^2\text{-P}_2)]$ as a P_2 ligand complex. On the contrary, the coordination of pentaphosphaferrocenes $[\text{Cp}^R\text{Fe}(\eta^5\text{-P}_5)]$ towards Au has been left untouched so far, despite its multifaceted application as building block in supramolecular chemistry. Therefore, synthetic approaches to the first Au containing assemblies of pentaphosphaferrocenes were developed. Thereby, systematic variations of the counterions (GaCl_4^- , SbF_6^- , TEF^-) and the Cp^R ligand (Cp^* , Cp^x , Cp^{Bn}) were carried out.

The GaCl_4^- containing products **20a** and **20b** were synthesized starting from $[(\text{tth})\text{AuCl}]$ and GaCl_3 as Cl abstractor (Scheme 7). Variation of the solvent from CH_2Cl_2 to *o*-DFB enabled isolation of the crystals in up to 86% yield. A series of solvatomorphs and polymorphs was characterized by X-ray crystallography. Compounds **20a** and **20b** constitute unprecedented 1D polymers with 1,2- and 1,3-coordinating P_5 building blocks and trigonally planar coordinated Au atoms and are thus the first coordination polymers of polyphosphorus ligand complexes and Au.



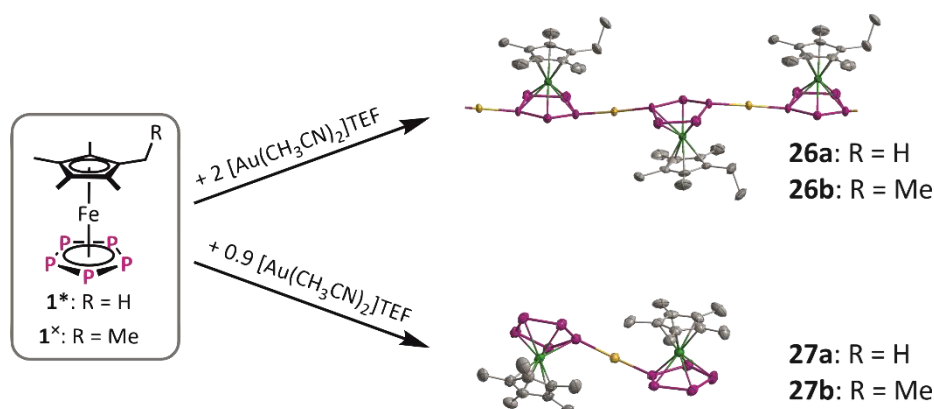
Scheme 7. Polymers obtained from self-assembly of **1*** or **1^x** with $[(\text{tth})\text{AuCl}]$ and GaCl_3 .

For reactions with SbF_6^- as a counterion, $[(\text{tht})_2\text{Au}]\text{SbF}_6$ was synthesized *in situ* following the reported method from $[(\text{tht})\text{AuCl}]$, AgSbF_6 and THT. As products of self-assembly with $\mathbf{1}^*$ a dimer **21a** and a 2D polymer **22** revealing a similar sum formula were formed (Scheme 8). Thus, they could not be synthesized deliberately e.g. by varying the stoichiometry. Additionally, a 1D polymer **23** was obtained from crystallization of the mother liquor. Remarkably, compound **22** comprises vacancies in the Au positions which are hence not fully occupied (s.o.f. < 1) but site occupancy factors sum up to an integer ($\sum \text{s.o.f.} = 2$). When C_{60} was added as a potential template, the cationic assembly **24** was obtained with three units of $\mathbf{1}^*$ coordinating to one Au atom, co-crystallizing with two molecules of C_{60} . Going to $\mathbf{1}^x$, the self-assembly takes place selectively and dimer **21b** is formed with a similar structure to **21a**. From reaction with $\mathbf{1}^{\text{Bn}}$, compound **25** is formed in which only one tht ligand is replaced by the P_5 ligand complex. In solution, **25** showed a highly dynamic behavior.



Scheme 8. Monomeric, dimeric and polymeric products obtained from self-assembly of $\mathbf{1}^*$, $\mathbf{1}^x$ or $\mathbf{1}^{\text{Bn}}$ with $[(\text{tht})_2\text{Au}]\text{SbF}_6$.

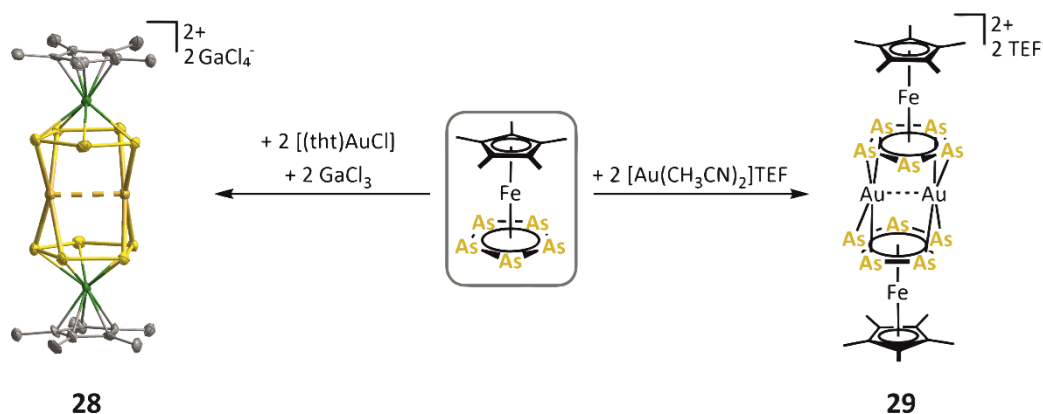
Moreover, 1D coordination polymers **26a** and **26b** were obtained when reacting **1*** or **1^x** with 2 eq. AuTEF, which was in hand as isolable $[\text{Au}(\text{CH}_3\text{CN})_2]\text{TEF}$ salt (Scheme 9). Unfortunately, crystallization was often hampered due to rapid precipitation but for the reaction with **1^x**, the precipitate was successfully identified as target polymer **26b**. Analogous reactions with less than 1 eq. AuTEF resulted in the formation of monomeric products **27a** and **27b**, in which two P₅ ligand complexes coordinate to one Au atom.



Scheme 9. Monomers and polymers obtained from self-assembly of **1*** or **1^x** with $[\text{Au}(\text{CH}_3\text{CN})_2]\text{TEF}$.

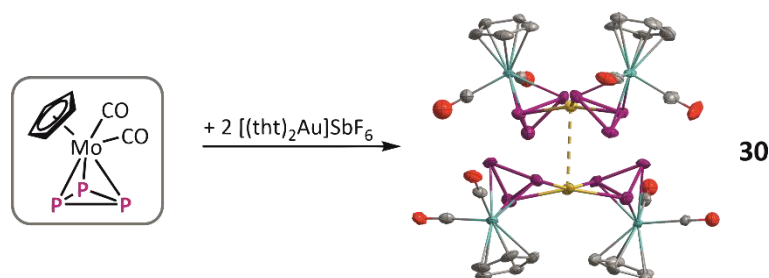
The molecular products and partially disaggregated polymeric assemblies of **1***, **1^x** and **1^{Bn}** and Au salts exhibit highly dynamic behavior in solution. Moreover, all products comprise Au centers with an either linear or planar coordination environment, thus impeding the formation of spherical aggregates in combination with planar P₅ building blocks.

Therefore, instead of P₅ ligand complexes **1**, also the self-assembly of $[\text{CpMo}(\text{CO})_2(\eta^3\text{-P}_3)]$ and $[\text{Cp}^*\text{Fe}(\eta^5\text{-As}_5)]$ with Au salts was investigated. The As₅ ligand complex $[\text{Cp}^*\text{Fe}(\eta^5\text{-As}_5)]$ is known to coordinate through its π -system rather than by the lone pairs of the As atoms. Indeed, this out-of-plane coordination was also observed in the reaction products of $[\text{Cp}^*\text{Fe}(\eta^5\text{-As}_5)]$ with AuGaCl₄ and AuTEF. In both cases, dimers (**28** and **29**) with Au₂ dumbbells in between two As₅ ligand complexes were obtained (Scheme 10).



Scheme 10. Dimers obtained from self-assembly of $[\text{Cp}^*\text{Fe}(\eta^5\text{-As}_5)]$ with Au salts.

In contrast, the reaction of $[\text{CpMo}(\text{CO})_2(\eta^3\text{-P}_3)]$ with $[(\text{tht})_2\text{Au}]\text{SbF}_6$ furnished crystals of dimer $[\{\text{CpMo}(\text{CO})_2(\mu, \eta^{3:2}\text{-P}_3)\}_2\text{Au}]_2(\text{SbF}_6)$ (**30**) with a different structural motif (Scheme 11). Here, two P_3 ligand complexes coordinate in an η^2 -mode to one Au atom and dimerization is provoked by unsupported $\text{Au}\cdots\text{Au}$ contacts.

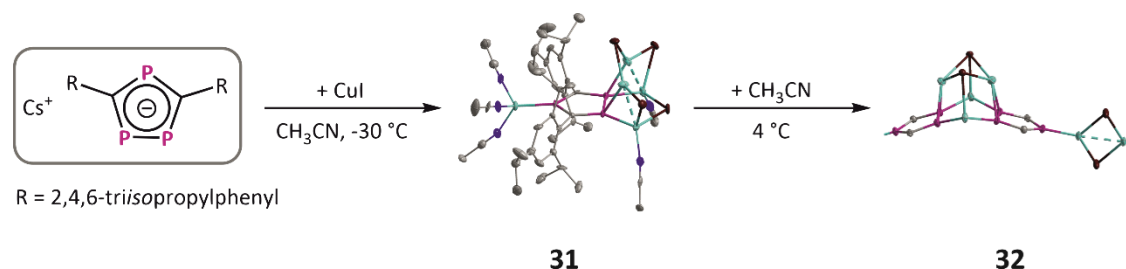


Scheme 11. Dimer obtained from self-assembly of $[\text{CpMo}(\text{CO})_2(\eta^3\text{-P}_3)]$ and $[(\text{tht})_2\text{Au}]\text{SbF}_6$.

In conclusion, $[\text{CpMo}(\text{CO})_2(\eta^3\text{-P}_3)]$ and $[\text{Cp}^*\text{Fe}(\eta^5\text{-As}_5)]$ both coordinate to Au in an out-of-plane fashion as aimed for. Nevertheless, the formation of spherical aggregates was not observed.

Coordination Behavior of Di- and Triphospholyl Ligands

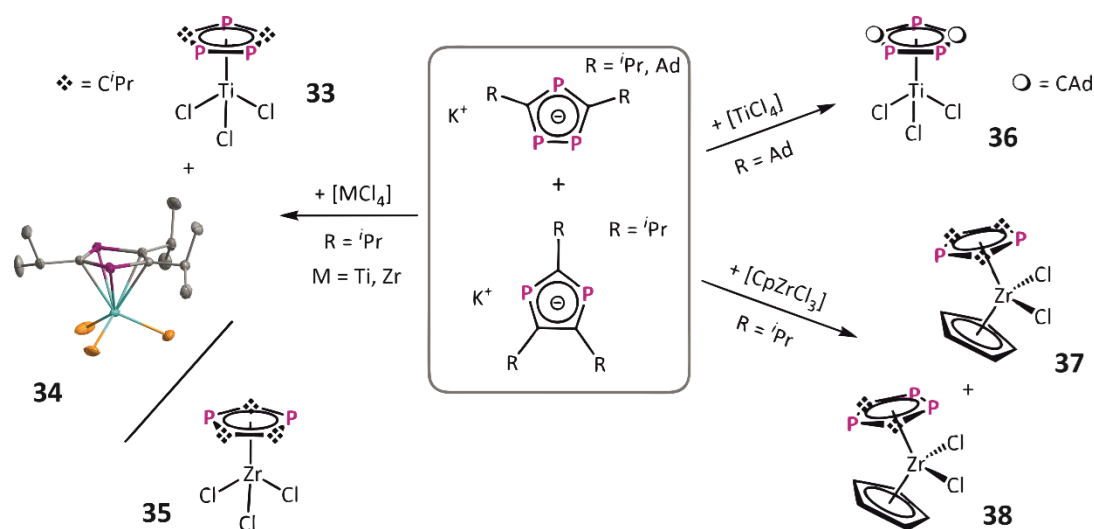
Apart from all-phosphorus P_5 ligands as in $[\text{Cp}^*\text{Fe}(\eta^5\text{-P}_5)]$ (**1***), also triphospholyl ligands may coordinate through their P lone pairs and thus act as building blocks in supramolecular chemistry. Hence, the Cs^+ salt of the 1,2,4-triphospholyl ligand $[\text{P}_3\text{C}_2\text{trip}_2]^-$ was reacted with CuI (Scheme 12). Thereby, the monomeric coordination product $[\{\mu, \eta^{1:2:2}\text{-P}_3\text{C}_2\text{trip}_2\}\{\text{Cu}(\text{CH}_3\text{CN})_3\}\{\text{Cu}(\text{CH}_3\text{CN})(\mu\text{-I})\}_2\{\text{Cu}(\mu\text{-I})\}_2] \cdot 2 \text{CH}_3\text{CN}$ (**31**) was obtained, comprising an asymmetric Cu_4I_4 'crown' motif due to the steric bulk of the trip residues. Interestingly, recrystallization from CH_3CN yielded a waved 1D coordination polymer $[(\mu_4, \eta^{1:1:1:2}\text{-P}_3\text{C}_2\text{trip}_2)_2\{\text{Cu}(\text{CH}_3\text{CN})(\mu_3\text{-I})\}_2\{\text{Cu}(\text{CH}_3\text{CN})\}_2\{\text{Cu}(\mu_2\text{-I})\}_2]_n \cdot 2n \text{CH}_3\text{CN}$ (**32**).



Scheme 12. Monomer and polymer obtained from self-assembly of $\text{Cs}[1,2,4\text{-P}_3\text{C}_2\text{trip}_2]$ with CuI.

Besides the use as supramolecular building blocks in combination with coinage metal salts, also the coordination behavior of phospholyl ligands towards early transition metals was investigated. Thereby, the salt metathesis reactions of $\text{K}[\text{P}_3\text{C}_2\text{R}_2]$ ($\text{R} = \text{Pr}, \text{Ad}$) and $\text{K}[\text{P}_2\text{C}_3\text{R}_3]$ ($\text{R} =$

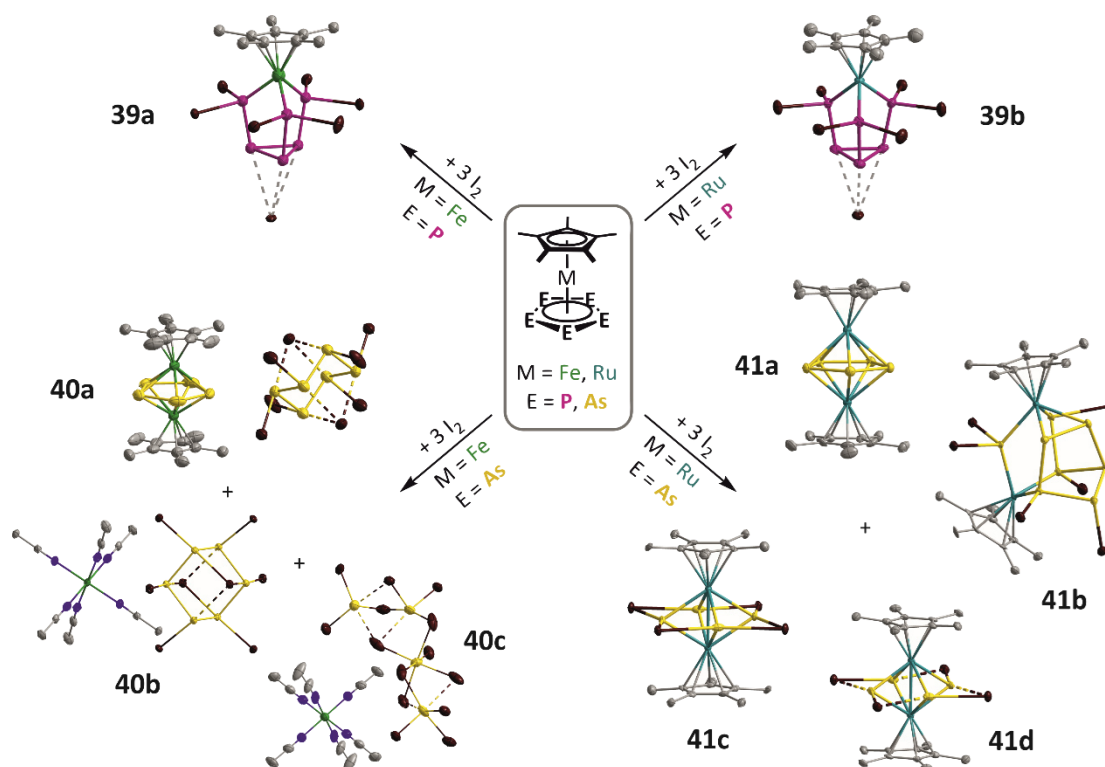
*i*Pr) salts with [TiCl₄], [ZrCl₄] and [CpZrCl₃], respectively, yielded a number of novel polyphospholyl complexes spanning [(η⁵-1,2,4-P₃C₂^{*i*}Pr₂)TiCl₃] (**33**), [(η⁵-1,3-P₂C₃^{*i*}Pr₃)TiCl₃] (**34**), [(η⁵-1,3-P₂C₃^{*i*}Pr₃)ZrCl₃] (**35**), [(η⁵-1,2,4-P₃C₂Ad₂)TiCl₃] (**36**), [Cp(η⁵-1,3-P₂C₃^{*i*}Pr₃)ZrCl₂] (**37**) and [Cp(η⁵-1,2,4-P₃C₂^{*i*}Pr₂)ZrCl₂] (**38**, Scheme 13). While the triphospholyl complex **33** proved to be unstable at room temperature, the diphospholyl analogue **34** was not. Remarkably, with complex **34**, a diphospholyl Ti complex was structurally characterized for the first time.



Scheme 13. Salt metathesis reactions of polyphospholyl salts and early transition metal halides.

Halogenation Reactions of *cyclo*-E₅-Complexes

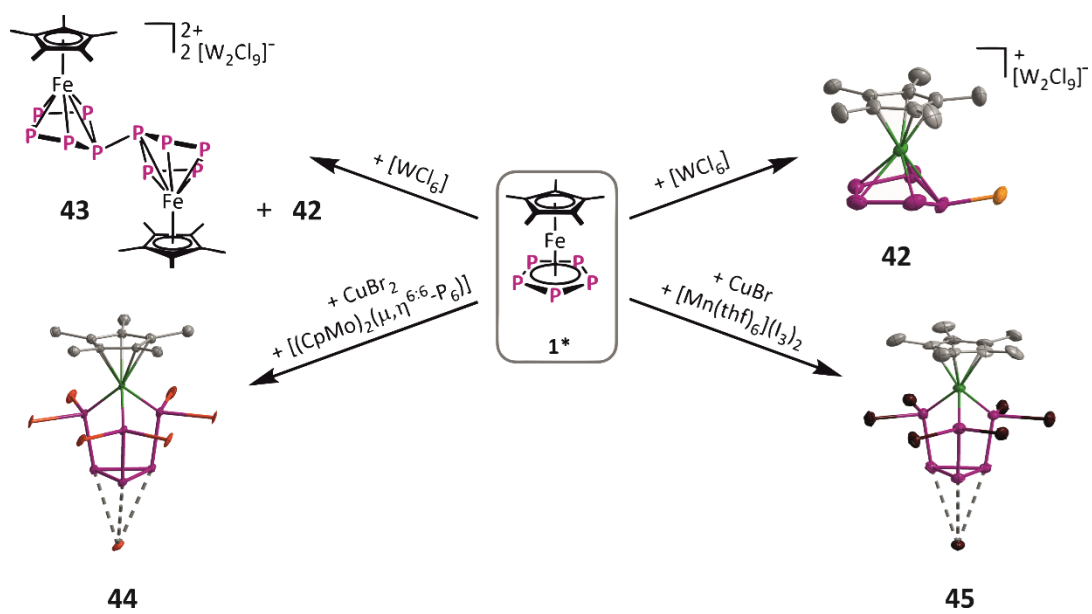
The reactions of P₄ and its complexes with I₂ have been shown to furnish interesting new polyphosphorus compounds through P-P bond cleavage and recombination steps. Hence, within this work, the iodination of polyphosphorus complexes other than P₄ complexes was investigated. The reactions of [Cp*Fe(η⁵-P₅)] (**1***) and its Ru analogue [Cp*Ru(η⁵-P₅)] with I₂ gave unprecedented P₆I₆ complexes [Cp*MP₆I₆]⁺ (**39a**: M = Fe; **39b**: M = Ru) as I⁻ salts (Scheme 14, top). For M = Fe, also the mixed I₃⁻ / I⁻ salt was structurally characterized. The P₆I₆ ligand within these complexes represents the first all-*cis* triphosphino-cyclotriphosphine. The analogous reaction with the As₅ complex [Cp*Fe(η⁵-As₅)] resulted in the concomitant crystallization of three compounds: [(Cp*Fe)₂(μ,η^{5:5}-As₅)] [As₆I₈] (**40a**), [Fe(CH₃CN)₆] [As₆I₈] (**40b**) and [Fe(CH₃CN)₆] [As₄I₁₄] (**40c**, Scheme 14, bottom left). The cation of compound **40a**, [(Cp*Fe)₂(μ,η^{5:5}-As₅)]²⁺, is the first dicationic Fe-As triple decker complex and reveals some Fe...Fe bonding interactions as well as paramagnetic behavior. Since this reaction led to the cleavage of most Fe-As bonds, the iodination of the Ru analogue [Cp*Ru(η⁵-As₅)] was also studied. Thereby, four concomitantly crystallizing products were obtained:



Scheme 14. Iodination reactions of *cyclo*-E₅-complexes [Cp**M*(η⁵-E₅)] (M = Fe, Ru; E = P, As).

[(Cp**Ru*)₂(μ,η^{5:5}-As₅)] [As₆I₈]_{0.5} (**41a**), [(Cp**Ru*)₂As₈I₆] (**41b**), [(Cp**Ru*)₂As₄I₄] (**41c** and **41d**, Scheme 14, bottom right). Remarkably, with compound **41a** the series of monocationic triple decker complexes [(Cp^R*M*)₂(μ,η^{5:5}-E₅)]⁺ (M = Fe, Ru; E = P, As) was completed. Compound **41b** was found to crystallize as a racemic mixture of both enantiomers, while [(Cp**Ru*)₂As₄I₄] crystallized as two structural isomers either with a symmetric (**41c**) or an unsymmetric (**41d**) As₄I₄ middle deck. This middle deck can be interpreted as a unique tetramer of {AsI} arsinidene units. Thus, it could be shown that iodination of *cyclo*-E₅ complexes leads to unprecedented polypnictogen scaffolds.

Encouraged by these results, also chlorination and bromination reactions of **1*** were investigated. Interestingly, P₄ was found to be set free as an intermediate during reactions of **1*** with PCl₅ and [WCl₆]. While the main product of the reaction with PCl₅ is PCl₃, different crystalline products of the reaction with [WCl₆] were formed depending on the reaction conditions. Thus, either [Cp**Fe*(η⁵-P₅Cl)] [W₂Cl₉] (**42**) crystallized or a co-crystallization of [(Cp**Fe*)₂(μ,η^{5:5}-P₁₀)] [W₂Cl₉]₂ (**43**) and **42** took place (Scheme 15). Moreover, the Br (**44**) or mixed Br/I (**45**) analogues of compound **39a** were obtained by reaction of **1*** with CuBr₂ and [(CpMo)₂(μ,η^{6:6}-P₆)] or CuBr and [Mn(thf)₆](I₃)₂.

Scheme 15. Further halogenation reactions of $[Cp^*Fe(\eta^5-P_5)]$ (**1***).

10 Appendices

10.1 Alphabetic List of Abbreviations

Å	Angstroem, $1 \text{ \AA} = 1 \cdot 10^{-10} \text{ m}$
°C	degree Celsius
1D	one-dimensional
2D	two-dimensional
3D	three-dimensional
Ad	adamantyl, $-\text{C}_{10}\text{H}_{15}$
a.d.p.	atomic displacement parameter
av.	average
Bn	benzyl, $-\text{CH}_2\text{C}_6\text{H}_5$
bp	boiling point
br (NMR)	broad
ⁿ Bu	<i>n</i> -butyl
^t Bu	<i>tert</i> -butyl
COSY	correlation spectroscopy
Cp	cyclopentadienyl, C_5H_5
Cp ^{''}	1,3-di- <i>tert</i> -butylcyclopentadienyl, $\text{C}_5\text{H}_3\text{tBu}_2$
Cp ^{'''}	1,2,4-tris- <i>tert</i> -butylcyclopentadienyl, $\text{C}_5\text{H}_2\text{tBu}_3$
Cp [°]	1- <i>tert</i> -butyl-3,4-dimethylcyclopentadienyl, $\text{C}_5\text{H}_2\text{Me}_2\text{tBu}_2$
Cp [*]	pentamethylcyclopentadienyl, C_5Me_5
Cp ^{BIG}	pentakis-4- <i>n</i> butylphenylcyclopentadienyl, $\text{C}_5(4\text{-nBuC}_6\text{H}_4)_5$
Cp ^{Bn}	pentabenzylcyclopentadienyl, $\text{C}_5(\text{CH}_2\text{Ph})_5$
Cp ^x	ethyltetramethylcyclopentadienyl, $\text{C}_5\text{Me}_4\text{Et}$
Cp ^R	substituted cyclopentadienyl ligand
CV	cyclic voltammetry
d	distance or day(s)
d (NMR)	doublet
δ	chemical shift
<i>o</i> -DCB	<i>ortho</i> -dichlorobenzene
<i>o</i> -DFB	<i>ortho</i> -difluorobenzene

DFT	density functional theory
<i>m</i> -DIB	1,3-diisopropylbenzene
DME	1,2-dimethoxyethane
DMF	dimethylformamide
dmsO	dimethylsulfoxide
DNA	deoxyribonucleic acid
dppp	bis(diphenylphosphino)propane
E	heavier element of the 15th group, E = P, As, Sb, Bi
e ⁻	electron
EI MS	electron impact mass spectrometry
en	ethylenediamine
EPR	electron paramagnetic resonance
ESI MS	electron spray ionization mass spectrometry
Et	ethyl
FAl ⁻	falanate, FAl{OC ₆ F ₁₀ (C ₆ F ₅) ₃ } ⁻
FD MS	field desorption ionization mass spectrometry
h	hour(s)
HMPA	hexamethylphosphoramide
HOMO	highest occupied molecular orbital
Hz	Hertz
<i>J</i> (NMR)	coupling constant
L	ligand (specified in text)
λ	wavelength
LUMO	lowest unoccupied molecular orbital
<i>m</i> (NMR)	multiplet
M	metal
<i>m/z</i>	mass to charge ratio
MAS	magic angle spinning
max.	maximum
Me	methyl
Mes	mesityl, 2,4,6-trimethylphenyl
MIM	mechanically interlocked material

MO	molecular orbital
MOF	metal-organic framework
MOP	metal-organic polyhedron
NMP	N-methyl-2-pyrrolidone
NMR	nuclear magnetic resonance
$\omega_{1/2}$	half width
OTf	triflate, CF_3SO_3^-
Ph	phenyl
P_n	polyphosphorus
POM	polyoxometallate
ppm	parts per million
<i>i</i> Pr	<i>iso</i> -propyl
q (NMR)	quartet
R	organic substituent
rms	root mean square
r.t.	room temperature
s (NMR)	singlet
SBB	supramolecular building block
SBU	secondary building unit
SCC	supramolecular coordination cage
sept (NMR)	septet
s.o.f.	site occupancy factor
t (NMR)	triplet
TEF ⁻	teflonate, $\text{Al}\{\text{OC}(\text{CF}_3)_3\}_4^-$
THF	tetrahydrofuran, $\text{C}_4\text{H}_8\text{O}$
THT	tetrahydrothiophene, SC_4H_8
trip	2,4,6-tri- <i>iso</i> -propylphenyl
vdW	van-der-Waals
VE	valence electrons
VT	various temperatures
WCA	weakly coordinating anion
X	any halide, X = Cl, Br, I

10.2 Curriculum Vitae

EDUCATION

since 01/2016	<p>Ph.D. studies in Inorganic Chemistry University of Regensburg (Germany)</p> <p>Ph.D. Thesis: <i>“Supramolecular Chemistry and Halogenation Reactions of Pentaphosphaferrocenes”</i> (Supervisor: Prof. Dr. Manfred Scheer)</p>
Apr 2016 – Jul 2016	<p>Research stay during the Ph.D. studies University of California, Berkeley (USA) (Supervisor: Prof. T. Don Tilley)</p>
Sep 2013 – Sep 2015	<p>Master of Science in Chemistry University of Regensburg (Germany)</p> <p>Master Thesis: <i>“Coordination behavior of polyphospholyl anions”</i> (Supervisor: Prof. Dr. Manfred Scheer)</p>
May 2011 – Sep 2013	<p>Bachelor of Science in Chemistry University of Regensburg (Germany)</p> <p>Bachelor Thesis: <i>“Synthesis and coordination behavior of the phospholyl ligands $[P_3C_2R_2]^-$ ($R = Me, {}^tBu, Mes$)”</i> (Supervisor: Prof. Dr. Manfred Scheer)</p>
May 2011	<p>Abitur (A-levels) Gymnasium der Schulstiftung Seligenthal, Landshut (Germany)</p>

SCHOLARSHIPS

Jun 2017 – Feb 2020	PhD scholarship - Studienstiftung des deutschen Volkes
Sep 2017	Conference Scholarship - Gesellschaft Deutscher Chemiker (German Chemical Society)
Apr 2017	Conference Scholarship - International PhD Program of the University of Regensburg (iPUR)
Apr 2016 – Jul 2016	Scholarship - German Academic Exchange Service

CONFERENCES

Aug 2019	Talk – Wissenschaftliches Kolloquium von Arbeitsgruppen für Anorganische Chemie 2019 in Hirschegg, Austria
Apr 2019	Poster – 16 th European Workshop on Phosphorus Chemistry (EWPC) in Bristol, United Kingdom
Feb 2019	Poster – 17 th Ferrocene-Colloquium in Rostock, Germany
Jul – Aug 2018	Talk – 43 rd International Conference on Coordination Chemistry in Sendai, Japan
Jul 2018	Talk – 28 th International Conference on Organometallic Chemistry in Florence, Italy
Sep 2017	Poster - GDCh Wissenschaftsforum Chemie, Berlin, Germany
Aug 2017	Talk – Wissenschaftliches Kolloquium von Arbeitsgruppen für Anorganische Chemie 2017 in Hirschegg, Austria
Apr 2017	Talk – 253 rd ACS National Meeting, San Francisco, USA
Feb 2017	Talk – 15 th Ferrocene Colloquium, Mainz, Germany

10.3 Acknowledgments

Zuletzt möchte ich mich bei folgenden Personen bedanken:

- Prof. Dr. Manfred Scheer für die Gelegenheit an so einem interessanten Thema zu arbeiten und auf internationale Tagungen fahren zu können, sowie die exzellenten Arbeitsbedingungen
- Prof. Dr. Henri Brunner (Zweitgutachter), Prof. Dr. Frank-Michael Matysik (Drittprüfer) und Apl. Prof. Dr. Rainer Müller (Vorsitz) für die Bereitschaft, den Prüfungsausschuss zu stellen
- Dr. Eugenia Peresyphina and Dr. Sc. Alexander V. Virovets for thorough proofreading, the countless night and weekend shifts and nevertheless truly untiring dedication to get even the most complicated data sets publishable. This work would not have been possible without you!
- Dr. Gábor Balász für seine wertvollen Ratschläge und die Hilfe mit EPR-Spektren
- Dr. Martin Piesch für die Hilfe mit Programmen, Computern und für die DFT-Rechnungen
- Der Studienstiftung des Deutschen Volkes für das Promotionsstipendium und neben der finanziellen auch der großartigen ideellen Förderung
- Prof. Dr. T. Don Tilley for hosting me at UC Berkeley and for the great supervision
- Prof. Dr. Werner Kremer für die zahlreichen MAS NMR Messungen
- Allen Mitarbeitern der zentralen Analytik und Werkstätten
- Allen aktuellen und ehemaligen Mitglieder des Arbeitskreises, insbesondere Anna, Babse, Christoph, Claudia, Felix, Julian, Kevin, Lena, Luis, Maria, Martin, Matze, Michi, Sabrina und allen anderen, die zu einer fröhlichen und konstruktiven Arbeitsatmosphäre beigetragen haben
- Dr. Claudia Heindl, Dr. Barbara Hiltl, Dr. Amélie Nicolay, Dr. Rebecca Grünbauer, Kevin Grill und Sabrina Dinauer für die gute Laborstimmung
- Meine Mitreisenden auf Konferenzen und anschließenden Urlauben: Luis, Anna, Matthias und Babse für die coole Zeit weit weg
- Maria, Claudia, Felix, Tobi, Andrea, Dani, Martin P. und Martin W. für die entspannenden Mittagspausen und die Ablenkung durch irgendwelche Spiele die Maria wieder aufgetrieben hat
- Maria und Julian für die emotionale Unterstützung insbesondere auf den letzten Metern
- The Wolf group for inviting me to all the switch Saturdays and group parties and making me have two groups of colleagues with twice the fun 😊
- Den Quersties (ich hoffe der nächste Italienurlaub steht noch?), der Zehnerleisbande und der Krimidinner-Truppe, durch die ich mich in Regensburg zuhause gefühlt habe.
- Jule und Mattcher für Cook'n'Cruise time, Katzenvideos und Wanderurlaube.

Ein ganz besonderer Dank gilt meiner Familie:

Meinen Eltern, die mich auf allen Wegen immer uneingeschränkt unterstützt haben und mir Halt gaben, und nicht zu vergessen das leckere Essen und das Dach über dem Kopf 😊

Meinen Geschwistern Kristina und Thomas, mit Markus und Sophie und meiner Nichte Paula, für's Zuhören, Ablenken, vor Augen führen was wirklich wichtig ist – und zuletzt auch hier wieder das Dach über dem Kopf!

Meinem Mann Christian. Ohne dich hätte ich wohl kaum die gesamte Studien- und Promotionszeit durchgestanden. Du warst immer für mich da, hast an mich geglaubt, mich unterstützt und mich -eigentlich ständig- zum Lachen gebracht. Danke, dass du seit dem ersten Semester immer an meiner Seite warst und mir tagtäglich ein Lächeln auf die Lippen zauberst.